University of Pennsylvania
ScholarlyCommons

Publicly Accessible Penn Dissertations

2017

Thermodynamic Analysis For Improving Understanding And Performance Of Hybrid Power Cycles Using Multiple Heat Sources Of Different Temperatures

Ting Yue
University of Pennsylvania, yuet06@gmail.com

Follow this and additional works at: https://repository.upenn.edu/edissertations

 Part of the Mechanical Engineering Commons, and the Oil, Gas, and Energy Commons

Recommended Citation

Yue, Ting, "Thermodynamic Analysis For Improving Understanding And Performance Of Hybrid Power Cycles Using Multiple Heat Sources Of Different Temperatures" (2017). *Publicly Accessible Penn Dissertations*. 2658.
https://repository.upenn.edu/edissertations/2658

This paper is posted at ScholarlyCommons. https://repository.upenn.edu/edissertations/2658
For more information, please contact repository@pobox.upenn.edu.

Thermodynamic Analysis For Improving Understanding And Performance Of Hybrid Power Cycles Using Multiple Heat Sources Of Different Temperatures

Abstract
Past studies on hybrid power cycles using multiple heat sources of different temperatures focused mainly on case studies and almost no general theory about this type of systems has been developed. This dissertation is a study of their general thermodynamic performance, with comparisons to their corresponding single heat source reference systems. The method used in the dissertation was step-wise: to first analyze the major hybrid power cycles (e.g. Rankine, Brayton, Combined Cycles, and their main variants) thermodynamically, without involving specific operation parameter values, and develop some generalized theory that is at least applicable to each type of system. The second step was to look for commonalities among these theories and develop the sought generalized theory based on these commonalities. A number of simulation case studies were performed to help the understanding and confirm the thermodynamic results. Exergo-economic analysis was also performed to complement the thermodynamic analysis with consideration of externalities, and was compared to the conventional economic analysis method. The generalized expressions for the energy/exergy efficiency differences between the hybrid and the corresponding single heat source systems were developed. The results showed that the energy and exergy efficiencies of the hybrid systems are higher than those of their corresponding single heat source reference systems if and only if the energy/exergy conversion efficiency (defined in the dissertation) of the additional heat source (AHS, can be any heat source that has lower temperature) is larger than that of the original heat source. Sensitivity analysis results showed the relations between the temperature and heat addition rate of the AHS and the energy/exergy efficiency of the hybrid systems. Other big advantages of hybrid systems, i.e. the effects on replacement of fossil fuel by renewable, nuclear and waste energy, lower emissions and depletion of fossil fuel, were revealed in the economic analysis, by considering the cost reduction from fuel saving and carbon tax. Simple criteria were developed to help compare the hybrid and reference systems and determine under which conditions the hybrid systems will have better thermodynamic or economic performance than the reference ones. The results and criteria can be used to help design the hybrid systems to achieve higher energy and/or exergy efficiencies and/or lower levelized electricity cost (LEC) before detailed design or simulation or experiment. So far, 3 archival journal papers and 3 conference papers were published from this dissertation work.

Degree Type
Dissertation

Degree Name
Doctor of Philosophy (PhD)

Graduate Group
Mechanical Engineering & Applied Mechanics

First Advisor
Noam Lior

This dissertation is available at ScholarlyCommons: https://repository.upenn.edu/edissertations/2658

Keywords
Exergo-economic analysis, Multiple heat sources with different temperatures, Power systems simulation, Thermal hybrid power cycles, Thermochemical hybrid power cycles, Thermodynamic analysis

Subject Categories
Engineering | Mechanical Engineering | Oil, Gas, and Energy

This dissertation is available at ScholarlyCommons: https://repository.upenn.edu/edissertations/2658

THERMODYNAMIC ANALYSIS FOR IMPROVING UNDERSTANDING AND PERFORMANCE OF HYBRID POWER CYCLES USING MULTIPLE HEAT SOURCES OF DIFFERENT TEMPERATURES

Ting Yue

A DISSERTATION

in

Mechanical Engineering and Applied Mechanics

Presented to the Faculties of the University of Pennsylvania

in

Partial Fulfillment of the Requirements for the

Degree of Doctor of Philosophy

2017

Supervisor of Dissertation

_____

Dr. Noam Lior
Professor, Department of Mechanical Engineering and Applied Mechanics

Graduate Group Chairperson

_____

Dr. Kevin T. Turner, Professor, Mechanical Engineering and Applied Mechanics and Materials Science and Engineering

Dissertation Committee
Dr. Haim H. Bau, Professor, Committee Chair, Department of Mechanical Engineering and Applied Mechanics, University of Pennsylvania
Dr. Warren D. Seider, Professor, Department of Chemical and Biomolecular Engineering, University of Pennsylvania
Dr. Gerard F. Jones, Professor, Department of Mechanical Engineering, Villanova University

THERMODYNAMIC ANALYSIS FOR IMPROVING UNDERSTANDING AND PERFORMANCE OF HYBRID POWER CYCLES USING MULTIPLE HEAT SOURCES OF DIFFERENT TEMPERATURES

COPYRIGHT

2017

Ting Yue

This work is licensed under the

Creative Commons Attribution-

NonCommercial-ShareAlike 3.0

License

To view a copy of this license, visit

https://creativecommons.org/licenses/by-nc-sa/3.0/us/

DEDICATION

To my loving parents, especially my Mother

for their support and caring, persistently and endlessly

ACKNOWLEDGMENT

First and foremost, I would like to express my sincere gratitude to my beloved academic advisor, Professor Noam Lior. It was a great honor to work under the guidance of Dr. Lior, at one of best universities in the world for the past years. With the help of his decades of experience in the field of power generation and many other related fields, Dr. Lior helped me define the topic, objective and scope of this dissertation and provided much guidance continuously over the years assisting me to overcome the many difficulties that were encountered during my research, with patience and immense knowledge. Dr. Lior also helped me improve my English pronunciation and writing skills, as well as my presentation skills. What's more, he also taught me about the culture in the US and invited me many times for leisure trips and holiday dinners, making my research life a little easier. There is an old saying in my country as "once a teacher, always a father", and Dr. Lior is like my father and will always be.

Besides my advisor, I would like to thank the rest of my thesis committee: Professor Haim Bau, Professor Warren Seider, and Professor Gerard Jones, for their time in reviewing my proposal and dissertation, and for their insightful comments and encouragement.

I would also like to thank all the professors who taught me courses at the University of Pennsylvania, including Dr. Lior, Dr. Lukes, Dr. Ayyaswamy, Dr. Carchidi, Dr. Kumar, Dr. Castañeda, Dr. Kothmann and Dr. Mylovanov.

Also, thank all the staff in the MEAM office, especially Maryeileen, Peter and Sue, who helped me many kinds of things, which are hard to count.

I would like to thank my fellow labmates, especially Yuejun, for the stimulation discussions, for all the work we have been working together, and for all the fun we had in the past years. Also, I would like to thank Professor Zhang Na for teaching me how to use the software and for all other help, such as accompanying my mom when she felt lonely in the US while I was working on my research and could not spend too much time with her.

What's more, I would like to thank the University of Pennsylvania, for admitting me as a PhD student, with the help of Dr. Lior. The university is one of the oldest and best university in the US. It provides modern and comprehensive facilities that made my research and life easier. To name a few, there are numerous food trucks all around the campus, providing cheap and tasty foods from all over the world. It also provides several modern playgrounds so that I can play soccer in the weekend for fun and to keep healthy. One of the playgrounds is even covered with an air tent in the winter so that people can play in there even there is heavy snow outside. Besides the infrastructures, the university is embedded with its unique culture, influencing all its students. For the past many years, I not only studied here but also lived here. This was a priceless experience for me and will surely positively influence my future life. I am really proud of being about to graduate as a PhD student from Penn and hope that Penn will be proud of me as one of her students in the future.

Last but not the least, I would like express my earnest appreciations to my parents. This dissertation is dedicated to them. Without their support, I could not have finished this dissertation. Their support is unconditional and persistent. I will do my best to pay back their love after graduation and make them happy.

Ting Yue

Philadelphia, PA

ABSTRACT

THERMODYNAMIC ANALYSIS FOR IMPROVING UNDERSTANDING AND PERFORMANCE OF HYBRID POWER CYCLES USING MULTIPLE HEAT SOURCES OF DIFFERENT TEMPERATURES

Ting Yue

Dr. Noam Lior

Past studies on hybrid power cycles using multiple heat sources of different temperatures focused mainly on case studies and almost no general theory about this type of systems has been developed. This dissertation is a study of their general thermodynamic performance, with comparisons to their corresponding single heat source reference systems. The method used in the dissertation was step-wise: to first analyze the major hybrid power cycles (e.g. Rankine, Brayton, Combined Cycles, and their main variants) thermodynamically, without involving specific operation parameter values, and develop some generalized theory that is at least applicable to each type of system. The second step was to look for commonalities among these theories and develop the sought generalized theory based on these commonalities. A number of simulation case studies were performed to help the understanding and confirm the thermodynamic results. Exergo-economic analysis was also performed to complement the thermodynamic analysis with consideration of externalities, and was compared to the conventional economic analysis method. The generalized expressions for the energy/exergy efficiency differences between the hybrid and the corresponding single heat source systems were developed. The results showed that the energy and exergy efficiencies of the hybrid systems are higher than those of their

corresponding single heat source reference systems if and only if the energy/exergy conversion efficiency (defined in the dissertation) of the additional heat source (AHS, can be any heat source that has lower temperature) is larger than that of the original heat source. Sensitivity analysis results showed the relations between the temperature and heat addition rate of the AHS and the energy/exergy efficiency of the hybrid systems. Other big advantages of hybrid systems, i.e. the effects on replacement of fossil fuel by renewable, nuclear and waste energy, lower emissions and depletion of fossil fuel, were revealed in the economic analysis, by considering the cost reduction from fuel saving and carbon tax. Simple criteria were developed to help compare the hybrid and reference systems and determine under which conditions the hybrid systems will have better thermodynamic or economic performance than the reference ones. The results and criteria can be used to help design the hybrid systems to achieve higher energy and/or exergy efficiencies and/or lower levelized electricity cost (LEC) before detailed design or simulation or experiment. So far, 3 archival journal papers and 3 conference papers were published from this dissertation work.

TABLE OF CONTENTS

LIST OF TABLES

LIST OF ILLUSTRATIONS

The flow and T-s diagrams of hybrid gas turbine power plants with intercooling are shown in Figs. 5-3 and 5-4, respectively. If there is no intercooling used, the operation cycle would have been 1-2-3-4-5-1. When the intercooling is used, compressed air from the low-pressure compressor (LP) at state 11 is cooled to state 12 and then compressed by the high-pressure (HP) compressor to state 2, at which the additional heat source is added. The operation cycle for the intercooled Brayton cycle is thus 1-11-12-2-3-4-5-1. Due to the pressure losses during heat addition from state 2 to state 3 and from state 3 to state 4, the pressure at the outlet of a component is lower than at its inlet. In addition, there is a pressure loss in the intercooler and all piping, so the air pressure at the intercooler outlet is lower than at its inlet. The temperature at outlet of the compressor is decreased from state 21 to

CHAPTER 1

INTRODUCTION

Most thermal power generation systems (e.g. fossil fuel, nuclear, solar, geothermal) use a single source of heat at a single temperature, and also use that heat source directly as heat. In some cases, the cost of the heat is related to the temperature, such as with solar heat collection equipment; the temperature of the heat source is limited by operational considerations, such as in nuclear reactors; the available temperature is well below the material endurance temperature, such as in geothermal heat sources; it is desired to employ renewable or other types of energy that reduces global warming gas emissions or/and reduces use of depletable fuels; waste heat at appropriate temperatures and price is available, such as in compounded internal combustion engines. It was found in these cases that gains in efficiency and reduction of emissions and cost could be achieved by power systems using multiple heat sources of different temperatures, which are called here "hybrid" systems.

Early work on hybrid power cycles was done by Lior and co-workers [1-5] who have analyzed and developed hybrid solar-powered/fuel assisted steam cycles and performed experiments with one of them (22.4 kW output), a concept similar to the one that was later (in the 1980s) used by the Luz company for the construction and successful operation of 9 solar-thermal power plants (SEGS) generating about 354 MWe (net) in southern California [6–8], that still operate competitively. The concept is successful because it uses solar

energy at the lower temperature level, where it is more economical, and augments it by smaller amount of heat from fuel combustion to: (1) raise the cycle temperature and thus efficiency, and (2) allow fuel heat backup when solar energy is not sufficiently available, without having to increase the number of collectors and thermal storage capacity. Furthermore, proper configuration of the systems' heat donors and receivers offers a closer match between their temperatures (smaller temperature differences between donors and receivers) and thus lower exergy losses. The energy and global warming crises have strongly increased the interest in such systems, especially solar-based, and several plants are in operating, construction or planning.

Another concept, of thermochemical hybridization, is explained in papers by Zhang, Lior and co-workers [9-12] and recent studies by others [13-15], and is discussed in CHAPTER 7 and CHAPTER 9.

Past studies on hybrid power cycles using multiple heat sources of different temperatures focused mainly on case studies and almost no general theory about this type of systems has been developed. This dissertation is a study of their general thermodynamic performance, with their comparison to their corresponding single temperature heat source reference system.

The method used in the dissertation is step-wise: to first analyze the major, most commonly used, hybrid power generation systems thermodynamically, without involving specific operation parameter values. In this way, some generalized theory that is at least applicable

to *this* type of system can be developed. The second step is to perform such an analysis for all the major types of power generation systems (e.g. Rankine, Brayton, Combined Cycles, and their main variants). The third step is to find commonalities between these theories (if any). The fourth and last step is to develop the sought generalized theory based on these commonalities.

A number of simulation case studies were performed to help the understanding and confirm the thermodynamic generalization of the results. Exergo-economic analysis was also performed to complement the thermodynamic analysis with consideration of the externalities and carbon tax, and was compared to the conventional economic analysis method.

The generalized expressions for the energy/exergy efficiency difference between the hybrid and the corresponding single heat source system were developed. The results showed that the energy and exergy efficiencies of the hybrid systems are higher than those of their corresponding single heat source reference systems if and only if the energy/exergy conversion efficiency (defined in the dissertation) of the additional heat source (AHS, can be any heat source that has lower temperature) is larger than that of the original heat source. Sensitivity analysis results showed the relation between the temperature and heat addition rate of the AHS and the energy/exergy efficiency of the hybrid systems, for different energy conversion efficiency of the AHS. Simple criteria were also developed to help compare the hybrid and reference system and determine under which conditions the hybrid systems will have better thermodynamic or economic performance than the reference ones.

The results and criteria found in the dissertation can be used to help design the hybrid systems to achieve higher energy and/or exergy efficiencies or lower levelized electricity cost (LEC) before detailed design or simulation or experiment. These are the main contributions from the author of the dissertation to the state of knowledge. None of this work has been done by others, to the best of the author's knowledge.

So far, 3 archival journal papers [16-18] and 3 conference papers were published from this dissertation work.

In this dissertation, CHAPTER 1 serves as a preparation of the thermodynamic analysis by defining and discussing the important criteria that could be used to evaluate and compare the performance of the hybrid systems and reference (single heat source) systems. Energy efficiency and exergy efficiencies were defined in this chapter, along with some other system performance criteria. The following chapters (CHAPTERS 3-9), were the main contributions of the dissertation to the state of knowledge, and are divided into two parts. The first part, containing CHAPTERS 3-7, is about the *thermodynamic* performance of the hybrid systems, and the second part, containing CHAPTERS 8-9, is about the *economic* performance of the hybrid systems. CHAPTER 10, the final, summarizes the conclusions and makes some recommendations about the hybrid power systems.

For the first part, the background review of thermal hybrid systems was made in CHAPTER 3, followed by the thermodynamic analysis of hybrid power generation systems based on Rankine cycles (CHAPTER 4), Brayton cycles (CHAPTER 5) and the combined

cycle (CHAPTER 6), respectively. CHAPTER 7, beginning with a background review of the thermochemical hybrid systems, was the thermodynamic analysis of the thermochemical hybrid systems, focusing on two representative thermochemical hybrid systems.

For the second part, the economic analysis of the thermal hybrid systems was made in CHAPTER 8, and of the thermochemical hybrid systems in CHAPTER 9, respectively. These two parts, especially the first parts that dealt with the thermodynamic analysis, contributed to the state of knowledge.

References for Chapter 1

[1] Koai K., Lior N., YeH H., Performance analysis of a solar-powered/fuel-assisted Rankine cycle with a novel 30hp turbine. Sol Energy 1984;(32)6:753-764.

[2] Lior N., Koai K., Solar-Powered/Fuel-Assisted Rankine Cycle Power and Cooling System: Simulation Method and Seasonal Performance. J Sol Energ-T ASME 1984;106:142-152.

[3] Lior N., Koai K., Solar-Powered/Fuel-Assisted Rankine Cycle Power and Cooling System: Sensitivity Analysis. J Sol Energ-T ASME 1984;106:447-456.

[4] Lior N., Solar energy and the steam Rankine cycle for driving and assisting heat pumps in heating and cooling modes. Energ Convers 1977;(16)3:111-123.

[5] Sherburne D., Lior N., Evaluation of minimum fuel consumption control strategies in the solar-powered fuel-assisted hybrid Rankine cycle. Proceedings ASES Ann. Meeting 1986:300-303.

[6] Kolb J., Evaluation of Power Production from the Solar Electric Generating Systems at Kramer Junction: 1988 to 1993. Proceedings of the Solar Engineering 1995; ASME Press New York: 1:499-504.

[7] Cohen G.H., Kearny O., Improved Parabolic Trough Solar Electric Systems Based on the Segs Experience. Proceedings of the American Solar Energy Society Conference 1994:147-150.

[8] Jensen C., Price H., Kearney D., The SEGS Power Plants: 1988 Performance. 1989 ASME International Solar Energy Conference San Diego CA.

[9] Hong H., Jin H., Ji J., Wang Z., Cai R., Solar thermal power cycle with integration of methanol decomposition and middle-temperature solar thermal energy. Sol Energy 2005;78:49-58.

[10] Jin H., Hong H., Sui J., Liu Q., Fundamental study of novel mid-and low-temperature solar thermochemical energy conversion. Sci China Ser E 2009;52(5):1135-1152.

[11] Zhang N., Lior N., Use of low/mid-temperature solar heat for thermochemical upgrading of energy, part I: application to a novel chemically-recuperated gas-turbine power generation (SOLRGT) system. J Eng Gas Turb Power 2012;134(7):072301.

[12] Zhang N., Lior N., Use of Low/Mid-Temperature Solar Heat for Thermochemical Upgrading of Energy, Part II: A Novel Zero-Emissions Design (ZE-SOLRGT) of the Solar Chemically-Recuperated Gas-Turbine Power Generation System (SOLRGT) guided by its Exergy Analysis. J Eng Gas Turb Power 2012;134(7):072302.

[13] Zhang H., Hong H., Gao J., Jin H., Mid-temperature Solar Hybridization CCHP with DME Fuelled-Chemical Looping Combustion. ECOS 2015: Proceedings of the 28th International Conference on Efficiency, Cost, Optimization, Simulation, and Environmental Impact of Energy Systems;2015 Jun 30- Jul 3;Pau, France.

[14] Hao Y., Kong H., A Solar Thermochemical Fuel Production System Integrated with Fossil Fuels. ECOS 2015: Proceedings of the 28th International Conference on

Efficiency, Cost, Optimization, Simulation, and Environmental Impact of Energy Systems;2015 Jun 30- Jul 3; Pau, France.

[15] Manente G., Lazzaretto A., Solar-aided precombustion CO_2 capture in natural gas combined cycles. ECOS 2015: Proceedings of the 28th International Conference on Efficiency, Cost, Optimization, Simulation, and Environmental Impact of Energy Systems;2015 Jun 30- Jul 3;Pau, France.

[16] Yue T., Lior N., Thermodynamic analysis of solar-assisted hybrid power generation systems integrated with thermochemical fuel conversion. Energy 2017(118):671-683.

[17] Yue T., Lior N., Exergo economic analysis of solar-assisted hybrid power generation systems integrated with thermochemical fuel conversion. Applied Energy 2017(191):204-222.

[18] Yue T., Lior N., Exergo-economic Competitiveness Criteria for Hybrid Power Cycles using Multiple Heat Sources of Different Temperatures. Energy 2017:1-19. Article in Press.

CHAPTER 2

ENERGY AND EXERGY PERFORMANCE CRITERIA

2.1. Introduction

Most thermal power cycles currently in use rely on a single temperature heat source. For example, in fossil fuel power plants, the high temperature is achieved through burning coal, fuel oil, or natural gas to generate power. This kind of plant is widely used because of its many benefits, such as long experience with design, control and maintenance, but it also has disadvantages, among which are emissions and exergy loss of about 30% in the combustion process are perhaps the most serious ones, notwithstanding depletion of fossil fuels, and for many fuel-importing countries the related energy insecurity. Many air pollutants such as NO_X, SO_X, and health threatening particulates, are created by burning fossil fuels, accompanied by carbon emission (CO_2 emission is 2,316 kg/ton for coal, 1.87 kg per cubic meter for natural gas, and 2.11 kg per liter for gasoline [1]), and cause the earth-threatening greenhouse effect pointing to the need for reducing the use of fossil fuels. They can be replaced by renewable heat sources or ones that produce lower or no emissions during the plant operation, or are more economical. Also, as will be discussed in the exergy analysis in Section 2.3, one of the important advantages of thermal hybrid power cycles compared with conventional fossil-fuel only power cycles is their ability to reduce this temperature difference and thus the associated exergy destruction by choosing heat sources

(such as from solar collectors, waste heat, or geothermal) that have temperatures closer to that of the working fluid.

For comparison, the highest temperature of the hybrid cycles, which use two or more heat sources, is kept the same as that of the reference power cycles (use a single heat source but with similar configuration), which is in practice at the maximal temperature the materials can tolerate. In this way, the theoretical maximal efficiency (which is the Carnot efficiency) is the same for both the conventional single heat source system and the hybrid systems studied here. In this way, the effect of using additional heat sources on the thermodynamic and economic performance of the conventional single heat source system can be studied and compared.

To study the thermodynamic performance of the hybrid systems and compare them with their corresponding single heat source systems, energy efficiency of the hybrid systems must be analyzed. Energy efficiency, or thermal efficiency that is commonly used in practice, is the most important thermodynamic performance criterion of power generation systems in general. It presents how much work can be produced from a certain amount of energy. It is thus of interest of study whether the hybrid have higher energy efficiency than the corresponding conventional single heat source systems, by how much, and how it is influenced by the temperature or the heat input of the additional heat source (AHS) of the hybrid systems.

Although energy efficiency is most widely used thermodynamic performance criterion, it is not perfect. The energy efficiency does not consider the ability of the heat source for doing work. Different heat sources may have different potential of doing work (called exergy) even if they have the same amount of energy. Considering that the hybrid power generation systems studied in this research use different kinds of heat sources or heat sources that have different temperatures, it is thus necessary to use the exergy analysis which complements the energy analysis, to fully study and reveal the advantages of hybrid power generation systems using multiple heat sources of different temperatures. Details about exergy analysis are discussed in Section 2.3.

This chapter serves as a preparation of the thermodynamic analysis by defining and discussing the important criteria that could be used to evaluate and compare the performance of the hybrid systems and reference (single heat source) systems. Energy efficiency and exergy efficiencies were defined in this chapter, along with some other system performance criteria. The following chapters (CHAPTERS 3-9), excluding the conclusions of the dissertation (CHAPTER 10), were the main contributions of the dissertation to the state of knowledge, and is divided into two parts. The first part, containing CHAPTERS 3 to 7, is about the *thermodynamic* performance of the hybrid systems, and the second part, containing CHAPTERS 8-9, is about the *economic* performance of the hybrid systems.

For the first part, the background review of the thermal hybrid system was made in CHAPTER 3, followed by the thermodynamic analysis of hybrid power generation systems

based on Rankine cycles (CHAPTER 4), Brayton cycles (CHAPTER 5) and the combined cycle (CHAPTER 6), respectively. CHAPTER 7, beginning with a background review of the thermochemical hybrid systems, is the thermodynamic analysis of the thermochemical hybrid systems, focusing on two representative thermochemical hybrid systems.

For the second part, the economic analysis of the thermal hybrid systems was made in CHAPTER 8, and of the thermochemical hybrid systems was made in CHAPTER 9, respectively. These two parts, especially the first parts that dealt with the thermodynamic analysis, contributed to the state of knowledge.

2.2. Energy analysis

The energy efficiency η of a power cycle is defined as the ratio between the total net power output of the system $\dot{W}_{\text{net}}$ and the total heat input rate $\dot{Q}_{\text{in}}$

$$\eta = \frac{\dot{W}_{\text{net}}}{\dot{Q}_{\text{in}}}. \tag{2.1}$$

If there are more than one heat sources in the system, Eq. (2.1) becomes

$$\eta_{\text{h}} = \frac{\dot{W}_{\text{net}}}{\sum_i \dot{Q}_i}, \tag{2.2}$$

in which $\dot{Q}_i$ is the heat input rate of the heat source i and η_{h} is the energy efficiency of the hybrid power cycle.

For example, when fuel or biomass is used as the heat source, the heat input rate of the fuel or biomass $\dot{Q}_{\mathrm{f}}$ is usually calculated by

$$\dot{Q}_{\mathrm{f}} = \dot{m}_{\mathrm{f}} \cdot \mathrm{LHV}, \tag{2.3}$$

in which $\dot{m}_{\mathrm{f}}$ [kg/s] is the mass flow rate of the fuel or biomass used in the system and LHV [kJ/kg] is the lower heating value of the fuel, which could be found in the tables or of the biomass, which is treated as known in this research. In Eq. (2.3), LHV is used instead of HHV which is the higher heating value of the fuel or biomass, because the water ($\mathrm{H_2O}$) formed during combustion of fuel or biomass usually leaves the system in the form of vapor and the latent heat contained in the vapor should thus not be included in the thermal analysis of the system.

It is very noteworthy that the most widely used energy efficiency definition, based on Eqs (2.2) and (2.3), does not consider the heat input source Q_i temperature, T_i, which is a critically important thermodynamic property and must be included in such analyses, typically using exergy efficiency, which we do in Section 2.3.

When geothermal or waste heat is used as the heat source, the heat input rate from the heat source to the system is the heat flow rate of the heat source and is usually easy to find.

When solar heat is used as the heat source, the solar radiation rate incident on the solar collector is

$$\dot{Q}_{\text{rad}} = I_{\text{s}} \cdot A_{\text{SC}}, \tag{2.4}$$

in which A_{SC} [m^2] is the effective radiation absorbing area of the solar collector normal to the direction of the solar flux I_{s} [kW/m^2]. I_{s} may be augmented by a solar concentrator.

Different from $\dot{Q}_{\text{rad}}$, $\dot{Q}_{\text{sol}}$ is the heat addition rate to the working fluid of the power cycle (both of which change with time and are defined as transient variables), which is expressed by

$$\dot{Q}_{\text{sol}} = \eta_{\text{receiver}} \cdot \eta_{\text{optical}} \cdot \dot{Q}_{\text{rad}}, \tag{2.5}$$

in which η_{receiver} is the solar receiver efficiency, which is the ratio between the heat transferred to the working fluid and the heat received by the solar receiver, and η_{optical} is the optical efficiency of the solar collector, which is the ratio between the heat received by the solar receiver and the incident solar radiation on the solar collector. The ratio between $\dot{Q}_{\text{sol}}$ and $\dot{Q}_{\text{rad}}$ can be called the solar collector efficiency η_{sc} and is the multiplication of the solar collector receiver efficiency and optical efficiency according to Eq. (2.5),

$$\eta_{\text{sc}} = \frac{\dot{Q}_{\text{sol}}}{\dot{Q}_{\text{rad}}} = \eta_{\text{receiver}} \cdot \eta_{\text{optical}}. \tag{2.6}$$

Thus for a power cycle using both fuel and solar as the heat sources, the energy efficiency of the hybrid power cycle η_{h} is expressed, according to Eqs (2.2), (2.3) and (2.6) as

$$\eta_{\mathrm{h}} = \frac{\dot{W}_{\mathrm{net}}}{\dot{Q}_{\mathrm{f}} + \dot{Q}_{\mathrm{rad}}} = \frac{\dot{W}_{\mathrm{net}}}{\dot{m}_{\mathrm{f}} \cdot \mathrm{LHV} + \frac{\dot{Q}_{\mathrm{sol}}}{\eta_{\mathrm{sc}}}}. \tag{2.7}$$

In Eq. (2.7), $\dot{Q}_{\mathrm{rad}}$ is used instead of $\dot{Q}_{\mathrm{sol}}$ as the solar heat input of the hybrid power generation systems. This is because that $\dot{Q}_{\mathrm{rad}}$ accounts for the optical losses in the solar receiver while $\dot{Q}_{\mathrm{sol}}$ does not. Also, this method relates the solar input with the area of solar collector through Eq. (2.4), whose cost is a major part of the solar hybrid power plant cost [2]. Also, if $\dot{Q}_{\mathrm{sol}}$ is used instead of $\dot{Q}_{\mathrm{rad}}$, it can be considered as a special case of Eq. (2.8) when $\eta_{\mathrm{sc}} = 1$.

2.3. Exergy analysis

Unlike energy which is conserved in a process, exergy, which is the potential for power generation [3] that is lost (or “destroyed” when it is rejected from the system without any further use) in processes, must be preserved. Systems should thus be carefully designed to minimize exergy destruction. This is especially important when different types of heat sources are used in one system since they may have different exergy value even if the energy content is the same, so using energy analysis alone cannot fully reflect this difference in the ability of doing work by each type of heat source.

For the following thermodynamic analysis, the relation between energy and exergy is defined here, by the "exergy factor" [4], ψ ,

$$\psi = \frac{B}{Q}, \tag{2.8}$$

in which B [kJ] is the total exergy content and Q [kJ] is the total energy content of the mass or heat flow.

Neglecting kinetic, potential, and nuclear exergy, which are often small or zero in comparison with the chemical exergy, the exergy factor of fuel at environment condition (ambient temperature and pressure) is

$$\psi_{\mathrm{f}} = \frac{b_{\mathrm{f}}}{\mathrm{LHV}}, \tag{2.9}$$

in which b_{f} [kJ/kg] is the specific exergy of fuel, which can be found in the tables [14] or calculated based on Eq. (2.9).

The exergy factor of such a heat flow (such as geothermal or waste heat), is, according the Carnot efficiency equation,

$$\psi_{\mathrm{h}} = \frac{\dot{B}_{\mathrm{h}}}{\dot{Q}_{\mathrm{h}}} = 1 - \frac{T_0}{T_{\mathrm{h}}}, \tag{2.10}$$

in which B_h [kJ/kg]and Q_h [kJ/kg] are the exergy and energy content of the heat flow, respectively, T_h [K] and T_0 [K] are the temperature of the heat flow and the environment, respectively.

A commonly accepted definition of the exergy of solar heat does not exist [4-13]. One way to calculate it is to use the temperature at the sun surface (about 5,800 K) as the temperature of the solar radiation, and on the other extreme to use the temperature associated with the working fluid (such as at the solar collector inlet, outlet, the average temperature in the solar collector, or even 10 K or 20 K above the solar collector inlet, outlet temperature, the average temperature in the solar collector) heated by the solar radiation. In any solar exergy definitions, the solar radiation exergy B_{rad} can be expressed using the solar exergy factor ψ_{rad} by

$$B_{rad} = \psi_{rad} Q_{rad}. \tag{2.11}$$

When the solar exergy is defined based on the working fluid temperature at the outlet of the solar collector, ψ_{rad} can be expressed, according to Eq. (2.10), by

$$\psi_{sol} = 1 - \frac{T_0}{T_{sol}}, \tag{2.12}$$

where T_{sol} [K] is the temperature at the outlet of the solar collector. When the solar exergy is defined based on the temperature at the solar surface, the solar exergy factor is expressed by

$$\psi_{ss} = 1 - \frac{T_0}{T_{ss}}, \tag{2.13}$$

in which T_{ss} is the effective temperature at the solar surface, at about 5,800 K. Other solar exergy definitions obviously result in different values of ψ_{rad}.

Either of the two types solar exergy definitions introduced above were used widely by researchers worldwide. Each definition has its advantages and drawbacks. The first definition can be used to compare with other heat sources, such as geothermal or waste heat, since they have similar temperatures that are related with temperature of the working fluid. This definition, however, does not consider the exergy loss in the solar collectors, which is different and based on solar collector efficiency. Also, if the first definition is used, different solar collector outlet temperatures also influence the calculated solar exergy and thus the system exergy efficiency, which makes it hard to compare between different systems, since the solar collector outlet temperatures often varies from case to case. The second definition, using the sun surface temperature as the solar temperature, does not have this issue, since it does not depend on the solar collector efficiency or outlet temperature, which makes it easier to compare between different systems. This definition, however,

overestimates the potential of doing work of solar radiation, since no solar collector can generate heat at the temperature of the sun surface.

I suggest that commercial users or other researchers should use the second definition when solar heat is used as the heat source in power generation systems, for the following reasons:

1) it makes it easier to compare between the performance of different systems;
2) it leaves room for technology advances when the solar collector may generate heat that is comparable to the temperature of the sun surface in the future;
3) it provides the opportunities to compare the solar thermal (hybrid) systems with the space power generation systems using solar radiation outside the atmosphere, and the photovoltaic power plants which convert the solar radiation directly to the electricity;

This dissertation, however, will also include the analysis using the first definition of solar exergy. This is because the dissertation focuses on an inclusive thermodynamic analysis considering various types of heat sources, including the geothermal and waste heat and the results using the first definition can also be applied to other types of heat sources, whose temperatures are easily defined.

The exergy efficiency of a hybrid power cycle using both fuel and solar as the heat sources, ε_{h}, is expressed, according to Eqs (2.11) and (2.6) as

$$\varepsilon_{\mathrm{h}} = \frac{\dot{W}_{\mathrm{net}}}{\dot{B}_{\mathrm{f}} + \dot{B}_{\mathrm{rad}}} = \frac{\dot{W}_{\mathrm{net}}}{\dot{m}_{\mathrm{f}} \cdot b_{\mathrm{f}} + \frac{\psi_{\mathrm{rad}} \dot{Q}_{\mathrm{sol}}}{\eta_{\mathrm{sc}}}}. \tag{2.14}$$

Recognizing that the exergy destruction rate during heat transfer ($\dot{B}_{\mathrm{d}}$) is proportional to the temperature difference as expressed using [14],

$$\dot{B}_{\mathrm{d}} = \int_0^{\dot{Q}} \left(\frac{1}{T_{\mathrm{heated}}} - \frac{1}{T_{\mathrm{heating}}} \right) T_0 \delta \dot{Q}, \tag{2.15}$$

in which $\delta \dot{Q}$ and $\dot{Q}$ [kW] are the infinitesimal and total heat transfer rate, respectively; T_{heated} and T_{heating} [K] are the temperature of heated (the cycle working fluid in our case) and heating (the heat source) during the heat transfer between them, one of the important advantages of thermal hybrid power cycles compared with conventional fossil-fuel only power cycles is their ability to reduce this temperature difference and thus the associated exergy destruction by choosing heat sources (such as from solar collectors, waste heat, or geothermal) that have temperature closer to the working fluid.

2.4. Other performance criteria

To analyze and compare the performance of the power cycles using single and more heat sources, other performance criteria are useful besides the energy efficiency and exergy efficiency introduced before.

a) AHS heat input fraction of total energy input

$$X_{\text{AHS}} = \frac{\dot{Q}_{\text{AHS}}}{\dot{Q}_{\text{in}}}. \tag{2.16}$$

Each variable has the same meaning as defined before. It shows the fraction of the heat input from input relative to the total energy input.

When solar heat is used as the AHS and fuel is used as the original heat source, the solar share is defined as

$$X_{\text{sol}} = \frac{\dot{Q}_{\text{rad}}}{\dot{Q}_{\text{in}}} = \frac{\dot{Q}_{\text{rad}}}{\dot{m}_{\text{f}} \cdot \text{LHV} + \dot{Q}_{\text{rad}}}. \tag{2.17}$$

b) Fuel savings ratio

$$S_{\text{f}} = 1 - \frac{\dot{m}_{\text{f}}}{\dot{m}_{\text{f,0}}}, \tag{2.18}$$

in which $\dot{m}_{\text{f,0}}$ and $\dot{m}_{\text{f}}$ [kg/s] are the mass flow rates of fuel in the reference (single heat source) and hybrid (multiple heat sources) power cycles, respectively.

It defines the energy quantity of fuel saved if the AHS is used while producing the same amount of net power output. It also is proportional to the quantity of emissions that would have been saved if the added heat source didn't generate CO_2, SO_X etc. during operation such as solar power, since the emission is proportional to the amount of fossil

fuel used (the operation of solar or geothermal device etc. doesn't generate direct emissions, but does embodied ones).

c) Solar-to-electricity efficiency

$$\eta_{se} = \frac{\dot{W}_{net} - \eta_0 \left(\dot{m}_f \cdot \mathrm{LHV} \right)}{\dot{Q}_{rad}}, \tag{2.19}$$

in which $\dot{W}_{net}$ [kW] is the net power output of the hybrid power cycles, η_0 is the energy efficiency of an appropriate chosen reference (single heat source) power cycle using the same amount of fuel in the hybrid power cycles, and the second term in the numerator stands for the net power output produced in that reference system.

This parameter shows how much of the solar energy is converted to net power output of the system. Itis also called the net incremental solar efficiency by some researchers [15].

References for Chapter 2

[1] Carbon Dioxide Emissions Coefficients - Available at:<http://www.eia.gov/environment/emissions/co2_vol_mass.cfm> [accessed 02.17.2017].

[2] Sheu E.J., Mitsos A., Eter A.A., Mokheimer E.M.A., Habib M.A., Al-Qutub A., A Review of Hybrid Solar-Fossil Fuel Power Generation Systems and Performance Metrics. J Sol Energ-T ASME 2012;134:041006.

[3] Moran M.J., Shapiro H.N., Fundamentals of Engineering Thermodynamics, 6th ed. US: John Wiley & Sons;2008.

[4] Petela R., Exergy of Heat Radiation. J Heat Trans-T ASME 1964;86:187-192.

[5] Spanner D.C., Introduction to Thermodynamics, London: Academic Press;1964.

[6] Jeter S.M., Maximum conversion efficiency for the utilization of direct solar radiation. Sol Energy 1981;26(3):231-236.

[7] Parrott J.E., Theoretical upper limit to the conversion efficiency of solar energy. Sol Energy 1978;21:227-229.

[8] De Vos A., Pauwels H., Comment on a thermodynamical paradox presented by P. Wurfel. J Phys C Solid State 1983;16:6897-6909.

[9] Winter C.J., Sizmann R.L., Vant-hull L.L., Solar power plants, New York:Springer;1991.

[10] Landsberg P.T., Tonge G., Thermodynamics of the conversion of diluted radiation. J Phys A-Math Gen 1979;12:551-562.

[11] Zamfirescu C., Dincer I., How Much Exergy Can One Obtain From Incident Solar Radiation. J Appl Phys 2009;105:044911.

[12] Baghernejad A., Yaghoubi M., Exergy analysis of an integrated solar combined cycle system. Renew Energ 2010;35:2157-2164.

[13] Hong H., Jin H., Ji J., Wang Z., Cai R., Solar thermal power cycle with integration of methanol decomposition and middle-temperature solar thermal energy. Sol Energy 2005;78:49-58.

[14] Szargut J., Exergy Method, WIT, 2005.

[15] Sheu E.J., Mitsos A., Eter A.A., Mokheimer E.M.A., Habib M.A., Al-Qutub A., A Review of Hybrid Solar-Fossil Fuel Power Generation Systems and Performance Metrics, J Sol Energ-T ASME 2012;134(4):041006.

CHAPTER 3

THERMAL HYBRID POWER CYCLES

BACKGROUND REVIEW

3.1. Developments and status of thermal hybrid power cycles

Perhaps the first studies of such hybrid systems were in the 1970's when Lior and coworkers [1-5] proposed, analyzed, constructed and tested a 30 hp prototype of the hybrid solar-powered/fuel assisted power cycle (SSPRE) under USDOE sponsorship. The same concept/principle was later used, in the 1980-s, by the Luz Company for the construction and successful operation of solar-thermal power plants still producing about 380 MWe in southern California, which are considered to still be the only cost-competitive (albeit with some tax subsidies) solar thermal power generation system built [6–8]. The concept is successful because it uses solar energy at the lower temperature level, where it is more economical, and augments it by smaller amount of heat from fuel combustion to: (1) raise the cycle temperature and thus efficiency, and (2) allows fuel heat backup when solar energy is not sufficiently available, without having to increase the number of collectors and the thermal storage capacity. The flow diagram of SSPRE with operating parameters at design point is shown in Fig. 3-1 (redrawn based on [1]).

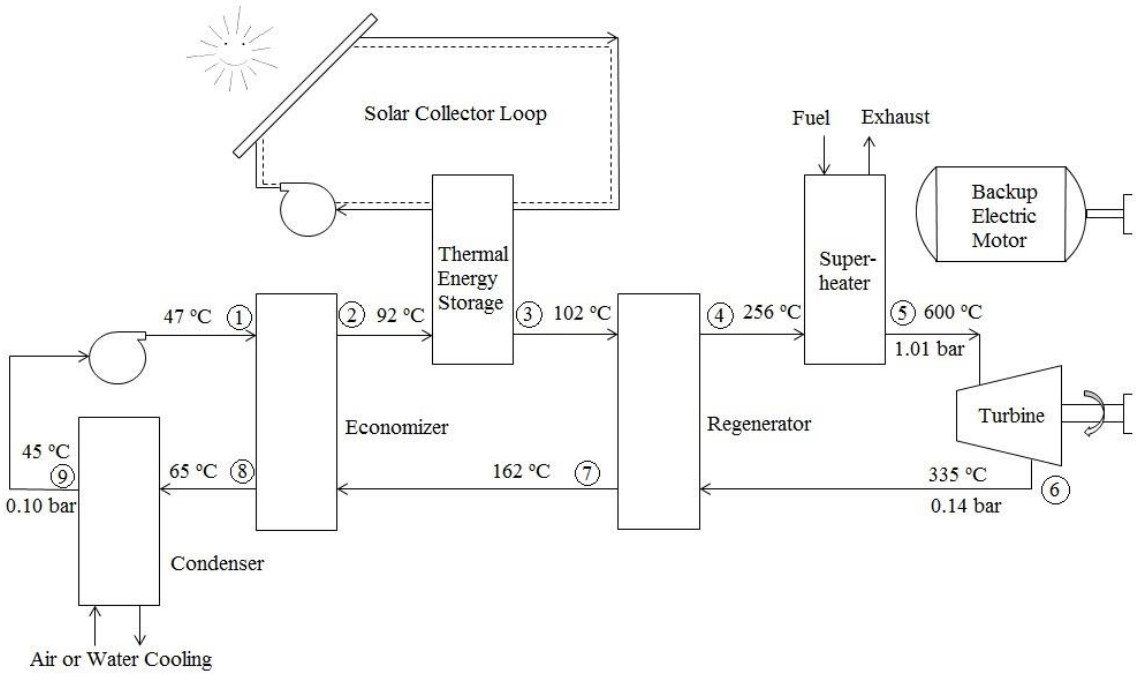

Fig. 3-1 Flow diagram of the SSPRE power/cooling system with design points (redrawn based on [1])

The system used solar heat generated from solar collectors to heat the working fluid (water) to around 100 °C and then boil it at about atmospheric pressure before the steam was superheated to 600 °C by burning of natural gas. It incorporated an economizer and regenerator to recuperate the turbine exhaust energy to heat the working fluid. The results showed that the efficiency of the basic power cycle was 18.3% at design, more than double as compared to organic fluid cycles operating at similar solar input temperatures, at the expense of adding only 20% non-solar energy. It was also shown to offer better thermodynamic matching with the energy sinks in the power cycle so that less exergy was destroyed in the process of working fluid heating,

Different types of hybrid systems relying on this concept were proposed and investigated since then, the main general types include solar-fossil fuel, biomass-fossil fuel, nuclear-fossil fuel, geothermal-fossil fuel, nuclear-gas turbine exhaust gas, diesel fuel-exhaust gas, geothermal-biomass and solar-gas turbine exhaust gas, solar-biomass, solar-geothermal. By far, solar thermal power is the most widely studied renewable heat sources in hybrid power systems due to its wide range of achievable temperature and various existing and new technologies available in the market [9,10] including many types of solar collectors [11,12] and thermal storage [13,14]. Some authors [15] has already studied the different options for solar hybridization but were focusing on concentrating solar thermal power and from a "source point of view" considering solar thermal power hybridization with coal, natural gas, geothermal, etc., and not from a thermodynamic point of view, which categorizes solar hybridization based on the way power is generated as this chapter does. Solar-assisted hybrid cycles were therefore sorted here in the following three sub categories based on the way power is generated and considering all types of solar thermal power generation method (concentrating and non-concentrating): solar assisted vapor cycles, solar assisted gas cycles, and solar assisted combined cycles. All the other types of thermal hybrid power generation systems (thermal hybridization option without the use of solar thermal power) will be sorted in the fourth group.

3.1.1. The solar assisted vapor turbine cycles

In this type of hybrid cycle (e.g. SSPRE [1]), solar heat is usually employed as the lower temperature heat source, being added between the outlet of the working fluid pump and

inlet of the boiler, so that the working fluid (such as water/steam or organic fluid) can be preheated before heated by the combustion of fossil fuel (usually coal or natural gas) or biomass. Solar heat, however, could also be used as higher temperature heat source when integrated with other lower temperature heat sources such as geothermal or nuclear. Table 1 shows a brief description for each system described in the published literature, in the order of the level of the lower temperature heat source.

As can be seen from Table 3-1, the temperatures of lower and higher temperature heat sources are different for some cycles but the same for others. We can thus further group these cycles in two categories: “Partially” hybrid cycles and “fully” hybrid cycles.

a) “Partially” hybrid cycles

In this type of cycles, solar thermal energy is the only heat source at design conditions, and other heat sources (such as fossil fuel or biomass) are employed only when solar energy alone cannot meet the design conditions. Strictly speaking, this is not a “hybrid cycle” at design conditions since only one heat source is then in effect, but since solar is an intermittent heat source whose power fluctuates with time, the cycle cannot work solely on solar for 24 hours at design conditions if no heat storage is in use. We may thus consider this type of cycles as a “partially” hybrid, which become “fully hybrid” only when solar energy cannot meet the demand (but still may provide some of the input thermal power) and other heat sources are in use. The systems proposed in Ref. [35-38] belong to this category. For such systems, the corresponding “Note” column in Table 3-1 says “Designed

solar share is 100%". Also, for this type of hybrid cycles, the temperatures of lower and higher temperature heat sources are the same at designed conditions, as shown in Table 1.

b) "Fully" hybrid cycles

Unlike "Partially" hybrid cycles, "fully" hybrid cycles use multiple heat sources at different temperatures even at design conditions. SSPRE [1] and cycles which do not belong to "Partially" hybrid cycles are all "fully" hybrid cycles.

Table 3-1 shows that so far solar heat was used as the higher temperature heat source only when the lower temperature heat source was geothermal power. The first solar-geothermal hybrid power plant used for power generation is claimed to be modeled and analyzed in 2006 [16]; this review confirmed that by finding no earlier papers about solar-geothermal hybrid system for power generation. In this system, geothermal power was introduced in addition to the original solar thermal power to increase steam flow used for power generation. Two alternative configurations were discussed and analyzed on an annual basis for a 10% increase in steam flow. Due to the lack of specific operating and performance parameters, however, it was not included in the summary table. In other solar-geothermal hybrid power generation systems found in the literatures, the temperature of geothermal heat is 90 °C [17,54] or 150 °C [20,21].

In [17] and [54], two combined heat and power (CHP) systems were analyzed using either evacuated tube solar collectors (ETC) or ETC as well as direct-steam parabolic trough solar collectors (PTC) to superheat different types of organic working fluids to 157 °C after

geothermal preheating. The results showed that the share of solar input energy is about 70%, but the energy efficiency is only about 9-13%. [20] introduced a hybrid cycle using geothermal heat at 150 °C as the lower temperature heat source and solar heat at 270 °C collected by solar parabolic trough concentrating collectors the higher temperature heat source. For the geothermal only cycle, the cycle efficiency and net power output were 13.60% and 4,606 kW respectively. After adding a solar field, they became 9.76% and 8,988.8 kW respectively for operation in Imperial, CA, USA. The net power output of the cycles was almost doubled but the efficiency decreased by 3.84%, largely due to the low solar radiation-to-heat efficiency (56.64%). Analysis in other locations (San Diego, CA, USA; Palermo, Sicily, Italy; Pisa, Tuscany, Italy) showed similar results. At the same geothermal temperature at 150 °C as the previous system, another hybrid geothermal-solar power plant was also studied, used especially in hot and arid climates [21]. Unlike the previous one using R134a as working fluid, this cycle uses Isopentane. The solar concentrating temperature from solar parabolic trough concentrating collectors also higher at 390 °C. The results showed that the efficiency rose to 12.36% and the power output became 1,496 kW, which is 62.7～76.3% higher annually than the stand-alone geothermal plant depending on the plant location. They both had a solar share of more than 60% at design conditions. Considering the relatively large capital cost of geothermal and solar thermal power and the relatively low power generation efficiency of only a dozen percentages, however, geothermal-solar hybrid systems may not be promising.

Except for geothermal hybrid power cycle, almost all solar hybrid vapor cycles use solar heat as the lower temperature heat source. In this type of system, fuel was often used as higher temperature heat source, but solar heat at higher temperature could also be used. For example, [26, 27] introduced a combined solar thermal power plant by adding an additional solar collector. An auxiliary boiler was also considered in the hybrid solar power plant, in order to reach the designed power generation capacity when solar irradiation was low due to technical or environmental reasons. In the new power plant, steam was heated up to 294 °C compared with 265 °C in the original plant. Both solar collectors were parabolic trough types and used oil as heat transfer fluid (HTF). The new plant also doubled the power output the plant from 250 kW to 500 kW. A transient study showed a month by month result of the new power plant. It was found that the energy efficiency ranges from 20% in January to 42% in June and solar share ranges from 16% in January to 62% in June. The energy efficiency of this new solar thermal power plant with the original one, however, was not compared. It was thus unknown whether the new hybrid system higher energy efficiency than the original one.

Although, as introduced above, solar heat at higher temperature could be used as higher temperature heat source when geothermal or solar heat at lower temperature was used as lower temperature heat source, most solar assisted hybrid system used solar heat as lower temperature heat source and fuel as higher temperature heat source. The earliest studied hybrid system of this type was found to be SSPRE [1] and has been introduced before. Many others were also studied as well. In this type of hybrid system, different types of fuel

could be used and could be further sorted into two groups: renewable fuel, such as biomass and non-renewable fuel, such as coal and natural gas.

First, using renewable fuel, a solar-biomass hybrid power system was analyzed in [23]. In the system, the oil heated by a parabolic trough solar field was used to replace the extraction steam to preheat the feed water (entering a biomass boiler where the feedwater was heated to 535 °C) and the previous extraction steam thus saved could continue to do work in the lower stages of turbine. The solar heat added to a 12 MW biomass power plant was 160～429 kW (1.3～3.6%) based on the solar temperature from 65.5～217.5 °C. The exergy of biomass was 29,307 kJ/kg and the exergy of solar radiation falling on the solar collectors was defined as

$$\Delta E_{\mathrm{s}} = I_{\mathrm{b,n}} \cos\theta_i A_{\mathrm{c}} \left(1 - \frac{T_{\mathrm{a}}}{T_{\mathrm{s}}}\right), \tag{3.1}$$

in which ΔE_{s} was the additional solar exergy added to the biomass plant, $I_{\mathrm{b,n}}$ was the direct normal insolation (DNI) (W/m^2), θ_i was incident angle of collector aperture (°), A_{c} was the aperture area of solar field (m^2), T_{a} was air temperature (K) and T_{s} was solar temperature, which was taken to be 6,000 K. The study showed an increase in exergy efficiency with solar temperature. A similar analysis was also done with the capacity of the biomass plant increased to 30 MW and a different set of solar temperatures and found the same trend. It was thus concluded that the best way to use solar heat was to replace the

extraction steam at the highest stage possible. Since most steam power plant used multiple stages of heat regeneration through extraction steams to increase energy efficiency of the thermal power plant, the results shown in this reference were widely applicable in giving guidance on replacing extraction steam with solar heat and are therefore valuable.

Another case using biomass as higher temperature heat source was shown in [35]. The proposed hybrid solar-biomass plant was a “partially” hybrid system and natural gas could also be used instead of biomass. Biomass or natural gas was only burned when solar radiation was not enough. The designed temperature of oil in solar collector was from 292 °C to 392 °C and the turbine inlet temperature was 375 °C. There was not a full thermodynamic analysis of the plant, and thus there was no information about the efficiency and solar share of the whole plant. Based on an annual analysis, solar produced 28.6% of the total electricity and the other part of electricity came from biomass (62.4%) and natural gas (9.0%).

Besides integrating with parabolic trough solar collector, biomass could also be integrated with a solar tower. In a steam cycle [38] that integrates biomass and a central receiver system (CRS), atmospheric air was heated by the CRS to 680 °C and is then used to superheat steam to 480 °C for power generation. This system was a “partially” hybrid system in which biomass is burned only when solar radiation could not meet the demand to heat the HTF (atmospheric air) to the designed temperature at 680 °C. 4 different configurations (4 MW CRS integrated with 4 MW or 10 MW biomass plant without 3 hours thermal storage) and 3 different control strategies (CS) for 4 MW hybrid solar-

biomass plant with 3h storage were considered and a 24 hours analysis was done. It was found that the 4 MW hybrid power plant with CS3 control strategy had a higher efficiency and capacity factor than a conventional 4 MW CRS power plant. For the 10 MW power plant, the hybrid system led to a 17% reduction in biomass consumption than a typical biomass power plant. This result was significant as the price of biomass continues to increase.

Compared with renewable fuel such as biomass, non-renewable fuel or fossil fuel, such as coal, oil, and natural gas, was more widely used as higher temperature heat source in solar hybrid power systems. This is mainly due to its advantages over renewable fuel such as easier to get, lower price and higher energy density. More importantly, this was because the configuration of the original power plant doesn't need much change when lower temperature solar heat was integrated directly into it, and most existing steam power plant was fossil fuel powered, rather than biomass powered.

Besides SSPRE, which was introduced in Section 3.1, there were only a few hybrid system experiments, and Fig. 3-2 shows the flow diagram of one of them [22].

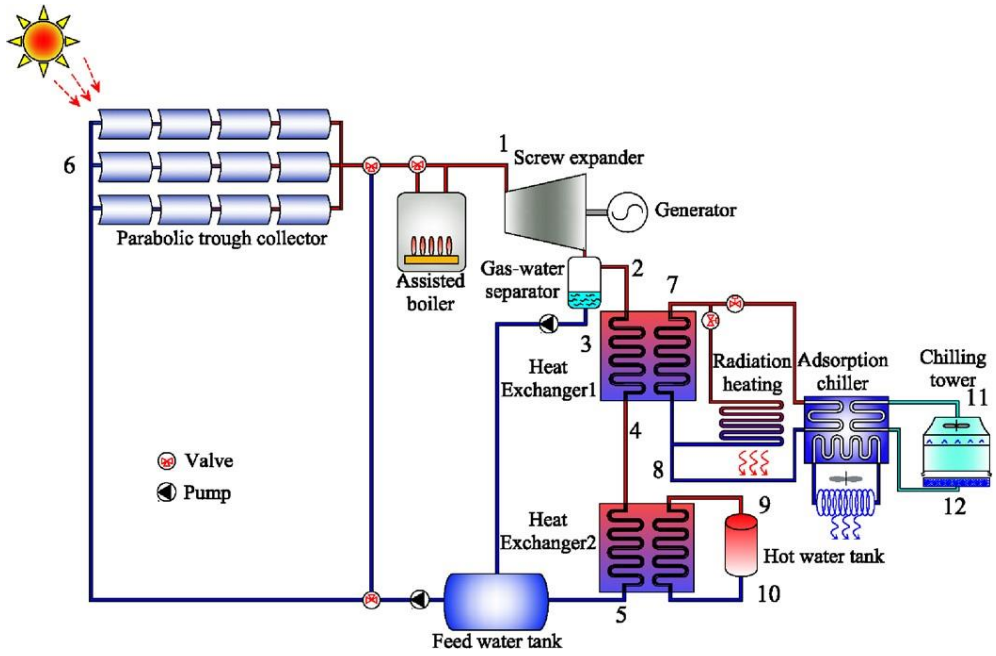

Fig. 3-2 Flow diagram of the solar heating, cooling and power generation system [22]

To maintain the designed power generation output at 23.5 kW, natural gas in the assisted boiler was used when solar heat was insufficient to heat the working fluid to the designed top temperature at 180 °C. On an annual basis, this was a fully hybrid cycle, since the solar share at design conditions was not 100% (it was 95.2% in summer and 94.0% in winter). The experiments showed that the energy efficiency was 27.3% in summer and 63.8% in winter and the exergy efficiency was 9.9% in summer and 16.9% in winter. The energy and exergy efficiencies were, however, not defined in normal practice as the ratio of the electricity output with the total energy or exergy input; instead, the generated cooling and heating energy/exergy was included as the output besides electricity. Based on the data given in the reference, however, we calculated the power generation efficiency to be 6.2%

in summer and 8.3% in winter. This was relative low, mainly due to the low top temperature of the system (180 °C).

Unlike the system shown above, most of the hybrid system studies were theoretical, without experiments. In a 4-E (Energy, Exergy, Environment, and Economic) analysis of solar thermal aided coal-fired power plants [24], two types of plants were considered: 500 MW subcritical and 600 MW supercritical power plants. A direct (DSG technology) or indirect (HTF) technology solar aided feed water heater (SAFWH) were added to each of these reference plants to replace one or all of the feedwater heater(s). The extraction streams used to preheat in the feedwater heater can thus be saved for power generation. Each subtype could operate in two different modes: power boosting mode, when fuel input rate was fixed and more power could be generated; and fuel conservation mode when power output was fixed but less fuel would be used. The efficiency was calculated based on fuel consumption and solar input was not considered, so it was not included in the summary table. Economic analysis showed that LEC for subcritical power plant with SAFWH ($0.036/kWh) is higher than that without SAFWH ($0.034/kWh) and for supercritical power plant with SAFWH ($0.037/kWh) is higher than that without SAFWH ($0.035/kWh). This results showed that adding solar aided feed water heater increased the cost of the original fossil power plants, for both subcritical and supercritical power plants.

Many other analyses also investigated the effect of replacing extraction steams from steam turbines with the thermal heat from thermal oil heated by a solar parabolic trough concentrating collector. In [25], 4 schemes for conventional power plants using solar aided

power generation (SAPG) technology, including a power boost mode and a fuel saving mode (introduced in the former case) for each scheme, were investigated. The results showed an increase in power output but decrease in energy efficiency. It is surprising, however, that the fuel consumption rate was found to be smaller in power boost mode than in fuel saving mode. It should have been discussed. Also, the resulting solar share suggested that using solar energy to replace high pressure extraction steam produced more work but also with lower energy efficiency, than to replace low pressure one. This result showed that higher pressure extraction steam should be replaced with solar heat rather than lower pressure one.

In [28,29], the performance of the hybrid system was analyzed by first replacing only the last stage of extraction steam using solar flat-plate collectors at 110 °C and then replacing all of the three extraction streams using solar evacuated tube collectors at 286 °C in a three stage regenerative Rankine power plant. The results showed the power output increased 2.5% and 30.04%, respectively. It was also found that the thermal efficiencies of solar energy for both hybrid systems (defined as additional power generated by solar energy divided by solar heat input) were larger than those of the solar only Rankine cycle using the same operating parameters (such as solar temperature, condensing temperature).

In [31], three preheating options for solar to be integrated in a traditional fossil fuel power plant were studied: solar heat replacing low pressure feed water heaters, replacing high pressure feed water heaters, and replacing high pressure feed water heaters together with part of the economizer of the boiler. Solar heat was designed to heat the working fluid to

159 °C, 249 °C and 319 °C respectively. The net electric efficiency in each arrangement was found to be 33.05%, 35.39% and 35.69%, respectively, compared with the efficiency of base case (without solar heat input) of 35.67%. The net power output of the system also changed with different types of configurations. It was suggested that the best option for future plants was the third one and for existing plants was the second one considering all the effects such as efficiency, solar share and modification of existing plants.

In [33], a 330 MW solar-aided coal-fired power generation system (SACPG) with various solar field areas and thermal energy storage capacity was studied on an annual basis under different loads, and optimized. There were 3 high-pressure feedwater heaters and 4 low-pressure feedwater heaters in addition to a deaerator in the system. Solar heat at 283 °C was used to replace each of the HP extraction steam from relatively lower temperature to higher one, and to replace all of the HP extraction steams when solar heat was sufficient. The superheated steam was heated by coal and the steam turbine inlet was set to 537 °C. It was found that that the overall energy efficiency of SACPG system was 42.41%, 41.59% and 38.84%, for 100%, 75%, and 50% loads, respectively. The results also showed that (1) the highest solar-to-electricity efficiency was achieved when all of the HP extraction steams were replaced by solar heat; (2) the installation of thermal energy storage (TES) increased the annual solar-to-electricity efficiency compared with the system without TES; (3) the levelized electricity cost (LEC) of the system with TES decreased first then increased with solar field sizes increasing, and the minimum LEC was $62.9/MWh for 100% load, $65.4/MWh for 75% load and $73.0/MWh for 50% load. It was thus concluded that

TES was an important sub-system for SACPG to overcome the intermittency of solar energy as well as to use solar energy in a more efficient way by achieving higher solar-to-electricity efficiency. The cost of TES, however, was an obstacle and developing low-cost TES was an important direction to make SACPG more promising in economic viewpoint.

In [32], a modern thermal power station with integration of a solar concentrator field to reduce fuel consumption was studied in two cases: feed water preheated by solar field from the condenser outlet to 241 °C and to 328 °C. It was found that the fuel consumption in the boiler was reduced by 10.7% and 25.6%, respectively.

In [34], a 300 MW lignite fired power plant combined with line-focus parabolic trough collectors filed was proposed and analyzed. Thermal oil at 390 °C produced by solar parabolic trough concentrating collector was used to provide heat to high pressure feed water heater. The blend off steam was thus saved to produce work in the turbine. Simulation was done for various solar field areas between 90,000 m^2 to 120,000 m^2. Plant efficiency was found to be 34.87-36.74% for different solar field areas, which were all higher than the reference plant with no solar heat (33.3%). The solar share was small at between 2.15-7.91%.

Unlike the above systems which focused on regenerative steam with extraction steams, some analysis dealed with simple Rankine cycle integrated with solar heat. For example, In [36], five types of solar hybrid power plants with thermal energy storage were introduced, three of which belong to solar assisted vapor cycle and the others belong to solar assisted

combined cycle, which was discussed in Section 3.1.3. The configurations of the three solar assisted vapor cycles were roughly the same, and the main difference between them was heat transfer fluid (HTF) and the types of solar collectors suitable to the HTF. For molten salt and pressurized CO_2, solar tower was used since higher temperature was needed (565 °C and 600 °C, respectively), and thermal oil was used in solar parabolic trough concentrating collector, since the temperature was not very high (393 °C). It was found that the efficiencies were 37.2%, 42.5% and 43.0%, respectively, when no thermal storage was used.

Besides that, a novel hybrid receiver-combustor system (HRC) using a combined solar receiver-combustor module compared with a traditional one (SGH) was introduced in [39]. The module was designed to heat the working fluid to 540 °C/180 bar. Two types of hybrid systems (novel and traditional) with 4 subtypes were analyzed: SGH with 13 hours storage (SGH13), SGH with 1 hour storage (SGH1), HRC with 0.5 hour storage (HRC0.5) and HRC with 13 hours storage (HRC13) to compare with the two base systems: solar power tower system (SPT) and gas-fired boiler plant (GB). The efficiency of SPT was inferred as 17.8% and of GB is 35.5% but the efficiencies for the hybrid systems were not calculated.

Sometimes, solar energy could be used without a heat exchanger to transfer solar heat to the working fluid. In [30], direct steam generation (DSG) collector was used in the study of performance of a hybrid power generation system (solar-gas) at three different sites assumed to in Australia (Alice Springs, Darwin and Dubbo). DSG collector is a type of parabolic trough collector, which consists of a water and steam mixture (two phase flow)

in a very long horizontal or segmented inclined pipe heated by solar radiation directly without the use of additional heat. Three arrangements of hybrid power plant were studied: Boiling process (solar heat is 310 °C and collector was paralleled with gas-fired boiler), Preheating process (solar heat is 209 °C and collector was paralleled with feed water heaters), and Preheating-boiling process (solar heat was 310 °C and collector was paralleled with the boiler and feed water heaters). The top temperatures (boiler outlet steam temperatures) of the three arrangements were all 510 °C. It was found that with a horizontal, N-S tracking axis of DSG collector and boiling process arrangement, the solar energy contribution for plants located in Alice Springs or Darwin was 37% and for Dubbo was 33% due to low incident radiation during the winter in Dubbo.

Besides the above one, a “partially” solar hybrid system using DSG solar collector was introduced in [37]. With the help of solar radiation and an auxiliary heater, steam was heated up to 410 °C to generate power. Fuel back up in each of the 12 months in a year in 4 different locations was discussed and it was found that the highest backup fraction was 82% and lowest was 43%.The authors, however, did not show the energy efficiency of the system.

All of the systems introduced above were based on Rankine cycle, which is widely used in power generation industry. Kalina cycles, however, could also be used. Kalina cycles are thermodynamic cycles using a solution of 2 fluids with different boiling points for its working fluid and have been used by some researchers in hybrid power generation systems. Since the most widely used working fluid is the mixture of steam and ammonia and there

hasn't been much research for hybrid Kalina cycle, it was included in the category of solar assisted steam cycle. For example, a new thermodynamic cycle for combined power and cooling was proposed and analyzed using low and mid temperature solar collectors to preheat the ammonia and water mixture to 127 °C before the mixture was heated to 137 °C by a superheater [19]. The cycle used low cost flat-plate collectors or medium temperature concentrators (or other lower temperature heat source, such as geothermal resources or waste heat from existing power plants) to preheat the mixture, which has a low boiling point. The electricity generation efficiency was found to be 17.39% under the designed conditions with a solar share of as much as 92.6%. This analysis, however, did not consider the efficiency of the solar collection and superheater, so the efficiency was just cycle efficiency, not system efficiency.

Table 3-1. A summary of past studies of solar-assisted vapor power cycles

Descriptive name of system and reference	Lower temperature heat source		Higher temperature heat source		S/E*	Power, kW	Claimed power generation efficiency**	Efficiency improvement over single temperature system	Solar fraction of the total energy input***	Note****
	T,°C	type	T,°C	type						
Micro CHP system fueled by low-temperature geothermal and solar energy [17,18]	90	Geothermal	157	Solar evacuated tube	S	38.86	9.1%	-	74%	Single pressure; R134a
						36.38	9.78%		73.5%	Single pressure; R236fa
						39.96	13%		76.4%	Single pressure; R245fa
			-			33.58	6.9%		75.3%	Dual pressure; R134a

				Solar parabolic trough		32.46	7.4%		75.1%	Dual pressure; R236fa
						36.04	10.0%		78.7%	Dual pressure; R134a
Solar-powered /fuel-assisted Rankine cycle [1]	100	Solar flat-plate collector	600	Gas	S&E	22.37	18.3%	9.5% (solar)	20%	First model
New Thermodynamic Cycle for Combined Power and Cooling Using Low and Mid Temperature Solar Collectors [19]	127	Solar flat plate or medium temperature concentrator	137	Fossil fuel	S	73.3 (kJ/kg)	17.39% (elec.) 23.54% (nominal)	-	92.6%	Working fluid is ammonia-water mixture
A solar-geothermal hybrid plant based on an Organic Rankine Cycle [20]	150	Geothermal	270	Solar parabolic trough	S	8,989	9.76%	-3.84%	63%	Working fluid in ORC is R134a; HTF is synthetic oil; LEC is $0.19-0.36/kWh (2011)
						9,188	10.36%	-3.24%	62%	
						7,788	10.04%	-3.56%	56%	
						7,660	9.68%	-3.92%	57%	
Hybrid solar-geothermal power plant in hot and arid climates [21]	150	Geothermal	390	Solar parabolic trough	S	1496	12.36%	-	67.5%	Organic working fluid (Isopentane) LEC is $0.17/kWh (2013), 23% less than stand-alone enhanced geothermal system
Novel hybrid solar heating, cooling	<180		180	Natural gas	E	23.5	6.2%	-	95.2%	Summer

and power generation system [22]		Solar parabolic trough					8.3%		94.0%	Winter
Solar aided biomass power generation systems with parabolic trough field [23]	65.5	Solar parabolic trough	535	Biomass	S	12,160	35.22%	-1.48%	~4%	Eff. is exergy efficiency; LEC is $0.08/kWh (2011)
	108					12,266	35.52%	-1.18%		
	148					12,356	35.78%	-0.92%		
	186.5					12,396	35.90%	-0.80%		
	217.5					12,429	35.99%	-0.71%		
Solar thermal aided coal-fired power plants [24]	253.5	Solar parabolic trough	1786.7	Coal	S	575,800	-	-	-	Power boosting mode
						500,000				Fuel conservation mode
	253.2		1775.8			806,000				Power boosting mode
						600,000				Fuel conservation mode
Conventional power plant using solar aided power generation (SAPG) technology (power boost mode) [25]	260	Solar parabolic trough	530	Coal	S	219,720	44.19%	-0.41%	8.04%	Scheme 1
	215					205.020	44.52%	-0.08%	3.17%	Scheme 2
	160					207,880	44.58%	-0.01%	4.33%	Scheme 3
	90					202,400	44.58%	-0.02%	1.11%	Scheme 4
Shiraz solar thermal power plant (STPP) integrated with a new collector and an auxiliary boiler [26,27]	265	Solar parabolic trough	294	Solar parabolic trough	E&S	500	42% (June)-20% (Jan.)	-	62% (June)-16% (Jan.)	Both HTFs are oil
Solar aided three-stage regenerative	110	Solar flat-plate collector	538	Brown coal	S	1111.96 (kJ/kg)	46.98%	-2.53%	7.4%	No low-pressure extraction steam from turbine

Rankine system [28,29]	286	Solar evacuated-tube collector				1410.86 (kJ/kg)	43.52%	-5.99%	32.4%	No extraction steam from turbine
Solar thermal electric generation systems using parabolic trough [30]	310	Solar parabolic trough	510	Natural gas	S	22,800	-	-	37% 37% 33%	Alice Springs Darwin Dubbo
Solar thermal repowering of fossil fuel fired power plants [31]	159 249 319	Linear Fresnel collector	540	Heavy fuel oil	S	104,352 116,418 116,912	33.05% 35.39% 35.69%	-2.62% -0.28% 0.02%	12.5% 10.3% 20.7%	Different amount of CO_2 avoided annually
Thermal power station integrated with solar energy [32]	241 328	Solar parabolic trough	577	Coal	S	210,000	45.2% 42.5%	-5.8% -8.5%	20.8% 37.9%	Fossil fuel reduction is 10.7% Fossil fuel reduction is 25.6%
Solar-aided coal-fired power generation system (SACPG) [33]	283	Solar parabolic trough	537	Coal	S	330,203 247,649 165,124	42.41% 41.59% 39.84%	-	-	100% load; LEC $62.9/MWh (2015) 75% load; LEC $65.4/MWh (2015) 50% load; LEC $73.0/MWh (2015)
Solar aided power generation of a lignite fired power plant combined with line-focus parabolic trough collectors field [34]	390	Solar parabolic trough	540	Lignite	S	285,000 290,000 296,000 302,000	34.87% 35.21% 35.96% 36.74%	1.57% 1.91% 2.66% 3.44%	2.15% 4.00% 6.13% 7.91%	Solar field area is 30,000 m^2 Solar field area is 60,000 m^2 Solar field area is 90,000 m^2 Solar field area is 120,000 m^2; LEC is $0.100/kWh

Hybrid solar-biomass plants for power generation [35]	392	Solar parabolic trough	392	Biomass and natural gas	S	10,000	30.6% (Rankine cycle)	-	-	Designed solar share is 100%; LEC is $0.2/kWh (2011)
Parabolic Trough with thermal storage [36]	393	Solar parabolic trough	393	Fossil Fuel	S	30,000	37.2%	-	100%	Designed solar share is 100%
Hybrid -solar-fossil- parabolic trough power plant [37]	410	Solar parabolic trough	410	Fossil fuel	S	100,000	-	-	18%～57%	Designed solar share is 100%
Salt-Tower with thermal storage [36]	565	Solar tower	565	Fossil Fuel	S	30,000	42.5%	-	100%	Designed solar share is 100%
CO_2-Tower with thermal storage [36]	600	Solar tower	600	Fossil Fuel	S	30,000	43%	-	100%	Designed solar share is 100%
Volumetric air CRS and integration of a biomass waste direct burning boiler on steam cycle [38]	680	Solar tower	680	Biomass	S	4,000	18% (no storage)	8% (solar) -8% (bio)	31%	Designed solar share is 100%; All columns show annual values; LEC is $0.100-0.149 /kWh (2012)
							17% (CS1)	6% (solar) -1% (bio)	39%	
							15% (CS2)	4% (solar) -3% (bio)	24%	
							16% (CS3)	5% (solar) -2% (bio)	34%	
						10,000	24% (no storage)	14 (solar) -4% (bio)	14%	
							23% (3h storage)	12% (solar) -1% (bio)	20%	
A novel fuel-saver hybrid combining a	-	Solar tower	-	Natural gas	S	100,000	-	-	82% (SGH13)	LEC is $0.077/kWh

solar receiver with a combustor for a solar power tower [39]	34% (SGH1)	LEC is $0.0648/kWh
	34.1% (HRC0.5)	LEC is $0.059/kWh
	87.5% (HRC13)	LEC is $0.0728/kWh

* E: Experiment, S: Simulation.

** Efficiency is defined as net power output divided by total energy input (Eq. (2.2)), unless indicated otherwise.

*** Solar fraction is defined as solar energy input divided by total energy input (Eq. (2.17)).

**** LEC (levelized electricity cost) was converted to dollar value, based on the currency of the first day in the year published.

3.1.2. The solar assisted gas turbine cycles

In this type of hybrid cycle, solar heat is added between the outlet of the compressor and inlet to the combustor so that working fluid (air) can be preheated before being heated by the combustion of fossil fuel (usually natural gas) in the combustor. A summary of this type of hybrid cycles is in Table 3-2, in the order of temperature of the lower temperature heat source.

A typical flow diagram of a simulation is shown in Fig. 3-3. In the optimal design for hybrid solar gas turbine power plant (HSGTPP) [53], a solar air receiver was used to heat the compressed air from the compressor to 934 °C before being heated by natural gas in the combustor at 1,220 °C. The efficiency was found to be 35.3% and the solar share 65.1% at the design point (annual solar share 42.3%).

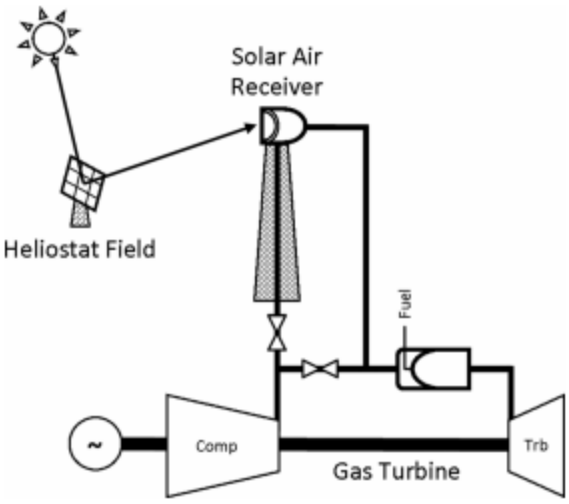

Fig. 3-3 Flow diagram of a hybrid solar gas-turbine power plant [53]

Other analyses was also done for configurations similar to Fig. 3-3. For a generic solar-fossil hybrid Brayton cycle [46], three types of solar collectors (parabolic trough, solar tower and Fresnel linear) were considered, each coupled with several kinds of heat transfer fluid (thermal oil, water/steam (DSG), molten salts, air (atmospheric), air (compressed), water/saturated steam, water/superheated steam, CO_2 and particles). Each combination had specific practical solar temperature ranges from 250 °C to 1,000 °C. The efficiencies for each configuration were calculated for turbine inlet temperatures of 827 °C to 1,427 °C, in steps of 100 °C. A simple analysis of a combined cycle with solar assistance in the top cycle concluded that such solar hybrid combined cycles had lower LEC than the solar hybrid Brayton cycle.

In another case, a hybrid solar gas turbine power plant (HSGTPP) was optimized to minimize the levelized electricity cost (LEC, $/MWh) [53]. After a series of case studies,

a solar tower was optimized to heat the compressed air to 934 °C and the combustor outlet temperature was optimized to 1,220 °C. The resulting efficiency was 35.3% with solar share being 65.1% at optimal point (annual solar share 24.9%). The “optimal” HSGTPP was then compared to two existing solar-assisted gas turbine systems and it was confirmed that it had the lowest LEC.

Hourly modeling was used to study the effects of the ambient temperature on the performance of a solar hybrid gas turbine systems [56]. The results showed that at the highest ambient temperature (about 29 °C in summer), the gas turbine outputs with and without solarization were 28.5 MW and 33.1 MW respectively, leading to a loss of 4.6 MW. It could be seen that using solar hybridization reduced power output. Also, the corresponding efficiency reduced from 37.8% to 36.6%. As assumed in the reference, with the highest temperature in winter is 15 °C in winter, the power outputs with and without solarization were 34.3 MW and 37.6 MW and corresponding efficiencies were 38.3% and 39.0%, respectively. The paper thus suggested that with solar energy input, the combination of pressure drops and airflow regulation would result in a lower electric power and efficiency, which agrees with the performance data provided by SOLGATE [47], although some fuel was saved during solar hybridization.

Apart from the configuration showed in Fig. 3-3, solar-assisted gas turbine cycles can have other configurations. In [52], three configurations for small-scale hybrid solar power plants were proposed: open-cycle design which is the same as Fig. 3-3, internally-fired recuperated design which added a heat exchange to use the exhaust gas to heat the

compressed air before heated by solar receiver, and externally-fired design which used solar heat and combustion heat to reheat the exhaust gas. Each design had a corresponding solar heat input (at 800 °C, 800 °C and 700 °C), turbine inlet temperatures (900 °C, 900 °C and 780 °C) and different compressor pressure ratios. A tradeoff between solar share and conversion efficiency for each design was found. The peak efficiency of each design at different pressure ratios was found to be 19.4%, 30.4% and 22.5%, respectively, with the respective annual solar share was 32.2%, 27% and 37.4%.

[54] introduced a novel air-based bottoming-cycle for water-free hybrid solar gas-turbine power plants (AB-HSGT). The top cycle part is the same as Fig. 3-3, but an air-based bottoming-cycle is added. The bottoming part consisted of an intercooled compressors and a turbine and utilizes the exhaust heat from the top cycle as the heat source. The solar temperature from the solar tower was 950 °C and the top temperature of the cycle was 1,400 °C. The exhaust gas temperature of the top gas turbine was 553 °C. The power output of the optimal design was 57.9 MW having an overall exergy efficiency of 29.9% (annual exergy efficiency was 38.5%) with solar share of 39.2% (annual solar share was 20.0%). It wasn't shown how the exergy was calculated. It was stated that the land use of the system, measured as the surface of land required per unit of electricity produced over the lifetime of the plant, was considerably lower than other renewable energy technologies, e.g. 1/7-1/5 of that of solar thermal power [40], because of the low solar share.

To attain a deeper understanding of solar-assisted power generation systems, the European Union (EU) funded a project to assess the performance of three prototype plants and

advanced software was used to optimize and predict their performance [49]. Two of them were about the solarized gas turbine cycle: Solar Mercury 50 (recuperated single shaft gas turbine) which used two pressurized air receivers to preheat the pressurized air to 630 °C and 800 °C, having a capacity of 4.2 MW, and Solar Heron H1 (intercooled recuperated two-shaft engine with reheat) which preheated the pressurized air and reheated the combustion gas to 800 °C, having a capacity of 1.4 MW. The third prototype plant was PGT10 which was a solarized combined cycle, which will be discussed in the next category. Each type of prototypes plants was assumed to be located in two places: Seville, Spain (annual DNI was 2,015 kWh/m^2) and Daggett, CA. USA (annual DNI was 2,790 kWh/m2). The calculated annual efficiency for Mercury 50 was 35.9% with solar share at design point 38% for both locations, and for Heron was 40.4% in Seville and 38.4% in Daggett with solar share at design point 75% for both locations.

The European Commission (EC) also funded a project called ECOSTARS, which involved solar hybridization with gas turbine. In [51], a conceptual solar hybrid gas turbine power plant assumed to be in France (PEGASE) was introduced and analyzed. A solar Central Receiver System (CRS) was used to heat the compressed air to 850 °C, after which the fuel was burned with the air in the combustor to 1,000 °C. The outlet electric power was 1,414 kW and the electrical efficiency was 35.1% for the original gas turbine. Solar thermal power of 2,463 kW was added to the turbine for a total of 4.9 MW incident solar thermal power on the field and provided 62% of the needed thermal power to the turbine. The

electricity efficiency for PEGASE was calculated to be 22.1%, which is 13% less than the original gas turbine.

Just as for some solar-assisted vapor cycle systems, solar-assisted gas turbine system can also be used to provide heating/cooling besides power generation. [48] introduced a solar-assisted small solar tower trigeneration system (solarized TURBEC T100) using a solar-hybrid microturbine to provide electricity and cooling and/or heating, which was suggested to be used for tourism installation (e.g. large hotel complexes). In this system, a small solar tower was used to preheat the pressurized air to 780 °C before the air and fuel were burned at 950 °C in the combustor. The system was stated to have an electric efficiency of 28%, which is 2% lower than the original microturbine without solar integration. Also, with the absorption chiller for cogeneration, the total efficiency increased by over 20%. Solar share at design point was calculated as 84% and the annual solar share was 29% with the most economical absorption chiller in the configuration.

Instead of using a solar air receiver or solar tower which utilizes solar heat at higher temperature (usually over 600 °C) as in the previous system, solar parabolic trough concentrating collector which utilizes mid-temperature (200～600 °C) can also be integrated in hybrid solar gas turbine. For example, a solar hybrid steam injection gas turbine (STIG) cycle was proposed in [44]. The system used solar heat at 240.4 °C to preheat the water injected to the combustor. The fuel was then mixed with the preheated steam and burned to get a turbine inlet temperature (TIT) at 1,200 °C. The solar STIG was

found to have an efficiency of 41.4% compared with 49.8% with a conventional STIG, but has 2,086 kW of net power output compared with just 513.9 kW for a conventional one. The big advantage of solar STIG compared with conventional one was thus the ability to preheat more injected water and produce more work.

Some solar hybrid gas cycles were reported to have the ability of carbon capture. [41-43] introduced a CO_2-capturing hybrid power-generation system, which used solar heat collected by parabolic trough to superheat the steam to be injected to the combustor with fuel and air to 223 °C. Turbine inlet temperature was set to 1,150 °C. Based on actual conditions in Osaka, Japan, the predicted maximum net generated power was 1.55 MW with total net exergy efficiency 20.9% (it was not show how it was calculated) and net energy efficiency on fuel energy base (net power divided by fuel input) 63.7%. The CO_2 generated during combustion was recovered by cooling the exhaust gas, and the CO_2 capture capability was said to be near 100%. There was, however, no information on the cost of the additional equipment for CO_2 capture, nor the consequent effect on system performance.

Another system with the ability to capture carbon emission was introduced in [45]. The novel hybrid oxy-fuel power cycle utilized solar thermal energy at 252.8 °C to produce saturated steam. The fuel (methane) and oxygen were mixed with the saturated steam and burned to generate combustion gas at 1,300 °C to produce power in two power turbines in series. The energy efficiency was found to be 38.51% with solar share of 59.85% at design point. An exergy analysis was performed, for which the exergy efficiency was defined as

$$\eta_{ex} = \frac{W_{net}}{Q_{fuel} + Q_{sol,th} \times \left(1 - \frac{T_0}{T_s + 20}\right)}, \quad (3.2)$$

where W_{net} was the cycle net output work, Q_{fuel} and $Q_{sol,th}$ were fuel energy and solar thermal energy to the cycle, respectively, T_0 was the atmosphere temperature, 15 °C and T_s was the temperature of saturated steam, 252.8 °C. The temperature of the solar heat source was defined as 20 °C higher than T_s, so $T_s + 20$ was the temperature of the solar heat. The exergy for AHPS was found to be 55.88% and the biggest exergy losses happened in the combustor (15.27%) and in the solar heat addition (9.52%). Using the zero emission Graz cycle, the carbon emission of the system was near zero. There was, however, also no information on the cost of the additional equipment for CO_2 capture, nor the consequent effect on system performance.

Most of the analyses were by simulation as the ones shown above. Still, there are some experiments done in this field and were shown below.

To prove the technical feasibility and verify the electricity cost reduction potential of solar-hybrid power system, the European Union conducted the SOLGATE (solar hybrid gas turbine electric power system) project [47]. One of a prototype plants was called Mercury 50. Two stages of solar preheating were used at 600 °C and 760 °C before the combustion of fuel at 1,090.49 °C. The efficiency was found to be 37.2% and the solar share 39.04%, at the design point.

Also as part of the SOLGATE project, an experiment was done on a solar-assisted gas turbine [50]. Compressed air in solar receivers was heated up to 810 °C and the solarized gas turbine produced a net electricity of 227 kW with a net efficiency of 18.2%, with no combustor casing or combustor inlet insulation, and a solar share of 60%. Also, a prototype solar powered gas turbine system installed in Spain was tested [55]. A pressurized solar receiver cluster of three modules was used to convert solar thermal power to heat, and a modified helicopter engine was used as the gas turbine. In test phase 1 when the solar receiver air outlet temperature was 800 °C, the electrical output was > 230 kW with efficiency of about 20%. The solar share was close to 60%. In test phase 2, solar temperature at 960 °C was achieved without turbine damage (unknown if blade cooling was used) and the solar share increased to 70%. Due to reduced turbine speed (95% of the nominal speed) and high ambient temperature, however, the electrical power production was just 165 kW, which was considerably lower than possible and the efficiency was only about 15%.

Table 3-2. A summary of past studies of solar-assisted gas power cycles

Descriptive name of system and reference	Lower temperature heat source		Higher temperature heat source		E/S*	Power, kW	Claimed power generation efficiency**	Efficiency improvement over single temperature system	Solar fraction of the total energy input***	Note****
	T,°C	type	T,°C	type						

A CO_2-capturing hybrid power-generation system [41, 42,43]	223	trough-type solar collector	1,150	Natural gas	S	1,550	20.9% (exergy efficiency)	-	-	Nearly 100% carbon capture ability
Solar hybrid Steam Injected Gas Turbine cycle (STIG) [44]	240.4	Solar parabolic trough	1,200	Natural gas	S	2,086.0	41.4%	-8.4%	43.4%	SAR=1.2 kg steam/kg air
A novel hybrid oxy-fuel power cycle utilizing solar thermal energy (AHPS) [45]	252.8	Solar	1,300	Natural gas	S	1,543.14 (kJ/kg)	38.51%	-	59.85%	Exergy efficiency is 55.88%
Hybridized Brayton cycles with current solar technologies [46]	550	Solar parabolic trough					31.60%		18%	HTF is molten salts
	565	Solar tower	1,227	Natural gas	S	-	31.35%	-	22%	HTF is molten salts
	500	Fresnel linear					31.39%		13%	HTF is superheated steam
Solar Hybrid Gas Turbine Electric Power System (Mercury 50) [47]	600 (1st) 760 (2nd)	Pressurized air receiver	1,090.46	Natural gas	E&S	3,943	37.2%	-3.1%	39.04%	Save 0.07 kg CO_2/kWh (annual solar share 10%)
Solar-Assisted Small Solar Tower Trigeneration System (solarized TURBEC T100) [48]	780	Solar tower	950	Natural gas	S	100	28%	-2%	84%	Cooling or heating at the same time

Solarized gas turbine prototype plant: Mercury50 unit [49]	630 (1st) 800 (2nd)	Pressurized air receiver	1,150	Natural gas	S	4,200	35.9% (Annually)	-4.4%	38%	LEC is $0.12/ kWh (2006)
Solarized gas turbine prototype plant: Heron H1 unit [49]	800 (preheat and reheat)	Pressurized air receiver	860 (preheat) 865 (Reheat)	Natural gas	S	1,400	40.4% (Seville) 38.4% (Daggett)	-2.5% -4.5%	75%	LEC is $0.227/ kWh (2006) LEC is $0.236/ kWh (2006)
Gas Turbine ‘‘Solarization’’- Modifications for Solar/Fuel Hybrid Operation [50]	810	Pressurized air receiver	1,080	Natural gas	E	227	18.2%	-	60%	
Hybrid Solar Gas Turbine Project using Central Receiver System (PEGASE) [51]	850	Central Receiver System	1,000	Natural gas	S	1,414	22.1%	-13.0%	62%	
Small-scale hybrid solar power plants using micro gas-turbine [52]	800		900				19.4%		32.2% (annually)	open-cycle design
	800	Solar tower	900	Natural gas	S	100	30.4%	-	27% (annually)	internally-fired recuperated design
	700		780				22.5%		37.4% (annually)	externally-fired design
Hybrid solar gas-turbine power plant (HSGTPP) [53]	934	Solar tower	1,220	Natural gas	S	15,000	35.3%	-	65.1%	LEC is $0.104 /kWhe (2012); Specific CO_2 emission is 0.4 kg/kWh

Air-Based Bottoming-Cycles for Water-Free Hybrid Solar Gas-Turbine Power Plants (AB-HSGT) [54]	950	Solar tower	1,400	Natural gas	S	57,900	29.9% (exergy efficiency)	-	39.2%	LEC is $0.109/kWh (2013); Specific CO_2 emission is 0.350 kg/kWh
Solar powered gas turbine system [55]	800 960	Solar air receiver	-	Fuel	E	230 165	20% 15%	-	60% 70%	
A solar hybrid gas turbine [56]	1,015 800	Solar tower	1,230 1,236	Natural gas	S	28,500 34,300	36.6% 38.3%	-1.2% -0.7%	70% 40%	Summer (ambient temperature at 29°C Winter (ambient temperature at 15°C)

* E: Experiment, S: Simulation.

** Efficiency is defined as net power output divided by total energy input (Eq. (2.2)), unless indicated otherwise.

*** Solar fraction is defined as solar energy input divided by total energy input (Eq. (2.17)).

**** LEC (levelized electricity cost) was converted to dollar value, based on the currency of the first day in the year published.

3.1.3. The solar assisted combined cycle

In this type of hybrid cycle, solar heat is either added in the steam cycle (bottoming part) or the gas cycle (topping part), or in both parts, but I found no publication of the latter, possibly because of complexity of design or control of the system. If solar heat is added to the steam cycle without changing the top cycle, the steam turbine power output (thus total and net) will increase; if it is added to the gas cycle without changing the bottom cycle,

less fuel will be needed (thus resulting in lower emissions). The first approach is also called the “power-booster” mode, and the second the “fuel-saver” mode. The sketch for solar assisted combined cycles is shown in Fig. 3-4 [74]. Option (I) is a “power-booster” mode and uses gas turbine exhaust gas as the higher temperature heat source (in the bottom part, not the combined cycle); while option (II) is the “fuel-saver” mode and uses natural gas as the higher temperature heat source. A summary of the features of this type of hybrid cycles is shown in Table 3, in the order of temperature of lower temperature heat source. Note that option (I) contains two higher temperature heat sources. The higher temperature heat source for the hybrid combined cycle is natural gas, but gas turbine exhaust gas can also be regarded as heat source if we only consider the bottom part and that is why it is also included in the table.

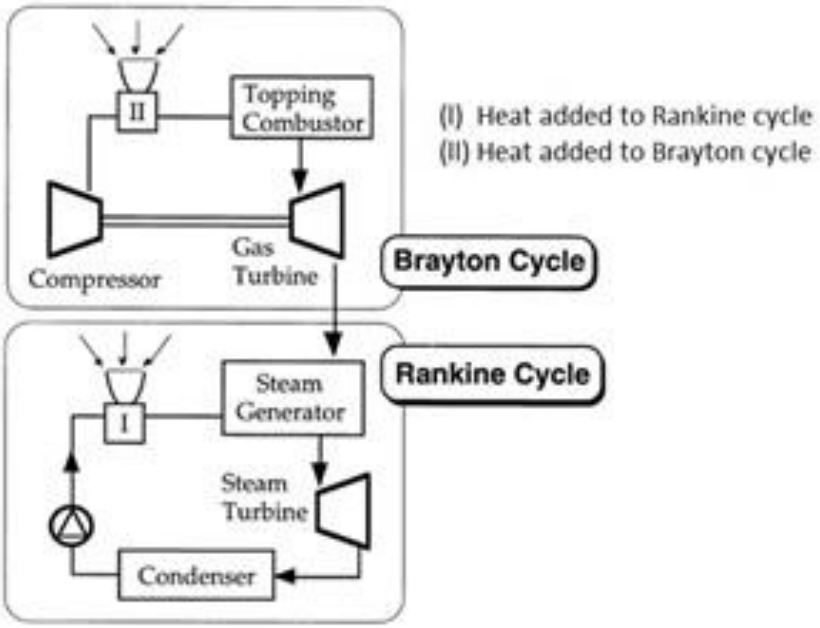

Fig. 3-4 Flow diagrams of hybrid combined cycle (adapted from [74])

In [74], an early work was done for both types of solar hybrid combined cycle by categorizing the types (Fig. 3-4), predicting the performances, and estimating the costs. Two solar hybrid combined cycle power plants having the capacity of 600 kWe and 34 MWe were analyzed. The temperature the solar tower (Irradiated Annular Pressurized Receiver) could achieve was 1,300 °C, but the operating temperatures were not specified, neither were the solar share. But the top temperatures of the cycles were given as 1,000 °C and 1,200 °C, respectively, and the annual efficiencies of the plants were 16.1% and 21.3%, respectively.

First, let's look at the first type of solar hybrid combined cycle system when solar thermal power is integrated in the bottom cycle. An exergy analysis was done for a solar

concentrator-aided natural gas fired combined cycle power plant [58]. The concentrator was a linear Fresnel reflecting (LFRSC) type. The solar exergy was calculated assuming solar temperature at 5,800 K. The insolation on the concentrator heated a heat transfer fluid (Therminol VP-1) from 260 °C to 311 °C, and was then used to preheat the feed water. The results showed that the power output increased from 293.59 MW to 325.29 MW due to the additional heat input from solar, but the energy efficiency was decreased from 54.47% to 41.69% due to the low solar collector efficiency. The exergy efficiency also decreased from 53.93% to 49.69%, thus by a smaller amount. Another finding is that exergy efficiency was higher than energy efficiency for the hybrid system, unlike the conventional system.

Apart from the previous one, another full cycle exergy analysis on an ISCCS was done in [64], but using a solar parabolic trough concentrating collector rather than Fresnel collector. The oil at the outlet of the collector had a maximal temperature of 393 °C, to heat the water to saturated vapor at 310.6 °C. The solar and fuel energy input were 114.96 MW and 736.04 MW, respectively, and the net power output was 392.93 MW, so the energy efficiency was 46.2% with solar energy share of 13.5%. With solar input exergy calculated using solar temperature, the exergy efficiency of solar collector was only 27%, which was the least efficient component in the plant. It was also argued that the energy and exergy efficiencies of ISCCS were higher than that of simple combined cycle without solar contribution and also Rankine cycle power plants using parabolic trough solar collectors, but no efficiency of those plants had been given or calculated in the paper.

For the same ISCCS as the previous described, other researchers [65] did a technical and economical assessment but with three integration schemes considered: 1) Integrated Solar Combined Cycle System with solar field that could produce heat at 33 MW (ISCC-33); 2) ISCCS with solar field that could produce heat at 67 MW (ISCC-67) and 3) ISCCS with solar field that could produce heat at 33 MW and Auxiliary Firing system (ISCC67-AF). Also, they were compared with three reference systems: Gas Turbine power plant (GT), Combined Cycle power plant (CC) and Solar Electric Generating System (SEGS). It was found that ISCC-67 was the best of all, with the highest generation capacity at 444 MW, highest annual net efficiency at 51.6% and lowest LEC of 2.035 ¢/kWh (2005).

For a proposed advanced Zero Emissions Power (AZEP) cycle, four different integration schemes using a parabolic trough were analyzed [59]: vaporization of high-pressure stream, heating of intermediate-pressure turbine inlet stream, heating of low-pressure turbine inlet stream, and preheating of high-pressure stream, and compared with a non-solar AZEP cycle. The solar heat source temperature varied with time and the highest one (369 °C) was included in the summary table, as was the net power output for each configuration. In all cases, the maximum solar share in a year was set to 30%. The authors focused on the power output of each configuration but didn't calculate the energy efficiency of any configuration, which should be done in comparing these configurations. It was found that the configuration with vaporization of high-pressure stream had the highest power output. The conclusion was similar as for solar hybrid vapor cycle.

A comprehensive study was done on investigating the performance of general Integrated Solar Combined Cycle System (ISCCS) with and without thermal energy storage (TES) in different operation modes [60]. For comparison, two locations (Barstow, California with high solar radiation and Tabernas, Spain with somewhat lower solar radiation) were considered, in comparison with solar-integrated not-combined Rankine cycle systems with the same nominal electricity output. It was found that the energy efficiency of ISCCS at design point with 100% storage (annual solar share was 9.4% in California and 6.4% in Spain) was 37.44%, and with no storage (annual solar share was 5.6% in California and 3.4% in Spain) was 36.72%, compared with a reference combined cycle plant having an efficiency of 36.19%. We could see that the energy efficiency for hybrid power plant was about 1% higher than fossil fuel only power plant and using thermal energy storage could further increase the efficiency by having higher solar share. Also, the economic analysis showed that the hybrid plant will have lower solar LEC than solar-only plants at the same sites and the same operation scheme.

Four years earlier, an analysis on ISCCS like the one described before was done but with different operation points [61]. The maximal temperature of heat transfer fluid (the type was not specified) in parabolic trough is 390 °C and the exhaust gas from gas turbine at 540 °C. The relation between steam cycle efficiency (defined as steam turbine power output divided by energy input from (solar + HRSG) and solar share for three different configurations, and also the influence of solar collector size on the levelized cost of electricity of the plants, were studied. It was found that the plant LEC was dependent on

the size of the solar field with a lower LEC for lower collector. According to the reference, the LEC of ISCCS with 15 to 24% of annual solar share was about 20% to 30% higher than similar size combined cycle plant.

An economic analysis on ISCCS using line-focus parabolic trough collectors to generate steam at 390 °C to either augment the power of the low-pressure steam turbine in the bottom cycle (power boost mode) or help save fuel in the top cycle (fuel saving mode) [62]. There was not much information about the thermodynamic performance of the hybrid system except for some operating parameters such as solar temperature, gas turbine inlet temperature (1,200 °C), gas turbine exhaust gas temperature (573.4 °C). The economic analysis was done for a one year period with hourly time steps considering different size of solar field from 30,000 m^2 to 180,000 m^2. It was shown that the LEC of ISCCS with different size of solar field ranges from 0.060-0.076 $/kWh (2013). It could be seen that when the size of solar field becomes 6 times larger, the cost of ISCCS was 26.7% higher.

[70,71] introduced an Integrated Solar Combined Cycle (ISCC) using Direct Steam Generation (DSG) which was coupled to the high-pressure level in the two-pressure levels Heat Recovery Steam Generation (HRSG) generating steam at 545 °C, and compared it to a conventional Combined Cycle Gas Turbine (CCGT). The annual simulation showed Annual global efficiencies ISCC power plant were 52.18% in Almería (ambient temperature at 25 °C) and 51.90% in Las Vegas (ambient temperature at 35 °C) which were both lower than that of the reference CCGT 53.2%. Solar share was calculated from the

data given in the reference. It was found that solar share is 3.0% in Almeria and 4.6% in Las Vegas, which had a higher ambient temperature.

To compare the effect of direct steam generation (DSG) technology with traditional heat transfer method using heat transfer fluid (HTF) in a parabolic trough concentrating solar collector, the performance of ISCCS for different technologies were studied in [63]. For DSG, water is heated directly by solar radiation, so that a heat exchanger or HTF are not required. That reduced the capital investment and eliminate the heat exchanger thermal and pressure losses, and thus raise the system efficiency and power output. It was proved by finding that annual efficiency and power output of ISCCS with DSG was 0.6% and 1.5% higher than ISCCS with HTF, respectively. Also, the LEC of ISCCS with DSG was also found to be lower than ISCCS with HTF by about 2.4%.

An analysis was done during the construction of the first ISCCS in Algeria before the plant broke ground in Oct. 2007 [66]. The hybrid power plant is now in operation since July 2011 according to NREL [57], and can work in three modes: Integrated solar combined cycle mode at solar hours (even with one gas turbine), conventional combined cycle mode at non-solar hours and gas turbine mode when the steam turbine is not functioning. The simulation results showed that the power plant could provide about 134 MW with efficiency of 57.5% at night with no solar input, and could reach 157 MW and 67% with solar input at daytime.

Like the previous one, an analysis was made based on an existing plant (Colon Solar project, Spain) [68]. Due to the liberalization of the electricity generation market, the project needed to be modified to an all-new combined cycle with solar energy integrated into a heat recovery boiler. A central receiver system was used in the plant. The total net power output of the plant was 70.4 MW with an efficiency of 51.5% compared with the efficiency of 54.0% when there was no solar radiation. The designed solar input was 21.8 MW, so the solar share was 16%.

Two types of solar hybrid combined cycles were analyzed in [67]. The first one used solar heat at 395 °C generated by parabolic trough concentrating collectors (oil as HTF) to supplement the energy required by the steam cycle; while the second one used solar heat at 450 °C generated by parabolic trough (molten salt as HTF) and two storage tanks at the outlet of the solar field to supplement the energy required by steam cycle. Both cycles had a predicted capacity of 137.8 MW and efficiencies of 46.4% and 48.3%, respectively. Correspondingly, the solar share was 57% and 64%, respectively.

An economic analysis was done for an ISCCS assumed to be in Egypt [69]. Two technologies were considered: solar parabolic trough concentrating collector field (HTF-trough) and air receiver tower with a heliostat field (air-tower). In HTF-trough type collector, the HTF (synthetic oil) was heated to 390 °C to boil a fraction of the feed water together with gas turbine exhaust gas. In the air-tower type, hot air heated by solar air receiver at 680 °C is mixed with gas turbine exhaust gas at 525 °C before HRSG. When the solar energy was insufficient, a duct burner was used. The authors did almost no

thermodynamic performance analysis, but investigated comprehensively in economic performance. The results showed that LEC for HTF-trough types was 3.076 ¢/kWh, which was 0.3% higher than that of air-tower types, 3.066 ¢/kWh, and both types were about 26% higher than the corresponding reference combined cycle systems.

As part of the SOLGATE project [47] introduced above, the performance of two prototype solarized combined cycle plants were analyzed [49]. One of them used two pressurized air solar receivers to preheat the compressed air to 610 °C and 800 °C, while the other one used three solar receivers to preheat at 600 °C, 800 °C and 1,000 °C, consecutively. The top temperatures were both 1,080 °C and the net power outputs were both 16.1 MW. The first prototype plant was assumed to be located in both the city of Seville, Spain and Daggett, USA while the second one in Daggett only. It was found that the annual efficiency was 44.9% and 43.4% for the first type in Seville and Daggett, respectively, and was 43.9% for the second type. The solar share for the second type (88%) was much higher than for the first type (57% and 58%, respectively).

After the review of solar hybridization in the bottom cycle, let's now look at the cases when solar thermal power is integrated in the top cycle of the combined cycle.

In [72], a solar-hybrid gas turbine-based power Tower system (REFOS) was built and tested in which a solar receiver was used to preheat compressed air to 800 °C. The turbine inlet temperature is 1,300 °C and the system was scaled to have a capacity of 30 MW. The analysis was based on two modes: daytime operation and full-time operation. The

efficiencies were almost the same (43.0% and 43.1%, respectively) but the solar shares were very different (28.6% and 15.0, respectively). The reason why solar share in daytime operation was higher than that in full-time operation was that more fuel was used in full-time operation due to lack of solar radiation in night time.

In [36], two types of solar hybrid combined cycle were analyzed, named Solar-Hybrid Combined Cycle (SHCC) system and Particle-Tower (PT) system, both of which used thermal energy storage. For each system, pressurized air was heated up to 850 °C and 995 °C, respectively. In the Particle-Tower, air was heated by solid media particles, which acted as the heat transfer fluid (HTF) through a heat exchanger. Both cycles could achieve a gross efficiency of about 45% and power output of about 30 MW. The influence of thermal storage capacity on solar share, specific CO_2 emissions and levelized electricity cost, was then studied. For SHCC, with solar share at 60.1%, the specific CO_2 emissions with thermal storage at 0 hour, 7.5 hours and 15 hours was 0.396 kg/kWh, 0.334 kg/kWh and 0.273 kg/kWh, respectively. For PT, with solar share at 79.7%, the specific CO_2 emissions with thermal storage at 0 hour, 7.5 hours and 15 hours was 0.379 kg/kWh, 0.297 kg/kWh and 0.219 kg/kWh, respectively. For SHCC, the LEC with thermal storage at 0 hour, 7.5 hours and 15 hours was \$0.098/kWh, \$0.112/kWh and \$0.128/kWh, respectively. For PT system, the LEC with thermal storage at 0 hour, 7.5 hours and 15 hours was \$0.098/kWh, \$0.113/kWh and \$0.129/kWh, respectively. It could be seen that compared with no thermal storage, adding 7.5 hours thermal storage decreased the carbon emissions by 16% for SHCC and 22% for PT, and 15 hours by 31% for SHCC and 42% for PT.

Adding 7.5 hours thermal storage increased LEC by 14% and 15 hours by 31% for both SHCC and PT. That was because adding thermal storage to the solar hybrid systems could reduce the usage of fuel, which was needed when there was not enough solar heat input (which is intermittent and influenced by the weather conditions) to make the system run at the design point. The more thermal storage was used, the less fuel was needed, and thus the less emission was generated by the systems.

In [73], the influence of the type of gas turbine and its arrangements on the performance of solar hybrid combined cycle was studied. A solar tower was simulated and used to preheat compressed air to 950 °C. Three different types of gas turbines were chosen: Siemens SGT-800, a modern heavy-duty machine with relatively high cycle efficiency and a single shaft configuration, Siemens SGT-750, a new advanced heavy duty unit with a two-shaft configuration consisting of a compressor turbine (used to drive the compressor) and a power turbine (used to produce power output), and GE LM6000PF, a high performance aeroderivative model presenting a higher sensitivity to inlet air temperature variation and a two-spool configuration. Each solarized combined cycles was also compared with the corresponding reference combined cycles without solar input using the same gas turbine. For each GT type, the system efficiency was about 50% with solar share of 34%, 36% and 31%, respectively, and the efficiency was about 0.7% lower than the corresponding fossil-fuel-only combined cycle power plant using the same gas turbine.

More detailed information about the above-reviewed solar assisted combined cycle is in Table 3-3.

Table 3-3. A summary of past studies of solar-assisted combined power cycles

Descriptive name of system and reference	Lower temperature heat source		Higher temperature heat source		E/S*	Power, kW	Claimed power generation efficiency**	Efficiency improvement over single temperature system	Solar fraction of the total energy input***	Note****
	T,°C	type	T,°C	type						
Solar concentrator aided natural gas fired combined cycle power plant [58]	311	Solar Linear Fresnel reflecting concentrator	551	Gas turbine exhaust gas	S	325,290	41.69%	-12.78%	10.7%	Exergy efficiency is 49.69%, which is 4.24% less than fossil fuel only plant
			1,072	Natural gas						
Solar hybridized advanced Zero Emissions Power (AZEP) cycle [59]	369	Solar parabolic trough	465	Gas turbine exhaust gas	S	465	-	-	30%	Vaporization
						475				Heating of intermediate-pressure stream
			1,200	Natural gas		470				Heating of low-pressure stream
						431				Preheating
Integrated solar combined cycle system (ISCCS) [60]	380	Solar parabolic trough	565	Gas turbine exhaust gas	S	310,000	36.72%	0.53%	5.6% in California; 3.4% in Spain	Without thermal storage
			-	Natural gas			37.44%	1.25%	9.4% in California; 6.4% in Spain	With 100% thermal storage
Advanced Solar-Fossil	390		540	Gas turbine	S	125,000	61.0%	-	24.3%	Collector size is 0.61 km2; LEC

Combined Power Plants (ISCCS) [61]		Solar parabolic trough	-	exhaust gas Natural gas		100,000	55.0%		14.5%	is $0.054/kWh (2000) Collector size is 0.28 km2; LEC is $0.055/kWh (2000)
Integrated solar combined cycle power plant in Greece using line-focus parabolic trough collectors [62]	390	Solar parabolic trough	573.4 1,200	Gas turbine exhaust gas Natural gas	S	50,000	-	-	-	LEC is $0.060-0.076/kWh for different size of collector area
Integrated solar combined cycle system with DSG technology compared with HTF technology [63]	390	Solar parabolic trough	690 1,247	Gas turbine exhaust gas Natural gas	S	451,460 444,800	~52.4% (Annual) ~51.8% (Annual)	~17% (compared with solar only system)	14.8% 15.1%	ISCCS-DSG; LEC is $0.7459/kWh (2010) ISCCS-HTF; LEC is $0.7645/kWh (2010)
Integrated solar combined cycle system (ISCCS) [64]	393	Solar parabolic trough	548.38 1,131.65	Gas turbine exhaust gas Natural gas	S	392,920	46.2%	-	13.5%	Exergy efficiency is 45.6%; solar exergy share is 12.4%
Integrated solar combined cycle	393		548.38	Gas turbine	S	407,000	50.9% (Annual)	1.6%	-	33 MWe solar field

system (ISCCS) [65]		Solar parabolic trough		exhaust gas		444,000	51.6% (Annual)	2.3%	67 MWe solar field
			1131.65	Natural gas		444,000	50.9% (Annual)	1.6%	67 MW e solar field and auxiliary firing system
First Integrated Solar Combined Cycle System in Algeria [66]	393	Solar parabolic trough	-	Gas turbine exhaust gas	S	147,000	67%	9.5%	-	Hybrid mode only at daytime
			-	Natural gas					
Co-located gas turbine/solar thermal hybrid for power production [67]	395	Solar parabolic trough	450	Gas turbine exhaust gas	S	137,800	46.4%	-	57%	HTF is oil; without thermal energy storage; LEC is $0.136/kWh (2014)
	450		-	Natural gas			48.3%		64%	HTF is molten salts; with thermal energy storage (3h); LEC is $0.154/kWh (2014)
The Colon solar project [68]	510	Central Receiver System	-	Gas turbine exhaust gas	E&S	70,400	51.5%	-2.5%	16%	IRR is 8.36%, assuming a 12% discount rate (1999)
			-	Natural gas					

Integrated solar combined cycle power plants using different types of solar field [69]	380	Solar parabolic trough	525	Gas turbine exhaust gas	S	124.13	-	-	-	LEC is $0.03076/kWh (2004)
	680	Solar volumetric air receiver	-	Natural gas						LEC is $0.03066/kWh (2004)
Integrated Solar Combined Cycle using Direct Steam Generation [70, 71]	545	Solar parabolic trough	555	Gas turbine exhaust gas	S	220,000	52.18% (Annually)	-1.02%	3.0%	Almería; LEC is $0.108/kWh (2011)
			1,177	Natural gas			51.90% (Annually)	-1.3%	4.6%	Las Vegas; LEC is $0.109/kWh (2011)
Solarized gas turbine prototype plant: PGT10 unit, 800 °C [49]	610 (1st) 800 (2nd)	Pressurized air receiver	1,080	Natural gas	S	16,100	44.9% (Annually)	0.3%	57%	Seville; LEC is $0.0747/kWh (2006)
							43.4% (Annually)	-1.2%	58%	Daggett; LEC is $0.0750/kWh (2006)
Solar-Hybrid Gas Turbine-based Power Tower Systems (REFOS) [72]	800	REFOS Receiver module	1,300	Natural gas	E&S	30,000	43.0%	-1.9%	28.6%	Daytime operation; LEC is $0.0695/ kWh (2002)
							43.1%		15.0%	Full-time operation; LEC is $0.0508/ kWh (2002)
	850	Solar tower	1,100		S	30,200	45.9%	-	60.1%	No storage;

Solar-Hybrid Combined Cycle (SHCC) with thermal energy storage [36]				Natural gas		29,500 28,800	44.8% 43.7%			LEC is $0.098/kWh 7.5h storage; LEC is $0.112/kWh 15h storage; LEC is $0.128/kWh
Solar Hybrid Combined Cycle with different Gas Turbine Model and Spool Arrangements [73]	950	Solar tower	1,285 1,210 1,280	Natural gas	S	55,380 36,800 41,260	50.7% 49.3% 50.7%	-0.7% -0.7% -0.6%	34.2% 36.3% 30.8%	GT type is Siemens SGT-800 GT type is Siemens SGT-750 GT type is GE LM6000PF
Particle- tower with thermal energy storage [36]	995	Solar tower	1,100	Natural gas	S	30,300	45.6% 45.2% 44.9%	-	79.7%	No storage; LEC is $0.098/kWh 7.5h storage; LEC is $0.113/kWh 15h storage; LEC is $0.129/kWh
Solarized gas turbine prototype plant: PGT10 unit, 1,000 °C [49]	600 (1st) 800 (2nd) 1,000 (3rd)	Pressurized air receiver	1,080	Natural gas	S	16,100	43.9%	-0.7%	88%	Daggett; LEC is $0.082/kWh (2006)

Solar-driven combined cycle power plant [74]	Irradiated Annular Pressurized Receiver	1,000 1,200	Natural gas	S	600 34,000	16.1% (Annually) 21.3% (Annually)	-	Lowest LEC is about $0.10/kWh (1997) LEC is $0.06-0.07/kWh (1997)

* E: Experiment, S: Simulation.

** Efficiency is defined as net power output divided by total energy input (Eq. (2.2)), unless indicated otherwise.

*** Solar fraction is defined as solar energy input divided by total energy input (Eq. (2.17)).

**** LEC (levelized electricity cost) was converted to dollar value, based on the currency of the first day in the year published.

3.1.4. Other types of thermal hybrid power cycles

Apart from solar assisted types of hybrid power cycles, other types of heat sources, such as biomass, nuclear, and geothermal, as well as waste heat from internal combustion engines (mostly diesel), can also be used in hybrid power cycles. A summary of these types of hybrid cycle is given in Table 3-4, grouped by the types of heat sources.

1) Geothermal with coal

As in solar assisted power cycles, conventional (hydro-thermal) geothermal heat sources usually has the lowest temperature in a hybrid system. In a geothermal-fossil hybrid power plant, geothermal heat at 103 °C and 147 °C at two different locations was used to produce hot water. The hot water was then used to preheat the feed water in steam power plant before superheated in the boiler [85,86]. The condition of the superheated steam at the

turbine inlet is 250 bar/540 °C. Reheat was also used at 560 °C to improve the efficiency of the power plant. To compare the performance of power plants under different geothermal temperature, two plants at different locations were considered. The one at Neustadt-Glewe, Germany, used geothermal water at 98 °C and the one at Soultz-sous-Forets, France, at 142 °C. The pinch temperatures in the geothermal heat exchanger were both 5 °C. A combined heat and power plant (CHP) in condensing mode (i.e., pure electricity generation) having an efficiency of 40.9% was used for comparison. Since the superheated steam conditions were different from that of the hybrid system, however, it cannot be used as a reference plant for comparison with the hybrid power plant. Also, the authors focused on geothermal energy conversion efficiency (electricity produced by geothermal heat divided by geothermal heat) didn't do a full cycle analysis, so full cycle efficiency was not known. It was found that the geothermal to electricity conversion efficiency was 8.06% and 13.34%, respectively, for the two locations.

2) Geothermal with biomass

Besides fossil fuel as in the previous analysis, biomass could also be combined with geothermal power in a hybrid power plant. In [87], two types of geothermal-biomass hybrid cycles were proposed and analyzed: Dual-fluid-hybrid cycle (DFH) using two different working fluids, which was actually a geothermal powered organic Rankine cycle topped by a biomass powered steam Rankine cycle, and Single-fluid hybrid cycle (HYB) using geothermal heat to preheat and biomass to superheat the working fluid (could be organic or steam). Four kinds of organic fluids and steam were studied as working fluid,

respectively, and a sensitivity analysis of energy efficiency, power output and efficiency of utilization of geothermal heat on geothermal water temperature from 80 °C to 100 °C (the pinch point in the geothermal heat exchanger was set to 5 °C). When the geothermal temperature was 100 °C, although not given directly, the geothermal energy supply share could be calculated by the given data as 9.7~45.7 % for different organic fluids used in the system. The organic Rankine cycle powered only by geothermal heat was used as the reference cycle. It was found that HYB using cyclohexane as working fluid had the highest energy efficiency (28%) and power output (9.7 MW). For comparison, a geothermal-only ORC using R236fa as working fluid was just 11% and 0.4 MW, respectively. This represented a 127% and 2,325% increase, respectively, in energy efficiency and power output.

3) Biomass with natural gas

In [88], several integration methods of a biomass boiler burning wet forest and agricultural residue (FAR) with two types of gas turbines in a combined cycle gas turbine (CCGT) plants were proposed and analyzed. The flow diagrams of the two integration methods could be seen in Fig. 3-5 and Fig. 3-6. One type of CCGT (01Ref) consists of 2 parallel gas turbines (GT) (2 GT was chosen to be compared with the case when only 1 GT was used), heat recovery steam generator (HRSG) and 1 steam turbine (ST), and the other one (02Ref) consists of 1 GT, HRSG and 1 ST with reheat and intercooling in GT. In the integrated power plant, a fraction of flue gases from a CCGT is extracted between GT and HRSG (primary flue gas), led to the boiler and used as combustion air and fluidization

medium (fully-fired configuration) or for preheating air and economizing in the steam cycle (parallel-powered configuration). Flue gas from the end of the HRSG (secondary flue gas) was used to dry the biomass fuel. A gasification option was also provided, which utilized turbine exhaust gas to drive biomass gasification in a gasifier. The results were that the efficiency of the hybrid cycle was higher than the corresponding stand-alone biomass power plant but lower than the corresponding conventional CCGT. For example, for the first type of CCGT, the energy efficiency of the fully-fired configuration shown in Fig. 3-5was 41.0%, which was 5.5% higher than biomass only power plant, but 16.1% lower than the corresponding CCGT power plant. For parallel-powered configuration shown in Fig. 3-6, the efficiency was 37.9%, which was 2.4% higher than biomass only power plant, but 19.2% lower than the corresponding CCGT power plant. More details could be found in Table 3-4.

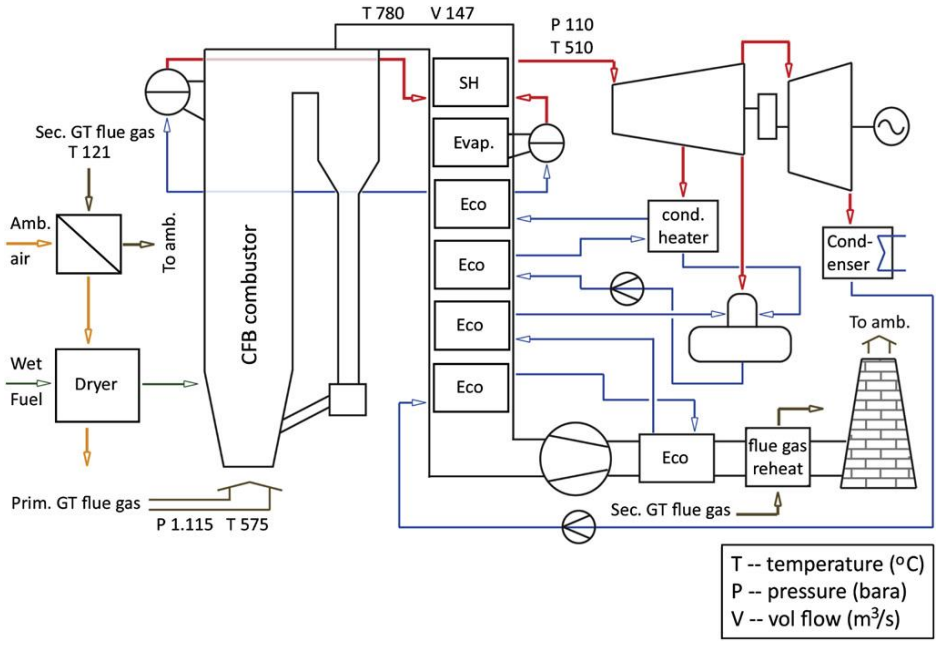

Fig. 3-5 Hybrid option biomass unit simplified scheme, 01HybFF configuration [88]

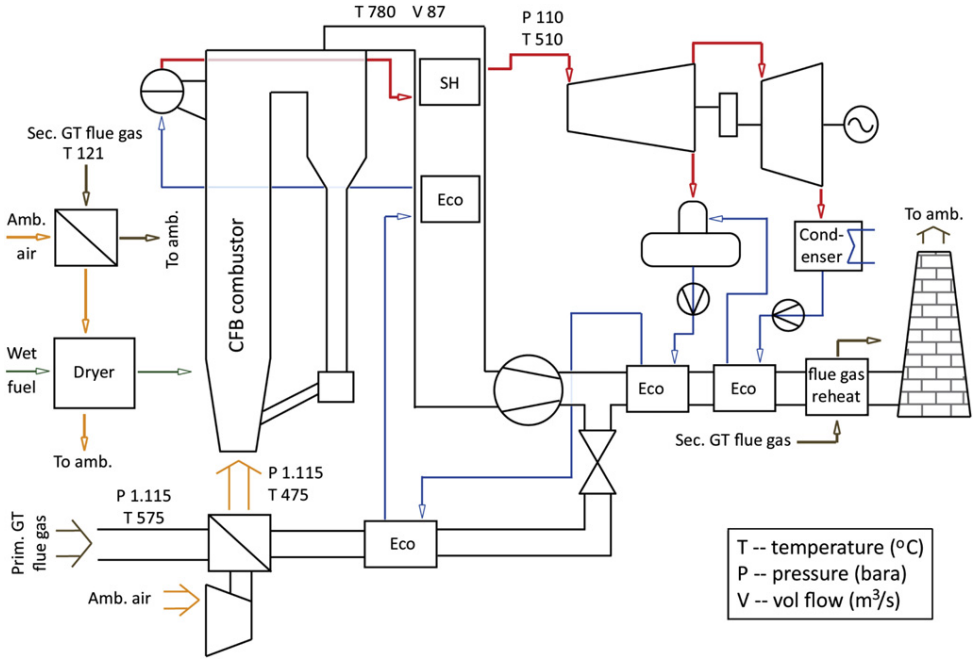

Fig. 3-6 Hybrid option biomass unit simplified scheme, 01HybPP configuration [88]

4) Nuclear with fuel

A number of studies and implementations were made of nuclear thermal hybrid power systems. Lior [89] made an energy, exergy and thermoeconomic analysis of a nuclear power plant superheated by fossil fuel. This plant was built and operated earlier at Indian Point, New York, was a pressurized water reactor generating core steam at 269 °C to produce steam at 234 °C at the outlet of the steam generator, which was superheated by an oil-fueled superheater to 540 °C, that was fed to the steam turbine. A total of 275 kW electricity was produced with 112 kW of that provided by the added fuel. The energy efficiency of the plant was 34.1% compared with 28.4% for the original plant that did not incorporate fossil fuel superheat. A sensitivity analysis of plant efficiency to the superheat temperature shown that the efficiency increased at a rate of about 7.7%/(100 °C superheat). An optimization on extraction steam from the turbine was also done in the paper, together with an economic evaluation.

An energetic and exergetic analysis on a hybrid combined nuclear power plant using a pressurized water reactor (PWR) was made [90,91]. In the system, nuclear heat at 273.4 °C was used to preheat the working fluid in the HRSG of the bottom cycle. Turbine exhaust gas at 343.4°C and 505.6 °C was used before and after nuclear preheating, respectively. The energy efficiency was found to be about 44% with a net power output of 1.84 GW.

In a comprehensive exergetic and economic comparison of a Pressurized Water Reactor (PWR) power plant and hybrid fossil fuel-PWR power plant [92], the nuclear-only system

was compared with the hybrid system using the same nuclear power plant but with additional natural gas or coal as higher temperature heat source. The nuclear only system, with top temperature of working fluid at 326.1 °C, was reported to have an exergy efficiency (power generation cost) of 38.5% (3.06% cent/kWh) for highest exergy efficiency and 37.6% (3.005% cent/kWh) when power generation cost when optimized for lowest power generation cost. The respective result for natural gas assisted (superheat to 480 °C) and coal assisted (superheat to 490 °C) hybrid power plant was reported to be 46.24% (3.431% cent/kWh) and 39.72% (3.495% cent/kWh), respectively, when exergy efficiency was optimized, and 44.16% (3.369% cent/kWh) and 38.46% (3.411% cent/kWh), respectively, when power generation cost was optimized.

Unlike the previously-described nuclear hybrid plants, which used nuclear power to preheat the working fluid in the steam cycle, [94] introduced a mobile hybrid gas turbine cogeneration power plant concept, which used a high temperature reactor (HTR) to preheat the compressed air for the gas turbine. The mobile system used a reactor outlet temperature at 800 °C to preheat the pressurized air to 700 °C and could further heat it to 1,000 °C using fuel oil. Hot exhaust gas from the gas turbine could also provide heat for hot water or desalination. A thermodynamic analysis when both heat sources were used was not performed, but instead the performance of the system when only nuclear or fuel was used were calculated. In the nuclear mode when only nuclear heat was used, the electrical generation efficiency was 32% and the power output 5 MW, while in the fuel mode when

only fuel was used, it was 40% and 5-6 MW, respectively. Both modes can provide heat output rate of 8 MW.

Besides integration with steam cycle and gas turbine as in the previous cases, nuclear could also be integrated with the combined cycle. [95] introduced a nuclear-assisted combined cycle (Nuclear assisted NGCC) in which nuclear power was used to preheat the compressed air in the gas turbine (top cycle). A gas cooled nuclear reactor was used to provide hot water at 900 °C to preheat the compressed air to 874 °C by a heat exchanger as shown in the flow diagram of the system Fig. 3-7. Usually nuclear power plant cannot provide such high temperature, however, certain types, such as high-temperature gas-cooled reactor could have an outlet temperature of 900 to 1,000 °C [75]. The inlet temperature for gas turbine is 1,400 °C and for the steam turbine 545 °C. The nuclear-assisted NGCC provided total power of 382 MW with the nuclear heat providing 46.3% of the total input thermal power. A sensitivity analysis found that the nuclear contribution increases with reactor outlet temperature for a fixed turbine inlet temperature. The energy efficiency for the whole plant is 59.1%, which is lower than for NGCC without nuclear (59.9%), but is higher than a conventional nuclear power plant (45%).

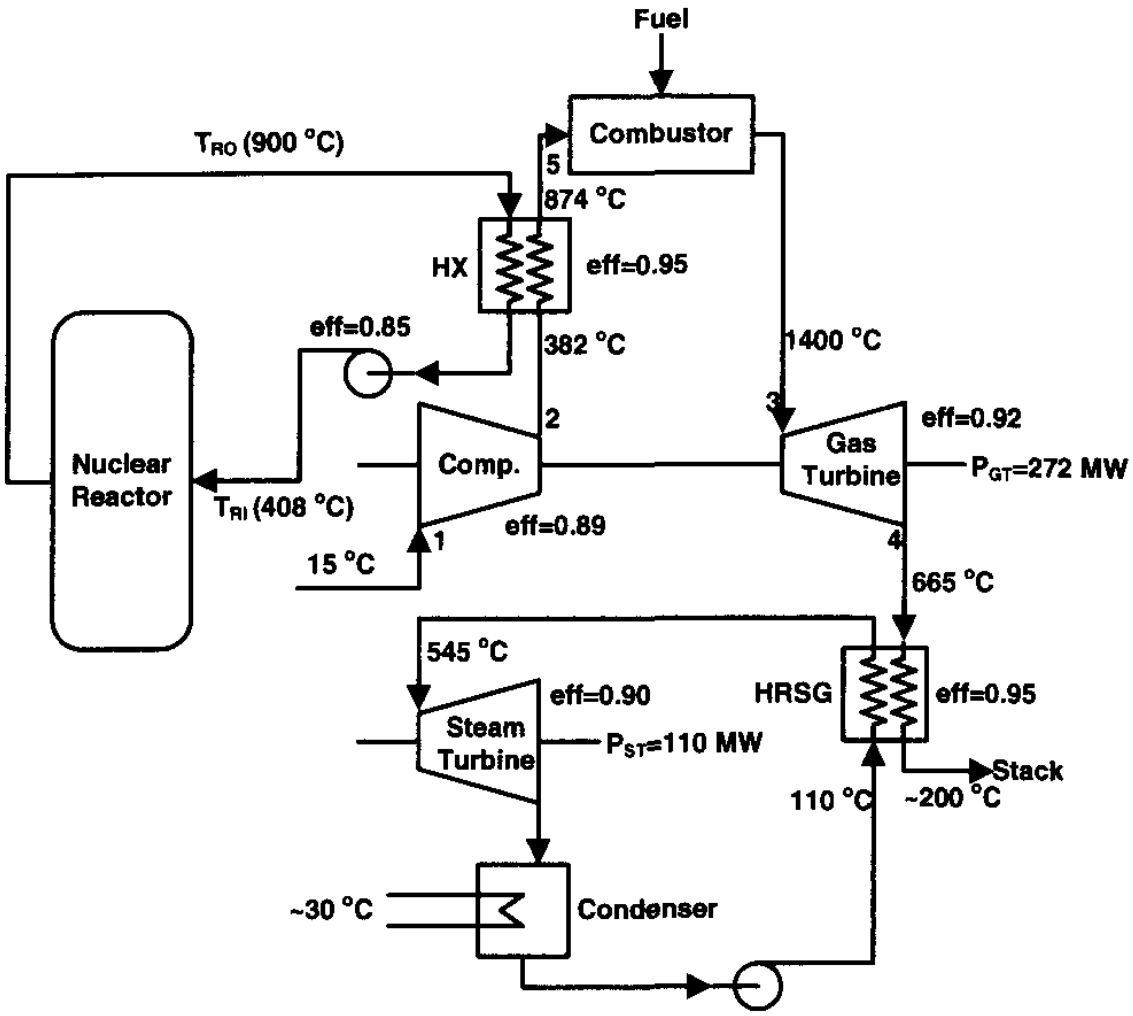

Fig. 3-7 Flow diagram of a nuclear-assisted combined cycle (Nuclear assisted NGCC) (RO: reactor outlet, RI: reactor inlet, eff: effectiveness/efficiency, HX: heat exchanger, Comp: compressor, GT: gas turbine, ST: steam turbine, HRSG: heat recovery steam generator, T: temperature, P: power) [95]

Also in [93], a Nuclear Air-Brayton Combined Cycle (NACC) was proposed, using a Fluroride-salt-cooled High-temperature Reactor (FHR). It could be operated in two modes:

base-load mode when only nuclear was used as heat source to heat the air to 670 °C, and peak electricity mode when natural gas (near-term), stored heat in thermal storage or hydrogen, were used to further heat the air to 1,065 °C. In the nuclear-only mode, the efficiency was reported to be 42% with power generation capacity of 100 MW; while in the hybrid mode, it could provide additional capacity of 142 MW. The efficiency of the hybrid system was not shown.

5) Nuclear with renewables

Apart from fuel, nuclear could also be integrated with renewable heat sources such as solar, geothermal or wind. Being able to take advantage of the differences between nuclear (base-load heat source) and renewables (variable electricity output), a novel hybrid nuclear renewable system for variable electricity production was introduced [76] and is shown in Fig. 3-8. In this system, the nuclear plant operated at full capacity with different mass flow rate of steam to turbines to match the electricity demand with production (renewables and nuclear). Excess steam at times of low electricity prices and electricity demand went to hybrid fuel production and storage systems. For example, the excess steam from the nuclear plant could be used to heat rock a kilometer underground to create an artificial geothermal heat source, which could also be used to produce electricity. The nuclear power plant used in the study was a pressurized water reactor, which had a maximal temperature of 273 °C. It was predicted that with relatively good match between nuclear production and electricity demand, this plant would have a competitive economic advantage relative to wind or solar energy power plants for a low-carbon world because of lower investments in energy storage

systems to meet variable electricity demand. Quantitative analysis to prove that was not performed.

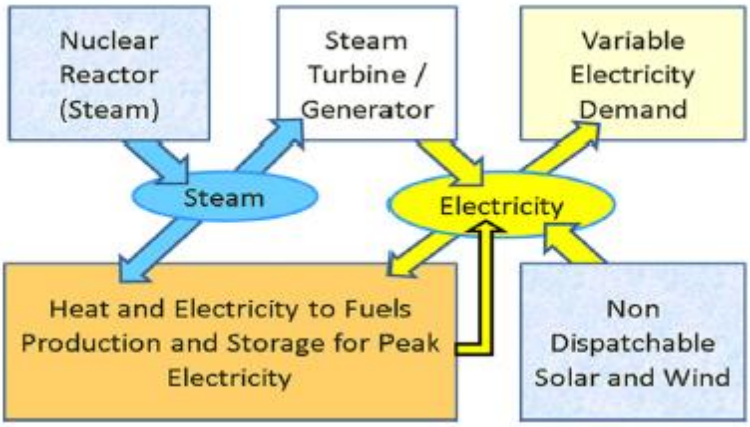

Fig. 3-8 Hybrid nuclear renewable system for variable electricity production [76]

6) Internal combustion engine compound systems

Internal combustion engine, or ICE, is an engine that produces work through internal fuel combustion. The waste heat from the engine combustion chamber and other parts of the engine, which is 60-70% of the fuel heat input into the ICE [77], whose temperature ranges from below 100 °C to over 500 °C, can serve as the heat source and be used produce additional power in addition to the power output from the ICE. Internal combustion engine (ICE) compound systems are also hybrid power cycles using multiple heat sources with different temperatures and much work have been done in this field.

In [96], the performances of 3 kinds of IC engine-organic Rankine cycle (ORC) combined cycles with different amounts of waste heats recovered at different temperatures was

studied. The first configuration utilized all of the five waste heat sources at different temperature (85 °C, 127 °C, 172 °C, 330 °C and 506 °C, from cooling water, intercooler, aftercooler, engine exhaust gas and Exhaust Gas Recirculation (EGR) cooler, respectively. The second configuration used the EGR gases and part of engine exhaust gas to drive a top Rankine cycle, and used other waste heat having relatively lower temperatures to drive a bottom Rankine cycle at the same time. The third configuration used only waste heat from the aftercooler, engine exhaust gas and EGR cooler to drive a Rankine cycle. The flow diagram of each configuration could be found in [96] and will not be introduced here. It was found the first configuration has the lowest power output (342 kW) and efficiency (41.3%) of the whole system and the second one has the highest power output (370 kW) and efficiency (44.69%).

Following the previous work, 3 kinds of innovative compound engine systems were configured [97], with flow diagrams shown in Fig. 3-9, Fig. 3-10 and Fig. 3-11, respectively:: (1) configurations without LP (low pressure) turbine, one with MP (medium pressure) EGR (exhaust gas recirculation); (2) configuration without LP turbine, with LP EGR, and (3) configuration without LP turbine, with LP EGR and high temperature Rankine cycle. The resulting efficiencies and power outputs showed no improvement over the 3 systems studied previously in [96]. It was concluded that the best configuration should be the third system since it had a relatively high efficiency and power output, but with a less complex configuration compared with the second system, which had a higher efficiency and power output.

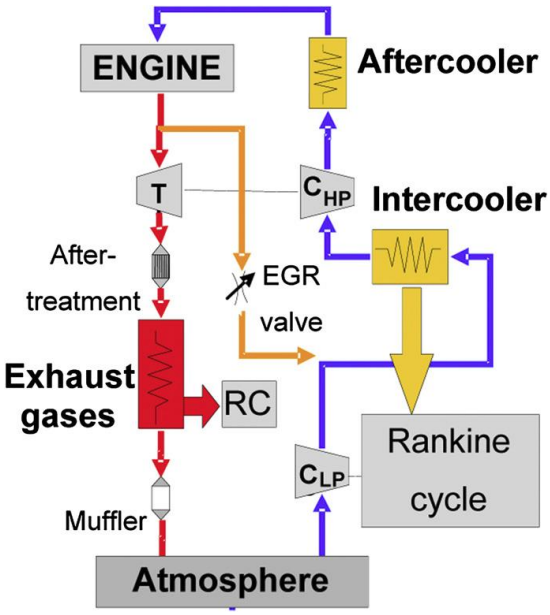

Fig. 3-9 Compounded IC engine power plant layout of the configuration without LP turbine, with MP EGR [97]

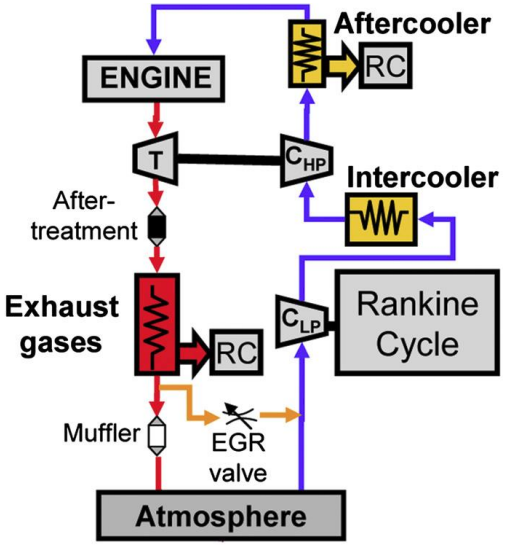

Fig. 3-10 Compounded IC engine power plant layout of the configuration without LP turbine, with MP EGR [97]

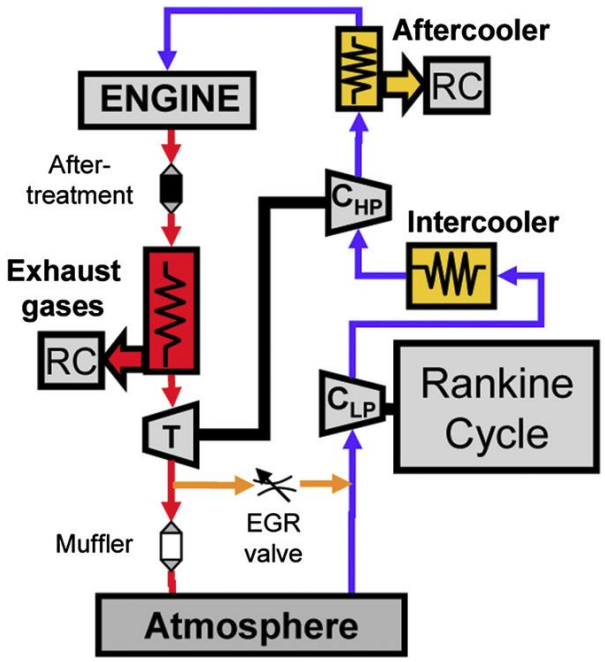

Fig. 3-11 Compounded IC engine power plant layout of the without LP turbine, with LP EGR and high temperature Rankine cycle configuration [97]

Another example is a combined diesel engine gas turbine system for distributed power generation [103]. The flow and T-s diagrams are shown in Fig. 3-12. In the system, part of the compressed air from low pressure compressor was used for the diesel engine combustion, and the other part was for further compression and used in gas turbine. The fuel for diesel engine acted as higher temperature heat source (point 5) and the fuel (natural gas) for the gas turbine acted as lower temperature heat source (point 12). This hybrid system used the thermal energy of the exhaust gas from diesel engine to generate additional power in a gas turbine. The optimization on the pressure ratios of three compressors with

the compression ratio (CR) of diesel engine fixed showed the cycle can had a maximal efficiency of 74.7% when $CR = 20$, and 77.3% when $CR = 30$.

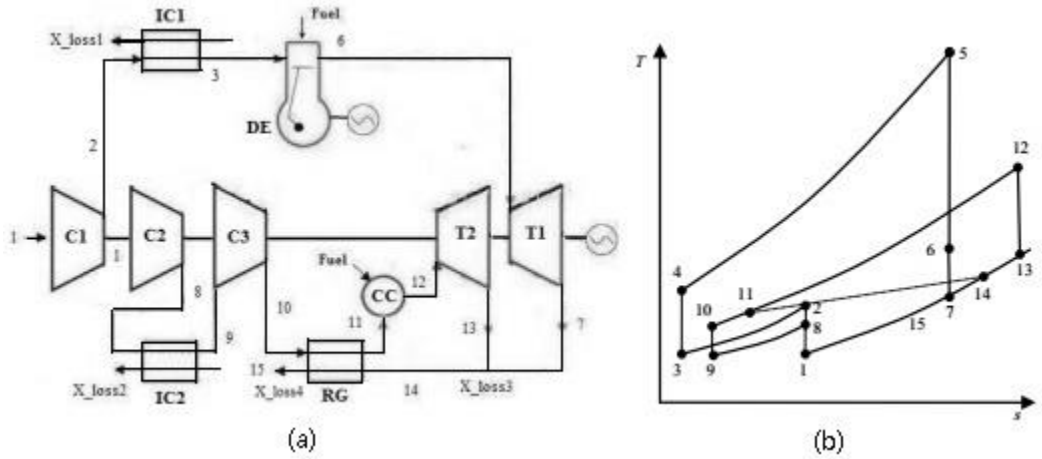

Fig. 3-12 Flow diagram (a) and T-s diagram (b) of a combined diesel-engine gas-turbine system with intercooling and regeneration [103] (DE: Diesel engine, C: compressor, T: turbine, CC: combustion chamber, IC: Intercooler, RG: regenerator)

The above-described analyses [96,97] considered the engine and the waste heat recovery system as a whole, by including the engine power output in the total power output and considered engine fuel input. Many studies, however, focused only on recovering the waste heat from the engine for augmenting power generation, and the engine exhaust gas is used as heat source in the waste heat recovery (WHR) system, without considering the engine output and fuel input. For those systems, only the efficiency of the WHR system (defined as the ratio between net power output and available energy in the exhaust gas of engine) is shown in Table 3-4, with “excluding engine” in the parentheses.

A review of organic Rankine cycles (ORC) driven by recovered internal combustion engine (ICE) exhaust waste heat [77], it was found that ORC was the most widely used waste heat recovery system in harvesting engine exhaust and engine coolant heat from ICE. It was also found that no single working fluid was best for all ORC's, since operating conditions, environmental impacts and concerns, and economic factors must be considered.

Furthermore, a recent study of an organic Rankine cycle system utilizing exhaust gas of a marine diesel engine showed that there was still no best choice of working fluid considering both power output and efficiency, even for one type of ICE exhaust gas driven ORC systems [99]. The authors optimized the system with and without pre-heater for 4 types of working fluid: R123ze, R245fa, R600 and R600a. The flow diagram is shown in Fig. 3-13. The results showed that the system using R245 as working fluid had the best performance in terms of the ratio between power output and total cost of system, which was 3% higher than the system using R1234ze. The system using R1234ze, however, had the best thermodynamic performance, with the maximum energy efficiency 2.2% higher than that for R600. Also, compared with conventional diesel oil feeding, the proposed ORC system could reduce 76% CO_2 emissions per kWh.

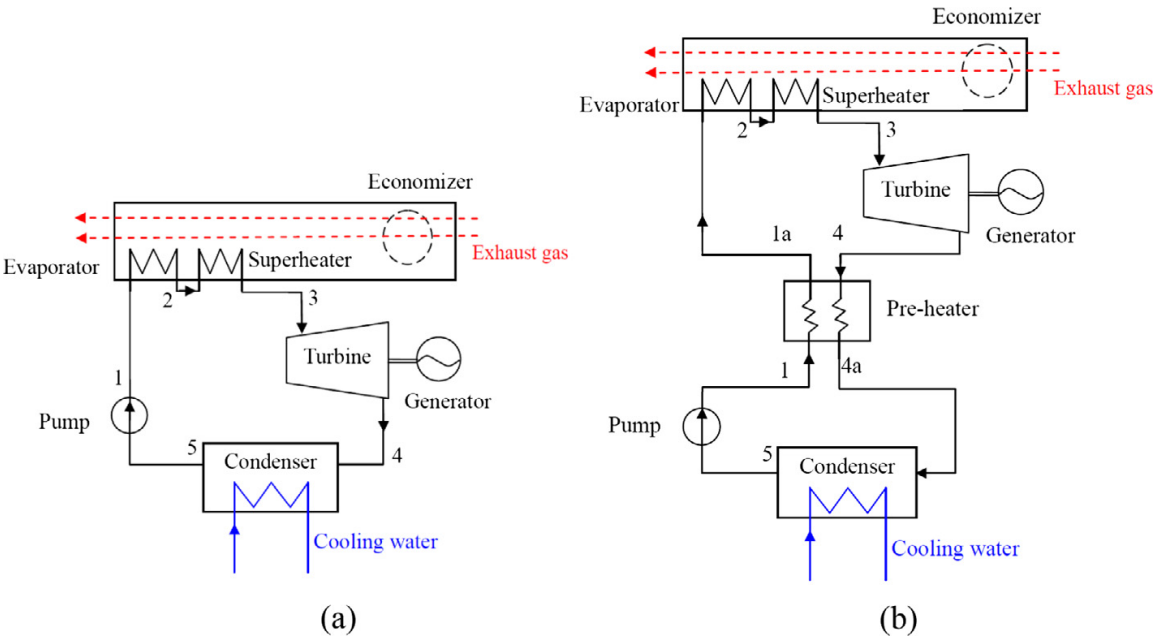

Fig. 3-13 Schematic diagrams of the ORC system (a) without pre-heater and (b) with pre-heater [99]

[98] introduced a combined thermodynamic cycle used for waste heat recovery of ICE. The system consisted of two cycles: organic Rankine cycle (ORC), for recovering the waste heat of lubricant at 175 °C and high-temperature exhaust gas at 500 °C, and a Kalina cycle, for recovering the waste heat of low-temperature cooling water at 135 °C. The performance of several types of working fluids in the higher temperature ORC was also analyzed. It was found that cyclopentane had a better performance than R113, since the efficiency was 20.83% when using cyclopentane as working fluid, higher than 16.51% when R113 was used, and the power output (347.8 kJ/kg) was also higher (261.52 KJ/kg).

The performance of a medium temperature organic Rankine cycle (ORC) recovering waste heat from heavy duty diesel engine (258 kW rated power) exhaust gas was analyzed in [101]. The organic fluid was chosen to be R123. The effect of temperature and mass flow rate of exhaust gas on the power output and efficiency of ORC was studied and it was found that an efficiency of up to 10-15% could be achieved. The ORC system, however, had no waste heat recovery effect when exhaust temperature was below 300 °C.

An organic Rankine cycle bottomed ICE was also analyzed, but using natural gas as fuel [102]. The engine without the ORC system generated 2,928 kW of electricity with turbine exhaust gas at 470 °C. Three configurations were analyzed to integrate with the engine: (1) ORC simple cycle powered by engine exhaust gases, (2) ORC simple cycle powered by engine exhaust gases and engine refrigerant water, and (3) ORC regenerated cycle powered by engine exhaust gases. The authors also considered the effect of the type of the working fluid and compared the performances of Benzene, R11 and R134a. Since only Benzene was used in all three investigated systems, the system performances with Benzene as organic fluid were included in Table 3-4. It was found that all three configurations are about 5% more efficient than the stand-alone engine and the third one is the best one among them with the highest power output and efficiency (47.1%).

Hydrogen can also be used as fuel for ICE. [104] introduced the hydrogen internal combustion engine (HICE) combined with open steam Rankine cycle to recover water and waste heat. Unlike diesel engines, HICE produce H_2O vapor as the main combustion product, besides the waste heat. The water produced by the HICE was used as the working

fluid in an open steam Rankine cycle, with the HICE exhaust gas as the heat source for the cycle. Two options for the cycle were also provided: without condenser (RS-1) and with condenser (RS-2). Water could be recycled if a condenser is used, but more work was needed to drive the air cooling fan. The energy efficiency for the recovery system was found to be higher for RS-2, but the overall efficiency for the combined system was almost the same, 2.9-3.7% higher than that of a conventional HICE without any recovery system, in the engine speed range of 1,500 rpm to 4,500 rpm. A sensitivity analysis was done on the turbine inlet temperature (TIT) and showed that the overall energy efficiency increased with TIT.

7) SOFC hybrid systems

Solid oxide fuel cells (SOFC) can also be used in hybrid power cycles. Early works were done by topping fuel cells on a Rankine cycle [78,79]. The flow diagram is shown in Fig. 3-14. In this system, hydrogen (stream 1) and ambient air (stream 2) were preheated by the preheaters to the needed reaction temperature (1020 °C) before entering the fuel-cell system, where the fuel was partially oxidized by the oxygen in the air. The high temperature fuel-cell exhaust gas (1170 °C for stream 6 and 1319 °C for stream 7) was then combusted in the combustion chamber so that the exhaust gas from the combustion chamber (at 1448 °C) was used to drive a power cycle. It was predicted that the exergy efficiency of the hybrid system ranged from 42.4-26.4%, depending on the current of the fuel-cell unit (maximized at 1.1 A), which was 0.9-4.9% higher than the conventional system without the fuel-cell unit at 41.5%.

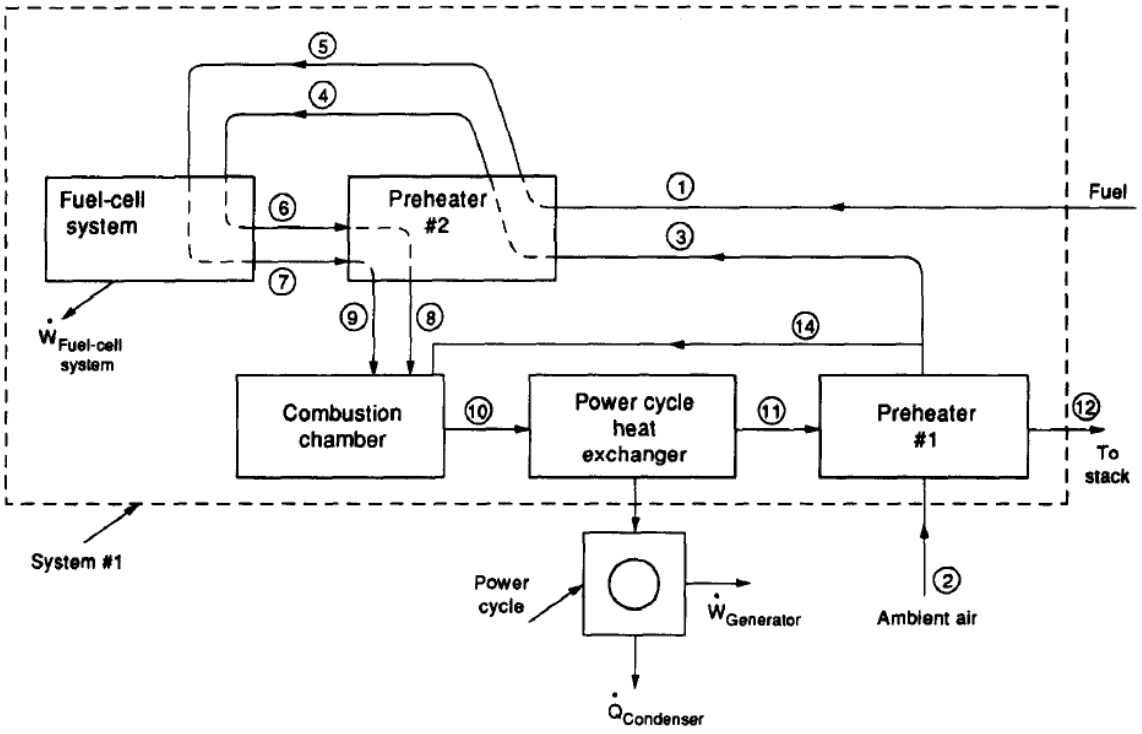

Fig. 3-14 Flow diagram of the fuel-cell-topped Rankine power cycle system [78]

[105] introduced a trigeneration plant based on a solid oxide fuel cell with an organic Rankine cycle. The flow diagram of the system is shown in Fig. 3-15. The cycle used the waste heat from a SOFC to drive an organic Rankine cycle using n-octane as working fluid for power generation, heating and cooling at the same time. The inlet flows of air, CH_4 and water to the SOFC were heated via a heat exchanger using the heat from a wood-burning boiler. The effects of inlet flow temperature and current density of the SOFC and inlet pressure of the turbine on the performances of the trigeneration system were studied. Under the design conditions, in which the inlet flow temperature of the SOFC was 757 °C, current density 0.8 A/cm^2 and turbine inlet pressure of 1,600 kPa, the electricity generation

efficiency was 30% and the trigeneration system efficiency (nominal efficiency) was 71%. The system could produce a total power of 520 kW, with SOFC contributing 460 kW.

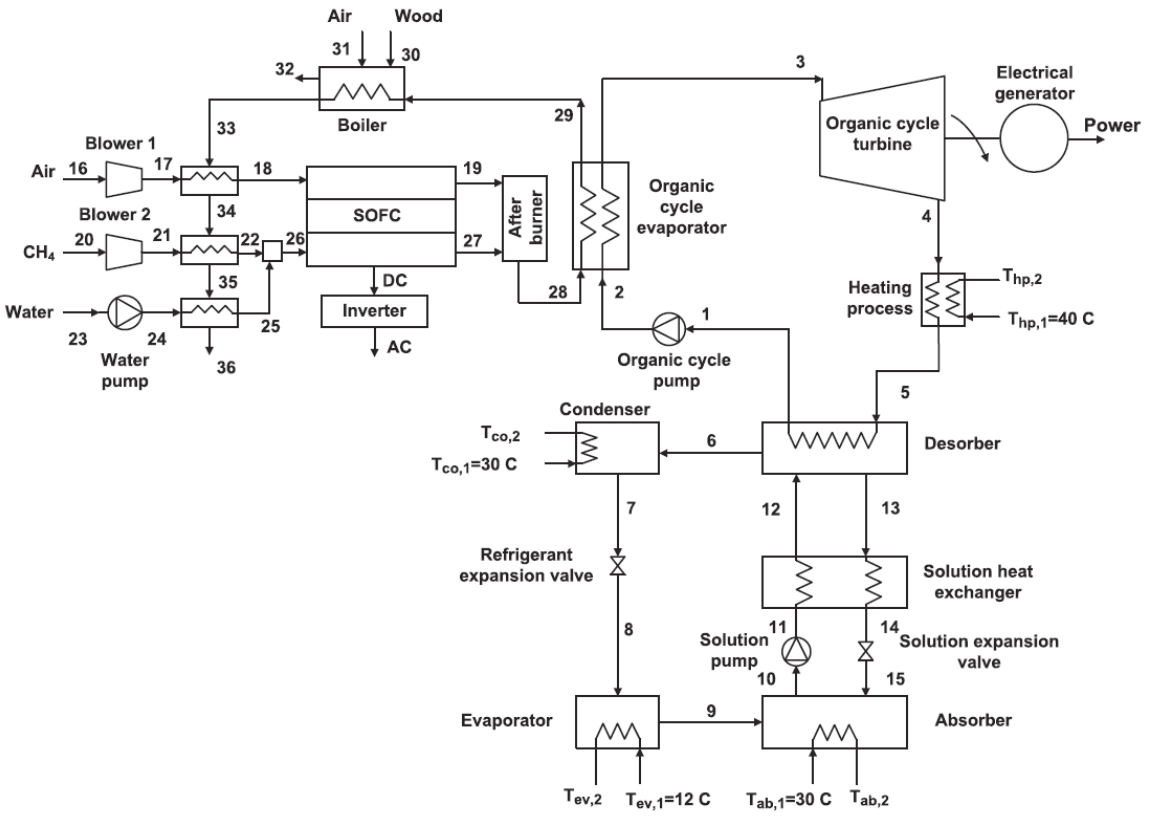

Fig. 3-15 Flow diagram of trigeneration plant with combined SOFC and organic Rankine cycle [105]

Another hybrid system involving SOFC was introduced in [106]. The flow diagram is shown in Fig. 3-16. It was a novel combined cycle integrating coal gasification, solid oxide fuel cell (SOFC), and chemical looping combustion (CLC), and it was the first analysis of hybrid system combining coal gasification, SOFC and CLC. Due to the integration of CLC,

CO_2 was inherently separated in the process of fuel conversion, so the proposed system had the ability to achieve almost 100% carbon capture performance. It was found that by using NiO as oxygen carrier in the CLC unit, at the baseline case with SOFC temperature of 900 °C, SOFC pressure of 15 bar, fuel utilization factor 0.85, fuel reactor temperature 900 °C and air reactor temperature 950 °C, the plant net power efficiency was predicted to reach 49.8% (based on coal LHV), including the energy penalties for coal gasification, oxygen production, and CO_2 compression. Also, a thorough exergy analysis of the system showed the largest exergy loss portion was the in the gasification process, followed by CO_2 compression and SOFC.

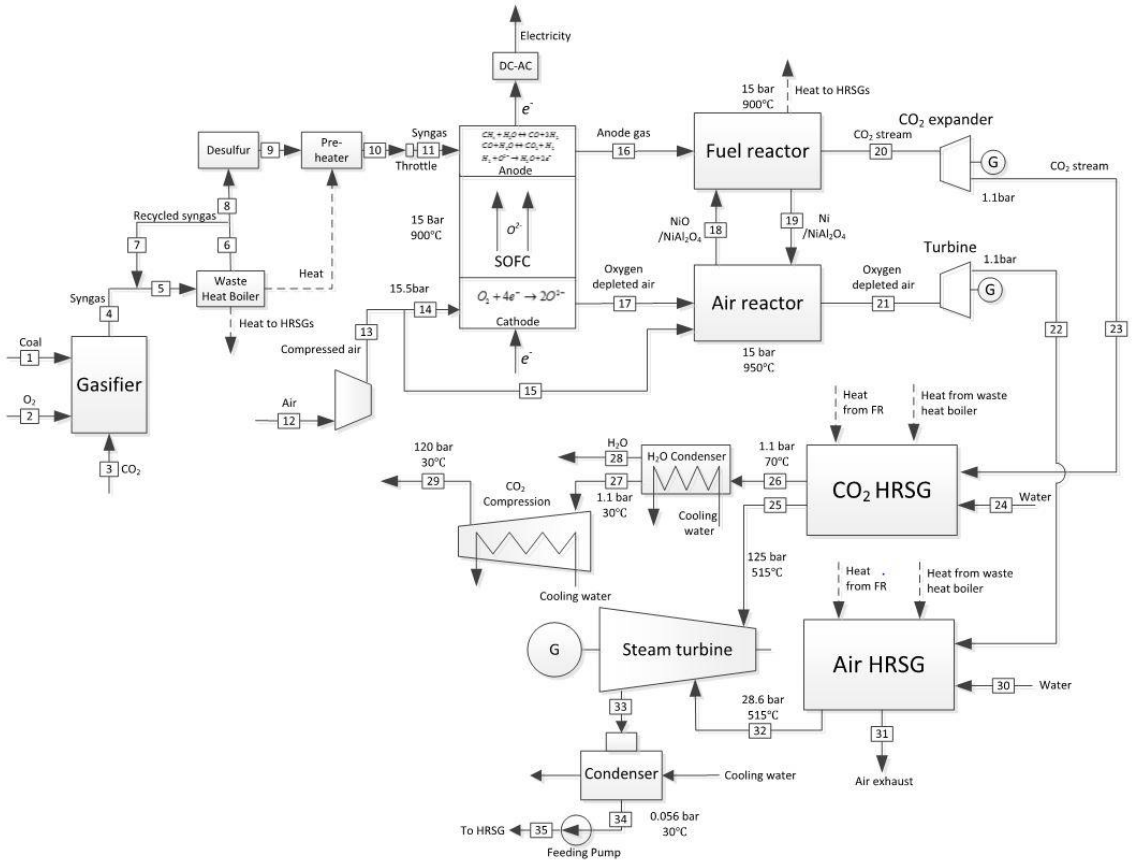

Fig. 3-16 Flow diagram of the power plant integrating coal gasification, SOFC, CLC and combined power cycle [106]

Besides the two SOFC hybrid systems introduced above, a recent and thorough review of hybrid SOFC-gas turbine (SOFC/GT) systems was done in [80]. The layout of SOFC/GT plant, according to the authors, depends on several design parameters, such as (1) operating temperature and pressure of the SOFC stack; (2) type of fuel and peculiarities of the fuel processing subsystem (steam reforming: internal/external, direct/indirect; partial oxidation, autothermal reforming, etc.); (3) production of steam required for the reforming process:

anode recirculation or heat recovery steam generator; (4) type of Brayton cycle: basic, intercooled and/or reheated. Other review papers on hybrid SOFC systems are also available, such as [81-83].

8) Unspecified heat source

There are also hybrid cycles that don't specify the type of heat sources. Y.M. Kim et al. [107] proposed and analyzed a novel power cycle using transcritical (or supercritical) CO_2 as the working fluid. The cycle used hot and cold tanks to store and release lower temperature heat. Heat was stored in the hot tank in the day and released from the hot tank to the cold tank at night, so the cycle could produce more work when the heat from higher temperature heat source is fixed. The higher temperature heat source could be nuclear, concentrated solar or fuel combustion. Also, a thermo-electric energy storage (TEES) system could be added by charging and discharging to improve the performance of the cycle. The flow diagrams Fig. 3-17 showed how it worked. The paper used nuclear power as the higher temperature heat source and hot/cold water tank as the lower temperature heat source as an example. The results showed that the efficiency was 40.3% without TEES and 40.9% with TEES, both of which were higher than two separate cycles working independently for the same heat source temperatures.

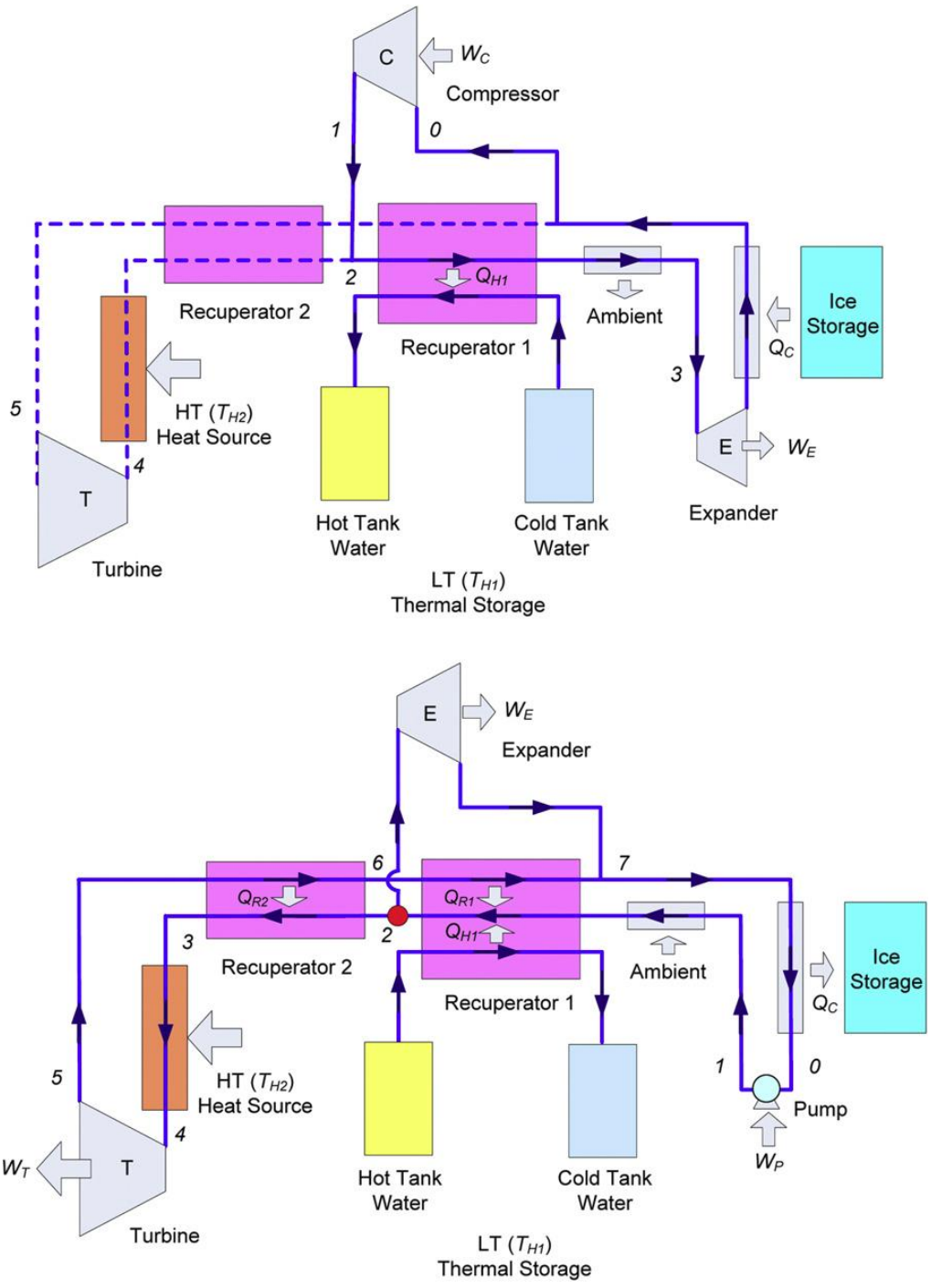

Fig. 3-17 Schematic of TEES LH T-CO2 cycles, charging mode (top) and discharging and generation mode (bottom) [107]

Also with unspecified heat source, [108] introduced a combined cycle power plant with integrated low temperature heat (LOTHECO) which utilized low temperature waste heat or solar heat to vaporize the water droplets in compressed air of gas turbine. The flow diagram showing the exergy flow of each stream is shown in Fig. 3-18. In an example, waste heat from a natural gas compressor station at 250 °C was used to vaporize the humid air steam to saturated steam at 169 °C. The designed power output of LOTHECO was 46.6 MW and efficiency of 57.6%, which was higher than CCGT (51.1%). The paper also compared it with simple gas turbine, steam injection gas turbine and humid air turbine, but didn't specify if they used the same operating parameters, such as turbine inlet temperature.

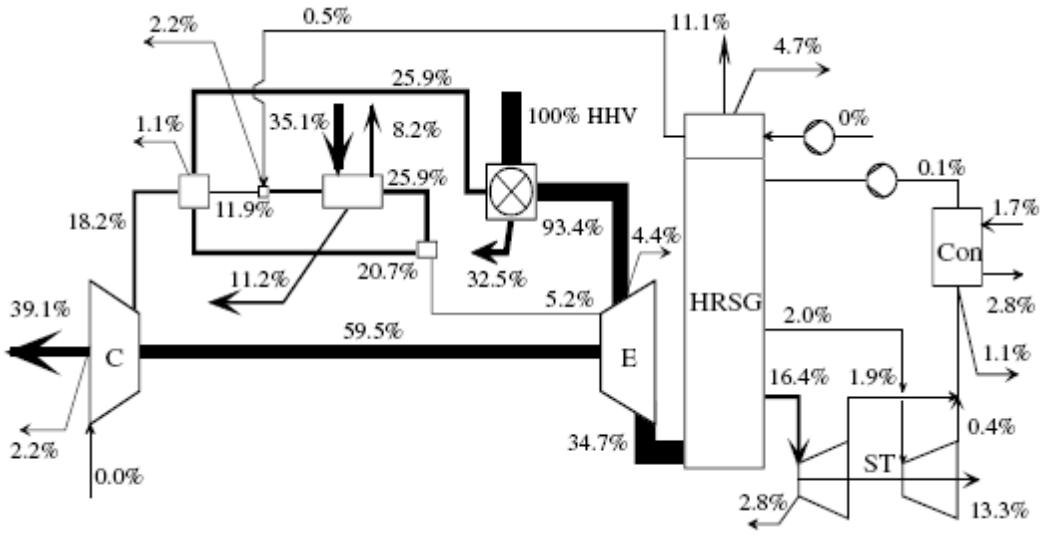

Fig. 3-18 Exergy flow diagram of the LOTHECO cycle [108]

[84] introduced a combined cooling, heating and power system with dual power generation units (D-CCHP) shown in Fig. 3-19. There were two power generation units (PGU) in this

system, one of which worked at base load while the other worked following the electric load. The waste heat generated by the two PGUs was used for cooling and heating in the building. Any supplemental thermal or electrical energy needs in the building were met by a boiler or purchased from the grid. The system was compared with a separate heating and power (SHP) configuration in nine geographic locations. It was found that the system was able to reduce the operation cost except for two locations, primary energy consumptions except for one location, and carbon dioxide emissions for two locations. It was thus concluded that the system had a potential to save money, energy and emissions.

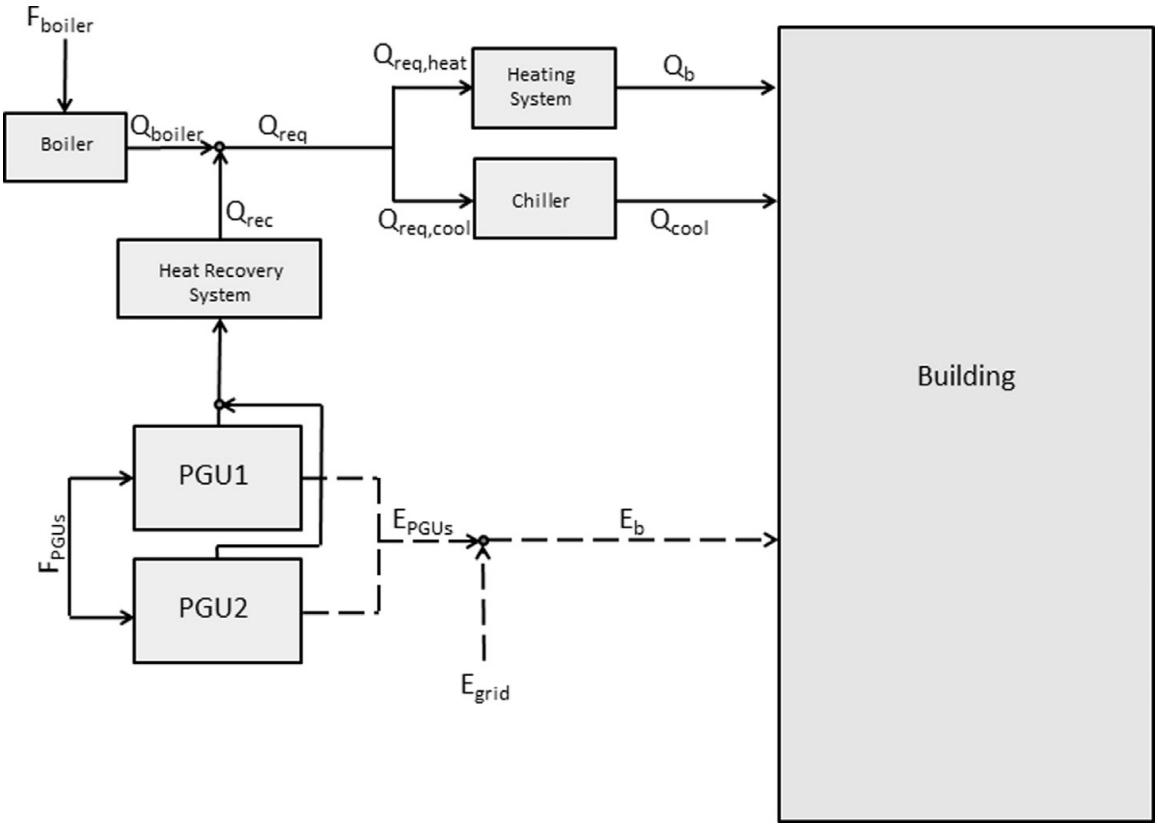

Fig. 3-19 Schematic of proposed D-CCHP configuration [84]

[109] introduced a hybrid power generation plant with the ability of CO_2 capture. The flow diagram is shown in Fig. 3-20. In the hybrid system, exhaust gas from gas turbine was used to capture CO_2 generated from pulverized coal (PC) power plant so that the extraction steam in the PC power plant could be saved for power generation. The details for carbon capture can be seen from Fig. 3-21. Three cases were studied for the system: (1) aeroderivative GT with HRSG+PC units with post-combustion CO_2 capture, (2) E-class GT with HRSG+PC units with post-combustion CO_2 capture and (3) F-class GT with HRSG and BP STG+PC units with post-combustion CO_2 capture and an additional back-pressure (BP) steam turbine generator (STG). The results showed that the efficiencies are lower than the reference PC power plant without CO_2 capture (the reason was not mentioned, but possibly because of additional pressure loss due to more complex configuration), but have higher power output and CO_2 capture ability. The third case was found to have the highest efficiency (36.6%, in terms of HHV) and power output (1.65 GW) of all three cases and was then compared with natural gas fired combined cycle (NGCC) system. It was found that while it captured 64.1% of the CO_2 produced from PC, the efficiency of hybrid system is much lower than that of NGCC (36.0% and 50.4%, respectively).

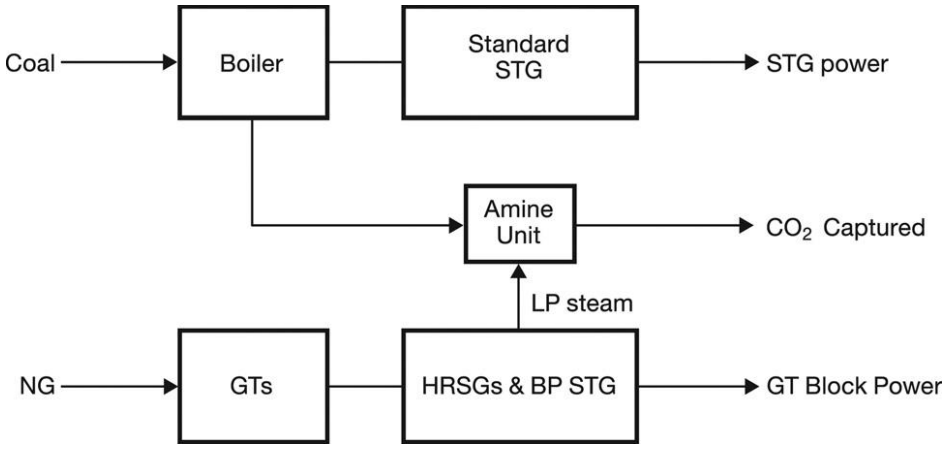

Fig. 3-20 Block flow diagram of hybrid power plant for CO_2 capture [109]

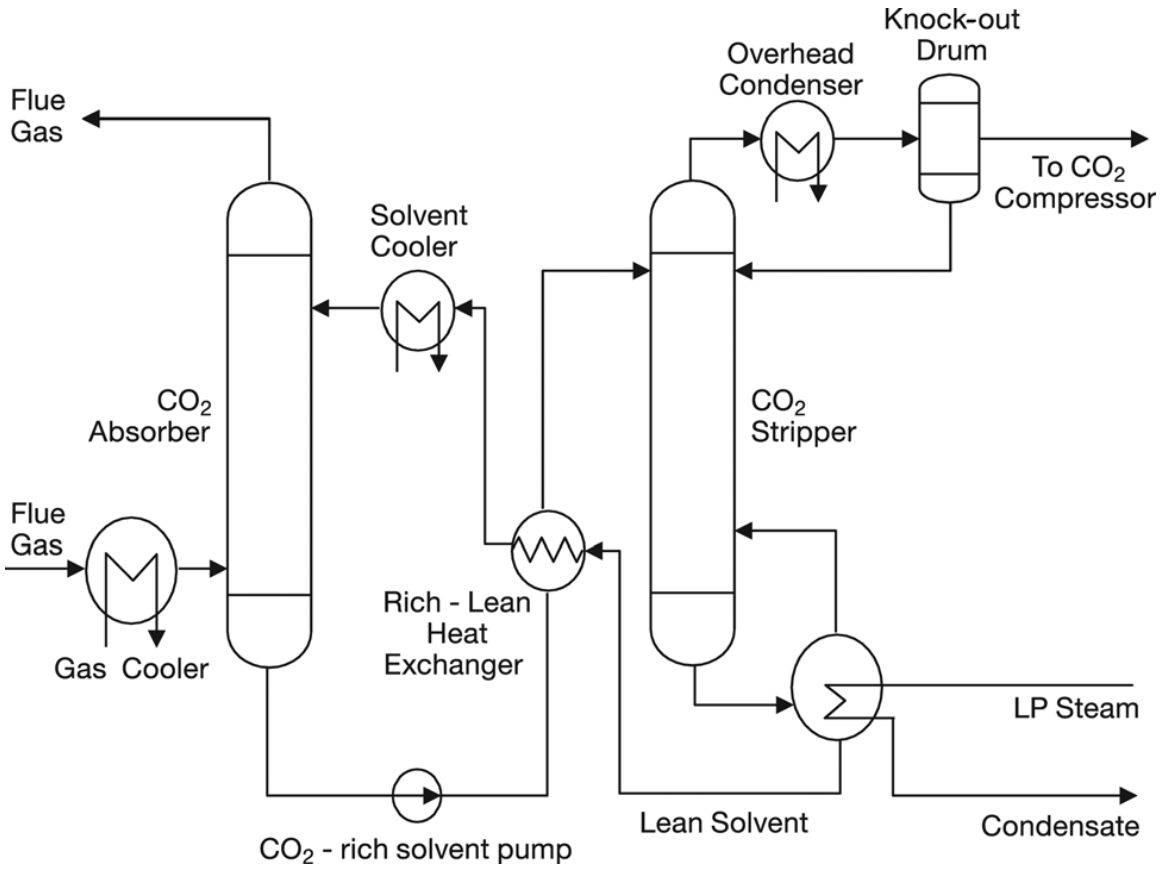

Fig. 3-21 Amine unit for CO_2 capture [109]

Table 3-4. A summary of past studies of hybrid power cycles without solar input

Descriptive name of system and reference	Low temperature heat source T,°C	Low temperature heat source type	Higher temperature heat source T,°C	Higher temperature heat source type	E/S*	Power, kW	Claimed power generation efficiency**	Efficiency improvement over single temperature system	Note***
Geothermal feedwater preheating in conventional power plants [85,86]	103	Geothermal	560 (Reheat)	Hard coal	S	520,000	8.06% (geothermal to electricity)	-	Neustad; LEC is $0.146/kWh (2002)
	147						13.34% (geothermal to electricity)		Soultz; LEC is $0.075/kWh (2002)
Dual-fluid-hybrid power plant co-powered by low-temperature geothermal water [87]	105	Geothermal	230	Biomass	S	9,700	28%	-	HYB cyclohexane
						-	23%	-	HYB water
						5,100	25%	14%	DFH R365mfc-water
						4,900	25%	14%	DFH R245mfc-water
						3,200	23%	12%	DFH R236mfc-water
Boiler integrated with 02Ref CCGT hybrid power plant [88]	575 (1st)121 (2nd)	Gas turbine Exhaust gas	510	Biomass	S	524,900	40.0%	4.5% (Biomass) -17.0% (CCGT)	Fully-fired; LEC is $0.191/ kWh (2010)
	1210	Natural gas					38.0%	3.5% (Biomass) -19.0% (CCGT)	Parallel-powered; LEC is $0.195/ kWh (2010)
Boiler integrated with 01Ref CCGT	575 (1st)121 (2nd)	Gas turbine exhaust gas	510	Biomass	S	861,600	41.0%	5.5% (Biomass) -16.1% (CCGT)	Fully-fired; LEC is $0.135/ kWh (2010)

hybrid power plant [88]	1267	Natural gas					37.9%	2.4% (Biomass) -19.2% (CCGT)	Parallel-powered; LEC is $0.140/ kWh (2010)
Nuclear power plant with fossil-fuel superheat [89]	269	Nuclear	540	oil	E&S	275	34.1%	5.7% (compared with nuclear only)	LEC is $0.026/ kWh (i=6.5%) and $0.030/ kWh (i=8.5%) (1997)
Novel hybrid Combined-Nuclear Power Plant (HCNPP) [90,91]	273.4	Nuclear	505.6 (1st) 343.4 (2nd)	Gas turbine exhaust gas	S	1,840,000	44%	11% (compared with nuclear only)	Total exergy destruction is 2281 MW
			1,087.0	Natural gas					
Hybrid fossil-PWR (Pressurized Water Reactor) plants [92]	321	Nuclear	480	Natural gas	S	1,000,000	46.24%	7.74%	Exergetic maximized; LEC $34.31/MWh (2010)
							44.16%	6.56%	LEC minimized; LEC $34.31/MWh (2010)
			490	Coal			39.72%	1.22%	Exergetic optimized; LEC $34.95/MWh (2010)
							38.46%	0.86%	Exergetic minimized; LEC $33.69/MWh (2010)
Nuclear Air-Brayton Combined Cycle (NACC) [93]	670	Nuclear	1,065	Natural gas	S	242,000	-	-	Hydrogen or stored heat could also be used instead of natural gas

Mobile hybrid (nuclear/oil-fired) gas turbine cogeneration power plant [94]	800	Nuclear	1,000	Fuel oil	S	5,000-6,000	32% (nuclear mode)-40% (fuel mode) 82-87% (nominal)	-	Also provide heat at 8 MW
Nuclear-assisted NGCC (natural-gas combined-cycle) [95]	900	Nuclear	1,400	Natural gas	S	382,000	59.1%	14.1% (compared with nuclear only) -0.8% (compared with NGCC)	LEC is $0.0644±0.0093/kWh (2007); CO_2 emission reduced by 46.3% compared with NGCC
Heavy Duty (HD) Diesel engine equipped with a bottoming Rankine cycle as a waste heat recovery system (classical) [96]	85	Cooling water	-	Diesel	E&S	342	41.30%	3.74%	All the waste heat sources
	127	Intercooler				370	44.69%	7.13%	Relatively high (low) temperature heat sources for top (bottom) Rankine cycle
	172	Aftercooler							
	330	Engine Exhaust gas				357	43.12%	5.56%	Waste heats from cooling water and intercooling not used
	509	Exhaust Gas Recirculation (EGR) cooler							
Heavy Duty (HD) Diesel engine equipped with a bottoming	85	Cooling water	-	Diesel	E&S	331	39.98%	2.42%	Without LP turbine with MP EGR
	127	Intercooler				335	40.46%	2.90%	Without LP turbine, with LP EGR
	172	Aftercooler							

Rankine cycle as a waste heat recovery system (innovative) [97]	330 509	Engine Exhaust gas Exhaust Gas Recirculation (EGR) cooler				290	35.02%	-2.54%	Without LP turbine, with LP EGR and high temperature
Combined thermodynamic cycle used for waste heat recovery of internal combustion engine [98]	135 175	Cooling water lubricant	500	Vehicle engine exhaust gas	S	347.8 (kJ/kg) 261.52 (kJ/kg)	20.83% (excluding engine) 16.51% (excluding engine)	-	Working fluid is cyclopentane Working fluid is R113
Organic Rankine cycle system utilizing exhaust gas of a marine diesel engine without pre-heater [99]	180	Diesel engine exhaust gases	-	Diesel	S	81.79 81.68 81.26 78.95	9.61% (excluding engine) 6.46% (excluding engine) 9.5% (excluding engine) 6.42% (excluding engine)	-	R1234ze R245fa R600 R600a
Organic Rankine cycle system utilizing exhaust gas of a marine diesel engine	180	Diesel engine exhaust gases	-	Diesel	S	89.72 87.05	10.51% (excluding engine) 10.08% (excluding engine)	-	R1234ze R245fa

with pre-heater [99]					87.32	10.21% (excluding engine)		R600
					88.76	10.37% (excluding engine)		R600a
A natural gas expansion plant integrated with an IC engine and an organic Rankine cycle [100]	405	Exhaust gas from engine	-	Pressurized natural gas	S	4,482	52.57%	2.97	Exhaust gas from ICE is used to drive ORC and two gas expanders to generate power; System CO_2 emission is 0.2559 kg/kWh
A medium-temperature waste-heat recovery system based on the organic Rankine cycle (ORC) [101]	470	Diesel engine exhaust gases	-	Diesel	S	273	15% (excluding engine)	-	Working fluid is R123
Internal Combustion Engine bottoming with Organic Rankine Cycles [102]	470	Diesel engine exhaust gases	-	Natural gas	S	3277.3	46.6%	4.8%	Simple cycle
						3314.0	47.1%	5.3%	Simple cycle with reheat
						3320.6	47.1%	5.3%	Regenerated cycle
	827	Natural gas	-	Diesel	S	1,333.9 (kJ/kg)	74.7%	-	Diesel engine $CR = 20$

A Combined Diesel-Engine Gas-Turbine System for Distributed Power Generation [103]						1,553.9 (kJ/kg)	77.3%		Diesel engine $CR = 30$
Hydrogen internal combustion engine	616					6.6	27.2%	2.9%	Engine speed is 1,500 rpm
combined with open steam Rankine cycle recovering water and waste heat [104]	769	HICE exhaust gas	-	Hydrogen	S	22.1	33.6%	3.7%	Engine speed is 4,500 rpm
Fuel-cell-topped Rankine power cycle system [78,79]	1020	Fuel	1448	Fuel	S	361,100	42.4%-46.4% (exergy efficiency)	0.9%-4.9%	Exergy efficiency maximized at fuel-cell current 1.1 A
Trigeneration plant based on solid oxide fuel cell and organic Rankine cycle [105]	727	Wood	-	Natural gas	S	520	30% (electricity) 71% (nominal)	-6%	Current density from SOFC is 0.8 A/cm^2
Novel combined	900	Coal	900	Anode gas	S	13,346	49.8%	>0	Nearly 100% carbon capture

cycle integrating coal gasification, solid oxide fuel cell, and chemical looping combustion [106]			950	Oxygen depleted air					
Transcritical CO_2 cycles using both low- and high-temperature heat sources [107]	122.2	Lower temperature thermal storage	600	Higher temperature heat source	S	150.4 (kJ/kg)	40.3%	5.2%	HTF is transcritical CO
	122					186.8 (kJ/kg)	40.9%	6.9%	With thermo-electric energy storage (TEES)
Combined cycle power plant with integrated low temperature heat (LOTHECO) [108]	250	Waste heat from industrial processes	-	Natural gas	S	46,600	57.6%	6.5%	LEC is $0.06-0.22/kWh depended on full load operation hours
Hybrid Power Generation Plant for CO_2 Capture [109]	-	Gas turbine exhaust gas	580	Coal	S	1,489,300	36.4%	-1.1%	Aeroderivative GT
						1,494,200	35.7%	-1.8%	E-class GT
			-	Natural gas		1,646,700	36.6%	-0.9%	F-class GT with Steam turbine

* E: Experiment, S: Simulation.

** Efficiency is defined as net power output divided by total energy input (Eq. (2.2)), unless indicated otherwise.

*** LEC (levelized electricity cost) was converted to dollar value, based on the currency of the first day in the year published.

3.2. Conclusions of the review of thermal hybrid power cycles

As can be easily seen from the tables, solar heat was used in thermal hybrid power generation systems for a wide range of temperatures (100-680 °C). In the lowest part of the range (100-157 °C), solar flat-plate and evacuated tube collector were used; in the mid-range temperature (180-550 °C), solar parabolic trough concentrating collector is most widely used, but Fresnel concentrating collectors are also usable; in the high-temperature range (>565 °C), solar towers were used. Although point-focus concentrators could also produce thermal temperature at 1,371 °C with the same principle as for solar tower [110] and can be used to drive Stirling engine or gas turbine system, it was not found in the past publications about hybrid power generation systems.

Most of the hybrid multi-temperature systems are reported to have a higher efficiency than those using only one heat source (lower temperature heat source). This is mostly because the use of fossil fuel combustion as a heat source raises the top temperature of the original cycle, and enables cascading use of input heats to reduce exergy losses. For example, in the ‘SSPRE’ cycle, the top temperature has been raised from 100 °C to 600 °C by burning fossil fuel, resulting in an efficiency increase of 80%. In solar hybrid gas turbine system, however, the efficiency was found to usually slightly decrease, by several percentage points due to pressure loss in additional equipment, in comparison with non-hybrid gas turbine systems. This small loss should be contrasted with the ability of such hybrid cycles to use solar energy, with the associated benefits.

The relation between the system energy efficiency at design point and the top temperature of the cycle for all the investigated system discussed in this section is shown in Fig. 3-22. This figure doesn't contain the system when energy efficiency at design point or top temperature of the cycle is unknown. The efficiencies of the same systems but with different parameters (such as geographic locations, working fluids, ambient temperatures) will be averaged and regarded as one system. It is clear shown in the figure that energy efficiency generally increases with the top temperature of cycle. The result confirmed the fact that hybrid cycles with additional higher temperature heat sources will generally have a higher energy efficiency than the corresponding single heat source cycles without it, due to higher top temperature of the hybrid system.

For the three solar-hybrid power system categories (vapor, gas and combined), the combined cycle has the highest efficiency (43-52%). The efficiencies of most of hybrid steam cycles are 10-40%, and of hybrid gas cycles are 20-40%. So the solar hybrid combined cycle is the most efficiency category.

The most efficient configuration among vapor cycle is Solar-aided three-stage regenerative Rankine system with solar heat replacing the low-pressure feed water heater [28], which was reported to have an efficiency of 46.98%. The second most efficient is 'Thermal power stations with solar energy' [32] that was reported to have an efficiency of 45.2% The 'Novel hybrid solar heating, cooling and power generation system' [22] was reported to have a nominal efficiency of 58.0%, but this definition of this efficiency includes the

produced heating, cooling and hot water energy as the “useful” power output, while the others use only power generation as the “useful” power output.

The most efficient configurations among hybrid gas cycles are ‘Solar hybrid Steam Injected Gas Turbine cycle (STIG) [44] which was reported to have an efficiency of 41.4%, and ‘Solarized gas turbine prototype plant: Heron H1 unit located in Seville’ [49] which was reported to have an efficiency of 40.4%. These are the only two hybrid gas cycles that were reported to have efficiency above 40%.

The most efficient configuration of hybrid combined gas cycles is the ‘Integrated solar combined cycle system (ISCCS)’ [60] which was reported to have an energy efficiency of 68.6% without thermal storage and 68.1% with thermal storage. According to the reference, the reason why the efficiency with thermal storage was lower than that without it is that adding storage required larger solar field to charge the storage, which led to higher parasitic power. Although adding thermal storage reduced energy efficiency, it, however, led to higher solar share. The second most efficient one is “First Integrated Solar Combined Cycle System in Algeria” [66] which was reported to have an efficiency of 67%.

The most efficient configuration of non-solar hybrid cycles reviewed here is the ‘Nuclear-assisted NGCC (natural-gas combined-cycle)’ [95] which was reported to have an efficiency of 59.1%. Some systems ([94,103,105]) were reported to have nominal efficiencies of over 70%, but their energy efficiency definition includes both power and heat as useful outputs, not electricity generation efficiency.

The best system for solar-aided hybrid system considering all aspects including efficiency, solar share and cost appears to be the ‘‘Integrated solar combined cycle system (ISCCS)’ [60], with an overall efficiency of over 68% and solar share of about 17%. The levelized cost of electricity was stated to be $0.049-0.053/kWh (in year 2004 dollars), one of the lowest ones.

The best system for non-solar-aided hybrid system considering all aspects including efficiency of the system, power output, efficiency improvement over single heat source system and cost seems to be the ‘Nuclear-assisted NGCC’ (natural-gas combined-cycle) [95], with an efficiency of 59.1%, high capacity (382 MW), large efficiency improvement due to the hybridization (14.1%) over the nuclear-power-only plant, and a low cost of electricity ($0.0644±0.0093/kWh in year 2007 dollars). The second promising one is ‘Combined cycle power plant with integrated low temperature heat (LOTHECO)’ [108] having an efficiency of 57.6%.

Hybrid power cycles have the ability of preserving fuel usage and saving carbon emissions. For example, a solar hybrid gas turbine electric power system (Mercury 50) [47] was reported to have the ability to save about 70 kg CO_2/MWh with an annual solar share of 10%, and a Nuclear-assisted NGCC (natural-gas combined-cycle) [95] was reported to have the ability to reduce 46.3% of CO_2 emissions compared with a fuel-only NGCC, with 59.1% of total energy input supplied by nuclear. Also, some hybrid systems were able to capture nearly all carbon emissions, such as the novel combined cycle integrating coal

gasification, solid oxide fuel cell, and chemical looping combustion [106] and a CO_2-capturing hybrid power-generation system [41-43].

Therefore, beyond the efficiency, it is noteworthy that use of solar, nuclear and geothermal in the hybrid system has the important advantage of lower emissions and preservation of depletable energy resources.

According to EIA [111], the levelized electricity cost (LEC) of all of the power generation methods using fossil fuel is between $72.6/MWh for advanced combined cycle burning natural gas and $144.4/MWh for advanced coal power plant with carbon capture and storage (CCS). The economic analyses for hybrid power generation systems have shown that the LEC of some of them are not very high relative to conventional and some may even be competitive already. For example, for solar aided biomass power generation systems with parabolic trough field [23], the predicted LEC was $80/MWh, and for a hybrid solar gas-turbine power plant (HSGTPP) [53], the LEC was predicted to be $104/MWh. The LEC of most solar hybrid systems, however, is still found to be high at least two times higher than that of advanced combined cycle, so there is still much room for cost reduction as the cost of solar collector goes down with technology advance suggested in [112].

Most of the studies done in this area are restricted to simulations and not experiments, and thus the results may not adequately reflect reality.

There are also some types of hybrid systems that could be used for water desalination, hydrogen production or heating/cooling alongside with power.

Despite the listed advantages of hybrid power systems, a decision to use them must also take into account a number of important issues in which hybrid systems will also have disadvantages, the main ones including more complex controls, higher embodied energy, and life-cycle issues, such as the disposal of additional equipment. Moreover, hybrid power systems that use renewable energy of intermittent and unsteady nature may require energy storage and typically conventionally fueled backup systems or power, and tend to lower the performance and increase the price in any case. All of these issues are thermodynamically sensible and must be considered carefully in the analysis and practical feasibility assessment of hybrid power plants, which generally are predicted to deliver significant improvements in efficiency at a reasonable cost and show good promise.

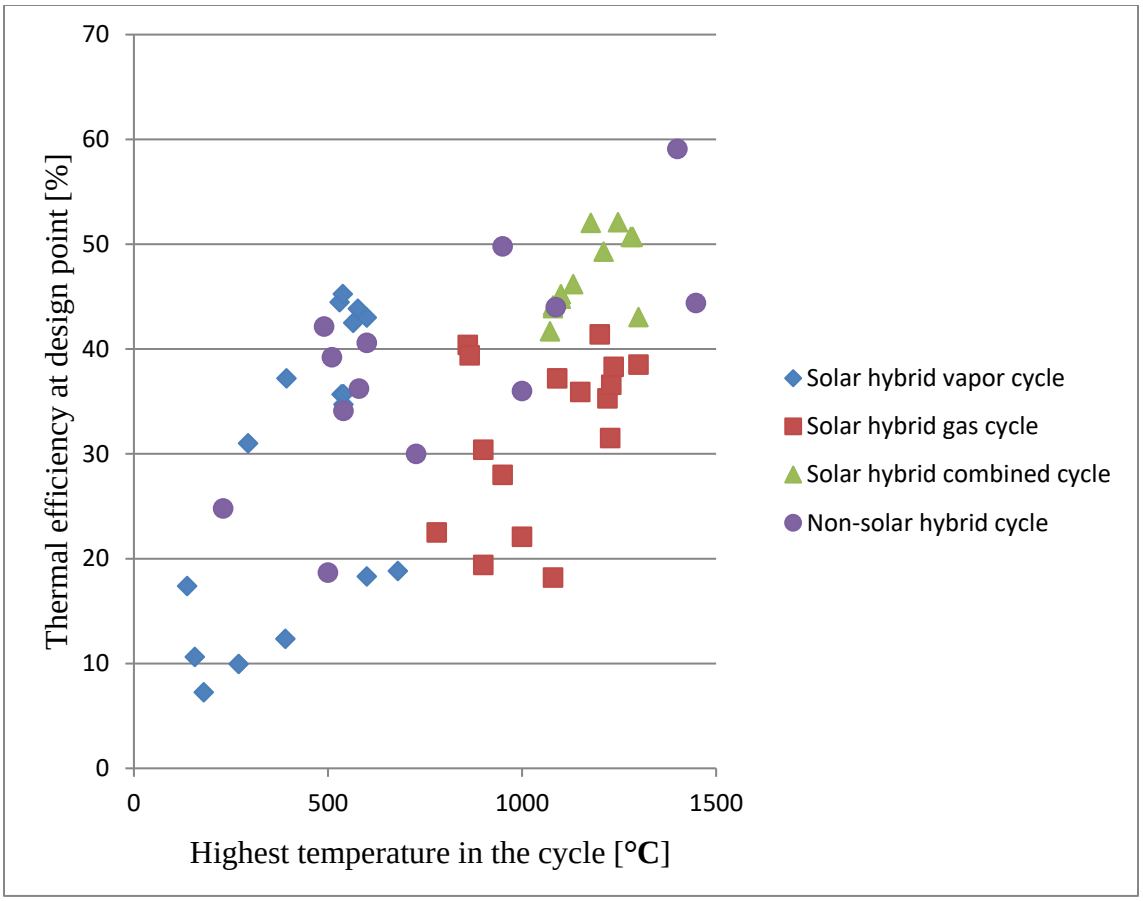

Fig. 3-22 Hybrid power plant energy efficiency at design point as a function of the highest temperature of working fluid in the cycle

References for Chapter 3

[1] Koai K., Lior N., Yeh H., Performance analysis of a solar-powered/fuel-assisted Rankine cycle with a novel 30hp turbine. Sol Energy 1984;(32)6:753-764.

[2] Lior N., Koai K., Solar-Powered/Fuel-Assisted Rankine Cycle Power and Cooling System: Simulation Method and Seasonal Performance. J Sol Energ-T ASME 1984;106:142-152.

[3] Lior N., Koai K., Solar-Powered/Fuel-Assisted Rankine Cycle Power and Cooling System: Sensitivity Analysis. J Sol Energ-T ASME 1984;106:447-456.

[4] Lior N., Solar energy and the steam Rankine cycle for driving and assisting heat pumps in heating and cooling modes. Energ Convers 1977;(16)3:111-123.

[5] Sherburne D., Lior N., Evaluation of minimum fuel consumption control strategies in the solar-powered fuel-assisted hybrid Rankine cycle. Proceedings ASES Ann. Meeting 1986:300-303.

[6] Kolb J., Evaluation of Power Production from the Solar Electric Generating Systems at Kramer Junction:1988 to 1993. Proceedings of the Solar Engineering 1995; ASME Press New York:1:499-504.

[7] Cohen G.H., Kearny O., Improved Parabolic Trough Solar Electric Systems Based on the Segs Experience. Proceedings of the American Solar Energy Society Conference 1994:147-150.

[8] Jensen C., Price H., Kearney D., The SEGS Power Plants:1988 Performance. 1989 ASME International Solar Energy Conference San Diego CA.

[9] Mills D., Advances in solar thermal electricity technology, Sol Energy 2004;76:19-31.

[10] Tian Y., Zhao C.Y., A review of solar collectors and thermal energy storage in solar thermal applications, Appl Energ 2013;104:538-553.

[11] Kalogirou S.A., Solar thermal collectors and applications, Prog Energ Combust 2004;30:231-295.

[12] Avila-Marin A.L., Fernandez-Reche J., Tellez F.M., Evaluation of the potential of central receiver solar power plants: Configuration, optimization and trends, Appl Energ 2013;112:274-288.

[13] Fernandez-Garcıa A., Zarza E., Valenzuela L., Perez M., Parabolic-trough solar collectors and their applications, Renew Sust Energ Rev 2010;14:1695-1721.

[14] Kuravi S., Trahan J., Goswami D.Y., Rahman M.M., Stefanakos E.K., Thermal energy storage technologies and systems for concentrating solar power plants, Prog Energ Combust 2013;39:285-319.

[15] Peterseim J.H., White S., Tadros A., Hellwig U., Concentrating solar power hybrid plants-Enabling cost effective synergies, Renew Energ 2014;67:178-185.

[16] Lentz A., Almanza R., Solar-geothermal hybrid system, Appl Therm Eng 2006;26:1537-1544.

[17] Tempesti D., Manfrida G., Fiaschi D., Thermodynamic analysis of two micro CHP systems operating with geothermal and solar energy, Appl Energ 2012;97:609-617.

[18] Ruzzenenti F., Bravi M., Tempesti D., Salvatici E., Manfrida G., Basosi R., Evaluation of the environmental sustainability of a micro CHP system fueled by low-temperature geothermal and solar energy, Energ Convers Manage 2014;78:611-616.

[19] Goswami D.Y., Xu F., Analysis of a New Thermodynamic Cycle for Combined Power and Cooling Using Low and Mid Temperature Solar Collectors, J Sol Energ-T ASME 1999;121:91-97.

[20] Astolfi M., Xodo L., Romano M., Macchi E., Technical and economical analysis of a solar-geothermal hybrid plant based on an Organic Rankine Cycle. Geothermics 2011;40:58-68.

[21] Zhou C., Doroodchi E., Moghtaderi B., An in-depth assessment of hybrid solar-geothermal power generation, Energ Convers Manage 2013;74:88-101.

[22] Zhai H., Dai Y.J., Wu J.Y., Wang R.Z., Energy and exergy analyses on a novel hybrid solar heating, cooling and power generation system for remote areas. Appl Energ 2009;86:1395-1404.

[23] Hou H., Yang, Y., Hu E., Song J., Dong C., Mao J., Evaluation of solar aided biomass power generation systems with parabolic trough field. Sci China Technol Sc 2011;54(6):1455-1461.

[24] Suresh M.V.J.J., Reddy K.S., Kolar A.K., 4-E (Energy, Exergy, Environment, and Economic) analysis of solar thermal aided coal-fired power plants, Energy Sustain Dev 2010;14:267-279.

[25] Yang Y., Yan Q., Zhai R., Kouzani A., Hu E., An efficient way to use medium-or-low temperature solar heat for power generation-integration into conventional power plant, Appl Therm Eng 2011;31:157-162.

[26] Nikni I., Yaghoubi M., Transient simulation for developing a combined solar thermal power plant, Appl Therm Eng 2012;37:196-207.

[27] Nikni I., Yaghoubi M., Transient analysis of integrated Shiraz hybrid solar thermal power plant, Renew Energ 2013;49:216-221.

[28] Ying Y., Hu E.J., Thermodynamic advantages of using solar energy in the regenerative Rankine power plant, Appl Therm Eng 1999;19:1173-1180.

[29] Hu E., Yang Y., Nishimura A., Yilmaz F., Kouzani A., Solar thermal aided power generation, Appl Energ 2010;87:2881-2885.

[30] Odeh S., Behnia M., Morrison G., Performance evaluation of solar thermal electric generation systems. Energ Convers Manage 2003;44(15):2425-2443.

[31] Popov D., An option for solar thermal repowering of fossil fuel fired power plants. Sol Energy 2011;85:344-349.

[32] Pai B.R., Augmentation of thermal power stations with solar energy, Sadhana, 1991;16(1):59-74.

[33] Wu J., Hou H., Yang Y., Hu E., Annual performance of a solar aided coal-fired power generation system (SACPG) with various solar field areas and thermal energy storage capacity, Appl Energ 2015;157:123-133.

[34] Bakos G.C., Tsechelidou Ch., Solar aided power generation of a 300 MW lignite fired power plant combined with line-focus parabolic trough collectors field, Renew Energ 2013;60:540-547.

[35] Servert J., San Miguel G., Lopez D., Hybrid solar - Biomass plants for power generation; technical and economic assessment. Global Nest J 2011;13(3):266-276.

[36] Giuliano S., Buck R., Eguiguren S., Analysis of Solar-Thermal Power Plants With Thermal Energy Storage and Solar-Hybrid Operation Strategy. J Sol Energy 2011;133:031007.

[37] Larraın T., Escobar R., Vergara J., Performance model to assist solar thermal power plant siting in northern Chile based on backup fuel consumption. Renew Energ 2010;35:1632-1643.

[38] Coelho B., Schwarzbozl P., Oliveira A. Mendes A., Biomass and central receiver system (CRS) hybridization: Volumetric air CRS and integration of a biomass waste direct burning boiler on steam cycle. Sol Energy 2012;86:2912-2922.

[39]Nathan G.J., Battye D.L., Ashman P.J., Economic evaluation of a novel fuel-saver hybrid combining a solar receiver with a combustor for a solar power tower, Appl Energ 2014;113:1235-1243.

[40] Müller S., Brown A., Ölz S., Renewable Energy-Policy Considerations for Deploying Renewables, IEA Publications, Paris, 2011.

[41] Pak P. S., A CO_2-capturing hybrid power-generation system with highly efficient use of solar thermal energy. Energy 1997;22(2/3):295-299.

[42] Pak P. S., Hatikawa T., Suzuki Y., A hybrid power generation system utilizing solar thermal energy with CO2 recovery based on oxygen combustion method. Energ Convers Manage 1995;36(6-9):823-826.

[43] Pak P. S., Hatikawa T., Suzuki Y., Characteristics and Economic Evaluation of a CO2-Capturing Solar Thermal Hybrid Power Generation System with Heat Storage, Electr Eng JPN, 1999;126(4):21-29.

[44] Livshits M., Kribus A., Solar hybrid steam injection gas turbine (STIG) cycle. Sol Energy 2012;86:190-199.

[45] Gou C.H., Cai R.X., Hong H., A novel hybrid oxy-fuel power cycle utilizing solar thermal energy. Energy 2007;32:1707-1714.

[46] Bernardos E., López I., Rodríguez J., Abánades A., Assessing the potential of hybrid fossil-solar thermal plants for energy policy making: Brayton cycles, Energ Policy, 2013;62:99-106.

[47] European Communities, Solar hybrid gas turbine electric power system (Final Publishable Report). 2005;31.

[48] Buck R., Friedmann S., Solar-Assisted Small Solar Tower Trigeneration Systems. J Sol Energy 2007;129:349-354.

[49] Schwarzbozl P., Buck R., Sugarmen C., Ring A., Crespo M., Altwegg P., Enrile J., Solar gas turbine systems: Design, cost and perspectives. Sol Energy 2006;80:1231-1240.

[50] Fisher U., Sugarmen C., Ring A., Sinai J., Gas Turbine ‘‘Solarization’’-Modifications for Solar/Fuel Hybrid Operation. J Sol Energ-T ASME 2004;126(3):872-878.

[51] Garcia P., Ferriere A., Flamant G., Costerg P., Soler R., Gagnepain B., Solar Field Efficiency and Electricity Generation Estimations for a Hybrid Solar Gas Turbine Project in France. J Sol Energ 2008;130:014502.

[52] Aichmayer L., Spelling J., Laumert B., Fransson T., Micro Gas-Turbine Design for Small-Scale Hybrid Solar Power Plants. J Eng Gas Turb Power 2013;135:113001.

[53] Spelling J., Laumert B., Fransson T., Optimal Gas-Turbine Design for Hybrid Solar Power Plant. J Eng Gas Turb Power 2012;134:092301.

[54] Sandoz R., Spelling J., Laumert B., Fransson T., Air-Based Bottoming-Cycles for Water-Free Hybrid Solar Gas-Turbine Power Plants. J Eng Gas Turb Power 2013;135:101701.

[55] Heller P., Pfander M., Denk T., Tellez F., Valverde A., Fernandez J., Ring A., Test and evaluation of a solar powered gas turbine system. Sol Energy 2006;80:1225-1230.

[56] Barigozzi G., Bonetti G., Franchini G., Perdichizzi A., Ravelli S., Thermal performance prediction of a solar hybrid gas turbine. Sol Energy 2012;86:2116-2127.

[57] ISCC Hassi R'mel, NREL. http://www.nrel.gov/csp/solarpaces/project_detail.cfm/projectID=44 <Nov. 1, 2015>

[58] Reddy V.S., Kaushik S.C., Tyagi S.K., Exergetic analysis of solar concentrator aided natural gas fired combined cycle power plant. Renew Energ 2012;39:114-125.

[59] Gunasekaran S, Mancini N.D., El-Khaja R., Sheu E.J., Mitsos A., Solar-thermal hybridization of advanced zero emissions power cycle. Energy 2014;65:152-165.

[60] Dersch J., Geyer M., Herrmann U., Jones S., Kelly B., Kistner R., Ortmanns W., Pitz-Paal R., Price H., Trough integration into power plants—a study on the performance and economy of integrated solar combined cycle systems. Energy 2004;29:947-959.

[61] Kane M., Favrat D., Ziegler K., Allani Y., Thermoeconomic Analysis of Advanced Solar-Fossil Combined Power Plants. Int J Appl Therm 2000;3(4):191-198.

[62] Bakos G.C., Parsa D., Technoeconomic assessment of an integrated solar combined cycle power plant in Greece using line-focus parabolic trough collectors. Renew Energ 2013;60:598-603.

[63] Nezammahalleh H., Farhadi F., Tanhaemami M., Conceptual design and techno-economic assessment of integrated solar combined cycle system with DSG technology. Sol Energy 2010;84:1696-1705.

[64] Baghernejad A., Yaghoubi M., Exergy analysis of an integrated solar combined cycle system. Renew Energ 2010;35:2157-2164.

[65] Hosseini R., Soltani M., Valizadeh G., Technical and economic assessment of the integrated solar combined cycle power plants in Iran. Renew Energ 2005;30:1541-1555.

[66] Behar O., Kellaf A., Mohamedi K., Belhamel M., Instantaneous performance of the first Integrated Solar Combined Cycle System in Algeria. Energ Proced 2011;6:185-193.

[67] Turchi C.S., Ma Z., Co-located gas turbine/solar thermal hybrid designs for power production. Renew Energ 2014;64:172-179.

[68] Silva M., Blanco M., Ruiz V., Integration of solar thermal energy in a conventional power plant: The Colon solar project, J Phys IV France 1999;9(Pr3)189-194.

[69] Horn M., Fuhring H., Rheinlander J., Economic analysis of integrated solar combined cycle power plants A sample case: The economic feasibility of an ISCCS power plant in Egypt. Energy 2004:29:935-945.

[70] Montes M.J., Rovira A., Muñoz M., Martínez-Val J.M., Performance analysis of an Integrated Solar Combined Cycle using Direct Steam Generation in parabolic trough collectors. Appl Energ 2011;88:3228-3238.

[71] Montes M.J., Rovira A., Muñoz M., Martínez-Val J.M., Proposal of an integrated solar combined cycle system using direct steam generation technology. In: Proc of 15th int solar PACES symp on sol therm conc technol, Berlin, Germany; 2009.

[72] Buck R., Brauning T., Denk T., Pfander M., Schwarzbozl P., Tellez F., Solar-Hybrid Gas Turbine-based Power Tower Systems (REFOS). J Sol Energ 2002;124:2-9.

[73] Barigozzi G., Bonetti G., Franchini G., Perdichizzi A., Ravelli S., Solar Hybrid Combined Cycle Performance Prediction Influence of Gas Turbine Model and Spool Arrangements. J Eng Gas Turb Power 2012;134:121701.

[74] Kribus A., Zaibel R., Carey.D., Segal.A., Karni.J., A solar-driven combined cycle power plant. Sol Energy 1998;62(2):121-129.

[75] High Temperature Gas Cooled Reactor Fuels and Materials, INTERNATIONAL ATOMIC ENERGY AGENCY VIENNA, 2010, http://www-pub.iaea.org/MTCD/publications/PDF/TE_1645_CD/PDF/TECDOC_1645.pdf

[76] Forsberg C., Hybrid systems to address seasonal mismatches between electricity production and demand in nuclear renewable electrical grids. Energ Policy 2013;62:333-341.

[77] Sprouse C. III, Depcik C., Review of organic Rankine cycles for internal combustion engine exhaust waste heat recovery. Appl Therm Eng 2013;51:711-722.

[78] Dunbar W. R., Lior N., Gaggioli R., Combining fuel cells with fuel-fired power plants for improved exergy efficiency. Energy 1991;16(10)1259-1274.

[79] Dunbar W. R., Lior N., Gaggioli R., The effect of the fuel-cell unit size on the efficiency of a fuel-cell-topped Rankine Cycle. J Energ Resour-ASME 1993;115:105-107.

[80] Buonomano A., Calise F., d'Accadia M.D., Palombo A., Vicidomini M., Hybrid solid oxide fuel cells-gas turbine systems for combined heat and power: A review. Appl Energ 2015;156:32-85.

[81] Zabihian F., Fung A., A review on modeling of hybrid solid oxide fuel cell systems. Int J Eng 2009;3:85-119.

[82] McPhail S.J., Aarva A., Devianto H., Bove R., Moreno A., SOFC and MCFC: commonalities and opportunities for integrated research. Int J Hydrogen Energ 2011;36(16):10337-10345.

[83] Zhang X., Chan S.H., Li G., Ho H.K., Li J., Feng Z., A review of integration strategies for solid oxide fuel cells. J Power Sources 2010;195:685-702.

[84] Knizley A.A., Mago P.J., Smith A.D., Evaluation of the performance of combined cooling, heating, and power systems with dual power generation units. Energ Policy 2014;66:654-665.

[85] Bruhn M., Hybrid geothermal-fossil electricity generation from low enthalpy geothermal resources: geothermal feedwater preheating in conventional power plants. Energy 2002;27:329-346.

[86] Bruhn M., Erbas K., Huenges E., Efficient geothermal-fossil hybrid electricity generation: geothermal feedwater preheating in conventional power plants. Bulletin d'Hydrogdoiogie 1999;17:403-413.

[87] Borsukiewicz-Gozdur A., Dual-fluid-hybrid power plant co-powered by low-temperature geothermal water. Geothermics 2010;39:170-176.

[88] Pihl E., Heyne S., Thunman H., Johnsson F., Highly efficient electricity generation from biomass by integration and hybridization with combined cycle gas turbine (CCGT) plants for natural gas. Energy 2010;35:4042-4052.

[89] Lior N., Energy, exergy and thermoeconomic analysis of the effects of fossil-fuel superheating in nuclear power plants. ENERG CONVERS MANAGE 1997;38(15-17):1585-1593.

[90] Alsairafi A., Energetic and exergetic analysis of a hybrid combined nuclear power plant. Int J Energy Res 2012;36:891-901.

[91] Alsairafi A.A., Effects of ambient conditions on the thermodynamic performance of hybrid nuclear-combined cycle power plant. Int J Energy Res 2013;37:211-227.

[92] Sayyaadi H., Sabzaligol T., Comprehensive exergetic and economic comparison of PWR and hybrid fossil fuel-PWR power plants. Energy 2010;35:2953-2964.

[93] Forsberg C., Strategies for a Low-Carbon Electricity Grid With Full Use of Nuclear, Wind and Solar Capacity to Minimize Total Costs. MIT-ANP-TR-162, August 2015, For Public Distribution. http://energy.mit.edu/wp-content/uploads/2015/08/MIT-ANP-TR-162.pdf

[94] McDonald C.F., Mobile hybrid (nuclear oil fired) gas turbine cogeneration power plant concept. Appl Therm Eng 1998;18(6):353-368.

[95] Jeong Y.H., Kazimi M.S., The synergetic effects of nuclear-assisted gas turbine power cycles. Nucl Technol 2007;160(2):233-243.

[96] Dolz V., Novella R., García A., Sánchez J., HD Diesel engine equipped with a bottoming Rankine cycle as a waste heat recovery system. Part 1: Study and analysis of the waste heat energy. Appl Therm Eng 2012;36:269-278.

[97] Serrano J.R., Dolz V., Novella R., Garcia A., HD Diesel engine equipped with a bottoming Rankine cycle as a waste heat recovery system. Part 2: Evaluation of alternative solutions. Appl Therm Eng 2012;36:279-287.

[98] He M., Zhang X., Zeng K., Gao K., A combined thermodynamic cycle used for waste heat recovery of internal combustion engine. Energy 2011;36:6821-6829.

[99] Yang M., Yeh R., Thermodynamic and economic performances optimization of an organic Rankine cycle system utilizing exhaust gas of a large marine diesel engine. Appl Energ 2015;149:1-12.

[100] Kostowski W.J., Usón S., Comparative evaluation of a natural gas expansion plant integrated with an IC engine and an organic Rankine cycle, Energ Convers Manage 2013;75:509-516.

[101] Wei M., Fang J., Ma C., Danish S.N., Waste heat recovery from heavy-duty diesel engine exhaust gases by medium temperature ORC system. Sci China Technol Sc 2011;54(10):2746-2753.

[102] Vaja I., Gambarotta A., Internal Combustion Engine (ICE) bottoming with Organic Rankine Cycles (ORCs). Energy 2010;35:1084-1093.

[103] El-Awad M., Siraj A., A Combined Diesel-Engine Gas-Turbine System for Distributed Power Generation. In: International Conference on Chemical, Biological and Medical Sciences (ICCBMS'2012) August 25-26, 2012 Kuala Lumpur (Malaysia).

[104] Yamada N., Mohamad M., Efficiency of hydrogen internal combustion engine combined with open steam Rankine cycle recovering water and waste heat. Int J Hydrogen Energ 2010;35:1430-1442.

[105] Al-Sulaiman F.A., Dincer I., Hamdullahpur F., Energy analysis of a trigeneration plant based on solid oxide fuel cell and organic Rankine cycle. Int J Hydrogen Energ 2010;35:5104-5113.

[106] Chen S, Lior N., Xiang W., Coal gasification integration with solid oxide fuel cell and chemical looping combustion for high-efficiency power generation with inherent CO2 capture. Appl Energ 2015;146(15):298-312.

[107] Kim Y.M., Kim C.G., Favrat D., Transcritical or supercritical CO2 cycles using both low- and high-temperature heat sources. Energy 2012;43:402-415.

[108] Kakaras E., Doukelis A., Leithner R., Aronis N., Combined cycle power plant with integrated low temperature heat (LOTHECO). Appl Therm Eng 2004;24:1677-1686.

[109] Deng S., Hynes R., Drover B., Hybrid Power Generation Plant for CO_2 Capture. J Eng Gas Turb Power 2014;136:052001.

[110] Concentrating Point Focus Solar Thermal Power Generation, http://www.gesyw.com/pdf/CPF%20Solar%20Thermal%20Power.pdf

[111] Levelized Cost and Levelized Avoided Cost of New Generation Resources in the Annual Energy Outlook 2015, EIA, June 2015, http://www.eia.gov/forecasts/aeo/pdf/electricity_generation.pdf

[112] Renewables 2015 Global Status Report, EIA, 2015, http://www.ren21.net/wp-content/uploads/2015/07/REN12-GSR2015_Onlinebook_low1.pdf

CHAPTER 4

THERMODYNAMIC ANALYSIS OF THERMAL HYBIRD POWER GENERATION SYSTEMS BASED ON RANKINE CYCLES

4.1. Hybrid power generation systems based on the simple Rankine cycle

Many types of hybrid power plants have been developed and analyzed, type by type (e.g. [1]), and some were built for testing and commercial operation [2]. Little work, however, was done to develop the generalized theory, which can be applicable to all (or many) types of hybrid power plants, or at least one type of power plants but without involving specific operation parameters. The main objective of this dissertation is therefore to develop some generalized quantitative theories to fill this gap and to help design various hybrid power plants.

The method we used here is step-wise: to first analyze the major, most commonly used, hybrid power generation systems thermodynamically, without involving specific operation parameter values. In this way, some generalized theory that is at least applicable to *this* type of system can be developed. The second step is to perform such an analysis for all the major types of power generation systems (e.g. Rankine, Brayton, Combined Cycles, and their main variants) The third step is to find commonalities between these theories (if any).

The fourth and last step is to develop the sought generalized theory based on these commonalities. As shown below 4.2.4, this approach indeed worked and led to the discovery of such a theory.

Based on the major types of power generation methods, the hybrid power generation systems based on the Rankine cycles, Brayton cycles and the combined cycle will be analyzed in sequence. The first, presented here, is for the hybrid systems based on Rankine cycles, mainly used in steam and organic and other working fluid power plants.

4.1.1. Introduction of hybrid power generation systems based on the simple Rankine cycle

The Rankine cycle is the most widely used type of power generation cycle in power plants, especially in steam power plants. Fig. 4-1 and Fig. 4-2 show, respectively, the flow diagrams of a very basic Rankine cycle and a correspondingly very basic hybrid Rankine cycle, which has one additional heat source (AHS). The T-s diagram of the hybrid Rankine cycle is shown in Fig. 4-3. Note that the “heat exchanger” in Fig. 4-2 may be part of the economizer of the boiler in Fig. 4-1 when there is no AHS. The economizer is part of a boiler in a steam power plant, which is used to preheat the working fluid using the combustion gas from the boiler. In essence, an economizer is also a heat exchanger.

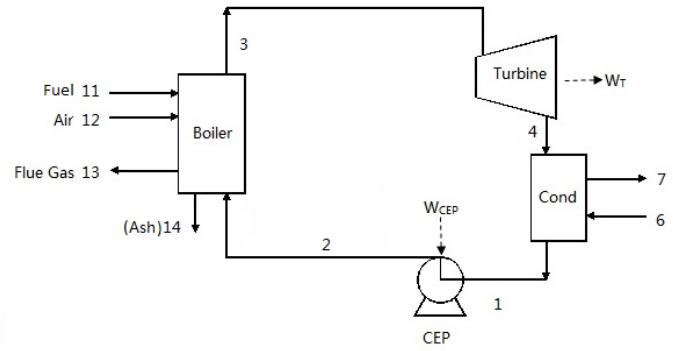

Fig. 4-1. Flow diagram of the reference (single heat source) power cycle based on the simple Rankine cycle without additional heat sources (AHS) (Cond: condenser, CEP: condensate extraction pump)

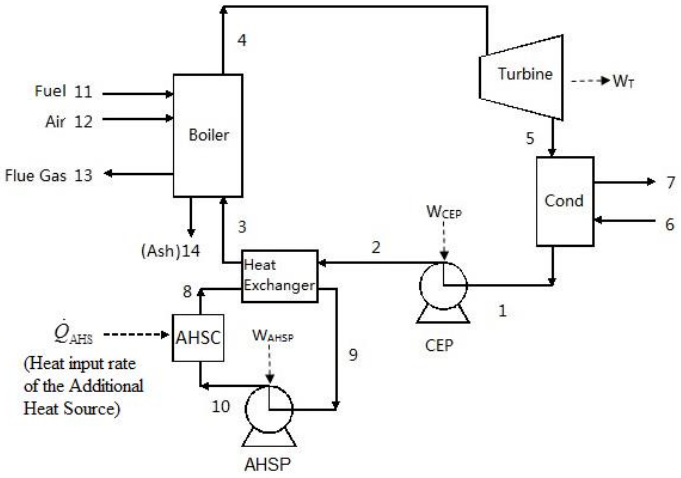

Fig. 4-2. Flow diagram of the hybrid power cycle based on the simple Rankine cycle with one additional heat source (AHS) (Cond: condenser, CEP: condensate extraction pump, AHSP: additional heat source pump, AHSC: additional heat source collection equipment) (The heat exchanger may be part of the economizer in the reference system when there is no AHS)

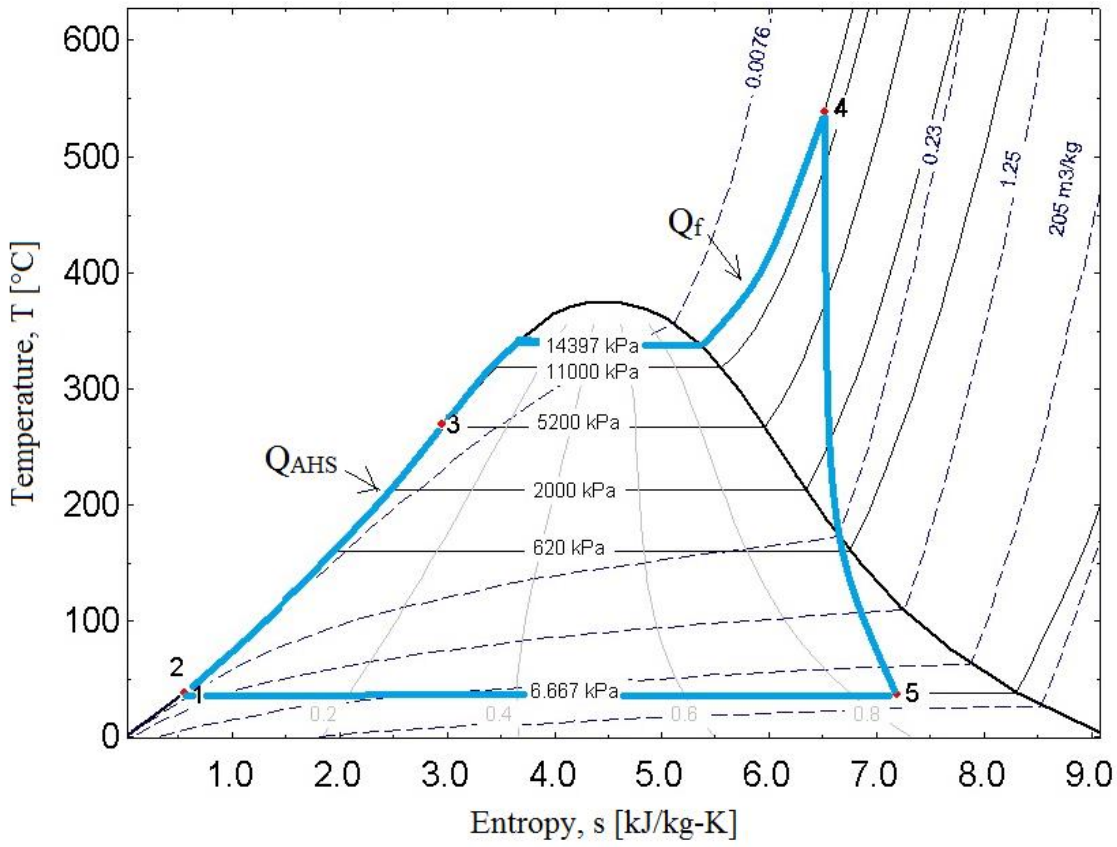

Fig. 4-3 The T-s diagram for the hybrid power generation systems based on the simple Rankine cycle in Fig. 4-2

The working fluid in the power cycles can either be water as normally used in the steam power plants, or other working fluids (most often organic) of different temperature and pressure boiling points. Water is used in this analysis, but the general method also applies to the other fluids.

In the Rankine cycle that has an AHS temperature lower than that of the boiler heat source, the water flow from the outlet of the main pump (CEP: condensate extraction pump) is heated by the AHS before being heated by the boiler.

A “heat exchanger” (Fig. 4-2) is not always needed, e. g. when solar heat is used as the AHS, it can be directly added to the working fluid. We call the basic Rankine cycle as the “main cycle”, and the one containing the AHS, such as solar collector as the “AHS cycle”.

Since the 2-heat sources flow diagram (Fig. 4-2) obviously becomes the same as the reference case (Fig. 4-1) if there is no AHS input, it is sufficient to analyze the 2-heat sources case.

4.1.2. Thermodynamic analysis of hybrid power generation systems based on the simple Rankine cycle

The thermodynamic analysis uses the following assumptions:

The kinetic and potential energy of the fluids are ignored in such power cycle analyses due to their small magnitude and impact on the system performance relative to the heat-caused enthalpy changes in the fluids. This will be demonstrated in the simulation following the thermodynamic analysis.

Since the composition of the working fluid almost doesn’t change, the enthalpy of the working fluid can be assumed to be that of pure water and its chemical exergy can be neglected.

The enthalpy difference between the outlet and inlet working fluid flows is thus equal to the heat input or work output.

The pressure drops in the pump, heat exchangers and all pipes are not taken into account but the pressure at each state point in the hybrid system is assumed to be the same as in the reference system, respectively. In practice, the pressure of the working fluid decreases during heat addition due to friction. Since the pressure drops in heat exchangers are only a few percent of the inlet pressure, they can be assumed to be zero in this first-step thermodynamic analysis. Furthermore, the following analysis shows that the results of the sensitivity analysis is valid even if the pressure drop is accounted for.

Each component, including the heat exchangers, is adiabatic with respect to its surroundings, (i.e., there is no heat loss to the environment). Since the heat loss is generally easily reducible and usually only a small fraction of the heat duty of the heat exchangers, most early-stage design processes ignore these heat losses.

The mechanical efficiencies of the pump and the steam turbine are 100%.

The isentropic efficiencies (which are different from mechanical efficiencies) of the pump and the steam turbine are constant and do not change with the heat addition rate or temperature of the AHS.

To facilitate the future thermodynamic analysis process, the energy conversion efficiency of the heat source (HS), or just called the “HS energy efficiency”, is defined as

$$\eta_{\mathrm{HS}} = \frac{\dot{Q}_{\mathrm{ADD}}}{\dot{Q}_{\mathrm{HS}}}, \tag{4.1}$$

where $\dot{Q}_{\mathrm{HS}}$ [kW] is the energy input rate of the heat source to the system (for example, $\dot{Q}_{\mathrm{AHS}}$ for the AHS) and $\dot{Q}_{\mathrm{ADD}}$ [kW] is the heat addition rate absorbed by the working fluid from the heat source (for example, $H_3 - H_2$ in Fig. 4-2). η_{HS} is the fraction of the heat from the heat source that is received by the working fluid.

The next step is to find the energy efficiency and exergy efficiency of the hybrid system and the reference system, respectively. Based on the enthalpy balance of the boiler and the heat exchanger (Fig. 4-2), the enthalpy increase of the working fluid during the heat addition process is, respectively,

$$\dot{Q}_{\mathrm{ADD,f}} = \dot{m}_{\mathrm{w}} \cdot \left(h_4 - h_3\right), \tag{4.2}$$

$$\dot{Q}_{\mathrm{ADD,AHS}} = \dot{m}_{\mathrm{w}} \cdot \left(h_3 - h_2\right), \tag{4.3}$$

in which $\dot{m}_{\mathrm{w}}$ [kg/s] is the mass flow rate of the working fluid (water).

When solar energy is used as the AHS, $\dot{Q}_{\mathrm{ADD,AHS}} = \dot{Q}_{\mathrm{sol}}$ and η_{HS} is η_{sc} defined in Eq. (2.6).

Using the assumptions listed at the beginning of Section 4.1.2 and based on Eqs (2.2) and (4.1)-(4.3), the energy efficiency of the hybrid system, η_{h}, is

$$\eta_{\mathrm{h}} = \frac{\dot{m}_{\mathrm{w}} \cdot \left[\left(h_4 - h_5 \right) - \left(h_2 - h_1 \right) \right]}{\dot{m}_{\mathrm{f}} \cdot \mathrm{LHV} + \dot{Q}_{\mathrm{ADD}} / \eta_{\mathrm{AHS}}} = \frac{\left(h_4 - h_5 \right) - \left(h_2 - h_1 \right)}{\dfrac{h_4 - h_3}{\eta_{\mathrm{B}}} + \dfrac{h_3 - h_2}{\eta_{\mathrm{AHS}}}}, \tag{4.4}$$

in which $\eta_{\mathrm{B}} = \dfrac{\dot{m}_{\mathrm{w}} \cdot \left(h_4 - h_3 \right)}{\dot{m}_{\mathrm{f}} \cdot \mathrm{LHV}}$ is the boiler efficiency and η_{AHS} is the energy conversion efficiency of the AHS, both of which were defined in Eq. (4.1). Note that in practice the isentropic efficiencies of the pump and the steam turbine are used to calculate the outlet specific enthalpies of the pump and the steam turbine, h_5 and h_2, respectively. These isentropic efficiency terms thus are not explicitly shown in Eq. (4.4).

Assuming the ambient temperature is T_0 and the AHS temperature is T_{AHS}, the exergy efficiency of the hybrid system, ε_{h}, based on Eq. (2.8), is

$$\varepsilon_{\mathrm{h}} = \frac{\dot{m}_{\mathrm{w}} \cdot \left[\left(h_4 - h_5 \right) - \left(h_2 - h_1 \right) \right]}{\dot{m}_{\mathrm{f}} \cdot b_{\mathrm{f}} + \psi_{\mathrm{AHS}} \cdot \dot{Q}_{\mathrm{AHS}}} = \frac{\left(h_4 - h_5 \right) - \left(h_2 - h_1 \right)}{\psi_{\mathrm{f}} \dfrac{h_4 - h_3}{\eta_{\mathrm{B}}} + \psi_{\mathrm{AHS}} \dfrac{h_3 - h_2}{\eta_{\mathrm{AHS}}}}. \tag{4.5}$$

If there is no AHS input in Fig. 4-2, $h_3 = h_2$, we will arrive at the general form of energy efficiency of the simple Rankine cycle system showed in Fig. 4-1 as

$$\eta_0 = \frac{\left(h_4 - h_5 \right) - \left(h_2 - h_1 \right)}{\dfrac{h_4 - h_2}{\eta_{\mathrm{B}}}}, \tag{4.6}$$

and the exergy efficiency will be

$$\varepsilon_0 = \frac{\left(h_4 - h_5\right) - \left(h_2 - h_1\right)}{\psi_{\mathrm{f}} \dfrac{h_4 - h_2}{\eta_{\mathrm{B}}}}. \tag{4.7}$$

The next step is to compare the energy and exergy efficiencies of the hybrid system and the reference system. To compare the hybrid and reference system, the top temperature of each system is kept the same, i.e. T_4 in Fig. 4-2 is the same as T_3 in Fig. 4-1. Considering the assumption that there is no pressure drop in the system (the pressure drop was considered in the simulation, though, and the simulation results confirmed that the assumption could be made in the equations' derivation here) and the fact that the specific enthalpy of the working fluid is the function of only temperature and pressure, i.e. $h = h\left(T, p\right)$, the specific enthalpy at each state point in the reference system will be the same as in the hybrid system. It further indicates that the specific enthalpy at each state point in the hybrid system (h_1, h_2, h_4 and h_5) will remain constant even if h_3 changes.

Based on Eqs (4.4) and (4.6), the difference between the energy efficiency of the hybrid system and the reference system is thus

$$\eta_{\mathrm{h}} - \eta_0 = \left[\left(h_4 - h_5\right) - \left(h_2 - h_1\right)\right] \frac{\left(h_3 - h_2\right)\left(\eta_{\mathrm{AHS}} - \eta_{\mathrm{B}}\right)}{\eta_{\mathrm{B}}\eta_{\mathrm{AHS}}\left(\dfrac{h_4 - h_3}{\eta_{\mathrm{B}}} + \dfrac{h_3 - h_2}{\eta_{\mathrm{AHS}}}\right)\left(h_4 - h_2\right)}. \tag{4.8}$$

It can thus be concluded that

$$\eta_h < \eta_0 \ \text{for} \left(\eta_{AHS} < \eta_B \right), \tag{4.9}$$

$$\eta_h = \eta_0 \ \text{for} \left(\eta_{AHS} = \eta_B \right), \tag{4.10}$$

$$\eta_h > \eta_0 \ \text{for} \left(\eta_{AHS} > \eta_B \right). \tag{4.11}$$

This indicates that for the same enthalpy states h_1 to h_5 in the hybrid and reference systems, the energy efficiency of the hybrid system is higher than that of the reference single heat source system if and only if the energy conversion efficiency of the AHS is larger than that of the boiler. Considering that the efficiency of the boiler, η_B, was increased over centuries, leaving little room for further improvement, Eq. (4.11) suggests that the system efficiency can be increased by adding an addition heat source that has a higher energy conversion efficiency. It is worth noting that, even if $\eta_{AHS} < \eta_f$, the hybrid systems still permit addition of lower temperature AHS, thus making good use of renewable and other heat sources, with all associated advantages, but without a prohibitive efficiency penalty, especially from the perspective of exergy usage as will be shown below.

Based on Eqs (4.5) and (4.7), the difference between the exergy efficiency of the hybrid system and the reference system is

$$\varepsilon_{\mathrm{h}}-\varepsilon_0=\left[\left(h_4-h_5\right)-\left(h_2-h_1\right)\right]\frac{\left(h_3-h_2\right)\left(\dfrac{\psi_{\mathrm{f}}}{\eta_{\mathrm{B}}}-\dfrac{\psi_{\mathrm{AHS}}}{\eta_{\mathrm{AHS}}}\right)}{\left(\psi_{\mathrm{f}}\dfrac{h_4-h_3}{\eta_{\mathrm{B}}}+\psi_{\mathrm{AHS}}\dfrac{h_3-h_2}{\eta_{\mathrm{AHS}}}\right)\left(h_4-h_2\right)}.$$

(4.12)

Define the exergy conversion efficiency of the boiler and the AHS, respectively, as

$$\eta'_{\mathrm{B}}=\frac{\eta_{\mathrm{B}}}{\psi_{\mathrm{f}}}, \tag{4.13}$$

$$\eta'_{\mathrm{AHS}}=\frac{\eta_{\mathrm{AHS}}}{\psi_{\mathrm{AHS}}}. \tag{4.14}$$

Equations (4.5) and (4.7) can thus be written, respectively, as

$$\varepsilon_{\mathrm{h}}=\frac{\left(h_4-h_5\right)-\left(h_2-h_1\right)}{\dfrac{h_4-h_3}{\eta'_{\mathrm{B}}}+\dfrac{h_3-h_2}{\eta'_{\mathrm{AHS}}}}, \tag{4.15}$$

$$\varepsilon_0=\frac{\left(h_4-h_5\right)-\left(h_2-h_1\right)}{\dfrac{h_4-h_2}{\eta'_{\mathrm{B}}}}, \tag{4.16}$$

which have the similar form as Eqs (4.4) and (4.6), except that the energy conversion efficiencies are replaced by the corresponding exergy conversion efficiencies defined in Eqs (4.13) and (4.14).

Equation (4.12) will also have the similar form as Eq. (4.8) as

$$\varepsilon_{\mathrm{h}}-\varepsilon_0=\left[\left(h_4-h_5\right)-\left(h_2-h_1\right)\right]\frac{\left(h_3-h_2\right)\left(\eta'_{\mathrm{AHS}}-\eta'_{\mathrm{B}}\right)}{\eta_{\mathrm{B}}\eta_{\mathrm{AHS}}\left(\frac{h_4-h_3}{\eta'_{\mathrm{B}}}+\frac{h_3-h_2}{\eta'_{\mathrm{AHS}}}\right)\left(h_4-h_2\right)}.$$

(4.17)

It can thus be concluded that

$$\varepsilon_{\mathrm{h}}<\varepsilon_0 \ \mathrm{for}\left(\eta'_{\mathrm{AHS}}<\eta'_{\mathrm{B}}\right), \tag{4.18}$$

$$\varepsilon_{\mathrm{h}}=\varepsilon_0 \ \mathrm{for}\left(\eta'_{\mathrm{AHS}}=\eta'_{\mathrm{B}}\right), \tag{4.19}$$

$$\varepsilon_{\mathrm{h}}>\varepsilon_0 \ \mathrm{for}\left(\eta'_{\mathrm{AHS}}>\eta'_{\mathrm{B}}\right). \tag{4.20}$$

This indicates that for the same enthalpy states h_1 to h_5 in the hybrid and reference systems, the exergy efficiency of the hybrid system is higher than that of the reference single heat source system if and only if the exergy conversion efficiency of the AHS is larger than that of the boiler. It could also be seen that while the energy efficiency has nothing to do with the temperature of the heat source T_{HS}, the exergy efficiency is influenced by T_{HS} if the exergy factor changes with the temperature of the heat source, such as for a heat flow. For a given boiler, b_{f} and LHV of the fuel and the boiler efficiency η_{B} are all constant. The ambient temperature T_0 is also relatively steady. So we can see from Eq. (4.5) that the exergy efficiency of hybrid system decreases with ψ_{AHS}. This

suggests that we can increase the exergy efficiency by decreasing ψ_{AHS}. For example, the temperature of the AHS when heat is used as the AHS should be as low as possible, given that other operation parameters, such as the top temperatures of the cycles, are fixed.

In conclusion, for the power generation systems based on the simple Rankine cycle and for the same enthalpy states h_1 to h_5 in the hybrid and reference systems, the energy (exergy) efficiency of the hybrid system is higher than that of the reference single heat source system if and only if the energy (exergy) conversion efficiency of the AHS is larger than that of the boiler. Also, increasing the AHS energy conversion efficiency will increase both the energy and exergy efficiency of the hybrid system, while decreasing the exergy factor of the AHS (temperature when the AHS is heat) will only increase the exergy efficiency but not the energy efficiency of the hybrid system.

4.1.3. Generalization to other types of heat sources for hybrid power generation systems based on the simple Rankine cycle

The above analysis is for the hybrid simple Rankine cycle system shown in Fig. 4-2 in which the heat source of reference system is fuel in the boiler and the additional heat source is in the form of heat, such as solar heat, waste heat or geothermal heat. It, however, could be generalized, considering that the additional heat source (AHS) can come from either fuel combustion or other sources, and the higher temperature heat source (HTHS) which is fuel used in the boiler in the studied hybrid simple Rankine cycle system doesn't need to

be fuel, but could be in the form of heat, such as solar heat collected at higher temperature (higher than that of the AHS).

When the heat source (whether it is the AHS or the HTHS) is in the form of heat, the exergy conversion efficiency of the heat source (HS) that is at temperature $T_{HS,}$ η'_{HS}, is

$$\eta'_{HS} = \frac{\eta_{HS}}{1 - \frac{T_0}{T_{HS}}}, \tag{4.21}$$

based on Eqs (4.14) and (2.10). T_0 is the dead state temperature.

When the heat source (whether it is the AHS or the HTHTS) is in the form of fuel, the exergy conversion efficiency of the heat source (HS), η'_{HS}, is

$$\eta'_{HS} = \frac{\eta_{HS}}{\frac{b_f}{LHV}}, \tag{4.22}$$

based on Eqs (4.13) and (2.9).

For either type of heat source, the energy conversion efficiency of the heat source η_{HS} is determined by Eq. (4.1).

Therefore, follow the same procedure as section 4.1.2, it can be easily concluded that

$$\eta_h < \eta_0 \text{ for} \left(\eta_{AHS} < \eta_{HTHS}\right), \tag{4.23}$$

$$\eta_{\mathrm{h}} = \eta_0 \ \text{for} \left(\eta_{\mathrm{AHS}} = \eta_{\mathrm{HTHS}} \right), \tag{4.24}$$

$$\eta_{\mathrm{h}} > \eta_0 \ \text{for} \left(\eta_{\mathrm{AHS}} > \eta_{\mathrm{HTHS}} \right), \tag{4.25}$$

and

$$\varepsilon_{\mathrm{h}} < \varepsilon_0 \ \text{for} \left(\eta'_{\mathrm{AHS}} < \eta'_{\mathrm{HTHS}} \right), \tag{4.26}$$

$$\varepsilon_{\mathrm{h}} = \varepsilon_0 \ \text{for} \left(\eta'_{\mathrm{AHS}} = \eta'_{\mathrm{HTHS}} \right), \tag{4.27}$$

$$\varepsilon_{\mathrm{h}} > \varepsilon_0 \ \text{for} \left(\eta'_{\mathrm{AHS}} > \eta'_{\mathrm{HTHS}} \right), \tag{4.28}$$

in which the energy and exergy conversion efficiency of the AHS and HTHS should be calculated, respectively, by

$$\eta_{\mathrm{AHS}} = \frac{\Delta H_{\mathrm{AHS}}}{Q_{\mathrm{AHS}}}, \tag{4.29}$$

$$\eta_{\mathrm{HTHS}} = \frac{\Delta H_{\mathrm{HTHS}}}{Q_{\mathrm{HTHS}}}, \tag{4.30}$$

$$\eta'_{\mathrm{AHS}} = \frac{\eta_{\mathrm{AHS}}}{\psi_{\mathrm{AHS}}} = \frac{\Delta H_{\mathrm{AHS}}}{B_{\mathrm{AHS}}}, \tag{4.31}$$

$$\eta'_{\mathrm{HTHS}} = \frac{\eta_{\mathrm{HTHS}}}{\psi_{\mathrm{HTHS}}} = \frac{\Delta H_{\mathrm{HTHS}}}{B_{\mathrm{HTHS}}}, \tag{4.32}$$

in which ΔH_{AHS} and ΔH_{HTHS} are the enthalpy increase of the working fluid heated by the AHS and HTHS, respectively; Q_{AHS} and Q_{HTHS} are the energy input from the AHS and HTHS to the power generation system, respectively; B_{AHS} and B_{HTHS} are the exergy input from the AHS and HTHS, respectively to the power generation system.

4.1.4. Sensitivity analysis of the hybrid power generation systems based on the simple Rankine cycle, with respect to the AHS

In this section we study the effects of the AHS on the efficiencies of the hybrid systems (Eqs (4.23)-(4.28)). In this analysis it is assumed that the turbine inlet temperature (TIT, T_4 in Fig. 4-2) and turbine outlet pressure (p_5), as well as the condensing temperature (T_1), condensing pressure (p_1) and pump pressure (p_2), are kept constant when $\dot{Q}_{\mathrm{AHS}}$ or T_{AHS} changes.

4.1.4.1. *Effect of the heat addition rate of the additional heat source, $\dot{Q}_{\mathrm{AHS}}$, on the energy efficiency of the hybrid power generation systems based on the simple Rankine cycle, η_{h}.*

To study the effect of the heat addition rate of the additional heat source, $\dot{Q}_{\mathrm{AHS}}$, on the energy efficiency of the hybrid power generation systems based on the simple Rankine cycle, η_{h}, we examine the partial derivative of the energy efficiency of the hybrid system, η_{h}, with respect to the heat addition rate of the AHS, $\dot{Q}_{\mathrm{AHS}}$. By examining the first and second order partial derivatives (the shapes of the curves), the results can be used to study

the hybrid system behavior and give guidance on system designing. For example, when the curve is upward and concave, it can be inferred that the objective function increases more strongly with the variable and will have a larger influence on the objective function when it is small. When the curve is downward and concave, it can be inferred that the variable has less influence on the objective function when it is small, and can be treated as a less important factor than other variables that has larger impact on the objective function. When there is a local maximum point on the curve, the system should be designed around that point to maximize the objective function, such as energy efficiency of the hybrid system.

From Eq. (4.4), the partial derivative of the energy efficiency of the hybrid system, η_h, with respect to the heat addition rate of the AHS, $\dot{Q}_{AHS}$, is thus

$$\frac{\partial \eta_h}{\partial \dot{Q}_{AHS}} = \frac{\partial \eta_h}{\partial h_3}\frac{\partial h_3}{\partial \dot{Q}_{AHS}} = \frac{\eta_h}{q_{in}}\left(\frac{1}{\eta_B} - \frac{1}{\eta_{AHS}}\right)\frac{\eta_{AHS}}{\dot{m}_w} = \frac{{\eta_h}^2}{\dot{W}_{net}}\left(\frac{\eta_{AHS}}{\eta_B} - 1\right), \quad (4.33)$$

in which $q_{in} = \frac{\dot{Q}_{in}}{\dot{m}_w}$ [kJ/kg] is the specific total heat input to the system.

Equation (4.33) shows that η_h increases with $\dot{Q}_{AHS}$ when $\eta_{AHS} > \eta_B$, and decreases with increasing $\dot{Q}_{AHS}$ when $\eta_{AHS} < \eta_B$.

While the first-order partial derivative shows whether the objective function (η_h) increases or decreases with the variable ($\dot{Q}_{AHS}$), it does not show whether the curve (η_h-$\dot{Q}_{AHS}$) is

concave[1] or convex[2] or straight[3]. Mathematically, when the first-order partial derivative is 0, there will be a local maximum point when the curve is concave and a local minimum point when the curve is convex. Also, when the slope of the curve is negative, a concave curve means that the objective function will decrease less with the variable at the beginning than later while a convex curve means that the objective function will decrease more with the variable at the beginning than later, and v.v. when the slope of the curve is positive. The second-order partial derivative is thus needed to show more information about the relation between the variable and the objective function and therefore help us design the hybrid systems.

The second-order partial derivative of the energy efficiency of the hybrid system with respect to the heat addition rate of the AHS is

$$\frac{\partial^2 \eta_{\mathrm{h}}}{\partial \dot{Q}_{\mathrm{AHS}}{}^2} = \frac{2\eta_{\mathrm{h}}{}^3}{\dot{W}_{\mathrm{net}}{}^2}\left(\frac{\eta_{\mathrm{AHS}}}{\eta_{\mathrm{B}}} - 1\right)^2 \geq 0. \tag{4.34}$$

Equation (4.34) shows that the η_{h}-$\dot{Q}_{\mathrm{AHS}}$ curve is convex unless $\eta_{\mathrm{AHS}} = \eta_{\mathrm{B}}$, in which case η_{h} doesn't change with $\dot{Q}_{\mathrm{AHS}}$.

---

[1] The curve is concave when the second partial derivative is negative, indicating there might be a maximum point.

[2] The curve is convex when the second partial derivative is positive, indicating there might be a minimum point.

[3] The curve is straight when the second partial derivative is 0, indicating the curve is straight.

4.1.4.2. *Effect of the temperature of the additional heat source, T_{AHS}, on the energy efficiency of the hybrid power generation systems based on the simple Rankine cycle, η_{h}.*

To study the effect of the temperature of the additional heat source, T_{AHS}, on the energy efficiency of the hybrid power generation systems based on the simple Rankine cycle, η_{h}, we examine the partial derivate of the energy efficiency of the hybrid system, η_{h}, with respect to the temperature of the AHS, T_{AHS}.

From Eq. (4.4), the partial derivative of the energy efficiency of the hybrid system, η_{h}, with respect to the temperature of the AHS, T_{AHS}, is

$$\frac{\partial \eta_{\mathrm{h}}}{\partial T_{\mathrm{AHS}}} = \frac{\partial \eta_{\mathrm{h}}}{\partial h_3}\frac{\partial h_3}{\partial T_{\mathrm{AHS}}} = \frac{\eta_{\mathrm{h}}}{q_{\mathrm{in}}}\left(\frac{1}{\eta_{\mathrm{B}}} - \frac{1}{\eta_{\mathrm{AHS}}}\right)\frac{\partial h_3}{\partial T_{\mathrm{AHS}}} = \frac{{\eta_{\mathrm{h}}}^2}{w_{\mathrm{net}}}\left(\frac{1}{\eta_{\mathrm{B}}} - \frac{1}{\eta_{\mathrm{AHS}}}\right)\frac{\partial h_3}{\partial T_{\mathrm{AHS}}}. \tag{4.35}$$

T_{AHS} in this equation can be expressed by $T_{\mathrm{AHS}} = T_3 + \Delta T_{\mathrm{HE}}$, with ΔT_{HE} defined as the temperature difference at the cold side of the heat exchanger in Fig. 4-2. In practice, ΔT_{HE} is designed so that it is neither too large nor too small considering both the efficiency and the cost of the heat exchanger. It could thus be assumed that ΔT_{HE} is constant and doesn't change with T_{AHS}.

Therefore,

$$\frac{\partial h_3}{\partial T_{\text{AHS}}} = \frac{\partial h_3}{\partial \left(T_3 + \Delta T_{\text{HE}} \right)} = \frac{\partial h_3}{\partial T_3} = c_{p,T_3}, \tag{4.36}$$

in which c_{p,T_3} [kJ/kg-K] is the specific heat at constant pressure of the working fluid (a function of temperature as shown in Fig. 4-4) at temperature T_3, when T_3 is not the boiling temperature ($T_3 \neq T_{\text{b}}$). When $T_3 = T_{\text{b}}$, however, $\frac{\partial h_3}{\partial T_3}$ cannot be defined since T_3 doesn't change in the phase change region when h_3 increases.

Equation (4.35) thus becomes

$$\frac{\partial \eta_{\text{h}}}{\partial T_{\text{AHS}}} = \frac{{\eta_{\text{h}}}^2}{w_{\text{net}}} \left(\frac{1}{\eta_{\text{B}}} - \frac{1}{\eta_{\text{AHS}}} \right) c_{p,T_3}, \tag{4.37}$$

when $T_3 \neq T_{\text{b}}$.

Since the specific heat at constant pressure is always positive, Eq. (4.37) shows that η_{h} increases with T_{AHS} when $\eta_{\text{AHS}} > \eta_{\text{B}}$, and decreases with increasing T_{AHS} when $\eta_{\text{AHS}} < \eta_{\text{B}}$.

From Eq. (4.37), the second-order partial derivative of the energy efficiency of the hybrid system, η_{h}, with respect to the temperature of the AHS, T_{AHS}, is

$$\frac{\partial^2 \eta_{\mathrm{h}}}{\partial T_{\mathrm{AHS}}{}^2} = \left(\frac{1}{\eta_{\mathrm{B}}} - \frac{1}{\eta_{\mathrm{AHS}}}\right)\left[\frac{2\eta_{\mathrm{h}}{}^3}{w_{\mathrm{net}}{}^2}\left(\frac{1}{\eta_{\mathrm{B}}} - \frac{1}{\eta_{\mathrm{AHS}}}\right)c_{p,T_3}{}^2 + \frac{\eta_{\mathrm{h}}{}^2}{w_{\mathrm{net}}}\frac{\partial c_{p,T_3}}{\partial T_3}\right]$$
$$= \left(\frac{1}{\eta_{\mathrm{B}}} - \frac{1}{\eta_{\mathrm{AHS}}}\right)\frac{\eta_{\mathrm{h}}{}^2}{w_{\mathrm{net}}}\left[\left(\frac{1}{\eta_{\mathrm{B}}} - \frac{1}{\eta_{\mathrm{AHS}}}\right)\frac{2\eta_{\mathrm{h}} c_{p,T_3}{}^2}{w_{\mathrm{net}}} + \frac{\partial c_{p,T_3}}{\partial T_3}\right], \tag{4.38}$$

when $T_3 \neq T_{\mathrm{b}}$. Equation (4.38) shows that the η_{h}-T_{AHS} curve is convex ($\frac{\partial^2 \eta_{\mathrm{h}}}{\partial T_{\mathrm{AHS}}{}^2} > 0$) when $\eta_{\mathrm{AHS}} > \eta_{\mathrm{B}}$ and $\frac{\partial c_{p,T_3}}{\partial T_3} > 0$, or when $\eta_{\mathrm{AHS}} < \eta_{\mathrm{B}}$ and $\frac{\partial c_{p,T_3}}{\partial T_3} < 0$.

To further analyze Eq. (4.38), c_{p,T_3} must be examined. According to the thermodynamic properties of water, the c_p-T diagram of water at 14 MPa (boiling pressure of the system described by Fig. 4-2) is shown in Fig. 4-4 [1]. As can be seen in Fig. 4-4, c_{p,T_3} first increases slowly with T_3, and then increases faster until it reaches the boiling point, T_{b}, after which c_{p,T_3} will decrease fast and then slowly with T_3.

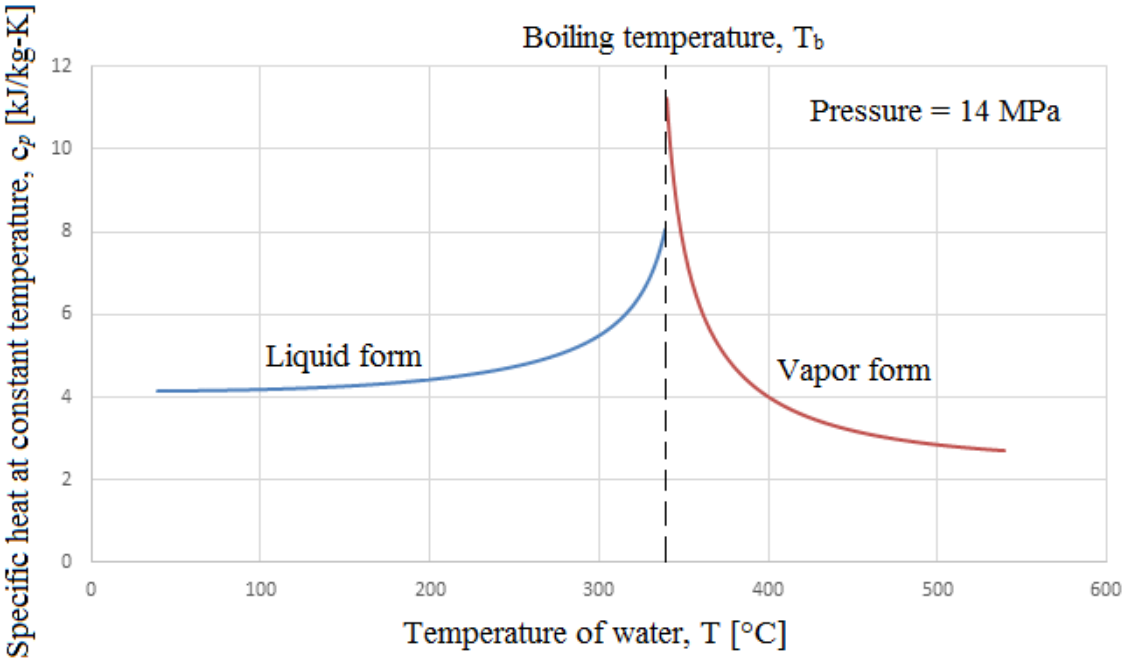

Fig. 4-4. The specific heat at constant pressure dependency on the water temperature (at 14 MPa) [1]

From Eq. (4.38), it can thus be seen that when $\eta_{\mathrm{AHS}} > \eta_{\mathrm{B}}$ and $T_3 < T_{\mathrm{b}}$,

$$\frac{\partial^2 \eta_{\mathrm{h}}}{\partial T_{\mathrm{AHS}}{}^2} > 0, \tag{4.39}$$

since c_{p,T_3} increases with T_3 when $T_3 < T_{\mathrm{b}}$ from Fig. 4-4.

When $\eta_{\mathrm{AHS}} < \eta_{\mathrm{B}}$ and $T_3 > T_{\mathrm{b}}$, Eq. (4.39) is also valid, since c_{p,T_3} decrease with T_3 when $T_3 > T_{\mathrm{b}}$ from Fig. 4-4.

The salient results from these subsections are summarized at the end in Section 4.1.4.5.

4.1.4.3. *Effect of the heat addition rate of the additional heat source, $\dot{Q}_{\mathrm{AHS}}$, on the exergy efficiency of the hybrid power generation systems based on the simple Rankine cycle, ε_{h}.*

To study the effect of the heat addition rate of the additional heat source, $\dot{Q}_{\mathrm{AHS}}$, on the exergy efficiency of the hybrid power generation systems based on the simple Rankine cycle, ε_{h}, we examine the partial derivative of the exergy efficiency of the hybrid system, ε_{h}, with respect to the heat addition rate of the AHS, $\dot{Q}_{\mathrm{AHS}}$.

From Eq. (4.15), the partial derivative of the exergy efficiency of the hybrid system, ε_{h}, with respect to the heat additional rate of the AHS, $\dot{Q}_{\mathrm{AHS}}$, is

$$\frac{\partial \varepsilon_{\mathrm{h}}}{\partial \dot{Q}_{\mathrm{AHS}}} = \frac{\partial \varepsilon_{\mathrm{h}}}{\partial h_3}\frac{\partial h_3}{\partial \dot{Q}_{\mathrm{AHS}}} = -\frac{\varepsilon_{\mathrm{h}}}{b_{\mathrm{in}}}\left[\frac{\partial\left(\frac{h_4-h_3}{\eta_{\mathrm{HTHS}}}\psi_{\mathrm{HTHS}}\right)}{\partial h_3} + \frac{\partial\left(\frac{h_3-h_2}{\eta_{\mathrm{AHS}}}\psi_{\mathrm{AHS}}\right)}{\partial h_3}\right]\frac{\eta_{\mathrm{AHS}}}{\dot{m}_{\mathrm{w}}}$$

$$= -\eta_{\mathrm{AHS}}\frac{\varepsilon_{\mathrm{h}}^{\,2}}{\dot{W}_{\mathrm{net}}}\left(\frac{\psi_{\mathrm{HTHS}}}{\eta_{\mathrm{HTHS}}} - \frac{h_4-h_3}{\eta_{\mathrm{HTHS}}}\frac{\partial \psi_{\mathrm{HTHS}}}{\partial h_3} - \frac{\psi_{\mathrm{AHS}}}{\eta_{\mathrm{AHS}}} - \frac{h_3-h_2}{\eta_{\mathrm{AHS}}}\frac{\partial \psi_{\mathrm{AHS}}}{\partial h_3}\right). \tag{4.40}$$

Unlike the energy efficiency analysis, different types of heat sources may result in different exergy efficiencies of the system. In this study, as in most types of thermal hybrid systems studied before, it is assumed that the additional heat source (AHS) is from heat and the

higher temperature heat source (HTHS) is from burning fuel, the exergy conversion efficiencies of which are defined in Eqs (4.21) and (4.22), respectively.

Using Eqs (4.21) and (4.22), Eq. (4.40) becomes

$$\frac{\partial \varepsilon_{\mathrm{h}}}{\partial \dot{Q}_{\mathrm{AHS}}} = \frac{\partial \varepsilon_{\mathrm{h}}}{\partial h_3}\frac{\partial h_3}{\partial \dot{Q}_{\mathrm{AHS}}} = -\eta_{\mathrm{AHS}}\frac{{\varepsilon_{\mathrm{h}}}^2}{\dot{W}_{\mathrm{net}}}\left\{\frac{\partial\left(\frac{h_4-h_3}{\eta_{\mathrm{B}}}\cdot\frac{b_{\mathrm{f}}}{\mathrm{LHV}}\right)}{\partial h_3}+\frac{\partial\left[\frac{h_3-h_2}{\eta_{\mathrm{AHS}}}\cdot\left(1-\frac{T_0}{T_{\mathrm{AHS}}}\right)\right]}{\partial h_3}\right\}$$

$$=\eta_{\mathrm{AHS}}\frac{{\varepsilon_{\mathrm{h}}}^2}{\dot{W}_{\mathrm{net}}}\left[\frac{1}{\eta_{\mathrm{B}}}\cdot\frac{b_{\mathrm{f}}}{\mathrm{LHV}}-\frac{1}{\eta_{\mathrm{AHS}}}\cdot\left(1-\frac{T_0}{T_{\mathrm{AHS}}}\right)-\frac{h_3-h_2}{\eta_{\mathrm{AHS}}}\frac{T_0}{{T_{\mathrm{AHS}}}^2}\frac{\partial T_{\mathrm{AHS}}}{\partial h_3}\right]$$

$$=\frac{{\varepsilon_{\mathrm{h}}}^2}{\dot{W}_{\mathrm{net}}}\left[\frac{\eta_{\mathrm{AHS}}}{\eta_{\mathrm{B}}}\cdot\frac{b_{\mathrm{f}}}{\mathrm{LHV}}-\left(1-\frac{T_0}{T_{\mathrm{AHS}}}\right)-\left(h_3-h_2\right)\frac{T_0}{{T_{\mathrm{AHS}}}^2}\frac{\partial T_{\mathrm{AHS}}}{\partial h_3}\right],$$

(4.41)

in which

$$\frac{\partial T_{\mathrm{AHS}}}{\partial h_3}=\frac{\partial\left(T_3+\Delta T_{\mathrm{HE}}\right)}{\partial h_3}=\frac{\partial T_3}{\partial h_3}=\frac{1}{c_{p,T_3}}, \tag{4.42}$$

when T_3 is not the boiling temperature ($T_3 \neq T_{\mathrm{b}}$), and

$$\frac{\partial T_{\mathrm{AHS}}}{\partial h_3}=0, \tag{4.43}$$

when T_3 is the boiling temperature ($T_3 = T_b$).

Equation (4.41) thus becomes

$$\frac{\partial \varepsilon_h}{\partial \dot{Q}_{AHS}} = \frac{{\varepsilon_h}^2}{\dot{W}_{net}} \left[\frac{\eta_{AHS}}{\eta_B} \cdot \frac{b_f}{LHV} - \left(1 - \frac{T_0}{T_{AHS}}\right) - \left(h_3 - h_2\right) \frac{T_0}{c_{p,T_3} {T_{AHS}}^2} \right], \quad (4.44)$$

when $T_3 \neq T_b$, and

$$\frac{\partial \varepsilon_h}{\partial \dot{Q}_{AHS}} = \frac{{\varepsilon_h}^2}{\dot{W}_{net}} \left[\frac{\eta_{AHS}}{\eta_B} \cdot \frac{b_f}{LHV} - \left(1 - \frac{T_0}{T_{AHS}}\right) \right], \quad (4.45)$$

when $T_3 = T_b$.

The second-order partial derivative of the exergy efficiency of the hybrid system, ε_h, with respect to the heat additional rate of the AHS, $\dot{Q}_{AHS}$, is

$$\begin{aligned} \frac{\partial^2 \varepsilon_h}{\partial {\dot{Q}_{AHS}}^2} = & \frac{2{\varepsilon_h}^3}{{\dot{W}_{net}}^2} \left[\frac{\eta_{AHS}}{\eta_B} \cdot \frac{b_f}{LHV} - \left(1 - \frac{T_0}{T_{AHS}}\right) - \left(h_3 - h_2\right) \frac{T_0}{c_{p,T_3} {T_{AHS}}^2} \right]^2 \\ & + \frac{{\varepsilon_h}^2}{\dot{W}_{net}} \left[-\frac{2T_0}{c_{p,T_3} {T_{AHS}}^2} + \left(h_3 - h_2\right) \frac{T_0}{{c_{p,T_3}}^2 {T_{AHS}}^3} \left(\frac{T_{AHS}}{c_{p,T_3}} \frac{\partial c_{p,T_3}}{\partial T_3} + 2 \right) \right] \frac{\eta_{AHS}}{\dot{m}_w}, \end{aligned} \quad (4.46)$$

when $T_3 \neq T_b$, and

$$\frac{\partial^2 \varepsilon_{\mathrm{h}}}{\partial \dot{Q}_{\mathrm{AHS}}{}^2} = \frac{2\varepsilon_{\mathrm{h}}{}^3}{\dot{W}_{\mathrm{net}}{}^2}\left[\frac{\eta_{\mathrm{AHS}}}{\eta_{\mathrm{B}}} \cdot \frac{b_{\mathrm{f}}}{\mathrm{LHV}} - \left(1 - \frac{T_0}{T_{\mathrm{AHS}}}\right)\right]^2, \tag{4.47}$$

when $T_3 = T_{\mathrm{b}}$.

To further analyze Eqs (4.44) and (4.46), different scenarios must be analyzed as T_3 is raised.

4.1.4.3.1. <u>Region in which the specific heat of working fluid at T_3 almost remains constant</u>

According to Fig. 4-4, for T_3 up to about 200 °C, c_{p,T_3} can be assumed to be constant, i.e.

$$\frac{\partial c_{p,T_3}}{\partial T_3} = 0. \tag{4.48}$$

In this case,

$$\frac{h_3 - h_2}{c_{p,T_3} T_{\mathrm{AHS}}} = \frac{\bar{c}_{p,T_2,T_3}\left(T_3 - T_2\right)}{c_{p,T_3} T_{\mathrm{AHS}}} = \frac{c_{p,T_3}\left(T_3 - T_2\right)}{c_{p,T_3} T_{\mathrm{AHS}}} = \frac{T_{\mathrm{AHS}} - \Delta T_{\mathrm{HE}} - T_2}{T_{\mathrm{AHS}}} = 1 - \frac{\Delta T_{\mathrm{HE}} + T_2}{T_{\mathrm{AHS}}}. \tag{4.49}$$

Equation (4.44) thus becomes

$$\begin{aligned} \frac{\partial \varepsilon_{\mathrm{h}}}{\partial \dot{Q}_{\mathrm{AHS}}} &= \frac{\varepsilon_{\mathrm{h}}{}^2}{\dot{W}_{\mathrm{net}}}\left[\frac{\eta_{\mathrm{AHS}}}{\eta_{\mathrm{B}}} \cdot \frac{b_{\mathrm{f}}}{\mathrm{LHV}} - \left(1 - \frac{T_0}{T_{\mathrm{AHS}}}\right) - \left(1 - \frac{\Delta T_{\mathrm{HE}} + T_2}{T_{\mathrm{AHS}}}\right)\frac{T_0}{T_{\mathrm{AHS}}}\right] \\ &= \frac{\varepsilon_{\mathrm{h}}{}^2}{\dot{W}_{\mathrm{net}}}\left[\frac{\eta_{\mathrm{AHS}}}{\eta_{\mathrm{B}}} \cdot \frac{b_{\mathrm{f}}}{\mathrm{LHV}} - 1 + \frac{T_0\left(\Delta T_{\mathrm{HE}} + T_2\right)}{T_{\mathrm{AHS}}{}^2}\right]. \end{aligned} \tag{4.50}$$

From Eq. (4.50), it is known that $\frac{\partial \varepsilon_{\mathrm{h}}}{\partial \dot{Q}_{\mathrm{AHS}}} > 0$ when

$$\frac{\eta_{\mathrm{AHS}}}{\eta_{\mathrm{B}}} \cdot \frac{b_{\mathrm{f}}}{\mathrm{LHV}} - 1 + \frac{\left(\Delta T_{\mathrm{HE}} + T_2\right) T_0}{T_{\mathrm{AHS}}{}^2} > 0 \tag{4.51}$$

or

$$\frac{\eta_{\mathrm{AHS}}}{\eta_{\mathrm{B}}} \cdot \frac{b_{\mathrm{f}}}{\mathrm{LHV}} > 1 - \frac{\left(\Delta T_{\mathrm{HE}} + T_2\right) T_0}{T_{\mathrm{AHS}}{}^2} \tag{4.52}$$

or

$$\begin{aligned} \eta_{\mathrm{AHS}} &> \frac{\eta_{\mathrm{B}}}{\frac{b_{\mathrm{f}}}{\mathrm{LHV}}} \left(1 - \frac{\left(\Delta T_{\mathrm{HE}} + T_2\right) T_0}{T_{\mathrm{AHS}}{}^2}\right) \\ &= \frac{\eta_{\mathrm{B}}}{\psi_{\mathrm{f}}} \left(1 - \frac{\left(\Delta T_{\mathrm{HE}} + T_2\right) T_0}{T_{\mathrm{AHS}}{}^2}\right) = \eta'_{\mathrm{B}} \left(1 - \frac{\left(\Delta T_{\mathrm{HE}} + T_2\right) T_0}{T_{\mathrm{AHS}}{}^2}\right). \end{aligned} \tag{4.53}$$

When

$$\frac{\eta_{\mathrm{AHS}}}{\eta_{\mathrm{B}}} \cdot \frac{b_{\mathrm{f}}}{\mathrm{LHV}} \geq 1, \tag{4.54}$$

Eq. (4.51) is always satisfied, but when

$$\frac{\eta_{\mathrm{AHS}}}{\eta_{\mathrm{B}}} \cdot \frac{b_{\mathrm{f}}}{\mathrm{LHV}} < 1, \tag{4.55}$$

Eq. (4.51) can be rewritten as

$$T_{\mathrm{AHS}} < \left[\frac{\left(\Delta T_{\mathrm{HE}} + T_2\right) T_0}{1 - \dfrac{\eta_{\mathrm{AHS}}}{\eta_{\mathrm{B}}} \cdot \dfrac{b_{\mathrm{f}}}{\mathrm{LHV}}} \right]^{\frac{1}{2}}. \tag{4.56}$$

From Eq. (4.78), it is also known that $\dfrac{\partial \varepsilon_{\mathrm{h}}}{\partial \dot{Q}_{\mathrm{AHS}}} < 0$ when

$$\frac{\eta_{\mathrm{AHS}}}{\eta_{\mathrm{B}}} \cdot \frac{b_{\mathrm{f}}}{\mathrm{LHV}} - 1 + \frac{\left(\Delta T_{\mathrm{HE}} + T_2\right) T_0}{{T_{\mathrm{AHS}}}^2} < 0 \tag{4.57}$$

or

$$\frac{\eta_{\mathrm{AHS}}}{\eta_{\mathrm{B}}} \cdot \frac{b_{\mathrm{f}}}{\mathrm{LHV}} < 1 - \frac{\left(\Delta T_{\mathrm{HE}} + T_2\right) T_0}{{T_{\mathrm{AHS}}}^2} \tag{4.58}$$

or

$$\begin{aligned} \eta_{\mathrm{AHS}} &< \frac{\eta_{\mathrm{B}}}{\dfrac{b_{\mathrm{f}}}{\mathrm{LHV}}} \left(1 - \frac{\left(\Delta T_{\mathrm{HE}} + T_2\right) T_0}{{T_{\mathrm{AHS}}}^2} \right) \\ &= \frac{\eta_{\mathrm{B}}}{\psi_{\mathrm{f}}} \left(1 - \frac{\left(\Delta T_{\mathrm{HE}} + T_2\right) T_0}{{T_{\mathrm{AHS}}}^2} \right) = \eta'_{\mathrm{B}} \left(1 - \frac{\left(\Delta T_{\mathrm{HE}} + T_2\right) T_0}{{T_{\mathrm{AHS}}}^2} \right). \end{aligned} \tag{4.59}$$

When

$$\frac{\eta_{\mathrm{AHS}}}{\eta_{\mathrm{B}}}\cdot\frac{b_{\mathrm{f}}}{\mathrm{LHV}}<1, \tag{4.60}$$

Eq. (4.57) can be rewritten as

$$T_{\mathrm{AHS}}>\left[\frac{\left(\Delta T_{\mathrm{HE}}+T_2\right)T_0}{1-\dfrac{\eta_{\mathrm{AHS}}}{\eta_{\mathrm{B}}}\cdot\dfrac{b_{\mathrm{f}}}{\mathrm{LHV}}}\right]^{\frac{1}{2}}. \tag{4.61}$$

The second-order partial derivative of the exergy efficiency of the hybrid system, ε_{h}, with respect to $\dot{Q}_{\mathrm{AHS}}$ is

$$\begin{aligned}\frac{\partial^2\varepsilon_{\mathrm{h}}}{\partial\dot{Q}_{\mathrm{AHS}}{}^2}&=\left\{\frac{2\varepsilon_{\mathrm{h}}{}^3}{\dot{W}_{\mathrm{net}}{}^2}\left[\frac{\eta_{\mathrm{AHS}}}{\eta_{\mathrm{B}}}\cdot\frac{b_{\mathrm{f}}}{\mathrm{LHV}}-1+\frac{\left(\Delta T_{\mathrm{HE}}+T_2\right)T_0}{T_{\mathrm{AHS}}{}^2}\right]^2+\frac{\varepsilon_{\mathrm{h}}{}^2}{\dot{W}_{\mathrm{net}}}\left[-2\frac{\left(\Delta T_{\mathrm{HE}}+T_2\right)T_0}{T_{\mathrm{AHS}}{}^3}\frac{\eta_{\mathrm{AHS}}}{C_{p,T_3}}\right]\right\}\\&=\frac{2\varepsilon_{\mathrm{h}}{}^3}{\dot{W}_{\mathrm{net}}{}^2}\left\{\left[\frac{\eta_{\mathrm{AHS}}}{\eta_{\mathrm{B}}}\cdot\frac{b_{\mathrm{f}}}{\mathrm{LHV}}-1+\frac{\left(\Delta T_{\mathrm{HE}}+T_2\right)T_0}{T_{\mathrm{AHS}}{}^2}\right]^2-\frac{\dot{W}_{\mathrm{net}}}{\varepsilon_{\mathrm{h}}}\frac{\left(\Delta T_{\mathrm{HE}}+T_2\right)T_0}{T_{\mathrm{AHS}}{}^3}\frac{\eta_{\mathrm{AHS}}}{C_{p,T_3}}\right\}\\&=\frac{2\varepsilon_{\mathrm{h}}{}^3c_{p,T_3}{}^2\eta_{\mathrm{AHS}}{}^2}{w_{\mathrm{net}}{}^2}\left\{\left[\frac{\eta_{\mathrm{AHS}}}{\eta_{\mathrm{B}}}\cdot\frac{b_{\mathrm{f}}}{\mathrm{LHV}}-1+\frac{\left(\Delta T_{\mathrm{HE}}+T_2\right)T_0}{T_{\mathrm{AHS}}{}^2}\right]^2-\frac{\dot{W}_{\mathrm{net}}}{\varepsilon_{\mathrm{h}}}\frac{\eta_{\mathrm{AHS}}\left(\Delta T_{\mathrm{HE}}+T_2\right)T_0}{C_{p,T_3}T_{\mathrm{AHS}}{}^3}\right\}.\end{aligned} \tag{4.62}$$

From Eqs (4.62), it is known that

$$\frac{\partial^2 \varepsilon_{\mathrm{h}}}{\partial \dot{Q}_{\mathrm{AHS}}{}^2} < 0, \tag{4.63}$$

when

$$\frac{\eta_{\mathrm{AHS}}}{\eta_{\mathrm{B}}} \cdot \frac{b_{\mathrm{f}}}{\mathrm{LHV}} - 1 + \frac{\left(\Delta T_{\mathrm{HE}} + T_2\right) T_0}{T_{\mathrm{AHS}}{}^2} = 0 \tag{4.64}$$

or

$$\frac{\partial \varepsilon_{\mathrm{h}}}{\partial \dot{Q}_{\mathrm{AHS}}} = 0 \tag{4.65}$$

from Eq. (4.50). This means that there might be a local maximum point on the ε_{h} - $\dot{Q}_{\mathrm{AHS}}$ curve.

What's more, as can be seen from Eq. (4.64), the temperature of the AHS T_{AHS} at the local maximal point (if exists) increases with the energy conversion efficiency of the AHS η_{AHS}.

4.1.4.3.2. *<u>Region in which the specific heat of working fluid at T_3 increases rapidly</u>*

When T_3 continues to increase, c_{p,T_3} cannot be assumed to be constant. Rewrite Eq. (4.44) as

$$\frac{\partial \varepsilon_{\mathrm{h}}}{\partial \dot{Q}_{\mathrm{AHS}}} = \frac{\varepsilon_{\mathrm{h}}{}^2}{\dot{W}_{\mathrm{net}}} \left[\frac{\eta_{\mathrm{AHS}}}{\eta_{\mathrm{B}}} \cdot \frac{b_{\mathrm{f}}}{\mathrm{LHV}} - 1 + \frac{T_0}{T_{\mathrm{AHS}}} \left(1 - \frac{h_3 - h_2}{c_{p,T_3} T_{\mathrm{AHS}}} \right) \right]. \tag{4.66}$$

Since

$$h_3 - h_2 = \int_{T_2}^{T_3} c_{p,T} \mathrm{d}T, \tag{4.67}$$

it can be found from Fig. 4-4 that

$$\frac{\partial\left(\frac{h_3 - h_2}{c_{p,T_3} T_{\mathrm{AHS}}}\right)}{\partial T_{\mathrm{AHS}}} \approx \frac{\partial\left(\frac{h_3 - h_2}{c_{p,T_3} T_3}\right)}{\partial T_{\mathrm{AHS}}} = \frac{\partial\left(\frac{h_3 - h_2}{c_{p,T_3} T_3}\right)}{\partial T_3} < 0, \tag{4.68}$$

meaning that $\frac{h_3 - h_2}{c_{p,T_3} T_{\mathrm{AHS}}}$ will decrease with increasing T_{AHS}. Using Eq. (4.44) and comparing with Eq. (4.49), we can see that the value of $\frac{\partial \varepsilon_{\mathrm{h}}}{\partial \dot{Q}_{\mathrm{AHS}}}$ is higher than when c_{p,T_3} is assumed to be constant. This further suggests that the ε_{h} - $\dot{Q}_{\mathrm{AHS}}$ curve is above the ε_{h} - $\dot{Q}_{\mathrm{AHS}}$ curve in which c_{p,T_3} were assumed to be constant.

4.1.4.3.3. <u>*Phase change region*</u>

When T_3 reaches the boiling point, i.e. $T_3 = T_{\mathrm{b}}$, from Eq. (4.47),

$$\frac{\partial^2 \varepsilon_{\mathrm{h}}}{\partial \dot{Q}_{\mathrm{AHS}}^{\ 2}} \geq 0, \tag{4.69}$$

meaning that the ε_{h}-$\dot{Q}_{\mathrm{AHS}}$ curve is convex during the phase change region ($T_3 = T_{\mathrm{b}}$).

4.1.4.3.4. Region in which the specific heat of working fluid at T_3 is close to the turbine inlet temperature, T_{TI}

When T_3 is close to the turbine inlet temperature, T_{TI}, it can be assumed that

$$h_3 - h_2 = \eta_{AHS} q_{in}. \tag{4.70}$$

Using Eq. (4.70), Eq. (4.44) becomes

$$\begin{aligned}\frac{\partial \varepsilon_h}{\partial \dot{Q}_{AHS}} &= \frac{\varepsilon_h}{\dot{B}_{in}}\left[\frac{\eta_{AHS}}{\eta_B}\cdot\frac{b_f}{LHV} - \left(1-\frac{T_0}{T_{AHS}}\right) - \left(h_3 - h_2\right)\frac{T_0}{c_{p,3}T_{AHS}^{\ 2}}\right] \\ &= \frac{\eta_{AHS}\varepsilon_h}{\dot{B}_{in}}\left(\frac{1}{\eta_B}\cdot\frac{b_f}{LHV} - \frac{1-\frac{T_0}{T_{AHS}}}{\eta_{AHS}} - \frac{q_{in}T_0}{c_{p,3}T_{AHS}^{\ 2}}\right).\end{aligned} \tag{4.71}$$

Considering

$$\begin{aligned}&\frac{1}{\eta_B}\cdot\frac{b_f}{LHV} - \frac{1-\frac{T_0}{T_{AHS}}}{\eta_{AHS}} - \frac{q_{in}T_0}{c_{p,3}T_{AHS}^{\ 2}} \\ &< \frac{1}{\eta_B}\cdot\frac{b_f}{LHV} - \left(1-\frac{T_0}{T_{AHS}}\right) - \frac{q_{in}T_0}{c_{p,3}T_{AHS}^{\ 2}} = \frac{1}{\eta_B}\cdot\frac{b_f}{LHV} - 1 - \frac{T_0}{T_{AHS}}\left(\frac{q_{in}}{c_{p,3}T_{AHS}} - 1\right)\end{aligned} \tag{4.72}$$

and in normal practice

$$\frac{1}{\eta_{\mathrm{B}}} \cdot \frac{b_{\mathrm{f}}}{\mathrm{LHV}} \approx 1, \tag{4.73}$$

$$q_{\mathrm{in}} > c_{p,3} T_{\mathrm{AHS}}, \tag{4.74}$$

it is known that when $T_3 \approx T_{\mathrm{TI}}$,

$$\frac{\partial \varepsilon_{\mathrm{h}}}{\partial \dot{Q}_{\mathrm{AHS}}} < 0, \tag{4.75}$$

meaning that ε_{h} will decrease with increasing $\dot{Q}_{\mathrm{AHS}}$ when T_3 is large enough. This further indicates that there is a local maximum ε_{h} when $T_{\mathrm{b}} \le T_3 < T_{\mathrm{TI}}$.

4.1.4.4. *Effect of the temperature of the additional heat source, T_{AHS}, on the exergy efficiency of the hybrid power generation systems based on the simple Rankine cycle, ε_{h}.*

To study the effect of the temperature of the additional heat source, T_{AHS}, on the exergy efficiency of the hybrid power generation systems based on the simple Rankine cycle, ε_{h}, we examine the partial derivatives of the exergy efficiency of the hybrid system, ε_{h}, with respect to the temperature of the AHS, T_{AHS}.

When $T_3 \neq T_{\mathrm{b}}$, from Eq. (4.5), the partial derivative of the exergy efficiency of the hybrid system, ε_{h}, with respect to the temperature of the AHS, T_{AHS}, is

$$\frac{\partial \varepsilon_{\mathrm{h}}}{\partial T_{\mathrm{AHS}}} = \frac{\partial \varepsilon_{\mathrm{h}}}{\partial h_3}\frac{\partial h_3}{\partial T_{\mathrm{AHS}}} = \frac{\varepsilon_{\mathrm{h}}}{b_{\mathrm{in}}}\left[\frac{1}{\eta_{\mathrm{B}}}\cdot\frac{b_{\mathrm{f}}}{\mathrm{LHV}} - \frac{1}{\eta_{\mathrm{AHS}}}\cdot\left(1-\frac{T_0}{T_{\mathrm{AHS}}}\right) - \frac{h_3-h_2}{\eta_{\mathrm{AHS}}}\frac{T_0}{c_{p,T_3}{T_{\mathrm{AHS}}}^2}\right]c_{p,T_3}$$
$$= \frac{{\varepsilon_{\mathrm{h}}}^2}{w_{\mathrm{net}}}\left[\frac{1}{\eta_{\mathrm{B}}}\cdot\frac{b_{\mathrm{f}}}{\mathrm{LHV}}c_{p,T_3} - \frac{1}{\eta_{\mathrm{AHS}}}\cdot\left(1-\frac{T_0}{T_{\mathrm{AHS}}}\right)c_{p,T_3} - \frac{h_3-h_2}{\eta_{\mathrm{AHS}}}\frac{T_0}{{T_{\mathrm{AHS}}}^2}\right].$$

(4.76)

When $T_3 = T_{\mathrm{b}}$, $\dfrac{\partial \varepsilon_{\mathrm{h}}}{\partial T_{\mathrm{AHS}}}$ cannot be defined since c_{p,T_3} is not continuous at this point as can be seen from Fig. 4-4 and $c_{p,T_3} = \dfrac{\partial h_3}{\partial T_{\mathrm{AHS}}}$ thus doesn't have meaning.

When $T_3 \neq T_{\mathrm{b}}$, the second-order partial derivative of the exergy efficiency of the hybrid system, ε_{h}, with respect to the temperature of the AHS, T_{AHS}, is

$$\begin{aligned}
\frac{\partial^2 \varepsilon_{\mathrm{h}}}{\partial {T_{\mathrm{AHS}}}^2} &= \frac{2{\varepsilon_{\mathrm{h}}}^3}{{w_{\mathrm{net}}}^2}\left[\frac{1}{\eta_{\mathrm{B}}}\cdot\frac{b_{\mathrm{f}}}{\mathrm{LHV}}c_{p,T_3} - \frac{1}{\eta_{\mathrm{AHS}}}\cdot\left(1-\frac{T_0}{T_{\mathrm{AHS}}}\right)c_{p,T_3} - \frac{h_3-h_2}{\eta_{\mathrm{AHS}}}\frac{T_0}{{T_{\mathrm{AHS}}}^2}\right]^2 \\
&- \frac{{\varepsilon_{\mathrm{h}}}^2}{w_{\mathrm{net}}}\left[\begin{array}{l}\dfrac{1}{\eta_{\mathrm{B}}}\cdot\dfrac{b_{\mathrm{f}}}{\mathrm{LHV}}\dfrac{\partial c_{p,T_3}}{\partial T_{\mathrm{AHS}}} - \dfrac{1}{\eta_{\mathrm{AHS}}}\cdot\dfrac{T_0}{{T_{\mathrm{AHS}}}^2}c_{p,T_3} \\ -\dfrac{1}{\eta_{\mathrm{AHS}}}\cdot\left(1-\dfrac{T_0}{T_{\mathrm{AHS}}}\right)\dfrac{\partial c_{p,T_3}}{\partial T_{\mathrm{AHS}}} - \dfrac{c_{p,T_3}}{\eta_{\mathrm{AHS}}}\dfrac{T_0}{{T_{\mathrm{AHS}}}^2} + 2\dfrac{h_3-h_2}{\eta_{\mathrm{AHS}}}\dfrac{T_0}{{T_{\mathrm{AHS}}}^3}\end{array}\right] \\
&= \frac{2\varepsilon_{\mathrm{h}}}{{b_{\mathrm{in}}}^2}\left[\frac{1}{\eta_{\mathrm{B}}}\cdot\frac{b_{\mathrm{f}}}{\mathrm{LHV}}c_{p,T_3} - \frac{1}{\eta_{\mathrm{AHS}}}\cdot\left(1-\frac{T_0}{T_{\mathrm{AHS}}}\right)c_{p,T_3} - \frac{h_3-h_2}{\eta_{\mathrm{AHS}}}\frac{T_0}{{T_{\mathrm{AHS}}}^2}\right]^2 \\
&- \frac{\varepsilon_{\mathrm{h}}}{b_{\mathrm{in}}}\left\{\left[\frac{1}{\eta_{\mathrm{B}}}\cdot\frac{b_{\mathrm{f}}}{\mathrm{LHV}} - \frac{1}{\eta_{\mathrm{AHS}}}\cdot\left(1-\frac{T_0}{T_{\mathrm{AHS}}}\right)\right]\frac{\partial c_{p,T_3}}{\partial T_{\mathrm{AHS}}} - 2\frac{c_{p,T_3}}{\eta_{\mathrm{AHS}}}\frac{T_0}{{T_{\mathrm{AHS}}}^2} + 2\frac{h_3-h_2}{\eta_{\mathrm{AHS}}}\frac{T_0}{{T_{\mathrm{AHS}}}^3}\right\},
\end{aligned} \tag{4.77}$$

When $T_3 = T_\mathrm{b}$, $\dfrac{\partial^2 \varepsilon_\mathrm{h}}{\partial T_\mathrm{AHS}{}^2}$ cannot be defined, since $\dfrac{\partial \varepsilon_\mathrm{h}}{\partial T_\mathrm{AHS}}$ cannot be defined as previously mentioned.

To further analyze Eqs (4.76) and (4.77), different scenarios must be analyzed respectively as T_3 rises.

4.1.4.4.1. *Region in which the specific heat of working fluid at T_3 almost remains constant*

According to Fig. 4-4, for T_3 up to about 200 °C and using Eq. (4.49), Eq. (4.76) can be written as

$$\begin{aligned}
\frac{\partial \varepsilon_\mathrm{h}}{\partial T_\mathrm{AHS}} &= \frac{\varepsilon_\mathrm{h}{}^2}{w_\mathrm{net}}\left[\frac{1}{\eta_\mathrm{B}}\cdot\frac{b_\mathrm{f}}{\mathrm{LHV}} - \frac{1}{\eta_\mathrm{AHS}}\cdot\left(1-\frac{T_0}{T_\mathrm{AHS}}\right) - \frac{c_{p,T_3}\left(T_3-T_2\right)}{\eta_\mathrm{AHS}}\frac{T_0}{c_{p,T_3}T_\mathrm{AHS}{}^2}\right]c_{p,T_3} \\
&= \frac{\varepsilon_\mathrm{h}{}^2}{w_\mathrm{net}}\left[\frac{\eta_\mathrm{AHS}}{\eta_\mathrm{B}}\cdot\frac{b_\mathrm{f}}{\mathrm{LHV}} - \left(1-\frac{T_0}{T_\mathrm{AHS}}\right) - \frac{\left(T_\mathrm{AHS}-\Delta T_\mathrm{HE}-T_2\right)T_0}{T_\mathrm{AHS}{}^2}\right]\frac{c_{p,T_3}}{\eta_\mathrm{AHS}} \\
&= \frac{\varepsilon_\mathrm{h}{}^2}{w_\mathrm{net}}\left[\frac{\eta_\mathrm{AHS}}{\eta_\mathrm{B}}\cdot\frac{b_\mathrm{f}}{\mathrm{LHV}} - 1 + \frac{\left(\Delta T_\mathrm{HE}+T_2\right)T_0}{T_\mathrm{AHS}{}^2}\right]\frac{c_{p,T_3}}{\eta_\mathrm{AHS}}.
\end{aligned} \tag{4.78}$$

The second-order partial derivative of the exergy efficiency of the hybrid system ε_h with respect to the temperature of the AHS T_AHS is

$$\frac{\partial^2 \varepsilon_{\mathrm{h}}}{\partial T_{\mathrm{AHS}}{}^2} = \left\{ \begin{array}{l} \dfrac{2\varepsilon_{\mathrm{h}}{}^3}{w_{\mathrm{net}}{}^2}\left[\dfrac{\eta_{\mathrm{AHS}}}{\eta_{\mathrm{B}}} \cdot \dfrac{b_{\mathrm{f}}}{\mathrm{LHV}} - 1 + \dfrac{(\Delta T_{\mathrm{HE}} + T_2)T_0}{T_{\mathrm{AHS}}{}^2} \right]^2 c_{p,T_3}{}^2 \\ + \dfrac{\varepsilon_{\mathrm{h}}{}^2}{w_{\mathrm{net}}}\left[-2\dfrac{(\Delta T_{\mathrm{HE}} + T_2)T_0}{T_{\mathrm{AHS}}{}^3} c_{p,T_3} \right] \end{array} \right\}$$

$$= \frac{2\varepsilon_{\mathrm{h}}{}^3}{w_{\mathrm{net}}{}^2}\left\{ \left[\frac{\eta_{\mathrm{AHS}}}{\eta_{\mathrm{B}}} \cdot \frac{b_{\mathrm{f}}}{\mathrm{LHV}} - 1 + \frac{(\Delta T_{\mathrm{HE}} + T_2)T_0}{T_{\mathrm{AHS}}{}^2} \right]^2 c_{p,T_3}{}^2 - \frac{w_{\mathrm{net}}}{\varepsilon_{\mathrm{h}}} \frac{(\Delta T_{\mathrm{HE}} + T_2)T_0}{T_{\mathrm{AHS}}{}^3} c_{p,T_3} \right\}$$

$$= \frac{2\varepsilon_{\mathrm{h}}{}^3 c_{p,T_3}{}^2}{w_{\mathrm{net}}{}^2}\left\{ \left[\frac{\eta_{\mathrm{AHS}}}{\eta_{\mathrm{B}}} \cdot \frac{b_{\mathrm{f}}}{\mathrm{LHV}} - 1 + \frac{(\Delta T_{\mathrm{HE}} + T_2)T_0}{T_{\mathrm{AHS}}{}^2} \right]^2 - \frac{w_{\mathrm{net}}}{\varepsilon_{\mathrm{h}}} \frac{(\Delta T_{\mathrm{HE}} + T_2)T_0}{c_{p,T_3} T_{\mathrm{AHS}}{}^3} \right\}. \tag{4.79}$$

From Eqs (4.79) and (4.78), it is known that

$$\frac{\partial^2 \varepsilon_{\mathrm{h}}}{\partial T_{\mathrm{AHS}}{}^2} < 0, \tag{4.80}$$

when

$$\frac{\partial \varepsilon_{\mathrm{h}}}{\partial T_{\mathrm{AHS}}} = 0. \tag{4.81}$$

This means that there might be a maximum point on the ε_{h}-T_{AHS} curve.

What's more, as can be seen from Eqs (4.78) and (4.81), the temperature of the AHS, T_{AHS}, at the maximum point (if exists) increases with the energy conversion efficiency of the AHS η_{AHS}.

4.1.4.4.2. Region in which the specific heat of working fluid at T_3 increases rapidly

When T_3 continues to increase so that c_{p,T_3} cannot be assumed to be constant, using Eqs (4.76) and (4.68), and comparing with Eq. (4.78), we can see that the value of $\frac{\partial \varepsilon_{\mathrm{h}}}{\partial T_{\mathrm{AHS}}}$ is higher than when c_{p,T_3} is assumed to be constant. This further suggests that the ε_{h}-T_{AHS} curve is above the ε_{h}-T_{AHS} curve when c_{p,T_3} were assumed to be constant.

4.1.4.4.3. Region in which the specific heat of working fluid at T_3 is close to the turbine inlet temperature, T_{TI}

When $T_3 \approx T_{\mathrm{TI}}$, substituting Eq. (4.70) into Eq. (4.76), we have

$$\frac{\partial \varepsilon_{\mathrm{h}}}{\partial T_{\mathrm{AHS}}} = \frac{\varepsilon_{\mathrm{h}}}{b_{\mathrm{in}}}\left[\frac{1}{\eta_{\mathrm{B}}} \cdot \frac{b_{\mathrm{f}}}{\mathrm{LHV}} - \frac{1}{\eta_{\mathrm{AHS}}} \cdot \left(1 - \frac{T_0}{T_{\mathrm{AHS}}}\right) - q_{\mathrm{in}} \frac{T_0}{c_{p,T_3} T_{\mathrm{AHS}}^{\ 2}}\right] c_{p,T_3}. \quad (4.82)$$

According to Eqs (4.72)-(4.74), it is known that when $T_3 \approx T_{\mathrm{TI}}$,

$$\frac{\partial \varepsilon_{\mathrm{h}}}{\partial T_{\mathrm{AHS}}} < 0, \quad (4.83)$$

meaning that ε_{h} will decrease with increasing T_{AHS} when T_3 is large enough. This further indicates that there is a local maximum ε_{h} when $T_{\mathrm{b}} \le T_3 < T_{\mathrm{TI}}$.

In fact, when $T_3 \neq T_{\mathrm{b}}$, since

$$\frac{\partial \varepsilon_{\mathrm{h}}}{\partial T_{\mathrm{AHS}}} = \frac{\partial \varepsilon_{\mathrm{h}}}{\partial \dot{Q}_{\mathrm{AHS}}} \frac{\partial \dot{Q}_{\mathrm{AHS}}}{\partial T_{\mathrm{AHS}}} = \frac{\partial \varepsilon_{\mathrm{h}}}{\partial \dot{Q}_{\mathrm{AHS}}} \frac{C_{p,T_3}}{\eta_{\mathrm{AHS}}}, \tag{4.84}$$

we can see that $\frac{\partial \varepsilon_{\mathrm{h}}}{\partial T_{\mathrm{AHS}}}$ and $\frac{\partial \varepsilon_{\mathrm{h}}}{\partial \dot{Q}_{\mathrm{AHS}}}$ have the same sign, meaning that the ε_{h}-T_{AHS} curve will rise when the ε_{h}-$\dot{Q}_{\mathrm{AHS}}$ curve rises and the ε_{h}-T_{AHS} curve will fall down when the ε_{h}-$\dot{Q}_{\mathrm{AHS}}$ curve falls down. When

$$\frac{\partial \varepsilon_{\mathrm{h}}}{\partial \dot{Q}_{\mathrm{AHS}}} = 0, \tag{4.85}$$

there is

$$\frac{\partial \varepsilon_{\mathrm{h}}}{\partial T_{\mathrm{AHS}}} = 0. \tag{4.86}$$

Also, since

$$\frac{\partial^2 \varepsilon_{\mathrm{h}}}{\partial T_{\mathrm{AHS}}{}^2} = \frac{\partial\left(\frac{\partial \varepsilon_{\mathrm{h}}}{\partial \dot{Q}_{\mathrm{AHS}}} \frac{C_{p,T_3}}{\eta_{\mathrm{AHS}}}\right)}{\partial T_{\mathrm{AHS}}} = \frac{\partial^2 \varepsilon_{\mathrm{h}}}{\partial \dot{Q}_{\mathrm{AHS}}{}^2}\left(\frac{C_{p,T_3}}{\eta_{\mathrm{AHS}}}\right)^2 + \frac{\partial \varepsilon_{\mathrm{h}}}{\partial \dot{Q}_{\mathrm{AHS}}} \frac{\partial C_{p,T_3}}{\partial T_{\mathrm{AHS}}} \frac{1}{\eta_{\mathrm{AHS}}} \tag{4.87}$$

and $\frac{\partial^2 \varepsilon_{\mathrm{h}}}{\partial \dot{Q}_{\mathrm{AHS}}{}^2} < 0$ when $\frac{\partial \varepsilon_{\mathrm{h}}}{\partial \dot{Q}_{\mathrm{AHS}}} = 0$ from previous results (Eqs (4.63)-(4.65)), we can see that

$$\frac{\partial^2 \varepsilon_{\mathrm{h}}}{\partial T_{\mathrm{AHS}}{}^2} < 0, \tag{4.88}$$

when

$$\frac{\partial \varepsilon_{\mathrm{h}}}{\partial T_{\mathrm{AHS}}} = \frac{\partial \varepsilon_{\mathrm{h}}}{\partial \dot{Q}_{\mathrm{AHS}}} = 0, \tag{4.89}$$

meaning that there might be local maximum point on the ε_{h}-T_{AHS} curve.

4.1.4.5. *Conclusions of the sensitivity analysis of the hybrid power generation systems based on the simple Rankine cycle, with respect to the AHS*

The results in Sections 4.1.4.1-4.1.4.4 are summarized in Table 4-1.

Table 4-1. Summary results of the sensitivity analysis of the hybrid power generation systems based on the simple Rankine cycle with respect to the AHS

Conditions	Results	Comments
$\eta_{\mathrm{AHS}} \neq \eta_{\mathrm{B}}$	$\frac{\partial^2 \eta_{\mathrm{h}}}{\partial \dot{Q}_{\mathrm{AHS}}{}^2} > 0$	The η_{h}-$\dot{Q}_{\mathrm{AHS}}$ curve is convex
$\eta_{\mathrm{AHS}} = \eta_{\mathrm{B}}$	$\frac{\partial^2 \eta_{\mathrm{h}}}{\partial \dot{Q}_{\mathrm{AHS}}{}^2} = 0$	The η_{h}-$\dot{Q}_{\mathrm{AHS}}$ is a straight line

$\eta_{\text{AHS}} > \eta_{\text{B}}$ and $T_3 < T_{\text{b}}$	$\frac{\partial^2 \eta_{\text{h}}}{\partial T_{\text{AHS}}{}^2} > 0$	The η_{h}-T_{AHS} curve is convex
$\eta_{\text{AHS}} < \eta_{\text{B}}$ and $T_3 > T_{\text{b}}$	$\frac{\partial^2 \eta_{\text{h}}}{\partial T_{\text{AHS}}{}^2} > 0$	The η_{h}-T_{AHS} curve is convex
$\frac{\partial c_{p,T_3}}{\partial T_3} = 0$ and $T_{\text{AHS}} < \left[\frac{\left(\Delta T_{\text{HE}} + T_2\right) T_0}{1 - \frac{\eta_{\text{AHS}}}{\eta_{\text{B}}} \cdot \frac{b_{\text{f}}}{\text{LHV}}} \right]^{\frac{1}{2}}$	$\frac{\partial \varepsilon_{\text{h}}}{\partial \dot{Q}_{\text{AHS}}} > 0$	The ε_{h}-$\dot{Q}_{\text{AHS}}$ curve is convex
$\frac{\partial c_{p,T_3}}{\partial T_3} = 0$ and $T_{\text{AHS}} > \left[\frac{\left(\Delta T_{\text{HE}} + T_2\right) T_0}{1 - \frac{\eta_{\text{AHS}}}{\eta_{\text{B}}} \cdot \frac{b_{\text{f}}}{\text{LHV}}} \right]^{\frac{1}{2}}$	$\frac{\partial \varepsilon_{\text{h}}}{\partial \dot{Q}_{\text{AHS}}} < 0$	The ε_{h}-$\dot{Q}_{\text{AHS}}$ curve is concave

$\frac{\partial c_{p,T_3}}{\partial T_3} = 0$ and $\frac{\partial \varepsilon_h}{\partial \dot{Q}_{AHS}} = 0$	$\frac{\partial^2 \varepsilon_h}{\partial \dot{Q}_{AHS}^{\ 2}} < 0$ and $\frac{\partial^2 \varepsilon_h}{\partial T_{AHS}^{\ 2}} < 0$	There might be a local maximum ε_h when $T_3 < T_b$
$\frac{\partial c_{p,T_3}}{\partial T_3} > 0$	The value of $\frac{\partial \varepsilon_h}{\partial \dot{Q}_{AHS}}$ ($\left(\frac{\partial \varepsilon_h}{\partial T_{AHS}}\right)$) is higher than the value of $\frac{\partial \varepsilon_h}{\partial \dot{Q}_{AHS}}$ ($\left(\frac{\partial \varepsilon_h}{\partial T_{AHS}}\right)$) when c_{p,T_3} is assumed to be constant	The ε_h - $\dot{Q}_{AHS}$ (ε_h - T_{AHS}) curve is above the ε_h - $\dot{Q}_{AHS}$ (ε_h - T_{AHS}) curve in which c_{p,T_3} were assumed to be constant when $T_3 < T_b$
$T_3 = T_b$	$\frac{\partial^2 \varepsilon_h}{\partial \dot{Q}_{AHS}^{\ 2}} \geq 0$	Phase change region
$T_3 \approx T_{TI}$	$\frac{\partial \varepsilon_h}{\partial \dot{Q}_{AHS}} < 0$ and $\frac{\partial \varepsilon_h}{\partial T_{AHS}} < 0$	There is a local maximum ε_h when $T_b \leq T_3 < T_{TI}$

Table 4-1 can be used to give guidance for hybrid systems design in the following ways:

1) When the curve is convex, it means that adding the same amount of AHS ($\dot{Q}_{\mathrm{AHS}}$) or increasing the same amount of AHS temperature (T_{AHS}) to the already hybridized system will have higher energy efficiency (η_{h}) and exergy efficiency (ε_{h}) than to a non-hybridized reference system.
2) When the curve is concave, it means that it is better to add $\dot{Q}_{\mathrm{AHS}}$ or increase T_{AHS} for the non-hybridized system. It also indicates that the energy and exergy efficiency of the system may decline when adding too much $\dot{Q}_{\mathrm{AHS}}$ or increasing T_{AHS} too much (the extent to which "how much" is determined based on the operation parameters of the system and cannot be determined using thermodynamic analysis alone. As an example, the actual values of $\dot{Q}_{\mathrm{AHS}}$ and T_{AHS} that decrease the systems efficiencies are shown in the simulation results in Section 4.1.5). This finding lets designers have the idea that increasing $\dot{Q}_{\mathrm{AHS}}$ or T_{AHS} may not keep systems efficiencies increasing, even if it does at the beginning.
3) When there is a maximal point on a curve, it means that there is local point, at which the energy or exergy efficiency is maximized, at least locally for a certain range (may also be gloabally maximum in the whole range of the variable). The location of the maximum varies depending on the operation parameter of the system, but the designers will know the existence of this point, from the thermodynamic results

summarized in Table 4-1 (can be found in the “comments” column when “local maximum” is mentioned), before detailed calculation, and are thereby encouraged to find this point.

To demonstrate and help understanding of the thermodynamic results summarized in Table 4-1, a series of simulation studies was performed. It is shown in Section 4.1.5.2 how the energy and exergy efficiencies change with $\dot{Q}_{\mathrm{AHS}}$ and T_{AHS}. The designers will then have confidence on the thermodynamic results and are able to use the graphs shown in the simulation to determine which $\dot{Q}_{\mathrm{AHS}}$ and T_{AHS} to choose for attaining higher energy or exergy efficiency.

4.1.5. Simulation of hybrid power generation systems based on the simple Rankine cycle

To confirm the previous thermodynamic analysis results and show explicitly the relation between η_{h} or ε_{h} and $\dot{Q}_{\mathrm{AHS}}$ or T_{AHS}, the following simulation examples are made using Aspen Plus® [1].

4.1.5.1. *Validation*

Before using the simulation model to analyze the hybrid power generation systems based on the simple Rankine cycle, the model and its results are validated. To do that, the simulation model was first run using the operation parameters given in the reference paper from an outside source used for the validation comparison. The results from the simulation

were then compared with the results given by the outside reference. The simulation model is said to be validated when the relative errors are small (e.g. less than 1%). The reference Rankine cycle is configured based on Fig. 4-1, whose operation parameters are mainly based on a real steam power plant analysis [2] and shown in Table 4-2. The measures often designed to increase the efficiency or net power output of the plant such as reheat, regeneration, and multi-stage steam turbine etc. in the real power plant are not included in the plant and its simulation. The analysis was performed for a water mass flow rate of 1 kg/s, and the mass flow rate of CH_4 and air are adjusted by the software (trial and error) so that the turbine inlet temperature reaches the design value of 540 °C. The simulation results for each state point in Fig. 4-1 are shown in Table 4-3.

Table 4-2. Important input parameters for simulation in the reference power generation systems based on the simple Rankine cycle (*Fig. 4-1*)

Name	Value
Mass flow rate of water $\left(\dot{m}_{w}\right)$	1 kg/s
Mass flow rate of CH_4 $\left(\dot{m}_{f}\right)$	0.06843 kg/s
Mass flow rate of air $\left(\dot{m}_{a}\right)$	1.413 kg/s (20% excess air)
Mass flow rate of cooling water $\left(\dot{m}_{cw}\right)$	36 kg/s

Air and CH_4 inlet temperatures $(T_a,\ T_f)$	17 °C
Air and CH_4 inlet pressures $(p_a,\ p_f)$	100 kPa
Turbine inlet temperature (T_3)	540 °C
Condenser outlet pressure (p_4)	6.667 kPa
Pump outlet pressure (p_1)	14.3965 MPa
Condensate extraction pump efficiency (η_{CEP})	0.98
Turbine isentropic efficiency (η_T)	0.85

Table 4-3. Aspen Plus simulation results for each state point in Fig. 4-1

State	m [kg/s]	T [C]	p [kPa]	h [kJ/kg]	s [kJ/kg-K]
1	1	38.1	6.667	159.6	0.5469
2	1	38.6	14,396.5	174.4	0.5479915
3	1	540.0	14,396.5	3,429.8	6.514969

4	1	38.1	6.667	2,229.0	7.195786
CH4	0.06843	17	100	11,306.7	4.34376
Air	1.413	17	100	15,962.3	9.547446
Flue gas	1.48143	120	100	13,549.8	9.736563
6	36	24.5	3,102	105.6	0.359419
7	36	37.8	5,471	163.1	0.540556

To validate the simulation results generated by Aspen Plus, we repeat the calculation processes described in the thermodynamic analysis by using the Engineering Equation Solver (EES [3]) that also contains steam and air properties. The state points and calculation results are shown in Fig. 4-5, in which numbers written in the squares are the input values and the others are the calculated output values (the calculation results). Comparison of some important results given by these two methods are given in Table 4-4. It can be seen that the results are quite close to each other, with differences probably caused by different property methods used and calculation approximation errors, etc. Such small differences are within the error band of the analysis. The simulation made by Aspen was thereby validated, and Aspen Plus will be used alone to simulate the remaining types of systems in this chapter.

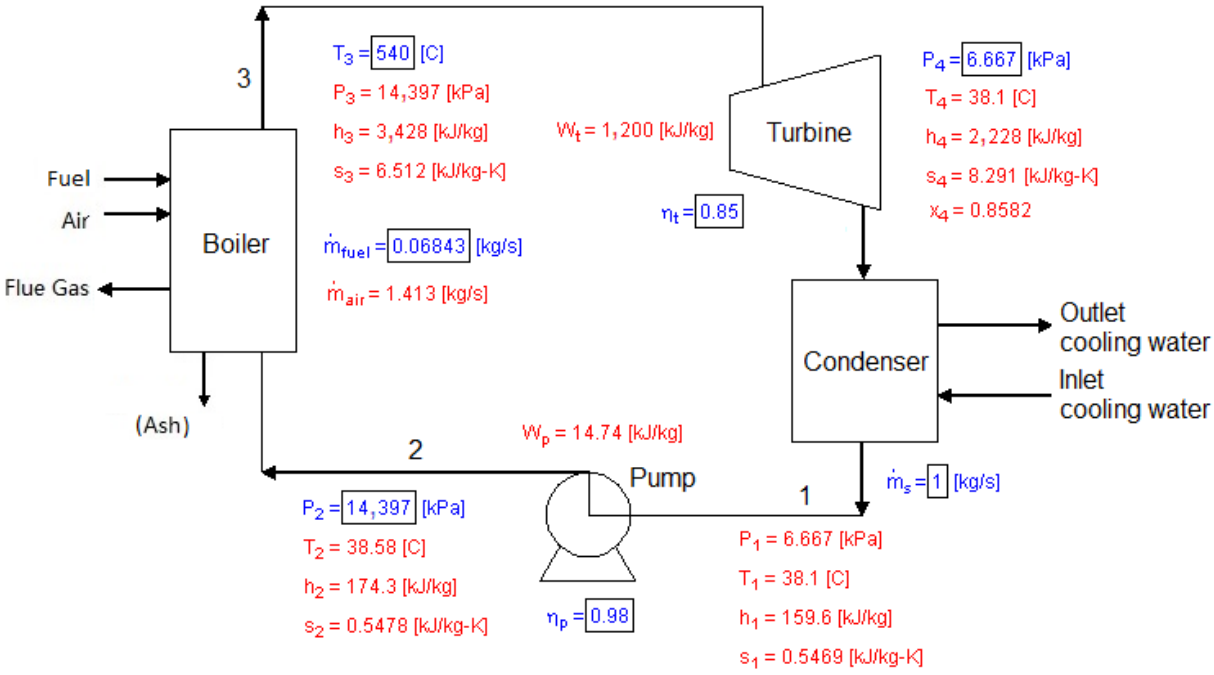

Fig. 4-5 The simple Rankine systems results by using EES (equivalent to manual validation) based on the shown state points

Table 4-4. Comparison of the results obtained by using Aspen Plus and EES.

Results	Aspen	EES
Energy input rate $\dot{Q}_{in}$ (kW)	3,431.42	3,431.00
Exergy input rate $\dot{B}_{in}$ (kW)	3,577.65	3,578.00
Turbine power output $\dot{W}_T$ (kW)	1,200.77	1,200.00

Pump power input $\dot{W}_{CEP}$ (kW)	14.79	14.74
Energy efficiency η_0 (%)	34.56	34.55
Exergy efficiency ε_0 (%)	33.15	33.13

4.1.5.2. *Simulation results of the hybrid power generation systems based on the simple Rankine cycle*

The simulation is done by Aspen Plus and its PR-BM thermodynamic model[4] was selected to calculate the thermodynamic properties. The main assumptions for the simulation are listed in Table 4-2. To consider the effect of pressure loss in reality, the pressure losses for all heat exchange processes are, as often assumed in such systems, 2% of the inlet pressure.

The power system energy efficiency, η_h, was computed for energy conversion efficiencies of the AHS, η_{AHS}, of 40%, 60%, 80%, 95.2% and 100%. η_{AHS} = 95.2% is the energy conversion efficiency of the fuel, i.e. the boiler efficiency, based on the assumptions in Table 4-2. $\eta_{AHS} = 100\%$ represents the ideal case in which all of the AHS heat input is absorbed by the working fluid and used to increase its enthalpy.

Fig. 4-3 showed the computed T-s diagram for the hybrid power generation systems based on the simple Rankine cycle. It can be seen that heat from the additional heat

[4] PR-BM is an enhanced model relative to PR which is widely used by researcher in simulation involving carbohydrate (methane).

source (Q_{AHS}) is used to heat the working liquid from state point 2 to 3, and the heat from burning the fuel (Q_{f}) is used to further heat the working fluid from state point 3 (liquid phase) to 4 (superheated steam).

The relation between the energy efficiency of the hybrid system, η_{h}, and the additional heat source (AHS) heat addition rate, $\dot{Q}_{\text{AHS}}$, (based on the chosen value of η_{AHS}) for the hybrid power generation systems based on the simple Rankine cycle was shown in Fig. 4-6. The results show that for the same enthalpy states h_1 *to* h_5 in the hybrid and reference systems, the energy efficiency of the hybrid system is higher than that of the reference system (in which $\dot{Q}_{\text{AHS}} = 0$) if and only if the energy conversion efficiency of the AHS is higher than that of the original heat source (fuel). This result demonstrates and confirms Eqs (4.9)-(4.11). Fig. 4-6 also shows that the energy efficiency of the hybrid increases with $\dot{Q}_{\text{AHS}}$ when Eq. (4.9) is satisfied and decreases with increasing $\dot{Q}_{\text{AHS}}$ when Eq. (4.11) is satisfied. This result demonstrates and confirms Eq. (4.33). When $\eta_{\text{AHS}} \neq \eta_{\text{B}}$, the convexity of the curves in Fig. 4-6 demonstrates and confirms Eq. (4.34).

Considering that the simulation includes the effects of the pressure loss in the heat transfer process and the equation derivations mostly do not, the correspondence of the simulation results and equation derivations shows that the effects of the pressure loss can indeed be ignored in the thermodynamic analysis.

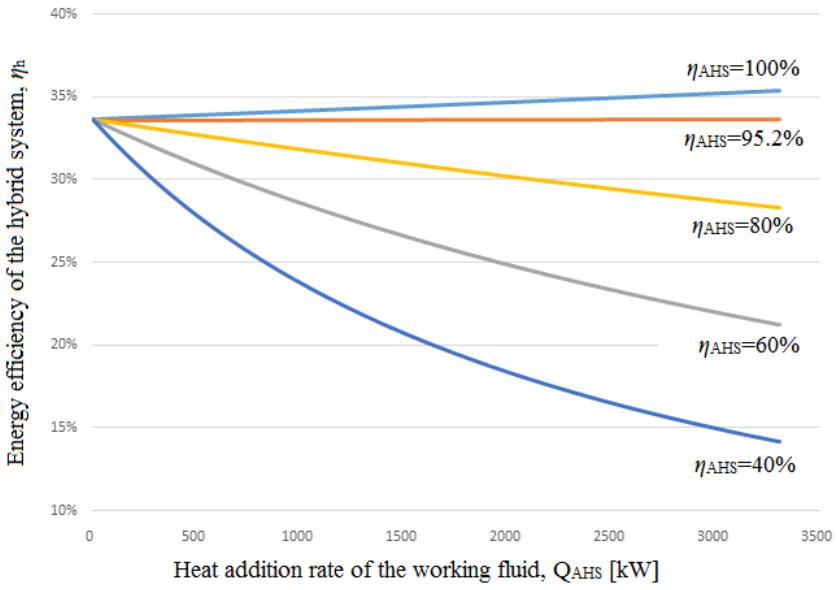

Fig. 4-6. The relation between the energy efficiency of the hybrid system, η_h, and the additional heat source (AHS) heat addition rate, $\dot{Q}_{AHS}$, for the hybrid power generation systems based on the simple Rankine cycle (η_{AHS} is the energy conversion efficiency of the AHS)

Fig. 4-7 shows the relation between the energy efficiency of the hybrid system, η_h, and the temperature of the additional heat source (AHS), T_{AHS}, for the hybrid power generation systems based on the simple Rankine cycle. The results showed that η_h changes with T_{AHS} in almost the same way as with $\dot{Q}_{AHS}$ in Fig. 4-6, except that there is a sharp change of η_h at $T_{AHS} = 358\,°C$, which is the vaporization temperature of the working fluid at the pressure at about 14 MPa, because this is the phase change region in which the temperature does not change even though the enthalpy of the working fluid rises. For $\eta_{AHS} \neq \eta_B$ and

the AHS is used to vaporize the working fluid, the heat addition rate of the AHS, $\dot{Q}_{\mathrm{AHS}}$, affects the hybrid system energy efficiency, η_{h}, based on Eq. (4.33), while the temperature of the AHS T_{AHS} does not change, thus resulting in a sharp change in η_{h} with T_{AHS} in Fig. 4-7. Based on Eqs (4.9) and (4.11), the step is up when $\eta_{\mathrm{AHS}} = 100\% > \eta_{\mathrm{B}} = 95.3\%$ and is down when $\eta_{\mathrm{AHS}} < \eta_{\mathrm{B}} = 95.3\%$. When the phase change pressure is higher than the critical pressure of the working fluid (22.06 MPa for water), there is no sharp change of η_{h} if T_{AHS} is changed.

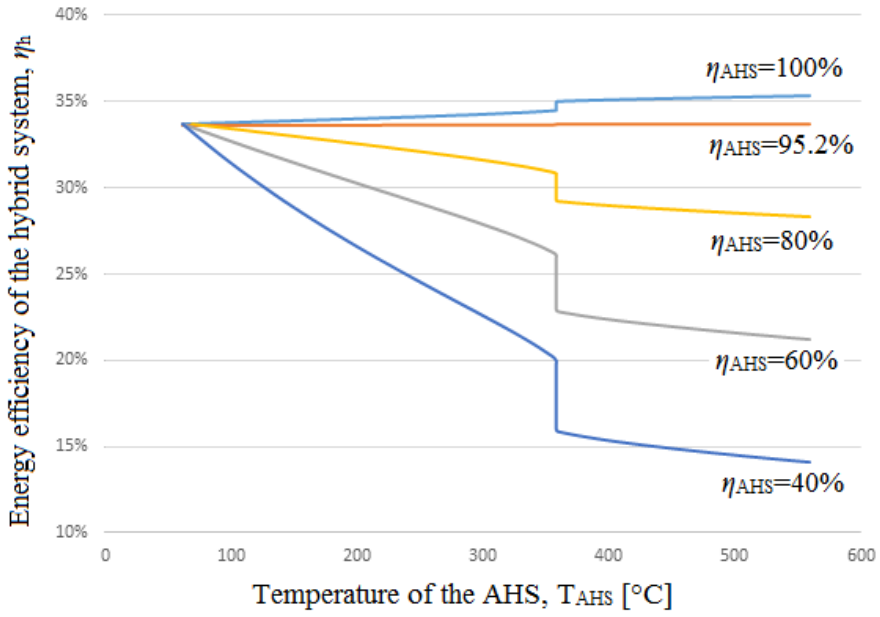

Fig. 4-7. The relation between the energy efficiency of the hybrid system, η_{h}, and the temperature of the additional heat source (AHS), T_{AHS}, for the hybrid power generation systems based on the simple Rankine cycle (η_{AHS} is the energy conversion efficiency of the AHS)

Fig. 4-8 showed the relation between the exergy efficiency of the hybrid system, ε_{h}, and the additional heat source (AHS) heat addition rate, $\dot{Q}_{\mathrm{AHS}}$, for the hybrid power generation systems based on the simple Rankine cycle. It can be seen that there might be a local maximum when $\dot{Q}_{\mathrm{AHS}}$ is small. When $\eta_{\mathrm{AHS}} = 40\%$, there is a maximum point. When $\eta_{\mathrm{AHS}} = 60\%$, there is also a maximum point, (though hard to see in the figure) at $T_{\mathrm{AHS}} = 1,202$ °C. These results demonstrate and confirm Eqs (4.63)-(4.65). When $\eta_{\mathrm{AHS}} > 60\%$, there is no maximum point when the AHS is not used to vaporize the working fluid (i.e. when $\dot{Q}_{\mathrm{AHS}}$ is lower than 1,600 kW). When the AHS is used to vaporize the working fluid (i.e. when $\dot{Q}_{\mathrm{AHS}}$ is between 1,600 to 2,700 kW), the curves are convex, confirming Eq. (4.69). When the AHS is also used to superheat the working fluid (i.e. when $\dot{Q}_{\mathrm{AHS}}$ is higher than 2,700 kW), there is a maximum point when the η_{AHS} is high enough, confirming Eq. (4.75).

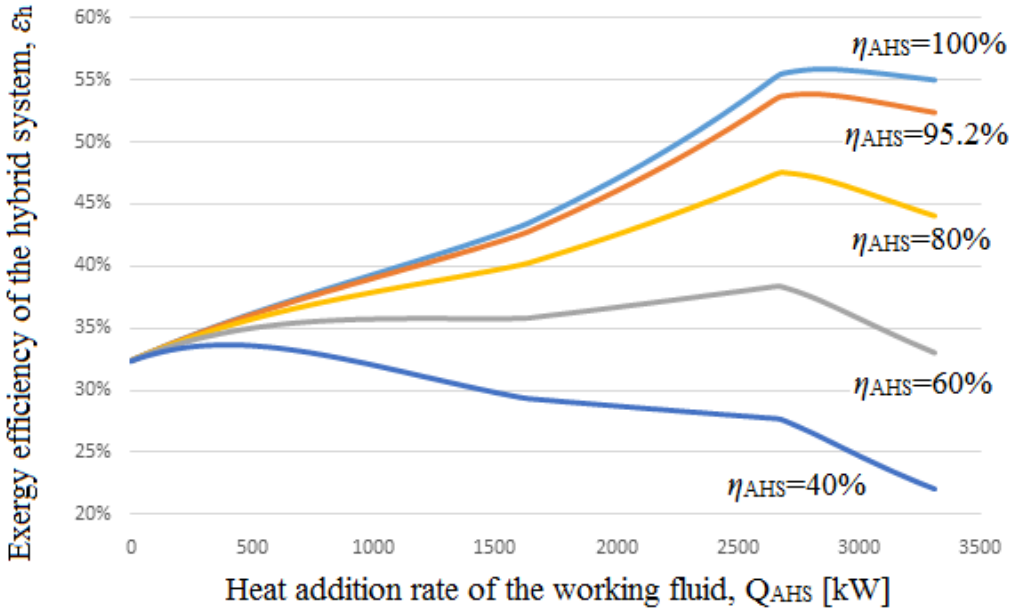

Fig. 4-8. The relation between the exergy efficiency of the hybrid system, ε_h, and the additional heat source (AHS) heat addition rate, $\dot{Q}_{AHS}$, for the hybrid power generation systems based on the simple Rankine cycle (η_{AHS} is the energy conversion efficiency of the AHS)

Fig. 4-9 showed the relation between the exergy efficiency of the hybrid system, ε_h, and the temperature of the additional heat source (AHS), T_{AHS}, for a hybrid power generation systems based on the simple Rankine cycle. The shapes of the curves are almost the same as ones in Fig. 4-8, except that there is a step-jump in the phase change region and the slopes are slightly different based on Eq. (4.84). Based on Eq. (4.45), the step is up when $\frac{\eta_{AHS}}{\eta_B}\cdot\frac{b_f}{LHV}>\left(1-\frac{T_0}{T_{AHS}}\right)$ and down when $\frac{\eta_{AHS}}{\eta_B}\cdot\frac{b_f}{LHV}<\left(1-\frac{T_0}{T_{AHS}}\right)$.

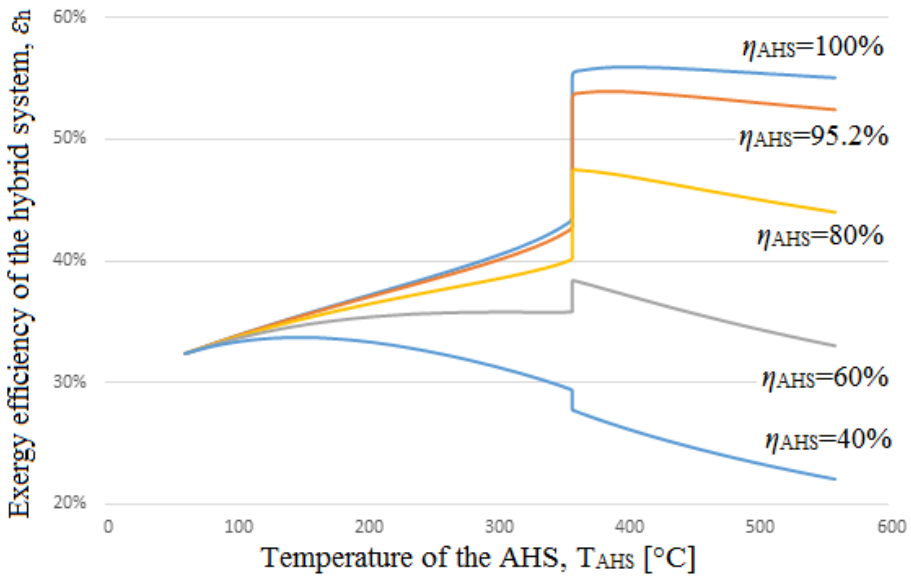

Fig. 4-9. The relation between the exergy efficiency of the hybrid system, ε_h, and the temperature of the additional heat source (AHS), T_{AHS}, for the hybrid power generation systems based on the simple Rankine cycle (η_{AHS} is the energy conversion efficiency of the AHS)

Designers can use Fig. 4-8 and Fig. 4-9 to help design the hybrid system shown in Fig. 4-2. When the energy conversion efficiency of the AHS, η_{AHS}, is not too low (such as larger than 40% in the simulation here), the designers will know that adding a small amount of AHS to the reference system will increase the exergy efficiency, meaning that the hybrid system will have a higher exergy efficiency than the reference system shown in Fig. 4-1. When the η_{AHS} is not large enough, say 40-60%, there will be a local maximum point, in the preheating region (when the working fluid is in the form of liquid). Designers should try to find this point if they want to achieve the highest system exergy efficiency. On the

other hand, in the phase change region, the designers will know that the exergy efficiency changes monotonically with the $\dot{Q}_{\text{AHS}}$, and there is no need to waste time in calculating the exergy efficiency of the system in this region. When the working fluid is superheated, there is always a local maximum point, since the curve is always downwarding. Designers can thereby focus more on the beginning of the superheated phase, and no need to worry about the remaining region. These understandings and strategies save designers lots of time and effort in finding the maximum point and therefore help them design the hybrid system.

4.1.6. Conclusions about the hybrid power generation systems based on the simple Rankine cycle

The results from the thermodynamic analysis and simulation of hybrid power generation systems based on the simple Rankine showed that

- for the same enthalpy states in the hybrid and reference systems, the energy efficiency of the hybrid system is higher than that of the reference single heat source system if and only if the energy conversion efficiency (defined in Eq. (4.1)) of the AHS is larger than that of the heat source used in the reference single heat source system, i.e. $\eta_{\text{h}} < \eta_0$ for $\left(\eta_{\text{AHS}} < \eta_{\text{HTHS}}\right)$, $\eta_{\text{h}} = \eta_0$ for $\left(\eta_{\text{AHS}} = \eta_{\text{HTHS}}\right)$ and $\eta_{\text{h}} > \eta_0$ for $\left(\eta_{\text{AHS}} > \eta_{\text{HTHS}}\right)$;
- for the same enthalpy states in the hybrid and reference systems, the exergy efficiency of the hybrid system is higher than that of the reference single heat source

system if and only if the exergy conversion efficiency (defined in Eqs (4.21) and (4.22)) of the AHS is larger than that of the heat source used in the reference single heat source system, i.e. $\varepsilon_{\mathrm{h}} < \varepsilon_0$ for $\left(\eta'_{\mathrm{AHS}} < \eta'_{\mathrm{HTHS}}\right)$, $\varepsilon_{\mathrm{h}} = \varepsilon_0$ for $\left(\eta'_{\mathrm{AHS}} = \eta'_{\mathrm{HTHS}}\right)$ and $\varepsilon_{\mathrm{h}} > \varepsilon_0$ for $\left(\eta'_{\mathrm{AHS}} > \eta'_{\mathrm{HTHS}}\right)$;

- the η_{h}-$\dot{Q}_{\mathrm{AHS}}$ curve is convex unless $\eta_{\mathrm{AHS}} = \eta_{\mathrm{B}}$, in which case η_{h} doesn't change with $\dot{Q}_{\mathrm{AHS}}$;
- when $T_3 < T_{\mathrm{b}}$ and $\eta_{\mathrm{AHS}} > \eta_{\mathrm{B}}$, η_{h} will increase with T_{AHS}, the η_{h}-T_{AHS} curve is convex and the convexity increases with T_{AHS};
- when $T_3 > T_{\mathrm{b}}$ and $\eta_{\mathrm{AHS}} < \eta_{\mathrm{B}}$, η_{h} will decrease with increasing T_{AHS}, the η_{h}-T_{AHS} curve is convex and the convexity increases with T_{AHS};
- when $T_3 < T_{\mathrm{b}}$, there might be a local maximum point on the ε_{h}-$\dot{Q}_{\mathrm{AHS}}$ curve and T_{AHS} at the local maximum point (if exists) increases with η_{AHS};
- when $T_3 < T_{\mathrm{b}}$, the ε_{h}-$\dot{Q}_{\mathrm{AHS}}$ curve is above the ε_{h}-$\dot{Q}_{\mathrm{AHS}}$ curve in which c_{p,T_3} were assumed to be constant;
- When $T_3 = T_{\mathrm{b}}$ (in the phase change region), the ε_{h}-$\dot{Q}_{\mathrm{AHS}}$ curve is convex;
- when $T_3 \geq T_{\mathrm{b}}$, there is a local maximum point in the ε_{h}-$\dot{Q}_{\mathrm{AHS}}$ curve;
- when $T_3 < T_{\mathrm{b}}$, there might be a local maximum point on the ε_{h}-T_{AHS} curve and T_{AHS} at the local maximum point (if exists) increases with η_{AHS};

- when $T_3 < T_b$, the ε_h-T_{AHS} curve is above the ε_h-T_{AHS} curve in which c_{p,T_3} were assumed to be constant;
- when $T_3 \geq T_b$, there is a local maximum point in the ε_h-T_{AHS} curve.

The results suggest that

- an effort that should be made to increase the energy conversion efficiency of the AHS, η_{AHS}, is emphasized, since it is critical for improving the hybrid system energy/exergy efficiency relative to a non-hybrid reference system at the same AHS temperature or heat addition rate as shown in Fig. 4-6-Fig. 4-9;
- when η_{AHS} is low, such as 40% (only for the simulated cases and may be different for other cases), the temperature of the AHS T_{AHS} should be designed around the maximum point of the ε_h - T_{AHS} curve in which case the AHS is used to preheat the working fluid ($T_3 < T_b$): higher T_{AHS} will result in higher energy efficiency but lower exergy efficiency, and lower T_{AHS} will result in both lower energy and exergy efficiencies, as shown in Fig. 4-7 and Fig. 4-9;
- when η_{AHS} is higher, such as 60% or 80% (only for the simulated cases and may be different for other cases), T_{AHS} should either be designed around the local maximum point in the region $T_3 < T_b$, or designed so that the AHS is used to just vaporize the working fluid but not superheat it, since using the AHS to superheat

the working fluid will result in both lower energy and exergy efficiencies, as shown in Fig. 4-7 and Fig. 4-9;

- when η_{AHS} is even higher and comparable to η_{B}, such as 95.2% and 100% in the ideal case (only for the simulated cases and may be different for other cases), the AHS should be used not only to vaporize but also superheat the working fluid and T_{AHS} should be designed around the local maximum point in the region $T_3 > T_{\mathrm{b}}$, as shown in Fig. 4-7 and Fig. 4-9.

Other systems with the same configuration as Fig. 4-2 but with different operation parameters may follow similar characteristics as shown in Fig. 4-6 -Fig. 4-9 and the conclusions may be generalized to those systems, since the systems must follow the same thermodynamic equations that are derived in Section 4.1.2, such as Eq. (4.37).

4.2. Hybrid power generation systems based on a Rankine cycle with reheat

4.2.1. Introduction of hybrid power generation systems based on the Rankine cycle with reheat

Reheat is usually used in modern steam power plants to avoid excess moisture at the end of steam expansion process to protect the turbine, and to raise the system power generation rate without necessarily increasing the efficiency. In cases where the mean temperature of the cycle is also increased by reheating, the energy efficiency also increases. The flow

diagram of a Rankine cycle with reheat (reference system) is shown in Fig. 4-10. Note that the power output is from both the high-pressure (HP) and low-pressure (LP) turbines, $\dot{W}_{\mathrm{HPT}}+\dot{W}_{\mathrm{LPT}}=\dot{m}_{\mathrm{w}}\cdot\left[\left(h_4-h_{15}\right)+\left(h_{16}-h_5\right)\right]$, in which $\dot{m}_{\mathrm{w}}$ is the mass flow rate of the working fluid.

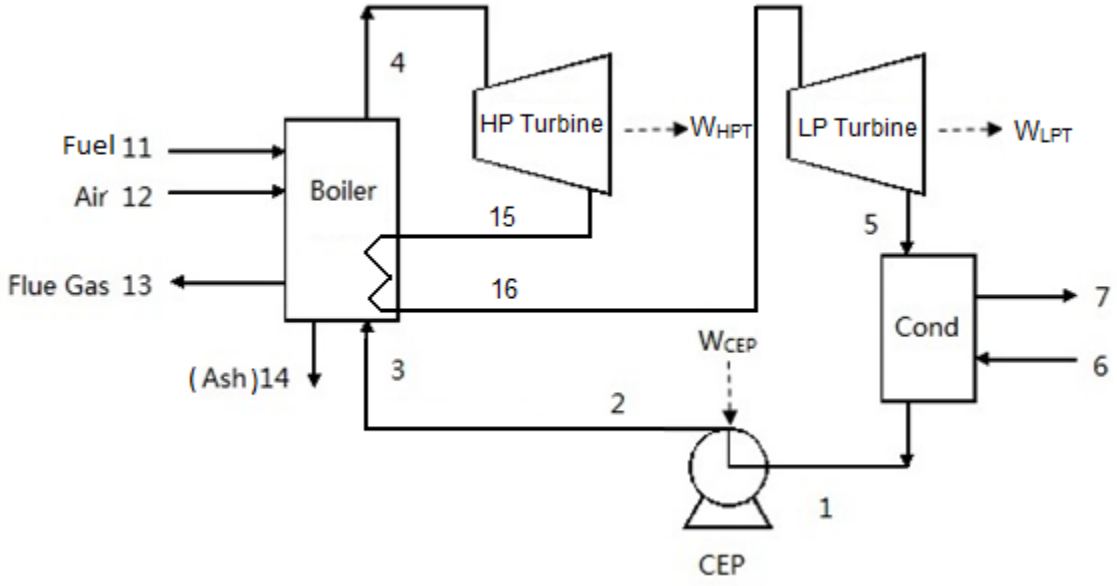

Fig. 4-10. Flow diagram of the reference (single heat source) power cycle based on a Rankine cycle with reheat without the additional heat source (AHS) (Cond: condenser, CEP: condensate extraction pump, HP: high-pressure, LP: low-pressure)

Based on the reference system, a hybrid power generation system with reheat can be created by adding an additional heat source (AHS) to the reference system, as shown in Fig. 4-11.

Theoretically, the AHS can be added between the HP and LP turbines so that the heat from the AHS is used to reheat the working fluid at the outlet of the HP turbine. This method, however, is not common since some of the AHS, such as geothermal and waste heat, are typically not available at that high temperature (over 500 °C), and the cost to attain that high temperature is also higher than using lower temperature, such as with solar heat. The AHS should thus be added in the place as in Fig. 4-11, instead of between stream 15 and 16 to reheat the working fluid.

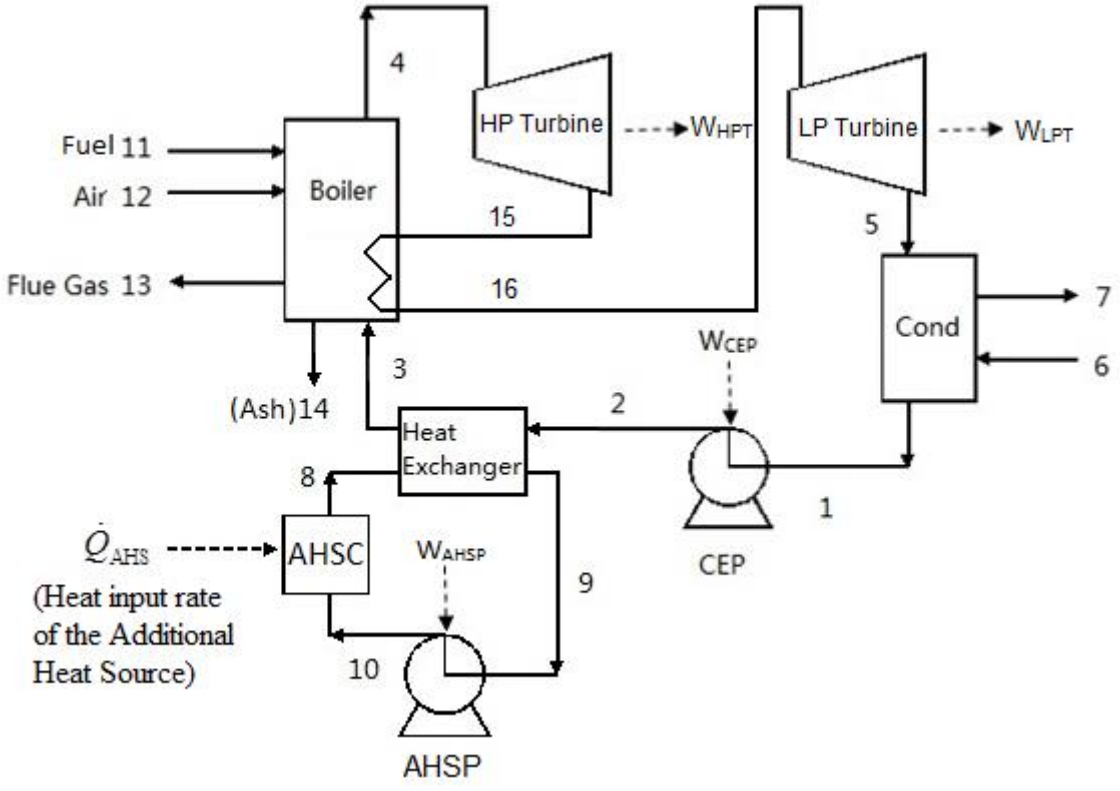

Fig. 4-11. Flow diagram of hybrid steam power plant with reheat assisted by an additional heat source (AHS) (Cond: condenser, CEP: condensate extraction pump,

AHSP: additional heat source pump, HP: high-pressure, LP: low-pressure) (The heat exchanger may be part of the economizer in the reference system when there is no AHS)

4.2.2. Thermodynamic analysis of hybrid power generation systems based on the Rankine cycle with reheat

Using the same method as for the simple Rankine cycle, shown in detail in Section 4.1, the energy and exergy efficiencies for the hybrid system are expressed, respectively, as

$$\eta_{\mathrm{h}} = \frac{\dot{m}_{\mathrm{w}} \cdot \left[\left(h_4 - h_{15} \right) + \left(h_{16} - h_5 \right) - \left(h_2 - h_1 \right) \right]}{\dot{m}_{\mathrm{f}} \cdot \mathrm{LHV} + \dot{Q}_{\mathrm{ADD}} / \eta_{\mathrm{AHS}}} = \frac{\left(h_4 - h_{15} \right) + \left(h_{16} - h_5 \right) - \left(h_2 - h_1 \right)}{\dfrac{\left(h_4 - h_3 \right) + \left(h_{16} - h_{15} \right)}{\eta_{\mathrm{B}}} + \dfrac{h_3 - h_2}{\eta_{\mathrm{AHS}}}}, \tag{4.90}$$

$$\varepsilon_{\mathrm{h}} = \frac{\dot{m}_{\mathrm{w}} \cdot \left[\left(h_4 - h_{15} \right) + \left(h_{16} - h_5 \right) - \left(h_2 - h_1 \right) \right]}{\dot{m}_{\mathrm{f}} \cdot b_{\mathrm{f}} + \psi_{\mathrm{AHS}} \cdot \dot{Q}_{\mathrm{AHS}}} = \frac{\left(h_4 - h_{15} \right) + \left(h_{16} - h_5 \right) - \left(h_2 - h_1 \right)}{\psi_{\mathrm{f}} \dfrac{\left(h_4 - h_3 \right) + \left(h_{16} - h_{15} \right)}{\eta_{\mathrm{B}}} + \psi_{\mathrm{AHS}} \dfrac{h_3 - h_2}{\eta_{\mathrm{AHS}}}}, \tag{4.91}$$

and for the reference system are expressed, respectively, as

$$\eta_0 = \frac{\left(h_4 - h_{15} \right) + \left(h_{16} - h_5 \right) - \left(h_2 - h_1 \right)}{\dfrac{\left(h_4 - h_3 \right) + \left(h_{16} - h_{15} \right)}{\eta_{\mathrm{B}}}}, \tag{4.92}$$

$$\varepsilon_0 = \frac{\left(h_4 - h_{15}\right) + \left(h_{16} - h_5\right) - \left(h_2 - h_1\right)}{\psi_{\mathrm{f}} \dfrac{\left(h_4 - h_3\right) + \left(h_{16} - h_{15}\right)}{\eta_{\mathrm{B}}}}. \tag{4.93}$$

Comparing Eqs (4.90) - (4.93) for the systems with reheat with Eqs (4.4)-(4.7) for the systems without reheat, it can be seen that they are have similar forms except that the specific power output is $\left(h_4 - h_{15}\right) + \left(h_{16} - h_5\right)$ instead of $\left(h_4 - h_5\right)$ and the specific enthalpy increase of the working fluid corresponding to the original heat source (fuel) is $\left(h_4 - h_3\right) + \left(h_{16} - h_{15}\right)$ instead of $\left(h_4 - h_3\right)$ for the hybrid system and $\left(h_4 - h_2\right) + \left(h_{16} - h_{15}\right)$ instead of $\left(h_4 - h_2\right)$ for the reference system. Using the same method as in Section 4.1, it is easy to realize that the results for the systems with reheat also apply to the ones without reheat, since h_{15} and h_{16} can assumed to be constant when $\dot{Q}_{\mathrm{AHS}}$ or T_{AHS} changes.

4.2.3. Simulation of hybrid power generation systems based on the Rankine cycle with reheat

Besides the basic assumptions listed in Table 4-2, two additional assumptions are made for the reheat system:

As commonly done (but not mandatory), the reheat temperature is the same as the top temperature of the cycle, i.e. $T_{16} = T_4$;

the reheat pressure p_{15} is 3.8 MPa, which is the square root of the turbine inlet pressure, i.e. $p_{15} = \sqrt{p_4}$ (the energy efficiency is maximized if reheat pressure is the square root of the turbine inlet pressure [3]);

the pressure loss during reheat is 2%, $p_{16} = 0.98\, p_{15}$.

It was found that the results for the hybrid power generation systems based on the Rankine cycle is similar to the results for the hybrid power generation systems based on the simple Rankine cycle as in Fig. 4-6-Fig. 4-9. The comparison results between the hybrid systems with and without reheat are, however, shown below.

4.2.4. Comparison between the hybrid Rankine cycle with and without reheat

Although the shapes of the efficiency curves for the hybrid cycle with and without reheat are similar, they are quantitatively different, as can be better seen when they are shown in the same figure (Fig. 4-12-Fig. 4-15). For clearer view, only two cases are chosen for these two types of hybrid systems: $\eta_{\text{AHS}} = 100\%$ and $\eta_{\text{AHS}} = 60\%$.

As can be seen from Fig. 4-12 and Fig. 4-13, the energy efficiency of the reheated hybrid power generation system is higher by approximately 2 percentage points than that of the system without reheat, for the same AHS heat addition rate, $\dot{Q}_{\text{AHS}}$, or temperature, T_{AHS}, since reheat increases the mean heat addition temperature of the power cycle in this

simulation from 208 °C to 223 °C. That difference (for the same η_{AHS}) almost does not change as a function of $\dot{Q}_{\mathrm{AHS}}$ and T_{AHS}.

The trends of exergy efficiency are more complicated than those of the energy efficiency, when η_{AHS} is large (=100%), as can be seen from Fig. 4-14 and Fig. 4-15. This is because that in the system with reheat, the working fluid is reheated by the fuel and the exergy destruction rate in the reheat process is unchanged as $\dot{Q}_{\mathrm{AHS}}$ and T_{AHS} increases. Since ε_{h} increases with $\dot{Q}_{\mathrm{AHS}}$ when η_{AHS} is large as shown in Fig. 4-8 and Fig. 4-14, the exergy efficiency change as more AHS is used will be smaller in the system with reheat than in the system without reheat. Thus, when η_{AHS} is large enough, the ε_{h} - $\dot{Q}_{\mathrm{AHS}}$ curves may, as seen, intersect for the system with and without reheat

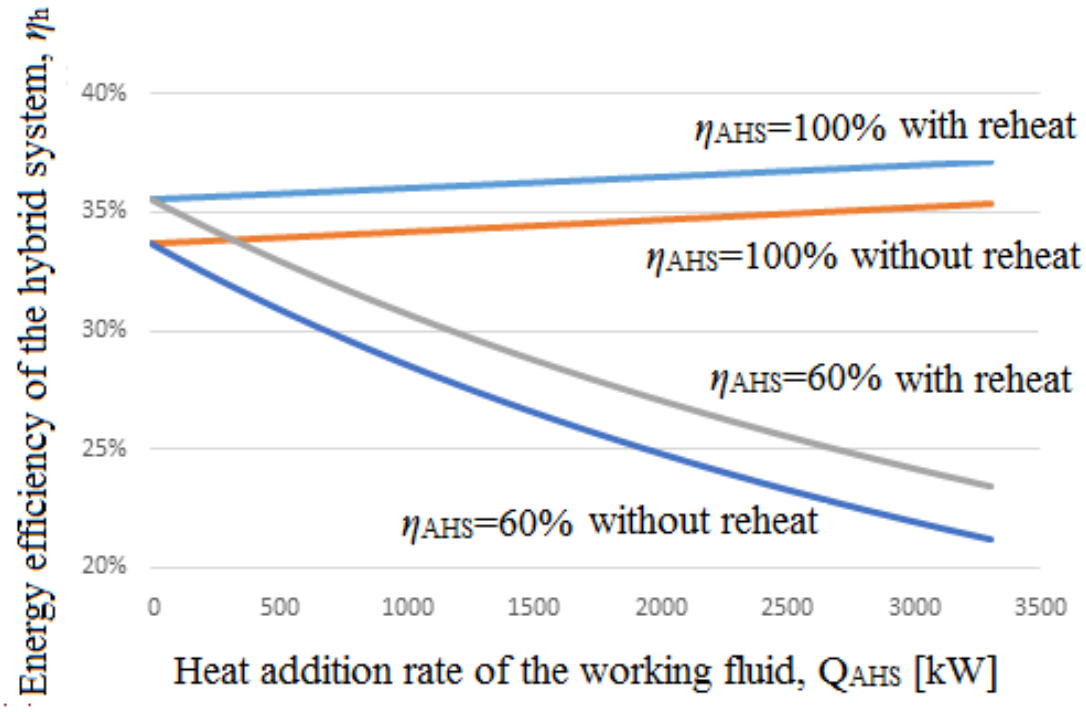

Fig. 4-12. Comparison results between the energy efficiency of the hybrid system, η_h, and the additional heat source (AHS) heat addition rate, $\dot{Q}_{AHS}$, for the hybrid power generation systems based on the Rankine cycles with and without reheat (η_{AHS} is the energy conversion efficiency of the AHS)

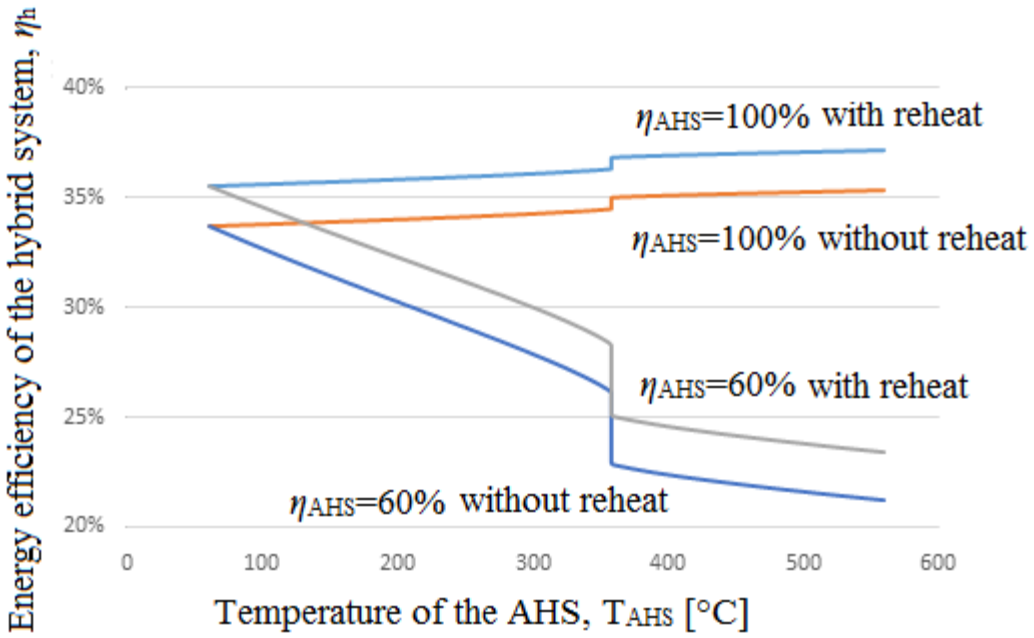

Fig. 4-13. Comparison results between the energy efficiency of the hybrid system, η_h, and the temperature of the additional heat source (AHS), T_{AHS}, for the hybrid power generation systems based on the Rankine cycles with and without reheat (η_{AHS} is the energy conversion efficiency of the AHS)

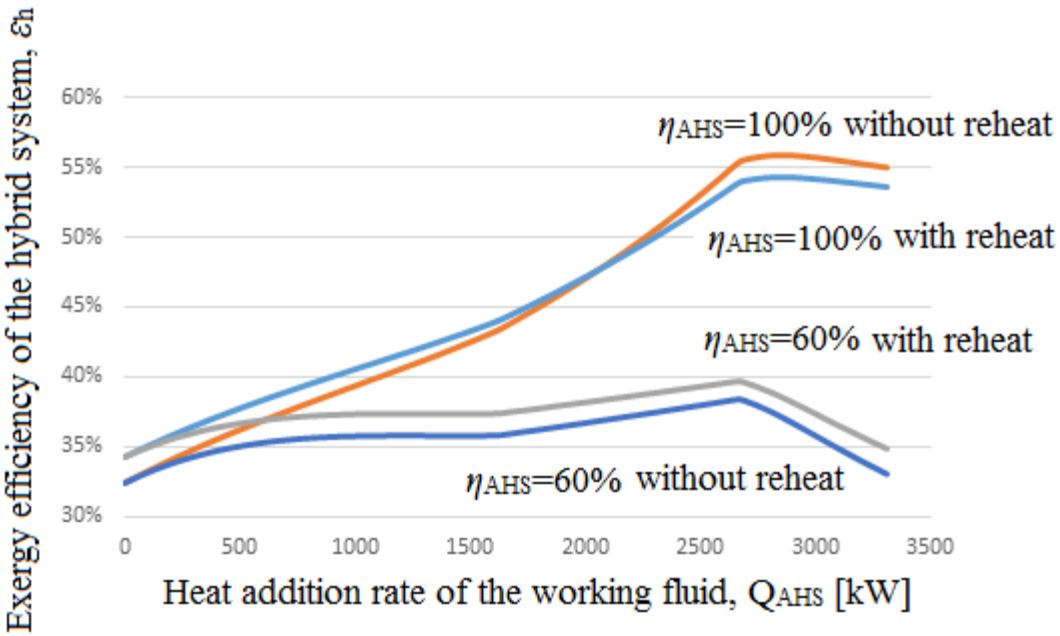

Fig. 4-14. Comparison results between the exergy efficiency of the hybrid system, ε_h, and the additional heat source (AHS) heat addition rate, $\dot{Q}_{AHS}$, for the hybrid power generation systems based on the Rankine cycles with and without reheat (η_{AHS} is the energy conversion efficiency of the AHS)

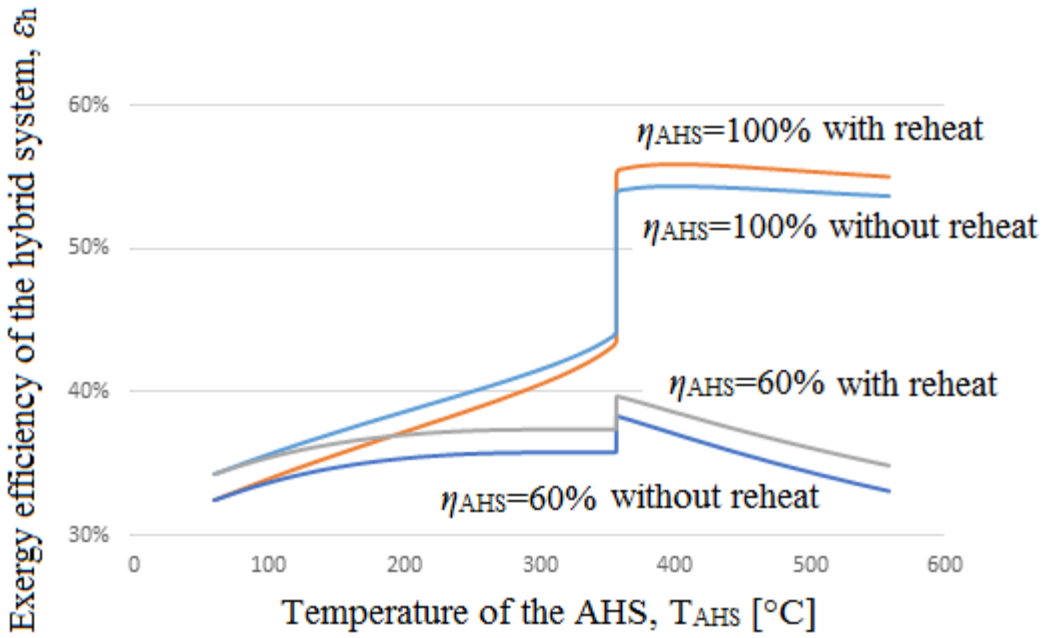

Fig. 4-15. Comparison results between the exergy efficiency of the hybrid system, ε_h, and the temperature of the additional heat source (AHS), T_{AHS}, for the hybrid power generation systems based on the Rankine cycles with and without reheat (η_{AHS} is the energy conversion efficiency of the AHS)

4.3. Hybrid power generation systems based on the Rankine cycle with heat regeneration

Besides "reheat", "regeneration", shown in Fig. 4-16, is another typical configuration used in steam power plants [4]. Steam is extracted from the turbine at one or more points of different temperatures to preheat the boiler feedwater mainly three reasons: to raise the energy efficiency of the power plant, reduce thermal shock in the boiler and eliminate

hazardous chemicals in boiler feedwater. Regeneration is realized by closed or open (direct contact) feedwater heaters. The feedwater heater may be low-pressure (LP) if it is located upstream of the boiler feed pump, or high-pressure (HP) if it is downstream.

4.3.1. Introduction of hybrid power generation systems based on the Rankine cycle with heat regeneration

The flow diagrams of the two hybrid systems with the AHS replacing the HP and LP feedwater heater, respectively, are shown in Fig. 4-17 and Fig. 4-18. In the first system, called here the hybrid system 1, the HP feedwater heater is replaced by an AHS to heat the working fluid from state 2 to 3, and in the second system, called here the hybrid system 2, the LP feedwater heater is replaced by an AHS to heat the working fluid from state 10 to 11. In both cases, the saved extraction stream continues to expand in the turbine to produce extra work.

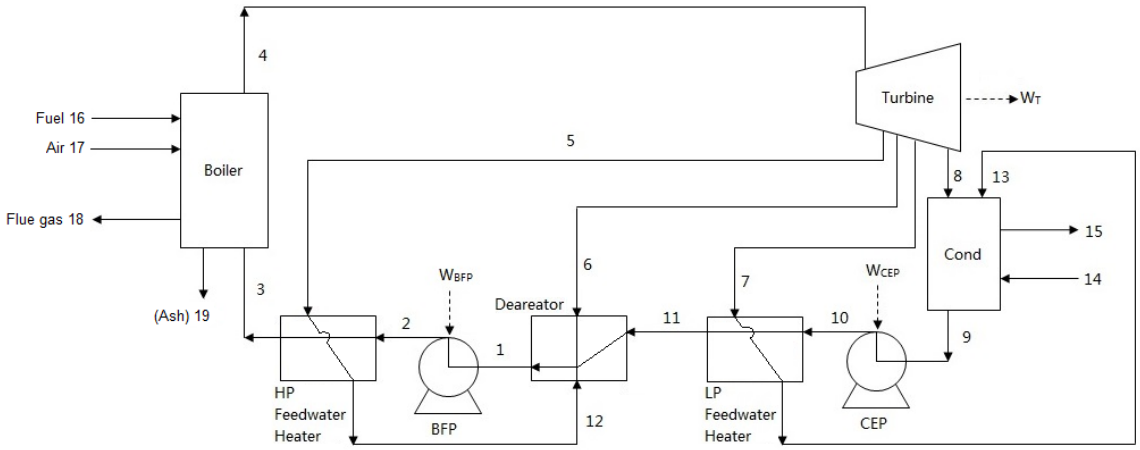

Fig. 4-16. Flow diagram of the reference steam power plant with regeneration by 2 closed feedwater heaters and one open feedwater heaters (Cond: condenser, CEP: condensate extraction pump, BFP: boiler feedwater pump, HP: high-pressure, LP: low-pressure)

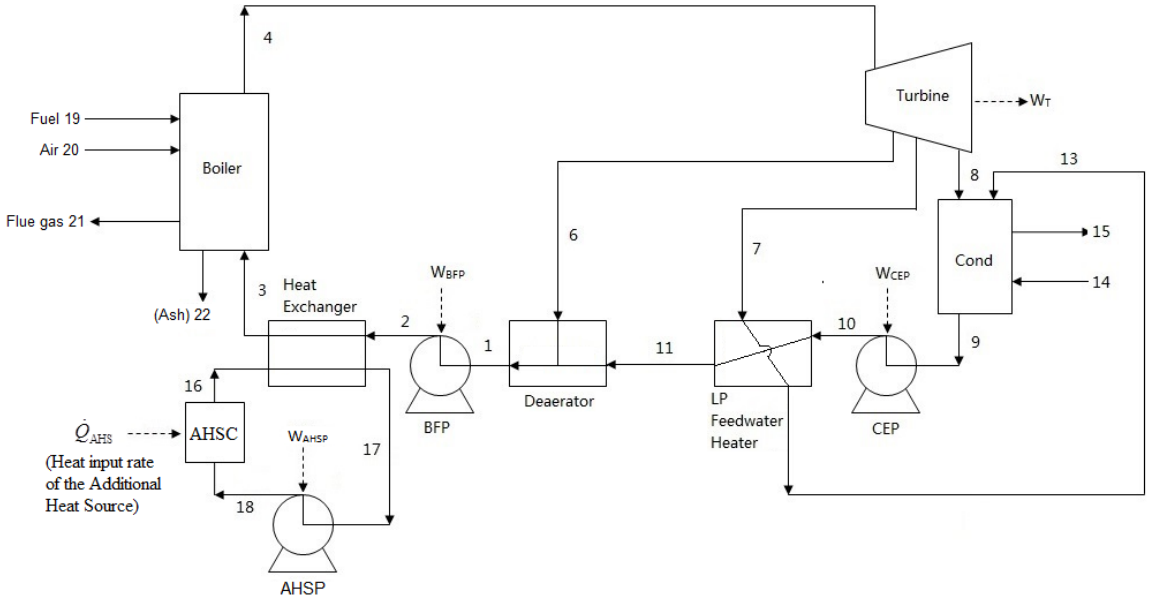

Fig. 4-17. Flow diagram of the first examined kind of hybrid regenerative steam power plant in which the closed high-pressure feedwater heater was replaced by an additional heat source (AHS) (Cond: condenser, CEP: condensate extraction pump, BFP: boiler feedwater pump, AHSC: additional heat source collection equipment, AHSP: additional heat source pump, LP: low-pressure)

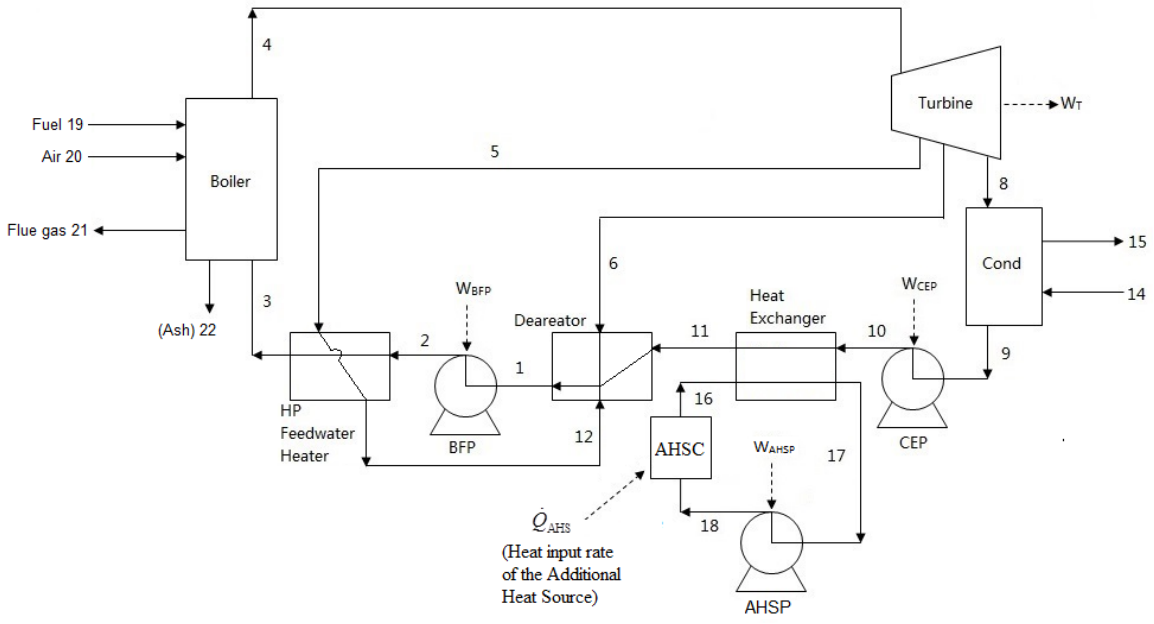

Fig. 4-18. Flow diagram of the second examined kind of hybrid regenerative steam power plant in which the closed low-pressure feedwater heater was replaced by an AHS (Cond: condenser, CEP: condensate extraction pump, BFP: boiler feedwater pump, AHSC: additional heat source collection equipment, AHSP: additional heat source pump, HP: high-pressure)

4.3.2. Thermodynamic analysis of hybrid power generation systems based on the Rankine cycle with heat regeneration

For the reference system shown in Fig. 4-16, the mass flow rate for each extraction stream from the steam turbine could be defined, respectively, as

$$\dot{m}_5 = y'\dot{m}_w, \tag{4.94}$$

$$\dot{m}_6 = y''\dot{m}_w, \tag{4.95}$$

$$\dot{m}_7 = y'''\dot{m}_w, \tag{4.96}$$

in which $\dot{m}_w = \dot{m}_4$ [kg/s] is mass flow rate of working fluid entering the turbine and y', y'', y''' is the extraction fraction of each extraction stream from the turbine.

Application of mass and energy balances to the control volume enclosing each feedwater heater gives, respectively,

$$y' = \frac{h_3 - h_2}{h_5 - h_{12}}, \tag{4.97}$$

$$0 = y''h_6 + (1 - y' - y'')h_{11} + y'h_{12} - h_1, \tag{4.98}$$

$$y''' = \frac{(1 - y' - y'')(h_{11} - h_{10})}{h_7 - h_{13}}, \tag{4.99}$$

in which Eq. (4.98) could be written as

$$y'' = \frac{(h_1 - h_{11}) - y'(h_{12} - h_{11})}{h_6 - h_{11}}. \tag{4.100}$$

The specific power output from the steam turbine of the reference system is

$$w_{\text{net},0} = \left[\left(h_4 - h_8 \right) - y' \left(h_5 - h_8 \right) - y'' \left(h_6 - h_8 \right) - y''' \left(h_7 - h_8 \right) \right] - \left[\left(h_2 - h_1 \right) + \left(1 - y' - y'' \right) \left(h_{10} - h_9 \right) \right]. \tag{4.101}$$

The energy efficiency of the reference system is

$$\eta_0 = \frac{\dot{W}_{\text{net},0}}{\dot{Q}_{\text{f}}} = \frac{w_{\text{net},0}}{\dfrac{\left(h_4 - h_3 \right)}{\eta_{\text{B}}}}. \tag{4.102}$$

The exergy efficiency of the reference system is

$$\varepsilon_0 = \frac{\dot{W}_{\text{net},0}}{\dot{B}_{\text{f}}} = \frac{w_{\text{net},0}}{\dfrac{\left(h_4 - h_3 \right)}{\eta_{\text{B}}} \dfrac{b_{\text{f}}}{\text{LHV}}}. \tag{4.103}$$

For the hybrid system 1, i.e. when the HP feedwater heater is replaced by an AHS, as shown in Fig. 4-17, application of mass and energy balance to the control volume enclosing the AHS heat exchanger and each feedwater heater give, respectively,

$$\eta_{\text{AHS},1} \dot{Q}_{\text{AHS},1} = \dot{Q}_{\text{ADD},1} = \dot{m}_{\text{w}} \left(h_3 - h_2 \right), \tag{4.104}$$

$$0 = y_1'' h_6 + \left(1 - y_1'' \right) h_{11} - h_1, \tag{4.105}$$

$$y_1''' = \frac{\left(1 - y_1'' \right) \left(h_{11} - h_{10} \right)}{h_7 - h_{13}}, \tag{4.106}$$

in which the subscript 1 stands for the case when HP feedwater is replaced by an AHS and Eq. (4.105) becomes

$$y_1'' = \frac{h_1 - h_{11}}{h_6 - h_{11}}. \tag{4.107}$$

The specific power output from the steam turbine of the hybrid system 1 is

$$\begin{aligned} w_{\text{net},1} &= w_{\text{net},0} + \Delta w_{\text{net},1} \\ &= \left[\left(h_4 - h_8\right) - y'\left(h_5 - h_8\right) - y''\left(h_6 - h_8\right) - y'''\left(h_7 - h_8\right) \right] \\ &- \left[\left(h_2 - h_1\right) + \left(1 - y' - y''\right)\left(h_{10} - h_9\right) \right] + y'''\left(h_7 - h_8\right) \\ &= \left[\left(h_4 - h_8\right) - y'\left(h_5 - h_8\right) - y''\left(h_6 - h_8\right) \right] - \left[\left(h_2 - h_1\right) + \left(1 - y' - y''\right)\left(h_{10} - h_9\right) \right]. \end{aligned} \tag{4.108}$$

The energy efficiency of the hybrid system 1 is

$$\eta_{\text{h},1} = \frac{\dot{W}_{\text{net},1}}{\dot{Q}_{\text{f}} + \dot{Q}_{\text{AHS},1}} = \frac{w_{\text{net},1}}{\dfrac{\left(h_4 - h_3\right)}{\eta_{\text{B}}} + \dfrac{\left(1 - y' - y''\right)\left(h_{11} - h_{10}\right)}{\eta_{\text{AHS},1}}}. \tag{4.109}$$

The exergy efficiency of the hybrid system 1 is

$$\varepsilon_{\text{h},1} = \frac{\dot{W}_{\text{net},1}}{\dot{B}_{\text{f}} + \dot{B}_{\text{AHS},1}} = \frac{w_{\text{net},1}}{\dfrac{\left(h_4 - h_3\right)}{\eta_{\text{B}}}\dfrac{b_{\text{f}}}{LHV} + \dfrac{\left(1 - y' - y''\right)\left(h_{11} - h_{10}\right)}{\eta_{\text{AHS},1}}\left(1 - \dfrac{T_0}{T_{\text{AHS},1}}\right)}. \tag{4.110}$$

For the hybrid system 2, i.e. when the LP feedwater heater is replaced by an AHS, as shown in Fig. 4-18, application of mass and energy balance to the control volume enclosing the AHS heat exchanger and each feedwater heater give, respectively,

$$y_2' = \frac{h_3 - h_2}{h_5 - h_{12}}, \tag{4.111}$$

$$0 = y_2'' h_6 + \left(1 - y_2' - y_2''\right) h_{11} + y_2' h_{12} - h_1, \tag{4.112}$$

$$\eta_{\text{AHS},2} \dot{Q}_{\text{AHS},2} = \dot{Q}_{\text{ADD},2} = \dot{m}_{\text{w}} \left(1 - y_2' - y_2''\right)\left(h_{11} - h_{10}\right), \tag{4.113}$$

in which the subscript 2 stands for the case when the LP feedwater is replaced by AHS and Eq. (4.112) could be written as

$$y_2'' = \frac{\left(h_1 - h_{11}\right) - y_2'\left(h_{12} - h_{11}\right)}{h_6 - h_{11}}. \tag{4.114}$$

The specific power output from the steam turbine of the hybrid system 2 is

$$\begin{aligned} w_{\text{net},2} &= w_{\text{net},0} + \Delta w_{\text{net},2} \\ &= \left[\left(h_4 - h_8\right) - y'\left(h_5 - h_8\right) - y''\left(h_7 - h_8\right) - y'''\left(h_7 - h_8\right)\right] \\ &- \left[\left(h_2 - h_1\right) + \left(1 - y' - y''\right)\left(h_{10} - h_9\right)\right] + y'\left[\left(h_5 - h_8\right) - \left(h_{10} - h_9\right)\right] \\ &= \left[\left(h_4 - h_8\right) - y''\left(h_5 - h_8\right) - y'''\left(h_7 - h_8\right)\right] - \left[\left(h_2 - h_1\right) + \left(1 - y''\right)\left(h_{10} - h_9\right)\right]. \end{aligned} \tag{4.115}$$

The energy efficiency of the hybrid system 2 is

$$\eta_{\mathrm{h},2}=\frac{\dot{W}_{\mathrm{net},2}}{\dot{Q}_{\mathrm{f}}+\dot{Q}_{\mathrm{AHS},2}}=\frac{w_{\mathrm{net},2}}{\frac{\left(h_4-h_3\right)}{\eta_{\mathrm{f}}}+\frac{\left(h_3-h_2\right)}{\eta_{\mathrm{AHS},2}}}. \tag{4.116}$$

The exergy efficiency of the hybrid system 2 is

$$\varepsilon_{\mathrm{h},2}=\frac{\dot{W}_{\mathrm{net},2}}{\dot{B}_{\mathrm{f}}+\dot{B}_{\mathrm{AHS},2}}=\frac{w_{\mathrm{net},2}}{\frac{\left(h_4-h_3\right)}{\eta_{\mathrm{B}}}\frac{b_{\mathrm{f}}}{\mathrm{LHV}}+\frac{\left(h_3-h_2\right)}{\eta_{\mathrm{AHS},2}}\left(1-\frac{T_0}{T_{\mathrm{AHS},2}}\right)}. \tag{4.117}$$

The next objective is compare the energy/exergy efficiency of the hybrid system 1 and 2.

Assuming the specific power output of the two hybrid systems are equal, i.e. $w_{\mathrm{net},1}=w_{\mathrm{net},2}$ and neglecting pump works, which are small compared to the turbine power output, we have

$$y_1'\left(h_5-h_8\right)+y_1''\left(h_6-h_8\right)=y_2''\left(h_6-h_8\right)+y_2'''\left(h_7-h_8\right). \tag{4.118}$$

Assuming also the efficiency of AHS are the same, i.e.

$$\eta_{\mathrm{AHS},1}=\eta_{\mathrm{AHS},2}, \tag{4.119}$$

we have $\eta_{\mathrm{h},2}>\eta_{\mathrm{h},1}$, according to Eqs (4.109) and (4.116), when

$$\left(h_3-h_2\right)<\left(1-y_1'-y_1''\right)\left(h_{11}-h_{10}\right) \tag{4.120}$$

or

$$\left[\frac{h_6-h_1}{h_6-h_{11}}-\left(\frac{h_3-h_2}{h_5-h_{12}}\right)\left(\frac{h_6-h_{12}}{h_6-h_{11}}\right)\right]\left(\frac{h_{11}-h_{10}}{h_3-h_2}\right)>1 \tag{4.121}$$

or

$$\left(\frac{h_3-h_2}{h_5-h_{12}}\right)\left(\frac{h_7-h_{13}}{h_{11}-h_{10}}\right)\left(\frac{h_5-h_8}{h_7-h_8}\right)\left(\frac{h_{11}-h_{10}}{h_3-h_2}\right)>1 \tag{4.122}$$

or

$$\left(\frac{h_7-h_5}{h_5-h_{12}}\right)\left(\frac{h_5-h_8}{h_7-h_8}\right)>1. \tag{4.123}$$

Similarly to the analysis for the previous analysis, we have

$$\frac{h_5-h_8}{h_5-h_{12}}>\frac{h_7-h_8}{h_7-h_5}. \tag{4.124}$$

So similar to the analysis in the previous study, we have the same conclusion that

$$\eta_{\mathrm{h},2}>\eta_{\mathrm{h},1}, \tag{4.125}$$

when $w_{\mathrm{net},2}=w_{\mathrm{net},1}$.

This means that replacing higher pressure extracted steam will achieve higher system energy efficiency than replacing lower pressure extracted steam, when both extracted steam, if replaced, increases the same amount of net power output.

Similarly, for the exergy efficiency, we can conclude that when $w_{\text{net},2} = w_{\text{net},1}$,

$$\varepsilon_{\text{h},2} > \varepsilon_{\text{h},1}, \tag{4.126}$$

when

$$\left(\frac{h_7 - h_5}{h_5 - h_{12}}\right)\left(\frac{h_5 - h_8}{h_7 - h_8}\right)\left(\frac{T_{\text{AHS},2} - T_0}{T_{\text{AHS},1} - T_0}\right) > 1, \tag{4.127}$$

which isn't always satisfied. If, however, solar temperature at the sun surface is used as the heat source temperature for solar, $T_{\text{AHS},1} = T_{\text{AHS},2} = T_{\text{ss}} = 5760\ \text{K}$, we have

$$\left(\frac{h_{63} - h_{31}}{h_{61} - h_{51}}\right)\left(\frac{h_{61} - h_7}{h_{63} - h_7}\right)\left(\frac{T_{\text{ss}} - T_0}{T_{\text{ss}} - T_0}\right) > 1, \tag{4.128}$$

which is always satisfied as in the energy analysis section. This means

$$\varepsilon_{\text{h},2} > \varepsilon_{\text{h},1}, \tag{4.129}$$

when $w_{\text{net},2} = w_{\text{net},1}$.

This means that when solar heat is used as the AHS and the temperature of solar heat is defined as the sun surface temperature, replacing higher pressure extracted steam will achieve higher system exergy efficiency than replacing lower pressure extracted steam, when both extracted steams, if replaced, increase the same amount of net power output.

4.4. Conclusions of the thermodynamic analysis of hybrid power generation systems based on Rankine cycles

This chapter mainly examines the thermodynamic features and performance of hybrid power generation systems based on Rankine cycles. The main conclusions for the hybrid power generation systems based on the simple Rankine cycle were summarized in Section 4.1.6 and are not repeated here. For the hybrid power generation systems based on the Rankine cycle with reheat, the thermodynamic analysis showed that they have similar characteristics with the hybrid power generation systems based on the simple Rankine cycle, in terms of the relation between the temperature of the AHS, T_{AHS}, the heat addition rate of the AHS, $\dot{Q}_{\mathrm{AHS}}$, and the energy/exergy efficiency of the hybrid system, for different energy conversion efficiency of the AHS, η_{AHS}.

For the hybrid power generation systems based on the Rankine cycle with heat regeneration, it was found in the thermodynamic analysis that replacing higher pressure extracted steam will achieve higher system energy efficiency than replacing lower pressure extracted steam, when both extracted steams, if replaced, increase the same amount of net power output.

When solar heat is used as the AHS and the temperature of the solar heat is defined as the sun surface, this result also applies to the exergy efficiency of the hybrid system. The results suggested that it is better to replace the higher pressure extracted steams with the AHS than the lower pressure ones in terms of energy efficiency. From the exergy point of view, however, it is not always the case and a simple criterion to decide which extracted steam to replace is Eq. (4.127).

References for Chapter 4

[1] ASPN PLUS: V9, Aspen Technology, Inc., http://www.aspentech.com/products/engineering/aspen-plus/.

[2] Ameri M., Ahmadi P., Hamidi A., Energy, exergy and exergoeconomic analysis of a steam power plant: A case study. Int J Energ Res 2009;33:499-512.

[3] EES: Engineering Equation Solver, Academic commercial V10.091, http://www.fchart.com/ees/.

[4] Woodruff E.B., Lammers H.B., Lammers T.F., Steam power plant operation, 8th edition, New York US: McGraw-Hill; 2005.

CHAPTER 5

THERMODYNAMIC ANALYSIS OF THERMAL HYBIRD POWER GENERATION SYSTEMS BASED ON BRAYTON CYCLES

5.1. Hybrid power generation systems based on the simple Brayton cycle

5.1.1. Introduction of hybrid power generation systems based on the simple Brayton cycle

The flow and T-s diagrams of the considered hybrid gas turbine system based on simple Brayton cycle is shown in Fig. 5-1 and Fig. 5-2, respectively. For simplicity, additional heat source equipment is shown collectively as AHSC in Fig. 5-1 and “Fuel” stands for natural gas, methane, or other gas or liquid fuel that could be burned in gas turbines combustor.

In this system, air is pressurized in the compressor before heated by AHS and fuel. The high temperature high pressure combustion gas from the combustor outlet is then used to drive the turbine. The compressor and the turbine usually attach to one shaft and the net power output of the system is the turbine shaft work minus compressor work. The flue gas could be used to preheat the pressurized air as well and will be dealt with in the next section.

When there is no AHS input, the hybrid simple Brayton cycle reduces to the reference system, which is the simple Brayton cycle.

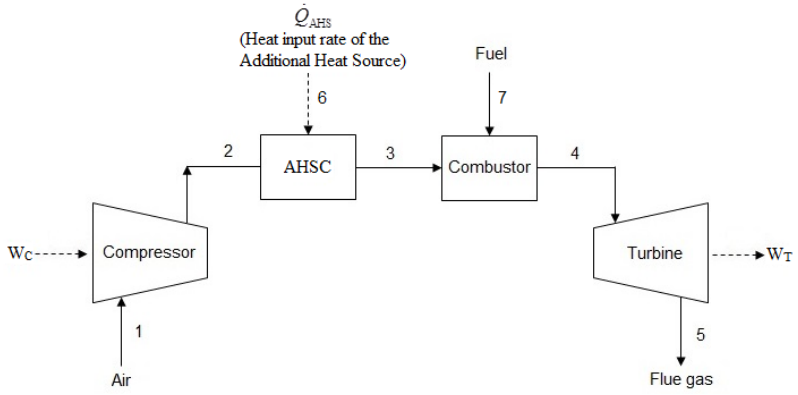

Fig. 5-1. Flow diagram of the hybrid gas turbine power plant based on a simple Brayton cycle with an additional heat source (AHS) (AHSC: additional heat source collection equipment)

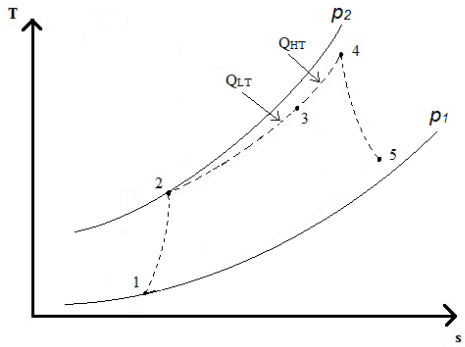

Fig. 5-2. T-s diagram of the hybrid gas turbine power plant based on a simple Brayton cycle with an additional heat source (AHS) (Q_{LT}: heat input from the additional heat source, Q_{HT}: heat input from the fuel in the combustor, ——: isobars, - - - -: real processes)

5.1.2. Thermodynamic analysis of hybrid power generation systems based on the simple Brayton cycle

In reality, introducing the AHS for the simple Brayton cycle may change the isentropic efficiency of the compressor and will thus change the specific enthalpy at the outlet of the compressor, h_2. What's more, introducing the AHS will also change the mass flow rate of the needed fuel in the combustion process, $\dot{m}_f$, and will thus change the composition of the flue gas (stream 4 in Fig. 5-1) after the combustion process. Introducing the AHS will also change the pressure drop in the heat addition process (from the compressor outlet to the turbine inlet) and may thus result in different pressures in the turbine inlet, p_4.

Determination of all the operation parameters of a system, such as the temperature and pressure, at each state points in the power cycles requires experiments or even information that a company may make available only to its customers.

Considering that this research is a preliminary thermodynamic analysis and is intended to serve only as a guideline for designing hybrid power cycles before detailed simulation or experiments, there is no need to provide exact values or expressions to calculate the operation parameters for each state point in the power cycles at this stage and certain assumptions can be made to help with the thermodynamic analysis instead. It is assumed that the addition of the AHSC will not change:

1) the isentropic efficiency of the compressor,

2) the pressure drop during the heat addition process (from the compressor outlet to the turbine inlet), or the pressure at the turbine inlet, p_4,
3) and the composition of the flue gas after combustion, considering that the mass flow rate of fuel is small compared to that of air in gas turbine (fuel-air ratio about 2%).

Considering that the compressor inlet air (stream 1) conditions are the same for the reference system and the hybrid system and the top temperature of the cycles are kept the same, it can be further concluded from the above assumptions that the specific enthalpies at each state point in the power cycles remains constant.

Besides the above assumptions, the thermodynamic analysis uses the following assumptions similar to those in Section 4.1.2:

- The kinetic and potential energy of the fluids are ignored in such power cycle analyses due to their small magnitude and impact on the system performance relative to the heat-caused enthalpy changes in the fluids.
- Each component in the power cycles is adiabatic with respect to its surroundings, (i.e., there is no heat loss to the environment). Since the heat loss is generally easily reducible and usually only a small fraction of the heat duty of the heat exchangers, most early-stage design processes ignore these heat losses.
- The mechanical efficiencies of the compressor and the turbine are 100%.

The following analyses are based on these assumptions. The objective, same as before for the analysis of the Rankine cycles, is to compare the energy/exergy efficiency of the hybrid and the reference system.

According to the mass and energy balance in the control volume enclosing the combustor for the hybrid system in Fig. 5-1,

$$\eta_{\mathrm{CC}}\dot{m}_{\mathrm{f}}\mathrm{LHV}+\dot{m}_{\mathrm{f}}h_7+\dot{m}_{\mathrm{a}}h_3=\left(\dot{m}_{\mathrm{a}}+\dot{m}_{\mathrm{f}}\right)h_4, \tag{5.1}$$

in which η_{CC} is the energy efficiency of the combustor defined as the ratio between fuel energy input and enthalpy increase of working fluid, $\dot{m}_{\mathrm{a}}$ [kg/s] and $\dot{m}_{\mathrm{f}}$ [kg/s] are the mass flow rate of combustor inlet air and fuel, respectively, LHV [kJ/kg] is the lower heating value of the combustor inlet fuel.

Based on the enthalpy balance of the AHSC and the combustor (Fig. 5-1), the enthalpy increase of the working fluid during the heat addition process is, respectively,

$$\dot{Q}_{\mathrm{ADD,f}}=\left(\dot{m}_{\mathrm{a}}+\dot{m}_{\mathrm{f}}\right)h_4-\left(\dot{m}_{\mathrm{f}}h_7+\dot{m}_{\mathrm{a}}h_3\right)=\eta_{\mathrm{CC}}\dot{Q}_{\mathrm{ADD}}=\eta_{\mathrm{CC}}\dot{m}_{\mathrm{f}}\mathrm{LHV}, \tag{5.2}$$

$$\dot{Q}_{\mathrm{ADD,AHS}}=\dot{m}_{\mathrm{a}}\left(h_3-h_2\right)=\eta_{\mathrm{AHS}}\dot{Q}_{\mathrm{AHS}}. \tag{5.3}$$

When solar energy is used as the AHS, $\dot{Q}_{\mathrm{ADD,AHS}}=\dot{Q}_{\mathrm{sol}}$ and η_{HS} is η_{sc} defined in Eq. (2.6).

For later use, define the fuel-air ratio, f, as the ratio of mass flow rate of air and that of fuel in a combustion process, or

$$f = \frac{\dot{m}_{\mathrm{f}}}{\dot{m}_{\mathrm{a}}}. \tag{5.4}$$

Using Eq. (5.2), the fuel-air ratio for the hybrid system is thus

$$f = \frac{\dot{m}_{\mathrm{f}}}{\dot{m}_{\mathrm{a}}} = \frac{h_4 - h_3}{\eta_{\mathrm{CC}}\mathrm{LHV} - \left(h_4 - h_7\right)}. \tag{5.5}$$

Using the assumptions listed at the beginning of Section 5.1.2 and based on Eqs (2.2) and (4.1)-(4.3), the energy efficiency of the hybrid system, η_{h}, is

$$\eta_{\mathrm{h}} = \frac{\left(\dot{m}_{\mathrm{a}} + \dot{m}_{\mathrm{f}}\right)\left(h_4 - h_5\right) - \dot{m}_{\mathrm{a}}\left(h_2 - h_1\right)}{\dot{m}_{\mathrm{f}}\mathrm{LHV} + \dfrac{\dot{m}_{\mathrm{a}}\left(h_3 - h_2\right)}{\eta_{\mathrm{AHS}}}} = \frac{\left(1 + f\right)\left(h_4 - h_5\right) - \left(h_2 - h_1\right)}{f \cdot \mathrm{LHV} + \dfrac{h_3 - h_2}{\eta_{\mathrm{AHS}}}}, \tag{5.6}$$

in which the fuel-air ratio for the hybrid system, f, is determined using Eq. (5.5).

Assuming the dead state temperature is T_0 and the AHS temperature is T_{AHS}, the exergy efficiency of the hybrid system, ε_{h}, based on Eq. (2.8), is

$$\varepsilon_{\mathrm{h}} = \frac{\left(\dot{m}_{\mathrm{a}} + \dot{m}_{\mathrm{f}}\right)\left(h_4 - h_5\right) - \dot{m}_{\mathrm{a}}\left(h_2 - h_1\right)}{\dot{m}_{\mathrm{f}} \cdot b_{\mathrm{f}} + \dfrac{\dot{m}_{\mathrm{a}}\left(h_3 - h_2\right)}{\eta_{\mathrm{AHS}}}\left(1 - \dfrac{T_0}{T_{\mathrm{AHS}}}\right)} = \frac{\left(1 + f\right)\left(h_4 - h_5\right) - \left(h_2 - h_1\right)}{f \cdot b_{\mathrm{f}} + \dfrac{h_3 - h_2}{\eta_{\mathrm{AHS}}}\left(1 - \dfrac{T_0}{T_{\mathrm{AHS}}}\right)}. \tag{5.7}$$

If there is no AHS input in Fig. 5-1, $h_3 = h_2$, the general form of energy efficiency of the simple Brayton cycle system is

$$\eta_0 = \frac{(1+ f_0)(h_4 - h_5) - (h_2 - h_1)}{f_0 \cdot \mathrm{LHV}}, \tag{5.8}$$

and the exergy efficiency is

$$\varepsilon_0 = \frac{(1+ f_0)(h_4 - h_5) - (h_2 - h_1)}{f_0 \cdot b_\mathrm{f}}, \tag{5.9}$$

in which the fuel-air ratio for the reference system, f_0, is

$$f_0 = \frac{\dot{m}_{\mathrm{f},0}}{\dot{m}_\mathrm{a}} = \frac{h_4 - h_2}{\eta_{\mathrm{CC}}\mathrm{LHV} - (h_4 - h_7)}. \tag{5.10}$$

The next step is to compare the energy efficiencies of the hybrid system and the reference system.

Based on Eqs (5.6) and (5.8), the ratio between the energy efficiency of the hybrid system and the reference system is

$$\frac{\eta_\mathrm{h}}{\eta_0} = \frac{(1+ f)(h_4 - h_5) - (h_2 - h_1)}{(1+ f_0)(h_4 - h_5) - (h_2 - h_1)} \frac{f_0 \cdot \mathrm{LHV}}{f \cdot \mathrm{LHV} + \dfrac{h_3 - h_2}{\eta_{\mathrm{AHS}}}}. \tag{5.11}$$

Using the assumption that the fuel-air ratio is only about 2% in practice, or

$$f < f_0 \approx 0.02 < 1. \tag{5.12}$$

Eq. (5.11) becomes

$$\frac{\eta_{\mathrm{h}}}{\eta_0} \approx \frac{f_0 \cdot \mathrm{LHV}}{f \cdot \mathrm{LHV} + \dfrac{h_3 - h_2}{\eta_{\mathrm{AHS}}}} = \frac{\dfrac{h_4 - h_2}{\eta_{\mathrm{CC}}\mathrm{LHV} - \left(h_4 - h_7\right)}\mathrm{LHV}}{\dfrac{h_4 - h_3}{\eta_{\mathrm{CC}}\mathrm{LHV} - \left(h_4 - h_7\right)}\mathrm{LHV} + \dfrac{h_3 - h_2}{\eta_{\mathrm{AHS}}}}, \tag{5.13}$$

which is = 1 when

$$\eta_{\mathrm{AHS}} = \eta_{\mathrm{CC}} - \frac{h_4 - h_7}{\mathrm{LHV}}, \tag{5.14}$$

and > 1 when

$$\eta_{\mathrm{AHS}} > \eta_{\mathrm{CC}} - \frac{h_4 - h_7}{\mathrm{LHV}}, \tag{5.15}$$

and < 1 when

$$\eta_{\mathrm{AHS}} < \eta_{\mathrm{CC}} - \frac{h_4 - h_7}{\mathrm{LHV}}. \tag{5.16}$$

In practice, the energy efficiency of the combustor is close to 1 (99%), since the heat loss from the combustor is small compared to the heat duty of the combustion process, i.e.

$$\eta_{\mathrm{CC}} \approx 1. \tag{5.17}$$

As will be shown in the simulation,

$$\frac{h_4 - h_7}{\text{LHV}} << 1. \tag{5.18}$$

Thus,

$$\eta_{\text{CC}} - \frac{h_4 - h_7}{\text{LHV}} \approx \eta_{\text{CC}} \approx 1, \tag{5.19}$$

and can be concluded that $\eta_{\text{h}} < \eta_0$, since $\eta_{\text{AHS}} < \eta_{\text{CC}} - \dfrac{h_4 - h_7}{\text{LHV}}$ in most cases.

The next step is to compare the exergy efficiencies of the hybrid system and the reference system.

Based on Eqs (5.7) and (5.9), the ratio between the energy efficiency of the hybrid system and the reference system is

$$\frac{\varepsilon_{\text{h}}}{\varepsilon_0} = \frac{(1+f)(h_4 - h_5) - (h_2 - h_1)}{(1+f_0)(h_4 - h_5) - (h_2 - h_1)} \frac{f_0 \cdot b_{\text{f}}}{f \cdot b_{\text{f}} + \dfrac{h_3 - h_2}{\eta_{\text{AHS}}}\left(1 - \dfrac{T_0}{T_{\text{AHS}}}\right)}, \tag{5.20}$$

which is 1 when

$$\eta'_{\text{AHS}} = \eta'_{\text{CC}} - \frac{h_4 - h_7}{b_{\text{f}}}, \tag{5.21}$$

and ≥ 1 when

$$\eta'_{\text{AHS}} > \eta'_{\text{CC}} - \frac{h_4 - h_7}{b_{\text{f}}}, \tag{5.22}$$

and ≤ 1 when

$$\eta'_{\text{AHS}} < \eta'_{\text{CC}} - \frac{h_4 - h_7}{b_{\text{f}}}, \tag{5.23}$$

in which η'_{AHS} and η'_{CC} are the exergy conversion efficiencies of the AHS and the combustor, defined before respectively in Eqs (4.21) and (4.22).

Considering that $b_{\text{f}} \approx \text{LHV}$ for fuel, it can thus be seen that

$$\eta'_{\text{CC}} - \frac{h_4 - h_7}{b_{\text{f}}} \approx \eta'_{\text{CC}} \approx \eta_{\text{CC}} \approx 1. \tag{5.24}$$

This means that $\varepsilon_{\text{h}} > \varepsilon_0$ when $\eta'_{\text{AHS}} > 1$, or

$$\eta_{\text{AHS}} > 1 - \frac{T_0}{T_{\text{AHS}}}. \tag{5.25}$$

For example, when $T_0 = 300\ \mathrm{K}$ and $T_{\mathrm{AHS}} = 1,200\ \mathrm{K}$, η_{AHS} has to be larger than 0.75 for $\varepsilon_{\mathrm{h}} > \varepsilon_0$.

5.2. Hybrid power generation systems based on the Brayton cycle with intercooling

5.2.1. Introduction of hybrid power generation systems based on the Brayton cycle with intercooling

Intercooling is widely used in Brayton power systems since it reduces the power consumption of the compressor by lowering the temperature of the compressed air, and thus increases the net power output of the gas turbine. Lowering the temperature of the pressurized air outlet from the compressor leaves more room for utilizing the AHS at lower temperatures, such as when using solar parabolic trough concentrating collectors instead of higher concentration (and hence more expensive) solar systems such as dish or tower.

The flow and T-s diagrams of hybrid gas turbine power plants with intercooling are shown in Figs. 5-3 and 5-4, respectively. If there is no intercooling used, the operation cycle would have been 1-2-3-4-5-1. When the intercooling is used, compressed air from the low-pressure compressor (LP) at state 11 is cooled to state 12 and then compressed by the high-pressure (HP) compressor to state 2, at which the additional heat source is added. The operation cycle for the intercooled Brayton cycle is thus 1-11-12-2-3-4-5-1. Due to the pressure losses during heat addition from state 2 to state 3 and from state 3 to state 4, the

pressure at the outlet of a component is lower than at its inlet. In addition, there is a pressure loss in the intercooler and all piping, so the air pressure at the intercooler outlet is lower than at its inlet. The temperature at outlet of the compressor is decreased from state 21 to state 2. So there is more flexibility for choosing the temperature and the type of AHS since the temperature of the AHS must be higher than the temperature of pressurized air at the compressor outlet. Also, since the intercooling decreased the temperature at the compressor outlet, more regeneration can be gained from the gas turbine exhaust gas at state 5.

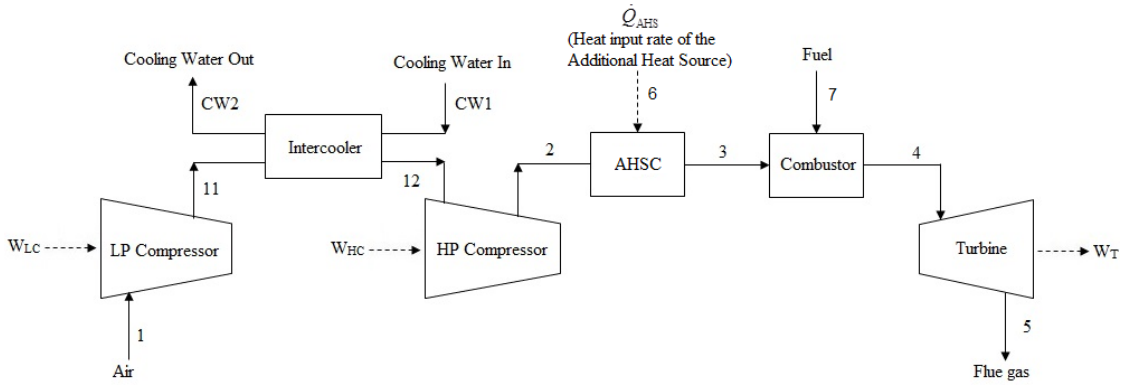

Fig. 5-5. Flow diagram of the hybrid gas turbine power plant based on the Brayton cycle with intercooling with an additional heat source (AHS) (AHSC: additional heat source collection equipment, LP: low-pressure, HP: high-pressure)

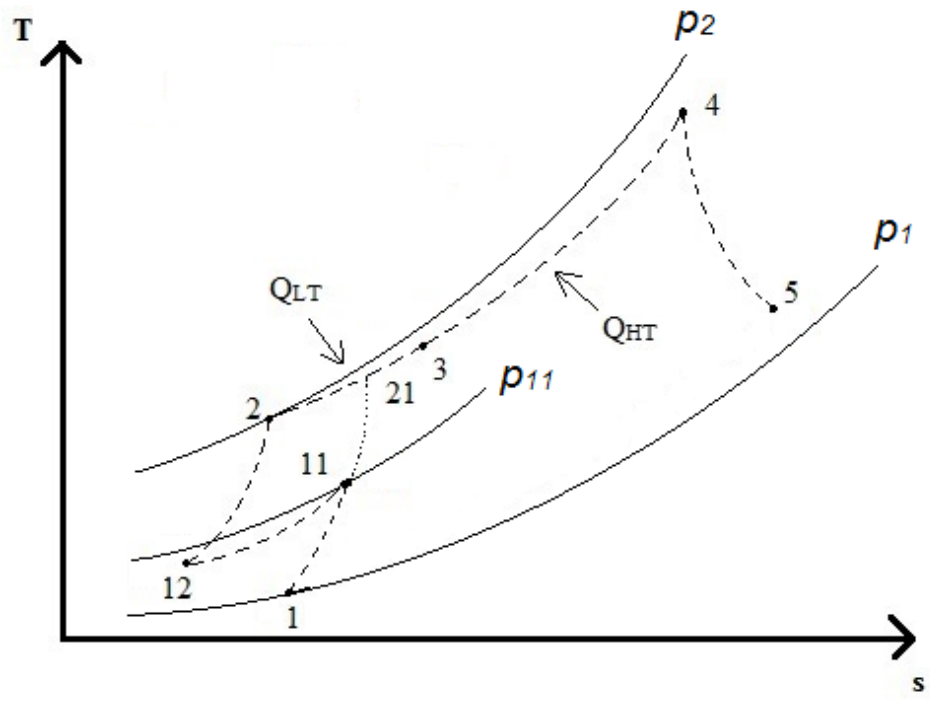

Fig. 5-6. T-s diagram of hybrid gas turbine power plant based on the Brayton cycle with intercooling with an additional heat source (AHS)(Q_{LT}: heat input from the additional heat source, Q_{HT}: heat input from the fuel in the combustor, ——: isobars, - - - -: real processes)

5.2.2. Thermodynamic analysis of hybrid power generation systems based on the Brayton cycle with intercooling

Using the same assumptions and method in Section 5.1.2, the energy and exergy efficiency for the hybrid Brayton cycle with intercooling are, respectively,

$$\eta_{\mathrm{h}} = \frac{(1+f)(h_4 - h_5) - \left[(h_{11} - h_1) + (h_2 - h_{12})\right]}{f \cdot \mathrm{LHV} + \dfrac{h_3 - h_2}{\eta_{\mathrm{AHS}}}}, \tag{5.26}$$

$$\varepsilon_{\mathrm{h}} = \frac{(1+f)(h_4 - h_5) - \left[(h_{11} - h_1) + (h_2 - h_{12})\right]}{f \cdot b_{\mathrm{f}} + \dfrac{h_3 - h_2}{\eta_{\mathrm{AHS}}}\left(1 - \dfrac{T_0}{T_{\mathrm{AHS}}}\right)}, \tag{5.27}$$

and for the reference system are, respectively,

$$\eta_0 = \frac{(1+f_0)(h_4 - h_5) - \left[(h_{11} - h_1) + (h_2 - h_{12})\right]}{f_0 \cdot \mathrm{LHV}}, \tag{5.28}$$

$$\varepsilon_0 = \frac{(1+f_0)(h_4 - h_5) - \left[(h_{11} - h_1) + (h_2 - h_{12})\right]}{f_0 \cdot b_{\mathrm{f}}}. \tag{5.29}$$

Using the same method in Section 5.1.2, we have the same results as for the simple Brayton cycle, i.e. $\eta_{\mathrm{h}} < \eta_0$ in most cases ($\eta_{\mathrm{AHS}} < \eta_{\mathrm{CC}} - \dfrac{h_4 - h_7}{\mathrm{LHV}}$) and $\varepsilon_{\mathrm{h}} > \varepsilon_0$ when $\eta_{\mathrm{AHS}} > 1 - \dfrac{T_0}{T_{\mathrm{AHS}}}$.

5.3. Hybrid power generation systems based on the Brayton cycle with reheat

5.3.1. Introduction of hybrid power generation systems based on the Brayton cycle with reheat

Reheat is also widely used in Brayton cycles since it increases the power output and the turbine exhaust gas temperature, which can be used in heat regeneration or a bottom cycle. The flow diagram and the qualitative T-s diagram of the hybrid Brayton cycle with reheat with the additional heat source (Q_{LT} in Fig. 5-8) are shown in Fig. 5-7 and Fig. 5-8, respectively. In this system, three heat sources Q_{LT}, $Q_{HT,1}$ and $Q_{HT,2}$ are used to heat the working fluid. As can be seen from the diagram, the HP Turbine exhaust gas at state 5 is reheated by heat source $Q_{HT,2}$ to state 42, from which it is expanded in the LP Turbine to state 5. The reheat-system turbine exit temperature T_5 is higher than the turbine exit temperature if no reheat was applied, T_{50}, and thus offers higher potential for heat regeneration or for use in combined cycle systems that will be discussed in CHAPTER 6.

The reason why the AHSC is not added in the upstream of combustor 2 is that this hybridization method raises the temperature needed for the AHS as can be seen from Fig. 5-8 ($T_{41}>T_2$). This increases the cost of the AHSC (the cost of solar collectors generally increases with the temperature it can achieve) and will thus not be considered here.

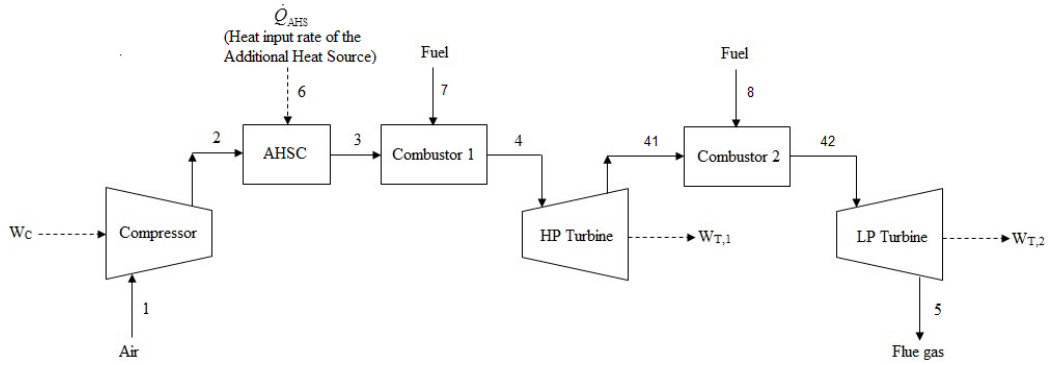

Fig. 5-7. Flow diagram of the reheat Brayton-based hybrid gas turbine power plant with an additional heat source (AHS) used to preheat the pressurized air (AHSC: additional heat source collection equipment, LP: low-pressure, HP: high-pressure)

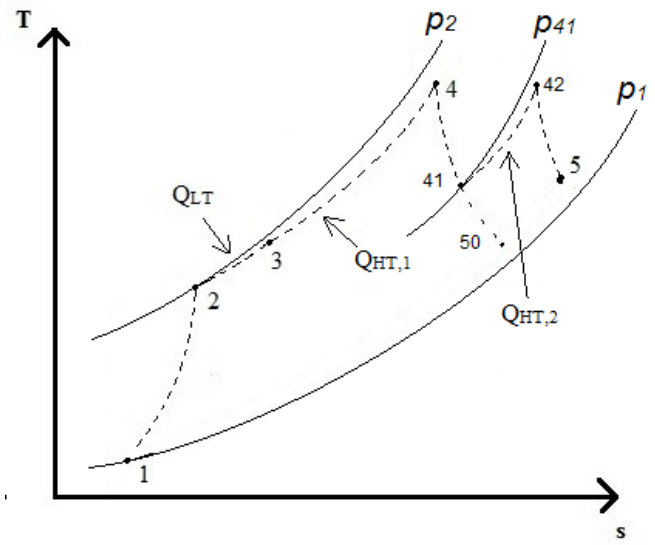

Fig. 5-8. Qualitative T-s diagram of the reheat Brayton-based hybrid gas turbine power plant with an additional heat source (AHS) (Q_{LT}: heat input from the additional heat source, $Q_{HT,1}$: heat input from the fuel in the combustor, $Q_{HT,2}$: heat input from the reheater, ——: isobars, - - - -: real processes)

5.3.2. Thermodynamic analysis of hybrid power generation systems based on the Brayton cycle with reheat

According to the mass and energy balance in the control volume enclosing the combustor 2 for the hybrid system in Fig. 5-7,

$$\eta_{\mathrm{CC}}\dot{m}_{\mathrm{f},2}\mathrm{LHV}+\dot{m}_{\mathrm{f},2}h_8+\left(\dot{m}_{\mathrm{a}}+\dot{m}_{\mathrm{f},1}\right)h_{41}=\left(\dot{m}_{\mathrm{a}}+\dot{m}_{\mathrm{f},1}+\dot{m}_{\mathrm{f},2}\right)h_{42}. \tag{5.30}$$

Thus

$$f_2=\frac{\dot{m}_{\mathrm{f},2}}{\dot{m}_{\mathrm{a}}+\dot{m}_{\mathrm{f},1}}=\frac{h_{42}-h_{41}}{\eta_{\mathrm{CC}}\mathrm{LHV}-\left(h_{42}-h_8\right)}. \tag{5.31}$$

For the reference system, similarly,

$$f_{0,2}=\frac{\dot{m}_{\mathrm{f},0,2}}{\dot{m}_{\mathrm{a}}+\dot{m}_{0,\mathrm{f},1}}=\frac{h_{42}-h_{41}}{\eta_{\mathrm{CC}}\mathrm{LHV}-\left(h_{42}-h_8\right)}=f_2. \tag{5.32}$$

Using the same assumptions and method in Section 5.1.2, the energy and exergy efficiency for the hybrid Brayton cycle with intercooling are, respectively,

$$\eta_{\mathrm{h}}=\frac{\left(1+f_1\right)\left(h_4-h_{41}\right)+\left(1+f_1\right)\left(1+f_2\right)\left(h_{42}-h_5\right)-\left(h_2-h_1\right)}{\left(f_1+f_2+f_1f_2\right)\cdot\mathrm{LHV}+\dfrac{h_3-h_2}{\eta_{\mathrm{AHS}}}}, \tag{5.33}$$

$$\varepsilon_{\mathrm{h}}=\frac{(1+f_1)(h_4-h_{41})+(1+f_1)(1+f_2)(h_{42}-h_5)-(h_2-h_1)}{(f_1+f_2+f_1f_2)\cdot b_{\mathrm{f}}+\dfrac{h_3-h_2}{\eta_{\mathrm{AHS}}}\left(1-\dfrac{T_0}{T_{\mathrm{AHS}}}\right)}, \qquad (5.34)$$

and for the reference system are, respectively,

$$\eta_0=\frac{(1+f_0)(h_4-h_{41})+(1+f_0)(1+f_2)(h_{42}-h_5)-(h_2-h_1)}{(f_0+f_2+f_0f_2)\cdot \mathrm{LHV}}, \qquad (5.35)$$

$$\varepsilon_{\mathrm{h}}=\frac{(1+f_0)(h_4-h_{41})+(1+f_0)(1+f_2)(h_{42}-h_5)-(h_2-h_1)}{(f_0+f_2+f_0f_2)\cdot b_{\mathrm{f}}}. \qquad (5.36)$$

Using the same method in Section 5.1.2, we obtain the same results as for the simple Brayton cycle, i.e. $\eta_{\mathrm{h}}<\eta_0$ when $\eta_{\mathrm{AHS}}<\eta_{\mathrm{CC}}-\dfrac{h_4-h_7}{\mathrm{LHV}}$ and $\varepsilon_{\mathrm{h}}>\varepsilon_0$ when $\eta_{\mathrm{AHS}}>1-\dfrac{T_0}{T_{\mathrm{AHS}}}$.

5.4. Hybrid power generation systems based on the Brayton cycle with heat regeneration

5.4.1. Introduction of hybrid power generation systems based on the Brayton cycle with heat regeneration

Heat regeneration, or just regeneration, is widely used in Brayton cycle power plants, where the turbine exhaust gas is used to preheat the pressurized air at the compressor outlet by a regenerator. The efficiency of an ideal cycle will typically be improved thereby since less heat input is needed while the work output remains the same. In real systems, the regenerator causes a pressure drop that will lower the turbine inlet pressure, which can be restored by additional compressor work investment. The efficiency of the regenerative Brayton cycle is nevertheless still likely to increase because the effect of the typical pressure loss on the system efficiency is much more than compensated by the effect of the regenerative heat input.

If regeneration is coupled with intercooling and/or reheat, as often done in Brayton power systems in practice, the efficiency can be improved further due to lower pressurized air temperature at the outlet of the compressor and/or higher turbine exhaust gas temperature [1]. The flow and T-s diagrams of the hybrid Brayton cycle with heat regeneration with the additional heat source is shown in Fig. 5-9 and Fig. 5-10, respectively. The reason why the AHS is used downstream of the regenerator rather than upstream is to increase the energy use of the turbine exhaust gas: to enable such heat transfer, the temperature of flue gas must be higher than the temperature of the pressurized air at the inlet of the regenerator (T_{51} must be higher than T_2, Fig. 5-10), so if AHS is added upstream of the regenerator, the

temperature of the pressurized air at the inlet of the regenerator will be higher and consequently also the temperature of flue gas, allowing less heat regeneration.

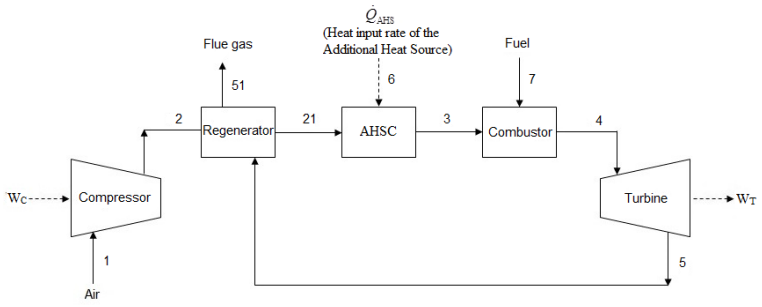

Fig. 5-9. Flow diagram of hybrid gas turbine power plant based on the Brayton cycle with heat regeneration, with an additional heat source (AHS) (AHSC: additional heat source collection equipment)

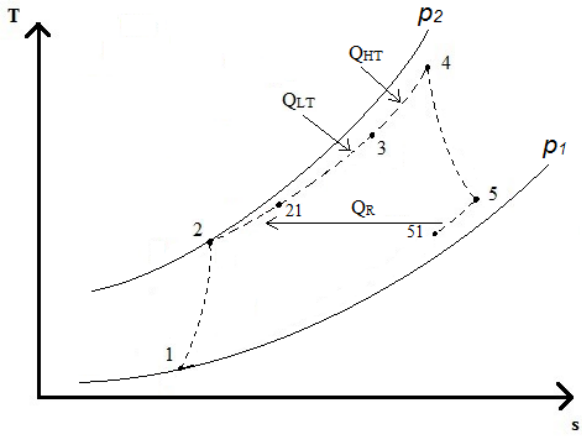

Fig. 5-10. Qualitative T-s diagram of the regenerative Brayton-based hybrid gas turbine power plant with an additional heat source (AHS) (Q_{LT}: heat input from the additional heat source, Q_{HT}: heat input from the fuel in the combustor, Q_R: heat duty of the regenerator, ——: isobars, - - - -: real processes)

5.4.2. Thermodynamic analysis of hybrid power generation systems based on the Brayton cycle with heat regeneration

Using the same assumptions and method as in Section 5.1.2, the energy and exergy efficiency for the hybrid Brayton cycle with intercooling are, respectively,

$$\eta_{\mathrm{h}} = \frac{(1+f)(h_4 - h_5) - (h_2 - h_1)}{f \cdot \mathrm{LHV} + \dfrac{h_3 - h_{21}}{\eta_{\mathrm{AHS}}}}, \tag{5.37}$$

$$\varepsilon_{\mathrm{h}} = \frac{(1+f)(h_4 - h_5) - (h_2 - h_1)}{f \cdot b_{\mathrm{f}} + \dfrac{h_3 - h_{21}}{\eta_{\mathrm{AHS}}}\left(1 - \dfrac{T_0}{T_{\mathrm{AHS}}}\right)}, \tag{5.38}$$

and for the reference system are, respectively,

$$\eta_0 = \frac{(1+f_0)(h_4 - h_5) - (h_2 - h_1)}{f_0 \cdot \mathrm{LHV}}, \tag{5.39}$$

$$\varepsilon_0 = \frac{(1+f_0)(h_4 - h_5) - (h_2 - h_1)}{f_0 \cdot b_{\mathrm{f}}}. \tag{5.40}$$

Using the same method as in Section 5.1.2, we have the same results as for the simple Brayton cycle, i.e. $\eta_h < \eta_0$ in most cases ($\eta_{AHS} < \eta_{CC} - \frac{h_4 - h_7}{LHV}$) and $\varepsilon_h > \varepsilon_0$ when $\eta_{AHS} > 1 - \frac{T_0}{T_{AHS}}$.

5.5. Simulation of hybrid power generation systems based on the Brayton cycle with intercooling, reheat and heat regeneration

5.5.1. Introduction of hybrid power generation systems based on the Brayton cycle with intercooling, reheat and heat regeneration

The flow diagram of the hybrid power generation system based on the Brayton cycle with intercooling, reheat and heat regeneration is shown in Fig. 5-11. The studied system uses 3 heat sources and has intercooling, reheat and regeneration process in addition to the simple Brayton cycle.

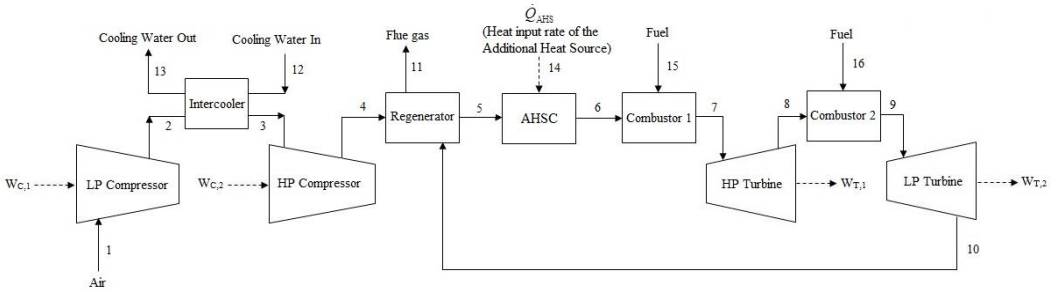

Fig. 5-11. Flow diagram of the hybrid gas turbine power plant based on the Brayton cycle with intercooling, reheat and heat regeneration, with an additional heat source

(AHS) (AHSC: additional heat source collection equipment, LP: low-pressure, HP: high-pressure)

The flow diagram of the reference power generation system based on the Brayton cycle with intercooling, reheat and heat regeneration is shown in Fig. 5-12. The only difference from the hybrid system is that there is no AHS and the state point 5 and 6 in the hybrid system are the same point in the reference system.

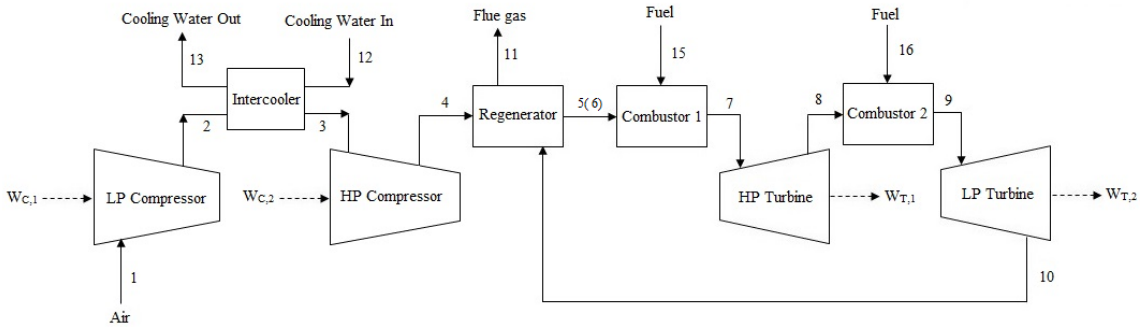

Fig. 5-12. Flow diagram of the reference gas turbine power plant based on the Brayton cycle with intercooling, reheat and heat regeneration (LP: low-pressure, HP: high-pressure)

5.5.2. Validation

Before using the Aspen simulation model to analyze the hybrid power generation systems based on the studied system, the model and its results need to be validated. To do that, the simulation model was first run using the operation parameters given in the outside reference used for the validation comparison. The results from the simulation were then

compared with the results given by the outside reference. The simulation model is considered to be validated when the relative errors are acceptably small (e.g. less than 1%). A similar example is given in Moran [1], with the same configuration as Fig. 5-11 with operation parameters and assumptions, but with no AHS. The assumptions made in the example are listed here:

1) Each component is analyzed as a control volume at steady state;
2) There are no pressure drops for flow through heat exchangers;
3) The compressor and turbine are adiabatic;
4) Kinetic and potential energy effects are negligible;
5) The working fluid is air modeled as an ideal gas.

Of these assumptions, the last one cannot be fulfilled by the simulation model, since when fuel is added and combusted, the mass flow rate and composition of working fluid will change; while the working fluid remains the same throughout the process in the book example. This will thus induce some difference in the results.

The operation parameters specified by the reference are summarized in Table 5-1.

Table 5-1. Operation parameter summary for the validation reference system [1]

Operation parameter	Value	Unit
Mass flow rate of inlet air	5.807	kg/s
Temperature of inlet air	300	K

Pressure of inlet air	100	kPa
Intercooler operation pressure	300	kPa
Reheater operation pressure	300	kPa
Turbine inlet temperatures	1,400	K
High pressure compressor inlet temperature	300	K
Pressure ratio across the two-stage compressor	10	
Pressure ratio across the two-stage turbine	10	
Isentropic efficiency of each compressor and turbine stage	80%	
Regenerator effectiveness	80%	

In the simulation, the mass flow of fuel is determined by the enthalpy balance in the combustor to ensure the temperature of combustion gas at the outlet of combustor is 1,400 K as given in the reference. The composition of natural gas is chosen as in an example in Moran's book [1] and is shown in Table 5-2. The lower heating value (LHV) of this fuel is the weighted total of the LHV of each component with respect to their composition and is calculated as 41,809 kJ/kg.

Table 5-2. Composition of the fuel used in the validation [1]

Component	Percentage
CH_4	80.62%
C_2H_6	5.41%
C_3H_8	1.87%
C_4H_{10}	1.6%
N_2	10.5%

The comparison results between the reference and simulation are shown in Table 5-3. The relative difference is only a few percent. Considering the mass flow rate change of working fluid (mass flow rate of fuel is 1.6% of mass flow rate of inlet air, given by simulation) as discussed before, the simulation model was validated.

Table 5-3. Comparison results between the reference and simulation for the validation system

Performance criteria	Reference [1]	Simulation	Relative difference
Mass flow rate of fuel [kg/s]	0	0.095	-

Compressor power input [kW]	1,704	1,705	0.06%
Turbine power output [kW]	3,750	3,851	2.6%
Net power output [kW]	2,046	2,146	4.7%
Total energy input rate [kW]	4,622	4,750	2.7%
Energy efficiency	0.443	0.452	2.0%

As an illustration, the T-s diagram of the validated reference system (Fig. 5-12) is shown in Fig. 5-13. When the AHS is introduced, point 6 will move upward along the line from point 5, as far as point 7 in which case combustor 1 is not needed, depending on how much AHS is used in the hybrid system.

Note that in the validation process, no pressure drop is considered, which is not the case in reality. Pressure drops in heat exchangers can have negative influence on system performance. The next step is study the exergy destruction in each component of the system to determine the potential of improvement, while considering pressure drops.

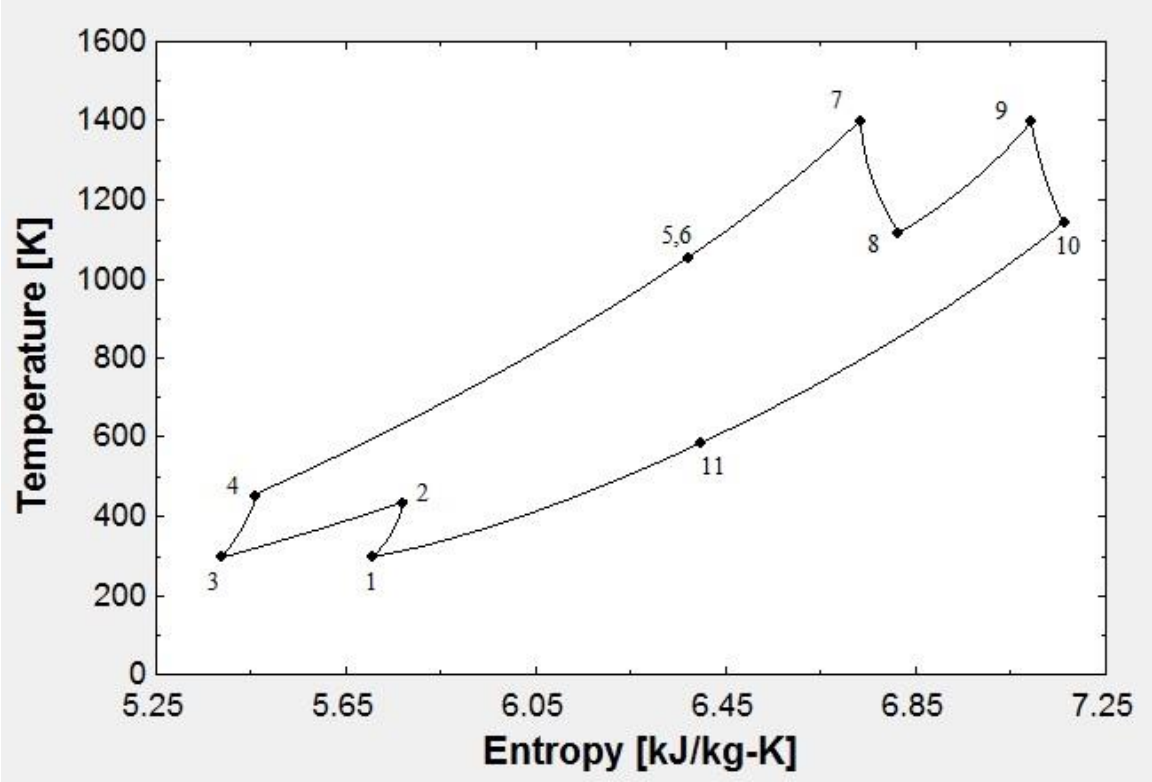

Fig. 5-13. T-s diagram of the validation system in Fig. 5-12 using the assumptions in Table 5-1

5.5.3. Reference system simulation

Before doing component exergy analysis for the system, we need to construct the system using practical operation parameters. We will first simulate the reference system in which no AHS is used and then study the effect after the introduction of the AHS.

The operation parameters for the reference system are summarized in Table 5-4.

Table 5-4. Operation parameters for the reference power generation systems based on the Brayton cycle with intercooling, reheat and heat regeneration

Operation parameter	Value	Unit
Mass flow rate of inlet air (normalized)	1	kg/s
Temperature of inlet air	288	K
Pressure of inlet air	101.3	kPa
Turbine inlet temperatures	1,623	K
High pressure compressor inlet temperature	288	K
Pressure ratio across the two-stage compressor	17	
Pressure ratio across the two-stage turbine	17	
Isentropic efficiency of each compressor stage	88%	
Isentropic efficiency of each turbine stage	90%	
Combustor energy efficiency	98%	
Compressor mechanical efficiency	98%	
Turbine mechanical efficiency	98%	

Air intake system pressure drop*	2%	
Exhaust system pressure drop*	3%	
LPC compression ratio	4	
HPC expansion ratio	4	
Intercooler hot side pressure drop*	5%	
Regenerator cold side pressure drop*	2.5%	
Combustor 1 pressure drop*	5%	
Combustor 2 pressure drop*	5%	
Regenerator hot side pressure drop*	2.5%	
Regenerator pinch point temperature	10	K

* Pressure drop is defined as the difference of the outlet and inlet pressure of a component relative to the inlet pressure of that component.

The calculated energy efficiency is 55.8%, which is smaller than 58.9% when no pressure drop is considered. We can see that there is an absolute 3.1% change for energy efficiency when considering the effect of pressure drops on system performance.

The T-s diagrams showing both the reference system with and with pressure drop are shown in Fig. 5-14. The symbol (×) indicates the points calculated with pressure drops; while the round symbol (◦) indicates the points calculated without pressure drops. For the same design point, the point calculated with pressure drop (× symbol) is placed to the right side to the point without pressure drop (◦symbol), since the pressure drop introduces entropy increases during the heat transfer process.

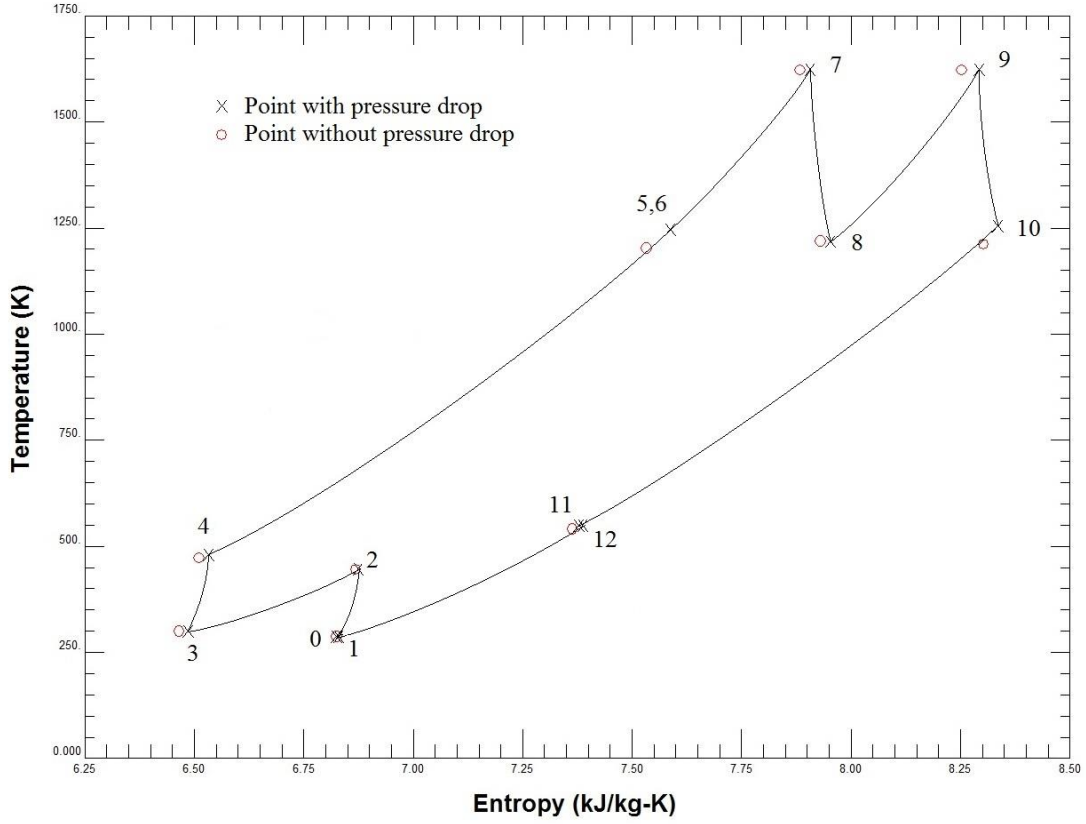

Fig. 5-14. T-s diagram of the reference power generation systems based on the Brayton cycle with intercooling, reheat and heat regeneration (×: pressure drops considered, ◦: pressure drops not considered)

The physical properties at each design point calculated with pressure drops are summarized in Table 5-5. Other main operation data are summarized in Table 5-6.

Table 5-5. Physical properties at each design point for the reference power generation systems based on the Brayton cycle with intercooling, reheat and heat regeneration, with pressure drops

Design point	Mass flow rate [kg/s]	Temperature [K]	Pressure [kPa]	Specific enthalpy [kJ/kg]	Specific entropy [kJ/kg-K]
0	1.0000	288	101.3	288.3	6.82
1	1.0000	288	99.3	288.3	6.83
2	1.0000	446	397.1	448.1	6.87
3	1.0000	300	377.2	299.6	6.49
4	1.0000	481	1,687.7	482.9	6.53
5	1.0000	1,246	1,645.5	1,334.2	7.59
6	1.0000	1,246	1,645.5	1,334.2	7.59
7	1.0122	1,623	1,603.3	1,882.1	7.91
8	1.0122	1,219	400.8	1,380.5	7.95

9	1.0259	1,623	380.8	1,983.6	8.29
10	1.0259	1,256	107.1	1,514.1	8.33
11	1.0259	551	104.4	684.1	7.38
12	1.0259	551	101.3	684.1	7.39

Table 5-6. Simulation results for the reference power generation systems based on the Brayton cycle with intercooling, reheat and heat regeneration, with pressure drops

	Value	Unit
Mass flow rate of fuel for Combustor 1	0.012	kg/s
Mass flow rate of fuel for Combustor 2	0.014	kg/s
Total compressor power input	350	kW
Total turbine power output	960	kW
Net power output	611	kW
Heat addition rate for Combustor 1	512	kW
Heat addition rate for Combustor 2	582	kW
Total heat addition rate	1,094	kW

Energy efficiency	55.81	%

5.5.4. Reference system exergy analysis

Before making exergy analysis for reference system, we need to find the chemical exergy of fuel. The chemical exergy equation for mixture is widely known [1] as

$$\bar{b}_{\text{ch}} = \sum_{i=1}^{j} y_i \bar{b}_{i,\text{ch}} + \bar{R}T_0 \sum_{i=1}^{j} y_i \ln y_i \tag{5.41}$$

in which $\bar{b}_{i,\text{ch}}$ [kJ/kmol] and y_i is the standard chemical exergy and mole fraction of species i, $\bar{R}$ [kJ/kmol-K] is universal gas constant and T_0 [K] is dead state temperature.

Based on the composition of the fuel used in the simulation (given in Table 5-2) and standard chemical exergy of its component given in [1], the chemical exergy of the fuel used in the simulation is

$$\begin{aligned}\bar{b}_{\text{ch}} &= \sum_{i=1}^{j} y_i \bar{b}_{i,\text{ch}} + \bar{R}T_0 \sum_{i=1}^{j} y_i \ln y_i = 0.8062(831{,}650) + 0.0541(1{,}495{,}840) \\ &+0.0187(2{,}154{,}000) + 0.016(2{,}805{,}800) + 0.105(720) \\ &+(8.314)(288)\begin{bmatrix} 0.8062\ln(0.8062) + 0.0541\ln(0.0541) \\ +0.0187\ln(0.0187) + 0.016\ln(0.016) + 0.105\ln(0.105) \end{bmatrix} \\ &= 834{,}952 \text{ kJ/kmol}\end{aligned} \tag{5.42}$$

The specific chemical exergy of the fuel is thus

$$b_{\text{ch}} = 52,045 \text{ kJ/kg} \tag{5.43}$$

The chemical exergy flow from the fuel, $\dot{B}_{\text{ch}}$ [kW], can thus be found using

$$\dot{B}_{\text{ch}} = \dot{m}_{\text{f}} b_{\text{ch}} \tag{5.44}$$

in which $\dot{m}_{\text{f}}$ [kg/s] is the mass flow rate of fuel, which is calculated from the simulation.

Since the fuel is simulated to be injected at environmental temperature and pressure, the physical exergy of fuel is 0. Neglecting kinetic exergy and potential exergy, which is small compared with chemical exergy, the total exergy of the injected fuel can thus be regarded as its chemical exergy.

Inlet air is assumed to be at environmental temperature, pressure and composition, so its physical and chemical exergy are both 0. Since our interest is in the exergy destruction in each component and the velocity and height of fluid cannot be determined by the simulation, the kinetic exergy and potential exergy will be neglected. The total exergy flow of the air into the system is thus 0.

The exergy destruction in component is defined by the difference between the total inlet exergy flow rate and total outlet exergy flow rate. The results, together with exergy destruction breakdown, are summarized in Table 5-7 and Fig. 5-15.

Table 5-7. Component exergy breakdown for the reference power generation systems based on the Brayton cycle with intercooling, reheat and heat regeneration

Component	Exergy destruction rate [kW]	Exergy destruction fraction
Compressor inlet	1.7	0.4%
Low-pressure compressor	16.3	3.4%
Intercooler	33.7	7.1%
High-pressure compressor	17.5	3.7%
Regenerator	23.2	4.9%
Combustor 1	147.4	31.2%
High-pressure turbine	24.6	5.2%
Combustor 2	174.7	36.9%
Low-pressure turbine	31.3	6.6%
Turbine outlet	2.7	0.6%
TOTAL	473.2	100.0%

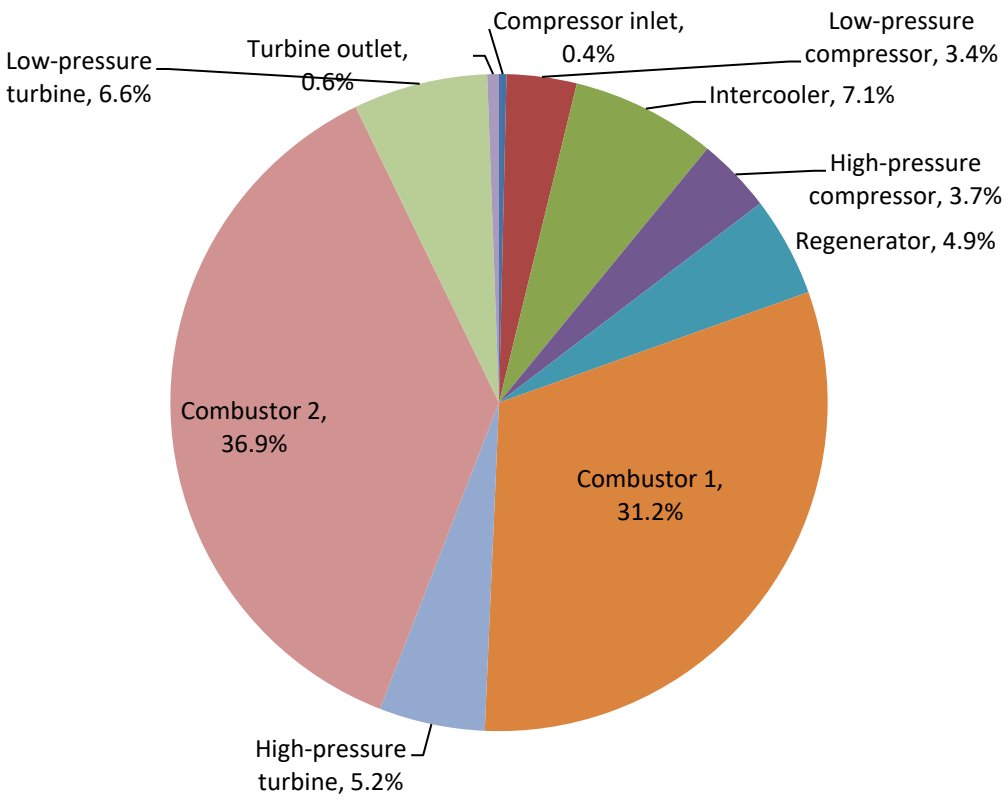

Fig. 5-15. Component exergy destruction breakdown for the reference power generation systems based on the Brayton cycle with intercooling, reheat and heat regeneration

We can see that the two combustors have the most exergy destruction fractions of the total exergy destruction of the system, with each combustor accounts for about 1/3 of the total exergy destruction. This is largely due to the irreversible chemical reactions and large temperature difference during heat transfer in the combustors, when we use the combustors to heat the working fluid by burning fuel. This suggests that we should try to minimize the exergy destruction in the combustors. One way to achieve that is perhaps to use a lower

temperature heat source to partially preheat the working fluid before heated by burning fuel. This may reduce the fuel usage and thus the exergy destruction in the combustion process. As will be shown in the next section, it indeed reduces the exergy destruction in the combustors.

5.5.5. Hybrid system exergy analysis

As we can see from Fig. 5-11, when an additional heat source (AHS) is added between the regenerator and combustor 1, less fuel will be needed in combustor 1 to heat the working fluid to the designed maximum temperature of the system. If there is enough AHS input, no fuel for combustor 1 is needed and this is the maximal amount of possible added AHS. We will first determine this maximum value.

In the reference system, we have assumed that the pressure drop of combustor 1 is 5% of the pressure at the outlet of the high-pressure compressor. In the hybrid system, we may assume that the pressure at the outlet of combustor 1 remains the same for the hybrid and the reference system.

The pressure drop of the AHSC may vary depending on the type of AHSC, directly or indirectly using a heat exchanger. Based on the previous available date about pressure drops for the intercooler and regenerator, which is 5% and 2.5%, respectively, for pressurized air side, we may assume the pressure drop of the AHSC for pressurized air side as 3%.

5.5.5.1. *Limiting case for the AHS heat input*

When the AHS is solely used to preheat the working fluid to HPT designed inlet temperature and no fuel is needed in combustor 1, the amount of the AHS needed reaches its maximum amount, and this case will be regarded as the limiting case. For comparison, we have assumed that the energy conversion efficiency of LTHS is the same as that for combustor 1 (98%), while it could be lower in practice, which will be discussed in the next section.

5.5.5.1.1. Energy analysis

The physical properties at each design point calculated with pressure drops are summarized in Table 5-8. Other main results are summarized in Table 5-9.

Table 5-8. Physical properties at each design point in Fig. 5-11 for the hybrid power generation systems based on the Brayton cycle with intercooling, reheat and heat regeneration in the limiting case

Design point	Mass flow rate [kg/s]	Temperature [K]	Pressure [kPa]	Specific enthalpy [kJ/kg]	Specific entropy [kJ/kg-K]
0	1.000000	288	101.3	1.2258	288.31
1	1.000000	288	99.3	1.2013	288.31
2	1.000000	446	397.1	3.0967	448.10

3	1.000000	300	377.2	4.3851	299.76
4	1.000000	481	1,687.7	12.1550	482.96
5	1.000000	1,255	1,645.5	4.5475	1344.20
6	1.000000	1,623	1,594.8	3.4111	1787.70
7	1.000000	1,623	1,510.5	3.2311	1787.70
8	1.000000	1,211	377.6	1.0851	1291.50
9	1.013334	1,623	358.7	0.7633	1889.60
10	1.013334	1,265	107.1	0.2926	1443.70
11	1.013334	523	104.4	0.6896	593.54
12	1.013334	523	101.3	0.6689	593.54

Table 5-9. Operation data for the hybrid power generation systems based on the Brayton cycle with intercooling, reheat and heat regeneration in the limiting case

	Value	Unit
Mass flow rate of fuel for combustor 1	0	kg/s
Mass flow rate of fuel for combustor 2	0.013	kg/s

Total compressor power input	350	kW
Total turbine power output	929	kW
Net power output	579	kW
Heat addition rate from the AHS	452	kW
Heat addition rate for combustor 1	0	kW
Heat addition rate for combustor 2	569	kW
Total heat addition rate	1,021	kW
Energy efficiency	56.69	%

We can see that, compared to the reference system,

1) Compressor power inputs remained the same, since air inlet condition and compressor configurations remained the same;
2) Turbine power output decreased by 31 kW (3%), due to the decrease in the mass flow rate of the working fluid in the turbine (without the addition of fuel added in combustor 1);
3) Net power output decreased by 32 kW (5%), due to the decrease in turbine power output;
4) AHS (combustor 1) heat addition rate decreased by 69 kW (13%), since higher energy conversion efficiency for the AHSC (100%) compared with combustor 1

(98%), and higher regenerated temperature (1,265 K for hybrid system and 1256 K for the reference system);

5) Combustor 2 heat addition rate decreased by 13 kW (2%), due to lower mass flow rate of working fluid in the high-pressure turbine;
6) Total heat addition rate decreased by 73 kW (7%), due to decrease in heat additional rates for the AHSC (combustor 1) and combustor 2;
7) Energy efficiency increased from 55.81% to 56.69%, since decrease in heat additional rate (7%) is larger than decrease in net power output (5%), but such small difference is within the error band of the analysis.

The energy-related results indicate that replacingcombustor 1 with the AHSC whose energy conversion efficiency is 100% and higher than that of the combustors (98%) reduces the mass flow rate of working fluid (since less fuel is injected into the combustor) and thus the net power output (since the turbine power output is proportional to the mass flow rate of the working fluid), but increases the energy efficiency of the system (from Eq. (5.15)). There is also little room to improve the energy efficiency of the hybrid system since the energy conversion efficiency of the AHSC has already been maximized to 100% in this analysis. The efficiency of the combustor also has little room to improve since it is already very high (98%) after having been developed for so many decades. The feasible ways to improve the energy efficiency of the hybrid system is to increase the top temperature of the system or the turbine inlet temperature (TIT) and increase the isentropic efficiencies of the compressor and turbine by doing experiments or detailed simulation within the compressor and turbine. All of these methods are beyond the scope of the dissertation and my ability.

5.5.5.1.2. <u>Exergy analysis</u>

The calculation method of exergy destruction rate for every component is the same as in reference system exergy analysis in Section 5.5.4, except for the AHSC.

From the energy analysis, we have known the heat input rate for the AHSC. The exergy input rate, however, does not solely depend on the heat input rate, but also an "effective temperature T_{eff} " of the heat source. Using Carnot efficiency, the exergy input rate for the AHSC can be calculated by

$$\dot{B}_{\text{AHS}} = \dot{B}_{14} = \dot{Q}_{\text{AHS}}\left(1-\frac{T_0}{T_{\text{eff}}}\right) = \dot{Q}_{14}\left(1-\frac{T_0}{T_{\text{eff}}}\right) \tag{5.45}$$

in which $T_0 = 288\ \text{K}$ is the dead state temperature.

Thus, the exergy destruction rate in the AHSC can be calculated by

$$\dot{B}_{\text{D,AHSC}} = \dot{B}_5 + \dot{B}_{14} - \dot{B}_6 \tag{5.46}$$

For the solar heat source, the effective temperature can be regarded as the temperature at sun surface, which is about 5,800 K. For hot fluid as heat source, such as pressurized air in the solar tower, the effective temperature is the temperature of the fluid. For complete discussion, we will consider two scenarios:

1) The sun surface temperature is defined as the AHS temperature when solar heat is used as the AHS, i.e. $T_{\text{eff}} = T_{\text{ss}} = 5{,}800\ \text{K}$;
2) The temperature of the hot fluid is defined as the AHS temperature and is 10 K higher than the temperature at the AHSC outlet, i.e. $T_{\text{eff}} = T_6 + 10 = 1633\ \text{K}$.

The exergy destruction rate breakdown in each component in the hybrid system are shown in Fig. 5-16 and Fig. 5-17, respectively, for the above two scenarios, with emphasis on the AHSC.

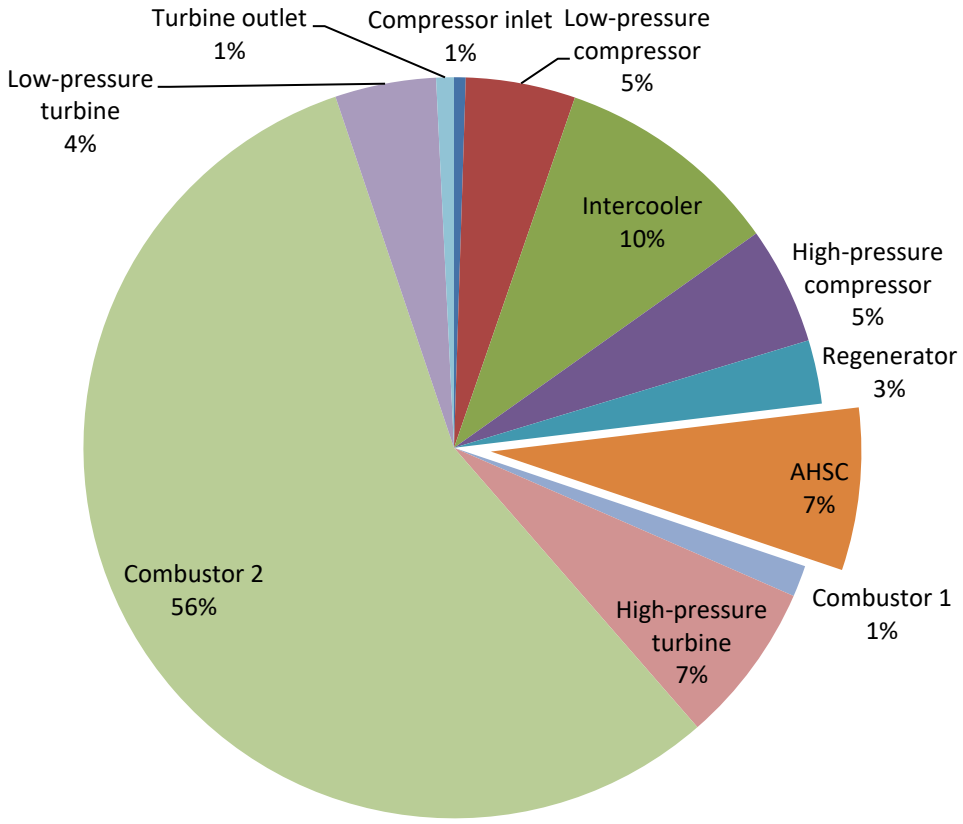

Fig. 5-16 The exergy destruction rate breakdown in each component for the hybrid power generation systems based on the Brayton cycle with intercooling, reheat and heat regeneration in the limiting case (the AHS temperature is defined as the sun surface temperature when solar heat is used as the AHS)

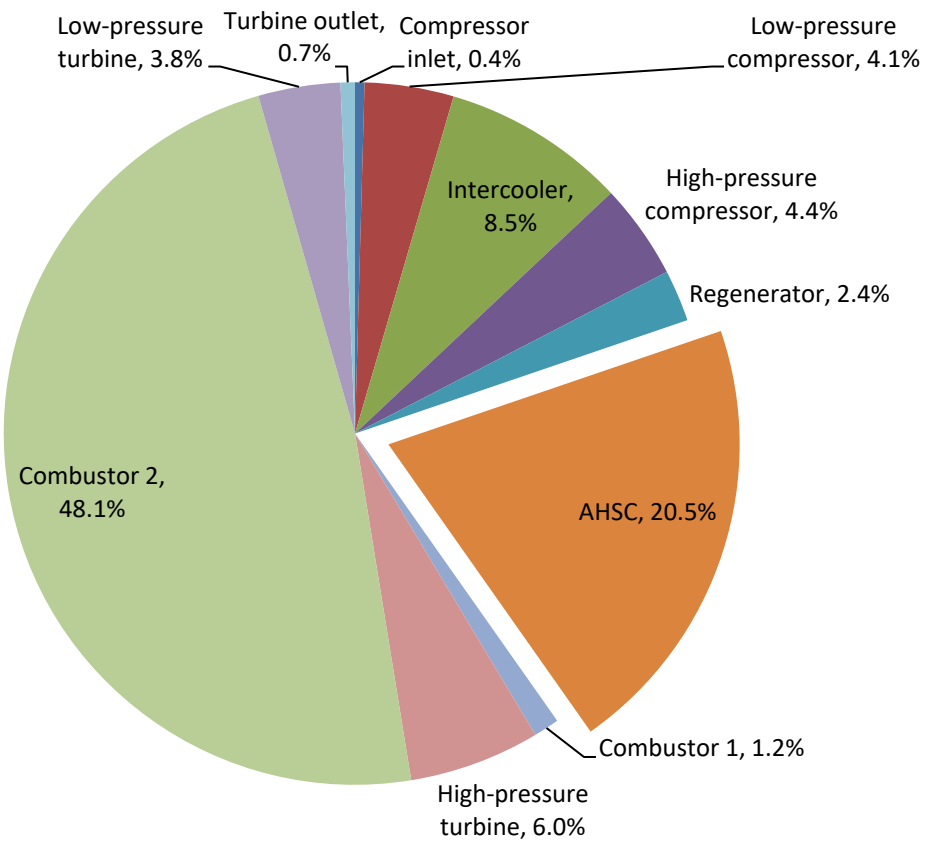

Fig. 5-17. The exergy destruction rate breakdown in each component for the hybrid power generation systems based on the Brayton cycle with intercooling, reheat and heat regeneration in the limiting case (the AHS temperature is defined as 10 K higher than the AHSC outlet temperature)

It can be seen that when the AHS temperature is defined as the sun surface temperature, the exergy destruction rate in the AHSC is "larger" than if defined based on the outlet temperature of the AHSC (10 K higher in the case study but could be other values in

practice). It should be noted that this is only a matter of definition of the AHS temperature. While it is not practical to use solar heat at the sun surface temperature (about 5,800 K), the AHSC-based AHS temperature also has its drawback since it does not consider the full potential of doing work from solar energy. For example, the heat from the AHSC that generates higher temperature can do more work than the same amount of heat from the AHSC that generates lower temperature. It will thus make it hard to compare the performance of two solar-assisted power generation systems using solar heat at different temperatures. Both methods have been used by researchers and there is no agreement on which method to use in the future. This study shows the difference between the results from different definition of the AHS temperature.

Although some results (such as the exergy destruction rate in the AHSC and the system exergy efficiency) are different based on different solar exergy definitions, it does not mean that the performance of the system will change based on different solar exergy definitions. The solar exergy definition is only used in determining the exergy destruction rate in the AHSC and will not affect other equipment analysis results (such as the exergy destruction rate in the combustors).

Different system exergy efficiencies are not comparable to each other unless they use the same solar exergy definition. This, however, does not invalidate the results from the previous thermodynamic analysis. The thermodynamic analysis has already included the effect of solar exergy definition in the determination of the exergy conversion efficiency

of the AHS, η'_{AHS}. The comparisons of the hybrid system and the reference system and the sensitivity analysis of the hybrid system were all based on different η'_{AHS}.

The results also showed that the exergy destruction fraction in the AHSC of the total exergy destruction of the hybrid system is less than exergy destruction fraction of the combustor 1 of the total exergy destruction in the reference system (the numbers can be easily read from Figs. 5-18-5-19 and will not be repeated here). This is mainly because the exergy destruction in the combustor during fuel combustion is higher than that in the AHSC in which the temperature difference between the heat source (solar heat) and the working fluid (pressurized air) is small.

5.5.5.2. *Sensitivity analysis for the hybrid system*

After considering the limiting case when the amount of low temperature heat source reaches its maximum value, we now study the influence of the AHS on the energy efficiency of the hybrid system, η_{h}, by doing sensitivity analysis of the energy efficiency of the hybrid system with respect to the

1) AHS input fraction of the total energy input, X_{AHS}, (defined in Eq. (2.17));
2) AHS exergy input rate, $\dot{B}_{\text{AHS}}$, (defined in Eq. (5.45) and the temperature of the AHS is assumed to be 10 K higher than the outlet temperature of the AHSC);
3) AHS temperature (expressed by a dimensionless parameter as $\frac{T_6 - T_5}{T_7}$ in Fig. 5-11);

4) AHS energy conversion efficiency, η_{AHS}.

Fig. 5-20 shows the relation between the energy efficiency of the hybrid Brayton system, η_h, and the AHS input fraction of total energy input, X_{AHS}, for different energy conversion efficiency of the AHS, η_{AHS}. It can be seen that when η_{AHS} is 40%, 60% and 80%, adding the AHS will lower η_h. When $\eta_{AHS} = 100\%$, adding the AHS will increase η_h. This was shown in the results from the thermodynamic analysis before in Eqs (5.15) and (5.16).

It can also be seen from Fig. 5-20 that for a contain X_{AHS}, higher η_{AHS} will increase η_h. This suggests that it is worthwhile to increase η_{AHS} from the thermodynamic perspective. For example, when $X_{AHS} = 29\%$, doubling η_{AHS} from 40% to 80% will increase η_h by an absolute value of 7%, from 47% to 54%.

Fig. 5-21 shows the relation between the energy efficiency of the hybrid Brayton system, η_h, and the exergy input rate from the AHS, $\dot{B}_{AHS}$, for different energy conversion efficiency of the AHS, η_{AHS}. Fig. 5-22 shows the relation between the energy efficiency of the hybrid Brayton system, η_h, and the dimensionless parameter as $\frac{T_6 - T_5}{T_7}$ in Fig. 5-11, for different energy conversion efficiency of the AHS, η_{AHS}. These three figures show that the overall performance of the hybrid cycles decreases except for unrealistically high AHS efficiencies.

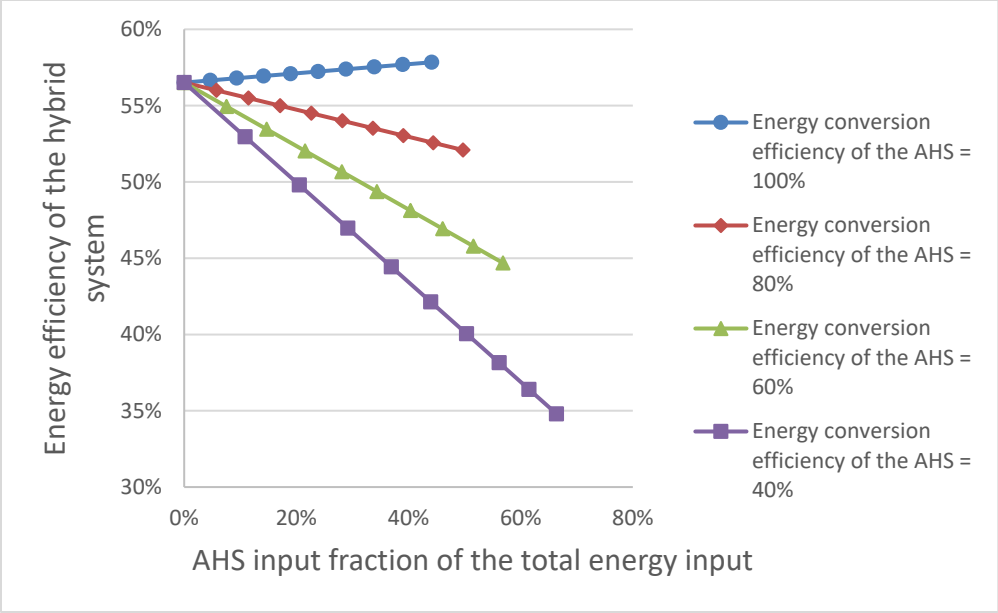

Fig. 5-20. The relation between the energy efficiency of the hybrid system and the AHS input fraction of total energy input for different energy conversion efficiencies of the AHS

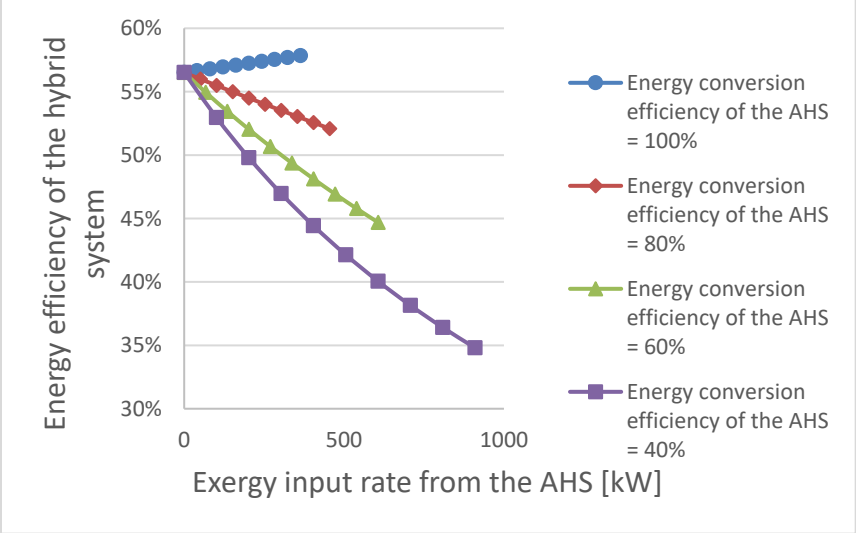

Fig. 5-21. The relation between the energy efficiency of the hybrid system and the AHS exergy input rate for different energy conversion efficiencies of the AHS

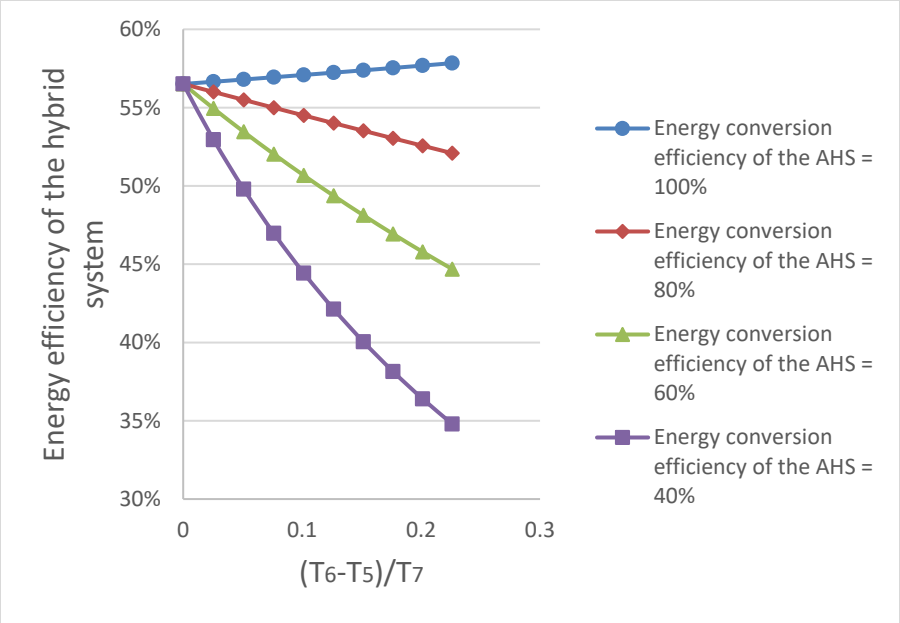

Fig. 5-22. The relation between the energy efficiency of the hybrid system and the dimensionless parameter $\frac{T_6 - T_5}{T_7}$ *in Fig. 5-11 for different energy conversion efficiency of the AHS*

5.6. Conclusions of the thermodynamic analysis of hybrid power generation systems based on Brayton cycle

This chapter mainly examines the thermodynamic features and performance of hybrid power generation systems based on Brayton cycles. The thermodynamic analysis for the hybrid power generation systems based on the simple Brayton cycle, Brayton cycle with intercooling, Brayton cycle with reheat and Brayton cycle with heat regeneration was done, respectively.

The results showed that the energy efficiency of the hybrid system is lower that of the single heat source reference system when $\eta_{\text{AHS}} < \eta_{\text{CC}} - \frac{h_4 - h_7}{\text{LHV}}$. Considering that $\eta_{\text{CC}} - \frac{h_4 - h_7}{\text{LHV}}$ is close to 1 and $\eta_{\text{AHS}} \le 1$, adding the AHS to the single heat source Brayton cycles will lower the energy efficiency of the reference system as Table 3-2 showed in the background review. The exergy efficiency, however, is not the case, and $\varepsilon_{\text{h}} > \varepsilon_0$ when $\eta'_{\text{AHS}} < \eta'_{\text{CC}} - \frac{h_4 - h_7}{b_{\text{f}}}$ or roughly $\eta_{\text{AHS}} > 1 - \frac{T_0}{T_{\text{AHS}}}$. For example, when $T_{\text{AHS}} = 800\ ^\circ\text{C}$ and $T_0 = 15\ ^\circ\text{C}$, $\varepsilon_{\text{h}} > \varepsilon_0$ when $\eta_{\text{AHS}} > 0.73$.

Following the validation, a detailed simulation for the hybrid power generation systems based on the Brayton cycle with intercooling, reheat and heat regeneration was done in the dissertation. The results were compared for with and without the consideration of pressure drops in the system and showed that the energy efficiency dropped 3.1% if pressure drops were considered in the system. The results from the exergy analysis for each major component of the single heat source reference system showed that the majority (68.1%) of the exergy destructions happened in the combustors, in which fuel was burned. Considering that, using the AHS to help heat the working fluid may decrease the exergy destruction in the combustors and raise the exergy efficiency of the system. Another simulation was thus done to test the performance of the hybrid system. The results showed that the total exergy destruction of the system decreased by 16% (when the temperature of the solar heat is

defined as the sun surface temperature), or 28% (when the temperature the AHS is 10 K higher than the temperature of the working fluid at the outlet of the AHSC). The sensitivity analysis of the energy efficiency of the hybrid system with respect to the AHS input fraction of the total energy input, exergy input rate from the AHS and the dimensionless parameter $\frac{T_6 - T_5}{T_7}$ in Fig. 5-11, for different energy conversion efficiency of the AHS was also done. The results can be used to help researcher study the performance of the hybrid power generation systems based on the Brayton cycles and suggested that effort should be made in increasing η_{AHS}.

References for Chapter 5

[1] Moran M.J., Shapiro H.N., Boettner D.D., Bailey M.B., Fundamentals of Engineering Thermodynamics, 8th ed. Wiley, 2014.

CHAPTER 6

THERMODYNAMIC ANALYSIS OF THERMAL HYBIRD POWER GENERATION SYSTEMS BASED ON THE COMBINED CYCLES

In combined-cycle power plants, the high temperature (typ. > ~500 °C) gas turbine exhaust gas is used as the heat source for the Rankine cycle that could generate additional power besides the gas turbine. The energy efficiency of commercial combined cycle power plants is as high as about 60%, which is much higher than efficiencies of individual Rankine or Brayton cycle. Combined cycle power plants are therefore used increasingly.

Hybrid combined cycles could be configured in ways shown in Fig. 6-1, by adding heat sources in the topping cycle (Brayton), or the bottoming cycle (Rankine), or in both. The T-s diagram of a hybrid combined cycle with AHS added in both the topping cycle and the bottoming cycle is shown in Fig. 6-2. When the additional heat source (AHS) is added in the topping cycle and fix the bottoming cycle, less fuel is needed while the net power output of the system remains roughly the same. In this case, the hybrid combined cycle power plant is often said to be in fuel-saving mode. When the AHS is added in the bottoming cycle and fix the topping cycle, the fuel use in the top cycle remains the same, but the power generation from the bottom cycle increases due to the higher energy input. In this case, the hybrid combined cycle power plant is in the power-boost mode. In fact, it is easy

to know that when the net power outputs are fixed for all cycles, both modes reduce the fuel usage. This research, however, does not fix the net power output, since the objective here is to compare the energy and exergy efficiencies of the power cycles, which are the more important criteria in assessing the performance of power cycles than the net power output.

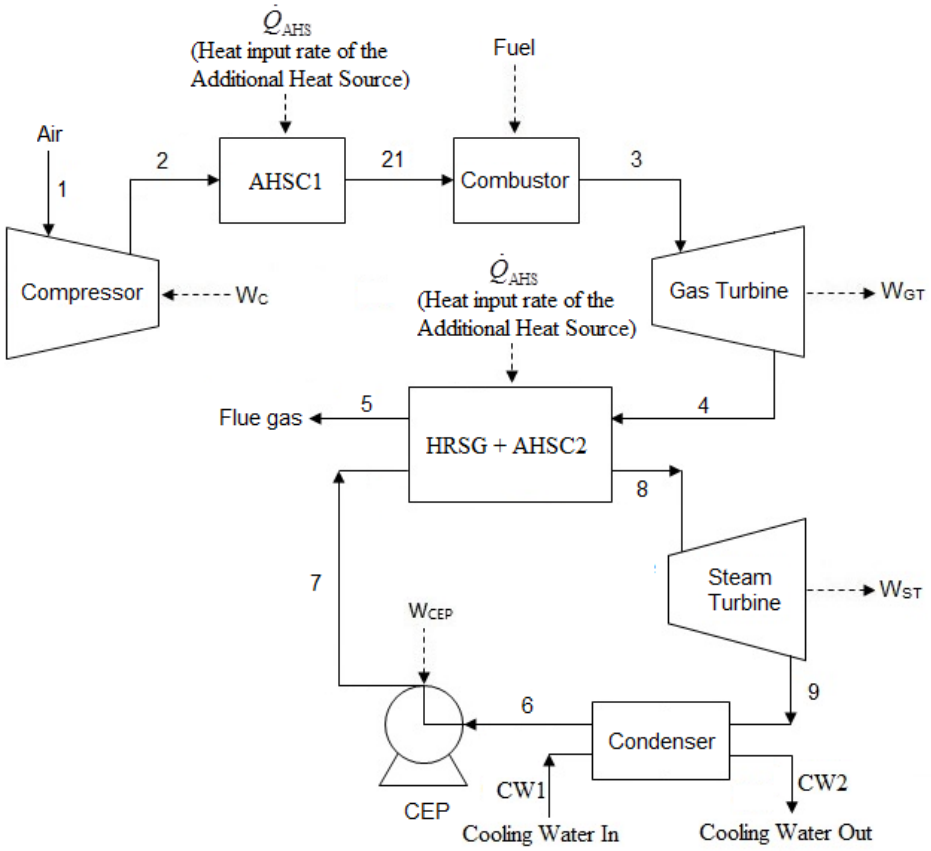

Fig. 6-1. Flow diagrams of hybrid combined cycle with three ways to add the additional heat source(s) (AHS): added to Brayton cycle as AHS1, added to the Rankine cycle as AHS2, and added to both cycles (HRSG: heat recovery steam generator, CEP: condensate extraction pump, AHSC: additional heat source collection equipment)

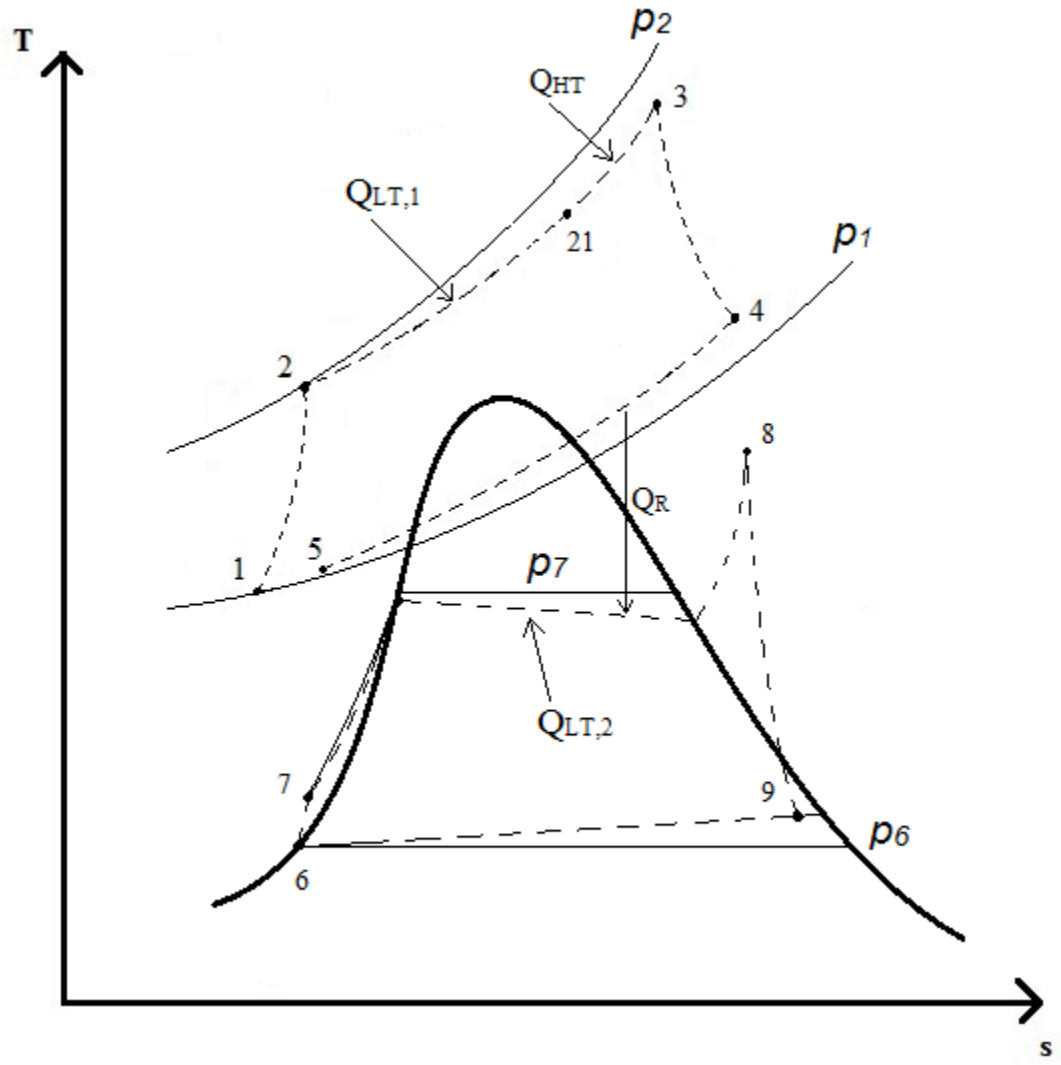

Fig. 6-2. Qualitative T-s diagram of the hybrid combined cycle plant with two additional heat sources (AHS) ($Q_{LT,1}$: heat input from the additional heat source at the topping cycle, $Q_{LT,2}$: heat input from the additional heat source at the bottoming cycle, Q_{HT}: heat input from the fuel in the combustor, Q_R: heat duty of the heat recovery steam generator, ——: isobars, - - - -: real processes)

6.1. Hybrid power generation systems based on the combined cycle with the AHS added in the topping (Brayton) cycle

6.1.1. Introduction of the hybrid power generation systems based on the combined cycle with the AHS added in the topping (Brayton) cycle

The flow diagram of the hybrid power generation systems based on the combined cycle with the AHS added in the topping cycle (Brayton) is shown in Fig. 6-3. It could be seen that the topping cycle of the combined cycle is the hybrid simple gas turbine cycle system which was analyzed in CHAPTER 5. HRSG stands for "heat recovery steam generator" composed of several heat exchangers and a steam generator (drum), and is used to heat the working fluid in the bottoming cycle from state 7 to state 8 using the energy contained in the exhaust gas from the gas turbine in the topping cycle. In the reference system (conventional combined cycle power plant without the AHS), the only heat source is the fuel added in the gas turbine in the topping cycle. The heat source for the bottoming cycle is the heat from the gas turbine exhaust gas and no additional fuel is needed to drive it.

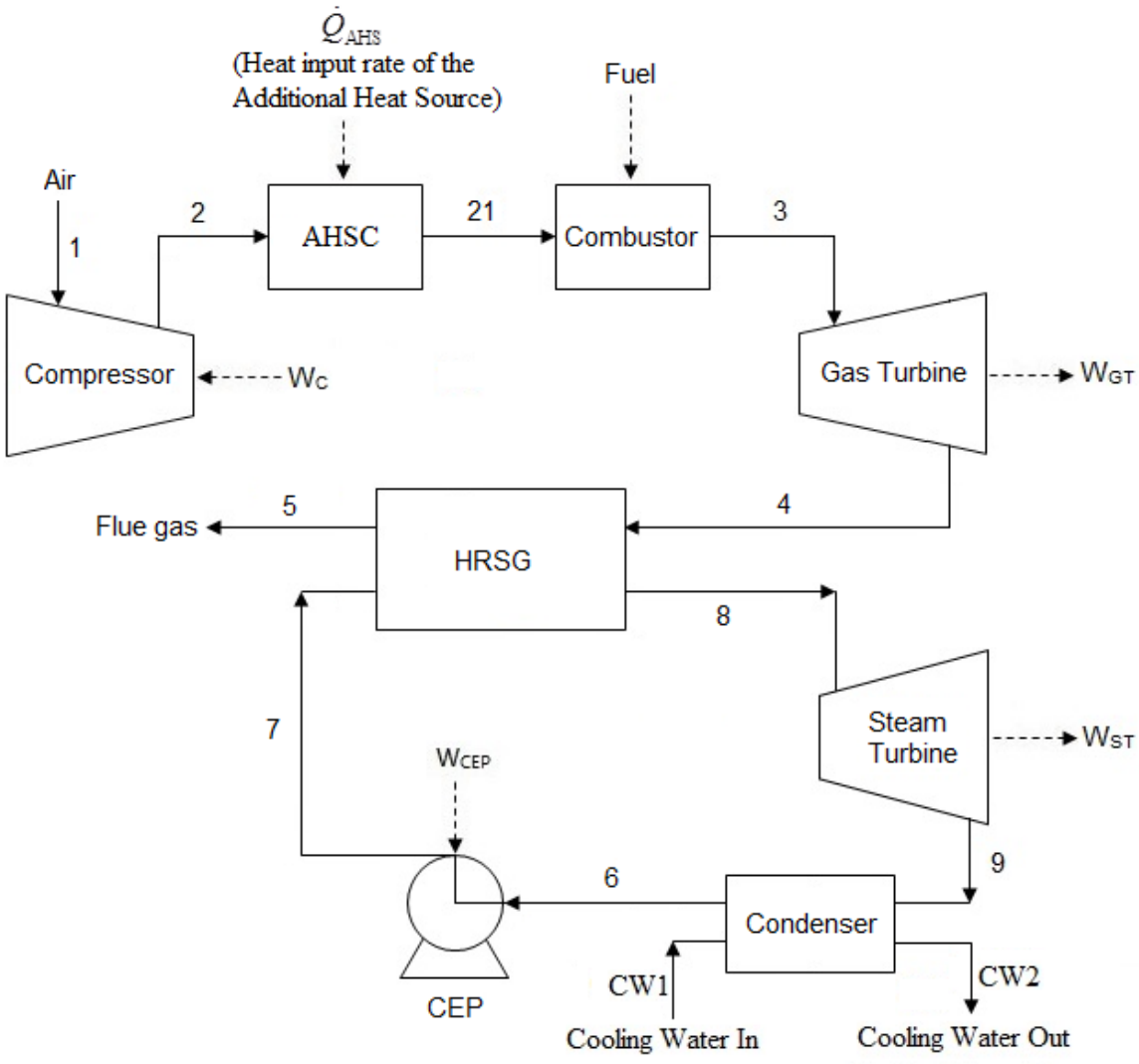

Fig. 6-3. Flow diagram of the hybrid combined cycle power plant with the additional heat source (AHS) added in the topping (Brayton) cycle (HRSG: heat recovery steam generator, CEP: condensate extraction pump, AHSC: additional heat source collection equipment)

6.1.2. Thermodynamic analysis of the hybrid power generation systems based on the combined cycle with the AHS added in the topping (Brayton) cycle

According the energy balance for the control volume enclosing HRSG in Fig. 6-3, for the hybrid and the reference system (Fig. 6-3 but without the AHSC), respectively,

$$\left(\dot{m}_{\mathrm{a}}+\dot{m}_{\mathrm{f}}\right)\left(h_4-h_5\right)=\dot{m}_{\mathrm{bc}}\left(h_8-h_7\right), \tag{6.1}$$

$$\left(\dot{m}_{\mathrm{a}}+\dot{m}_{\mathrm{f,0}}\right)\left(h_4-h_5\right)=\dot{m}_{\mathrm{bc,0}}\left(h_8-h_7\right), \tag{6.2}$$

in which $\dot{m}_{\mathrm{bc}}=\dot{m}_8$ [kg/s] is the mass flow rate of the working fluid in the bottoming cycle.

Thus we have

$$\frac{h_4-h_5}{h_8-h_7}=\frac{\dot{m}_{\mathrm{bc}}}{\dot{m}_{\mathrm{a}}+\dot{m}_{\mathrm{f}}}=\frac{\dot{m}_{\mathrm{bc,0}}}{\dot{m}_{\mathrm{a}}+\dot{m}_{\mathrm{f,0}}} \tag{6.3}$$

or

$$\frac{\dot{m}_{\mathrm{bc}}}{\dot{m}_{\mathrm{bc,0}}}=\frac{\dot{m}_{\mathrm{a}}+\dot{m}_{\mathrm{f}}}{\dot{m}_{\mathrm{a}}+\dot{m}_{\mathrm{f,0}}}=\frac{\dot{m}_{\mathrm{a}}\left(1+f\right)}{\dot{m}_{\mathrm{a}}\left(1+f_0\right)}=1-\frac{f_0-f}{1+f_0}, \tag{6.4}$$

in which f and f_0 are defined before, respectively, as the fuel-air ratio for the hybrid and the reference system in Eqs (5.5) and (5.10).

Using Eq. (6.4), we have

$$\frac{\dot{m}_{\mathrm{bc}}}{\dot{m}_{\mathrm{bc},0}} = 1 - \frac{f_0 - f}{1 + f_0} \approx 1. \tag{6.5}$$

Therefore, the net power output from the bottoming cycle is

$$\frac{\dot{W}_{\mathrm{net,bc}}}{\dot{W}_{\mathrm{net,bc},0}} = \frac{\dot{W}_{\mathrm{ST}} - \dot{W}_{\mathrm{CEP}}}{\dot{W}_{\mathrm{ST},0} - \dot{W}_{\mathrm{CEP},0}} = \frac{\dot{m}_{\mathrm{bc}}\left[\left(h_8 - h_9\right) - \left(h_7 - h_6\right)\right]}{\dot{m}_{\mathrm{bc},0}\left[\left(h_8 - h_9\right) - \left(h_7 - h_6\right)\right]} \approx 1, \tag{6.6}$$

in which the subscript bc stands for the bottoming cycle of the combined cycle, $\dot{W}_{\mathrm{ST}}$ [kW] and $\dot{W}_{\mathrm{CEP}}$ [kW] are the power output of the steam turbine and the power input to the CEP, respectively.

Using the same assumptions and method in Section 5.1.2, the energy and exergy efficiency for the hybrid combined cycle with the AHS added in the topping (Brayton) cycle are, respectively,

$$\eta_{\mathrm{h}} = \frac{\left(1 + f\right)\left(h_3 - h_4\right) - \left(h_2 - h_1\right) + \dfrac{\dot{m}_{\mathrm{bc}}}{\dot{m}_{\mathrm{a}}}\left[\left(h_8 - h_9\right) - \left(h_7 - h_6\right)\right]}{f \cdot \mathrm{LHV} + \dfrac{h_{21} - h_2}{\eta_{\mathrm{AHS}}}}, \tag{6.7}$$

$$\varepsilon_{\mathrm{h}}=\frac{(1+f)(h_3-h_4)-(h_2-h_1)+\frac{\dot{m}_{\mathrm{bc}}}{\dot{m}_{\mathrm{a}}}\left[(h_8-h_9)-(h_7-h_6)\right]}{f\cdot b_{\mathrm{f}}+\frac{h_{21}-h_2}{\eta_{\mathrm{AHS}}}\left(1-\frac{T_0}{T_{\mathrm{AHS}}}\right)}, \qquad (6.8)$$

and for the reference system are, respectively,

$$\eta_0=\frac{(1+f_0)(h_3-h_4)-(h_2-h_1)+\frac{\dot{m}_{\mathrm{bc},0}}{\dot{m}_{\mathrm{a}}}\left[(h_8-h_9)-(h_7-h_6)\right]}{f_0\cdot \mathrm{LHV}}, \qquad (6.9)$$

$$\varepsilon_0=\frac{(1+f_0)(h_3-h_4)-(h_2-h_1)+\frac{\dot{m}_{\mathrm{bc},0}}{\dot{m}_{\mathrm{a}}}\left[(h_8-h_9)-(h_7-h_6)\right]}{f_0\cdot b_{\mathrm{f}}}. \qquad (6.10)$$

Using the same method in Section 5.1.2 and Eq. (6.6) we have the same results as for the simple Brayton cycle, i.e. $\eta_{\mathrm{h}}<\eta_0$ when $\eta_{\mathrm{AHS}}<\eta_{\mathrm{CC}}-\frac{h_4-h_7}{\mathrm{LHV}}$ and $\varepsilon_{\mathrm{h}}>\varepsilon_0$ when $\eta_{\mathrm{AHS}}>1-\frac{T_0}{T_{\mathrm{AHS}}}$.

6.2. Hybrid power generation systems based on the combined cycle with the AHS added in the bottoming (Rankine) cycle

6.2.1. Introduction of the hybrid power generation systems based on the combined cycle with the AHS added in the bottoming (Rankine) cycle

Besides integration into the topping cycle, the additional heat source (AHS) can also be integrated into the bottoming cycle in a combined cycle power plant. AHS is usually integrated into the heat recovery steam generator (HRSG) to preheat or vaporize some of the HRSG feedwater. HRSG can be single-pressure type as shown in Fig. 6-4 or multi-pressure type as shown in Fig. 6-5. Increasing the number of these pressure levels increases the combined cycle efficiency at the expense of system complexity and cost. Small combined cycle power plants have only one pressure level while large ones often use dual-pressure or even triple-pressure HRSG. Sometimes a duct burner as shown in Fig. 6-4 is used to maintain a steady power output when the AHS, such as solar power, input is not sufficient to maintain a steady power output. When no back-up fuel is used, the power output is variable because of solar input fluctuation.

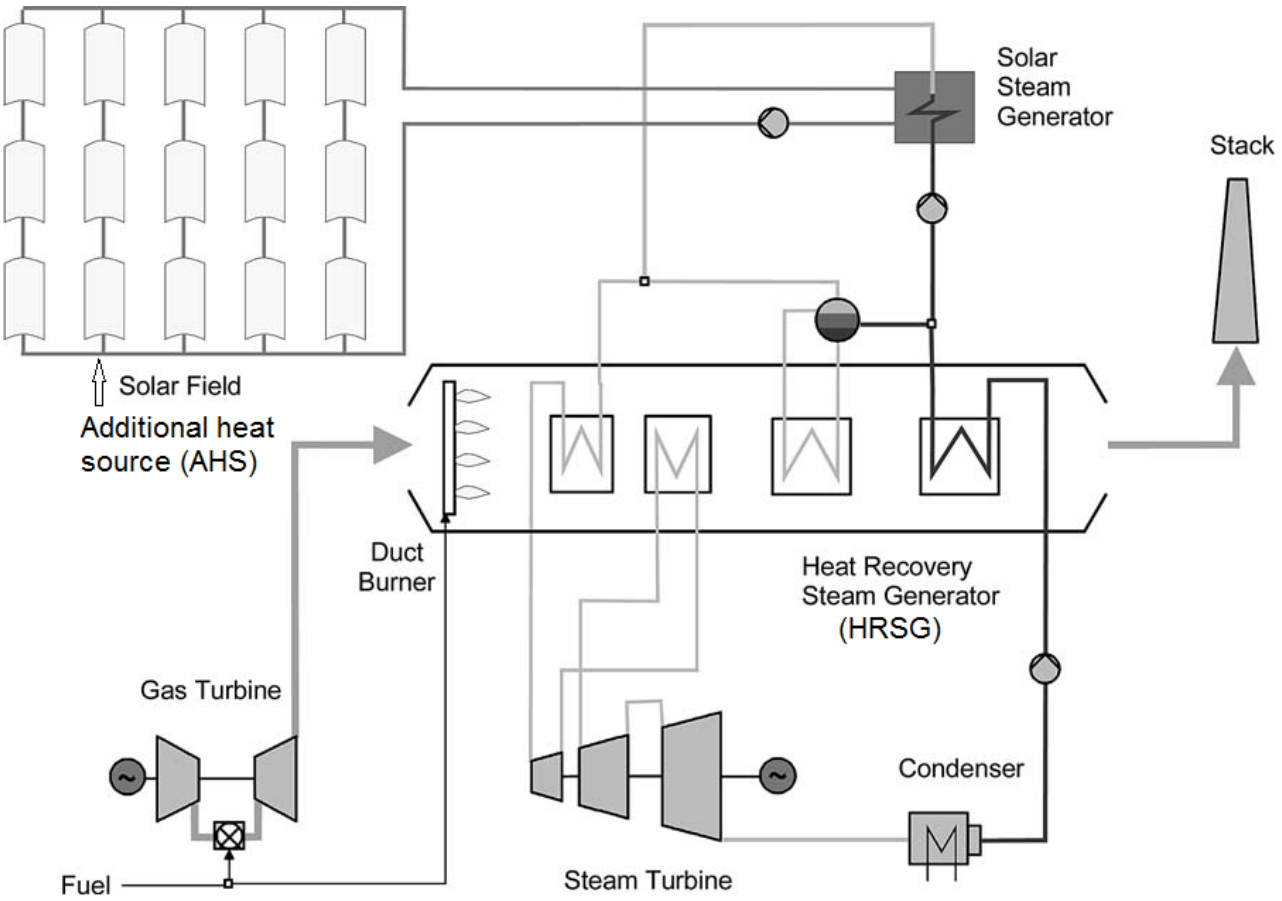

Fig. 6-4. Flow diagram of a hybrid combined cycle power plant with single-pressure HRSG with the additional heat source (AHS) added in the bottoming cycle (Adapted from [1])

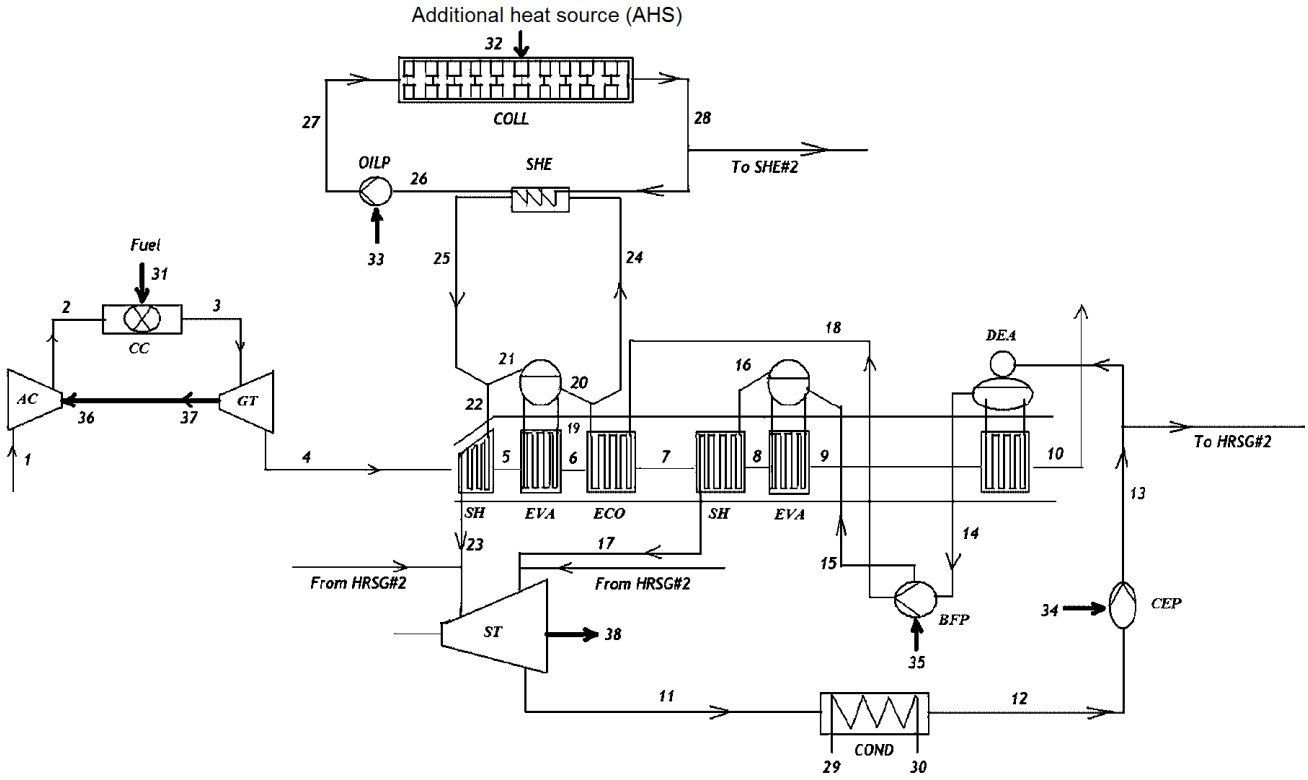

Fig. 6-5. Flow diagram of a hybrid combined cycle power plants with a dual-pressure HRSG with the additional heat source (AHS) added in the bottoming cycle (Adapted from [2]) (AC: air compressor, CC: combustion chamber; GT: gas turbine, SH: superheater, EVA: evaporator, ECO: economizer, BFP: boiler feedwater pump, DEA: deaerator, HRSG: heat recovery steam generator, CEP: condensate extraction pump, COND: condenser, ST: steam turbine, SHE: solar heat exchanger, OILP: oil pump, COLL: solar collector)

The heat from the additional heat source is added to the working fluid in the bottoming cycle together with the heat from the gas turbine exhaust gas, regardless of the HRSG configuration. As can be seen from Fig. 6-4 and Fig. 6-5, the AHSC can be added in various

locations in the HRSG and may thus have different temperature requirement. When the AHS is used to heat the working fluid at lower temperature, the temperature requirement of the AHS is also lower, and vice versa. For generality, the flow diagram of the combined cycle power plant with the AHSC added in the HRSG is simplified as Fig. 6-6, in which the HRSG and the AHSC are shown together in the "HRSG+AHSC" block.

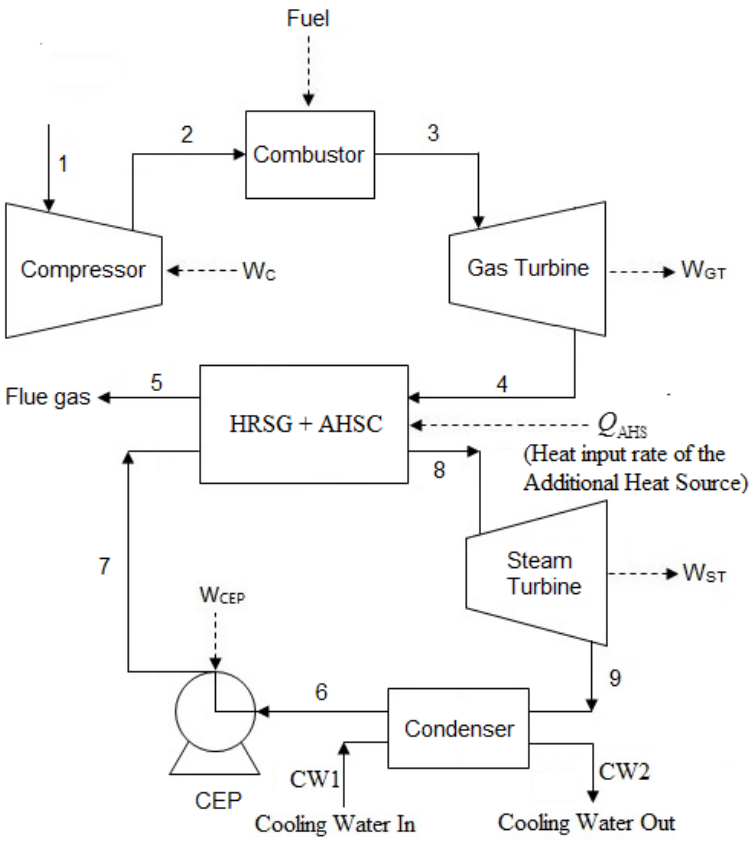

Fig. 6-6. Flow diagram of the hybrid combined cycle power plant with the additional heat source (AHS) added in the topping (Brayton) cycle (HRSG: heat recovery steam generator, CEP: condensate extraction pump, AHSC: additional heat source collection equipment)

6.2.2. Thermodynamic analysis of the hybrid power generation systems based on the combined cycle with the AHS added in the bottoming (Rankine) cycle

Using the same assumptions and method in Section 5.1.2, the energy and exergy efficiency for the hybrid combined cycle with the AHS added in the bottoming (Rankine) cycle are, respectively,

$$\eta_{\mathrm{h}}=\frac{\left(1+f_0\right)\left(h_3-h_4\right)-\left(h_2-h_1\right)+\frac{\dot{m}_{\mathrm{bc}}}{\dot{m}_{\mathrm{a}}}\left[\left(h_8-h_9\right)-\left(h_7-h_6\right)\right]}{f_0\cdot\mathrm{LHV}+\frac{\dot{Q}_{\mathrm{ADD}}}{\eta_{\mathrm{AHS}}}}, \tag{6.11}$$

$$\varepsilon_{\mathrm{h}}=\frac{\left(1+f_0\right)\left(h_3-h_4\right)-\left(h_2-h_1\right)+\frac{\dot{m}_{\mathrm{bc}}}{\dot{m}_{\mathrm{a}}}\left[\left(h_8-h_9\right)-\left(h_7-h_6\right)\right]}{f_0\cdot b_{\mathrm{f}}+\frac{\dot{Q}_{\mathrm{ADD}}}{\eta_{\mathrm{AHS}}}\left(1-\frac{T_0}{T_{\mathrm{AHS}}}\right)}. \tag{6.12}$$

According the energy balance for the control volume enclosing HRSG+AHS in Fig. 6-4, for the hybrid and the reference system, respectively,

$$\dot{m}_{\mathrm{fg}}\left(h_4-h_5\right)+\dot{Q}_{\mathrm{ADD}}=\dot{m}_{\mathrm{bc}}\left(h_8-h_7\right)=\frac{\dot{W}_{\mathrm{ST}}}{h_8-h_9}\left(h_8-h_7\right)=\frac{\dot{W}_{\mathrm{CEP}}}{h_6-h_9}\left(h_7-h_6\right), \tag{6.13}$$

$$\dot{m}_{\text{fg}}\left(h_4-h_5\right)=\dot{m}_{\text{bc},0}\left(h_8-h_7\right)=\frac{\dot{W}_{\text{ST},0}}{h_8-h_9}\left(h_8-h_7\right)=\frac{\dot{W}_{\text{CEP},0}}{h_6-h_9}\left(h_7-h_6\right), \quad (6.14)$$

in which $\dot{m}_{\text{fg}}=\dot{m}_5=\left(1+f_0\right)\dot{m}_{\text{a}}$ [kg/s] is the mass flow rate of system flue gas and is the same for the hybrid and the reference system since the topping cycle is the same for both systems.

Combining Eqs (6.13) and (6.14),

$$\dot{Q}_{\text{ADD}}=\left(\dot{m}_{\text{bc}}-\dot{m}_{\text{bc},0}\right)\left(h_8-h_7\right), \quad (15)$$

$$\dot{W}_{\text{ST}}-\dot{W}_{\text{ST.0}}=\dot{Q}_{\text{ADD}}\frac{h_8-h_9}{h_8-h_7}, \quad (16)$$

$$\dot{W}_{\text{CEP}}-\dot{W}_{\text{CEP.0}}=\dot{Q}_{\text{ADD}}\frac{h_7-h_6}{h_8-h_7}. \quad (17)$$

Thus the difference between the energy efficiency of the hybrid system and the reference system is

$$
\begin{aligned}
\eta_{\mathrm{h}}-\eta_0 &= \frac{\dot{W}_{\mathrm{GT}}-\dot{W}_{\mathrm{C}}-\dot{W}_{\mathrm{ST}}-\dot{W}_{\mathrm{CEP}}}{\dot{Q}_{\mathrm{f}}+\dot{Q}_{\mathrm{AHS}}} - \frac{\dot{W}_{\mathrm{GT}}-\dot{W}_{\mathrm{C}}-\dot{W}_{\mathrm{ST,0}}-\dot{W}_{\mathrm{CEP,0}}}{\dot{Q}_{\mathrm{f}}} \\
&= \frac{\dot{Q}_{\mathrm{f}}\left[\left(\dot{W}_{\mathrm{ST}}-\dot{W}_{\mathrm{CEP}}\right)-\left(\dot{W}_{\mathrm{ST,0}}-\dot{W}_{\mathrm{CEP,0}}\right)\right]-\dot{Q}_{\mathrm{AHS}}\left(\dot{W}_{\mathrm{GT}}-\dot{W}_{\mathrm{C}}-\dot{W}_{\mathrm{ST,0}}-\dot{W}_{\mathrm{CEP,0}}\right)}{\left(\dot{Q}_{\mathrm{f}}+\dot{Q}_{\mathrm{AHS}}\right)\dot{Q}_{\mathrm{f}}} \\
&= \frac{\dot{Q}_{\mathrm{f}}\left[\dfrac{\left(h_8-h_9\right)-\left(h_7-h_6\right)}{h_8-h_7}\eta_{\mathrm{AHS}}\dot{Q}_{\mathrm{AHS}}\right]-\dot{Q}_{\mathrm{AHS}}\left(\eta_0\dot{Q}_{\mathrm{f}}\right)}{\left(\dot{Q}_{\mathrm{f}}+\dot{Q}_{\mathrm{AHS}}\right)\dot{Q}_{\mathrm{f}}} \\
&= \frac{\dot{Q}_{\mathrm{AHS}}}{\dot{Q}_{\mathrm{f}}+\dot{Q}_{\mathrm{AHS}}}\left[\frac{\left(h_8-h_9\right)-\left(h_7-h_6\right)}{h_8-h_7}\eta_{\mathrm{AHS}}-\eta_0\right] \\
&= X_{\mathrm{AHS}}\left(\eta_{\mathrm{bc}}\eta_{\mathrm{AHS}}-\eta_0\right),
\end{aligned}
\tag{6.18}
$$

in which X_{AHS} is the AHS input fraction of total energy input and was defined in Eq. (2.16), and η_{bc} is the energy efficiency of the bottom cycle defined as

$$
\eta_{\mathrm{bc}} = \frac{\left(h_8-h_9\right)-\left(h_7-h_6\right)}{h_8-h_7}. \tag{6.19}
$$

Since in practice the energy efficiency of the combined cycle is always larger than that of its bottoming cycle, or

$$
\eta_0 > \eta_{\mathrm{bc}}, \tag{6.20}
$$

and considering

$$\eta_{\text{AHS}} \leq 1, \tag{6.21}$$

we have

$$\eta_0 > \eta_{\text{bc}} > \eta_{\text{bc}}\eta_{\text{AHS}}. \tag{6.22}$$

So from Eq. (6.18),

$$\eta_{\text{h}} < \eta_0, \tag{6.23}$$

and η_{h} increases with η_{AHS} but decreases with X_{AHS}.

Also, Eq. (6.18) can be written as

$$\eta_{\text{h}} = \left(1 - X_{\text{AHS}}\right)\eta_0 + \left(X_{\text{AHS}}\right)\eta_{\text{bc}}\eta_{\text{AHS}}, \tag{6.24}$$

meaning that the energy efficiency of the hybrid combined cycle system, η_{h}, is the weighted total of the energy efficiency of the conventional combined cycle system, η_0, and that of the bottoming (Rankine) cycle system whose heat source is the AHS, and the weighting factors are the heat input fractions of the total energy input, respectively, of the hybrid system.

From Eqs (6.12) and (6.10), the difference between the exergy efficiency of the hybrid system and the reference system is

$$
\begin{aligned}
\varepsilon_{\mathrm{h}}-\varepsilon_0 &= \frac{\dot{W}_{\mathrm{GT}}-\dot{W}_{\mathrm{C}}-\dot{W}_{\mathrm{ST}}-\dot{W}_{\mathrm{CEP}}}{\dot{B}_{\mathrm{f}}+\dot{B}_{\mathrm{AHS}}}-\frac{\dot{W}_{\mathrm{GT}}-\dot{W}_{\mathrm{C}}-\dot{W}_{\mathrm{ST,0}}-\dot{W}_{\mathrm{CEP,0}}}{\dot{B}_{\mathrm{f}}} \\
&= \frac{\dot{B}_{\mathrm{f}}\left[\left(\dot{W}_{\mathrm{ST}}-\dot{W}_{\mathrm{CEP}}\right)-\left(\dot{W}_{\mathrm{ST,0}}-\dot{W}_{\mathrm{CEP,0}}\right)\right]-\dot{B}_{\mathrm{AHS}}\left(\dot{W}_{\mathrm{GT}}-\dot{W}_{\mathrm{C}}-\dot{W}_{\mathrm{ST,0}}-\dot{W}_{\mathrm{CEP,0}}\right)}{\left(\dot{B}_{\mathrm{f}}+\dot{B}_{\mathrm{AHS}}\right)\dot{B}_{\mathrm{f}}} \\
&= \frac{\dot{B}_{\mathrm{f}}\left[\frac{\left(h_8-h_9\right)-\left(h_7-h_6\right)}{h_8-h_7}\eta'_{\mathrm{AHS}}\dot{B}_{\mathrm{AHS}}\right]-\dot{B}_{\mathrm{AHS}}\left(\varepsilon_0\dot{B}_{\mathrm{f}}\right)}{\left(\dot{B}_{\mathrm{f}}+\dot{B}_{\mathrm{AHS}}\right)\dot{B}_{\mathrm{f}}} \\
&= \frac{\dot{B}_{\mathrm{AHS}}}{\dot{B}_{\mathrm{f}}+\dot{B}_{\mathrm{AHS}}}\left[\frac{\left(h_8-h_9\right)-\left(h_7-h_6\right)}{h_8-h_7}\eta'_{\mathrm{AHS}}-\varepsilon_0\right] \\
&= X'_{\mathrm{AHS}}\left(\eta_{\mathrm{bc}}\eta'_{\mathrm{AHS}}-\varepsilon_0\right),
\end{aligned}
\tag{6.25}
$$

in which η'_{AHS} is the exergy conversion efficiency of the AHS defined in Eq. (4.14) and

$$
X'_{\mathrm{AHS}}=\frac{\dot{B}_{\mathrm{AHS}}}{\dot{B}_{\mathrm{f}}+\dot{B}_{\mathrm{AHS}}} \tag{6.26}
$$

is the AHS exergy input fraction of the total exergy input.

Therefore, $\varepsilon_{\mathrm{h}}>\varepsilon_0$ when

$$
\eta_{\mathrm{bc}}\eta'_{\mathrm{AHS}}-\varepsilon_0>0 \tag{6.27}
$$

or

$$\eta_{\text{bc}} \frac{\eta_{\text{AHS}}}{\psi_{\text{AHS}}} - \frac{\eta_0}{\psi_{\text{f}}} > 0 \tag{6.28}$$

or

$$\eta_{\text{AHS}} > \frac{\psi_{\text{AHS}}}{\psi_{\text{f}}} \frac{\eta_0}{\eta_{\text{bc}}} = \frac{1 - \dfrac{T_0}{T_{\text{AHS}}}}{\psi_{\text{f}}} \frac{\eta_0}{\eta_{\text{bc}}} \tag{6.29}$$

or

$$T_{\text{AHS}} < \frac{T_0}{1 - \eta_{\text{AHS}} \dfrac{\psi_{\text{f}} \eta_{\text{bc}}}{\eta_0}}. \tag{6.30}$$

6.3. Conclusions of the thermodynamic analysis of hybrid power generation systems based on the combined cycle

There are two ways to add the AHS in the power generation systems based on the combined cycle.

When the AHS is added in the topping cycle (Brayton cycle) of the combined cycle (the fuel-saving mode), the analysis and results are similar to those in CHAPTER 5 for the hybrid power generations based on Brayton cycles. The energy efficiency of the hybrid system is larger than that of the conventional single heat source system when

$\eta_{\mathrm{AHS}} < \eta_{\mathrm{CC}} - \dfrac{h_4 - h_7}{\mathrm{LHV}}$, and the exergy efficiency of the hybrid system is larger than that of the conventional single heat source system when $\eta_{\mathrm{AHS}} > 1 - \dfrac{T_0}{T_{\mathrm{AHS}}}$. The results can be used as easy criteria to determine whether the energy or exergy efficiency of the hybrid system is larger than that of the conventional single heat source combined cycle system, without the necessity of detailed calculation/simulation/experiment for the hybrid system.

When the AHS is added in the bottoming cycle (Rankine cycle) of the combined cycle (power-boost mode), the energy efficiency of the hybrid system is smaller than that of the conventional single heat source system. It increases with the η_{AHS} but decreases with increasing addition heat source share, X_{AHS}. The exergy efficiency of the hybrid system, however, is larger than that of the conventional single heat source system when $T_{\mathrm{AHS}} < \dfrac{T_0}{1 - \eta_{\mathrm{AHS}} \dfrac{\psi_{\mathrm{f}} \eta_{\mathrm{bc}}}{\eta_0}}$. This result suggests that the temperature of the AHS, T_{AHS}, should be designed so that it is smaller than $\dfrac{T_0}{1 - \eta_{\mathrm{AHS}} \dfrac{\psi_{\mathrm{f}} \eta_{\mathrm{bc}}}{\eta_0}}$, from the perspective of exergy efficiency of the system. This guide thus saves much design effort before the detail design of the hybrid power generation systems based on the combined cycle when the AHS is added in the bottoming cycle. For example, when $\eta_{\mathrm{AHS}} = 0.8$, $\psi_{\mathrm{f}} = 1.04$, $\eta_{\mathrm{bc}} = 0.4$, $\eta_0 = 0.55$ and $T_0 = 15\ ^{\circ}\mathrm{C}$, the maximum AHS temperature is 456 °C for $\varepsilon_{\mathrm{h}} > \varepsilon_0$.

References for Chapter 6

[1] Dersch J., Geyer M., Herrmann U., Jones S.A., Kelly B., Kistner R., Ortmanns W., Pitz-Paal R., Price H., Trough integration into power plants—a study on the performance and economy of integrated solar combined cycle systems. Energy 2004;29:947-959.

[2] Baghernejadand A., Yaghoubi M., Multi-objective exergoeconomic optimization of an Integrated Solar Combined Cycle System using evolutionary algorithms. Int J Energ Res 2011;35:601-615.

CHAPTER 7

THERMODYNAMIC ANALYSIS OF THERMOCHEMICAL HYBRID POWER GENERATION SYSTEMS

7.1. Introduction of thermochemical hybrid power generation systems

Different from the typical thermal hybrid systems that may involve chemical reactions in the heat addition process only, if fuel combustion is used, thermochemical hybrid systems are designed to include chemical reactions, typically to convert some hydrocarbon to readily-usable fuel, altogether to result in a more efficient and less polluting power generation system. In this type of system, lower temperature heat, such as solar, geothermal, or waste, is converted by such chemical reactions to the chemical exergy of the ultimately-combusted fuel (such as syngas).

Compared with thermal hybridization, thermochemical hybridization can have also the advantage that it can allow conversion of the exergy of intermittent heat sources (such as solar) to much higher fuel chemical exergy that is therefore much easier to store and transport than the energy/exergy of such input heat sources. Furthermore, low/mid temperature solar heat (~200 °C) is high enough to be used by a syngas-producing reforming process, thus potentially reducing the total cost relative to conventional solar

thermal power plants that necessarily use more expensive solar collection equipment due to their higher solar temperature.

Comprehensive work has been done on the hybrid power generation systems integrated with thermochemical fuel conversion. Methane is the most widely used fuel in such hybrid systems due to its high heating value, large reserve, low price and easiness to transport. The reforming temperature that is required to reform methane to the syngas, however, is over 600 °C, indicating high solar collector cost, since the cost of the solar collectors usually increases with the solar temperature of the solar collectors. To reduce the cost of the solar collectors, fuels that require lower reforming temperatures than methane were studied and methanol is the most widely studied among them. This is because methanol can be mass produced from coal gasification or chemical synthesis of syngas and easy to transport due to its liquid form in environmental conditions. Other type of fuel can also be used in the reforming process such as petroleum coke (petcoke) [1], coal [2] and biomass [3] and heat sources other than solar can also be used, such as waste heat [4]. Table 7-1 summarized the thermochemical hybrid systems studied in the past (modified based on [14]).

Table 7-1. A summary of past studies of thermochemical hybrid power generation systems

System	Chemical	Additional Heat source	Turbine inlet	CO_2	Performance

description	reaction	Type	Tempera-ture (°C)	Role	temperature (°C)	capture	
Gas turbine cycle with methane re-forming [5]	CH4 + 2H2O → CO2 + 4H2	Solar	800-1,000	Chemical reaction process heat	-	None	Fossil fuel saving: 25-40%
Combined cycle with methane reforming [6]	CH4 + 2H2O → CO2 + 4H2	Solar	600-900	Chemical reaction process heat	1,327	None	Annual thermal efficiency: 47.6% Solar share: 9.6%
Steam injected gas turbine cycle with nature gas reforming [7]	CH4 + 2H2O → CO2 + 4H2	Solar	600	Chemical reaction process heat	1,288	None	Natural gas saving: <20%
Combined cycle with solar methanol decomposition [29]	CH3OH → CO + 2H2	Solar	200-400	Chemical reaction process heat	1,300	None	Solar to electricity efficiency: 18-35% Exergy efficiency: 50-60% CO2 emission: 310 g/kW h
HAT cycle with Methanol decomposition [8]	CH3OH → CO + 2H2	Solar	175-210	Chemical reaction process heat	1,200	None	Solar to electricity efficiency: 25-39% Exergy efficiency: 59.2% Thermal

							efficiency: 53.6%
Chemically recuperated gas turbine cycle with solar methane reforming [15,9]	$CH_4 + 2H_2O \rightarrow CO_2 + 4H_2$	Solar	~220	Latent heat of reactant H_2O evaporation	1,300	None	Thermal efficiency: 51.2-53.6% Solar to electricity efficiency:25-38% Fossil fuel saving: 20%
Combined cycle with solar methane membrane reforming [10]	$CH_4 + 2H_2O \rightarrow CO_2 + 4H_2$	Solar	~550	Chemical reaction process heat	1,300	Membrane reaction/separation	CO_2 emission: 25 g/kW h Exergy efficiency: 58% Thermal efficiency: 51.6% Fossil fuel saving: 31.2% Solar share: 28.2% Solar to electricity efficiency: 36.4%
Zero-emission oxy-fuel combustion hybrid cycle [17,11]	$CH_4 + 2H_2O \rightarrow CO_2 + 4H_2$	Solar	200-400	Latent heat of reactant H_2O evaporation	1,308	Oxy-fuel combustion	Thermal efficiency: 50.7% CO_2 capture ratio: ~100%
Hybrid methanol-	(1) CH_3OH	Solar	150-500	Chemical reaction	1,327	Chemical looping combustion	Exergy efficiency: 58.4% Solar to electricity

fueled chemical looping combustion [12,13]	+ MxOy → M + CO2 + H2O (2) M + O2 → MxOy			process heat			efficiency: 22.3% CO_2 emission: 130 g/kW h
Combined cycle with solar methanol decomposition [14]	CH3OH → CO + 2H2	Solar	200-250	Chemical reaction process heat	1,308	Pre-combustion	CO_2 emission: 33.8 g/kW h Exergy efficiency: 53.8% Thermal efficiency: 51.1% Fossil fuel saving: 27.3% Solar thermal share: 17.6% Solar to electricity efficiency: 49.2%
Combined cycle with solar methanol reforming [14]	CH3OH +H2O → CO2 + 3H2	Solar	200-250	Chemical reaction process heat	1,308	Pre-combustion	CO_2 emission: 33.4 g/kW h Exergy efficiency: 55.1% Thermal efficiency: 50.9% Fossil fuel saving: 30.5% Solar thermal share: 21.5% Solar to electricity

							efficiency: 45%
Solar thermal gasification of coal for hybrid solar-fossil power and fuel production [2]	$CHxOy + (1 - y) H2O = (x/2 + 1 - y) H2 + CO$	Solar	1,077	Chemical reaction process heat	-	None	CO_2 emission: 0.96 kg/kW h Exergy efficiency: 33% Thermal efficiency: 35%
Polygeneration system for methanol production and power generation with solar-biomass thermal gasification [3]	-	Solar	900	Chemical reaction process heat	-	None	Exergy efficiency: 50.69%
Chemically Recuperated Gas Turbine [4]	$CH4 + 2H2O \rightarrow CO2 + 4H2$	Waste heat	596	Chemical reaction process heat	1,308	None	Thermal efficiency: 47.3%

7.2. Thermochemical hybrid systems using methane as fuel

Unlike the thermal hybrid systems whose configurations can be classified into several categories for further analysis, thermochemical hybrid systems have various configurations that are harder to be grouped together. In this research, two case studies are introduced about how this type of systems works and what advantages they have. “Solar thermochemical upgrading” is explained and discussed, followed by more general thermodynamic analysis of thermochemical hybrid systems. The first case analyzed in this chapter focuses on a novel Chemically-Recuperated Gas-Turbine Power Generation (SOLRGT) System proposed and described in [15-17].

7.2.1. System introduction

The flow diagram of SOLRGT is shown in Fig. 7-1, and all used operating parameters, such as temperature, pressure and chemical parameters, are from [15]. It can be seen from the flow diagram that solar heat collected by a parabolic concentrating solar collection equipment at 200-250 °C is used to generate the steam needed for the following reforming reaction, thereby converting the solar heat to that of the steam internal energy (stream 6 in Fig. 7-1), which is then converted to the chemical exergy of the syngas generated in the reformer, by using that steam, methane, and exhaust heat from the system gas turbine. The fuel conversion process is by the reactions:

$$CH_4 + H_2O \leftrightarrow CO + 3H_2 \qquad \Delta H = 206.11 \text{ kJ/mol} \tag{7.1}$$

$$CO + H_2O \leftrightarrow CO_2 + H_2 \qquad \Delta H = -41.17 \text{ kJ/mol} \tag{7.2}$$

Reaction (7.1) is the methane reforming process, which is endothermic, with that heat provided by the gas turbine exhaust gas (stream 16 in Fig. 7-1), at about 600 °C. At this temperature, 20-50% conversion of methane (stream 10) is realizable and higher conversion is achieved with more steam (stream 6), higher temperature and lower pressure in the reformer. Reaction (7.2) is a shift reaction, which is exothermic and heat released from it partially provides the heat needed for the methane reforming process of Eq. (7.1), in addition to the heat from gas turbine exhaust heat.

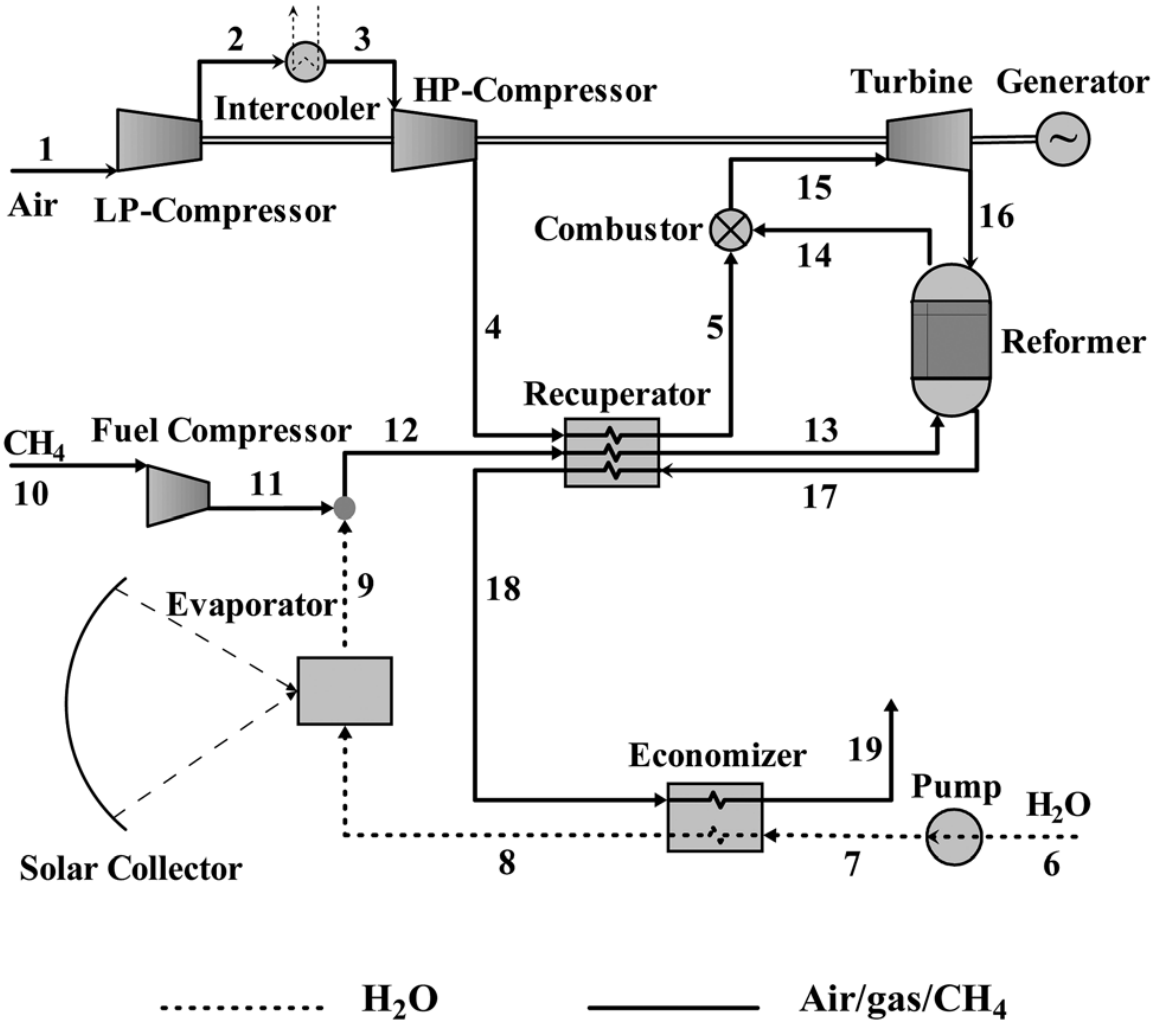

Fig. 7-1. Schematic diagram of the SOLRGT cycle [15]

The produced hydrogen-rich syngas (about 19% H_2, 8% CH_4, 68% H_2O, 4% CO_2 and < 1% CO when the steam/methane mole ratio is 6.1) from the reformer is then burned in the combustor with the compressed air recuperated by the reformer exhaust gas. As Eqs (7.1) and (7.2) show, both reactions are bi-directional, and the reactants composition shows that they are not complete (not all of the methane is converted). The high temperature and pressure (1,308 °C, 14.55 bar) produced syngas is then burned to generate power by the turbine that drives an electricity generator.

To increase the efficiency of the system, internal heat recovery is incorporated, in cascade, as shown in Fig. 7-2. The high temperature gas turbine exhaust gas (stream 16 in Fig. 7-1) is first used to provide the heat needed in the reformer for the methane reforming reaction. The exhaust heat from the reformer (stream 17) is then used to preheat the pressurized air (stream 4) from the compressor. At last, the heat from the gas turbine exhaust heat is used to preheat the pressurized water in the economizer (stream 7). The temperature of the exhaust gas leaving the system is about 163 °C.

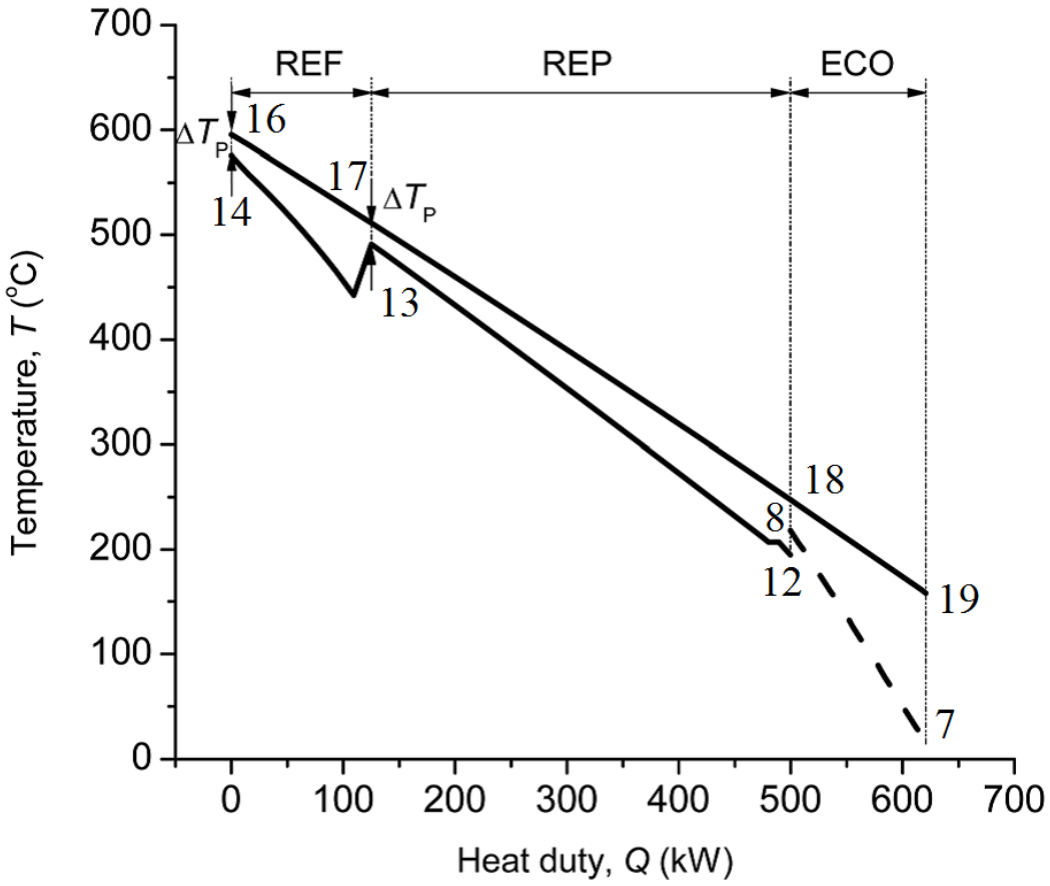

Fig. 7-2. Heat recuperation T-Q diagram for the SOLRGT system [15] (REF: reformer, REP: recuperator, ECO: economizer)

A non-hybrid equivalent of the SOLRGT thermochemical system, which uses only one type of heat source (methane) without the additional heat source is introduced for comparative analysis. It is the chemically-recuperated gas turbine (CRGT) system [18] shown in Fig. 7-3 with compressor intercooling (not shown in the figure), called IC-CRGT.

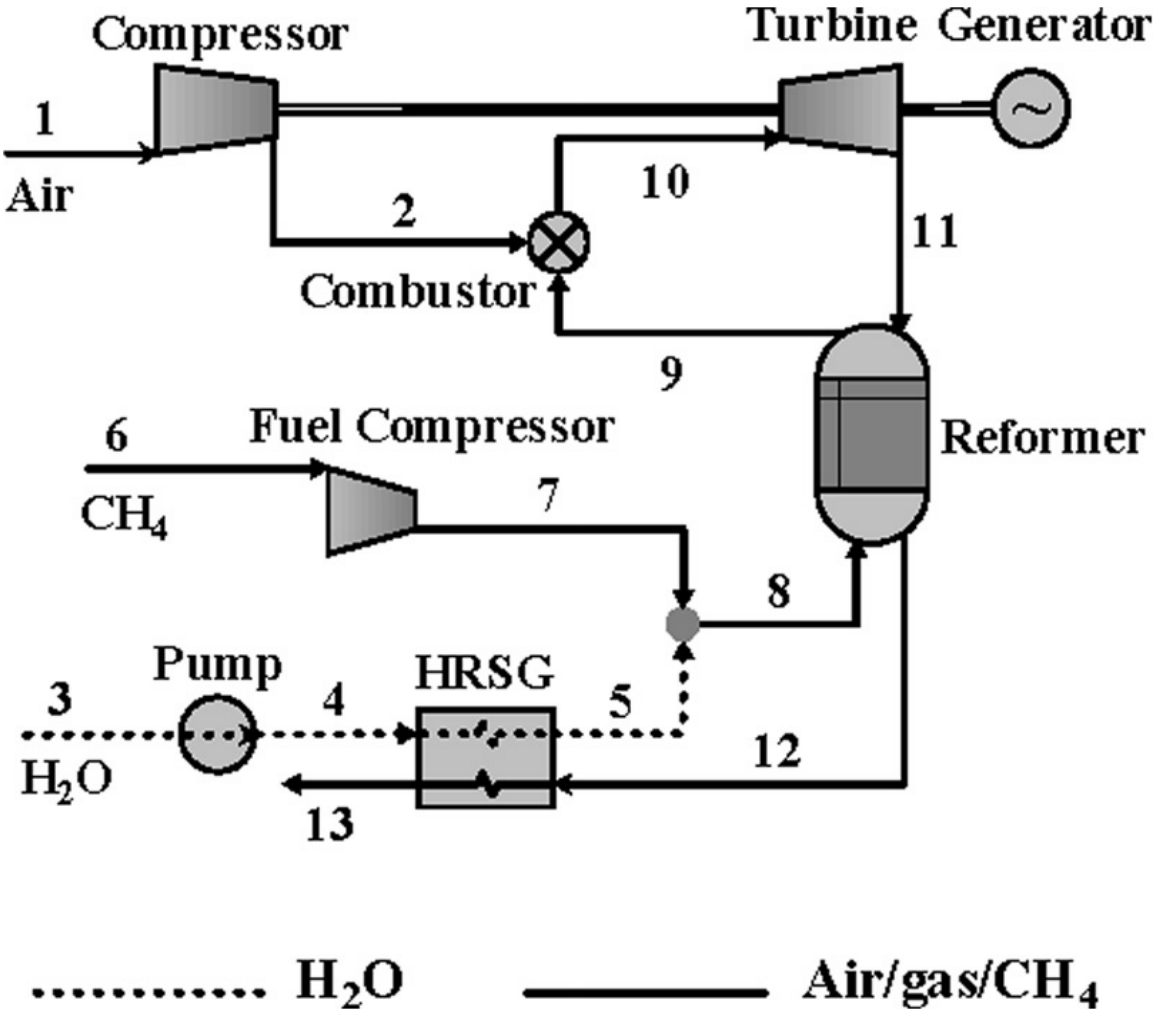

Fig. 7-3. Schematic diagram of the basic CRGT cycle [18] (HRSG: heat recovery steam generator)

Fig. 7-3 shows that the CRGT flow diagram is roughly the same as SOLRGT, except that the incoming water (stream 3 in Fig. 7-3) needed for the reforming is preheated and vaporized by the gas turbine exhaust gas (stream 12), instead of by solar heat as in SOLRGT. Compared with SOLRGT, this characteristic introduced more exergy

destruction in the heating of the incoming water because of the higher temperature differences between the heating and heated streams than those in the SOLRGT, as can be seen by comparing the T-Q diagrams in Fig. 7-4 (for CRGT) and 2 (for SOLRGT).

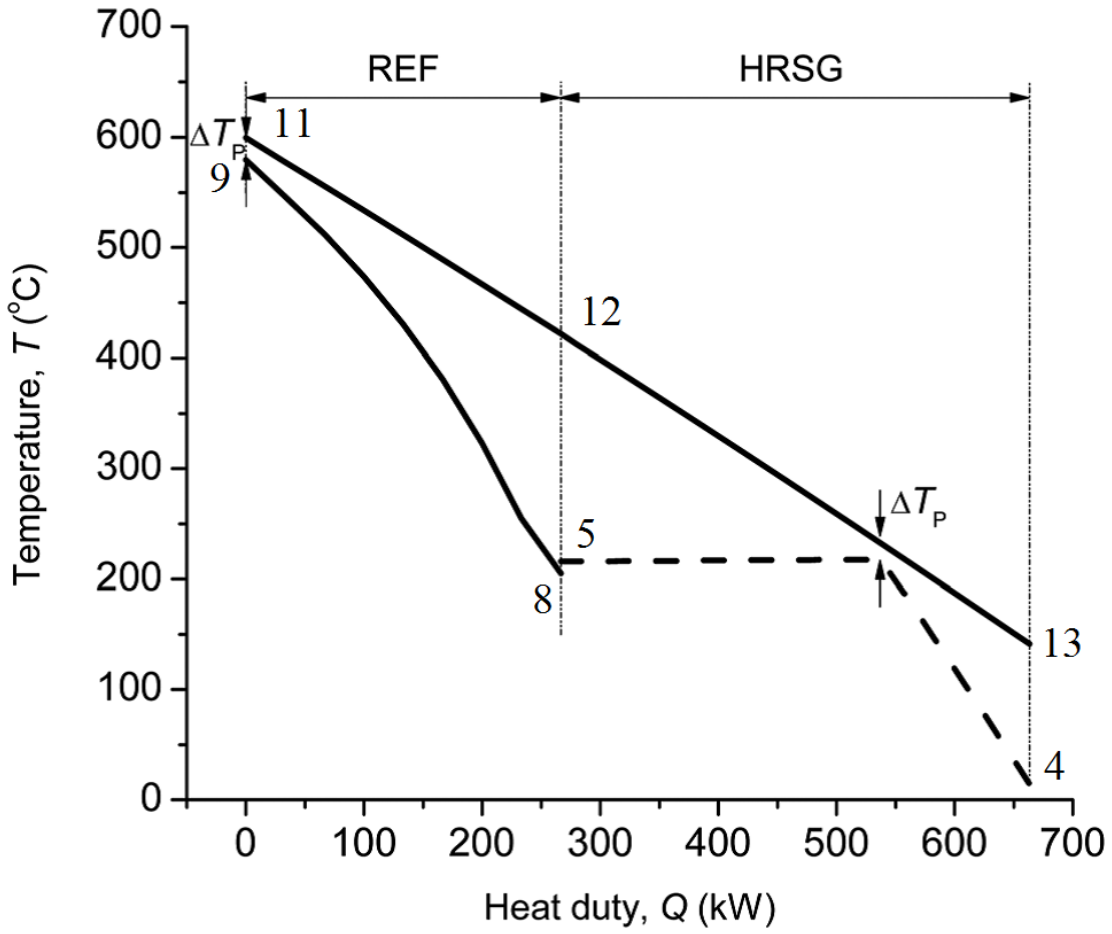

Fig. 7-4. Heat recuperation T-Q diagram for the IC-CRGT system [15] (REF: reformer, HRSG: heat recovery steam generator)

In the IC-CRGT system, the exhaust heat from the hot side of the reformer (states 11 to 13 in Fig. 7-4) is used to preheat and vaporize the pressurized incoming water (stream 3 in

Fig. 7-3, states 4 to 9 in Fig. 7-4) in the HRSG. Since the temperature of water doesn't change during vaporization while the temperature of the heating gas does, the temperature, difference between the heating and heated fluid is relatively large, as shown in Fig. 7-4, or it can be said that the temperature match during the heat transfer process is worse. Since the exergy destruction during heat transfer increases with the temperature difference between the heating and heated fluid, there is a relatively larger exergy destruction when using combustion gas to vaporize the incoming water. As seen from Fig. 3, the temperature match in the SOLRGT, is better than in the IC-CRGT, but in addition to the temperature differences the exergy destruction rate requires the knowledge of the specific temperatures and the temperature-dependent heat capacities of the heating and heated fluids, as well as the varying mass flow rate of the heated fluid during the process. Also, this method cannot be used to calculate the exergy destruction in the reforming process. The total exergy destruction shown in the processes described in Figs. 2 and 4 is therefore calculated as the difference between the exergy decrease of heating fluid (turbine exhaust gas) and the exergy increase of the heated fluid (water and steam-fuel mixture).

Our calculations (summarized in Table 1) show that the exergy destruction rate in the heat transfer and reforming processes shown in Fig. 7-2 is 44.8 kW, which is 18% smaller than in the processes shown in Fig. 7-4 (54.6 kW). Using the state points given in the references, the exergy decrease of gas turbine exhaust gas is $B_{16} - B_{19} = 332.0 \text{ kW}$ for the SORLGT and $B_{16} - B_{19} = 334.6 \text{ kW}$ for the IC-CRGT. For the SOLRGT, the exergy increase of the incoming water in the economizer is $B_8 - B_7 = 44.4 \text{ kW}$, the fuel-steam

mixture exergy increase in the recuperator is $B_{13} - B_{12} = 54.4$ kW, the pressurized air exergy increase in the recuperator is $B_5 - B_4 = 133.0$ kW. For the exergy increase in the cold side of reformer, chemical exergy is considered since the composition of the working fluid changes in the reforming process. It was calculated that the physical exergy increase is 14.2 kW and the chemical exergy increase is 41.2 kW. Thus the total exergy increase of the cold side of the heated fluid is 44.4+54.4+133.0+14.2+41.2=287.2 kW. So the exergy destruction shown in Fig. 7-2 is 332.0-287.2=44.8 kW. For the IC-CRGT, the exergy increase of the heated fluid (water/steam) in the HRSG is $B_8 - B_7 = 157.9$ kW. In the reformer, the physical exergy increase of the heated fluid is 71.2 kW and the chemical exergy increase of the heated fluid is 50.9 kW. Thus the total exergy increase of the cold side of the heated fluid is 157.9+71.2+50.9=280.0 kW. So the exergy destruction shown in Fig. 7-4 is 334.6-280.0=54.6 kW.

Table 7-2. Exergy destruction calculation summary for the heat transfer and reforming process in the T-Q diagrams for the SOLRGT and IC-CRGT

	Total exergy decrease of heating fluid (turbine exhaust gas)	Exergy increase of the heated fluid(s)	Exergy destruction
SOLRGT	$B_{16} - B_{19} = 332.0$ kW	Incoming water in the economizer	44.8 kW

		$B_8 - B_7 = 44.4$ kW Fuel-steam mixture in the Recuperator $B_{13} - B_{12} = 54.4$ kW Pressurized air in the Recuperator $B_5 - B_4 = 133.0$ kW Physical exergy increase in the reformer: 14.2 kW Chemical exergy increase in the reformer: 41.2 kW Incoming water in the HRSG	
IC-CRGT	$B_{11} - B_{13} = 334.6$ kW	$B_8 - B_7 = 157.9$ kW Physical exergy increase in the reformer: 71.2 kW	54.6 kW

Chemical exergy increase

in the reformer: 50.9 kW

SOLRGT has another advantage over the IC-CRGT: in the IC-CRGT system, the heat from the gas turbine exhaust gas (stream 11 in Fig. 7-3) is used to both reform the methane and vaporize the incoming water (stream 3). In the SOLRGT system, however, an additional heat source (solar heat) is used to vaporize the incoming water, and some of the gas turbine exhaust heat can be used to preheat the pressurized air. This will increase the temperature of the pressurized air at the combustor inlet and reduce the fuel demand in the combustion process, resulting higher system efficiency.

Yet another advantage of SOLRGT over the IC-CRGT, is the ability to produce larger power output. In both systems, the power output of the turbine increases with the mass flow rate of working fluid through the turbine, so the power output of the turbine increases with higher steam-methane ratio for the same mass flow rate of the fuel. In the IC-CRGT, the heat to vaporize the incoming water is provided by the turbine exhaust gas; while in the SOLRGT, it is provided by an additional heat source. This means that the SOLRGT can vaporize more incoming water than the IC-CRGT and thus have a higher steam-methane ratio, resulting in a higher power output from the turbine.

Summarizing, the main features of the SOLRGT are:

(1) Solar heat at only 200-250 °C can be used for the methane reforming process, much lower than heat at above 800 °C needed if methane is reformed directly. Since the cost of the solar collection equipment rises with the generated temperature, this results in a lower cost of required solar collection equipment. Also, compared with fossil-fuel-only power plants, SOLRGT reduces carbon emissions when the additional heat source does not generate carbon emissions, such as when using solar, geothermal or waste heat.

(2) SOLRGT has a better temperature match (smaller temperature difference between heating and heated fluid) in its heat exchangers as can seen from Fig. 7-2 and thus lower exergy destruction during heat transfer process from Eq. (2.15), when compared with the IC-CRGT.

(3) Compared with CRGT, which has only one heat source (methane), SOLRGT uses an additional heat source (solar heat) to vaporize the incoming water. This leaves more energy from the gas turbine exhaust gas to heat the pressurized air at the outlet of the compressor, leading to smaller energy requirement for raising the temperature of the combustion gas to the designed turbine inlet temperature (1,300 °C), and consequently reducing the fuel consumption and increasing the system efficiency.

(4) In IC-CRGT, the steam-methane ratio cannot be very high, since there may not be enough energy in the gas turbine exhaust gas to vaporize the water in addition to preheating the pressurized air and reforming the fuel. Due to the use of the

additional heat source (solar heat) in vaporizing the water, however, higher steam-methane ratio can be achieved simultaneously in the SOLRGT. Since higher steam-methane ratio usually results in higher power output, the SOLRGT has a potential to produce more power than the IC-CRGT system.

7.2.2. Thermodynamic analysis of SOLRGT

One of the advantages of thermochemical hybrid systems was interpreted as the ability to "upgrade" the energy quality of the additional heat, such as solar [15]. The indirect upgrading process is shown in Fig. 7-5. There are two steps in the upgrading process: first from solar heat to steam internal heat and then from steam internal heat to syngas chemical exergy.

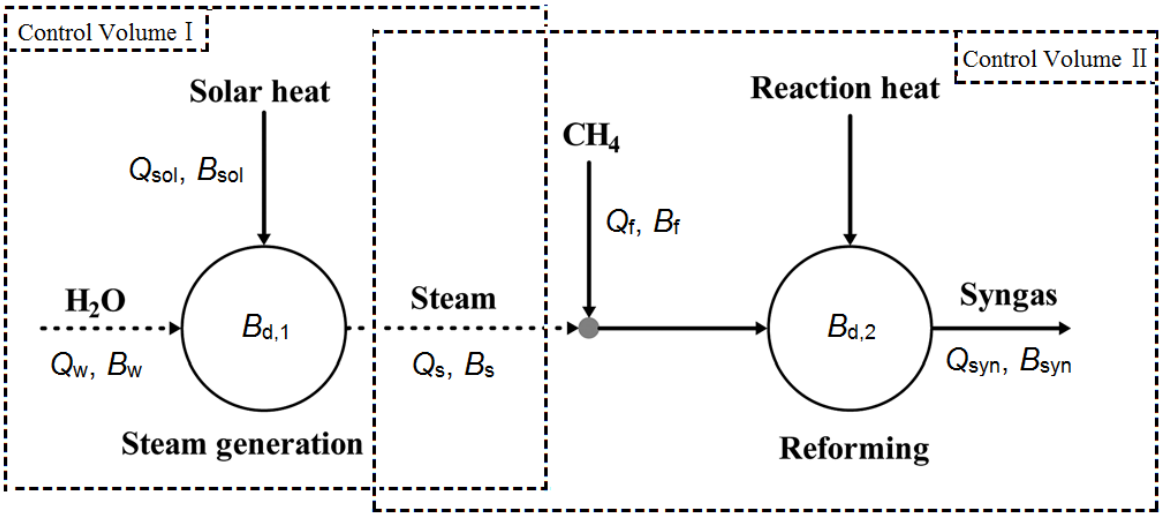

Fig. 7-5. Indirect upgrading the low/mid-level solar heat (Adapted from [15])

For control volume Ⅰ shown in Fig. 7-5, the energy balance and exergy balance equations could be written, respectively, as

$$H_{\mathrm{w}} + Q_{\mathrm{sol}} = H_{\mathrm{s}}, \tag{7.3}$$

$$B_{\mathrm{w}} + B_{\mathrm{sol}} = B_{\mathrm{s}} + B_{\mathrm{d,1}}. \tag{7.4}$$

Similarly, for control volume Ⅱ, the energy balance and exergy balance equations could be written, respectively, as

$$H_{\mathrm{f}} + H_{\mathrm{s}} + Q_{\mathrm{rec}} = H_{\mathrm{syn}}, \tag{7.5}$$

$$B_{\mathrm{f}} + B_{\mathrm{s}} + B_{\mathrm{rec}} = B_{\mathrm{syn}} + B_{\mathrm{d,2}}, \tag{7.6}$$

in which $B_{\mathrm{d,1}}$ and $B_{\mathrm{d,2}}$ are the exergy destruction in the steam generation and reforming processes, respectively. The enthalpy change relative to a reference condition, ΔH, contains changes in both chemical and thermal energy, and the exergy change relative to a reference condition, ΔB, contains both chemical and thermal exergy changes.

Following [19], we use the "*energy level*" concept, Λ, defined as the ratio of the changes of the exergy and the enthalpy in a process,

$$\Lambda \equiv \frac{\Delta B}{\Delta H}, \tag{7.7}$$

where ΔB and ΔH are the changes of exergy and enthalpy in a process, respectively. The concept of Λ is useful in exergy analysis because it represents the exergy change relative to the corresponding energy change in thermal processes, and thus directly gives the relation between them. When the reference state (environmental condition) is defined as the same for all process, the symbol Δ could be omitted in Eq. (7.7) and B and H stand for the exergy and enthalpy of the stream, respectively.

For the transferred heat, the *energy level* Λ_{tr} could be determined by the Carnot equation as

$$\Lambda_{\text{tr}} = 1 - \frac{T_0}{T_{\text{tr}}}, \tag{7.8}$$

in which T_0 and T_{tr} are the temperatures of environment and the transferred heat, respectively.

For solar heat, Λ_{sol} could be expressed using Eq. (7.8) as

$$\Lambda_{\text{sol}} = 1 - \frac{T_0}{T_{\text{sol}}}, \tag{7.9}$$

in which T_{sol} is the solar temperature, or the temperature of the solar heat.

According to the definition of Λ, Λ_{sol} can also be expressed by

$$\Lambda_{\text{sol}} = \frac{\text{Solar exergy}}{\text{Solar energy}}, \tag{7.10}$$

which will be used in later analysis.

The Λ of the fuel, such as methane, shown in Eq. (7.11), is the ratio of its specific chemical exergy (b_{f}) and its lower heating value (LHV), both of which can be found in the references, e.g. [20].

$$\Lambda_{\text{f}} = \frac{b_{\text{f}}}{\text{LHV}}. \tag{7.11}$$

Using the concept of Λ, Eqs (7.3)-(7.6) could thus be simplified to find the Λ difference between the solar heat input and the produced syngas. It is shown in the following analysis that the Λ of the solar heat input is increased to that of syngas by the indirect thermochemical upgrading process shown in Fig. 7-5.

According to the definition of Λ,

$$B_{\text{w}} = H_{\text{w}}\Lambda_{\text{w}} \tag{7.12}$$

$$B_{\text{sol}} = Q_{\text{sol}}\Lambda_{\text{sol}} \tag{7.13}$$

$$B_{\text{s}} = H_{\text{s}}\Lambda_{\text{s}} \tag{7.14}$$

$$B_{\text{f}} = H_{\text{f}}\Lambda_{\text{f}} \tag{7.15}$$

$$B_{\text{rec}} = Q_{\text{rec}} \Lambda_{\text{rec}} \tag{7.16}$$

$$B_{\text{syn}} = H_{\text{syn}} \Lambda_{\text{syn}} \tag{7.17}$$

According to [21], the exergy destruction during heat transfer is caused by the Λ difference between the energy donor (the heat source that releases energy) and the energy acceptor (the heat sink that absorbs energy), that could be expressed by

$$B_{\text{d}} = \Delta H_{\text{ea}} \left(\Lambda_{\text{ed}} - \Lambda_{\text{ea}} \right), \tag{7.18}$$

in which ΔH_{ea} is the enthalpy change of energy acceptor, and Λ_{ed} and Λ_{ea} are the Λ of the energy donor and energy acceptor, respectively.

In the steam generation process, exergy is destroyed when solar radiation is used to generate steam. The energy donor is the solar radiation incident on the solar collection equipment, and the energy acceptor is the steam that is generated. Thus, the exergy destruction rate in this process is

$$B_{\text{d,1}} = Q_{\text{sol}} \left(\Lambda_{\text{sol}} - \Lambda_{\text{sg}} \right), \tag{7.19}$$

in which Λ_{sg} and Λ_{sol} are the Λ of the steam generation heat and the solar heat, respectively.

In the reforming process, exergy is destroyed due to the chemical reactions and the temperature differences during the heat transfer. The energy donor is the gas turbine exhaust gas that provides part of the heat needed for the endothermic reaction and the energy acceptor is the chemical reaction. Thus the exergy destruction in reforming is,

$$B_{\mathrm{d},2} = Q_{\mathrm{rec}}\left(\Lambda_{\mathrm{ex}} - \Lambda_{\mathrm{rec}}\right), \tag{7.20}$$

in which Λ_{ex} and Λ_{rec} are the Λ of the external heat input to the reformer and the reaction heat, respectively.

Using Eqs (7.3) to (7.20), the total Λ difference between the solar heat input and the produced syngas is,

$$\Lambda_{\mathrm{syn}} - \Lambda_{\mathrm{sol}} = \frac{H_{\mathrm{f}}}{H_{\mathrm{s}}}\left(\Lambda_{\mathrm{f}} - \Lambda_{\mathrm{syn}}\right) - \frac{Q_{\mathrm{rec}}}{H_{\mathrm{s}}}\left(\Lambda_{\mathrm{syn}} - \Lambda_{\mathrm{rec}}\right) - \frac{H_{\mathrm{w}}}{Q_{\mathrm{sol}}}\left(\Lambda_{\mathrm{s}} - \Lambda_{\mathrm{w}}\right) - \left(\Lambda_{\mathrm{sol}} - \Lambda_{\mathrm{sg}}\right). \tag{7.21}$$

Based on the assumptions and justifications in [15], we can quantify this difference for this case from knowing that:

1) the fuel enthalpy input H_{f} is approximately equal to its lower heating value (802.3 kJ/mol), which is much higher than the reforming heat Q_{rec} (98.8 kJ per mol of methane

used for the system) and the water enthalpy H_w (89.0 kJ per mol of methane used for the system);

2) the Λ of methane, $\Lambda_f = 1.05$;

3) the average Λ of the reaction heat, $\Lambda_{rec} = 0.6$ as driven through the turbine exhaust heat at 500 °C (which is also the average temperature inside the reformer);

4) the Λ of the syngas, $\Lambda_{syn} = 0.83 \text{ to } 0.9$, depending on the syngas composition;

5) the Λ of the solar heat, $\Lambda_{sol} \approx 0.4$ using Eq. (7.8), when the temperature of the solar heat is defined as the temperature at the outlet of the solar collection equipment and is assumed to be 220 °C; In fact, the temperature of the solar heat may be defined in other ways and the detail is discussed in Section 7.2.3;

6) $\left(\Lambda_s - \Lambda_w\right) \approx -0.003$ and $\left(\Lambda_{sol} - \Lambda_{sg}\right) \approx 0.04$ are small compared with $\left(\Lambda_f - \Lambda_{syn}\right) \approx 0.4$ and $\left(\Lambda_{syn} - \Lambda_{rec}\right) \approx 0.4$, because of the small temperature difference between saturated steam and water, and between the solar heat (defined using the collector outlet temperature at 220 °C) and the steam generation process absorbed heat.

7) $H_s = 295.9$ kJ/(mol methane used for the system), so $\frac{H_f}{H_s} \approx 2.7$ and $\frac{Q_{rec}}{H_s} \approx 0.33$;

8) $Q_{\text{sol}} = 206.9$ kJ/mol methane used for the system), so $\frac{H_{\text{w}}}{Q_{\text{sol}}} \approx 0.43$.

The first term on the right side of Eq. (7.21) is thus much larger than the other terms there, so $\left(\Lambda_{\text{syn}} - \Lambda_{\text{sol}}\right) > 0$. This demonstrates that, the Λ of the solar heat input is indeed upgraded by this thermochemical process to the higher Λ of the produced syngas. When the solar heat temperature is used at 220 °C as in SOLRGT, the relative upgrade is $\left(\Lambda_{\text{syn}} - \Lambda_{\text{sol}}\right) / \Lambda_{\text{sol}} \approx 1.2$.

7.2.3. Effect of the solar Λ definition on the value of Λ difference between the produced syngas and the input solar heat

As shown in Section 7.2.2, the equations for calculating the Λ difference between the produced syngas and the input solar heat include one that is used to calculate the Λ of the solar heat, Λ_{sol} such as Eq. (7.8) used in [15], in which T_{tr} was chosen as the temperature of the steam generated by the solar heat, i.e. 220 °C. The solar Λ is often called the "solar exergy factor" [22] since it is also defined as the ratio between the solar exergy and its energy. The solar energy that is absorbed by the system (equal to the enthalpy increase of the working fluid heated by solar collectors) is easy to determine but not the solar exergy, with the discussion about the appropriate way to calculate it having started decades ago still remaining unresolved. For example, some publications, e.g. [23], recommend that the Λ of the solar heat (i.e. this solar exergy factor) is to be determined by using the

temperature at the sun surface, i.e. about 5,500 °C, in Eq. (7.8). Other expressions for the solar exergy factor were also proposed [22-26]. Different forms of the solar Λ expressions and different choices of the solar temperature will obviously result in different values of the solar Λ (Λ_{sol}), so the Λ of the produced syngas in SOLRGT may not always be higher than that of the solar Λ calculated in ref. [15]. Consequently, a conclusion in [15] that SOLRGT increases the Λ of the input solar heat to that of the produced syngas, while true for the way that the input solar heat was defined there, will be different for other solar Λ definitions.

According to the definition of exergy, using the temperature at the sun surface gives the theoretical maximum work that can be obtained by using solar radiation While use of such high temperatures in the definition may be currently impractical for heat-driven energy devices, it could be employed when using methods that do not use solar energy as heat, such as photovoltaic (PV) cells, which convert solar radiation directly to pure exergy (electricity).

A practical way to define solar exergy is to use in Eq. (7.8) the top temperature of the solar-heated material (e.g., the system working fluid), here the solar-generated steam in SOLRGT. While this is not the absolute maximum of thermodynamic solar exergy, not even the maximum among different type of the solar thermal collectors that could be used for the same purpose, it is the maximal solar exergy for the considered system, and this definition is used by many.

An alternative option is to choose the highest temperature that the working fluid can attain in practice as the temperature of the solar heat to determine the solar radiation Λ. This choice averts the above-discussed problem associated with choosing the sun surface temperature, since it is achievable in practice. It also averts the problem associated with using the solar collection equipment outlet temperature since this temperature would be the same for all thermal power cycles using solar heat. It still leaves, however, a problem: that temperature is not fixed and will change as technology advances. No one used this method in their research yet.

Considering the advantages and disadvantages of these methods, we suggest that using the sun surface temperature as the solar temperature would be the best. It is the same for all solar thermal power plants, and allows comparison of the solar thermal power plants with solar PV power plants though they have no working fluid. It is currently also a most widely used method to calculate solar exergy and the results are thus easy to compare with other works.

For comparison, let us call the solar *energy level* used in section 7.2.2, in which the solar temperature is assumed to be the solar collector outlet temperature, i.e. 220 °C, as the *solar heat energy level* Λ_{sol}. Let us then call the solar *energy level* that uses the sun surface temperature, i.e. 5,500 °C, as the *solar surface energy level* Λ_{ss}.

We now examine the indirect thermochemical upgrading process again, but replacing the solar heat Λ (that is now Λ_{sol}) with the solar surface Λ (that is now Λ_{ss}). The derivations

are the same except that $\left(\Lambda_{ss} - \Lambda_{sg}\right)$ cannot be neglected because $\Lambda_{ss} \approx 0.95$ when using the sun surface temperature as the solar temperature in Eq. (7.9). Since Λ_{syn} is 0.83 to 0.9 [15], depending on syngas composition.

$$\Lambda_{syn} < \Lambda_{ss}, \tag{7.22}$$

i.e. the Λ of the solar surface heat is not "upgraded"

It can thus be concluded that collector outlet temperature defined "solar heat" (as well as other heat sources such as waste or geothermal heat) is upgraded by the thermochemical process, but not the solar surface temperature based "solar surface heat".

An interesting question is the temperature at which the additional heat input (such as the solar in SOLRGT) is not upgraded to the Λ of the produced syngas. This temperature can be found by setting the Λ of the syngas equal to the Λ of the additional heat input. According to the results from the SOLRGT, the average of the Λ of the syngas is 0.865. The temperature of the additional heat input (here T_h) can thus be found using

$$\Lambda_h = 1 - \frac{T_0}{T_h} = \Lambda_{syn} = 0.865. \tag{7.23}$$

If the ambient temperature is $T_h = 298.15$ K, the temperature of the additional heat input is calculated from Eq. (7.23) to be $T_h = 2208.5$ K, or $1935\ ^{\circ}\mathrm{C}$, which, incidentally, is

higher than the temperature of geothermal heat, waste heat, or at the solar collection equipment outlet in most, if not all, cases.

7.3. Thermochemical hybrid system using methanol as fuel

Apart from methane (CH_4) that is commonly used as fuel in power plants, including thermochemical ones such as SOLRGT [27] discussed in Section 7.2, where it is reformed to syngas and allows the effective use of soar heat as a secondary emissions-free input, other fuels could also be used, such as methanol (CH_3OH), which is often made from coal as an easy to transport and use intermediate fuel and can then be thermochemically reformed to syngas that can then be burned in power generation systems. Compared with methane, one of the advantages to use methanol for reforming is that it has a lower reforming temperature: methane reforming generally requires a temperature of around 700 - 1,000 °C with Nickel-based catalyst and is impossible below 327 °C [18], while methanol could be decomposed easily (with a catalyst) at temperatures of 200 - 300 °C [28] as introduced in Section 7.2.

Methane can be reformed directly by using solar heat at the needed high temperatures (700 - 1,000 °C), but SOLRGT requires the additional solar heat that thus reduces the cost of the solar heat collection. At the same time, this type of indirect reforming process makes the systems more complex and requires the use of the heat from gas turbine exhaust gas and thus makes less of this heat available for internal heat recovery or for use in a bottoming cycle, such as the heat source for Rankine cycle as in a combined cycle. The system

described and analyzed in this chapter resolves these two issues by using methanol, instead of methane, as the reformed reactant, and by consequently adding a bottoming cycle that uses the gas turbine exhaust gas as its heat source. This system allows the use of the solar heat at about 200 °C to convert the methanol to syngas, and the gas turbine exhaust gas that was used in SOLRGT to provide energy needed for the methane reforming reaction is thus saved to be the heat source for making the bottoming cycle, and thus the combined cycle, more efficient.

The studied system [29] is a methanol-fueled solar-assisted chemically-recuperated combined cycle that we will call here SOLRMCC (called in [5] “solar thermal power cycle with solar decomposition of methanol”) for short. Other cycles of this type (but with different configurations) are described in [30,31]. Its flow diagram is shown in Fig. 7-6. Compared with Fig. 7-8 showing the general thermochemical process, SOLRMCC has only two inlet streams, fuel (methanol) and solar heat collected by the solar collection equipment.

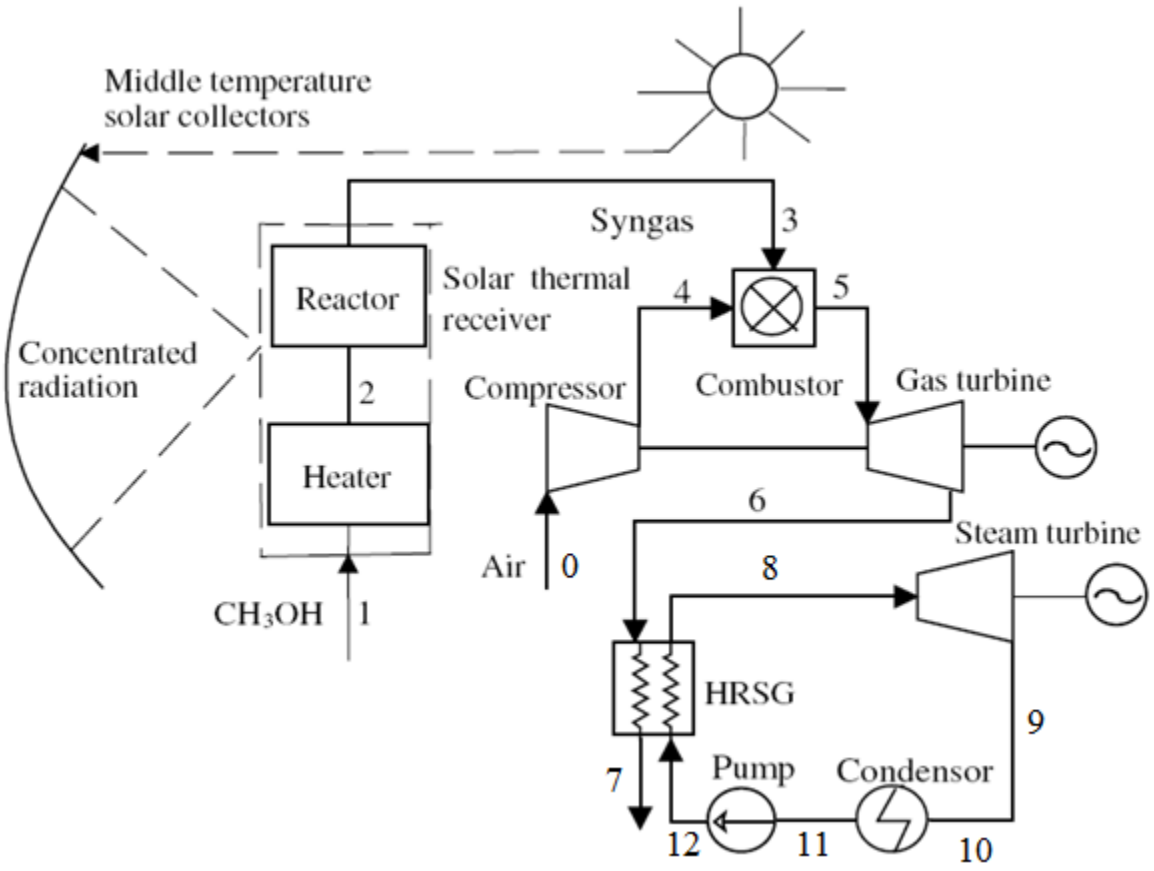

Fig. 7-6. Flow diagram for solar thermal power cycle with solar decomposition of methanol, SOLRMCC [29] (HRSG: heat recovery steam generator)

Features of the hybrid solar thermal power cycle with solar decomposition of methanol:

(1) Upgrade of *energy level* (Λ) from solar heat to chemical energy.

The *energy level* is defined by Eq. (7.11) and for liquid methanol LHV (the lower heating value) = 19,920 kJ/kg and the standard molar chemical exergy (b_f) at 298 K and 1.0 atm = 718,000 kJ/kmol (from [8]), so the liquid methanol energy level is

$$\Lambda_{\mathrm{f}} = \frac{718{,}000}{19{,}920 \times 32.04} = 1.125. \tag{7.24}$$

The difference between the *energy level* of the produced syngas and of the solar energy input [29] is

$$\Lambda_{\mathrm{syn}} - \Lambda_{\mathrm{sol}} = \frac{\mathrm{LHV}}{Q_{\mathrm{sol}}}\left(\Lambda_{\mathrm{f}} - \Lambda_{\mathrm{syn}}\right) - \left(\Lambda_{\mathrm{sol}} - \Lambda_{\mathrm{rec}}\right), \tag{7.25}$$

in which Λ_{syn}, Λ_{sol}, Λ_{f} and Λ_{rec} are the *energy levels* of the syngas, solar heat, fuel and methanol decomposition reaction, respectively, and Q_{sol} is the solar heat absorbed by the methanol decomposition reaction.

When the average temperature of the solar heat (collector outlet) is close to the temperature of the reaction heat at 200-300 °C, the value of $\left(\Lambda_{\mathrm{sol}} - \Lambda_{\mathrm{rec}}\right)$ in Eq. (7.25) is relatively small to $\left(\Lambda_{\mathrm{f}} - \Lambda_{\mathrm{syn}}\right) \approx 1.125 - 0.88 = 0.245$, and since $\frac{\mathrm{LHV}}{Q_{\mathrm{sol}}} \approx 4.6$ [29], this equation yields

$$\Lambda_{\mathrm{syn}} > \Lambda_{\mathrm{sol}}. \tag{7.26}$$

This means that the *energy level* of the solar input heat is upgraded to that of the syngas. It was stated in [29] that the Λ energy level of the syngas is 120% higher (2.2-fold) than that of the solar input heat for the conditions and solar exergy definition used in [29]. In other

words, the thermochemical reaction upgraded the “quality” of the solar thermal input energy 2.2-fold.

This relative magnitude of “thermochemical upgrading”, defined as $\left(\Lambda_{syn}-\Lambda_{sol}\right)/\Lambda_{sol}$, however, may be different for different chosen temperatures of the solar heat (or the solar collection equipment average temperature), as could be seen from Fig. 7-7, in which the “upgraded energy level” is defined as $\left(\Lambda_{syn}-\Lambda_{sol}\right)/\Lambda_{sol}$. It can be seen that the highest “upgraded energy level” happens when the temperature of the solar heat is 200-300 ℃ and is lower when outside this temperature range. This is caused by the relatively large exergy destruction in thermochemical process due to relatively large temperature difference between solar heat and methanol decomposition reaction.

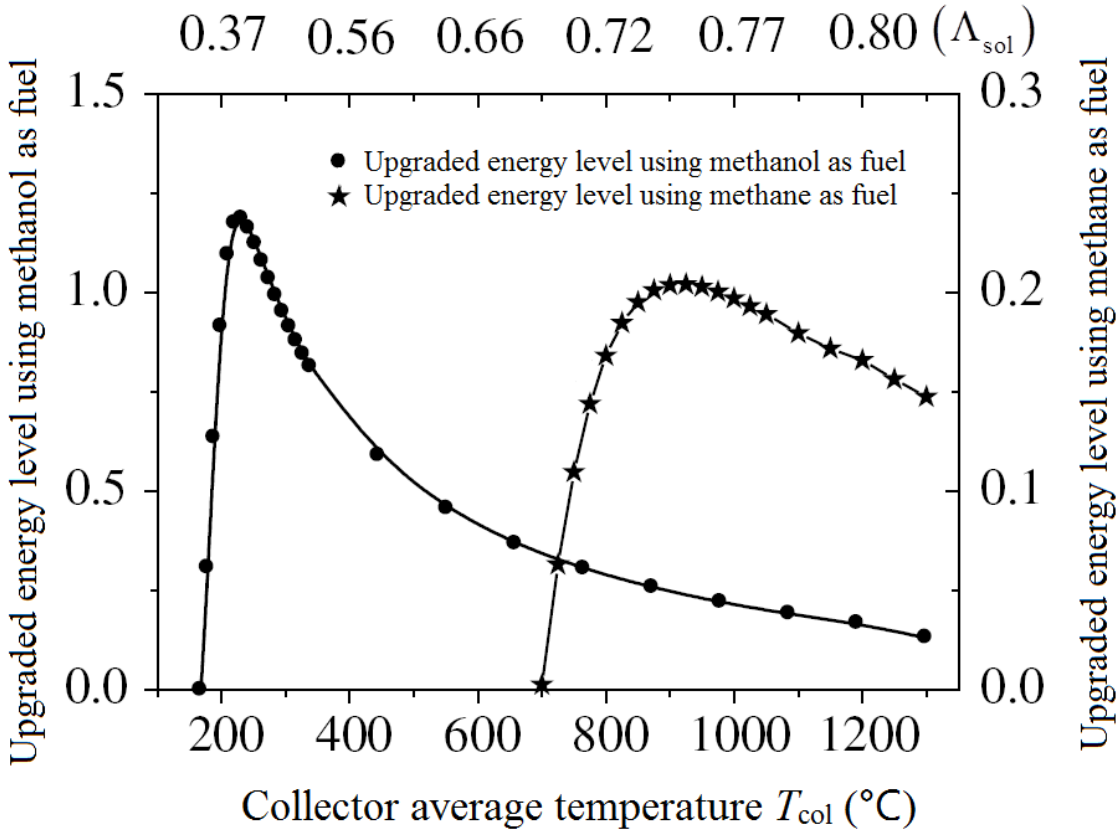

Fig. 7-7. The relationship between the upgraded level of the solar heat and the collector temperature for reforming of methanol and methane (adapted from [29]) (The ordinate is the upgraded energy level defined as $\left(\Lambda_{syn}-\Lambda_{sol}\right)/\Lambda_{sol}$

Note that similarly to the result for SOLRGT, the *energy level* of the solar heat is upgraded to the Λ of the syngas only when the magnitude of the solar temperature is defined as the temperature associated with the solar collection equipment. For example, reference [29] used the "collector average temperature" as the temperature for the solar heat. When the solar temperature is defined as the sun surface temperature, the Λ of the solar heat will be

0.95, which will be roughly the same as that of the syngas. Thus using this definition, the Λ of the solar energy is not upgraded.

(2) Potential for reducing chemical exergy loss in combustion

In the studied system [29], methanol is utilized by an indirect process: methanol decomposition to syngas and subsequent combustion of this produced syngas combustion. It was calculated in [29] that at the temperature of 1,300 °C, when methanol is directly burned, the exergy loss is 202.54 kJ/mol-CH_3OH. This loss is ~14.5% of the chemical exergy of the methanol. When methanol is used indirectly as in the SOLRMCC and burned at the same temperature in the combustor, however, the exergy loss is lowered to 167.91 kJ/mol-CH_3OH (including 13.26 kJ/mol-CH_3OH in the process of methanol decomposition and 154.61 kJ/mol-CH_3OH in the process of syngas combustion). There is thus a 17% reduction in the exergy loss using indirect combustion method as in the SOLRMCC, compared with the exergy loss using direct combustion method.

(3) Significant improvement in middle-temperature solar heat use for electricity generation

A useful performance criterion for evaluating the relative effect of using a solar-assisted hybrid system relative to a conventional one that also not use solar assistance amount of electricity generated from solar energy, i.e. net solar-to-electric efficiency is

$$\eta_{se} = \frac{\dot{W}_h - \dot{W}_{ref}}{\dot{Q}_{rad}}, \tag{7.27}$$

in which $\dot{W}_{\mathrm{h}}$ and $\dot{W}_{\mathrm{ref}}$ are the power outputs of the studied hybrid system and of a reference system (conventional gas turbine combined cycle with the same input of methanol fuel as the hybrid system), respectively and $\dot{Q}_{\mathrm{rad}}$ is the energy input rate from the solar radiation [15-17].

The predicted net solar-to-electric efficiency of the hybrid system. η_{se}, is higher than 30% when the solar collection equipment temperature is about 220-300 °C, and maybe as high as 35% when the turbine inlet temperature is 1,300 °C and the solar collection equipment temperature is 220 °C. This is attributed to the conversion of low-level solar energy into high-level chemical exergy, which is then used in the high efficiency gas turbine process.

In this system, solar heat collected by the solar collection equipment (parabolic trough) at 220 °C was used to provide the heat needed for producing syngas. One part of the heat was used to preheat, vaporize and superheat liquid methanol before the produced methanol vapor entered the receiver-reactor. The other part of heat was then used to drive the endothermic reaction:

$$\mathrm{CH_3OH} \rightarrow \mathrm{CO} + 2\mathrm{H_2} \qquad \Delta\mathrm{H}=62\ \mathrm{kJ/mol} \tag{7.28}$$

at a temperature of 220 °C and at a pressure of 17 bar.

The energy level of the syngas produced by the SOLRMCC is 0.95, which is higher than in the SOLRGT (0.83~0.9). Substituting $\Lambda_{\mathrm{syn}} = 0.95$ into Eq. (7.23), the temperature of

the additional heat input is calculated to be $T_h = 5{,}963\ \mathrm{K}\ (5{,}690\ ^\circ\mathrm{C})$, which, incidentally, is higher than the temperature of geothermal heat, waste heat, or at the solar collection equipment outlet in most, if not all, cases.

7.4. Thermodynamic background of thermochemical upgrading

7.4.1. Background and generalization of the thermochemical process

It was shown in Section 7.2 that the *energy level* (Λ) of input heat sources can be "upgraded" to that of the syngas, with specific attention to solar heat in the solar thermochemical hybrid systems. This is clearly useful since thus the same amount solar heat (energy) acquires a higher exergy due to the reforming process in the solar thermochemical hybrid power systems, and thus has higher potential for generating work. It was also shown that although it is true for heat sources whose *energy level* temperature is uniquely defined, such as geothermal or waste heat, it isn't necessarily true for solar heat whose temperature is not. In this section we generalize the thermodynamic background of the thermochemical process used in the above-introduced SOLRGT and SOLRMCC power systems, and explains the dependency of Λ on the heat source temperature definition. The explanation starts by expressing the Λ of syngas in terms of the thermodynamic properties of each inlet stream.

The thermochemical process used in SOLRGT (Fig. 7-5) and in SOLRMCC (Fig. 7-6) can be generalized as described by the control volume in Fig. 7-8, in which the steam

generation and reforming processes are lumped together. In Fig. 7-8, the fuel is not constrained to methane as used in SOLRGT, the heat input (used to vaporize the incoming water) is not constrained to solar, and heat sources like waste or geothermal heat could also be used, and the higher temperature heat (used for the reforming reaction) is not constrained to gas turbine exhaust has heat. The product of the thermochemical process is syngas, typically containing H_2, CO and possibly some unconverted fuel, H_2O and CO_2. The enthalpy H and exergy E of each stream brought into the control volume are also shown.

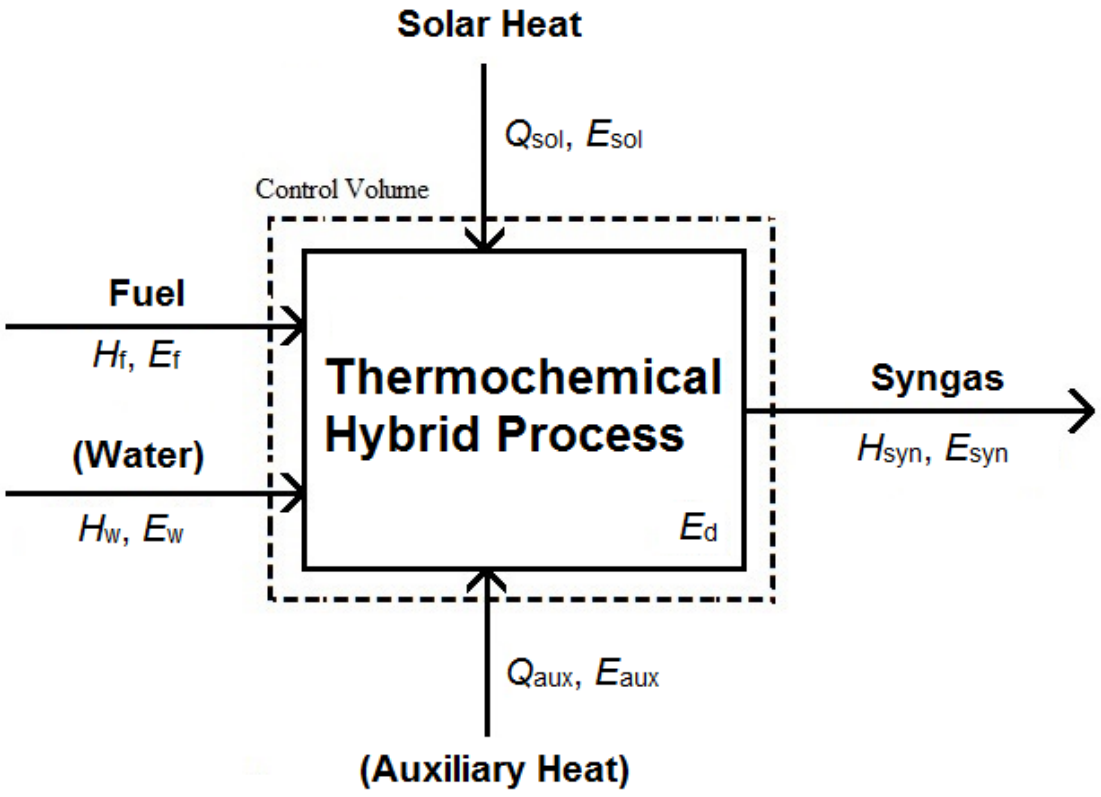

Fig. 7-8. Generalized energy and exergy streams diagram for the thermochemical hybrid process

7.4.2. Thermodynamic interpretation of the Λ of syngas

To further generalize the system described by Fig. 7-8, the solar heat and auxiliary heat shown in it can be replaced by any lower temperature heat (LT) and higher temperature heat (HT). Based on which temperature is used to define it, the solar heat can be either LT or HT compared to other heat sources, as further discussed below.

Based on the enthalpy and exergy balance of the control volume shown in Fig. 7-8, respectively,

$$H_{\mathrm{w}} + H_{\mathrm{f}} + Q_{\mathrm{LT}} + Q_{\mathrm{HT}} = H_{\mathrm{syn}}, \tag{7.29}$$

$$B_{\mathrm{w}} + B_{\mathrm{f}} + B_{\mathrm{LT}} + B_{\mathrm{HT}} - B_{\mathrm{d}} = B_{\mathrm{syn}}. \tag{7.30}$$

Based on the Λ definition Eq. (7.7),

$$B_{\mathrm{w}} = H_{\mathrm{w}}\Lambda_{\mathrm{w}} \tag{7.31}$$

$$B_{\mathrm{f}} = H_{\mathrm{f}}\Lambda_{\mathrm{f}} \tag{7.32}$$

$$B_{\mathrm{LT}} = Q_{\mathrm{LT}}\Lambda_{\mathrm{LT}} \tag{7.33}$$

$$B_{\mathrm{HT}} = Q_{\mathrm{HT}}\Lambda_{\mathrm{HT}} \tag{7.34}$$

$$B_{\mathrm{syn}} = H_{\mathrm{syn}}\Lambda_{\mathrm{syn}}. \tag{7.35}$$

Substitution of Eq. (7.31)-(7.35) to Eq. (7.30) gives

$$H_{\mathrm{w}}\Lambda_{\mathrm{w}} + H_{\mathrm{f}}\Lambda_{\mathrm{f}} + Q_{\mathrm{LT}}\Lambda_{\mathrm{LT}} + Q_{\mathrm{HT}}\Lambda_{\mathrm{HT}} - B_{\mathrm{d}} = H_{\mathrm{syn}}\Lambda_{\mathrm{syn}}. \tag{7.36}$$

The energy input fraction for each input stream to the control volume is defined here as

$$\varphi_i = \frac{H_i}{H_{\mathrm{w}} + H_{\mathrm{f}} + Q_{\mathrm{LT}} + Q_{\mathrm{HT}}} = \frac{H_i}{H_{\mathrm{syn}}}, \tag{7.37}$$

in which the subscript i could stand for the steam of water, fuel, the additional heat or higher temperature heat. Since

$$\sum_i H_i = H_{\mathrm{syn}} \tag{7.38}$$

or

$$\sum_i \varphi_i = 1, \tag{7.39}$$

then

$$0 < \varphi_i < 1. \tag{7.40}$$

Substitution of Eq. (7.37) into Eq. (7.36) then gives

$$\varphi_{\mathrm{w}}\Lambda_{\mathrm{w}} + \varphi_{\mathrm{f}}\Lambda_{\mathrm{f}} + \varphi_{\mathrm{LT}}\Lambda_{\mathrm{LT}} + \varphi_{\mathrm{HT}}\Lambda_{\mathrm{HT}} - B_{\mathrm{d}}/H_{\mathrm{syn}} = \Lambda_{\mathrm{syn}}. \tag{7.41}$$

Considering that real processes always incur some exergy destruction, E_{d}, where

$$B_{\mathrm{d}} > 0, \tag{7.42}$$

Eq. (7.42) becomes

$$\varphi_{\mathrm{w}}\Lambda_{\mathrm{w}} + \varphi_{\mathrm{f}}\Lambda_{\mathrm{f}} + \varphi_{\mathrm{LT}}\Lambda_{\mathrm{LT}} + \varphi_{\mathrm{HT}}\Lambda_{\mathrm{HT}} > \Lambda_{\mathrm{syn}}. \tag{7.43}$$

Since the first and second law of thermodynamics expressed in Eqs (7.29) and (7.30), respectively, are used here, without any other assumptions, Eq. (7.43) must always be satisfied. This means that there is a thermodynamic upper bound of the Λ of the syngas $\Lambda_{\mathrm{syn,max}}$, which is

$$\Lambda_{\mathrm{syn,max}} = \varphi_{\mathrm{w}}\Lambda_{\mathrm{w}} + \varphi_{\mathrm{f}}\Lambda_{\mathrm{f}} + \varphi_{\mathrm{LT}}\Lambda_{\mathrm{LT}} + \varphi_{\mathrm{HT}}\Lambda_{\mathrm{HT}}, \tag{7.44}$$

according to (7.43).

If the thermochemical process is ideal, i.e. not accompanied by exergy destruction, $E_{\mathrm{d}} = 0$, Eq. (7.41) is reduced to

$$\varphi_{\mathrm{w}}\Lambda_{\mathrm{w}} + \varphi_{\mathrm{f}}\Lambda_{\mathrm{f}} + \varphi_{\mathrm{LT}}\Lambda_{\mathrm{LT}} + \varphi_{\mathrm{HT}}\Lambda_{\mathrm{HT}} = \Lambda_{\mathrm{syn}}. \tag{7.45}$$

The Λ of the syngas, Λ_{syn}, can be expressed using the enthalpy fraction φ_i and the Λ_i of each input stream of thermochemical process.

Thus far, the expression of the Λ of the syngas in real processes, Eq. (7.41), and ideal processes, Eq. (7.45), were found. The next step is to evaluate the last term on the left hand side of Eq. (7.41). $\left(-B_{\mathrm{d}}/H_{\mathrm{syn}}\right)$ to determine by how much the real process expressed by Eq. (7.41) deviates from the ideal process expressed by Eq. (7.45).

7.4.3. Examination of the exergy destruction during the thermochemical process in SOLRGT

Sections 7.4.1 and 7.4.2 deal with the general form of thermochemical hybrid processes and are not restricted to the SOLRGT. To assess the exergy destruction during the thermochemical hybrid process, values are introduced in Eq. (7.41) for determining the magnitude of $B_{\mathrm{d}}/H_{\mathrm{syn}}$ relative to Λ_{syn}. Explanation of the *energy level* of the solar heat input on the definition of its temperature follows.

7.4.3.1. *Solar temperature defined by using the solar collection equipment or working fluid*

Using the SOLRGT as an example, the exergy destruction during a thermochemical process can be calculated using Eqs (7.19) and (7.20), where the Λ of the solar heat is defined by Eq. (7.9) (about 220 °C in [27], i.e. $T_{\mathrm{sol}} = 220$ °C), the total exergy destruction in the indirect thermochemical process in SOLRGT is about 7 kJ/(mol methane used for the system), and $B_{\mathrm{d}}/H_{\mathrm{syn}} = 0.006$, much smaller than the Λ of the syngas, which is

between 0.83 to 0.9. $B_{\mathrm{d}}/H_{\mathrm{syn}}$ could thus be neglected in Eqs (7.41) and (7.45) can then be used to estimate the Λ of the syngas Λ_{syn}.

7.4.3.2. *Solar temperature defined by using the sun surface temperature*

Since there are different definitions of solar exergy, the amount of exergy destruction in the solar heat addition process is different based on the chosen definition. This is because the temperatures (or the Λ) of the working fluid at the outlet of the solar collection equipment are the same regardless of the value of solar temperature but the value of solar exergy input varies with the definitions of solar temperature. For the ease of analysis, the total exergy destruction can thus be divided into two categories: one associated with the solar heat addition process $B_{\mathrm{d,sol}}$ and one associated with other processes $B_{\mathrm{d,other}}$, such as the reforming process. Eq. (7.41) can thus be rewritten as

$$\varphi_{\mathrm{w}}\Lambda_{\mathrm{w}}+\varphi_{\mathrm{f}}\Lambda_{\mathrm{f}}+\left(\varphi_{\mathrm{LT}}\Lambda_{\mathrm{LT}}-E_{\mathrm{d,sol}}/H_{\mathrm{syn}}\right)+\varphi_{\mathrm{HT}}\Lambda_{\mathrm{HT}}-B_{\mathrm{d,other}}/H_{\mathrm{syn}}=\Lambda_{\mathrm{syn}}, \tag{7.46}$$

in which $B_{\mathrm{d,sol}}+B_{\mathrm{d,other}}=B_{\mathrm{d}}$ and the third term in the left hand side of Eq. (7.46) represents the contribution to the Λ of the syngas Λ_{syn} from the solar input.

Since all the other terms except $\left(\varphi_{\mathrm{LT}}\Lambda_{\mathrm{LT}}-B_{\mathrm{d,sol}}/H_{\mathrm{syn}}\right)$ don't vary with the definition of solar temperature, $\left(\varphi_{\mathrm{LT}}\Lambda_{\mathrm{LT}}-B_{\mathrm{d,sol}}/H_{\mathrm{syn}}\right)$ is also fixed for all definitions of solar exergy.

Using the results from section 3.1.1, $\left(\varphi_{\mathrm{LT}}\Lambda_{\mathrm{LT}} - B_{\mathrm{d,sol}}/H_{\mathrm{syn}}\right) - B_{\mathrm{d,other}}/H_{\mathrm{syn}}$ is thus roughly the same with the value of $\varphi_{\mathrm{LT}}\Lambda_{\mathrm{LT}}$ which is calculated using the solar collector (or working fluid) temperature as the solar temperature. It can thus be concluded that Eq. (7.45) can be used to estimate the Λ of the syngas, as long as the solar Λ, Λ_{LT}, is calculated using the solar collector (or working fluid) temperature as the solar temperature.

The fact that $\left(\varphi_{\mathrm{LT}}\Lambda_{\mathrm{LT}} - B_{\mathrm{d,sol}}/H_{\mathrm{syn}}\right)$ doesn't change with the value of solar exergy level (or solar exergy definition) also explains thermodynamically why the Λ of the syngas Λ_{syn} is not always higher than the Λ of the solar energy Λ_{sol} (Λ_{LT}). Since the solar energy input is well defined and doesn't change with the definition of solar exergy, $\left(\varphi_{\mathrm{LT}}\Lambda_{\mathrm{LT}} - B_{\mathrm{d,sol}}/H_{\mathrm{syn}}\right)$ remaining unchanged indicates that the exergy destruction in the solar heat addition process $B_{\mathrm{d,sol}}$ increases with the Λ of the solar input Λ_{LT}. The value of Λ_{LT} is thus independent of Λ_{syn} and can be either higher or lower than Λ_{syn}, depending on the definition of solar exergy, or Λ_{LT}.

Generally, higher temperature differences between the heating and heated fluids lead to smaller heat exchangers and thus to lower capital costs, but they raise the heat transfer exergy losses and consequently reduce the system exergy efficiency and energy cost. When reduction of energy use is the dominant objective, the temperature differences are designed to be small in the thermochemical hybrid process. Equation (7.45) can then be used in a

process to determine the Λ of the syngas and should thus apply to other thermochemical hybrid processes as well.

7.4.3.3. *Thermodynamic meaning of the Λ of the syngas*

Since the enthalpy and *energy level* of the inlet streams in Fig. 7-8 are independent of each other, the *energy level* of the syngas Λ_{syn} could be regarded as the weighted average of the *energy levels* of each of the input streams, Λ_i, and the weighting factors for each input stream are the energy input fraction of each input stream φ_i, defined by Eq. (7.37), which is positive and the sum of the energy input fractions is 1 according to Eq. (7.39), i.e.

$$\sum_i \varphi_i \Lambda_i = \Lambda_{syn}, \tag{7.47}$$

$$\sum_i \varphi_i = 1. \tag{7.48}$$

Without further information, it can thus be concluded that the weighted average, which is the Λ of the syngas Λ_{syn} in Eq. (7.47), must be between the lowest $\Lambda_{i,min}$ and highest Λ $\Lambda_{i,max}$ of all input streams, i.e.

$$\Lambda_{i,min} < \Lambda_{syn} < \Lambda_{i,max}. \tag{7.49}$$

7.5. Advantages of solar thermochemical hybridization

7.5.1. Significant simplification of the solar energy storage and transportation.

Conversion of the intermittent and varying solar energy to the high specific energy/exergy synfuel by solar thermochemical systems allows compact and lower cost energy storage of the fuel, optimally controlled rate of use of the fuel, and easy transportation of the energy.

7.5.2. Reduction of the solar heat temperature needed for power generation plants, and consequently of the hybrid system cost.

Using solar energy for even a fraction of the energy needed for power generation plants reduces emissions, including those of greenhouse gases, and conserves depletable fuels. Direct use of solar heat in such plants needs it at turbine inlet temperatures between say 500 and 1,300 °C for steam and gas systems, respectively, and is thus expensive. Solar thermochemical hybrid systems, such as the SOLRGT and SOLRMCC, allow lower temperatures (down to about 200 °C) and thus cost, efficient use of solar energy in such systems.

7.5.3. Increase of the solar-to-electricity efficiency (η_{se}).

The solar-to-electricity efficiency of a thermochemical hybrid system using both fuel and solar as heat sources, is defined by Eq. (7.27). In a solar-only power plant where solar heat is the only heat source, the solar-to-electricity efficiency is the same as the power generation efficiency of the power plant,

$$\eta_{\text{sol-only}} = \frac{\dot{W}_{\text{sol-only}}}{\dot{Q}_{\text{rad}}}. \tag{7.50}$$

in which $\dot{W}_{\text{sol-only}}$ [kW] is the power output of the solar-only power plant and $\dot{Q}_{\text{rad}}$ [kW] is the heat input rate from the solar radiation.

Using Eqs (7.27) and (7.50), the difference between the solar-to-electricity efficiency of the hybrid system and the solar only system, or the increase of the solar-to-electricity efficiency through solar thermochemical hybridization, can be calculated by

$$\begin{aligned}
\eta_{\text{se}} - \eta_{\text{sol-only}} &= \frac{\dot{W}_{\text{h}} - \dot{W}_{\text{ref}}}{\dot{Q}_{\text{rad}}} - \frac{\dot{W}_{\text{sol-only}}}{\dot{Q}_{\text{rad}}} \\
&= \frac{\eta_{\text{h}}\left(\dot{m}_{\text{f}}\,\text{LHV}+\dot{Q}_{\text{rad}}\right) - \eta_0 \dot{m}_{\text{f}}\,\text{LHV} - \eta_{\text{sol-only}}\dot{Q}_{\text{rad}}}{\dot{Q}_{\text{rad}}} \\
&= \frac{\dot{m}_{\text{f}}\,\text{LHV}\left(\eta_{\text{h}} - \eta_0\right) + \dot{Q}_{\text{rad}}\left(\eta_{\text{h}} - \eta_{\text{sol-only}}\right)}{\dot{Q}_{\text{rad}}} \\
&= \frac{\dot{m}_{\text{f}}\,\text{LHV}}{\dot{Q}_{\text{rad}}}\left(\eta_{\text{h}} - \eta_0\right) + \left(\eta_{\text{h}} - \eta_{\text{sol-only}}\right),
\end{aligned} \tag{7.51}$$

in which $\dot{m}_{\text{f}}\,\text{LHV}/\dot{Q}_{\text{rad}}$ is the ratio of the fuel heat input to the solar heat input into the hybrid system. Generally, the solar share of a solar hybrid power plant, a widely used performance criterion for solar hybrid systems, is defined as

$$X_{\text{sol}} = \frac{\dot{Q}_{\text{rad}}}{\dot{m}_{\text{f}}\text{LHV}+\dot{Q}_{\text{rad}}} = \frac{1}{\dfrac{\dot{m}_{\text{f}}\text{LHV}}{\dot{Q}_{\text{rad}}}+1}, \tag{7.52}$$

which is 0 for the fuel only power plants, 1 for the solar only power plants and between 0 and 1 for the solar hybrid power plants. In Eq. (7.52), $\dot{m}_{\text{f}}\text{LHV}/\dot{Q}_{\text{rad}}$ can be expressed by the solar share expression, X_{sol}, as

$$\frac{\dot{m}_{\text{f}}\text{LHV}}{\dot{Q}_{\text{rad}}} = \frac{1-X_{\text{sol}}}{X_{\text{sol}}}, \tag{7.53}$$

whose theoretical range is from zero to infinity. For a practical range of X_{sol}, say between 0.2 and 0.8

$$0.25 < \frac{\dot{m}_{\text{f}}\text{LHV}}{\dot{Q}_{\text{rad}}} < 4. \tag{7.54}$$

Using Eq. (7.53), Eq. (7.51) can be written as

$$\eta_{\text{se}} - \eta_{\text{sol-only}} = \frac{1-X_{\text{sol}}}{X_{\text{sol}}}\left(\eta_{\text{h}} - \eta_{0}\right) + \left(\eta_{\text{h}} - \eta_{\text{sol-only}}\right). \tag{7.55}$$

Equation (7.55) shows that whether the solar-to-electricity efficiency increases through the solar thermochemical hybridization depends on the relative magnitude of three terms, X_{sol}, $\eta_{\text{h}} - \eta_{0}$ and $\eta_{\text{h}} - \eta_{\text{sol-only}}$.

For comparison, assume that the highest temperature in the solar thermochemical hybrid system is the same as that of the reference fuel-only system (conventional gas turbine power plant) and they use the same amount of fuel. Since the fuel only system and the hybrid system use the same type of power generation cycle (Brayton) in the considered SOLRGT and SOLRMCC and have the same highest cycle temperature, their energy efficiencies should approximately be the same. In fact, according to [15], the energy efficiency of the SOLRGT is 45.9%, while for the fuel only reference system (IC-CRGT) it is 46.7%.

Also for comparison, assume that the temperatures of solar heat generated by the solar collectors are the same for both the hybrid system and the solar only power generation system (solar power plants). Since the temperature that can be achieved by burning the syngas, say over 1,200 °C, is much higher than the temperature of the solar heat produced by the solar collectors, say 220 °C, the energy efficiency of the hybrid system is higher than that of the solar only power plant whose only heat source is solar heat produced at 220 °C. Thus there is

$$\eta_0 \approx \eta_{\mathrm{h}} > \eta_{\text{sol-only}}. \tag{7.56}$$

It can thus be concluded that $(\eta_0 - \eta_{\mathrm{h}})$ is small compared to $(\eta_{\mathrm{h}} - \eta_{\text{sol-only}})$. Considering Eq. (7.54), the magnitude of the first term on the right hand side of Eq. (7.55) is small

compared with the second term. This means that $(\eta_{se} - \eta_{sol\text{-}only})$ has the same sign as $(\eta_h - \eta_{sol\text{-}only})$. Considering Eq. (7.56), it is known that

$$\eta_{se} > \eta_{sol\text{-}only}, \tag{7.57}$$

meaning that the solar-to-electricity efficiency of the solar thermochemical hybrid systems is higher than that of the solar-only power generation systems when the temperature of the solar heat input is the same for both systems. This suggests that solar heat input should be used together with the fuel in the thermochemical hybrid systems rather than used alone.

In the SOLRGT, the solar-to-electricity efficiency was calculated in [15] to be 29.1%, while it is 20.5% if the same solar collector (same collector outlet temperature, collector efficiency and heat transfer efficiency) were used (calculated based on [32]). The solar-to-electricity thus increases 42% relatively (8.6 percentage points) if solar heat at 220 °C was used in the SOLRGT, compared to the solar-only power plant.

7.6. Conclusions of thermodynamic analysis of thermochemical hybrid power generation systems

This chapter examines the thermodynamic features and performance of thermochemical hybridization of power generation systems, and demonstrates it for two previously proposed and analyzed specific solar-hybridized systems, SOLRGT that incorporates reforming of methane, and SOLRMCC that incorporates reforming of methanol, both of

which using use low temperature solar heat (at ~220 °C) to help reform or decompose the fuel to syngas, which is then used for power generation.

The main conclusions are:

- The *energy level* (Λ) of the produced syngas from the reforming process (ratio of the exergy and enthalpy of the syngas) is approximately equal to the weighted average of the *energy levels* of all heat source input streams (Fig. 7-8, e.g., fuel, solar, gas turbine exhaust gas). The weighting factors are the enthalpy ratio of each input stream relative to the total heat input (or the enthalpy of the syngas) (Eq. (7.45)).
- The magnitude of the exergy destruction in the thermochemical process can be neglected compared to the magnitude of the exergy of the syngas, as long as the Λ of solar input is defined using the solar collector equipment or working fluid as the solar temperature.
- This finding thus also suggests that increasing the solar share (solar input relative to the total input) lowers the Λ of the syngas, which is undesirable. There is thus a tradeoff between the solar share and the energy/exergy efficiency of the solar thermochemical hybrid system.
- Solar thermochemical hybrid systems designed for using higher temperature solar heat are thus good for increasing the *energy level* (Λ) of the syngas.
- Since the cost of solar collection equipment generally increases with the temperature it provides, there is also a tradeoff between the thermodynamic performance of the system and the cost of the system.

- Solar thermochemical hybrid systems have the potential to increase the "solar-to-electricity" efficiency, which is an important criterion assessing how much power could be produced using solar heat. Eq. (7.55) provides an easy way to determine whether the solar-to-electricity efficiency increased or not through the thermochemical hybridization process.
- The thermodynamic analysis in this chapter has shown that the solar-to-electricity efficiency of the solar thermochemical hybrid systems is generally larger than that of the solar-only power plants when the temperature of the solar heat input is the same in both types of systems. For example, the solar-to-electricity efficiency increases by 42% relatively if solar heat at 220 °C was used in the SOLRGT, compared to the solar-only power plant. This suggests that in terms of solar-to-electricity efficiency, solar heat at a given temperature should be used for power generation together with the fuel through the reforming process rather than used alone.
- The extent of "upgrading" of the *energy level* Λ of the solar heat input in such hybrid systems depends on the solar exergy definition. It was demonstrated that the Λ of the solar heat input, in which its temperature is defined as the average of the solar collector or the solar-heated working fluid temperature, can be considered to be upgraded by the indirect thermochemical process to that of the produced syngas, but that such "thermochemical upgrading" doesn't take place if Λ of the solar heat input is defined by the sun surface temperature of 5,500 °C, or for any other heat input source above 1,935 °C when the energy

level of the syngas is 0.865 such as in the SOLRGT, or above 2,211 °C when the energy level of the syngas is 0.88 such as in the SOLRMCC.

References for Chapter 7

[1] Trommer D., Noembrini F., Fasciana M., Rodringuez D., Morales A., Romero M., Steinfeld A., Hydrogen production by steam-gasification of petroleum coke using concentrated solar power—I. Thermodynamic and kinetic analyses. Int J Hydrogen Energ 2005;30(6):605-618.

[2] Ng Y.C., Lipiński W., Thermodynamic analyses of solar thermal gasification of coal for hybrid solar-fossil power and fuel production. Energy 2012;4(1):720-731.

[3] Bai Z., Liu Q., Li H., Jin H., Performance Analysis of a Polygeneration System for Methanol Production and Power Generation with Solar-biomass Thermal Gasification. Enrgy Proced 2014;61:1561-1564.

[4] Kesser F.K., Hoffman A.M., Baughn W.J., Analysis of a basic chemically recuperated gas turbine power plant. J Eng Gas Turb Power 1994;116(2):277-284.

[5] Tamme R., Buck R., Epstein M., Fisher U., Sugarmen C., Solar upgrading of fuels for generation of electricity. J Sol Energ Eng 2001;123(2):160-163.

[6] Sheu E.J., Mitsos A., Optimization of a hybrid solar-fossil fuel plant: Solar steam reforming of methane in a combined cycle. Energy 2013;51:193-202.

[7] Bianchini A., Pellegrini M., Saccani C., Solar steam reforming of natural gas integrated with a gas turbine power plant. Sol Energy 2013;96:46-55.

[8] Zhao H., Yue P., Performance analysis of humid air turbine cycle with solar energy for methanol decomposition. Energy 2011;36:2372-80.

[9] Li Y., Zhang N., Lior N., Cai R., Yang Y., Performance analysis of a near zero CO2 emission solar hybrid power generation system. Appl Energ 2013;112:727-736.

[10] Li Y., Zhang N., Cai R., Low CO2-emissions hybrid solar combined-cycle power system with methane membrane reforming. Energy 2013;58:36-44.

[11] Luo C., Zhang N., Zero CO2 emission SOLRGT power system. Energy 2012;45:312-23.

[12] Hong H., Jin H., Liu B., A novel solar-hybrid gas turbine combined cycle with inherent CO2 separation using chemical-looping combustion by solar heat source. J Sol Energy Eng 2006;128(3):275-84.

[13] Hong H., Han T., Jin H., A low temperature solar thermochemical power plant with CO2 recovery using methanol-fueled chemical looping combustion. J Sol Energy Eng 2010;132(3):031002.

[14] Li Y., Zhang N., Lior N., Performance comparison of two low-CO2 emission solar/methanol hybrid combined cycle power systems. Appl Energ 2015:155:740-752.

[15] Zhang N., Lior N., Use of Low/Mid-Temperature Solar Heat for Thermochemical Upgrading of Energy, Part I: Application to a Novel Chemically-Recuperated Gas-Turbine Power Generation (SOLRGT) System, J Eng Gas Turb Power 2012;134:072301.

[16] Zhang N., Lior N., Use of Low/Mid-Temperature Solar Heat for Thermochemical Upgrading of Energy, With Application to a Novel Chemically-Recuperated Gas-Turbine Power Generation (SOLRGT) System. Proceedings of the ASME 2009 International Mechanical Engineering Congress and Exposition, November 13-19, Lake Buena Vista, FL, Paper No. IMECE2009-13037.

[17] Zhang N., Lior N., Use of Low/Mid-Temperature Solar Heat for Thermochemical Upgrading of Energy, Part II: A Novel Zero-Emissions Design (ZE-SOLRGT) of the Solar Chemically-Recuperated Gas-Turbine Power Generation System (SOLRGT) guided by its Exergy Analysis," ASME J Eng Gas Turb Power 2012;134:072302.

[18] Abdallah H., Harvey S., Thermodynamic Analysis of Chemically Recuperated Gas Turbines. Int J Therm Sci 2001;40:372-384.

[19] Ishida M., Thermodynamics Made Comprehensible, Nova Science. New York, 2002.

[20] Szargut J., Exergy Method: Technical and Ecological Applications. WIT Press, 2005. ISBN 1-85312-753-1.

[21] Ishida M., Process system synthesis and available information. Proceeding of TAIES'97, Beijing, 1997, 370-376.

[22] Petela R., Exergy of Heat Radiation. J Heat Transfer 1964;86:187-192.

[23]Reddy V. S., Kaushik S.C., Tyagi S.K., Exergetic analysis of solar concentrator aided natural gas fired combined cycle power plant. Renew Energ 2012;(39):114-125.

[24] Parrott J. E., Theoretical upper limit to the conversion efficiency of solar energy. Sol Energy 1978;21:227-229.

[25] Winter C. J., Sizmann R.L., Vant-hull L.L., Solar power plants. New York: Springer; 1991.

[26] Zamfirescu C., Dincer I., How Much Exergy Can One Obtain From Incident Solar Radiation. J Appl Phys 2009;105:044911.

[27] Zhang N., Lior N., Use of Low/Mid-Temperature Solar Heat for Thermochemical Upgrading of Energy, Part I: Application to a Novel Chemically-Recuperated Gas-Turbine Power Generation (SOLRGT) System. J Eng Gas Turb Power 2012;134:072301.

[28] Nakagaki T., Ogawa T., Murata K., Nakata Y., Development of methanol steam reformer for chemical recuperation. ASME J Eng Gas Turb Power 2001;123:727-733.

[29] Hong H., Jin H., Ji J., Wang Z., Cai R., Solar thermal power cycle with integration of methanol decomposition and middle-temperature solar thermal energy. Sol Energy 2005;78:49-58.

[30] Li Y., Zhang N., Cai R., Performance Comparison of Two Low CO_2 Emission Solar/Methanol Hybrid Power Systems, Proceedings of International Conference on Sustainable Energy and Environmental Protection (SEEP 2012), Dublin, Ireland, June 5-8, 2012.

[31] Hong H., Han T., Jin H., A Low Temperature Solar Thermochemical Power Plant With CO_2 Recovery Using Methanol-Fueled Chemical Looping Combustion. J Sol Energy-T ASME, 2010;132:031002.

[32] Glatzmaier G., Summary Report for Concentrating Solar Power Thermal Storage Workshop, Technical Report, NREL/TP- 5500-52134, August 2011;http://www.nrel.gov/docs/fy11osti/52134.pdf

CHAPTER 8

EXERGO-ECONOMIC ANALYSIS FOR THERMAL HYBIRD POWER GENERATION SYSTEMS

While thermal hybrid power cycles may have thermodynamic performance advantages over conventional single heat source power generation systems, it is of course important to assess also their economic viability. Usually there is a trade-off between the performance and cost of equipment in a system, e.g., in heat exchangers exergy destruction decreases with the reduction of the temperature difference between the cold and hot streams, but the latter requires larger heat exchange area and heat transfer coefficient and thus incurs higher cost.

Another important economic consideration is the potential for saving depletable fuel and reducing emissions (including of greenhouse gases) by hybrid power systems using renewable heat sources or other heat sources that generate no emissions, both features having important economic impact when considering the rise of fuel price and carbon tax (or other monetary penalty for CO_2 emissions).

Past studies focused only on the exergo-economic analysis of specific thermal hybrid systems but no general theory about the performance of this class of hybrid systems was developed. This chapter developed the general theory and equations for exergo-economic evaluation of such hybrid power generation systems (based on thermodynamics and the

SPECO method), discusses the results, and draws conclusions about their possible improvements. Major types of power generation cycles were studied, including hybrid Rankine cycles (with and without reheat and regeneration), hybrid Brayton cycles (with and without intercooling, reheat and regeneration) and hybrid combined cycles. Positive and negative prices of externalities were included. The study found that for all the types of hybrid power cycles studied, the difference between the levelized electricity costs (LEC-s) of the hybrid system and the corresponding single heat source reference system could be generalized by two equations: one for the fuel-saving mode when the additional heat sources (AHS, beyond one) are used to save fuel, and the other for power-boost mode when the AHS is added to generate more power. These equations can be, and were, used to find the fuel price and the values of the price-beneficial externalities at which the LEC of the hybrid system becomes lower than that of the reference system. Considering that the price of the non-renewable fuel will increase in the long run, that the cost of AHS equipment will decrease as technologies improve, and that the cost of undesirable externalities will be increased, the LEC of the hybrid systems will become lower. The results also show that higher carbon and other environmental taxes/penalties will boost the economic competitiveness of the hybrid systems and provide guidance for government in determining their magnitudes.

8.1. Economic analysis methods for thermal hybrid systems

8.1.1. The energo-economic analysis method

Energo-economic economic analysis that is historically and currently the most widely used by researchers and in practice to determine the economic feasibility of power generation and other energy-considering systems, is called by us and some others 'energo-economic' analysis (instead of the historically popular but thermodynamically incorrect "thermoeconomic" analysis name). In this method applied to power generation system as is the case in this study, the levelized electricity cost (LEC), from a power generation system is usually defined as

$$\text{LEC} = \frac{\text{Annual levelized cost of system (\$)}}{\text{Annual generation of electricity (kWh)}}, \tag{8.1}$$

$$c_{\text{P}} = \frac{\kappa \cdot C_{\text{Inv}} + C_{\text{O\&M}} + C_{\text{f}}}{H \cdot \dot{W}_{\text{net}} \cdot \eta_{\text{gen}}}, \tag{8.2}$$

in which c_{P} [\$/kJ] is the LEC of the system, C_{Inv} [\$] is the total investment cost of the system, $C_{\text{O\&M}}$ [\$] and C_{f} [\$] are, respectively, the annual operation and maintenance (O&M) cost and annual fuel cost of the system, H [h] is the total operation time of the system in a year, $\dot{W}_{\text{net}}$ [kW] is the net power output of the system. κ is the capital recovery factor, which depends on the interest rate as well as system expected lifetime and is determined by

$$\kappa = \frac{i(1+i)^n}{(1+i)^n - 1}, \tag{8.3}$$

in which i is the interest rate (for example, $i = 0.08$ when the interest rate is 8%) and n is the lifetime of the system in years. The capital recovery factor is widely used in economic analysis. The meaning of this term is to annualize the initial capital investment, with consideration of the time value of money, as if the investment were invested every year, and with the same amount, throughout the lifetime of the system.

η_{gen} is the electricity generator efficiency defined as the ratio of work input and electricity output of the generator, which in this chapter is assumed to be = 1 (0.95 to 0.99 in practice).

Equation (8.2) thus becomes

$$c_{\text{p}} = \frac{\kappa \cdot C_{\text{Inv}} + C_{\text{O\&M}} + C_{\text{f}}}{H \cdot \dot{W}_{\text{net}}}. \tag{8.4}$$

The energo-economic analysis method of calculating the LEC serves as the method to be compared with the exergo-economic analysis method.

8.1.2. The exergo-economic analysis method

Although the energo-economic analysis method is widely used, it doesn't relate the thermodynamic aspects of a system fully to the economic ones and thus gives no suggestion on how to improve the economic performance of the system by changing the operation

parameters, such as the temperature of the heat sources. The “exergo-economic” analysis method, which a cost analysis method that is based on exergy, rather than energy, costs, embeds in it the thermodynamic parameters, such as working fluid temperature, pressure and concentrations that distinguish exergy from energy. It thus allows direct examination of the effects of changing these thermodynamic parameters on the costs.

Exergo-economic analysis, which we use here, assigns exergy-related costs to economic analysis. It is often performed by using the Specific Exergy Costing (SPECO) methodology [1] which is therefore selected for this study. The basics of the SPECO method are described in [1], and other details are available in [2]. The SPECO analysis proceeds in two steps:

Step 1: identification of each component and the corresponding fuel and product

The words product and the fuel are defined here by considering the desired result produced by the component and the resources expended to generate this result [1]. Examples of components are pumps, turbines and heat exchangers. The product is defined to be equal to all the exergy

i. streams’ values to be considered at the outlet (including the exergy of energy streams generated in the component), plus
ii. increases between each component’s inlet and outlet (i.e. the exergy additions to the respective material streams) that are in accord with the purpose of the component,

and the fuel is defined to be equal to all the exergy

i. values to be considered at the inlet (including the exergy of energy streams supplied to the component), plus
ii. decreases between inlet and outlet (i.e. the exergy removals from the respective material streams), minus
iii. increases (between inlet and outlet) that are not in accord with the purpose of the component.

Step 2: Construction of cost equations

Defining cost rate as the time-rate at which money is invested and earned due to exergy inflows and outflows, and due to the investment in equipment and to operating (excluding fuel, which is already included in the exergy flows) and maintenance (O&M) expenses during the system life, cost balance equations of each component are constructed. These are based on the fact that the total of cost rates associated with all existing exergy streams is equal to the sum of cost rates associated with all entering exergy streams plus the appropriate charges due to capital investment and operation and maintenance expenses (including labor cost) [1].

There are two types of cost equations used in the SPECO method. One is the cost balance equation of component k , written according to the exergy streams entering or existing the

component, including the material exergy streams, work exergy streams and heat exergy streams,

$$\sum_{e}\left(c_e\dot{B}_e\right)_k + c_{\mathrm{w},k}\dot{W}_k = c_{\mathrm{q},k}\dot{B}_{\mathrm{q},k} + \sum_{i}\left(c_i\dot{B}_i\right)_k + \dot{Z}_k, \tag{8.5}$$

in which $\dot{B}_e$ [kW] and $\dot{B}_i$ [kW] are the associated rates of exergy transfer (exergy streams) with exiting and entering streams of matter (calculated based on state points in real processes with consideration of possible pressure drops), $\dot{W}$ [kW] and $\dot{B}_q$ [kW] are the exergy transfer rates associated with power output and entering heat transfer, respectively. c_e, c_i, c_w and c_q denote average costs per unit of exergy [$/kJ] for the corresponding exergy stream. $\dot{Z}_k$ [$/s] is the cost rate associated with the possessing, operating and maintaining the component and calculated by

$$\dot{Z}_k = \frac{\kappa \cdot Z_k \cdot \left(1+\varphi\right)}{H}, \tag{8.6}$$

in which κ is the capital recovery factor defined in Eq. (8.3), H [s] is the total operation time per year and φ is the maintenance factor defined as the ratio of operation and maintenance (O&M) cost $C_{\mathrm{O\&M}}$ and total investment cost C_{Inv}, i.e.

$$\varphi = \frac{C_{\mathrm{O\&M}}}{C_{\mathrm{Inv}}}. \tag{8.7}$$

The numerator of Eq. (8.6) stands of the levelized annual cost of component k including both the capital cost and the O&M cost and the denominator is the operation time of power plants. So the ratio between them stands for the cost rate associated with the component.

Z_k (or sometimes written as I_k) are usually called the "cost functions", whose variables are component operation parameters such as isentropic efficiency and inlet temperature. For common components, these cost functions can be found in various publications such as [2], [3] and [4]. When a cost function Z_k is not available, $\dot{Z}_k$ can also be calculated using the purchased cost of the component by assuming the total cost of each component is proportional to its purchased equipment cost $Z_{P,k}$ [5] as

$$\dot{Z}_k = \left(\frac{\kappa \cdot C_{\text{Inv}} + C_{\text{O\&M}}}{3600H} \right) \frac{Z_{P,k}}{\sum_k Z_{P,k}}, \tag{8.8}$$

in which the purchased equipment cost $Z_{P,k}$ [$] of component k can be found in [2].

In essence, the Z term used in the SPECO method is the sum of the cost of annualized purchasing cost and O&M cost of the component. The values can be found by conventional economic analysis, with consideration of the time value of money, as well (through the capital recovery factor κ).

Besides Eq. (8.5), the cost balance equation can also be written using the concepts of fuel and product defined in Step 1 for each component as

$$\sum_{\mathrm{P}}\left(c_{\mathrm{P}}\dot{B}_{\mathrm{P}}\right)_k=\sum_{\mathrm{F}}\left(c_{\mathrm{F}}\dot{B}_{\mathrm{F}}\right)_k+\dot{Z}_k, \tag{8.9}$$

in which c_{F} [$/kJ] and c_{P} [$/kJ] are called the average unit cost of fuel and product, respectively, and $\dot{B}_{\mathrm{F}}$ [kW] and $\dot{B}_{\mathrm{P}}$ [kW] are exergy transfer rates associated with fuel and product streams (including material streams and energy streams) of the component, respectively.

Eqs. (8.5) and (8.9) are both valid, although having different forms representing different physical meaning. Equation (8.5) distinguishes the form of energy flow and groups the energy flows into material flow, work flow and heat flow. Equation (8.9), however, does not distinguish whether an energy flow is material or work or heat, but groups the energy flow based on the direction of the flow alone. In Eq. (8.9), when the flow flows into a component, it is regarded as "Fuel (F)", and when the flow flows out of a component, it is regarded as "Product (P)". In practice, a heat flow can either flow into or out of a component. When it flows into the studied component, it is treated as a positive value in Eq. (8.5) but as a "Fuel" in Eq. (8.9). When it flows out of the studied component, it is treated as a negative value in Eq. (8.5) but as a "Product" in Eq. (8.9). A work flow can also either flow into or out of a component. When it flows into the studied component, it is treated as a negative value in Eq. (8.5) but as a "Fuel" in Eq. (8.9). When it flows out of the studied component, it is treated as a positive value in Eq. (8.5) but as a "Product" in Eq. (8.9).

Defining the cost rate associated with exergy stream as

$$\dot{C}_i = c_i \dot{B}_i = c_i \left(\dot{m}_i b_i \right) \tag{8.10}$$

$$\dot{C}_e = c_e \dot{B}_e = c_e \left(\dot{m}_e b_e \right) \tag{8.11}$$

$$\dot{C}_{\mathrm{w}} = c_{\mathrm{w}} \dot{W} \tag{8.12}$$

$$\dot{C}_{\mathrm{q}} = c_{\mathrm{q}} \dot{B}_{\mathrm{q}} \tag{8.13}$$

$$\dot{C}_{\mathrm{F}} = c_{\mathrm{F}} \dot{B}_{\mathrm{F}} \tag{8.14}$$

$$\dot{C}_{\mathrm{P}} = c_{\mathrm{P}} \dot{B}_{\mathrm{P}}, \tag{8.15}$$

so there is one cost balance equation for each component. As assumed by the SPECO method, the average cost per unit exergy of fuel and $\dot{Z}_k$ are known for component k, but none of the average costs per unit exergy of product is known, requiring as many equations as unknowns to solve for all average cost per unit exergy of product. These equations are called auxiliary equations and are constructed by F rule and P rule, the details of which could be found in [2] and will not be shown here.

With the help of the auxiliary equations, the problem having the same number of unknown and equations is closed. Case studies indicating how this method can be used have been demonstrated in several archival papers such as [6] and [7]. In this chapter, the SPECO

method will be used in this study to calculate and compare the cost of electricity of hybrid system, $c_{P,h}$, and that of the fuel-only reference system, $c_{P,0}$.

8.2. Hybrid power generation systems based on the Rankine cycle

8.2.1. Hybrid power generation systems based on the simple Rankine cycle

The goal is to find the LEC difference between the hybrid and the reference system (without AHS) using the exergo-economic analysis method. To achieve that, the LEC expression for both systems needs to be developed using the SPECO method introduced in the previous section. The fuel, product and auxiliary equation for each component is first determined. The cost function can then be built for each component. Manipulation of those cost balance equations will arrive at the LEC equation for each system. Further analysis could then be made based on it and conclusions could be drawn. The fuel, product and necessary auxiliary equations for each component for applying the SPECO method are summarized in Table 8-1. The cost balance equations can be constructed using Eq. (8.9) and are shown below the table.

Table 8-1. Fuel, product and auxiliary equation for each component in the hybrid simple Rankine cycle system (Fig. 4-2)

Component	Fuel	Product	Auxiliary equation	No. of streams

				Inlet	Outlet
Condensate extraction pump (CEP)	$\dot{C}_{w,CEP}$	$\dot{C}_2 - \dot{C}_1$	-	2	1
Heat Exchanger	$\dot{C}_8 - \dot{C}_9$	$\dot{C}_3 - \dot{C}_2$	$c_9 = c_8$ (F rule)	2	2
Boiler	$\left(\dot{C}_{11} + \dot{C}_{12}\right) - \left(\dot{C}_{13} + \dot{C}_{14}\right)$	$\dot{C}_4 - \dot{C}_3$		3	3
Turbine	$\dot{C}_4 - \dot{C}_5$	$\dot{C}_{w,T}$	$c_5 = c_4$ (F rule)	1	2
Condenser (Cond)	$\dot{C}_5 - \dot{C}_1$	$\dot{C}_7 - \dot{C}_6$	$c_1 = c_5$ (F rule)	2	2
Additional heat source collection equipment (AHSC)	$\dot{C}_{q,AHS}$	$\dot{C}_8 - \dot{C}_{10}$	-	2	1
Additional heat source pump (AHSP)	$\dot{C}_{w,AHSP}$	$\dot{C}_{10} - \dot{C}_9$	-	2	1

Cost Balance equations:

Condensate extraction pump (CEP):

$$\dot{C}_2 - \dot{C}_1 = \dot{C}_{\mathrm{w,CEP}} + \dot{Z}_{\mathrm{CEP}} \tag{8.16}$$

Heat exchanger:

$$\dot{C}_3 - \dot{C}_2 = \dot{C}_8 - \dot{C}_9 + \dot{Z}_{\mathrm{HE}} \tag{8.17}$$

Boiler:

$$\dot{C}_4 - \dot{C}_3 = \left(\dot{C}_{11} + \dot{C}_{12}\right) - \left(\dot{C}_{13} + \dot{C}_{14}\right) + \dot{Z}_{\mathrm{B}} \tag{8.18}$$

Turbine:

$$\dot{C}_{\mathrm{w,T}} = \dot{C}_4 - \dot{C}_5 + \dot{Z}_{\mathrm{T}} \tag{8.19}$$

Condenser (Cond):

$$\dot{C}_7 - \dot{C}_6 = \dot{C}_5 - \dot{C}_1 + \dot{Z}_{\mathrm{COND}} \tag{8.20}$$

Additional heat source collection equipment (AHSC):

$$\dot{C}_8 - \dot{C}_{10} = \dot{C}_{\mathrm{q,AHS}} + \dot{Z}_{\mathrm{AHSC}} \tag{8.21}$$

Additional heat source pump (AHSP):

$$\dot{C}_{10} - \dot{C}_9 = \dot{C}_{\mathrm{w,AHSP}} + \dot{Z}_{\mathrm{AHSP}} \tag{8.22}$$

Adding Eqs (8.16)-(8.22) together results in cancelation of some of their unknowns as shown in Eq. (8.23):

$$\dot{C}_{\mathrm{w,T}} - \dot{C}_{\mathrm{w,CEP}} - \dot{C}_{\mathrm{w,AHSP}} = \left(\dot{C}_{11} + \dot{C}_{12}\right) - \left(\dot{C}_{13} + \dot{C}_{14}\right) + \dot{C}_{\mathrm{q,AHS}} - \left(\dot{C}_{7} - \dot{C}_{6}\right) + \dot{Z}_{\mathrm{CEP}} + \dot{Z}_{\mathrm{HE}} + \dot{Z}_{\mathrm{B}} + \dot{Z}_{\mathrm{T}} + \dot{Z}_{\mathrm{COND}} + \dot{Z}_{\mathrm{AHSC}} + \dot{Z}_{\mathrm{AHSP}}. \quad (8.23)$$

The boiler inlet combustion air is generally free and thus its cost is zero,

$$c_{\mathrm{a}} = c_{12} = 0. \quad (8.24)$$

The higher temperature heat source (fuel) usually generates flue gas (stream 13 in Fig. 4-2) after burning in the boiler. When flue gas is not utilized in further process and is ultimately emitted to the atmosphere as in normal practice, the cost associated with the flue gas could be regarded as 0,

$$c_{\mathrm{fg}} = c_{13} = 0. \quad (8.25)$$

If, however, the flue gas is utilized in other processes, such as providing heat, the cost rate of flue gas will reduce the cost of the electricity generated by the hybrid system since it could be regarded as a gainful product of the system additional to the generated electricity. Conversely, if the flue gas is taxed or penalized in some way, its cost will raise the cost of the electricity.

The other product from the boiler is ash (stream 14 in Fig. 4-2) when coal is used as the fuel in the boiler. Since it usually has no sale value, the cost associated with ash could be regarded as 0, i.e.

$$c_{\text{ash}} = c_{14} = 0 \tag{8.26}$$

The flue gas and/or ash are, however, undesirable externalities (interactions with the environment that industry is not obliged to pay), and this analysis method is an opportunity to quantify here the externalities relative to the electricity cost, using Eq. (8.23).

In practice, the mass flow rate of air is usually proportional to the mass flow rate of fuel in the boiler. The mass flow rate of the combustion gas should thus be proportional to that of the fuel, so

$$\frac{\dot{C}_{\text{fg}}}{\dot{C}_{\text{f}}} = \frac{c_{\text{fg}}\dot{m}_{\text{fg}}b_{\text{fg}}}{c_{\text{f}}\dot{m}_{\text{f}}b_{\text{f}}} = \frac{c_{\text{fg}}b_{\text{fg}}}{c_{\text{f}}b_{\text{f}}}\left(1+\frac{1}{f}\right) = c'_{\text{fg}}, \tag{8.27}$$

in which $c_{\text{f}} = c_{11}$ [\$/kJ] is the cost of fuel (fuel price), $\dot{m}_{\text{f}}$ [kg/s] and b_{f} [kJ/kg] are, respectively, the mass flow rate and specific exergy of fuel, $\dot{m}_{\text{fg}}$ [\$/s] and b_{fg} [kJ/kg] are, respectively, the mass flow rate and specific exergy of flue gas, f is the fuel-air ratio.

Since the mass flow rate of ash (if any) from the boiler is also proportional to the mass flow rate of fuel,

$$\frac{\dot{C}_{\text{ash}}}{\dot{C}_{\text{f}}} = \frac{c_{\text{ash}}\dot{m}_{\text{ash}}b_{\text{ash}}}{c_{\text{f}}\dot{m}_{\text{f}}b_{\text{f}}} = c'_{\text{ash}}, \tag{8.28}$$

in which $\dot{m}_{\text{ash}}$ [kg/s] and b_{ash} [kJ/kg] are, respectively, the mass flow rate and specific exergy of ash.

Sometimes carbon tax could be imposed on power generation plants that emit CO_2, which is proportional to the amount of CO_2 emitted to the atmosphere, i.e.

$$\dot{C}_{\text{ct}} = c_{\text{CO}_2}\dot{m}_{\text{CO}_2}, \tag{8.29}$$

in which $\dot{C}_{\text{ct}}$ [\$/s] is the carbon tax imposed on the system, c_{CO_2} [\$/kg] is the specific cost for carbon emission, and $\dot{\text{m}}_{\text{CO}_2}$ [kg/s] is the carbon emission rate to the environment.

Since the mass flow rate of carbon dioxide is proportional to that of the fuel,

$$\frac{\dot{C}_{\text{ct}}}{\dot{C}_{\text{f}}} = \frac{c_{\text{CO}_2}\dot{m}_{\text{CO}_2}}{c_{\text{f}}\dot{m}_{\text{f}}b_{\text{f}}} = c'_{\text{ct}}. \tag{8.30}$$

As suggested in [2], the average unit cost of electricity consumption could be assumed to be the same as that of electricity generation and all equal to the levelized electricity cost, i.e.

$$c_{\text{w,CEP}} = c_{\text{w,AHSP}} = c_{\text{w,T}} = c_{\text{P}}. \tag{8.31}$$

Using Eq. (8.27), (8.28), (8.30) and (8.31), Eq. (8.23) could be simplified to

$$c_{\mathrm{P}}\dot{W}_{\mathrm{net}} = c'_{\mathrm{f}}\dot{m}_{\mathrm{f}}b_{\mathrm{f}} + c_{\mathrm{q,AHS}}\dot{B}_{\mathrm{AHS}} - \Delta\dot{C}_{\mathrm{cw}} + \dot{Z}_{\mathrm{CEP}} + \dot{Z}_{\mathrm{HE}} + \dot{Z}_{\mathrm{B}} + \dot{Z}_{\mathrm{T}} + \dot{Z}_{\mathrm{COND}} + \dot{Z}_{\mathrm{AHSC}} + \dot{Z}_{\mathrm{AHSP}}, \tag{8.32}$$

in which c'_{f} [kg/kJ] is the specific cost associated with fuel including the fuel price and externalities (cost of flue gas and ash) and carbon tax

$$c'_{\mathrm{f}} = c_{\mathrm{f}}\left(1 + c'_{\mathrm{fg}} + c'_{\mathrm{ash}} + c'_{\mathrm{ct}}\right), \tag{8.33}$$

$\dot{W}_{\mathrm{net}} = \dot{W}_{\mathrm{T}} - \dot{W}_{\mathrm{CEP}} - \dot{W}_{\mathrm{AHSP}}$ [kW] is the net power output of the hybrid system, $\Delta\dot{C}_{\mathrm{cw}} = \dot{C}_7 - \dot{C}_6$ [$/s] is the increase of cost rate associated with the cooling water due to heat reception in the condenser, in which the cost rate associated with the outlet flow (stream 7), $\dot{C}_7$, could be regarded as 0 when the cooling water is not used afterwards, $c_{\mathrm{q,AHS}}$ [$/kJ] is the specific cost of the additional heat source (AHS), which is 0 when solar, geothermal energy or other "free" heat source is used as AHS (the cost of equipment to harvest the energy is included in $\dot{Z}_{\mathrm{AHSC}}$), and $\dot{B}_{\mathrm{AHS}}$ [kJ/s] is the exergy flow rate of the AHS into the system.

Once the LEC of the hybrid system was calculated, the LEC of the reference system when there is only one heat source and no AHS (such as in conventional steam power plants) could be found using the same method by

$$c_{\mathrm{P},0}\dot{W}_{\mathrm{net},0} = c'_{\mathrm{f}}\dot{m}_{\mathrm{f},0}b_{\mathrm{f}} - \Delta\dot{C}_{\mathrm{cw},0} + \dot{Z}_{\mathrm{CEP},0} + \dot{Z}_{\mathrm{B},0} + \dot{Z}_{\mathrm{T},0} + \dot{Z}_{\mathrm{COND},0}, \tag{8.34}$$

in which the superscript 0 stands for reference system and $\dot{W}_{\mathrm{net},0} = \dot{W}_{\mathrm{T}} - \dot{W}_{\mathrm{CEP}}$ [kW] is the net power output of the reference system.

The LEC increase of the hybrid system relative to the reference system (may be either positive or negative), $\left(c_{\mathrm{P}} - c_{\mathrm{P},0}\right)$, can thus be calculated based on Eqs (8.32) and (8.34).

In the hybrid and reference system, the boiler efficiency (or the temperature of the flue gas) is kept constant, so the energy balance equations of the boiler for the hybrid and reference system are, respectively,

$$\eta_{\mathrm{B}}\left(\dot{m}_{\mathrm{f}}\mathrm{LHV}\right) = \dot{m}_{\mathrm{w}}\left(h_4 - h_3\right), \tag{8.35}$$

$$\eta_{\mathrm{B}}\left(\dot{m}_{\mathrm{f},0}\mathrm{LHV}\right) = \dot{m}_{\mathrm{w}}\left(h_4 - h_2\right), \tag{8.36}$$

in which η_{B} is the boiler efficiency defined as the ratio between the enthalpy increase of the working fluid and the energy input from the fuel.

From Eqs (8.35) and (8.36), the mass flow rate of the fuel for the reference system could be expressed by

$$\dot{m}_{\mathrm{f},0} = \dot{m}_{\mathrm{f}}\frac{h_4 - h_2}{h_4 - h_3}. \tag{8.37}$$

In the hybrid system, the additional heat source heat exchanger is used to replace part of the economizer in the reference system (an economizer is often part of a boiler). In the reference system, the economizer is designed to preheat the boiler feed water from T_2 to a fixed temperature, say T_{ECO}; while in the hybrid system, the preheating process is accomplished by two heat exchangers: the additional heat source heat exchanger and part of the reference system economizer. Thus,

$$\dot{Q}_{\mathrm{ECO},0} = \dot{Q}_{\mathrm{ADD}} + \dot{Q}_{\mathrm{ECO}} = \dot{m}_{\mathrm{w}} \cdot \left(h_{\mathrm{ECO}} - h_2 \right), \tag{8.38}$$

in which h_{ECO} [kJ/kg] is the specific enthalpy of working fluid at T_{ECO}, $\dot{Q}_{\mathrm{ECO}}$ and $\dot{Q}_{\mathrm{ECO},0}$ [kW] are the heat transfer rates in the economizer in the hybrid and the reference systems, respectively.

Following [3] (Appendix 9.3), the cost of a heat exchanger is proportional to the n_{HE} order of the heat transfer rate in the heat exchanger, in which n_{HE} is a constant for a specific type of heat exchanger whose value could be found in [3]. Thus, according to Eq. (8.38),

$$\frac{\dot{Z}_{\mathrm{ECO}} + \dot{Z}_{\mathrm{HE}} - \dot{Z}_{\mathrm{ECO},0}}{\dot{Z}_{\mathrm{ECO},0}} = \frac{\dot{Q}_{\mathrm{ECO}}^{n_{\mathrm{HE}}} + \dot{Q}_{\mathrm{ADD}}^{n_{\mathrm{HE}}} - \dot{Q}_{\mathrm{ECO},0}^{n_{\mathrm{HE}}}}{\dot{Q}_{\mathrm{ECO},0}^{n_{\mathrm{HE}}}} = \frac{\left(\dot{Q}_{\mathrm{ECO},0} - \dot{Q}_{\mathrm{ADD}} \right)^{n_{\mathrm{HE}}} + \dot{Q}_{\mathrm{ADD}}^{n_{\mathrm{HE}}} - \dot{Q}_{\mathrm{ECO},0}^{n_{\mathrm{HE}}}}{\dot{Q}_{\mathrm{ECO},0}^{n_{\mathrm{HE}}}}, \tag{8.39}$$

which is positive when $n_{\mathrm{HE}} < 1$ as is for usual type of heat exchanger for economizers, such as shell and tube.

The other part of the boiler is the same for both hybrid and reference systems, so for the boiler

$$\begin{aligned}&\dot{Z}_{\mathrm{B}} + \dot{Z}_{\mathrm{HE}} - \dot{Z}_{\mathrm{B},0} = \dot{Z}_{\mathrm{ECO}} + \dot{Z}_{\mathrm{HE}} - \dot{Z}_{\mathrm{ECO},0} \\ &= \frac{\dot{Z}_{\mathrm{ECO},0}}{\dot{Q}_{\mathrm{ECO},0}^{n_{\mathrm{HE}}}}\left[\left(\dot{Q}_{\mathrm{ECO},0} - \dot{Q}_{\mathrm{ADD}}\right)^{n_{\mathrm{HE}}} + \dot{Q}_{\mathrm{ADD}}^{n_{\mathrm{HE}}} - \dot{Q}_{\mathrm{ECO},0}^{n_{\mathrm{HE}}}\right].\end{aligned} \tag{8.40}$$

Using Eqs (8.37) and (8.40), the difference between the LEC between the hybrid and reference system is thus

$$\begin{aligned}&c_{\mathrm{P}}\dot{W}_{\mathrm{net}} - c_{\mathrm{P},0}\dot{W}_{\mathrm{net},0} = c_{\mathrm{f}}' b_{\mathrm{f}}\left(\dot{m}_{\mathrm{f}} - \dot{m}_{\mathrm{f},0}\right) + c_{\mathrm{q,AHS}}\dot{E}_{\mathrm{AHS}} + \dot{Z}_{\mathrm{AHSC}} + \dot{Z}_{\mathrm{AHSP}} \\ &+ \frac{\dot{Z}_{\mathrm{ECO},0}}{\dot{Q}_{\mathrm{ECO},0}^{n_{\mathrm{HE}}}}\left[\left(\dot{Q}_{\mathrm{ECO},0} - \dot{Q}_{\mathrm{ADD}}\right)^{n_{\mathrm{HE}}} + \dot{Q}_{\mathrm{ADD}}^{n_{\mathrm{HE}}} - \dot{Q}_{\mathrm{ECO},0}^{n_{\mathrm{HE}}}\right] \\ &= -c_{\mathrm{f}}' b_{\mathrm{f}}\dot{m}_{\mathrm{f}}\frac{h_3 - h_2}{h_4 - h_3} + c_{\mathrm{q,AHS}}\dot{B}_{\mathrm{AHS}} \\ &+ \dot{Z}_{\mathrm{AHS}} + \frac{\dot{Z}_{\mathrm{ECO},0}}{\dot{Q}_{\mathrm{ECO},0}^{n_{\mathrm{HE}}}}\left[\left(\dot{Q}_{\mathrm{ECO},0} - \dot{Q}_{\mathrm{ADD}}\right)^{n_{\mathrm{HE}}} + \dot{Q}_{\mathrm{ADD}}^{n_{\mathrm{HE}}} - \dot{Q}_{\mathrm{ECO},0}^{n_{\mathrm{HE}}}\right],\end{aligned} \tag{8.41}$$

in which $\dot{Z}_{\mathrm{AHS}} = \dot{Z}_{\mathrm{AHSC}} + \dot{Z}_{\mathrm{AHSP}}$ is the cost rate of equipment associated with the AHS.

The energy balance equation for the heat exchanger in Fig. 4-2

$$\eta_{\mathrm{AHS}}\dot{Q}_{\mathrm{AHS}} = \dot{Q}_{\mathrm{ADD}} = \dot{m}_{\mathrm{w}} \cdot \left(h_3 - h_2\right), \tag{8.42}$$

in which η_{AHS} is called here the energy conversion efficiency of the AHS or just the efficiency of the AHS, defined as the ratio between the enthalpy increase of the working fluid and of the AHS energy input, i.e.

$$\eta_{\text{AHS}} = \frac{\dot{Q}_{\text{ADD}}}{\dot{Q}_{\text{AHS}}}, \tag{8.43}$$

in which $\dot{Q}_{\text{AHS}}$ [kW] is the external heat input rate to the additional heat source collection equipment (AHSC), and $\dot{Q}_{\text{ADD}}$ [kW] is the enthalpy increase of working fluid based on energy conservation for the heat exchanger in Fig. 4-2 as shown in Eq. (8.42). Typical values of η_{AHS} are about 0.5 for solar heat [8] and can be close to 1 for waste heat (since the heat loss mostly occurs in the heat exchanger).

Considering Eq. (8.35), there is

$$\dot{m}_{\text{w}} = \frac{\eta_{\text{B}}\left(\dot{m}_{\text{f}}\,\text{LHV}\right)}{h_4 - h_3} = \frac{\eta_{\text{AHS}}\dot{Q}_{\text{AHS}}}{h_3 - h_2} \tag{8.44}$$

or

$$\dot{m}_{\text{f}} b_{\text{f}} = \frac{\eta_{\text{AHS}}\psi_{\text{f}}}{\eta_{\text{B}}\psi_{\text{AHS}}}\left(\frac{h_4 - h_3}{h_3 - h_2}\right)\dot{B}_{\text{AHS}}, \tag{8.45}$$

in which ψ_{f} and ψ_{AHS} are, respectively, the exergy factors of the fuel and of the AHS, defined as

$$\psi_{\mathrm{f}} = \frac{b_{\mathrm{f}}}{\mathrm{LHV}} \tag{8.46}$$

for the fuel, and

$$\psi_{\mathrm{AHS}} = \frac{\dot{B}_{\mathrm{AHS}}}{\dot{Q}_{\mathrm{AHS}}} \tag{8.47}$$

for the AHS, which is expressed by the Carnot efficiency $\left(1-\frac{T_0}{T_{\mathrm{AHS}}}\right)$ when heat such as waste or geothermal is used as the AHS.

Substitution of Eqs (8.45) and (8.47) into Eq. (8.41) gives

$$\begin{aligned} c_{\mathrm{P}}\dot{W}_{\mathrm{net}} - c_{\mathrm{P},0}\dot{W}_{\mathrm{net},0} &= \left[-c'_{\mathrm{f}}\psi_{\mathrm{f}}\left(\frac{\eta_{\mathrm{AHS}}}{\eta_{\mathrm{B}}}\right) + c_{\mathrm{q,AHS}}\psi_{\mathrm{AHS}} \right]\dot{Q}_{\mathrm{AHS}} \\ &+ \dot{Z}_{\mathrm{AHS}} + \frac{\dot{Z}_{\mathrm{ECO},0}}{\dot{Q}_{\mathrm{ECO},0}^{n_{\mathrm{HE}}}}\left[\left(\dot{Q}_{\mathrm{ECO},0} - \dot{Q}_{\mathrm{ADD}}\right)^{n_{\mathrm{HE}}} + \dot{Q}_{\mathrm{ADD}}^{n_{\mathrm{HE}}} - \dot{Q}_{\mathrm{ECO},0}^{n_{\mathrm{HE}}} \right]. \end{aligned} \tag{8.48}$$

Considering that the pump work is negligible compared with turbine output work in a steam power plant (1-2%), i.e.

$$\dot{W}_{\mathrm{CEP}}, \dot{W}_{\mathrm{AHSP}} << \dot{W}_{\mathrm{T}}, \tag{8.49}$$

the net power output of the reference and hybrid system is then the same, i.e.

$$\dot{W}_{\text{net},0} \approx \dot{W}_{\text{net}}. \tag{8.50}$$

Using Eqs (8.43) and (8.50), Eq. (8.48) could thus be simplified as

$$\Delta c_{\text{P}} = c_{\text{P}} - c_{\text{P},0} = \frac{\left\{ \begin{array}{l} \left(-c'_{\text{f}} \dfrac{\psi_{\text{f}}}{\eta_{\text{B}}} + c_{\text{q,AHS}} \dfrac{\psi_{\text{AHS}}}{\eta_{\text{AHS}}} \right) \dot{Q}_{\text{ADD}} + \dot{Z}_{\text{AHS}} \\ + \dfrac{\dot{Z}_{\text{ECO},0}}{\dot{Q}_{\text{ECO},0}^{n_{\text{HE}}}} \left[\left(\dot{Q}_{\text{ECO},0} - \dot{Q}_{\text{ADD}} \right)^{n_{\text{HE}}} + \dot{Q}_{\text{ADD}}^{n_{\text{HE}}} - \dot{Q}_{\text{ECO},0}^{n_{\text{HE}}} \right] \end{array} \right\}}{\dot{W}_{\text{net},0}}. \tag{8.51}$$

It could therefore be concluded that for a given reference system, the difference between the LEC-s of the hybrid and the reference system, Δc_{P}, increases with the cost rate of the AHS, $c_{\text{q,AHS}}$, and the cost rate associated with the equipment of the AHS, $\dot{Z}_{\text{AHS}}$, but decreases with the cost associated with fuel, c'_{f} (defined in Eq. (8.33) and includes fuel cost, carbon emission cost and the cost/benefit from flue gas and/or ash), the energy conversion efficiency of the AHS, η_{AHS}, and the exergy factor of the AHS, ψ_{AHS} (calculated using Eq. (8.46) when AHS is fuel, or Eq. (8.47) when AHS is heat).

8.2.2. Hybrid power generation systems based on the Rankine cycle with reheat

For the hybrid power generation systems based on the Rankine cycle with reheat shown in Fig. 4-11, the summation of the cost balance equation for each component and applying the auxiliary equations gives

$$\begin{aligned}\dot{C}_{\mathrm{w,T}}-\dot{C}_{\mathrm{w,CEP}}-\dot{C}_{\mathrm{w,AHSP}}&=\left(\dot{C}_{11}+\dot{C}_{12}\right)-\left(\dot{C}_{13}+\dot{C}_{14}\right)+\dot{C}_{\mathrm{q,AHS}}-\left(\dot{C}_{7}-\dot{C}_{6}\right)\\&+\dot{Z}_{\mathrm{CEP}}+\dot{Z}_{\mathrm{HE}}+\dot{Z}_{\mathrm{B}}+\dot{Z}_{\mathrm{T}}+\dot{Z}_{\mathrm{COND}}+\dot{Z}_{\mathrm{AHSC}}+\dot{Z}_{\mathrm{AHSP}},\end{aligned}\tag{8.52}$$

in which $\dot{C}_{\mathrm{w,T}}=\dot{C}_{\mathrm{w,HPT}}+\dot{C}_{\mathrm{w,LPT}}$ is the cost rate associated with the total turbine power output from the HP and LP turbines.

It could be seen that Eq. (8.52) has the same form as Eq. (8.23). Following the same analysis as for the hybrid simple Rankine cycle system, the difference between the LEC-s of the hybrid Rankine cycle system with reheat and of the single heat source Rankine cycle system with reheat that doesn't have the additional heat source is the same as Eq. (8.51).

Using the same method used in Section 8.2.1, the difference between the LEC-s of the hybrid Rankine cycle system with reheat and of the single heat source Rankine cycle system with reheat that doesn't have the additional heat source is also expressed by Eq. (8.51).

8.2.3. Hybrid power generation systems based on the Rankine cycle with heat regeneration

For the hybrid power generation systems based on the Rankine cycle with heat regeneration shown in Fig. 4-17 and Fig. 4-18. The summation of the cost balance equation for each component and applying the auxiliary equations gives

$$\begin{aligned}\dot{C}_{\mathrm{w,T}}-\dot{C}_{\mathrm{w,BFP}}-\dot{C}_{\mathrm{w,CEP}}&=\dot{C}_{\mathrm{f}}-\left(\dot{C}_{15}-\dot{C}_{14}\right)+\dot{Z}_{\mathrm{BFP}}\\&+\dot{Z}_{\mathrm{HPF}}+\dot{Z}_{\mathrm{B}}+\dot{Z}_{\mathrm{T}}+\dot{Z}_{\mathrm{COND}}+\dot{Z}_{\mathrm{CEP}}+\dot{Z}_{\mathrm{LPFH}}+\dot{Z}_{\mathrm{D}}.\end{aligned}\tag{8.53}$$

Using the assumptions made in section 8.2, Eq. (8.53) could be rewritten as

$$\begin{aligned}c_{\mathrm{P},0}\dot{W}_{\mathrm{net},0}&=c_{\mathrm{f}}\dot{m}_{\mathrm{f}}b_{\mathrm{f}}\left(1+c'_{\mathrm{fg}}+c'_{\mathrm{ash}}+c'_{\mathrm{ct}}\right)-\Delta\dot{C}_{\mathrm{cw}}\\&+\dot{Z}_{\mathrm{CEP}}+\dot{Z}_{\mathrm{HE}}+\dot{Z}_{\mathrm{B}}+\dot{Z}_{\mathrm{T}}+\dot{Z}_{\mathrm{C}}+\dot{Z}_{\mathrm{AHSC}}+\dot{Z}_{\mathrm{AHSP}},\end{aligned}\tag{8.54}$$

in which $\dot{W}_{\mathrm{net},0}=\dot{W}_{\mathrm{T}}-\dot{W}_{\mathrm{BFP}}-\dot{W}_{\mathrm{CEP}}$ is the net power output of the reference system.

Similarly, the equation for the first hybrid system when HP feedwater heater is replaced by AHS is

$$\begin{aligned}c_{\mathrm{P},1}\dot{W}_{\mathrm{net},1}&=c'_{\mathrm{f}}\dot{m}_{\mathrm{f},1}b_{\mathrm{f}}+\dot{C}_{\mathrm{AHS},1}-\Delta\dot{C}_{\mathrm{cw},1}+\dot{Z}_{\mathrm{AHSC},1}+\dot{Z}_{\mathrm{AHSP},1}\\&+\dot{Z}_{\mathrm{BFP},1}+\dot{Z}_{\mathrm{LPF},1}+\dot{Z}_{\mathrm{B},1}+\dot{Z}_{\mathrm{T},1}+\dot{Z}_{\mathrm{COND},1}+\dot{Z}_{\mathrm{CEP},1}+\dot{Z}_{\mathrm{D},1},\end{aligned}\tag{8.55}$$

in which the subscript 1 stands for the hybrid system when HP feedwater heater is replaced by AHS and $\dot{W}_{\text{net},1} = \dot{W}_{\text{T},1} - \dot{W}_{\text{BFP},1} - \dot{W}_{\text{CEP},1} - \dot{W}_{\text{AHSP},1}$ is the net power output of the first hybrid system.

Also, the equation for the second hybrid system when LP feedwater heater is replaced by AHS is

$$\begin{aligned} c_{\text{P},2}\dot{W}_{\text{net},2} &= c'_{\text{f}}\dot{m}_{\text{f},2}b_{\text{f}} + \dot{C}_{\text{AHS},2} - \Delta\dot{C}_{\text{cw},2} + \dot{Z}_{\text{AHSC},2} + \dot{Z}_{\text{AHSP},2} \\ &+ \dot{Z}_{\text{BFP},2} + \dot{Z}_{\text{HPF},2} + \dot{Z}_{\text{B},2} + \dot{Z}_{\text{T},2} + \dot{Z}_{\text{COND},2} + \dot{Z}_{\text{CEP},2} + \dot{Z}_{\text{D},2}, \end{aligned} \tag{8.56}$$

in which the subscript 2 stands for the hybrid system when LP feedwater heater is replaced by AHS and $\dot{W}_{\text{net},2} = \dot{W}_{\text{T},2} - \dot{W}_{\text{BFP},2} - \dot{W}_{\text{CEP},2} - \dot{W}_{\text{AHSP},2}$ is the net power output of the second hybrid system.

Since the working fluid conditions at boiler inlet and outlet is kept the same for all of the three systems,

$$\dot{m}_{\text{f}} = \dot{m}_{\text{f},1} = \dot{m}_{\text{f},2}, \tag{8.57}$$

$$\dot{Z}_{\text{B}} = \dot{Z}_{\text{B},1} = \dot{Z}_{\text{B},2}. \tag{8.58}$$

According to [3], the cost of turbine varies with mass flow rate, temperature of inlet flow, pressures of inlet and outlet flow and turbine efficiency, so in all three system, the turbine cost are the same, i.e.

$$\dot{Z}_{\mathrm{T}} = \dot{Z}_{\mathrm{T},1} = \dot{Z}_{\mathrm{T},2}, \tag{8.59}$$

the cost of feed water pump is

$$Z_{\mathrm{FWP}} = 32 \times 0.000435 \times M^{0.55} \Delta P^{0.55} \left(\frac{\eta_{\mathrm{p}}}{1-\eta_{\mathrm{p}}} \right)^{1.05}, \tag{8.60}$$

in which M [kg/s] is the mass flow rate of pump feedwater, ΔP [kPa] is the pressure increases of the flow and η_{p} is the adiabatic efficiency of the pump.

Since the pump cost is small compared with turbine cost and the change in pump cost also small compared with turbine cost, it could be assumed that

$$\dot{Z}_{\mathrm{BFP}} = \dot{Z}_{\mathrm{BFP},1} = \dot{Z}_{\mathrm{BFP},2} \tag{8.61}$$

$$\dot{Z}_{\mathrm{CEP}} = \dot{Z}_{\mathrm{CEP},1} = \dot{Z}_{\mathrm{CEP},2} \tag{8.62}$$

$$\dot{W}_{\mathrm{net},1} - \dot{W}_{\mathrm{net},0} = \dot{W}_{\mathrm{T},1} - \dot{W}_{\mathrm{T},0} \tag{8.63}$$

$$\dot{W}_{\mathrm{net},2} - \dot{W}_{\mathrm{net},0} = \dot{W}_{\mathrm{T},2} - \dot{W}_{\mathrm{T},0}. \tag{8.64}$$

For the deaerator, according to [9], the cost of deaerator is proportional to the mass flow rate of feed water of the deaerator. For all of three systems, the mass flow rate of feed water

of the deaerator is the same as the total mass flow rate of working fluid $\dot{m}_{\mathrm{w}}$ entering the boiler, which is kept constant, so

$$\dot{Z}_{\mathrm{D},1} = \dot{Z}_{\mathrm{D},2} = \dot{Z}_{\mathrm{D}}. \tag{8.65}$$

The difference between Eq. (8.54) and (8.55) is thus

$$\begin{aligned} &c_{\mathrm{P},1}\dot{W}_{\mathrm{net},1} - c_{\mathrm{P},0}\dot{W}_{\mathrm{net},0} = \dot{C}_{\mathrm{AHS},1} + \dot{Z}_{\mathrm{AHS},1} \\ &-\left(\Delta\dot{C}_{\mathrm{cw},1} - \Delta\dot{C}_{\mathrm{cw}}\right) + \left(\dot{Z}_{\mathrm{COND},1} - \dot{Z}_{\mathrm{COND}}\right) + \left(\dot{Z}_{\mathrm{HE},1} - \dot{Z}_{\mathrm{HPF}}\right), \end{aligned} \tag{8.66}$$

in which $\dot{Z}_{\mathrm{AHS},1} = \dot{Z}_{\mathrm{AHSC},1} + \dot{Z}_{\mathrm{AHSP},1}$ is the cost rate of equipment associated with the AHS for the hybrid system when HP feedwater heater is replaced by the AHS.

Similarly, The difference between Eq. (8.54) and (8.55) is thus

$$\begin{aligned} &c_{\mathrm{P},2}\dot{W}_{\mathrm{net},2} - c_{\mathrm{P},0}\dot{W}_{\mathrm{net},0} = \dot{C}_{\mathrm{AHS},2} + \dot{Z}_{\mathrm{AHS},2} \\ &-\left(\Delta\dot{C}_{\mathrm{cw},2} - \Delta\dot{C}_{\mathrm{cw}}\right) + \left(\dot{Z}_{\mathrm{COND},2} - \dot{Z}_{\mathrm{COND}}\right) + \left(\dot{Z}_{\mathrm{HE},2} - \dot{Z}_{\mathrm{LPF}}\right), \end{aligned} \tag{8.67}$$

in which $\dot{Z}_{\mathrm{AHS},2} = \dot{Z}_{\mathrm{AHSC},2} + \dot{Z}_{\mathrm{AHSP},2}$ is the cost rate of equipment associated with the AHS for the hybrid system when LP feedwater heater is replaced by the AHS.

Since the price of cooling water is the same for all systems and the inlet and outlet conditions of cooling water is also kept the same, the cost of cooling water is proportional to the heat duty of the condenser $\dot{Q}_{\mathrm{COND}}$, i.e.

$$\frac{\Delta\dot{C}_{\text{cw}}}{\dot{Q}_{\text{COND}}}=\frac{c_{\text{cw}}\dot{m}_{\text{cw}}\left(b_{14}-b_{15}\right)}{\dot{Q}_{\text{COND}}}=\text{constant},\tag{8.68}$$

in which c_{cw} [\$/kJ] is the price of cooling water, $\dot{m}_{\text{cw}}$ [kg/s] is the mass flow rate of cooling water, b_{14} [kJ/kg] and b_{15} [kJ/kg] is the specific exergy of inlet and outlet cooling water, respectively. Thus,

$$\frac{\Delta\dot{C}_{\text{cw},1}-\Delta\dot{C}_{\text{cw}}}{\Delta\dot{C}_{\text{cw}}}=\frac{\dot{Q}_{\text{COND},1}-\dot{Q}_{\text{COND}}}{\dot{Q}_{\text{CONDSS}}},\tag{8.69}$$

$$\frac{\Delta\dot{C}_{\text{cw},2}-\Delta\dot{C}_{\text{cw}}}{\Delta\dot{C}_{\text{cw}}}=\frac{\dot{Q}_{\text{COND},2}-\dot{Q}_{\text{COND}}}{\dot{Q}_{\text{COND}}},\tag{8.70}$$

in which the heat transfer rate in condenser in each system is, respectively,

$$\begin{aligned}\dot{Q}_{\text{COND}}&=\dot{m}_{\text{w}}\left(1-y'-y''-y'''\right)\left(h_8-h_9\right)+\dot{m}_{\text{w}}y'''\left(h_{13}-h_9\right)\\&=\dot{m}_{\text{w}}\left[\left(1-y'-y''\right)\left(h_8-h_9\right)-y'''\left(h_8-h_{13}\right)\right],\end{aligned}\tag{8.71}$$

$$\begin{aligned}\dot{Q}_{\text{COND},1}&=\dot{m}_{\text{w}}\left(1-y_1''-y_1'''\right)\left(h_8-h_9\right)+\dot{m}_{\text{w}}y_1'''\left(h_{13}-h_9\right)\\&=\dot{m}_{\text{w}}\left[\left(1-y_1''\right)\left(h_8-h_9\right)-y_1'''\left(h_8-h_{13}\right)\right],\end{aligned}\tag{8.72}$$

$$\dot{Q}_{\text{COND},2}=\dot{m}_{\text{w}}\left(1-y_2'-y_2''\right)\left(h_8-h_9\right),\tag{8.73}$$

and

$$\begin{aligned}
&\dot{Q}_{\mathrm{COND},1}-\dot{Q}_{\mathrm{COND}}=\dot{m}_{\mathrm{w}}\left[\left(-y_1''+y'+y''\right)\left(h_8-h_9\right)-\left(y_1'''-y'''\right)\left(h_8-h_{13}\right)\right]\\
&=\dot{m}_{\mathrm{w}}\frac{h_3-h_2}{h_5-h_{12}}\frac{h_6-h_{12}}{h_6-h_{11}}\left[\left(h_8-h_9\right)-\frac{h_8-h_{13}}{h_7-h_{13}}\left(h_{11}-h_{10}\right)\right]\\
&=\dot{m}_{\mathrm{w}}y'\frac{h_6-h_{12}}{h_6-h_{11}}\left[\left(h_8-h_9\right)-\frac{h_8-h_{13}}{h_7-h_{13}}\left(h_{11}-h_{10}\right)\right]\\
&<\dot{m}_{\mathrm{w}}y'\left(h_8-h_9\right),
\end{aligned}\tag{8.74}$$

$$\begin{aligned}
&\dot{Q}_{\mathrm{COND},2}-\dot{Q}_{\mathrm{COND}}=\dot{m}_{\mathrm{w}}\left[\left(-y_2'-y_2''+y'+y''\right)\left(h_8-h_9\right)+y'''\left(h_8-h_{13}\right)\right]\\
&=\dot{m}_{\mathrm{w}}y'''\left(h_8-h_{13}\right)<\dot{m}_{\mathrm{w}}y'''\left(h_8-h_9\right).
\end{aligned}\tag{8.75}$$

According to [23], the cost rate of condenser Z_{C} is proportional to the mass flow rate of working fluid through the hot side of the condenser, so

$$\frac{\dot{Z}_{\mathrm{COND},1}-\dot{Z}_{\mathrm{COND}}}{\dot{Z}_{\mathrm{COND}}}=\frac{\dot{m}_{9,1}-\dot{m}_9}{\dot{m}_9}=\frac{\left(1-y_1''\right)-\left(1-y'-y''\right)}{1-y'-y''}=y'\frac{h_6-h_{12}}{h_6-h_{11}},\tag{8.76}$$

$$\frac{\dot{Z}_{\mathrm{COND},2}-\dot{Z}_{\mathrm{COND}}}{\dot{Z}_{\mathrm{COND}}}=\frac{\dot{m}_{9,2}-\dot{m}_9}{\dot{m}_9}=\frac{\left(1-y_2'-y_2''\right)-\left(1-y'-y''\right)}{1-y'-y''}=0.\tag{8.77}$$

Feedwater heater and the heat exchanger used to preheat the working fluid by AHS could be assumed to be of the same type, e.g. shell and tube type heat exchanger. Since the mass flow rate of working fluid on the cold side is the same before and after replacing the feedwater heater with AHS, the cost of feedwater heater could be assumed to be equal to

that of the heat exchanger after the replacement, if the inlet and outlet condition of the hot side of the heat exchanger is designed to be the same as before the replacement. Thus,

$$\dot{Z}_{\mathrm{HE},1} = \dot{Z}_{\mathrm{HPF}}, \tag{8.78}$$

$$\dot{Z}_{\mathrm{HE},2} = \dot{Z}_{\mathrm{LPF}}. \tag{8.79}$$

Substitution of Eq. (8.76)-(8.79) into Eq. (8.66) and (8.67) gives

$$c_{\mathrm{P},1}\dot{W}_{\mathrm{net},1} - c_{\mathrm{P},0}\dot{W}_{\mathrm{net},0} = \dot{C}_{\mathrm{AHS},1} + \dot{Z}_{\mathrm{AHS},1} - \frac{\Delta\dot{C}_{\mathrm{cw}}}{\dot{Q}_{\mathrm{C}}}\left(\dot{Q}_{\mathrm{COND},1} - \dot{Q}_{\mathrm{COND}}\right) + y'\frac{h_6 - h_{12}}{h_6 - h_{11}}\dot{Z}_{\mathrm{COND}}, \tag{8.80}$$

$$c_{\mathrm{P},2}\dot{W}_{\mathrm{net},2} - c_{\mathrm{P},0}\dot{W}_{\mathrm{net},0} = \dot{C}_{\mathrm{AHS},2} + \dot{Z}_{\mathrm{AHS},2} - \frac{\Delta\dot{C}_{\mathrm{cw}}}{\dot{Q}_{\mathrm{COND}}}\left(\dot{Q}_{\mathrm{COND},2} - \dot{Q}_{\mathrm{COND}}\right). \tag{8.81}$$

In fact, it could be seen from Eq. (8.74) and (8.75) that

$$\dot{Q}_{\mathrm{COND},1} - \dot{Q}_{\mathrm{COND}} < \dot{m}_{\mathrm{w}} y'\left(h_8 - h_9\right), \tag{8.82}$$

$$\dot{Q}_{\mathrm{COND},2} - \dot{Q}_{\mathrm{COND}} < \dot{m}_{\mathrm{w}} y'''\left(h_8 - h_9\right). \tag{8.83}$$

Using Eq. (8.71) together with Eq. (8.82) and (8.83) and considering that the extraction fractions is usually small (about 5% [10]) compared to 1, it could be assumed that the cost of condenser is the same for all three systems, i.e.

$$\dot{Q}_{\mathrm{COND}} = \dot{Q}_{\mathrm{COND},1} = \dot{Q}_{\mathrm{COND},2}. \tag{8.84}$$

The third term in Eq. (8.80) and (8.81) can thus be neglected.

Next for the power output. Since extraction stream is saved from preheating working fluid, more work could be done in the turbine when the extraction stream flows through the turbine after replacing the feedwater heater by the AHS. The additional work done by the extraction stream in the turbine is expressed by

$$\begin{aligned}
\Delta\dot{W}_{\mathrm{net},1} &= \dot{W}_{\mathrm{net},1} - \dot{W}_{\mathrm{net},0}, \\
&= \dot{m}_{\mathrm{w}}\left[y'\left(h_5 - h_8\right) + \left(y'' - y_1''\right)\left(h_6 - h_8\right) + \left(y''' - y_1'''\right)\left(h_7 - h_8\right)\right] \\
&= \dot{m}_{\mathrm{w}} y'\left[\left(h_5 - h_8\right) - \frac{h_{12} - h_{11}}{h_6 - h_{11}}\left(h_6 - h_8\right) - \frac{h_{11} - h_{10}}{h_7 - h_{13}}\frac{h_6 - h_{12}}{h_6 - h_{11}}\left(h_7 - h_8\right)\right]
\end{aligned} \tag{8.85}$$

$$\begin{aligned}
\Delta\dot{W}_{\mathrm{net},2} &= \dot{W}_{\mathrm{net},2} - \dot{W}_{\mathrm{net},0} \\
&= \dot{m}_{\mathrm{w}}\left[\left(y' - y_2'\right)\left(h_5 - h_8\right) + \left(y'' - y_2''\right)\left(h_6 - h_8\right) + y'''\left(h_7 - h_8\right)\right] \\
&= \dot{m}_{\mathrm{w}} y'''\left(h_7 - h_8\right).
\end{aligned} \tag{8.86}$$

Using Eq. (4.104) and (4.113), change of net power output is related to the heat addition rate from the AHS to the working fluid, as

$$\Delta\dot{W}_{\text{net},1} = \frac{\dot{Q}_{\text{ADD},1}}{h_3 - h_2} y' \left[\left(h_5 - h_8\right) - \frac{h_{12} - h_{11}}{h_6 - h_{11}} \left(h_6 - h_8\right) - \frac{h_{11} - h_{10}}{h_7 - h_{13}} \frac{h_6 - h_{12}}{h_6 - h_{11}} \left(h_7 - h_8\right) \right]$$
$$= \frac{\dot{Q}_{\text{ADD},1}}{h_5 - h_{12}} \left[\left(h_5 - h_8\right) - \frac{h_{12} - h_{11}}{h_6 - h_{11}} \left(h_6 - h_8\right) - \frac{h_{11} - h_{10}}{h_7 - h_{13}} \frac{h_6 - h_{12}}{h_6 - h_{11}} \left(h_7 - h_8\right) \right],$$

(8.87)

$$\Delta\dot{W}_{\text{net},2} = \frac{\dot{Q}_{\text{ADD},2}}{\left(1 - y_2' - y_2''\right)\left(h_{11} - h_{10}\right)} y''' \left(h_7 - h_8\right) = \frac{\dot{Q}_{\text{ADD},2}}{h_7 - h_{13}} \left(h_7 - h_8\right). \quad (8.88)$$

Subtract $c_{\text{P},0}\Delta\dot{W}_{\text{net},1}$ on both sides of Eq. (8.80),

$$c_{\text{P},1} - c_{\text{P},0} = \frac{\dot{C}_{\text{AHS},1} + \dot{Z}_{\text{AHS},1} - \frac{\Delta\dot{C}_{\text{cw}}}{\dot{Q}_{\text{COND}}} \left(\dot{Q}_{\text{COND},1} - \dot{Q}_{\text{COND}}\right) + y' \frac{h_6 - h_{12}}{h_6 - h_{11}} \dot{Z}_{\text{COND}} - c_{\text{P},0}\Delta\dot{W}_{\text{net},1}}{\dot{W}_{\text{net},1}}.$$

(8.89)

Subtract $c_{\text{P},0}\Delta\dot{W}_{\text{net},2}$ on both sides of Eq. (8.81),

$$c_{\text{P},2} - c_{\text{P},0} = \frac{\dot{C}_{\text{AHS},2} + \dot{Z}_{\text{AHS},2} - \frac{\Delta\dot{C}_{\text{cw}}}{\dot{Q}_{\text{COND}}} \left(\dot{Q}_{\text{COND},2} - \dot{Q}_{\text{COND}}\right) - c_{\text{P},0}\Delta\dot{W}_{\text{net},2}}{\dot{W}_{\text{net},2}}, \quad (8.90)$$

in which $\Delta\dot{W}_{\text{net},1}$ and $\Delta\dot{W}_{\text{net},2}$ is shown in Eq. (8.87) and (8.88), respectively.

From Eq. (8.89) and (8.90), it could be seen that $c_{\mathrm{P},i} < c_{\mathrm{P},0}$ for $i = 1, 2$, if and only if

$$\dot{C}_{\mathrm{AHS},i} + \dot{Z}_{\mathrm{AHS},i} - \frac{\Delta \dot{C}_{\mathrm{cw}}}{\dot{Q}_{\mathrm{COND}}}\left(\dot{Q}_{\mathrm{COND,i}} - \dot{Q}_{\mathrm{COND}}\right) + i \cdot y' \frac{h_6 - h_{12}}{h_6 - h_{11}} \dot{Z}_{\mathrm{COND}} < c_{\mathrm{P},0} \Delta \dot{W}_{\mathrm{net},i}$$

(8.91)

or

$$\frac{\dot{C}_{\mathrm{AHS},i} + \dot{Z}_{\mathrm{AHS},i} - \frac{\Delta \dot{C}_{\mathrm{cw}}}{\dot{Q}_{\mathrm{COND}}}\left(\dot{Q}_{\mathrm{COND,i}} - \dot{Q}_{\mathrm{COND}}\right) + i \cdot y' \frac{h_6 - h_{12}}{h_6 - h_{11}} \dot{Z}_{\mathrm{COND}}}{\Delta \dot{W}_{\mathrm{net},i}} < c_{\mathrm{P},0}. \quad (8.92)$$

The numerator of the left hand side of (8.92) stands for the increase of the cost of the system by replacing the feedwater heater with the AHS. The inequality (8.92) thus means that the LEC of the such a hybrid system is lower than that of the single heat source reference system if and only if the ratio between the additional cost for replacing the feedwater heater (either HP or LP feedwater heater) by an AHS, and the additional net power output, is smaller than the LEC of the reference system. For example, when the cost rate increase due to replacing the feedwater heater with AHS is 5 \$/s, the additional power output is 100 MW, and the LEC of the reference system is 0.02 \$/kWh, or 0.056 \$/MJ, the LEC of the hybrid system will be lower that of the reference system, or the hybrid system is better than the reference system in terms of LEC, since 5/100 = 0.05 < 0.056.

8.2.4. Analysis of the LEC differences between the hybrid and the reference power generation Rankine-based systems

The above-derived formulations of the differences between the LEC-s of the Rankine-based hybrid and the reference power generation systems allow the drawing of additional generalized useful conclusions about these systems.

8.2.4.1. *Generalization of the differences between the LEC-s of the Rankine-based hybrid and the reference power generation systems*

It can be seen that Eqs (8.51), (8.89) and (8.90) have similar form. When fuel is saved by adding an additional heat source in the above shown system configurations like Fig. 4-2 and Fig. 4-11, they can be generalized as

$$\Delta c_{\mathrm{P}} = c_{\mathrm{P}} - c_{\mathrm{P},0} = \frac{\left(-c'_{\mathrm{f}} \frac{\psi_{\mathrm{f}}}{\eta_{\mathrm{B}}} + c_{\mathrm{q,AHS}} \frac{\psi_{\mathrm{AHS}}}{\eta_{\mathrm{AHS}}} \right) \dot{Q}_{\mathrm{ADD}} + \dot{Z}_{\mathrm{AHS}} + \Delta \dot{Z}_0}{\dot{W}_{\mathrm{net},0}}. \qquad (8.93)$$

When the power output increases by adding a heat source, such as when the additional heat source is used to replace feedwater heaters in the above shown system configurations like Fig. 4-17 and Fig. 4-18, the equations can be generalized as

$$\Delta c_{\mathrm{P}} = c_{\mathrm{P}} - c_{\mathrm{P},0} = \frac{c_{\mathrm{q,AHS}} \frac{\psi_{\mathrm{AHS}}}{\eta_{\mathrm{AHS}}} \dot{Q}_{\mathrm{ADD}} + \dot{Z}_{\mathrm{AHS}} + \Delta \dot{Z}_0 - c_{\mathrm{P},0} \Delta \dot{W}_{\mathrm{net}}}{\dot{W}_{\mathrm{net},0}}. \qquad (8.94)$$

In Eqs (8.93) and (8.94), $\dot{Z}_{\mathrm{AHS}}$ represents the cost rate associated with the components used to collect the additional heat source (such as solar collectors if there is a solar input) and their accessories (such as the associated circulation pump). The term $c_{\mathrm{q,AHS}} \dfrac{\psi_{\mathrm{AHS}}}{\eta_{\mathrm{AHS}}} \dot{Q}_{\mathrm{ADD}}$ represents the cost of the additional heat source itself, such as the cost to buy waste heat from other plants, but is zero if the heat source itself is free, such as for solar power or geothermal power. These two terms are present in both equations and their sum represents the total cost of using the additional heat source, including the cost of the source and the cost of the hardware. $\Delta \dot{Z}_0$ is the change of cost of the components that both the hybrid and the reference system have and represents the effect of introducing an additional heat source on the cost change of the original component. As previously analyzed for each system, it is small (if not zero) compared to the cost of the components in the reference system which uses only one heat source and maybe neglected. The term $-c'_{\mathrm{f}} \dfrac{\psi_{\mathrm{f}}}{\eta_{\mathrm{B}}} \dot{Q}_{\mathrm{ADD}}$ exists only in Eq. (8.93) and represents the cost reduction due to using less fuel in the hybrid system, including the cost to buy fuel, the externality associated with the flue gas and ash (if any) that results from burning the fuel, and the carbon tax that is imposed on the carbon dioxide emission from burning the fuel, as shown in Eq. (8.33).

$-c_{\mathrm{P},0} \Delta \dot{W}_{\mathrm{net}}$ exists only in Eq. (8.94) and represents the saving of cost by generating more power when introducing the additional heat source.

8.2.4.2. *Comparison of the Rankine-based hybrid to the reference power generation systems*

When fuel is saved by the hybridization (introducing the additional heat source), Eq. (8.93) shows that the LEC of the hybrid system is smaller than that of the reference system, if and only if[5]

$$\left(-c_{\mathrm{f}}'\frac{\psi_{\mathrm{f}}}{\eta_{\mathrm{B}}}+c_{\mathrm{q,AHS}}\frac{\psi_{\mathrm{AHS}}}{\eta_{\mathrm{AHS}}}\right)\dot{Q}_{\mathrm{ADD}}+\dot{Z}_{\mathrm{AHS}}+\Delta\dot{Z}_0<0 \tag{8.95}$$

or

$$c_{\mathrm{f}}'>\frac{\eta_{\mathrm{B}}}{\psi_{\mathrm{f}}}\left(c_{\mathrm{q,AHS}}\frac{\psi_{\mathrm{AHS}}}{\eta_{\mathrm{AHS}}}\dot{Q}_{\mathrm{ADD}}+\dot{Z}_{\mathrm{AHS}}+\Delta\dot{Z}_0\right). \tag{8.96}$$

This result provides the quantitative expression of the fact that once the type of the fuel and the reference system have been chosen, the hybrid system will have economic advantage over the reference system, if and only if the cost associated with fuel is larger than the increase of system cost incurred by adding the additional heat source. It could be achieved when fuel price, c_{f}, or carbon tax/penalty imposed on carbon emission of the power plant, c_{ct}, are high enough. This corresponds the fact that the hybrid systems may have economic competitiveness over conventional single heat source system because of

[5] Under the constrains of Eqs (8.49) and (8.50), and applies to all other such statements.

the potential for saving depletable fuel and reducing emissions (including of greenhouse gases) by hybrid power systems using renewable heat sources or other heat sources that generate no emissions, both features having important economic impact when considering the rise of fuel price and carbon tax (or other monetary penalty for CO_2 emissions). Although the values or range of c_{fg} or c_{ash} cannot be estimated without the actual operation parameters of the power generation system, typical values of c_{fg} have been calculated by some researchers (not for the Rankine cycle analyzed in this chapter). For example, c_{fg} is 17.84 €/GJ, or 22.06 $/GJ, for a novel zero-emission process generating hydrogen and electric power [11] and is 17.23 $/GJ for a trigeneration system [12].

Equation (8.96) shows that hybrid system's economic advantage over the conventional single heat source (non-hybrid) power generation system rises with the fuel price c_f and/or the carbon tax/penalty c_{ct}, and/or the drop of the cost of buying the heat source, $c_{q,AHS}$, to collect the additional heat source $\dot{Z}_{AHS}$, and the cost change of the components in the reference system $\Delta\dot{Z}_0$.

According to Eq. (8.94), when additional power is generated by the saving of the extraction streams in the regenerative Rankine cycle system by introducing the additional heat source, the LEC of the hybrid system is smaller than that of the reference system, if and only if

$$c_{\mathrm{q,AHS}}\frac{\psi_{\mathrm{AHS}}}{\eta_{\mathrm{AHS}}}\dot{Q}_{\mathrm{ADD}}+\dot{Z}_{\mathrm{AHS}}+\Delta\dot{Z}_0-c_{\mathrm{P},0}\Delta\dot{W}_{\mathrm{net}}<0 \tag{8.97}$$

or

$$\frac{c_{\mathrm{q,AHS}}\frac{\psi_{\mathrm{AHS}}}{\eta_{\mathrm{AHS}}}\dot{Q}_{\mathrm{ADD}}+\dot{Z}_{\mathrm{AHS}}+\Delta\dot{Z}_0}{\Delta\dot{W}_{\mathrm{net}}}=c_{\mathrm{P,AHS}}<c_{\mathrm{P},0}, \tag{8.98}$$

where $c_{\mathrm{P,AHS}}$ is "the incremental power generation cost". The numerator of the term at the left hand of inequality (8.98) stands for the increase of system cost by adding the AHS, and the denominator stands for the increase of power output by adding the AHS.

Inequality (8.98) thus means that the LEC of the hybrid system is lower than that of the reference system, if and only if $c_{\mathrm{P,AHS}}$ is smaller than the LEC of the reference system $c_{\mathrm{P},0}$. As a special case when solar power is used as the additional heat source, the cost of the heat source itself is 0, i.e. $c_{\mathrm{q,AHS}}=0$. If the additional heat source is added directly to the reference system, $\Delta\dot{Z}_0$ can also be regarded as 0, since the component cost are the same for the hybrid and the reference system. In this situation, inequality (8.98) is in fact the "solar LEC" [13] which is a widely used parameter in assessing the performance of solar or solar hybrid power plants, defined as the incremental cost divided by incremental power output. This means that the LEC of the solar hybrid system is lower than that of the reference system, if and only if the "solar LEC" is smaller than the LEC of the reference

system. This provides an easy way to compare the LEC of solar hybrid system with the reference system without calculating the actual LEC of the solar hybrid system.

The effect of carbon tax/penalty and externalities on the comparison of the LEC of the hybrid and the reference system is shown implicitly in the term $c_{\mathrm{P},0}$ as higher carbon tax/penalty and externalities will make it larger.

8.2.4.3. *Sensitivity analysis of the LEC-s differences between the Rankine-based hybrid and the reference power generation systems, to the temperature of the additional heat source*

Since the cost of the additional heat source often increases with its delivery temperature, the difference between the LEC of the Rankine-based hybrid and the reference power generation systems changes with the temperature of the additional heat source.

If the temperature of the additional heat source is higher by ΔT_{HE} [K] than the temperature of the working fluid heated by it, where the subscript HE refers to the heat exchanger that is used to transfer the heat from the additional heat source to the working fluid. ΔT_{HE} is typically about several dozen K. When a heat source is used to heat the working fluid directly, without the use of a heat exchanger, $\Delta T_{\mathrm{HE}} = 0$. According to Fig. 4-2,

$$T_3 + \Delta T_{\mathrm{HE}} = T_8 = T_{\mathrm{AHS}}, \tag{8.99}$$

in which the temperature of the additional heat source T_{AHS} is assumed to be the temperature of stream 8.

Using the definition of specific heat capacity at constant pressure

$$c_p = \left(\frac{\partial h}{\partial T} \right)_P , \tag{8.100}$$

and expressing $\dot{Q}_{\text{ADD}}$ by

$$\dot{Q}_{\text{ADD}} = \dot{m}_{\text{w}} \left(h_3 - h_2 \right), \tag{8.101}$$

The partial derivative of the heat addition rate to the working fluid from the additional heat source with respect to the temperature of the additional heat source is

$$\frac{\partial \dot{Q}_{\text{ADD}}}{\partial T_{\text{AHS}}} = \frac{\partial \left[\dot{m}_{\text{w}} \left(h_3 - h_2 \right) \right]}{\partial T_3} \cdot \frac{T_3}{T_{\text{AHS}}} = \dot{m}_{\text{w}} \frac{\partial h_3}{\partial T_3} \cdot \frac{T_{\text{AHS}} + \Delta T_{\text{HE}}}{T_{\text{AHS}}} = \dot{m}_{\text{w}} c_{p,3}, \tag{8.102}$$

in which $\dot{m}_{\text{w}}$ [kg/s] is the mass flow rate of working heated by the additional heat source and $c_{p,3}$ [kJ/kg-K] is the specific heat capacity at constant pressure of the working fluid at T_3.

The partial derivative of the difference between the LEC-s between the Rankine-based hybrid and reference power generation systems with respect to the temperature of the additional heat source is, based on Eqs (8.93) and (8.94),

$$\frac{\partial \Delta c_{\mathrm{P}}}{\partial T_{\mathrm{AHS}}} = \frac{-c_{\mathrm{f}}' \frac{\psi_{\mathrm{f}}}{\eta_{\mathrm{B}}} \dot{m}_{\mathrm{w}} c_{p,3} + \frac{\partial \dot{C}_{\mathrm{q,AHS}}}{\partial T_{\mathrm{AHS}}} + \frac{\partial \dot{Z}_{\mathrm{AHS}}}{\partial T_{\mathrm{AHS}}} + \frac{\partial \Delta \dot{Z}_0}{\partial T_{\mathrm{AHS}}}}{\dot{W}_{\mathrm{net},0}}, \tag{8.103}$$

$$\frac{\partial \Delta c_{\mathrm{P}}}{\partial T_{\mathrm{AHS}}} = \frac{-c_{\mathrm{P},0} \frac{\partial \Delta \dot{W}_{\mathrm{net}}}{\partial T_{\mathrm{AHS}}} + \frac{\partial \dot{C}_{\mathrm{q,AHS}}}{\partial T_{\mathrm{AHS}}} + \frac{\partial \dot{Z}_{\mathrm{AHS}}}{\partial T_{\mathrm{AHS}}} + \frac{\partial \Delta \dot{Z}_0}{\partial T_{\mathrm{AHS}}}}{\dot{W}_{\mathrm{net},0}}. \tag{8.104}$$

Typically, the cost of the AHS and the device for collecting the heat increases with the heat temperature, so

$$\frac{\partial \dot{C}_{\mathrm{q,AHS}}}{\partial T_{\mathrm{AHS}}} > 0, \tag{8.105}$$

$$\frac{\partial \dot{Z}_{\mathrm{AHS}}}{\partial T_{\mathrm{AHS}}} > 0. \tag{8.106}$$

As stated before in Section 8.2.4.2, if the additional heat source is added directly to the reference system, $\Delta \dot{Z}_0$ can be regarded as 0, since the component cost are the same for the hybrid and the reference system. The last term in the numerator of Eq. (8.104) can thus be dropped in this situation.

8.2.4.4. *Calculation example*

The previous sections deal with the thermodynamic analysis of hybrid power generation systems based on the Rankine cycle. In this section, the results from the thermodynamic

analysis are tested with numbers, using hybrid power generation systems based on the simple Rankine cycle as an example.

The assumptions are listed below:

1) The fuel used in the system is methane. The exergy factor of methane is $\psi_{\mathrm{f}} = 1.04$ and the specific exergy of methane is $b_{\mathrm{f}} = 51.975$ MJ/kg [14];
2) The specific cost of fuel (fuel cost) is $c_{\mathrm{f}} = 2.416 \times 10^{-6}$ \$/kJ-energy (New York, 7/13/2016) [15];
3) No ash is in the system since the fuel is methane, rather than solid fuel, such as coal;
4) The specific cost of flue gas is 0, i.e. $c_{\mathrm{fg}} = 0$, as suggested in [2] when the flue gas is emitted directly to the environment without further use;
5) The boiler efficiency is $\eta_{\mathrm{B}} = 0.855$ when the temperature of the flue gas is assumed to be 120 °C [16];
6) The mass flow rate of fuel of the reference system is $\dot{m}_{\mathrm{f},0} = 16.77$ kg/s and the power output is $\dot{W}_{\mathrm{net},0} = 315$ MW [17];
7) The power output of the hybrid system is the same as the reference one, i.e. $\dot{W}_{\mathrm{net}} = \dot{W}_{\mathrm{net},0} = 315$ MW;
8) The total cost rate of the components of the reference system is $\dot{Z}_0 = 6.101$ \$/s [18];

9) The cost rate of equipment collecting the additional heat source (solar) without thermal storage is $2.29\ \$/\mathrm{s}$ with temperature at the outlet of solar collector at 666.5 °C and a capacity of $\dot{Q}_{\mathrm{ADD}} = 51\ \mathrm{MW}$ [19];

10) 3 hours of thermal storage is used, resulting in 19.2% more than the AHS equipment cost without thermal storage [20];

11) The specific cost of the AHS (solar) is $c_{\mathrm{q,AHS}} = 0$ and the cost to collector it is included in $\dot{Z}_{\mathrm{AHS}}$;

12) The change of the cost rate of common components of the reference and the hybrid system is $\Delta\dot{Z}_0 = 0$;

13) The carbon tax rate imposed on carbon emissions is $c_{\mathrm{CO_2}} = 0$.

The mass flow rate of fuel of the hybrid system is calculated using Eq. (8.37) as

$$\dot{m}_{\mathrm{f}} = \left(1 - \frac{51}{16.77 \times 51.975 / 1.04 \times 0.855}\right) \times 16.77 = 15.576\ \mathrm{kg/s}. \quad (8.107)$$

Using the exergo-economic analysis method, the difference between the LEC of the hybrid and the reference system is, according to Eqs (8.51) and (8.33),

$$\Delta c_{\mathrm{P}} = \frac{\left\{\left(-c_{\mathrm{f}}\left(1+c'_{\mathrm{fg}}+c'_{\mathrm{ash}}+c'_{\mathrm{ct}}\right)\frac{\psi_{\mathrm{f}}}{\eta_{\mathrm{B}}}+c_{\mathrm{q,AHS}}\frac{\psi_{\mathrm{AHS}}}{\eta_{\mathrm{AHS}}}\right)\dot{Q}_{\mathrm{ADD}}+\dot{Z}_{\mathrm{AHS}}+\Delta Z_0\right\}}{\dot{W}_{\mathrm{net},0}}$$

$$= \frac{\left\{\left[-\frac{2.416\times10^{-6}}{1.04}\left(1+0+0+0\right)\frac{1.04}{0.855}+0\times\frac{\psi_{\mathrm{AHS}}}{\eta_{\mathrm{AHS}}}\right]\ 51{,}000+2.29\left(1+0.192\right)+0\right\}\$/\mathrm{s}}{315\ \mathrm{MW}}$$

$$= \frac{\left(-0.144+2.73+0\right)\$/\mathrm{s}}{315\ \mathrm{MW}} = 0.030\ \$/\mathrm{kWh}.$$

(8.108)

The first number in the numerator of Eq. (8.108), 0.144 $/s, represents the cost reduction from saving fuel by introducing the AHS, and the second number, 2.73 $/s, represents the cost of the additional equipment by introducing the AHS. The number 0 in Eq. (8.108) means the change of cost rate of the components that both the hybrid and the reference system have in common, as assumed previously. It can be seen from Eq. (8.108) that the cost saved from using less fuel is small (about 5%) compared to the addition equipment cost from the AHS.

Comparatively, using the energo-economic analysis method as in Eq. (8.4), the difference between the LEC of the hybrid and the reference system is

$$\Delta c_{\mathrm{P}} = \frac{\left[2.416\times10^{-6}\times\frac{51{,}975}{1.04}\times15.576+2.29\left(1+0.192\right)+6.101+0\right]\ \$/\mathrm{s}}{315\ \mathrm{MW}} - \frac{\left(2.416\times10^{-6}\times\frac{51{,}975}{1.04}\times16.77+6.101\right)\ \$/\mathrm{s}}{315\ \mathrm{MW}} = 0.030\ \$/\mathrm{kWh}.$$

(8.109)

It can be seen that the results from Eqs (8.108) and (8.109) are the same, meaning that the two economic methods give the same results and the exergo-economic analysis method was thus validated.

Using the above assumptions, it can be seen that the LEC of the hybrid system is higher that of the reference one, since $\Delta c_{\mathrm{P}} > 0$, under the used assumptions, and it is of interest to determine the assumptions/conditions values under which the LEC of the hybrid system becomes lower than that of the reference system ($\Delta c_{\mathrm{P}} < 0$). As seen from Eq. (8.51), some obvious conditions for that are an increase of the price of fuel. From Eq. (8.108),

$$\Delta c_{\mathrm{P}} = \frac{\left\{\left[-c_{\mathrm{f}}\left(1+c'_{\mathrm{fg}}+c'_{\mathrm{ash}}+c'_{\mathrm{ct}}\right)\frac{\psi_{\mathrm{f}}}{\eta_{\mathrm{B}}}+c_{\mathrm{q,AHS}}\frac{\psi_{\mathrm{AHS}}}{\eta_{\mathrm{AHS}}}\right]\dot{Q}_{\mathrm{ADD}}+\dot{Z}_{\mathrm{AHS}}+\Delta Z_0\right\}}{\dot{W}_{\mathrm{net,0}}}$$
$$= \frac{\left\{\left[-\frac{c_{\mathrm{f}}}{1.04}\left(1+0+0+0\right)\frac{1.04}{0.855}+0\times\frac{\psi_{\mathrm{AHS}}}{\eta_{\mathrm{AHS}}}\right]\ 51{,}000+2.29\left(1+0.192\right)+0\right\}\$/\mathrm{s}}{315\ \mathrm{MW}}$$
$$= \frac{\left(-59{,}649c_{\mathrm{f}}+2.73+0\right)\$/\mathrm{s}}{315\ \mathrm{MW}} < 0,$$

(8.110)

when $c_{\mathrm{f}} < 4.58\times10^{-5}$ \$/kJ-energy, meaning that $\Delta c_{\mathrm{P}} < 0$ when the price of fuel is higher than 4.58×10^{-5} \$/kJ-energy, which is 19-fold of the current level. Price that low is unlikely, at least in the near future, so other methods have to be done to make the hybrid systems economically competitive.

The previous calculations do not consider the effect of carbon tax rate, c_{ct}, on Δc_{P}, by assuming $c_{\mathrm{ct}} = 0$ in Eq. (8.33). Another way to make the hybrid systems have economic advantage over the reference ones (i.e. $\Delta c_{\mathrm{P}} < 0$) is imposing carbon tax ($c_{\mathrm{ct}} > 0$). Higher c_{ct} (thus higher c'_{ct} based on Eq. (8.30)) will make the term $c_{\mathrm{f}}\left(1+c'_{\mathrm{fg}}+c'_{\mathrm{ash}}+c'_{\mathrm{ct}}\right)$ in Eq. (8.108) larger and thus resulting in a smaller Δc_{P}, which is desired for the hybrid system. From Eq. (8.108) but without assuming $c_{\mathrm{ct}} = 0$,

$$\begin{aligned}\Delta c_{\mathrm{P}} &= \frac{\left\{\left[-c_{\mathrm{f}}\left(1+c'_{\mathrm{fg}}+c'_{\mathrm{ash}}+c'_{\mathrm{ct}}\right)\frac{\psi_{\mathrm{f}}}{\eta_{\mathrm{B}}}+c_{\mathrm{q,AHS}}\frac{\psi_{\mathrm{AHS}}}{\eta_{\mathrm{AHS}}}\right]\dot{Q}_{\mathrm{ADD}}+\dot{Z}_{\mathrm{AHS}}+\Delta Z_0\right\}}{\dot{W}_{\mathrm{net,0}}} \\ &= \frac{\left\{\left[-\frac{2.416\times10^{-6}}{1.04}\left(1+0+0+c'_{\mathrm{ct}}\right)\frac{1.04}{0.855}+0\times\frac{\psi_{\mathrm{AHS}}}{\eta_{\mathrm{AHS}}}\right]51{,}000+2.29\left(1+0.192\right)+0\right\}\text{\$/s}}{315\text{ MW}} \\ &= \frac{\left[-0.144\left(1+c'_{\mathrm{ct}}\right)+2.73+0\right]\text{\$/s}}{315\text{ MW}} < 0,\end{aligned} \tag{8.111}$$

when $c'_{\mathrm{ct}} > 17.96$.

For methane, $\frac{\dot{m}_{CO_2}}{\dot{m}_f} = \frac{44}{16} = 2.75$. Using Eq. (8.30), it can thus be found that $\Delta c_P < 0$ when

$$\frac{\dot{C}_{ct}}{\dot{C}_f} = \frac{c_{CO_2}\dot{m}_{CO_2}}{c_f \dot{m}_f b_f} = \frac{c_{CO_2}}{\frac{2.416\times10^{-6}}{1.04}\times 51{,}975} \times 2.75 = c'_{ct} > 18.96, \qquad (8.112)$$

or $c_{ct} > 0.79$ \$/kg$_{CO_2}$. This value is also too high to be feasible. For example, British Columbia is imposing a carbon tax rate of 0.03 \$/kg$_{CO_2}$ in 2012, which increases 0.005 \$/kg$_{CO_2}$ annually since 2008 [21], and this means that carbon tax rate has to increase 26-fold to the current value.

Reducing the AHS cost will also make the hybrid systems economic advantageous over the reference ones. From Eq. (8.108),

$$\begin{aligned}
\Delta c_P &= \frac{\left\{\left[-c_f\left(1+c'_{fg}+c'_{ash}+c'_{ct}\right)\frac{\psi_f}{\eta_B} + c_{q,AHS}\frac{\psi_{AHS}}{\eta_{AHS}}\right]\dot{Q}_{ADD} + \dot{Z}_{AHS} + \Delta Z_0\right\}}{\dot{W}_{net,0}} \\
&= \frac{\left\{\left[-\frac{2.416\times10^{-6}}{1.04}(1+0+0+0)\frac{1.04}{0.855} + 0\times\frac{\psi_{AHS}}{\eta_{AHS}}\right] 51{,}000 + \dot{Z}_{AHS} + 0\right\}\text{\$/s}}{315\text{ MW}} \\
&= \frac{\left[-0.144 + \dot{Z}_{AHS} + 0\right]\text{\$/s}}{315\text{ MW}} < 0,
\end{aligned} \qquad (8.113)$$

when $\dot{Z}_{\mathrm{AHS}} > 0.144$ \$/s, meaning that $\Delta c_{\mathrm{P}} < 0$ when the total cost rate of the AHS equipment is less than 0.144 \$/s, which is 5.3% of the current level. This seems to be hard to achieve unless there is breakthrough in technology.

Although each possibility introduced above seems hard to achieve, a combination of those factors may probably work. For example, the hybrid system is economically competitive to the reference system ($\Delta c_{\mathrm{P}} = 0$) if the fuel price quadruples the current level and the cost of the AHS equipment is cut to 27.5% of current level, with a carbon tax rate 10-fold of the value that is already imposed in British Columbia. The results are summarized in Table 8-2.

Table 8-2. Summary of the calculation example results

	Values	Notes
LEC difference between the hybrid and the reference system Δc_{P}		

	0.030 $/kWh	Exergo-economic analysis method using Eq. (8.37)
	0.030 $/kWh	Energo-economic analysis method using Eq. (8.4)

Conditions under which $\Delta c_P < 0$		
	$c_f > 4.58 \times 10^{-5}$ $/kJ-energy	Fuel price, at least 19-fold higher than the current level
	$c_{ct} > 0.79$ $/kg$_{CO_2}$	Carbon tax rate, at least 26-fold of the current level in British Columbia
	$\dot{Z}_{AHS} < 0.144$ $/s	Cost of the AHS equipment, at least 5.3% of the assumed value

One feasible way to have $\Delta c_{\mathrm{P}} = 0$	$c_{\mathrm{f}} = 9.664 \times 10^{-6}$ \$/kJ-energy (Quadruple of the current level) $c_{\mathrm{ct}} = 0.3$ \$/kg$_{\mathrm{CO_2}}$ (10-fold of the current value in British Columbia) $\dot{Z}_{\mathrm{AHS}} = 0.37$ \$/s (27.5% of the assumed value)

In theory, the Δc_{P} calculated based on the assumptions used above can be larger in other circumstance, such as with lower net power output of the system $\dot{W}_{\mathrm{net,0}}$, as can be seen from Eq. (8.51). The reason why a smaller power output is not chosen is because there wasn't a system studied in the publications that uses natural gas as fuel in steam power plant with lower power output. Another way to increase Δc_{P} is to increase the heat input from the AHS $\dot{Q}_{\mathrm{ADD}}$ (the cost of the AHS equipment $\dot{Z}_{\mathrm{AHS}}$ will also increase). Since the relation between $\dot{Q}_{\mathrm{ADD}}$ and $\dot{Z}_{\mathrm{AHS}}$ cannot be determined, however, existing data from previous publications by other researchers have to be used rather arbitrarily assumed. In summary, $\Delta c_{\mathrm{P}} = 0.030$ \$/kWh is the maximum value of Δc_{P} from the known data in the literature. It can be higher theoretically, such as with a lower output $\dot{W}_{\mathrm{net,0}}$ or higher AHS heat input $\dot{Q}_{\mathrm{ADD}}$ (and higher cost of the AHS equipment $\dot{Z}_{\mathrm{AHS}}$). Also, as can be seen from Eq. (8.51), the difficulty to get a negative Δc_{P} doesn't depend on the power output,

since the power output only appear in the denominator of Eq. (8.51) and doesn't affect the sign of Δc_{P}. It may not be difficult to get a negative Δc_{P} using other assumptions from the publications, such as when the cost rate of equipment collecting the additional heat source (solar) without thermal storage is $0.15\ \$/\mathrm{s}$ with temperature at the outlet of solar collector at 130.42 °C and a capacity of $\dot{Q}_{\mathrm{ADD}} = 57\ \mathrm{MW}$ [22], resulting a Δc_{P} at nearly 0.

8.3. Hybrid power generation systems based on the Brayton cycle

Economics of hybridization of Brayton cycle systems is analyzed below, starting with their simplest configuration, and followed by more advanced ones.

8.3.1. Hybrid power generation systems based on the simple Brayton cycle

The flow diagram of the considered hybrid gas turbine system based on simple Brayton cycle is shown in Fig. 5-1.

The summation of the cost balance equation for each component and applying the auxiliary equations gives

$$\dot{C}_{\mathrm{w,T}} - \dot{C}_{\mathrm{w,COMP}} = \dot{C}_1 + \dot{C}_{\mathrm{f}} + \dot{C}_{\mathrm{q,AHS}} - \dot{C}_5 + \dot{Z}_{\mathrm{COMP}} + \dot{Z}_{\mathrm{AHS}} + \dot{Z}_{\mathrm{CC}} + \dot{Z}_{\mathrm{T}}. \quad (8.114)$$

Again, assuming the cost of electricity generated and consumed are the same, i.e.

$$c_{\mathrm{w,COMP}} = c_{\mathrm{w,T}} = c_{\mathrm{P}}, \tag{8.115}$$

and since the cost of inlet air is zero, i.e.

$$\dot{C}_1 = 0, \tag{8.116}$$

Eq. (8.114) could be rewritten as

$$c_{\mathrm{P}}\dot{W}_{\mathrm{net}} = \dot{C}_{\mathrm{f}} + \dot{C}_{\mathrm{q,AHS}} - \dot{C}_5 + \dot{Z}_{\mathrm{COMP}} + \dot{Z}_{\mathrm{AHS}} + \dot{Z}_{\mathrm{CC}} + \dot{Z}_{\mathrm{T}}, \tag{8.117}$$

in which $\dot{W}_{\mathrm{net}} = \dot{W}_{\mathrm{T}} - \dot{W}_{\mathrm{COMP}}$ is the net power output of the hybrid system.

Similarly, for the reference gas turbine system without AHS,

$$c_{\mathrm{P},0}\dot{W}_{\mathrm{net},0} = \dot{C}_{\mathrm{f},0} - \dot{C}_{5,0} + \dot{Z}_{\mathrm{COMP},0} + \dot{Z}_{\mathrm{CC},0} + \dot{Z}_{\mathrm{T},0}, \tag{8.118}$$

in which the subscript 0 stands for conventional gas turbine system without AHS and $\dot{W}_{\mathrm{net},0} = \dot{W}_{\mathrm{T},0} - \dot{W}_{\mathrm{COMP},0}$ is the net power output of the reference system.

Since gas turbine is usually built as a whole from the factory and its component (compressor, combustor and turbine) is highly integrated with each other, it could be assumed that the gas turbine used in the hybrid and reference system is the same, i.e.

$$\dot{Z}_{\mathrm{COMP}} + \dot{Z}_{\mathrm{CC}} + \dot{Z}_{\mathrm{T}} = \dot{Z}_{\mathrm{COMP},0} + \dot{Z}_{\mathrm{CC},0} + \dot{Z}_{\mathrm{T},0}. \tag{8.119}$$

Subtraction of Eq. (8.118) from Eq. (8.117) gives

$$c_{\mathrm{P}}\dot{W}_{\mathrm{net}} - c_{\mathrm{P},0}\dot{W}_{\mathrm{net},0} = \left(\dot{\mathrm{C}}_{\mathrm{f}} - \dot{\mathrm{C}}_{\mathrm{f},0}\right) - \left(\dot{\mathrm{C}}_{5} - \dot{\mathrm{C}}_{5,0}\right) + \dot{\mathrm{C}}_{\mathrm{q,AHS}} + \dot{\mathrm{Z}}_{\mathrm{AHS}}. \qquad (8.120)$$

The second term on the right hand side of Eq. (8.120) is the change of externality of the system when the flue gas (stream 5 in Fig. 5-1) is not used in other place

$$\dot{C}_{\mathrm{fg}} - \dot{C}_{\mathrm{fg},0} = \dot{C}_{5} - \dot{C}_{5,0} = c_{5}\dot{m}_{5}b_{5} - c_{5,0}\dot{m}_{5,0}b_{\mathrm{f},0} = \dot{m}_{\mathrm{a}}\left[c_{5}b_{5}\left(1+f\right) - c_{5,0}b_{\mathrm{f},0}\left(1+f_{0}\right)\right]. \qquad (8.121)$$

The first term on the right hand side of Eq. (8.120) is

$$\dot{\mathrm{C}}_{\mathrm{f}} - \dot{\mathrm{C}}_{\mathrm{f},0} = c_{\mathrm{f}}''\dot{m}_{\mathrm{f}}b_{\mathrm{f}} - c_{\mathrm{f}}''\dot{m}_{\mathrm{f},0}b_{\mathrm{f}} = c_{\mathrm{f}}''b_{\mathrm{f}}\left(\dot{m}_{\mathrm{f}} - \dot{m}_{\mathrm{f},0}\right), \qquad (8.122)$$

in which c_{f}'' is the specific cost associated with fuel including fuel price and carbon tax but excluding externalities

$$c_{\mathrm{f}}'' = c_{\mathrm{f}}\left(1 + c_{\mathrm{ct}}'\right), \qquad (8.123)$$

in which c_{ct}' is defined in Eq. (8.30).

According to mass and energy balance in the control volume enclosing the combustor for the hybrid and the reference system, respectively,

$$\eta_{\mathrm{CC}}\dot{m}_{\mathrm{f}}\mathrm{LHV} + \dot{m}_{\mathrm{f}}h_{7} + \dot{m}_{\mathrm{a}}h_{3} = \left(\dot{m}_{\mathrm{a}} + \dot{m}_{\mathrm{f}}\right)h_{4}, \qquad (8.124)$$

$$\eta_{\mathrm{CC}}\dot{m}_{\mathrm{f},0}\mathrm{LHV} + \dot{m}_{\mathrm{f},0}h_{7} + \dot{m}_{\mathrm{a}}h_{2} = \left(\dot{m}_{\mathrm{a}} + \dot{m}_{\mathrm{f},0}\right)h_{4}, \qquad (8.125)$$

in which η_{CC} is the energy efficiency of the combustor defined as the ratio between fuel energy input and enthalpy increase of working fluid.

From Eq. (8.124) and (8.125),

$$\dot{m}_{\mathrm{f}} - \dot{m}_{\mathrm{f},0} = \frac{\dot{m}_{\mathrm{a}}\left(h_4 - h_3\right)}{\eta_{\mathrm{CC}}\mathrm{LHV} + h_{\mathrm{f}} - h_{\mathrm{TI}}} - \frac{\dot{m}_{\mathrm{a}}\left(h_4 - h_2\right)}{\eta_{\mathrm{CC}}\mathrm{LHV} + h_{\mathrm{f}} - h_{\mathrm{TI}}} = \frac{-\dot{m}_{\mathrm{a}}\left(h_3 - h_2\right)}{\eta_{\mathrm{CC}}\mathrm{LHV} + h_{\mathrm{f}} - h_{\mathrm{TI}}},$$

(8.126)

in which $h_{\mathrm{f}} = h_7$ [kJ/kg] is the specific enthalpy of fuel at combustor inlet and $h_{\mathrm{TI}} = h_4$ [kJ/kg] is the specific enthalpy of combustor gas at turbine inlet.

Also, according to mass and energy balance in the control volume enclosing AHS component in Fig. 5-1,

$$\eta_{\mathrm{AHS}}\dot{Q}_{\mathrm{AHS}} = \dot{Q}_{\mathrm{ADD}} = \dot{m}_{\mathrm{a}}\left(h_3 - h_2\right). \tag{8.127}$$

Substitution of Eq. (8.127) into Eq. (8.126) gives

$$\dot{m}_{\mathrm{f}} - \dot{m}_{\mathrm{f},0} = \frac{-\dot{Q}_{\mathrm{ADD}}}{\eta_{\mathrm{CC}}\mathrm{LHV} + h_{\mathrm{f}} - h_{\mathrm{TI}}}. \tag{8.128}$$

Substitution of Eq. (8.128) into Eq. (8.122) gives

$$\dot{\mathrm{C}}_{\mathrm{f}} - \dot{\mathrm{C}}_{\mathrm{f},0} = c_{\mathrm{f}}'' b_{\mathrm{f}} \frac{-\dot{Q}_{\mathrm{ADD}}}{\eta_{\mathrm{CC}}\mathrm{LHV} + h_{\mathrm{f}} - h_{\mathrm{TI}}}. \tag{8.129}$$

Since the mass flow rate of fuel is small compared to that of air in gas turbine (fuel-air ratio about 2%), the change of turbine power output due to change of mass flow rate of fuel is small compared to the turbine power output of the reference system. Considering that the compressor power input is roughly the same in the hybrid and reference systems because they operate with the same working parameters (inlet air flow rate, temperature, pressure, pressure ratio and isentropic efficiency), it could be assumed that their net power output is also the same, i.e.

$$\dot{W}_{\text{net}} = \dot{W}_{\text{net},0}. \tag{8.130}$$

Substitution of Eqs (8.43), (8.46), (8.47), (8.129) and (8.130) gives

$$\Delta c_{\text{P}} = c_{\text{P}} - c_{\text{P},0} = \frac{c_{\text{f}}'' \text{e}_{\text{f}} \dfrac{-\dot{Q}_{\text{ADD}}}{\eta_{\text{CC}} \text{LHV} + h_{\text{f}} - h_{\text{TI}}} + \dot{C}_{\text{q,AHS}} + \dot{Z}_{\text{AHS}} - \left(\dot{C}_{\text{fg}} - \dot{C}_{\text{fg},0}\right)}{\dot{W}_{\text{net},0}}$$

$$= \frac{\left(-c_{\text{f}}'' \dfrac{1}{\dfrac{\eta_{\text{CC}}}{\psi_{\text{f}}} - \dfrac{h_{\text{TI}} - h_{\text{f}}}{b_{\text{f}}}} + \dfrac{\psi_{\text{AHS}}}{\eta_{\text{AHS}}} c_{\text{q,AHS}} \right) \dot{Q}_{\text{ADD}} + \dot{Z}_{\text{AHS}} - \left(\dot{C}_{\text{fg}} - \dot{C}_{\text{fg},0}\right)}{\dot{W}_{\text{net},0}}. \tag{8.131}$$

The term $\dfrac{h_{\text{TI}} - h_{\text{f}}}{b_{\text{f}}}$ represents the fact that the fuel is mixed with the air in Brayton cycle system, while is not in Rankine cycle system. The term $\left(\dot{C}_{\text{fg}} - \dot{C}_{\text{fg},0}\right)$ accounts for the fact

that flue gas is emitted at the end of the system so the cost of each component of the system have an impact on the cost of the flue gas, while in Rankine cycle system the flue gas only flows through the boiler and is proportional to the cost rate of fuel as shown in Eq. (8.27). Considering the fact that $\frac{h_{\mathrm{TI}}-h_{\mathrm{f}}}{b_{\mathrm{f}}}<<1$ (about 2%) and $\dot{C}_{\mathrm{fg}}=\dot{C}_{\mathrm{fg},0}=0$ if externality is not included in the calculation of cost of electricity and the flue gas is not used elsewhere, Eq. (8.132) has a similar form as Eq. (8.51) for hybrid simple Rankine cycle.

8.3.2. Hybrid power generation systems based on the Brayton cycle with intercooling

The flow diagram of the hybrid gas turbine power plants with intercooling is shown in Fig. 5-5. The summation of the cost balance equation for each component and applying the auxiliary equations gives

$$\begin{aligned}&\dot{C}_{\mathrm{w,T}}-\dot{C}_{\mathrm{w,LC}}-\dot{C}_{\mathrm{w,HC}}=\dot{C}_1+\dot{C}_{\mathrm{f}}+\dot{C}_{\mathrm{q,AHS}}-\dot{C}_5\\&+\dot{Z}_{\mathrm{COMP}}+\dot{Z}_{\mathrm{AHS}}+\dot{Z}_{\mathrm{CC}}+\dot{Z}_{\mathrm{T}}+\left(\dot{C}_{\mathrm{cw1}}-\dot{C}_{\mathrm{cw2}}\right),\end{aligned}\tag{8.133}$$

in which $\dot{Z}_{\mathrm{COMP}}=\dot{Z}_{\mathrm{LC}}+\dot{Z}_{\mathrm{IC}}+\dot{Z}_{\mathrm{HC}}$ is the total cost rate of LP compressor, intercooler and HP compressor.

Again, assuming the cost of electricity generated and consumed are the same and considering the cost of inlet air is zero, Eq. (8.133) could be rewritten as

$$c_{\mathrm{P}}\dot{W}_{\mathrm{net}} = \dot{C}_{\mathrm{f}} + \dot{C}_{\mathrm{q,AHS}} - \dot{C}_5 + \dot{Z}_{\mathrm{COMP}} + \dot{Z}_{\mathrm{AHS}} + \dot{Z}_{\mathrm{CC}} + \dot{Z}_{\mathrm{T}} + \left(\dot{C}_{\mathrm{cw1}} - \dot{C}_{\mathrm{cw2}}\right). \quad (8.134)$$

The term of Eq. (8.134) is the cost rate increase of cooling water used in the intercooler and is calculated by

$$\dot{C}_{\mathrm{cw1}} - \dot{C}_{\mathrm{cw2}} = c_{\mathrm{cw}}\dot{m}_{\mathrm{cw}}\left(b_{\mathrm{cw1}} - b_{\mathrm{cw2}}\right), \quad (8.135)$$

in which $c_{\mathrm{cw}} = c_{\mathrm{cw1}} = c_{\mathrm{cw2}}$ [$/kJ], according to the F rule, is the specific cost of cooling water, $\dot{m}_{\mathrm{cw}} = \dot{m}_{\mathrm{cw1}} = \dot{m}_{\mathrm{cw2}}$ [kg/s] is the mass flow rate of cooling water, b_{cw1} and b_{cw2} [kJ/kg] are, respectively, the specific exergy of inlet and outlet cooling water.

Similarly, for the reference gas turbine system without AHS,

$$c_{\mathrm{P},0}\dot{W}_{\mathrm{net},0} = \dot{C}_{\mathrm{f},0} - \dot{C}_{5,0} + \dot{Z}_{\mathrm{COMP},0} + \dot{Z}_{\mathrm{CC},0} + \dot{Z}_{\mathrm{T},0} + \left(\dot{C}_{\mathrm{cw1},0} - \dot{C}_{\mathrm{cw2},0}\right). \quad (8.136)$$

Since the inlet condition of air (stream 1 in Fig. 5-5) and the operation parameters of compressor (pressure ratio and isentropic efficiency) is the same for the hybrid and the reference system, it could be assumed that the cost rate of cooling water is the same for both systems, i.e.

$$\dot{C}_{\mathrm{cw1}} - \dot{C}_{\mathrm{cw2}} = \dot{C}_{\mathrm{cw1},0} - \dot{C}_{\mathrm{cw2},0}. \quad (8.137)$$

Subtracting Eq. (8.136) from Eq. (8.134) and considering Eq. (8.137), (8.119) and (8.130), the difference between the LEC-s between the hybrid and the reference Brayton cycle

system with intercooling has the same form as Eq. (8.131) for that of Brayton cycle system without intercooling.

8.3.3. Hybrid power generation systems based on the Brayton cycle with reheat

The flow diagram of the hybrid Brayton cycle with reheat with the additional heat source is shown in Fig. 5-7. The summation of the cost balance equation for each component and applying the auxiliary equations gives

$$\begin{aligned}\dot{C}_{\mathrm{w,T,1}}+\dot{C}_{\mathrm{w,T,2}}-\dot{C}_{\mathrm{w,COMP}}&=\dot{C}_1+\dot{C}_{\mathrm{f,1}}+\dot{C}_{\mathrm{f,2}}+\dot{C}_{\mathrm{q,AHS}}-\dot{C}_5\\&+\dot{Z}_{\mathrm{COMP}}+\dot{Z}_{\mathrm{AHS}}+\dot{Z}_{\mathrm{CC,1}}+\dot{Z}_{\mathrm{T,1}}+\dot{Z}_{\mathrm{CC,2}}+\dot{Z}_{\mathrm{T,2}}.\end{aligned} \tag{8.138}$$

Using Eq. (8.115) and (8.116), Eq. (8.138) could be rewritten as

$$c_{\mathrm{P}}\dot{W}_{\mathrm{net}}=\dot{C}_{\mathrm{f,1}}+\dot{C}_{\mathrm{f,2}}+\dot{C}_{\mathrm{q,AHS}}-\dot{C}_5+\dot{Z}_{\mathrm{COMP}}+\dot{Z}_{\mathrm{AHS}}+\dot{Z}_{\mathrm{CC,1}}+\dot{Z}_{\mathrm{T,1}}+\dot{Z}_{\mathrm{CC,2}}+\dot{Z}_{\mathrm{T,2}}. \tag{8.139}$$

Similarly, for the reference gas turbine system without AHS,

$$c_{\mathrm{P,0}}\dot{W}_{\mathrm{net,0}}=\dot{C}_{\mathrm{f,1,0}}+\dot{C}_{\mathrm{f,2,0}}-\dot{C}_{5,0}+\dot{Z}_{\mathrm{COMP,0}}+\dot{Z}_{\mathrm{CC,0,1}}+\dot{Z}_{\mathrm{T,0,1}}+\dot{Z}_{\mathrm{CC,2,0}}+\dot{Z}_{\mathrm{T,2,0}}. \tag{8.140}$$

As assumed previously, the cost of gas turbine equipment is the same for system, so

$$\dot{Z}_{\mathrm{COMP}} + \dot{Z}_{\mathrm{CC},1} + \dot{Z}_{\mathrm{T},1} + \dot{Z}_{\mathrm{CC},2} + \dot{Z}_{\mathrm{T},2} = \dot{Z}_{\mathrm{COMP},0} + \dot{Z}_{\mathrm{CC},0,1} + \dot{Z}_{\mathrm{T},0,1} + \dot{Z}_{\mathrm{CC},2,0} + \dot{Z}_{\mathrm{T},2,0}.$$

(8.141)

According to mass and energy balance in the control volume enclosing the combustor 2 for the hybrid and the reference system, respectively,

$$\eta_{\mathrm{CC}}\dot{m}_{\mathrm{f},2}\mathrm{LHV} + \dot{m}_{\mathrm{f},2}h_8 + \left(\dot{m}_{\mathrm{a}} + \dot{m}_{\mathrm{f},1}\right)h_{41} = \left(\dot{m}_{\mathrm{a}} + \dot{m}_{\mathrm{f},1} + \dot{m}_{\mathrm{f},2}\right)h_{42}, \qquad (8.142)$$

$$\eta_{\mathrm{CC}}\dot{m}_{\mathrm{f},2,0}\mathrm{LHV} + \dot{m}_{\mathrm{f},2,0}h_8 + \left(\dot{m}_{\mathrm{a}} + \dot{m}_{\mathrm{f},1,0}\right)h_{41} = \left(\dot{m}_{\mathrm{a}} + \dot{m}_{\mathrm{f},1,0} + \dot{m}_{\mathrm{f},2,0}\right)h_{42}. \qquad (8.143)$$

From Eq. (8.142) and (8.143),

$$\dot{m}_{\mathrm{f},2} - \dot{m}_{\mathrm{f},2,0} = \frac{\left(\dot{m}_{\mathrm{a}} + \dot{m}_{\mathrm{f},1}\right)\left(h_{42} - h_{41}\right)}{\eta_{\mathrm{CC}}\mathrm{LHV} + h_{\mathrm{f},2} - h_{\mathrm{TI}}} - \frac{\left(\dot{m}_{\mathrm{a}} + \dot{m}_{\mathrm{f},1,0}\right)\left(h_{42} - h_{41}\right)}{\eta_{\mathrm{CC}}\mathrm{LHV} + h_{\mathrm{f},2} - h_{\mathrm{TI}}} = \frac{\left(\dot{m}_{\mathrm{f},1} - \dot{m}_{\mathrm{f},1,0}\right)\left(h_{42} - h_{41}\right)}{\eta_{\mathrm{CC}}\mathrm{LHV} + h_{\mathrm{f},2} - h_{\mathrm{TI}}},$$

(8.144)

in which $h_{\mathrm{f},2} = h_8$ [kJ/kg] is the specific enthalpy of fuel at inlet of combustor 2 and $h_{\mathrm{TI},2} = h_{42}$ [kJ/kg] is the specific enthalpy of combustor gas at LP turbine inlet.

Thus, adding Eq. (8.144) and (8.128),

$$\left(\dot{m}_{\mathrm{f},1}-\dot{m}_{\mathrm{f},1,0}\right)+\left(\dot{m}_{\mathrm{f},2}-\dot{m}_{\mathrm{f},2,0}\right)=\frac{-\dot{Q}_{\mathrm{ADD}}}{\eta_{\mathrm{CC}}\mathrm{LHV}+h_{\mathrm{f},1}-h_{\mathrm{TI},1}}\left(1+\frac{h_{42}-h_{41}}{\eta_{\mathrm{CC}}\mathrm{LHV}+h_{\mathrm{f},2}-h_{\mathrm{TI},2}}\right).$$

(8.145)

Using Eq. (8.130), the difference between the LEC-s of the hybrid and reference system based on Brayton cycle with reheat is

$$\begin{aligned}\Delta c_{\mathrm{P}} &= c_{\mathrm{P}}-c_{\mathrm{P},0}\\ &=\frac{c_{\mathrm{f}}''b_{\mathrm{f}}\dfrac{-\dot{Q}_{\mathrm{ADD}}}{\eta_{\mathrm{CC}}\mathrm{LHV}+h_{\mathrm{f},1}-h_{\mathrm{TI},1}}\left(1+\dfrac{h_{42}-h_{41}}{\eta_{\mathrm{CC}}\mathrm{LHV}+h_{\mathrm{f},2}-h_{\mathrm{TI},2}}\right)-\left(\dot{\mathrm{C}}_5-\dot{\mathrm{C}}_{5,0}\right)+\dot{\mathrm{C}}_{\mathrm{q,AHS}}+\dot{\mathrm{Z}}_{\mathrm{AHS}}}{\dot{W}_{\mathrm{net},0}}\\ &=\frac{\left(-c_{\mathrm{f}}''\dfrac{1+\dfrac{h_{42}-h_{41}}{\eta_{\mathrm{CC}}\mathrm{LHV}+h_{\mathrm{f},2}-h_{\mathrm{TI},2}}}{\dfrac{\eta_{\mathrm{CC}}}{\psi_{\mathrm{f}}}-\dfrac{h_{\mathrm{TI}}-h_{\mathrm{f}}}{b_{\mathrm{f}}}}+\frac{\psi_{\mathrm{AHS}}}{\eta_{\mathrm{AHS}}}c_{\mathrm{q,AHS}}\right)\dot{Q}_{\mathrm{ADD}}-\left(\dot{\mathrm{C}}_5-\dot{\mathrm{C}}_{5,0}\right)+\dot{\mathrm{Z}}_{\mathrm{AHS}}}{\dot{W}_{\mathrm{net},0}}.\end{aligned}$$

(8.146)

The term $\dfrac{h_{42}-h_{41}}{\eta_{\mathrm{CC}}\mathrm{LHV}+h_{\mathrm{f},2}-h_{\mathrm{TI},2}}$ shows the effect of adding an additional combustor and using additional fuel. According to Eq. (8.142),

$$\frac{h_{42}-h_{41}}{\eta_{\mathrm{CC}}\mathrm{LHV}+h_{\mathrm{f},2}-h_{\mathrm{TI},2}}=\frac{h_{42}-h_{41}}{\eta_{\mathrm{CC}}\mathrm{LHV}+h_{8}-h_{42}}=\frac{\dot{m}_{\mathrm{f},2}}{\dot{m}_{\mathrm{a}}+\dot{m}_{\mathrm{f},2}}<<1, \qquad (8.147)$$

since the mass flow rate of fuel $\dot{m}_{f,2}$ is small compared with that of the air $\dot{m}_a$.

Using Eq. (8.147), Eq. (8.146) has the same form as Eq. (8.131).

8.3.4. Hybrid power generation systems based on the Brayton cycle with heat regeneration

The flow diagram of the hybrid Brayton cycle with heat regeneration with the additional heat source is shown in Fig. 5-9. The summation of the cost balance equation for each component and applying the auxiliary equations gives

$$\dot{C}_{w,T} - \dot{C}_{w,C} = \dot{C}_1 + \dot{C}_f + \dot{C}_{q,AHS} - \dot{C}_{51} + \dot{Z}_{COMP} + \dot{Z}_R + \dot{Z}_{AHS} + \dot{Z}_{CC} + \dot{Z}_T. \tag{8.148}$$

Again, assuming the cost of electricity generated and consumed are the same, i.e.

$$c_{w,COMP} = c_{w,T} = c_P, \tag{8.149}$$

and since the cost of inlet air is zero, i.e.

$$\dot{C}_1 = 0. \tag{8.150}$$

Using Eqs (8.115) and (8.116), Eq. (8.150) could be rewritten as

$$c_P \dot{W}_{net} = \dot{C}_f + \dot{C}_{q,AHS} - \dot{C}_{51} + \dot{Z}_{COMP} + \dot{Z}_R + \dot{Z}_{AHS} + \dot{Z}_{CC} + \dot{Z}_T. \tag{8.151}$$

Similarly, for the reference gas turbine system without AHS,

$$c_{\mathrm{P},0}\dot{W}_{\mathrm{net},0} = \dot{C}_{\mathrm{f},0} - \dot{C}_{51,0} + \dot{Z}_{\mathrm{COMP},0} + \dot{Z}_{\mathrm{R},0} + \dot{Z}_{\mathrm{CC},0} + \dot{Z}_{\mathrm{T},0}. \tag{8.152}$$

According to mass and energy balance in the control volume enclosing the combustor for the hybrid and the reference system, respectively,

$$\eta_{\mathrm{CC}}\dot{m}_{\mathrm{f}}\mathrm{LHV} + \dot{m}_{\mathrm{f}}h_7 + \dot{m}_{\mathrm{a}}h_3 = \left(\dot{m}_{\mathrm{a}} + \dot{m}_{\mathrm{f}}\right)h_4, \tag{8.153}$$

$$\eta_{\mathrm{CC}}\dot{m}_{\mathrm{f},0}\mathrm{LHV} + \dot{m}_{\mathrm{f},0}h_7 + \dot{m}_{\mathrm{a}}h_{21} = \left(\dot{m}_{\mathrm{a}} + \dot{m}_{\mathrm{f},0}\right)h_4. \tag{8.154}$$

From Eqs (8.153) and (8.154),

$$\dot{m}_{\mathrm{f}} - \dot{m}_{\mathrm{f},0} = \frac{\dot{m}_{\mathrm{a}}\left(h_4 - h_3\right)}{\eta_{\mathrm{CC}}\mathrm{LHV} + h_{\mathrm{f}} - h_{\mathrm{TI}}} - \frac{\dot{m}_{\mathrm{a}}\left(h_4 - h_{21}\right)}{\eta_{\mathrm{CC}}\mathrm{LHV} + h_{\mathrm{f}} - h_{\mathrm{TI}}} = \frac{-\dot{m}_{\mathrm{a}}\left(h_3 - h_{21}\right)}{\eta_{\mathrm{CC}}\mathrm{LHV} + h_{\mathrm{f}} - h_{\mathrm{TI}}}. \tag{8.155}$$

Also, according to mass and energy balance in the control volume enclosing AHS component in Fig. 5-7,

$$\eta_{\mathrm{AHS}}\dot{Q}_{\mathrm{AHS}} = \dot{Q}_{\mathrm{ADD}} = \dot{m}_{\mathrm{a}}\left(h_3 - h_{21}\right). \tag{8.156}$$

Substitution of Eq. (8.156) into Eq. (8.155) gives Eq. (8.128) as in hybrid simple Brayton cycle analysis in section 3.1. Using Eqs (8.129) and (8.130), the difference between the

LEC-s of the hybrid and reference system based on Brayton cycle with heat regeneration is

$$\Delta c_{\mathrm{P}} = c_{\mathrm{P}} - c_{\mathrm{P},0} = \frac{\left(-c_{\mathrm{f}}'' \dfrac{1}{\dfrac{\eta_{\mathrm{CC}}}{\psi_{\mathrm{f}}} - \dfrac{h_{\mathrm{TI}} - h_{\mathrm{f}}}{b_{\mathrm{f}}}} + \dfrac{\psi_{\mathrm{AHS}}}{\eta_{\mathrm{AHS}}} c_{\mathrm{q,AHS}} \right) \dot{Q}_{\mathrm{ADD}} + \dot{Z}_{\mathrm{AHS}} - \left(\dot{C}_{\mathrm{fg}} - \dot{C}_{\mathrm{fg},0} \right)}{\dot{W}_{\mathrm{net},0}},$$

(8.157)

whose form is similar to Eq. (8.131) except that the cost rate difference of flue gas (the last term in the numerator) is calculated at the outlet of the regenerator instead of the gas turbine.

8.3.5. Analysis of the LEC differences between the hybrid and the reference power generation Brayton-based systems

Similar as in the analysis for Rankine cycle in section 8.2.4, the difference between the LEC-s of the hybrid and the reference power generation systems based on Brayton cycle shown in Eqs (8.131), (8.146) and (8.157) could also be generalized to Eq. (8.93). The analysis is thus the same as shown in section 8.2.4.

While we made similar calculation examples for the hybrid power generation systems based on the Brayton and combined cycles, they are lengthy and not presented here because the above-detailed method for the Rankine-based hybrids is the same, and because the

detailed example is adequate for demonstrating how the resulting equations can be used in practice for these cycles too.

8.4. Hybrid power generation systems based on the combined-cycle

8.4.1. Hybrid power generation systems based on the combined cycle with the AHS added in the topping (Brayton) cycle

The flow diagram of the hybrid power generation systems based on the combined cycle with the AHS added in the topping cycle (Brayton) is shown in Fig. 6-3. The summation of the cost balance equation for each component and applying the auxiliary equations gives

$$\dot{C}_{\mathrm{w,GT}} - \dot{C}_{\mathrm{w,COMP}} + \dot{C}_{\mathrm{w,ST}} - \dot{C}_{\mathrm{w,CEP}} = \dot{C}_1 + \dot{C}_{\mathrm{f}} + \dot{C}_{\mathrm{q,AHS}} - \dot{C}_5 - \left(\dot{C}_{\mathrm{cw2}} - \dot{C}_{\mathrm{cw1}}\right) + \dot{Z}_{\mathrm{COMP}} + \dot{Z}_{\mathrm{AHS}} + \dot{Z}_{\mathrm{CC}} + \dot{Z}_{\mathrm{GT}} + \dot{Z}_{\mathrm{HRSG}} + \dot{Z}_{\mathrm{ST}} + \dot{Z}_{\mathrm{COND}} + \dot{Z}_{\mathrm{CEP}}.$$

(8.158)

Again, assuming the cost of electricity generated and consumed are the same and the cost of inlet air is zero, Eq. (8.158) could be rewritten as

$$c_{\mathrm{P}}\dot{W}_{\mathrm{net}} = \dot{C}_{\mathrm{f}} + \dot{C}_{\mathrm{q,AHS}} - \dot{C}_5 - \left(\dot{C}_{\mathrm{cw2}} - \dot{C}_{\mathrm{cw1}}\right) + \dot{Z}_{\mathrm{COMP}} + \dot{Z}_{\mathrm{AHS}} + \dot{Z}_{\mathrm{CC}} + \dot{Z}_{\mathrm{GT}} + \dot{Z}_{\mathrm{HRSG}} + \dot{Z}_{\mathrm{ST}} + \dot{Z}_{\mathrm{COND}} + \dot{Z}_{\mathrm{CEP}}, \quad (8.159)$$

in which $\dot{W}_{\text{net}} = \dot{C}_{\text{w,GT}} - \dot{C}_{\text{w,COMP}} + \dot{C}_{\text{w,ST}} - \dot{C}_{\text{w,CEP}}$ is the net power output of the hybrid system.

Similarly, for the reference gas turbine system without AHS,

$$\begin{aligned} c_{\text{P},0}\dot{W}_{\text{net},0} &= \dot{C}_{\text{f},0} - \dot{C}_{5,0} - \left(\dot{C}_{\text{cw2},0} - \dot{C}_{\text{cw1},0}\right) \\ &+ \dot{Z}_{\text{COMP},0} + \dot{Z}_{\text{CC},0} + \dot{Z}_{\text{GT},0} + \dot{Z}_{\text{HRSG},0} + \dot{Z}_{\text{ST},0} + \dot{Z}_{\text{COND},0} + \dot{Z}_{\text{CEP},0}, \end{aligned} \tag{8.160}$$

in which $\dot{W}_{\text{net},0} = \dot{C}_{\text{w,GT},0} - \dot{C}_{\text{w,COMP},0} + \dot{C}_{\text{w,ST},0} - \dot{C}_{\text{w,CEP},0}$ is the net power output of the reference system.

According the energy balance for the control volume enclosing HRSG in Fig. 6-3, for the hybrid and the reference system, respectively,

$$\left(\dot{m}_{\text{a}} + \dot{m}_{\text{f}}\right)\left(h_4 - h_5\right) = \dot{m}_{\text{bc}}\left(h_8 - h_7\right), \tag{8.161}$$

$$\left(\dot{m}_{\text{a}} + \dot{m}_{\text{f},0}\right)\left(h_4 - h_5\right) = \dot{m}_{\text{bc},0}\left(h_8 - h_7\right), \tag{8.162}$$

in which $\dot{m}_{\text{bc}} = \dot{m}_8$ [kg/s] is the mass flow rate of working fluid in the bottoming cycle.

From Eqs (8.161) and (8.162),

$$\frac{h_4 - h_5}{h_8 - h_7} = \frac{\dot{m}_{\text{bc}}}{\dot{m}_{\text{a}} + \dot{m}_{\text{f}}} = \frac{\dot{m}_{\text{bc},0}}{\dot{m}_{\text{a}} + \dot{m}_{\text{f},0}} \tag{8.163}$$

or

$$\frac{\dot{m}_{\text{bc}}}{\dot{m}_{\text{bc,0}}}=\frac{\dot{m}_{\text{a}}+\dot{m}_{\text{f}}}{\dot{m}_{\text{a}}+\dot{m}_{\text{f,0}}}=\frac{\dot{m}_{\text{a}}\left(1+f\right)}{\dot{m}_{\text{a}}\left(1+f_0\right)}=1-\frac{f_0-f}{1+f_0}. \tag{8.164}$$

Since the fuel air ratio for a conventional gas turbine is small (about 2%), so $f < f_0 << 1$ and thus

$$\frac{\dot{m}_{\text{bc}}}{\dot{m}_{\text{bc,0}}}=1-\frac{f_0-f}{1+f_0}\approx 1. \tag{8.165}$$

Therefore, the power output from the steam turbine

$$\frac{\dot{W}_{\text{ST}}}{\dot{W}_{\text{ST,0}}}=\frac{\dot{m}_{\text{bc}}\left(h_8-h_9\right)}{\dot{m}_{\text{bc,0}}\left(h_8-h_9\right)}\approx 1, \tag{8.166}$$

and the component cost at bottoming cycle

$$\dot{Z}_{\text{HRSG}}+\dot{Z}_{\text{ST}}+\dot{Z}_{\text{C}}+\dot{Z}_{\text{CEP}}\approx\dot{Z}_{\text{HRSG,0}}+\dot{Z}_{\text{ST,0}}+\dot{Z}_{\text{COND,0}}+\dot{Z}_{\text{CEP,0}}, \tag{8.167}$$

since the operation parameter (temperature and pressure) for each component at bottoming cycle is the same.

Considering Eq. (8.130), the net power output of the hybrid and the reference combined cycle power plant is roughly the same. Thus, subtracting Eqs (8.160) from (8.159) and

considering Eqs (8.119), (8.167), (8.43) and (8.129), the difference between the LEC-s of the hybrid and reference system based on the combined cycle is

$$\Delta c_{\mathrm{P}} = c_{\mathrm{P}} - c_{\mathrm{P},0} = \frac{\left(-c_{\mathrm{f}}'' \dfrac{1}{\dfrac{\eta_{\mathrm{CC}}}{\psi_{\mathrm{f}}} - \dfrac{h_{\mathrm{TI}} - h_{\mathrm{f}}}{b_{\mathrm{f}}}} + \dfrac{\psi_{\mathrm{AHS}}}{\eta_{\mathrm{AHS}}} c_{\mathrm{q,AHS}} \right) \dot{Q}_{\mathrm{ADD}} + \dot{Z}_{\mathrm{AHS}} - \left(\dot{C}_{\mathrm{fg}} - \dot{C}_{\mathrm{fg},0} \right)}{\dot{W}_{\mathrm{net},0}},$$

(8.168)

in which $\dot{C}_{\mathrm{fg}} = \dot{C}_5$ and $\dot{C}_{\mathrm{fg},0} = \dot{C}_{5,0}$ [$/s] is the cost rate of system flue gas for the hybrid and the reference system, respectively. It could be seen that Eq. (8.168) is the same as Eq. (8.131) for the hybrid simple Brayton cycle system.

8.4.2. Hybrid power generation systems based on the combined cycle with the AHS added in the bottoming cycle (Rankine) cycle

The flow diagram of the combined cycle power plant with the AHS added in the HRSG is shown in Fig. 6-6. The summation of the cost balance equation for each component and applying the auxiliary equations gives

$$\begin{aligned} &\dot{C}_{\mathrm{w,GT}} - \dot{C}_{\mathrm{w,COMP}} + \dot{C}_{\mathrm{w,ST}} - \dot{C}_{\mathrm{w,CEP}} = \dot{C}_1 + \dot{C}_{\mathrm{f}} + \dot{C}_{\mathrm{q,AHS}} - \dot{C}_5 - \Delta\dot{C}_{\mathrm{cw}} \\ &+ \dot{Z}_{\mathrm{COMP}} + \dot{Z}_{\mathrm{AHS}} + \dot{Z}_{\mathrm{CC}} + \dot{Z}_{\mathrm{GT}} + \dot{Z}_{\mathrm{HRSG}} + \dot{Z}_{\mathrm{ST}} + \dot{Z}_{\mathrm{COND}} + \dot{Z}_{\mathrm{CEP}}, \end{aligned} \tag{8.169}$$

in which $\Delta\dot{C}_{\mathrm{cw}} = \dot{C}_{\mathrm{cw2}} - \dot{C}_{\mathrm{cw1}}$ is the cost rate increase of cooling water.

Again, assuming the cost of electricity generated and consumed are the same and the cost of inlet air is zero, Eq. (8.169) could be rewritten as

$$\begin{aligned} c_{\mathrm{P}}\dot{W}_{\mathrm{net}} &= \dot{C}_{\mathrm{f}} + \dot{C}_{\mathrm{q,AHS}} - \dot{C}_{5} - \Delta\dot{C}_{\mathrm{cw}} \\ &+\dot{Z}_{\mathrm{COMP}} + \dot{Z}_{\mathrm{AHS}} + \dot{Z}_{\mathrm{CC}} + \dot{Z}_{\mathrm{GT}} + \dot{Z}_{\mathrm{HRSG}} + \dot{Z}_{\mathrm{ST}} + \dot{Z}_{\mathrm{COND}} + \dot{Z}_{\mathrm{CEP}}. \end{aligned} \tag{8.170}$$

Similarly, for the reference gas turbine system without AHS,

$$\begin{aligned} c_{\mathrm{P,0}}\dot{W}_{\mathrm{net,0}} &= \dot{C}_{\mathrm{f,0}} - \dot{C}_{\mathrm{5,0}} - \Delta\dot{C}_{\mathrm{cw,0}} \\ &+\dot{Z}_{\mathrm{COMP,0}} + \dot{Z}_{\mathrm{CC,0}} + \dot{Z}_{\mathrm{GT,0}} + \dot{Z}_{\mathrm{HRSG,0}} + \dot{Z}_{\mathrm{ST,0}} + \dot{Z}_{\mathrm{COND,0}} + \dot{Z}_{\mathrm{CEP,0}}. \end{aligned} \tag{8.171}$$

Subtracting Eq. (8.171) from Eq. (8.170),

$$\begin{aligned} &c_{\mathrm{P}}\dot{W}_{\mathrm{net}} - c_{\mathrm{P,0}}\dot{W}_{\mathrm{net,0}} = \dot{C}_{\mathrm{q,AHS}} + \dot{Z}_{\mathrm{AHS}} - \left(\Delta\dot{C}_{\mathrm{cw}} - \Delta\dot{C}_{\mathrm{cw,0}}\right) \\ &+\left(\dot{Z}_{\mathrm{HRSG}} - \dot{Z}_{\mathrm{HRSG,0}}\right) + \left(\dot{Z}_{\mathrm{ST}} - \dot{Z}_{\mathrm{ST,0}}\right) + \left(\dot{Z}_{\mathrm{COND}} - \dot{Z}_{\mathrm{COND,0}}\right) + \left(\dot{Z}_{\mathrm{CEP}} - \dot{Z}_{\mathrm{CEP,0}}\right), \end{aligned}$$

(8.172)

in which the cost of the topping cycle for the hybrid and the reference system cancels out.

According the energy balance for the control volume enclosing HRSG+AHS in Fig. 6-4, for the hybrid and the reference system, respectively,

$$\dot{m}_{\mathrm{fg}}\left(h_4 - h_5\right) + \dot{Q}_{\mathrm{LT}} = \dot{m}_{\mathrm{bc}}\left(h_8 - h_7\right) = \frac{\dot{W}_{\mathrm{ST}}}{h_8 - h_9}\left(h_8 - h_7\right) = \frac{\dot{W}_{\mathrm{CEP}}}{h_6 - h_9}\left(h_7 - h_6\right),$$

(8.173)

$$\dot{m}_{\mathrm{fg}}\left(h_4-h_5\right)=\dot{m}_{\mathrm{bc},0}\left(h_8-h_7\right)=\frac{\dot{W}_{\mathrm{ST},0}}{h_8-h_9}\left(h_8-h_7\right)=\frac{\dot{W}_{\mathrm{CEP},0}}{h_6-h_9}\left(h_7-h_6\right), \quad (8.174)$$

in which $\dot{m}_{\mathrm{fg}}=\dot{m}_5$ [kg/s] is the mass flow rate of system flue gas and is the same for the hybrid and the reference system since the topping cycle is the same for both systems.

Combining Eqs (8.173) and (8.174),

$$\dot{Q}_{\mathrm{ADD}}=\left(\dot{m}_{\mathrm{bc}}-\dot{m}_{\mathrm{bc},0}\right)\left(h_8-h_7\right), \quad (8.175)$$

$$\dot{W}_{\mathrm{ST}}-\dot{W}_{\mathrm{ST.0}}=\dot{Q}_{\mathrm{ADD}}\frac{h_8-h_9}{h_8-h_7}, \quad (8.176)$$

$$\dot{W}_{\mathrm{CEP}}-\dot{W}_{\mathrm{CEP.0}}=\dot{Q}_{\mathrm{ADD}}\frac{h_7-h_6}{h_8-h_7}. \quad (8.177)$$

Using Eqs (16) and (17), Eq. (8.172) becomes

$$\Delta c_{\mathrm{P}}=c_{\mathrm{P}}-c_{\mathrm{P},0}=\frac{\begin{array}{c}\dot{C}_{\mathrm{q,AHS}}+\dot{Z}_{\mathrm{AHS}}-\left(\Delta\dot{C}_{\mathrm{cw}}-\Delta\dot{C}_{\mathrm{cw},0}\right)+\left(\dot{Z}_{\mathrm{HRSG}}-\dot{Z}_{\mathrm{HRSG},0}\right)\\ +\left(\dot{Z}_{\mathrm{ST}}-\dot{Z}_{\mathrm{ST},0}\right)+\left(\dot{Z}_{\mathrm{COND}}-\dot{Z}_{\mathrm{COND},0}\right)+\left(\dot{Z}_{\mathrm{CEP}}-\dot{Z}_{\mathrm{CEP},0}\right)-c_{\mathrm{P},0}\Delta\dot{W}_{\mathrm{net}}\end{array}}{\dot{W}_{\mathrm{net}}},$$

(8.178)

in which $\Delta\dot{W}_{\text{net}}$ [kW] is the difference of net power output of the hybrid and the reference system

$$\Delta\dot{W}_{\text{net}} = \dot{W}_{\text{net}} - \dot{W}_{\text{net},0} = \dot{Q}_{\text{ADD}} \frac{(h_8 - h_9) - (h_7 - h_6)}{h_8 - h_7}. \tag{8.179}$$

According to the cost functions given in [23], the cost the of steam turbine is proportional to the 0.7th power of the turbine power output, the cost of pump is proportional to the 0.71th power of the pump work, and the cost of condenser is proportional to the mass flow rate of working fluid. Since the steam turbine power output is proportional to the mass flow rate of the working fluid through the turbine, the pump work is proportional to the mass flow rate of the working fluid through the pump and the mass flow rate of the working fluid through the steam turbine and through the pump is the same, using Eqs (15)-(17), the relative difference of cost rate of the steam turbine, the condensate extraction pump and the condenser between the hybrid and the reference system are summarized in Table 8-3 below.

Table 8-3. Relative difference of the component cost rate between the hybrid and the reference combined cycle system

Component k	Relative difference of cost rate of component k, $\frac{\dot{Z}_k - \dot{Z}_{k,0}}{\dot{Z}_{k,0}}$, between the hybrid and the reference system	Equation number

Steam turbine (ST)	$\frac{\dot{m}_{\mathrm{bc}}^{0.7}-\dot{m}_{\mathrm{bc},0}^{0.7}}{\dot{m}_{\mathrm{bc},0}^{0.7}}=\left(\frac{\dot{m}_{\mathrm{bc}}}{\dot{m}_{\mathrm{bc},0}}\right)^{0.7}-1=\left[1+\frac{\dot{Q}_{\mathrm{ADD}}}{\dot{m}_{\mathrm{bc},0}\left(h_8-h_7\right)}\right]^{0.7}-1$	(8.180)
Condensate extraction pump (CEP)	$\frac{\dot{m}_{\mathrm{bc}}^{0.71}-\dot{m}_{\mathrm{bc},0}^{0.71}}{\dot{m}_{\mathrm{bc},0}^{0.7}}=\left(\frac{\dot{m}_{\mathrm{bc}}}{\dot{m}_{\mathrm{bc},0}}\right)^{0.71}-1=\left[1+\frac{\dot{Q}_{\mathrm{ADD}}}{\dot{m}_{\mathrm{bc},0}\left(h_8-h_7\right)}\right]^{0.71}-1$	(8.181)
Condenser (COND)	$\frac{\dot{m}_{\mathrm{bc}}-\dot{m}_{\mathrm{bc},0}}{\dot{m}_{\mathrm{bc},0}}=\frac{\dot{Q}_{\mathrm{ADD}}}{\dot{m}_{\mathrm{bc},0}\left(h_8-h_7\right)}$	(8.182)

Also according to the cost function for HRSG [23],

$$\dot{Z}_{\mathrm{HRSG}}-\dot{Z}_{\mathrm{HRSG},0}=c'_{\mathrm{HRSG}}\left(\dot{m}_{\mathrm{bc}}-\dot{m}_{\mathrm{bc},0}\right)=c'_{\mathrm{HRSG}}\frac{\dot{Q}_{\mathrm{ADD}}}{h_8-h_7}, \tag{8.183}$$

in which c'_{HRSG} [$/kg] is a constant.

For the cost of cooling water, since the mass flow rate of cooling water is proportional to the mass flow rate of the working fluid in the condenser,

$$\frac{\Delta\dot{C}_{\mathrm{cw}}-\Delta\dot{C}_{\mathrm{cw},0}}{\Delta\dot{C}_{\mathrm{cw}}}=\frac{\dot{m}_{\mathrm{bc}}-\dot{m}_{\mathrm{bc},0}}{\dot{m}_{\mathrm{bc},0}}=\frac{\dot{Q}_{\mathrm{ADD}}}{\dot{m}_{\mathrm{bc},0}\left(h_8-h_7\right)}. \tag{8.184}$$

Substitution of Eqs (8.179)-(8.184) into Eq. (8.178) gives

$$\Delta c_{\mathrm{P}} = c_{\mathrm{P}} - c_{\mathrm{P},0} = \left[\frac{\psi_{\mathrm{AHS}}}{\eta_{\mathrm{AHS}}} c_{\mathrm{q,AHS}} + \frac{+c'_{\mathrm{HRSG}} + \dot{Z}_{\mathrm{C},0} - \Delta \dot{C}_{\mathrm{cw},0} - c_{\mathrm{P},0} \dot{m}_{\mathrm{bc},0} \left[\left(h_8 - h_9 \right) - \left(h_7 - h_6 \right) \right]}{\dot{Q}_{\mathrm{ex}}} \right] \dot{Q}_{\mathrm{ADD}} + \left\{ \left[1 + \frac{\dot{Q}_{\mathrm{ADD}}}{\dot{Q}_{\mathrm{ex}}} \right]^{0.7} - 1 \right\} \dot{Z}_{\mathrm{ST},0} + \left\{ \left[1 + \frac{\dot{Q}_{\mathrm{ADD}}}{\dot{Q}_{\mathrm{ex}}} \right]^{0.71} - 1 \right\} \dot{Z}_{\mathrm{CEP},0} + \dot{Z}_{\mathrm{AHS}} = \frac{}{\dot{W}_{\mathrm{net}}},$$

(8.185)

in which $\dot{Q}_{\mathrm{ex}} = \dot{m}_{\mathrm{bc},0} \left(h_8 - h_7 \right)$ is the heat addition rate to the bottoming cycle from gas turbine exhaust gas.

8.4.3. Hybrid power generation systems based on the combined cycle with the AHS added in both the topping and bottoming cycles

When the AHS are added in both the topping and bottoming cycles of the combined cycle power plants as shown in Fig. 6-1, the summation of the cost balance equation for each component and applying the auxiliary equations gives

$$\dot{C}_{\mathrm{w,GT}} - \dot{C}_{\mathrm{w,COMP}} + \dot{C}_{\mathrm{w,ST}} - \dot{C}_{\mathrm{w,CEP}} = \dot{C}_1 + \dot{C}_{\mathrm{f}} + \dot{C}_{\mathrm{q,AHS},1} + \dot{Z}_{\mathrm{AHS},2} - \dot{C}_5 - \left(\dot{C}_{\mathrm{cw2}} - \dot{C}_{\mathrm{cw1}} \right) + \dot{Z}_{\mathrm{COMP}} + \dot{Z}_{\mathrm{AHS},1} + \dot{Z}_{\mathrm{AHS},2} + \dot{Z}_{\mathrm{CC}} + \dot{Z}_{\mathrm{GT}} + \dot{Z}_{\mathrm{HRSG}} + \dot{Z}_{\mathrm{ST}} + \dot{Z}_{\mathrm{COND}} + \dot{Z}_{\mathrm{CEP}}.$$

(8.186)

Again, assuming the cost of electricity generated and consumed are the same and the cost of inlet air is zero, Eq. (8.158) could be rewritten as

$$\begin{aligned} c_{\mathrm{P}}\dot{W}_{\mathrm{net}} &= \dot{C}_{\mathrm{f}} + \dot{C}_{\mathrm{q,AHS,1}} + \dot{C}_{\mathrm{q,AHS,2}} - \dot{C}_{5} - \left(\dot{C}_{\mathrm{cw2}} - \dot{C}_{\mathrm{cw1}}\right) \\ &+ \dot{Z}_{\mathrm{COMP}} + \dot{Z}_{\mathrm{AHS,1}} + \dot{Z}_{\mathrm{AHS,2}} + \dot{Z}_{\mathrm{CC}} + \dot{Z}_{\mathrm{GT}} + \dot{Z}_{\mathrm{HRSG}} + \dot{Z}_{\mathrm{ST}} + \dot{Z}_{\mathrm{COND}} + \dot{Z}_{\mathrm{CEP}}, \end{aligned} \tag{8.187}$$

in which $\dot{W}_{\mathrm{net}} = \dot{C}_{\mathrm{w,GT}} - \dot{C}_{\mathrm{w,COMP}} + \dot{C}_{\mathrm{w,ST}} - \dot{C}_{\mathrm{w,CEP}}$ is the net power output of the hybrid system.

Similarly, for the reference gas turbine system without AHS,

$$\begin{aligned} c_{\mathrm{P,0}}\dot{W}_{\mathrm{net,0}} &= \dot{C}_{\mathrm{f,0}} - \dot{C}_{5,0} - \left(\dot{C}_{\mathrm{cw2,0}} - \dot{C}_{\mathrm{cw1,0}}\right) \\ &+ \dot{Z}_{\mathrm{COMP,0}} + \dot{Z}_{\mathrm{CC,0}} + \dot{Z}_{\mathrm{GT,0}} + \dot{Z}_{\mathrm{HRSG,0}} + \dot{Z}_{\mathrm{ST,0}} + \dot{Z}_{\mathrm{COND,0}} + \dot{Z}_{\mathrm{CEP,0}}, \end{aligned} \tag{8.188}$$

in which $\dot{W}_{\mathrm{net,0}} = \dot{C}_{\mathrm{w,GT,0}} - \dot{C}_{\mathrm{w,COMP,0}} + \dot{C}_{\mathrm{w,ST,0}} - \dot{C}_{\mathrm{w,CEP,0}}$ is the net power output of the reference system.

Subtracting Eq. (8.188) from Eq. (8.187) and using Eqs (8.119), (8.43) and (8.129),

$$\begin{aligned} c_{\mathrm{P}}\dot{W}_{\mathrm{net}} - c_{\mathrm{P,0}}\dot{W}_{\mathrm{net,0}} &= \left(-c_{\mathrm{f}}'' \frac{1}{\dfrac{\eta_{\mathrm{CC}}}{\psi_{\mathrm{f}}} - \dfrac{h_{\mathrm{TI}} - h_{\mathrm{f}}}{b_{\mathrm{f}}}} + \frac{\psi_{\mathrm{AHS,1}}}{\eta_{\mathrm{AHS,1}}} c_{\mathrm{q,AHS,1}} \right) \dot{Q}_{\mathrm{ADD,1}} + \dot{C}_{\mathrm{q,AHS,2}} \\ &+ \dot{Z}_{\mathrm{AHS,1}} + \dot{Z}_{\mathrm{AHS,2}} - \left(\dot{C}_{\mathrm{fg}} - \dot{C}_{\mathrm{fg,0}}\right) - \left(\Delta\dot{C}_{\mathrm{cw}} - \Delta\dot{C}_{\mathrm{cw,0}}\right) + \left(\dot{Z}_{\mathrm{HRSG}} - \dot{Z}_{\mathrm{HRSG,0}}\right) \\ &+ \left(\dot{Z}_{\mathrm{ST}} - \dot{Z}_{\mathrm{ST,0}}\right) + \left(\dot{Z}_{\mathrm{COND}} - \dot{Z}_{\mathrm{COND,0}}\right) + \left(\dot{Z}_{\mathrm{CEP}} - \dot{Z}_{\mathrm{CEP,0}}\right). \end{aligned} \tag{8.189}$$

Using Eqs (8.180)-(8.184), Eq. (8.189) could be written as

$$\begin{aligned}\Delta c_{\mathrm{P}} &= c_{\mathrm{P}} - c_{\mathrm{P},0} \\ &\left(-c_{\mathrm{f}}'' \frac{1}{\frac{\eta_{\mathrm{CC}}}{\psi_{\mathrm{f}}} - \frac{h_{\mathrm{TI}} - h_{\mathrm{f}}}{b_{\mathrm{f}}}} + \frac{\psi_{\mathrm{AHS},1}}{\eta_{\mathrm{AHS},1}} c_{\mathrm{q,AHS},1} \right) \dot{Q}_{\mathrm{ADD},1} + \dot{Z}_{\mathrm{AHS},1} - \left(\dot{C}_{\mathrm{fg}} - \dot{C}_{\mathrm{fg},0} \right) \\ &+ \left[\frac{\psi_{\mathrm{AHS},2}}{\eta_{\mathrm{AHS},2}} c_{\mathrm{q,AHS},2} + \frac{+c'_{\mathrm{HRSG}} + \dot{Z}_{\mathrm{C},0} - \Delta \dot{C}_{\mathrm{cw},0}}{\dot{Q}_{\mathrm{ex}}} \right] \dot{Q}_{\mathrm{ADD},2} - c_{\mathrm{P}} \Delta \dot{W}_{\mathrm{net}} \\ &+ \left\{ \left[1 + \frac{\dot{Q}_{\mathrm{ADD},2}}{\dot{Q}_{\mathrm{ex}}} \right]^{0.7} - 1 \right\} \dot{Z}_{\mathrm{ST},0} + \left\{ \left[1 + \frac{\dot{Q}_{\mathrm{ADD},2}}{\dot{Q}_{\mathrm{ex}}} \right]^{0.71} - 1 \right\} \dot{Z}_{\mathrm{CEP},0} + \dot{Z}_{\mathrm{AHS},2} \\ &= \frac{}{\dot{W}_{\mathrm{net},0}},\end{aligned}$$

(8.190)

in which $\Delta \dot{W}_{\mathrm{net}}$ is the net power output differences of the hybrid and the reference system and is shown in Eq. (8.180).

8.4.4. Analysis of the LEC differences between the hybrid and the reference power generation combined cycle-based systems

Similar to the analysis for Rankine cycle in section 8.2.4, the difference between the LEC-s of the combined-cycle-based hybrid and reference power generation systems expressed by Eqs (8.168) and (8.185) could also be generalized to Eqs (8.93) and (8.94), respectively in the fuel-saving mode and power-boost mode. The analysis is thus the same as shown in section 8.2.4, and so are the results. It, however, cannot be used in the power generation

systems studied in section 8.4.3, because unlike other studied systems in this chapter which have only one additional heat source, there are 2 in the system studied in section 8.4.3. One of the additional heat source (AHS1) is used to save fuel, while the other additional heat source (AHS2) is used to increase the power output of the system. This means that the system operates in both the fuel-saving mode and the power-boost mode.

As discussed in section 8.2.4, the terms associated with the fuel (fuel price, carbon tax, cost associated with cooling water and externalities of flue gas and ash) are included explicitly in the expression of Δc_{P} in the fuel-saving mode, but are included implicitly in the power-boost mode (affect the LEC of the system). As could be seen from Eq. (8.190), however, the terms associated with the fuel (fuel price, carbon tax, cost associated with cooling water and externalities of flue gas and ash) exist both explicitly and implicitly.

8.5. Comparison between the exergo-economic analysis method and the energo-economic analysis method

Using the energo-economic analysis method as Eq. (8.4), the difference between the LEC of the hybrid and the reference power generation systems is expressed by

$$\Delta c_{\mathrm{P}} = c_{\mathrm{P}} - c_{\mathrm{P},0} = \frac{\kappa \cdot C_{\mathrm{Inv}} + C_{\mathrm{O\&M}} + C_{\mathrm{f}}}{H \cdot \dot{W}_{\mathrm{net}}} - \frac{\kappa \cdot C_{\mathrm{Inv},0} + C_{\mathrm{O\&M},0} + C_{\mathrm{f},0}}{H \cdot \dot{W}_{\mathrm{net},0}}, \quad (8.191)$$

in which the subscript 0 stands for the corresponding term in the reference single heat source system (i.e. without the additional hybridizing heat source).

Using Eq. (8.6), Eq. (8.191) could be rewritten as

$$\Delta c_{\mathrm{P}} = c_{\mathrm{P}} - c_{\mathrm{P,0}} = \frac{\dot{Z}_{\mathrm{TOT}} + \dot{Z}_{\mathrm{AHS}} + \dot{C}_{\mathrm{q,AHS}} + \dot{C}_{\mathrm{f}}}{\dot{W}_{\mathrm{net}}} - \frac{\dot{Z}_{\mathrm{TOT,0}} + \dot{C}_{\mathrm{f,0}}}{\dot{W}_{\mathrm{net,0}}}, \qquad (8.192)$$

in which $\dot{Z}_{\mathrm{TOT,0}}$ [$/s] is the total cost rate of the reference system, and $\dot{Z}_{\mathrm{TOT}}$ [$/s] is the total cost rate of the hybrid system without the component cost associated with the additional heat source, $\dot{Z}_{\mathrm{AHS}}$. As defined in section 8.2.4.1,

$$\dot{Z}_{\mathrm{TOT}} - \dot{Z}_{\mathrm{TOT,0}} = \Delta \dot{Z}_0. \qquad (8.193)$$

Comparing the results from the exergo-economic analysis method and the energo-economic analysis method, it could be seen that the exergo-economic analysis method is able to show:

1) the expressions for calculating the mass flow rate change of fuel, $\dot{m}_{\mathrm{f}} - \dot{m}_{\mathrm{f,0}}$, such as Eq. (8.37), which the energo-economic analysis cannot show since it doesn't consider the thermodynamic aspect of the power generation systems, such as the flow enthalpy and temperature, and doesn't have the corresponding terms to determine it;
2) the expressions for calculating the change of the net power output from the hybrid and the single heat source reference system, $\dot{W}_{\mathrm{net}} - \dot{W}_{\mathrm{net,0}}$, such as Eq. (8.180);

3) the expressions for calculating the cost change of the components that both the hybrid and the single heat source reference system have, $\Delta \dot{Z}_0$, such as Eq. (8.40);

4) the effect of the heat transfer rate from the additional heat source to the working fluid $\dot{Q}_{\mathrm{ADD}}$ on the change of LEC between the hybrid and the reference system Δc_{P}, such as Eqs (8.51), (8.131), (8.146), (8.157), (8.168) and (8.185);

5) the conditions under which the LEC of the hybrid system is competitive with the reference system, such as Eqs (8.96) and (8.98);

6) the effects of the temperature of the heat source on the LEC difference between the hybrid and the reference system, Δc_{P}, such as by Eqs (8.103) and (8.104);

7) the expressions for calculating the externalities, such as flue gas, using system operating parameters, in Eq. (8.27), ash in Eq. (8.29) and cooling water.

Having these advantages, the exergo-economic analysis method is clearly a better tool in comparing the economic performance of hybrid system using multiple heat sources of different temperatures and the conventional single heat source system, by giving more insights of the system, compared with the energo-economic analysis method.

8.6. Summary and conclusions of the exergo-economic analysis of thermal hybrid power generation systems

Exergo-economic analysis is used to compare the levelized cost of electricity (LEC) of hybrid power generation systems using multiple heat sources of different temperature with

the corresponding conventional single heat source systems. It is shown that for the three major types of power generation cycles, i.e. Rankine cycle, Brayton cycle and combined cycle, and their variants, such as reheat and heat regeneration, the difference between the LEC-s of the hybrid and the corresponding single heat source reference system could be generalized into two equations: when the additional heat source is used to save fuel (fuel-saving mode),

$$\Delta c_{\mathrm{P}} = c_{\mathrm{P}} - c_{\mathrm{P},0} = \frac{-c'_{\mathrm{f}} \dfrac{\psi_{\mathrm{f}}}{\eta_{\mathrm{B}}} \dot{Q}_{\mathrm{ADD}} + c_{\mathrm{q,AHS}} \dfrac{\psi_{\mathrm{AHS}}}{\eta_{\mathrm{AHS}}} \dot{Q}_{\mathrm{ADD}} + \dot{Z}_{\mathrm{AHS}} + \Delta \dot{Z}_0}{\dot{W}_{\mathrm{net},0}}, \quad (8.194)$$

and when the additional heat source is used to generate more power (power-boost mode),

$$\Delta c_{\mathrm{P}} = c_{\mathrm{P}} - c_{\mathrm{P},0} = \frac{-c_{\mathrm{P},0} \Delta \dot{W}_{\mathrm{net}} + c_{\mathrm{q,AHS}} \dfrac{\psi_{\mathrm{AHS}}}{\eta_{\mathrm{AHS}}} \dot{Q}_{\mathrm{ADD}} + \dot{Z}_{\mathrm{AHS}} + \Delta \dot{Z}_0}{\dot{W}_{\mathrm{net}}}. \quad (8.195)$$

The first term in the numerator of Eq. (8.194) stands for the saving from fuel (becomes zero when no fuel is saved, the power-boost mode), while the first term in Eq. (8.195) stands for the savings from generation of additional power from adding the AHS and is zero when no additional power is generated therefrom (fuel-saving mode) The second term for both equations stands for the cost of the additional heat source, the third term for both equations stands for the cost of the components for collecting or using the heat source, and the last term in both equations stands for the additional cost of the equipment component of the reference system (zero if the component of the reference system doesn't change).

Note that Eqs (8.194) and (8.195) are derived using the assumptions that the pump work is neglected (justifiably here) and the net power outputs for both the hybrid and the reference system are the same, i.e. Eqs (8.49) and (8.50).

In the fuel-saving mode, according to Eq. (8.96) the LEC of the hybrid system is lower than that of the reference system, if and only if

$$\begin{aligned} c'_{\mathrm{f}} &= c_{\mathrm{f}}\left[1+\frac{c_{\mathrm{fg}}b_{\mathrm{fg}}}{c_{\mathrm{f}}b_{\mathrm{f}}}\left(1+\frac{1}{f}\right)+\frac{c_{\mathrm{ash}}\dot{m}_{\mathrm{ash}}b_{\mathrm{ash}}}{c_{\mathrm{f}}\dot{m}_{\mathrm{f}}b_{\mathrm{f}}}+\frac{c_{\mathrm{CO_2}}\dot{m}_{\mathrm{CO_2}}}{c_{\mathrm{f}}\dot{m}_{\mathrm{f}}b_{\mathrm{f}}}\right] \\ &> \frac{\eta_{\mathrm{B}}}{\psi_{\mathrm{f}}}\left(c_{\mathrm{q,AHS}}\frac{\psi_{\mathrm{AHS}}}{\eta_{\mathrm{AHS}}}\dot{Q}_{\mathrm{ADD}}+\dot{Z}_{\mathrm{AHS}}+\Delta\dot{Z}_0\right), \end{aligned} \tag{8.196}$$

in which c_{f} (cost per unit exergy of fuel) is the price of fuel, c_{fg} (cost per unit exergy of flue gas) is the specific cost of flue gas of the system calculated using the SPECO method, c_{ash} (cost per unit exergy of ash) is the specific cost of ash of the system calculated using the SPECO method and $c_{\mathrm{CO_2}}$ (cost per unit weight of carbon dioxide emissions) is the carbon tax or penalty on the carbon emissions of the power generation systems. Equation (8.196) shows that increases of any of these specific costs will make the hybrid system more competitive with the reference system, in terms of LEC. Among these specific costs, c_{f} and $c_{\mathrm{CO_2}}$ are determined by the market and policy, respectively, while c_{fg} and c_{ash} are calculated using the SPECO method. The cost of externalities is determined by the markets or policy.

In the power-boost mode, the specific costs of fuel, flue gas, ash and carbon penalty are not explicitly shown in the final expression of ΔC_{P} as can be seen from Eq. (8.195). They, however, implicitly affects the ΔC_{P} in the term $C_{\mathrm{P,0}}$ as higher specific cost of fuel, flue gas, ash and carbon will increase the LEC of the reference system.

While flue gas and ash are often treated as externalities that have additional or zero cost for the power generation system, they can also be regarded as its gainful products of the power generation system. For the latter, for example, warm flue gas can be sold for providing heat for chemical plants, and ash can be sold for making cement or road asphalt.

Analysis of Eq. (8.194) shows that the LEC of the hybrid system is lower than that of the reference system if the price fuel and/or carbon tax is high enough. It was also shown in Eq. (8.194) that there is an inverse relation between the fuel price, c_{f} , and the LEC difference of the hybrid and the reference systems, Δc_{p}. This means that Δc_{p} decrease when c_{f} increases, and vice versa. It further suggests that higher fuel price in the future will make the hybrid system more economically advantageous than the corresponding reference system.

It is noteworthy that the above analysis was based on the current fuel price. In fact, it also holds in future scenarios when the fuel price changes. Eqs. (8.194) and (8.195) continue to be valid. If the fuel price rises in the future, the LEC difference between the hybrid and the reference systems (Δc_{p}) will decrease when compared with the "initial" LEC difference

calculated at time 0 (present value), and vice versa. This is because although the LEC of the hybrid system increases with higher fuel price, the LEC of the fuel-only system increases more, since it uses more fuel than the hybrid system. In other words, although the *absolute* LEC of the hybrid system increases due to higher fuel price, the *relative* LEC of the hybrid system compared to the fuel-only system deceases, due to smaller impact of the fuel price on the hybrid system that uses less fuel.

This result is shown explicitly in Eq. (8.96) when the additional heat source is used to save the use of fuel (fuel-saving mode). When the additional heat source is used to generate more power (power-boost mode), the result is shown implicitly in the LEC of the reference system $c_{\mathrm{P},0}$ in Eq. (8.98), considering that fuel price and carbon tax are included in the cost rate associated with fuel $\dot{C}_{\mathrm{f},0} = c'_{\mathrm{f}} \dot{m}_{\mathrm{f},0} b_{\mathrm{f}}$ in the calculation of $c_{\mathrm{P},0}$ such as in Eq. (8.34).

Sensitivity analysis of the difference between the LEC-s of the hybrid and the reference power generation systems with respect to the temperature of the additional heat source $\frac{\partial \Delta c_{\mathrm{P}}}{\partial T_{\mathrm{AHS}}}$ is shown in Eqs (8.103) and (8.104), respectively, for the fuel-saving mode and power-boost mode. It is shown that the sign of $\frac{\partial \Delta c_{\mathrm{P}}}{\partial T_{\mathrm{AHS}}}$ could be determined if the partial

derivative of the components related with the additional heat source with respect to the temperature of the additional heat source $\frac{\partial \dot{Z}_{\mathrm{AHS}}}{\partial T_{\mathrm{AHS}}}$ is known.

8.7. Recommendations and future trends of the exergo-economic analysis of thermal hybrid power generation systems

In addition to the equations developed in this study for allowing the calculation of the exergo-economic condition that make hybrid power systems competitive with conventional (non-hybrid) ones, the results show that making hybrid systems that use multiple heat sources of different temperatures economically competitive with the corresponding fuel-only conventional power generation system, the fuel price has to be high enough. Considering the fact that the current fuel prices do not in most cases include even a small fraction of the cost of fuel externalities (such as, but not limited to, carbon tax), inclusion of these would help protect the environment and make hybrid systems more economically competitive. Some governments are already imposing carbon taxes, which will also cause systems that use less fossil fuel to become more economically competitive.

Noting that the calculation example shown in Table 8-2 is representative of only a single hybrid system case and states chosen for ease of demonstration, the conditions for the LEC of this hybrid system to be equal to that of the reference single-heat-source system are that the fuel price has to rise 19-fold, or the cost of the AHS equipment has to be reduced to

5.3% of the current value, or the carbon tax rate has to increase to 26-fold of the value that is currently imposed in British Columbia, any of which is hard to reach.

More generally, while fuel price is largely determined by the market and accounting policies for externalities such as greenhouse gas emissions, the analysis shows that a rewarding effort is to decrease the cost associated with the components that collect and use the additional heat source, such as solar collectors when solar heat is used as the additional heat source, or heat collection grid systems when waste heat is used. As technology advances, there is still much room to decrease the cost of using the additional heat source (AHS), compared with the conventional fuel-only systems that have been developed for centuries and may have less room for reducing theirs.

Forecasting rising fuel price in the long term, higher taxing of externalities, and decreasing cost for implementing additional heat sources, hybrid systems using multiple heat source of different temperatures will thus increasingly become more economically competitive when compared with the conventional systems, especially for the hybrid systems that use heat sources that reduce generation of greenhouse gases and other undesirable emissions.

References for Chapter 8

[1] Lazzaretto A., Tsatsaronis G., SPECO: A systematic and general methodology for calculating efficiencies and costs in thermal systems. Energy 2006;31:1257-1289.

[2] Bejan A, Tsatsaronis G, Moran M., Thermal design and optimization. New York, US: John Wiley and Sons, Inc.; 1996.

[3] El-Sayed Y.M., The Thermoeconomics of Energy Conversions. Oxford, UK: Elsevier Ltd; 2003.

[4] Roosen P., Uhlenbruck S., Lucas K., Pareto optimization of a combined cycle power system as a decision support tool for trading off investment vs. operating costs. Int J Therm Sci 2003;42:553-560.

[5] Yildirim U., Gungor A., An application of exergoeconomic analysis for a CHP system. Int J Elec Power 2012;42250-256.

[6] Ahmadi P., Dincer I., Thermodynamic and exergoenvironmental analyses, and multi-objective optimization of a gas turbine power plant. Appl Therm Eng 2011;31:2529-2540.

[7] Yang Y., Wang L., Dong H., Xu G., Morosuk T., Tsatsaronis G., Comprehensive exergy-based evaluation and parametric study of a coal-fired ultra-supercritical power plant. Appl Energ 2013;112:1087-1099.

[8] Kalogirou A.S., Solar thermal collectors and applications. Prog Energy Combust 2004(30):231-295.

[9] Boehm R.F., Design analysis of thermal systems (Appendix D: Preliminary cost estimation data). New York US: John Wiley & Sons;1987.

[10] Dincer I., Zamfirescu C., Advanced Power Generation Systems. New York US: Elsevier;2014.

[11] Tsatsaronis G., Kapanke K., Marigorta M.B.A., Exergoeconomic estimates for a novel zero-emission process generating hydrogen and electric power. Energy 2008(33):321-330.

[12] Temir G., Bilge D., Thermoeconomic analysis of a trigeneration system. Appl Therm Eng 2004(24):2689-2699.

[13] Dersch J., Geyer M., Herrmann U., Jones S.A., Kelly B., Kistner R., Ortmanns W., Pitz-Paal R., Price, H., Trough integration into power plants—a study on the performance and economy of integrated solar combined cycle systems. Energy 2004;29:947-959.

[14] Szargut, J., Exergy Method: Technical and Ecological Applications. WIT Press, 2005.

[15] U.S. Energy Information Administration, 2016, “Natural Gas Weekly Update”, <http://www.eia.gov/naturalgas/weekly/#tabs-prices-2>.

[16] Cleaver-Brooks Inc., Boiler efficiency guide, 2010-Available at:< www.cleaver-brooks.com/reference-center/insights/boiler-efficiency-guide.aspx > [accessed 1.7.2016].

[17] Khoshgoftar Manesh M.H., Navid P., Baghestani M., Khamis Abadi S., Rosen M.A., Blanco, A.M., Amidpour M., Exergoeconomic and exergoenvironmental evaluation of the coupling of a gas fired steam power plant with a total site utility system. Energ Convers Manage 2014;77:469-483.

[18] U.S. Energy Information Administration, 2016, “Updated Capital Cost Estimates for Utility Scale Electricity Generating Plants”, <http://www.eia.gov/outlooks/capitalcost/pdf/updated_capcost.pdf>.

[19] Baghernejadand A., Yaghoubi M., Exergoeconomic analysis and optimization of an Integrated Solar Combined Cycle System (ISCCS) using genetic algorithm. Energ Convers Manage 2011;52:2193-2203.

[20] Zhang N., Lior N., Use of Low/Mid-Temperature Solar Heat for Thermochemical Upgrading of Energy, Part I: Application to a Novel Chemically-Recuperated Gas-Turbine Power Generation (SOLRGT) System. J Eng Gas Turb Power 2012;134:072301.

[21] Carbon Tax Center (British Columbia) - Available at:<http://www.carbontax.org/where-carbon-is-taxed/british-columbia/> [accessed 28.2.2016].

[22] Martin J.R., Rodriguez E.B., Paniagua I.L., Fernandez C.G., Thermoeconomic Evaluation of Integrated Solar Combined Cycle Systems (ISCCS). Entropy 2014;16:4246-4259.

[23] Baghernejadand A., Yaghoubi M., Exergoeconomic analysis and optimization of an Integrated Solar Combined Cycle System (ISCCS) using genetic algorithm. Energ Convers Manage 2011;52:2193-2203.

CHAPTER 9

EXERGO-ECONOMIC ANALYSIS FOR THERMOCHEMICAL HYBIRD POWER GENERATION SYSTEMS

This chapter examines economic performance of two previously proposed and analyzed thermochemical hybridized power generation systems: SOLRGT that incorporates reforming of methane, and SOLRMCC that incorporates methanol decomposition, both of which using use low temperature solar heat (at ~220 °C) to help convert the methane or methanol input to syngas, which is then burned for power generation. The solar heat is used "indirectly" in the methane reforming process, to vaporize the needed water for it, while it is used directly in the methanol decomposition process since methanol decomposition requires lower temperatures than methane reforming. This analysis resulted in an equation for each power system for determining the conditions under which the hybrid system will have a lower levelized electricity cost, and how it will change as a function of the fuel price, carbon tax rate, and the cost of the collection equipment needed for the additional heat source.

9.1. Exergo-economic analysis of the SOLRGT system

The goal is to find the LEC difference between that for the hybrid system (SOLRGT) and its corresponding reference systems (IC-CRGT and IC-HSTIG) using the operational

parameters of the systems. This is done by using the previously described SPECO method in Section 8.1.2. The fuel, product and auxiliary equation for each component are first determined and then the cost function can be built for each component. Manipulation of those cost balance equations will arrive at the LEC equation for each system. Further analysis could then be made based on it, and needed conclusions could be drawn.

The fuel, product and necessary auxiliary equations for each component for applying the SPECO method are summarized in Table 9-1. The cost balance equations are constructed using Eq. (8.9) and are shown below the table. The "additional heat source" stands for solar heat in SOLRGT but can be generalized to other heat sources, such as waste or geothermal heat, so the term "additional heat source" (AHS for short) is used below.

Table 9-1. Fuel, product and auxiliary equations for each component in the SOLRGT system in Fig. 7-1

Component	Fuel	Product	Auxiliary equation	No. of streams	
				Inlet	Outlet
LP-Compressor	$\dot{C}_{\mathrm{w,LPC}}$	$\dot{C}_2 - \dot{C}_1$	-	2	1
Intercooler	$\dot{C}_{\mathrm{cw,in}} - \dot{C}_{\mathrm{cw,out}}$	$\dot{C}_3 - \dot{C}_2$	$c_{\mathrm{cw,in}} = c_{\mathrm{cw,out}}$	2	2

			(F rule)		
HP-Compressor	$\dot{C}_{w,HPC}$	$\dot{C}_4 - \dot{C}_3$	-	2	1
Recuperator	$\dot{C}_{17} - \dot{C}_{18}$	$\left(\dot{C}_5 - \dot{C}_4\right) + \left(\dot{C}_{13} - \dot{C}_{12}\right)$	$c_{18} = c_{17}$ (F rule)	3	3
Combustor	$\dot{C}_5$	$\dot{C}_{15} - \dot{C}_{14}$	-	2	1
Turbine	$\dot{C}_{15} - \dot{C}_{16}$	$\dot{C}_{w,T}$	$c_{16} = c_{15}$ (F rule)	1	2
Reformer	$\dot{C}_{16} - \dot{C}_{17}$	$\dot{C}_{14} - \dot{C}_{13}$	$c_{17} = c_{16}$ (F rule)	2	2
Pump	$\dot{C}_{w,P}$	$\dot{C}_7 - \dot{C}_6$	-	2	1
Economizer	$\dot{C}_{18} - \dot{C}_{19}$	$\dot{C}_8 - \dot{C}_7$	$c_{19} = c_{18}$ (F rule)	2	2
Additional Heat Source	$\dot{C}_{q,AHS}$	$\dot{C}_9 - \dot{C}_8$	-	2	1
Fuel Compressor	$\dot{C}_{w,FC}$	$\dot{C}_{11} - \dot{C}_{10}$	-	2	1

Mixer	$\dot{C}_9 - \dot{C}_{11}$	$\dot{C}_{12}$	-	2	1

Cost balance equations:

LP-Compressor:

$$\dot{C}_2 - \dot{C}_1 = \dot{C}_{\mathrm{w,LPC}} + \dot{Z}_{\mathrm{LPC}} \tag{9.1}$$

Intercooler:

$$\dot{C}_3 - \dot{C}_2 = \left(\dot{C}_{\mathrm{cw,in}} - \dot{C}_{\mathrm{cw,out}}\right) + \dot{Z}_{\mathrm{IC}} \tag{9.2}$$

HP-Compressor:

$$\dot{C}_4 - \dot{C}_3 = \dot{C}_{\mathrm{w,HPC}} + \dot{Z}_{\mathrm{HPC}} \tag{9.3}$$

Recuperator:

$$\left(\dot{C}_5 - \dot{C}_4\right) + \left(\dot{C}_{13} - \dot{C}_{12}\right) = \left(\dot{C}_{17} - \dot{C}_{18}\right) + \dot{Z}_{\mathrm{REC}} \tag{9.4}$$

Combustor:

$$\left(\dot{C}_{15} - \dot{C}_{14}\right) = \dot{C}_5 + \dot{Z}_{\mathrm{CC}} \tag{9.5}$$

Turbine:

$$\dot{C}_{w,T} = \left(\dot{C}_{15} - \dot{C}_{16}\right) + \dot{Z}_{T} \tag{9.6}$$

Reformer:

$$\dot{C}_{14} - \dot{C}_{13} = \left(\dot{C}_{16} - \dot{C}_{17}\right) + \dot{Z}_{REF} \tag{9.7}$$

Pump:

$$\dot{C}_{7} - \dot{C}_{6} = \dot{C}_{w,P} + \dot{Z}_{P} \tag{9.8}$$

Economizer:

$$\dot{C}_{8} - \dot{C}_{7} = \left(\dot{C}_{18} - \dot{C}_{19}\right) + \dot{Z}_{E} \tag{9.9}$$

Additional heat source:

$$\dot{C}_{9} - \dot{C}_{8} = \dot{C}_{q,AHS} + \dot{Z}_{AHS} \tag{9.10}$$

Fuel compressor:

$$\dot{C}_{11} - \dot{C}_{10} = \dot{C}_{w,FC} + \dot{Z}_{FC} \tag{9.11}$$

Mixer:

$$\dot{C}_{12} = \dot{C}_{9} - \dot{C}_{11} \tag{9.12}$$

Adding Eqs (9.1)-(9.12) together results in cancelation of some of their unknowns as shown in Eq. (9.13):

$$\begin{aligned}&\dot{C}_{\mathrm{w,T}}-\left(\dot{C}_{\mathrm{w,LPC}}+\dot{C}_{\mathrm{w,HPC}}+\dot{C}_{\mathrm{w,P}}+\dot{C}_{\mathrm{w,FC}}\right)\\&=\dot{C}_{10}+\dot{C}_{1}+\dot{C}_{6}-\left(\dot{C}_{\mathrm{cw,out}}-\dot{C}_{\mathrm{cw,in}}\right)-\dot{C}_{19}+\dot{Z}_{\mathrm{TOT}},\end{aligned}\tag{9.13}$$

in which $\dot{Z}_{\mathrm{TOT}}$ is the total cost rate of SOLRGT including all components:

$$\dot{Z}_{\mathrm{TOT}}=\sum\nolimits_{k}\dot{Z}_{\mathrm{k}}.\tag{9.14}$$

Before further treatment of Eq. (9.13), we make two assumptions that are typical for power systems and to simplify the equations:

(1) $\dot{C}_{1}$, the cost rate associated with the inlet air of gas turbine, could be regarded as 0 since it is usually free to get from the ambient air;

(2) $\left(\dot{C}_{\mathrm{cw,out}}-\dot{C}_{\mathrm{cw,in}}\right)$ is the cost rate associated with the cooling water and is considered small compared with the cost rate associated with the fuel $\dot{C}_{\mathrm{f}}$. For example, in the case study in ref. [1], $\left(\dot{C}_{\mathrm{cw,out}}-\dot{C}_{\mathrm{cw,in}}\right)$ is (11.9-5.0) =6.9 $/h; while $\dot{C}_{\mathrm{f}}$ is 785.2 $/h;

The higher temperature heat source (fuel) usually generates flue gas (stream 13 in Fig. 7-1) after burning in the boiler. When the flue gas is not utilized in any further process and is ultimately emitted to the atmosphere as in normal practice, there are two ways to assessing

the cost associated with the flue gas. One ways is to calculate c_{fg} based on the cost balance equations. A simpler way is to set the specific cost of the flue gas to 0, i.e.

$$c_{fg} = c_{13} = 0. \tag{9.15}$$

This way of determining c_{fg}, however, is not recommended since it doesn't allow an estimation of the cost consequences of rejecting the flue gas to the surroundings and it also violates the F rule [1]. Either way is acceptable and the results apply to the final results of the analysis, although resulting in different values of calculated c_P. This also means that the c_P calculated from the exergo-economic method is not necessarily the same as from the energo-economic analysis method.

When not utilized in other processes, the flue gas is an undesirable externality (interaction with the environment that the power utility is not obliged to pay), and this analysis method is an opportunity to quantify here the "cost" of externalities and this is an advantage of using the exergo-economic analysis than the conventional energo-economic analysis method.

Sometimes carbon tax could be imposed on power generation plants that emit CO_2, which is proportional to the amount of CO_2 emitted to the atmosphere, i.e.

$$\dot{C}_{ct} = c_{CO_2} \dot{m}_{CO_2}, \tag{9.16}$$

in which $\dot{C}_{ct}$ [$/s] is the carbon tax imposed on the system, c_{CO_2} [$/kg] is the specific cost for carbon emission, and $\dot{m}_{CO_2}$ [kg/s] is the carbon emission rate to the atmosphere.

According to the combustion equation for methane

$$CH_4 + 2(1+0.2)O_2 = CO_2 + 2H_2O + 0.4O_2, \tag{9.17}$$

when methane is used as fuel and burned completely to carbon dioxide and steam (requiring excess air of at least 20% to ensure complete combustion), and no carbon capture method is used, the mass rate of CO_2 emission will be proportional to the fuel used in the system:

$$\frac{\dot{m}_{CO_2}}{\dot{m}_{CH_4}} = \frac{44}{16} = 2.75. \tag{9.18}$$

So

$$\dot{C}_{ct} = c_{CO_2}\dot{m}_{CO_2} = 2.75 c_{CO_2}\dot{m}_{CH_4} = 2.75 c_{CO_2}\dot{m}_a f, \tag{9.19}$$

in which $\dot{m}_a$ [kg/s] is the mass flow rate of inlet air (stream 1 in Fig. 7-1) and f is the fuel-air ratio.

As shown in [2], the average unit cost of electricity consumption could be assumed to be the same as that of electricity generation, and all to be equal to the levelized electricity cost, i.e.

$$c_{\mathrm{w,CEP}} = c_{\mathrm{w,AHSP}} = c_{\mathrm{w,T}} = c_{\mathrm{p}}. \tag{9.20}$$

Equation (9.13) can thus be rewritten as

$$c_{\mathrm{p,h}} = \frac{\dot{C}_{\mathrm{f}} + \dot{C}_{\mathrm{w}} - \dot{C}_{\mathrm{fg}} + \dot{C}_{\mathrm{q,AHS}} + \dot{Z}_{\mathrm{TOT}} + \dot{C}_{\mathrm{ct}}}{\dot{W}_{\mathrm{net}}}, \tag{9.21}$$

in which $\dot{C}_{\mathrm{f}} = \dot{C}_{10}$ is the cost rate of the fuel, $\dot{C}_{\mathrm{w}} = \dot{C}_{6}$ is the cost rate of incoming water and $\dot{C}_{\mathrm{fg}} = \dot{C}_{13}$ is the cost rate of flue gas of the system. For SOLRGT, $\dot{C}_{\mathrm{q,AHS}}$ can be regarded as 0 since solar radiation does not need to be paid, and the components for utilizing solar radiation, such as the solar collection equipment, have been taken into account in $\dot{Z}_{\mathrm{AHS}}$ and $\dot{Z}_{\mathrm{TOT}}$.

Although the final expression for the LEC of the system, Eq. (9.21), using the exergo-economic analysis method, contain only the external terms but not the internal ones that are inside the system, the internal terms inside the system which are listed in Table 9-1 are still needed, since that explains how Eq. (9.21) is derived. Without the help of the internal terms listed in Table 9-1, Eq. (9.21) cannot be written directly, even though it is similar to Eq. (8.4) of the energo-economic analysis method.

Without using the exergo-economic analysis method, one may write a similar equation to Eq. (9.21) based on Eq. (8.4), but people have no confidence if it is correct or not. No

researchers have ever expressed the LEC of a power generation system like Eq. (9.21) if the exergo-economic analysis method were not used.

What's more, without the use of the exergo-economic analysis method, the cost associated with the externalities, such as the flue gas, $\dot{C}_{fg}$ cannot be estimated appropriately. One of the internal cost balance equations, Eq. (9.4), shows how $\dot{C}_{fg}$ is estimated, if it is not set to 0 as the energo-economic analysis does. Different assumptions for $\dot{C}_{fg}$ will result in different results for the LEC of the system, which may be different from the result given by the energo-economic analysis.

9.2. Comparison the LEC of the SOLRGT with the reference single heat source thermochemical system (IC-CRGT)

It is of interest to compare the LEC for the SOLRGT with that for the system that does not use solar heat or does not include a thermochemical process. As introduced in section 7.2.1, the first reference system that is without solar heat is IC-CRGT shown in Fig. 7-3, and the second reference system is the non-thermochemical one (IC-HSTIG) which will be discussed in the next section. As a basis for comparison, the turbine inlet temperature and mass flow rate of the compressor inlet air are kept the same for all systems.

In the fuel-only reference system, solar heat is not used to vaporize the water, so more fuel is needed to maintain the turbine inlet temperature. Since water is vaporized by the gas

turbine exhaust gas in the reference system, less steam will be generated by the turbine exhaust gas heat in the SOLRGT system since it does not have as much thermal energy to vaporize both the needed water and heat the pressurized air. For the same reason, the methane conversion rate in the reference system will be lower because the turbine exhaust gas cannot provide as much heat as the SOLRGT system to the reforming process. Reference [15] specifically showed that, compared with SOLRGT, in the reference system the fuel flow rate increased from 0.02 kg/s to 0.026 kg/s, the water-to-methane mole ratio decreased from 6.1 to 5.02, and the methane conversion rate decreased from 0.378 to 0.340.

Using the same SPECO method as for SOLRGT, the resulting electricity cost expression for the reference system IC-CRGT is

$$c_{\mathrm{p},0} = \frac{\dot{C}_{\mathrm{f},0} + \dot{C}_{\mathrm{w},0} - \dot{C}_{\mathrm{fg},0} + \dot{Z}_{\mathrm{TOT},0} + \dot{C}_{\mathrm{ct},0}}{\dot{W}_{\mathrm{net},0}}, \tag{9.22}$$

in which the subscript 0 stands for the reference system.

From the results given in [15], the net power output of the reference system is 601.9 kJ/(kg air used in the system), which is about 1.6% more than that for SOLRGT, mainly because of the higher mass flow rate of working fluid by the turbine due to the increased fuel flow rate.

Since the mass flow rate of the fuel is small compared with the mass flow rate of the working fluid (fuel/air mass flow rate ratio is about 2%), it can be assumed that the cost

rate difference of each component between the reference system and SOLRGT is small compared to the total cost rate of SOLRGT.

The total cost rate of the reference system could thus be expressed by

$$\dot{Z}_{\mathrm{TOT},0} = \dot{Z}_{\mathrm{TOT}} - \dot{Z}_{\mathrm{AHS}}. \tag{9.23}$$

Next, for the difference of the cost rate of the fuel,

$$\dot{C}_{\mathrm{f}} - \dot{C}_{\mathrm{f},0} = c_{\mathrm{f}} b_{\mathrm{f}} \left(\dot{m}_{\mathrm{f}} - \dot{m}_{\mathrm{f},0} \right) = c_{\mathrm{f}} b_{\mathrm{f}} \dot{m}_{\mathrm{a}} \left(f - f_0 \right), \tag{9.24}$$

in which c_{f} [\$/kJ], b_{f} [kJ/kg] and $\dot{m}_{\mathrm{f}}$ [kg/s] are the specific cost of the fuel, specific chemical exergy of the fuel and mass flow rate of the fuel, respectively, f is the fuel/air ratio. $\dot{m}_{\mathrm{a}} = \dot{m}_1$ [kg/s] is the mass flow rate of air and is kept the same for both systems in this analysis.

The mass flow rate of the flue gas is the sum of the air, fuel and water mass flow rates, i.e.

$$\begin{aligned} \dot{m}_{\mathrm{fg}} &= \dot{m}_{\mathrm{a}} + \dot{m}_{\mathrm{f}} + \dot{m}_{\mathrm{w}} = \dot{m}_{\mathrm{a}} + f\dot{m}_{\mathrm{a}} + R_{\mathrm{sm}}\dot{m}_{\mathrm{f}} \\ &= \left(1 + f + fR_{\mathrm{sm}}\right)\dot{m}_{\mathrm{a}}, \end{aligned} \tag{9.25}$$

$$\begin{aligned} \dot{m}_{\mathrm{fg},0} &= \dot{m}_{\mathrm{a}} + \dot{m}_{\mathrm{f},0} + \dot{m}_{\mathrm{w},0} = \dot{m}_{\mathrm{a}} + f_0\dot{m}_{\mathrm{a}} + R_{\mathrm{sm},0}\dot{m}_{\mathrm{f},0} \\ &= \left(1 + f_0 + f_0 R_{\mathrm{sm},0}\right)\dot{m}_{\mathrm{a}}, \end{aligned} \tag{9.26}$$

in which $R_{\text{sm}} = \dfrac{\dot{m}_{\text{w}}}{\dot{m}_{\text{f}}}$ and $R_{\text{sm,0}} = \dfrac{\dot{m}_{\text{w,0}}}{\dot{m}_{\text{f,0}}}$ are the steam-methane mass ratios for the SOLRGT and the reference system, respectively.

Strictly speaking, the specific exergy of the flue gas is different for the reference and SOLRGT systems due to their different thermodynamic condition (temperature, pressure, and composition). Since the difference between the mass flow rate of the fuel in the reference and SOLRGT systems is small relative to the working fluid flow rate (0.6%) and the turbine inlet condition is fixed, it is assumed here that their exergies are the same. Thus the cost rate difference of the flue gas is, from Eqs (9.25) and (9.26),

$$\begin{aligned} \dot{C}_{\text{fg}} - \dot{C}_{\text{fg,0}} &= c_{\text{fg}} b_{\text{fg}} \left(\dot{m}_{\text{fg}} - \dot{m}_{\text{fg,0}} \right) \\ &= c_{\text{fg}} b_{\text{fg}} \dot{m}_{\text{a}} \left[\left(f - f_0 \right) + \left(f R_{\text{sm}} - f_0 R_{\text{sm,0}} \right) \right]. \end{aligned} \tag{9.27}$$

The cost rate associated with the additional heat source is

$$\dot{C}_{\text{q,AHS}} = c_{\text{q,AHS}} \dot{B}_{\text{AHS}}, \tag{9.28}$$

in which $c_{\text{q,AHS}}$ [$/kJ] is the specific cost of the additional heat source (AHS), which is 0 when the source energy itself, neglecting the cost of the needed systems for their collection or extraction, is free, such as in cases when solar or geothermal energy is used as AHS, and $\dot{B}_{\text{AHS}}$ [kW] is the exergy flow rate from the AHS into the system.

The cost rate of water (stream 6 in Fig. 7-1), according to the definition, is

$$\dot{C}_{\mathrm{w}} = c_{\mathrm{w}} b_{\mathrm{w}} \dot{m}_{\mathrm{w}} = c_{\mathrm{w}} b_{\mathrm{w}} \dot{m}_{\mathrm{f}} R_{\mathrm{sm}} = c_{\mathrm{w}} b_{\mathrm{w}} \dot{m}_{\mathrm{a}} f R_{\mathrm{sm}}. \tag{9.29}$$

Thus the cost rate difference of water between the SOLRGT and the reference systems is

$$\begin{aligned} \dot{C}_{\mathrm{w}} - \dot{C}_{\mathrm{w,0}} &= c_{\mathrm{w}} b_{\mathrm{w}} \dot{m}_{\mathrm{a}} f R_{\mathrm{sm}} - c_{\mathrm{w}} b_{\mathrm{w}} \dot{m}_{\mathrm{a}} f_0 R_{\mathrm{sm,0}} \\ &= c_{\mathrm{w}} b_{\mathrm{w}} \dot{m}_{\mathrm{a}} \left(f R_{\mathrm{sm}} - f_0 R_{\mathrm{sm,0}} \right). \end{aligned} \tag{9.30}$$

The cost rate of carbon tax is expressed by Eq. (9.19), so the difference between the carbon tax rate for the SOLRGT and for the reference system is

$$\dot{C}_{\mathrm{ct}} - \dot{C}_{\mathrm{ct,0}} = 2.75 c_{\mathrm{CO_2}} \dot{m}_{\mathrm{a}} \left(f - f_0 \right), \tag{9.31}$$

$$\dot{W}_{\mathrm{T}} = \dot{m}_{\mathrm{T}} \Delta h_{\mathrm{T}}, \tag{9.32}$$

in which $\dot{m}_{\mathrm{T}}$ is the total mass flow rate of the working fluid (combustion gas) and Δh_{T} is the specific enthalpy change of the working fluid through the turbine. Since the mass flow rate of water is independent of the mass flow rate of the fuel, there is no fixed relation between the turbine power output and thus the net power output of the SOLRGT and the reference system IC-CRGT.

Since the turbine power output is proportional to the mass flow rate of the working fluid and considering that the mass flow rate of air is kept the same for both systems, the power output ratio between the reference and SOLRGT system is

$$\frac{\dot{W}_{\mathrm{T},0}}{\dot{W}_{\mathrm{T}}}=\frac{\dot{m}_{\mathrm{a}}+\dot{m}_{\mathrm{w},0}+\dot{m}_{\mathrm{f},0}}{\dot{m}_{\mathrm{a}}+\dot{m}_{\mathrm{w}}+\dot{m}_{\mathrm{f}}}=\frac{1+f_0+f_0R_{\mathrm{sm},0}}{1+f+fR_{\mathrm{sm}}}. \tag{9.33}$$

Note that although the turbine power output ratio of the reference and the SOLRGT system can be explicitly written as Eq. (9.33), the ratio of the *net* power output of the system cannot, and we therefore define the ratio of the net power output of IC-CRGT and SOLRGT as λ, i.e.

$$\lambda=\frac{\dot{W}_{\mathrm{net},0}}{\dot{W}_{\mathrm{net,h}}}, \tag{9.34}$$

for further analysis. The results from [15] show that the net power output of IC-CRGT is about 1.6% higher than that of SOLRGT, or $\lambda=1.016$.

Using Eq. (9.34), the electricity cost difference between the hybrid system SOLRGT and the reference fuel-only system IC-CRGT is thus

$$\Delta c_{\mathrm{p}} = c_{\mathrm{p,h}} - c_{\mathrm{p,0}} = \frac{\dot{C}_{\mathrm{f}} + \dot{C}_{\mathrm{w}} - \dot{C}_{\mathrm{fg}} + \dot{C}_{\mathrm{q,AHS}} + \dot{Z}_{\mathrm{TOT}} + \dot{C}_{\mathrm{ct}}}{\dot{W}_{\mathrm{net}}} -$$

$$\frac{\dot{C}_{\mathrm{f,0}} + \dot{C}_{\mathrm{w,0}} - \dot{C}_{\mathrm{fg,0}} + \dot{Z}_{\mathrm{TOT,0}} + \dot{C}_{\mathrm{ct,0}}}{\dot{W}_{\mathrm{net,0}}}$$

$$= \frac{\begin{array}{l}\left(\lambda \dot{C}_{\mathrm{f}} - \dot{C}_{\mathrm{f,0}}\right) + \left(\lambda \dot{C}_{\mathrm{w}} - \dot{C}_{\mathrm{w,0}}\right) - \left(\lambda \dot{C}_{\mathrm{fg}} - \dot{C}_{\mathrm{fg,0}}\right) \\ + \dot{C}_{\mathrm{q,AHS}} + \dot{Z}_{\mathrm{AHS}} + \left(\dot{C}_{\mathrm{ct}} - \dot{C}_{\mathrm{ct,0}}\right)\end{array}}{\dot{W}_{\mathrm{net,0}}}$$

$$= \frac{\begin{array}{l}c_{\mathrm{f}} b_{\mathrm{f}} \dot{m}_{\mathrm{a}} \left(\lambda f - f_0\right) + c_{\mathrm{w}} b_{\mathrm{w}} \dot{m}_{\mathrm{a}} \left(\lambda f R_{\mathrm{sm}} - f_0 R_{\mathrm{sm,0}}\right) \\ - c_{\mathrm{fg}} b_{\mathrm{fg}} \dot{m}_{\mathrm{a}} \left[\left(\lambda f - f_0\right) + \left(\lambda f R_{\mathrm{sm}} - f_0 R_{\mathrm{sm,0}}\right)\right] \\ + \dot{C}_{\mathrm{q,AHS}} + \dot{Z}_{\mathrm{AHS}} + 2.75 c_{\mathrm{CO_2}} \dot{m}_{\mathrm{a}} \left(\lambda f - f_0\right)\end{array}}{\dot{W}_{\mathrm{net,0}}}$$

$$= \frac{\begin{array}{l}\dot{m}_{\mathrm{a}} \left(c_{\mathrm{f}} b_{\mathrm{f}} - c_{\mathrm{fg}} b_{\mathrm{fg}} + 2.75 c_{\mathrm{CO_2}}\right)\left(\lambda f - f_0\right) \\ + \dot{m}_{\mathrm{a}} \left(c_{\mathrm{w}} b_{\mathrm{w}} - c_{\mathrm{fg}} b_{\mathrm{fg}}\right)\left(\lambda f R_{\mathrm{sm}} - f_0 R_{\mathrm{sm,0}}\right) + c_{\mathrm{q,AHS}} \dot{B}_{\mathrm{AHS}} + \dot{Z}_{\mathrm{AHS}}\end{array}}{\dot{W}_{\mathrm{net,0}}}.$$

(9.35)

For SOLRGT to be competitive with the reference fuel-only system economically, Δc_{P} must be $\geqslant 0$, i.e.

$$\begin{array}{l}\dot{m}_{\mathrm{a}} \left(c_{\mathrm{f}} b_{\mathrm{f}} - c_{\mathrm{fg}} b_{\mathrm{fg}} + 2.75 c_{\mathrm{CO_2}}\right)\left(f_0 - \lambda f\right) \\ + \dot{m}_{\mathrm{a}} \left(c_{\mathrm{w}} b_{\mathrm{w}} - c_{\mathrm{fg}} b_{\mathrm{fg}}\right)\left(f_0 R_{\mathrm{sm,0}} - \lambda f R_{\mathrm{sm}}\right) \\ \geq c_{\mathrm{q,AHS}} \dot{B}_{\mathrm{AHS}} + \dot{Z}_{\mathrm{AHS}}.\end{array}$$

(9.36)

Based on the case in ref. [15], the values of the terms in Eq. (6.79) are $\lambda = 1.016$ $f_0 = 0.026$, $f = 0.02$, $R_{sm,0} = 5.02$ and $R_{sm} = 6.1$, so $f_0 - \lambda f = 0.0057$ and $f_0 R_{sm,0} - \lambda f R_{sm} = 0.0066$. Considering that $\lambda \approx 1$, or $\left(f_0 - \lambda f \right) \approx \left(f_0 - f \right)$, it could be assumed that

$$\left(f_0 - f \right) \approx \left(f_0 - \lambda f \right) \approx \left(f_0 R_{sm,0} - \lambda f R_{sm} \right). \tag{9.37}$$

Also, since the temperature of the incoming water is close to the ambient, the water specific exergy is small compared with that of the fuel, i.e. $b_w << b_f$. Since the water price is also small compared with that of the fuel, i.e. $c_w << c_f$, we can neglect the water cost rate term in Eq. (9.36) because

$$c_w b_w << c_f b_f. \tag{9.38}$$

Using (9.37) and (9.38), Eq. (9.36) can be simplified to

$$\left(c_f b_f - c_{fg} b_{fg} + 2.75 c_{CO_2} \right) \dot{m}_a \left(f_0 - f \right) \geq c_{q,AHS} \dot{B}_{AHS} + \dot{Z}_{AHS}. \tag{9.39}$$

This means that for SOLRGT to be economically competitive with its reference system, the cost saving from fuel reduction (saving fuel usage, reduce carbon tax and selling flue gas as by-product) by using the AHS must not be smaller than the total cost of the AHS and the SOLRGT components that were added to the reference system. As Eq. (9.36)

shows, this can be achieved by increasing the carbon tax rate c_{CO_2} and/or decreasing the AHS component cost $\dot{Z}_{\mathrm{AHS}}$, or if the fuel price c_{f} rises to the level of

$$c_{\mathrm{f}} > \frac{c_{\mathrm{q,AHS}}\dot{B}_{\mathrm{AHS}} + \dot{Z}_{\mathrm{AHS}}}{\left(f_0 - f\right)\dot{m}_{\mathrm{a}} b_{\mathrm{f}}} - 2.75 c_{\mathrm{CO}_2} + c_{\mathrm{fg}} b_{\mathrm{fg}} \tag{9.40}$$

Using this equation as a test example specific to the SOLRGT case [15], the use of Eq. (9.40) is demonstrated using the assumption shown in Table 9-2.

Table 9-2. Assumptions used in the analysis of the SOLRGT system in Fig. 7-1 with numbers

Variables	Values
Specific cost of the AHS (solar)	$c_{\mathrm{q,AHS}} = c_{\mathrm{solar}} = 0$
Carbon tax rate	$c_{\mathrm{CO}_2} = 0$
Specific cost of the flue gas	$c_{\mathrm{fg}} = 0$
Difference between the fuel-air ratio of IC-CRGT and SOLRGT	$f_0 - f = 0.026 - 0.02 = 0.006$ [15]
Mass flow rate of compressor inlet air	$\dot{m}_{\mathrm{a}} = 610$ kg/s [15]

Specific chemical exergy of fuel (methane)	$b_f = 831.6 \text{ kJ/mol} = 51.975 \text{ MJ/kg}$ [2]	

Using Eq. [15], the annual average investment cost of SOLRGT $C_{\text{inv,an}}$ is 25.5 M$, and that the solar block (consisting of the solar collection equipment field, thermal storage system which could provide heat for SOLRGT for 3 hours of operation when there is no solar heat input, and the solar evaporator) accounts for 54.0% of the total cost ($\chi_{\text{SB}} = 0.54$). So the cost rate of the solar block is

$$\dot{Z}_{\text{AHS}} = \frac{C_{\text{inv,an}}}{H}\chi_{\text{SB}} = \frac{\$25.5\times10^{6}}{365\times24\times3600 \text{ s}}\times0.54 = 0.437 \text{ \$/s.} \qquad (9.41)$$

Substituting the assumptions used in Table 9-2 and Eq. (9.41) into Eq. (9.40), shows that for SOLRGT to be economically competitive with the reference fuel-only system, c_f must be larger than 2.3×10^{-6} \$/kJ.

The average natural gas price in the US (on 11/23/2015) was 2.546 \$/(million BTU) or 2.7×10^{-6} \$/kJ, and was lowest at 1.7×10^{-6} \$/kJ in the US mid-Atlantic region [51]. This average fuel cost is already high enough for SOLRGT to be economic competitive, although not high enough in some regions. It is noteworthy that the price of gas in the US

(Henry Hub) is one of the lowest in the world, up to about 5-fold, it is obvious that SOLRGT under these conditions would be very competitive in most of the world.

If the fuel price is, however, 2.3×10^{-6} \$/kJ, one way to make SOLRGT economically advantageous is by imposing a carbon tax of

$$c_{\mathrm{CO_2}} \geq \frac{4}{11}\left[\frac{c_{\mathrm{q,AHS}}\dot{B}_{\mathrm{AHS}} + \dot{Z}_{\mathrm{AHS}}}{\dot{m}_{\mathrm{a}}\left(f_0 - f\right)} - c_{\mathrm{f}}b_{\mathrm{f}}\right] = 0.0113\ \$/\mathrm{kg_{CO_2}}. \qquad (9.42)$$

This is a practical tax value and some country/region has already imposed higher carbon tax. For example, British Columbia in Canada has imposed a carbon tax at 0.022 $/kg$_{CO_2}$ since July 2012 [3], which almost doubles the value given in Eq. (9.42).

Another way to make SOLRGT economically competitive is to decrease the cost of the solar block. Without carbon tax, and using the lowest fuel cost at1.7×10^{-6} \$/kJ, the cost of the solar block $\dot{Z}_{\mathrm{AHS}}$ must be

$$\dot{Z}_{\mathrm{AHS}} \leq \left(c_{\mathrm{f}}b_{\mathrm{f}} + 2.75c_{\mathrm{CO_2}}\right)\dot{m}_{\mathrm{a}}\left(f_0 - f\right) - c_{\mathrm{q,AHS}}\dot{B}_{\mathrm{AHS}} = 0.323\ \$/\mathrm{s}, \qquad (9.43)$$

which is only 26% lower than its above cited value, and is thus not unrealistic and is feasible as technology advances.

9.3. Comparison of the LEC of the SOLRGT with the reference hybrid non-thermochemical reference system (IC-HSTIG)

Besides the single heat source thermochemical reference system introduced before, it is of interest to compare the thermochemical system with the non-thermochemical hybrid system (that can be called the “thermal hybrid system”), i.e. using two heat sources but with no thermochemical process. Both the thermochemical hybrid systems introduced are based on a Brayton cycle, so the reference non-thermochemical hybrid system can be configured based on the steam-injected gas turbine power generation system (STIG). In the STIG, steam is injected into the combustor to increase the mass flow rate of the working fluid and thus increase the power output of the turbine. The AHS can be added in the STIG to preheat the water for the injected steam generation. The flow diagram of the reference non-thermochemical hybrid system, here called the intercooled hybrid steam injected gas turbine (IC-HSTIG), is shown in Fig. 9-1. As the figure shows, the pressurized incoming water (stream 7) is vaporized by the additional heat source before being superheated by the gas turbine exhaust gas. The superheated steam (stream 9) is then mixed with the fuel and air in the combustor. To compare with the performance of the SOLRGT, the turbine inlet temperature and the temperature of the AHS are the same as in the SOLRGT, respectively.

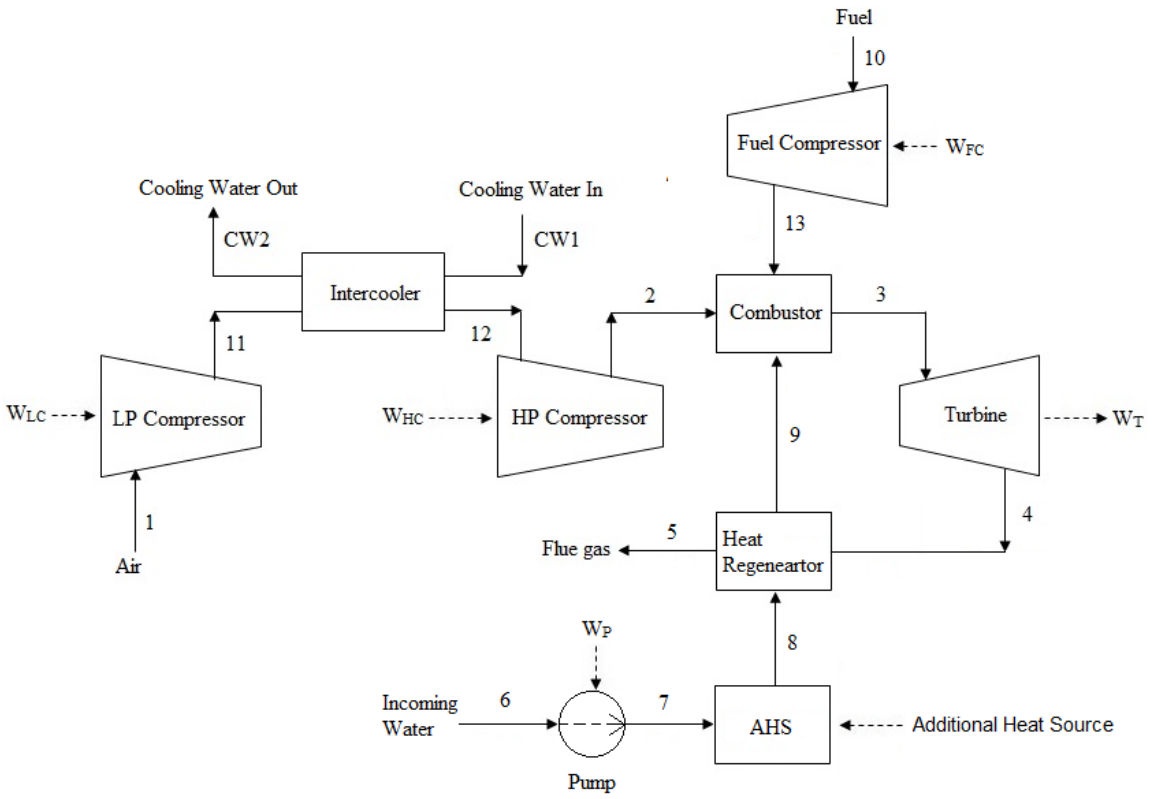

Fig. 9-1. Flow diagram of the reference non-thermochemical hybrid system IC-HSTIG (intercooled hybrid steam injection gas turbine power generation system)

When comparing the LEC for the SOLRGT with the non-thermochemical reference system IC-HSTIG shown in Fig. 9-1, the LEC for the latter is determined by using the same SPECO method as for SOLRGT, the LEC is expressed by

$$c'_{p,0} = \frac{\dot{C}'_{f,0} + \dot{C}'_{w,0} + \dot{C}'_{q,AHS,0} - \dot{C}'_{fg,0} + \dot{Z}'_{TOT,0} + \dot{C}'_{ct,0}}{\dot{W}'_{net,0}}, \qquad (9.44)$$

in which the subscript 0 stands for the reference system and the superscript prime stands for the reference system IC-HSTIG.

According to Fig. 7-1, the total energy addition rate to the SOLRGT, $\dot{Q}_{\text{in}}$, is the sum of the enthalpy of water, fuel and the heat from regenerated from the turbine exhaust gas (ignoring heat losses in each equipment since they are small compared to the heat duty of the equipment), i.e.

$$\dot{Q}_{\text{in}} = \left(\dot{m}_{\text{w}} h_{\text{w}} + \dot{W}_{\text{P}} + \dot{Q}_{\text{ADD}}\right) + \left(\dot{m}_{\text{f}} h_{\text{f}} + \dot{m}_{\text{f}} \text{LHV} + \dot{W}_{\text{FC}}\right) + \left(\dot{m}_{\text{fg}} h_{\text{ex}} - \dot{m}_{\text{fg}} h_{\text{fg}}\right), \tag{9.45}$$

in which $\dot{W}_{\text{P}}$ and $\dot{W}_{\text{FC}}$ are the power input of the pump and the fuel compressor, respectively, $\dot{Q}_{\text{ADD}}$ is the heat addition rate from the AHS to the system, $\dot{m}_{\text{w}} = \dot{m}_6$ is the mass flow rate of the incoming water, $\dot{m}_{\text{f}} = \dot{m}_{10}$ is the mass flow rate of the fuel, $\dot{m}_{\text{fg}} = \dot{m}_{16}$ is the mass flow rate of the flue gas, h_{ex} and h_{fg} are the specific enthalpies of the turbine exhaust gas and the flue gas, respectively.

Similarly, according to Fig. 9-1, the total energy addition rate to the IC-HSTIG, $\dot{Q}'_{\text{in},0}$, can be expressed by

$$\begin{aligned} \dot{Q}'_{\text{in},0} &= \left(\dot{m}'_{\text{w},0} h'_{\text{w},0} + \dot{W}'_{\text{P},0} + \dot{Q}'_{\text{ADD},0}\right) \\ &+ \left(\dot{m}'_{\text{f},0} h'_{\text{f},0} + \dot{m}'_{\text{f},0} \text{LHV} + \dot{W}'_{\text{FC},0}\right) + \left(\dot{m}'_{\text{fg},0} h'_{\text{ex},0} - \dot{m}'_{\text{fg},0} h'_{\text{fg},0}\right). \end{aligned} \tag{9.46}$$

For comparison, the mass flow rate of compressor inlet air and turbine inlet temperature is the same for both systems. By comparing Eqs (9.45) and (9.46), it can be concluded that each corresponding term in the two equations should be the same, i.e.

$$\dot{Q}'_{\text{in},0} = \dot{Q}_{\text{in}} \tag{9.47}$$

$$\dot{m}'_{\text{w},0} = \dot{m}_{\text{w}} \tag{9.48}$$

$$h'_{\text{w},0} = h_{\text{w}} \tag{9.49}$$

$$\dot{W}'_{\text{P},0} = \dot{W}_{\text{P}} \tag{9.50}$$

$$\dot{Q}'_{\text{ADD},0} = \dot{Q}_{\text{ADD}} \tag{9.51}$$

$$\dot{m}'_{\text{f},0} = \dot{m}_{\text{f}} \tag{9.52}$$

$$h'_{\text{f},0} = h_{\text{f}} \tag{9.53}$$

$$\dot{W}'_{\text{FC},0} = \dot{W}_{\text{FC}} \tag{9.54}$$

$$\dot{m}'_{\text{fg},0} = \dot{m}_{\text{fg}} \tag{9.55}$$

$$h'_{\text{ex},0} = h_{\text{ex}} \tag{9.56}$$

$$h'_{\mathrm{fg},0} = h_{\mathrm{fg}} \tag{9.57}$$

It is thus easy to know that

$$\dot{C}'_{\mathrm{f},0} = \dot{C}_{\mathrm{f}} \tag{9.58}$$

$$\dot{C}'_{\mathrm{w},0} = \dot{C}_{\mathrm{w}} \tag{9.59}$$

$$\dot{C}'_{\mathrm{q,AHS},0} = \dot{C}_{\mathrm{q,AHS}} \tag{9.60}$$

$$\dot{C}'_{\mathrm{fg},0} = \dot{C}_{\mathrm{fg}} \tag{9.61}$$

$$\dot{C}'_{\mathrm{ct},0} = \dot{C}_{\mathrm{ct}} \tag{9.62}$$

$$\dot{W}'_{\mathrm{net},0} = \dot{W}_{\mathrm{net}} \tag{9.63}$$

The cost rate of the corresponding equipment in the SOLRGT and IC-HSTIG are thus also the same. So the cost rate difference between the two systems is

$$\Delta\dot{Z}'_{\mathrm{TOT}} = \dot{Z}_{\mathrm{TOT}} - \dot{Z}'_{\mathrm{TOT},0} = \dot{Z}_{\mathrm{REC}} + \dot{Z}_{\mathrm{REF}} + \dot{Z}_{\mathrm{ECO}} - \dot{Z}_{\mathrm{HR}}, \tag{9.64}$$

in which $\dot{Z}_{\mathrm{REC}}$, $\dot{Z}_{\mathrm{REF}}$ and $\dot{Z}_{\mathrm{ECO}}$ are the cost rates of the recuperator, reformer and economizer of the SOLRGT system and $\dot{Z}_{\mathrm{HR}}$ is the cost rate of the heat regenerator of the IC-HSTIG system.

Comparing Eqs (9.21) and (9.44), the LEC difference of the SOLRGT and IC-HSTIG is

$$\Delta c'_{\mathrm{p}} = c_{\mathrm{p,h}} - c'_{\mathrm{p,0}} = \frac{\Delta \dot{Z}'_{\mathrm{TOT}}}{\dot{W}_{\mathrm{net}}}. \tag{9.65}$$

It can thus be concluded from Eq. (9.65) that the LEC for the thermochemical hybrid system (SOLRGT) is lower than that for the non-thermochemical hybrid system (IC-HSTIG) if $\Delta \dot{Z}'_{\mathrm{TOT}} < 0$, or $\dot{Z}_{\mathrm{REC}} + \dot{Z}_{\mathrm{REF}} + \dot{Z}_{\mathrm{ECO}} < \dot{Z}_{\mathrm{HR}}$ according to Eq. (9.64). It can also be seen that $\Delta c'_{\mathrm{p}}$ doesn't change with the fuel price, carbon tax rate or the AHS equipment cost.

9.4. Sensitivity analysis of the SOLRGT LEC to fuel price, carbon tax and the solar collection equipment price

From Eq. (9.21), the LEC for the SOLRGT $c_{\mathrm{p,h}}$ increases with the cost of the fuel $\dot{C}_{\mathrm{f}}$ and carbon tax $\dot{C}_{\mathrm{ct}}$, as well as the cost of the additional heat source (AHS) components $\dot{Z}_{\mathrm{AHS}}$ (part of the cost of all components in SOLRGT $\dot{Z}_{\mathrm{TOT}}$). To illustrate this characteristics, sensitivity analysis of the LEC for the SOLRGT to fuel price, carbon tax and cost of AHS component will be done. For SOLRGT, solar radiation is used as the AHS, so the AHS components include the solar collection equipment. Thermal storage may also be used and should strictly be included, but the majority of the AHS cost comes from the solar collection equipment (70% of total LHTS cost [15]). This analysis therefore focuses

only on the change of the solar collection equipment price rather than the total cost of all AHS components.

The assumption used are mostly from [15] and are summarized in Table 9-3.

Table 9-3. Economic analysis assumptions summary for the SOLRGT system in Fig. 7-1

	Values	Notes
Price of the methane	2.0 $/MMBtu	[4]
Plant operation life	30 years	[15]
Interest rate	8%	[15]
Price of the land	2.8 $/$m^2$	[15]
Annual O&M (cost of operation and maintenance)	4% of the investment capital cost of the system	[15]
Construction period	2 years	[15]

Finance	50% of the total investment cost is an interest-bearing loan and the other 50% is equity, and a loan interest rate of 8%, and the loan period (years) which is assumed to be equal to the system operation life, which means there is no loan payment during the construction period	[15]
Solar collection equipment cost	100.6 M$	[15]
Price of the methane variation	80-120% of the base price (0.144 $/Nm^3)	Assumed
solar collection equipment cost variation	100%, 75% or 50% of base cost (100.6 M$)	Assumed
Carbon tax rate variation	0 to 0.04$/kg$_{CO_2}$	Assumed based on [3]

The results are shown in Fig. 9-2. The two variables are fuel price relative to the current price at $2.0/MMBtu (assumed price/$2.0/MMBtu) and carbon tax rate, respectively. The

objective function is the levelized electricity cost (LEC) from the system calculated using Eq. (9.21). The upper, middle and lower surface in the figure were calculated when the solar collection equipment price is 100%, 75% and 50% of the base price (288.4 \$/m^2 [15]), respectively. Using Eq. (9.21) and the data in Table 9-3, the LECs of the SOLRGT are

$$\text{LEC}(\$/\text{kWh}) = \frac{a_i + 360.6 c_{\text{CO}_2} + 15.14 r_{\text{cf}}}{1052}, \tag{9.66}$$

in which $a_1 = 56.25$ when the solar collection equipment price is 100% of the base price, $a_2 = 50.92$ when the solar collection equipment price is 75% of the base price, $a_3 = 45.59$ when the solar collection equipment price is 50% of the base price, c_{CO_2} [\$/kg] is the specific cost for carbon emission and r_{cf} is the ratio between the assumed fuel price and the current fuel price.

Fuel price fluctuates, often with large amplitude and frequency. Equation (9.66) thus provides a good estimate of how the LEC of the hybrid cycle changes with the fuel price. For example, it can be seen from Eq. (9.66) that the LEC will increase by about 35% when the fuel price doubles from the current level, and will decrease by about 10% when the fuel price is half of the current level.

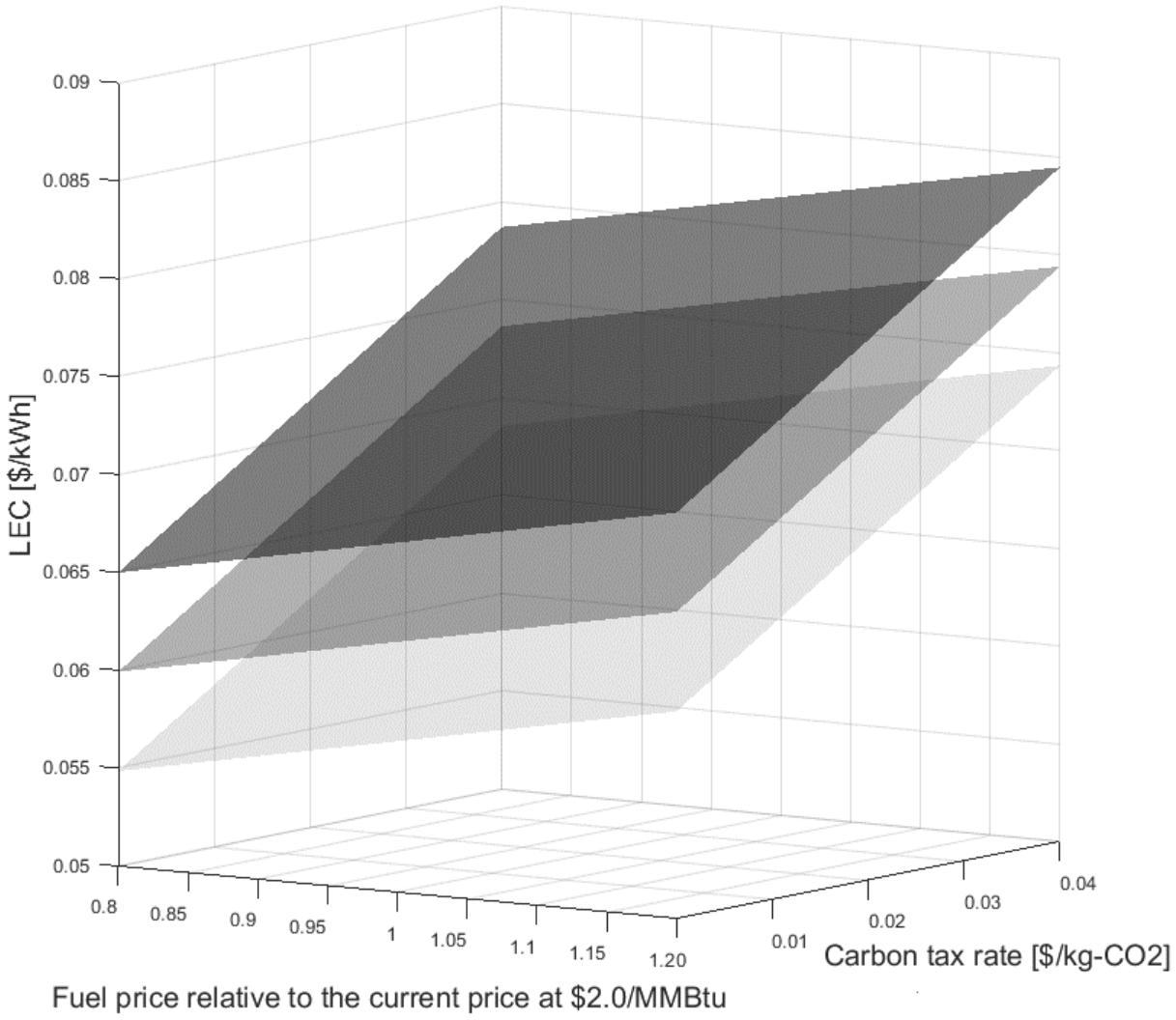

Fig. 9-2. Sensitivity analysis of levelized electricity cost (LEC) from SOLRGT to fuel price, carbon tax with different solar collection equipment price (100%, 75% and 50% of the base price for the upper, middle and lower surface, respectively)

It can be seen from Fig. 9-2 that for all the solar collection equipment prices considered in this study, the LEC for SOLRGT increases with both fuel price and carbon tax rate. For example, when there is no carbon tax and the solar collection equipment price is the same as the base price, the LEC for the system will decrease by about 4% (from 0.049 $/MWh to 0.047 $/MWh), if the fuel price decreases by 20% from the current price. When both fuel and solar collection equipment prices remain at their base price, the LEC for the system will increase by about 28% (from 0.049 $/MWh to 0.062 $/MWh) if the carbon tax rate is increased from 0 to 0.04$/kg$_{CO_2}$.

Besides fuel price and carbon tax rate, it is obvious (and shown in Fig. 9-2) that higher solar collection equipment price would raise the LEC. For example, when the fuel price is at its base value and the carbon tax rate is that in British Columbia in Canada, i.e. 0.022 $/kg$_{CO_2}$, reducing the solar collection equipment price to half of its base price, causes the COE of the system to decrease by about 12% (from 0.056 $/MWh to 0.050 $/MWh).

9.5. Exergo-economic analysis of the SOLRMCC

The exergo-economic analysis is now performed for the SOLRMCC system, in the same way as it was done for SOLRGT (in Section 9.1). The fuel, product and necessary auxiliary equations for each component for applying the SPECO method are summarized in Table 9-4. The cost balance equations can be constructed using Eq. (8.9) and are shown below the table.

Table 9-4. Fuel, product and auxiliary equations for each component in the SOLRMCC system in Fig. 7-6

Component	Fuel	Product	Auxiliary equation	No. of streams	
				Inlet	Outlet
Heater	$\dot{C}_{\text{q,AHS,1}}$	$\dot{C}_2 - \dot{C}_1$	-	2	1
Reactor	$\dot{C}_{\text{q,AHS,2}}$	$\dot{C}_3 - \dot{C}_2$	-	2	1
Compressor	$\dot{C}_{\text{w,C}}$	$\dot{C}_4 - \dot{C}_0$	-	2	1
Combustor	$\dot{C}_3$	$\dot{C}_5 - \dot{C}_4$	-	2	1
Gas Turbine	$\dot{C}_5 - \dot{C}_6$	$\dot{C}_{\text{w,GT}}$	$c_6 = c_5$ (F rule)	1	2
HRSG	$\dot{C}_6 - \dot{C}_7$	$\dot{C}_8 - \dot{C}_{12}$	$c_7 = c_6$ (F rule)	2	2
Steam Turbine	$\dot{C}_8 - \dot{C}_9$	$\dot{C}_{\text{w,ST}}$	$c_9 = c_8$	1	2
Condenser	$\dot{C}_{\text{cw,in}} - \dot{C}_{\text{cw,out}}$	$\dot{C}_{11} - \dot{C}_{10}$	$c_{\text{cw,in}} = c_{\text{cw,out}}$ (F rule)	2	2

Pump	$\dot{C}_{w,P}$	$\dot{C}_{12} - \dot{C}_{11}$	-	2	1

Cost balance equations:

Heater:

$$\dot{C}_2 - \dot{C}_1 = \dot{C}_{q,AHS,1} + \dot{Z}_H \tag{9.67}$$

Reactor:

$$\dot{C}_3 - \dot{C}_2 = \dot{C}_{q,AHS,2} + \dot{Z}_R \tag{9.68}$$

Compressor:

$$\dot{C}_4 - \dot{C}_0 = \dot{C}_{w,C} + \dot{Z}_C \tag{9.69}$$

Combustor:

$$\dot{C}_5 - \dot{C}_4 = \dot{C}_3 + \dot{Z}_{CC} \tag{9.70}$$

Gas Turbine:

$$\dot{C}_{w,GT} = \left(\dot{C}_5 - \dot{C}_6\right) + \dot{Z}_{GT} \tag{9.71}$$

HRSG:

$$\dot{C}_8 - \dot{C}_{12} = \left(\dot{C}_6 - \dot{C}_7\right) + \dot{Z}_{\text{HRSG}} \tag{9.72}$$

Steam Turbine:

$$\dot{C}_{\text{w,ST}} = \left(\dot{C}_8 - \dot{C}_9\right) + \dot{Z}_{\text{ST}} \tag{9.73}$$

Condenser:

$$\dot{C}_{11} - \dot{C}_{10} = \left(\dot{C}_{\text{cw,in}} - \dot{C}_{\text{cw,out}}\right) + \dot{Z}_{\text{COND}} \tag{9.74}$$

Pump:

$$\dot{C}_{12} - \dot{C}_{11} = \dot{C}_{\text{w,P}} + \dot{Z}_{\text{P}} \tag{9.75}$$

Adding Eqs (9.67)-(9.75) together results in cancelation of some of their unknowns as shown in Eq. (9.76):

$$\begin{aligned} &\left(\dot{C}_{\text{w,GT}} + \dot{C}_{\text{w,ST}}\right) - \left(\dot{C}_{\text{w,C}} + \dot{C}_{\text{w,P}}\right) \\ &= \dot{C}_1 + \dot{C}_0 - \dot{C}_7 + \dot{C}_{\text{q,AHS}} + \left(\dot{C}_{\text{cw,in}} - \dot{C}_{\text{cw,out}}\right) + \dot{Z}_{\text{TOT}}, \end{aligned} \tag{9.76}$$

in which $\dot{Z}_{\text{TOT}}$ is the total cost rate of the system including all components and considering time value of money and finance. $\dot{C}_{\text{q,AHS}}$ is the cost rate of the additional heat source and is the sum of $\dot{C}_{\text{q,AHS,1}}$ and $\dot{C}_{\text{q,AHS,2}}$.

Before further treatment of Eq. (9.13), we make two assumptions that are typical for power systems and to simplify the equations as in the SOLRGT.

When methanol is used as fuel and no carbon capture method is used, the amount of carbon emission will be proportional to the fuel used in the system, or specifically,

$$\frac{\dot{m}_{\mathrm{CO_2}}}{\dot{m}_{\mathrm{CH_3OH}}} = \frac{44}{32} = 1.375 \tag{9.77}$$

So

$$\dot{C}_{\mathrm{ct}} = c_{\mathrm{CO_2}} \dot{m}_{\mathrm{CO_2}} = 1.375 c_{\mathrm{CO_2}} \dot{m}_{\mathrm{CH_3OH}} = 1.375 c_{\mathrm{CO_2}} \dot{m}_{\mathrm{f}}. \tag{9.78}$$

Since all the carbon dioxide generated during the operation of the studied system comes from the usage of the fuel, carbon tax could also be regarded as the additional cost of the fuel in addition to the purchasing cost of the fuel c_{f} . So when carbon tax is considered, the cost rate of the fuel $\dot{C}_{\mathrm{f}}$ can be expressed by

$$\dot{C}'_{\mathrm{f}} = \dot{C}_{\mathrm{f}} + \dot{C}_{\mathrm{ct}} = c_{\mathrm{f}} b_{\mathrm{f}} \dot{m}_{\mathrm{f}} + 1.375 c_{\mathrm{CO_2}} \dot{m}_{\mathrm{f}} = \left(c_{\mathrm{f}} b_{\mathrm{f}} + 1.375 c_{\mathrm{CO_2}} \right) \dot{m}_{\mathrm{f}}. \tag{9.79}$$

Using Eq. (8.31), the LEC for the hybrid system with consideration of the carbon tax is

$$c_{\mathrm{p,h}} = \frac{\dot{C}_{\mathrm{f}} - \dot{C}_{\mathrm{fg}} + \dot{C}_{\mathrm{q,AHS}} + \dot{Z}_{\mathrm{TOT}} + \dot{C}_{\mathrm{ct}}}{\dot{W}_{\mathrm{net}}}. \tag{9.80}$$

It is of interest to compare the LEC for the hybrid with that from the system without solar heat input. The system without solar heat is the conventional gas turbine combined cycle system with methanol as fuel (this is assumed just for this analysis; Methanol is not commonly used as fuel for gas turbines, but was discussed, such as in [5]), with the same flow diagram as Fig. 7-6, without the solar heat source and its related components including the solar collection equipment, heater and reactor. The operating parameters are the same as in the hybrid system, including fuel and air inlet temperatures and pressures, mass flow rate of compressor inlet air, gas turbine and steam turbine inlet temperatures, compression ratio of gas turbine, isentropic efficiency of compressor, gas turbine, steam turbine and pump, flue gas temperature, cooling water inlet temperature and pressure, temperature of working fluid at condenser outlet and pump pressure ratio.

Using the same method as in the hybrid system, the resulting LEC expression for the reference system is

$$c_{\mathrm{p},0} = \frac{\dot{C}_{\mathrm{f},0} - \dot{C}_{\mathrm{fg},0} + \dot{Z}_{\mathrm{TOT},0} + \dot{C}_{\mathrm{ct},0}}{\dot{W}_{\mathrm{net},0}}, \tag{9.81}$$

in which the subscript 0 stands for the reference system.

Comparison of the LEC for the hybrid and reference system can be done by comparing each term in Eqs (9.80) and (9.81). In the following comparison, the turbine inlet temperature would be kept the same for both.

Methanol is the only fuel used in this hybrid and in its reference systems. In the hybrid system, the methanol is decomposed to CO and H_2 that are then burned; while in the reference system, the methanol is directly burned. According to species conservation, for both systems, the mole ratio of carbon dioxide and steam in the combustion gas is 1:2, since the mole ratio of carbon to hydrogen atoms is 1:4 in the methanol (CH_3OH) molecule and each carbon dioxide molecule (CO_2) has 1 carbon atom and each steam molecule (H_2O) has 2 hydrogen atoms. Besides methanol, gas turbine inlet air also contains some carbon and hydrogen. The mole ratio of CO_2 in the atmospheric dry air (without vapor) is typically only 0.03% [1]. Continuous operation of the gas turbine compressor requires removal of the moisture from the compressor inlet air, so the CO_2 and H_2O in the air can be neglected relative to their content in the methanol fuel.

To approach complete combustion of the fuel, the gas turbine inlet air flow is assumed to be 20% higher than needed for stoichiometric combustion. Since the gas temperature and pressure at the turbine inlet are assumed to be the same for the hybrid and reference system, so is thus the enthalpy. The energy balances of the combustor for the reference and hybrid systems, respectively, are thus

$$\dot{m}_{a,0}h_4+\dot{m}_{f,0}\mathrm{LHV}=\left(\dot{m}_{a,0}+\dot{m}_{f,0}\right)h_5, \tag{9.82}$$

and

$$\dot{m}_{a}h_4+\dot{m}_{f}\mathrm{LHV}+\dot{Q}_{sol}=\left(\dot{m}_{a}+\dot{m}_{f}\right)h_5, \tag{9.83}$$

in which h_4 [kJ/kg] and h_5 [kJ/kg] are the specific enthalpy of pressurized air and combustion gas relative to the reference state, respectively. $\dot{m}_{f,0}$ [kg/s] and $\dot{m}_f$ [kg/s] are the mass flow rate of the methanol fuel in the reference and hybrid system, respectively. LHV [kJ/kg] is the lower heating value of methanol. $\dot{Q}_{sol}$ [kW] is the solar heat input rate from the collector and

$$\dot{Q}_{sol} = \eta_{sc} \cdot \dot{Q}_{rad}, \tag{9.84}$$

in which $\dot{Q}_{rad}$ [kW] is the total solar radiation input rate on solar collection equipment and η_{sc} is the solar collection equipment efficiency.

Comparison of the reference and hybrid system on the same basis is based on assuming that the mass flow rate of air was kept the same for both systems, i.e. $\dot{m}_a = \dot{m}_{a,0}$, so

$$\dot{m}_{f,0}\mathrm{LHV} = \dot{m}_f \mathrm{LHV} + \dot{Q}_{sol} \tag{9.85}$$

Using the data from [29], the LHV of methanol = 676.29 kJ/mol, the solar radiation on the solar collectors was 147.88 kJ/mol-CH_3OH, and the solar collection equipment efficiency was 0.62. Substituting these numbers in Eq. (9.85) yields

$$\frac{\dot{m}_{f,0}}{\dot{m}_f} = 1.14 \tag{9.86}$$

Knowing the ratio of mass flow rate of the fuel for the hybrid and the reference system (Eq. (9.86)), the ratio of the cost rate of the fuel is

$$\frac{\dot{C}_{\mathrm{f},0}}{\dot{C}_{\mathrm{f}}} = \frac{c_{\mathrm{f}} b_{\mathrm{f}} \dot{m}_{\mathrm{f},0}}{c_{\mathrm{f}} b_{\mathrm{f}} \dot{m}_{\mathrm{f}}} = 1.14, \tag{9.87}$$

since the cost rate of the fuel $\dot{C}_{\mathrm{f}}$ [$/s] is defined as

$$\dot{C}_{\mathrm{f}} = c_{\mathrm{f}} b_{\mathrm{f}} \dot{m}_{\mathrm{f}}, \tag{9.88}$$

in which c_{f} [$/kJ] is the specific cost of the fuel (methanol) and b_{f} [kJ/kg] is the specific chemical exergy of the fuel (methanol) which are both the same for the hybrid and the reference system.

For the flue gas of the system, the temperature and pressure of the flue gas could be assumed to be the same for both systems. Considering the composition of the flue gas is roughly the same as that of the combustion gas, the specific exergy and specific cost of flue gas should also be the same, or

$$b_{\mathrm{fg},0} = b_{\mathrm{fg}} \tag{9.89}$$

$$c_{\mathrm{fg},0} = c_{\mathrm{fg}} \tag{9.90}$$

Since the mass flow rate of flue gas is the same as that of the combustion gas when no leakage is considered,

$$\frac{\dot{m}_{\mathrm{fg},0}}{\dot{m}_{\mathrm{fg}}} = \frac{\dot{m}_{\mathrm{f},0}}{\dot{m}_{\mathrm{f}}} = 1.14 \tag{9.91}$$

Therefore,

$$\frac{\dot{C}_{\mathrm{fg},0}}{\dot{C}_{\mathrm{fg}}} = \frac{c_{\mathrm{fg}} b_{\mathrm{fg}} \dot{m}_{\mathrm{fg}}}{c_{\mathrm{fg}} b_{\mathrm{fg}} \dot{m}_{\mathrm{fg},0}} = 1.14 \tag{9.92}$$

In this comparison, the turbine inlet temperature is fixed, but not the work output. So based on Eq. (9.86),

$$\frac{\dot{W}_{\mathrm{net},0}}{\dot{W}_{\mathrm{net}}} = \frac{366.44}{446.20} \cdot \frac{\dot{m}_{\mathrm{f},0}}{\dot{m}_{\mathrm{f}}} = 0.94, \tag{9.93}$$

in which the mass flow rate of fuel in the hybrid and the reference system are found in [29].

Next, the cost rate of each component of the system is compared. According to [1], most of the component cost is proportional to the mass flow rate of working fluid when the operation parameters, such as temperature and pressure, are the same. Remembering that it has been assumed that the excess air is the same for both systems (for example, 20% more than stoichiometric air), the ratio between each component cost for hybrid system and reference system will be the same as the ratio between the mass flow rates of the fuel, so

$$\frac{\dot{Z}_{\mathrm{TOT},0}}{\dot{Z}_{\mathrm{TOT}}-\dot{Z}_{\mathrm{AHS}}}=\frac{\dot{m}_{\mathrm{f},0}}{\dot{m}_{\mathrm{f}}}=1.14 \tag{9.94}$$

Defining the cost rate ratio between the additional heat source component (e.g. solar collection equipment) and the hybrid system as χ_{AHS}, or

$$\chi_{\mathrm{AHS}}=\frac{\dot{Z}_{\mathrm{AHS}}}{\dot{Z}_{\mathrm{TOT}}}, \tag{9.95}$$

results in

$$\frac{\dot{Z}_{\mathrm{TOT},0}}{\dot{Z}_{\mathrm{TOT}}-\dot{Z}_{\mathrm{AHS}}}=\frac{\dot{Z}_{\mathrm{TOT},0}}{\left(1-\chi_{\mathrm{AHS}}\right)\dot{Z}_{\mathrm{TOT}}}=1.14 \tag{9.96}$$

Substituting Eqs (9.87), (9.92), (9.93) and (9.96) into Eq. (9.80) and (9.81), the ratio between the electricity cost of the reference and the hybrid system is

$$\begin{aligned}\frac{c_{\mathrm{p},0}}{c_{\mathrm{p,h}}}&=\frac{\left(\dot{C}'_{\mathrm{f},0}-\dot{C}_{\mathrm{fg},0}+\dot{Z}_{\mathrm{TOT},0}\right)/\dot{W}_{\mathrm{net},0}}{\left(\dot{C}'_{\mathrm{f}}-\dot{C}_{\mathrm{fg}}+\dot{C}_{\mathrm{q,AHS}}+\dot{Z}_{\mathrm{TOT}}\right)/\dot{W}_{\mathrm{net}}}=\frac{\dot{W}_{\mathrm{net}}}{\dot{W}_{\mathrm{net},0}}\cdot\frac{\dot{C}'_{\mathrm{f},0}-\dot{C}_{\mathrm{fg},0}+\dot{Z}_{\mathrm{TOT},0}}{\dot{C}'_{\mathrm{f}}-\dot{C}_{\mathrm{fg}}+\dot{C}_{\mathrm{q,AHS}}+\dot{Z}_{\mathrm{TOT}}}\\&=0.94\frac{1.14\dot{C}'_{\mathrm{f}}-1.14\dot{C}_{\mathrm{fg}}+1.14\left(1-\chi_{\mathrm{AHS}}\right)\dot{Z}_{\mathrm{TOT}}}{\dot{C}'_{\mathrm{f}}-\dot{C}_{\mathrm{fg}}+\dot{C}_{\mathrm{q,AHS}}+\dot{Z}_{\mathrm{TOT}}}=1.07\left[\frac{\dot{C}'_{\mathrm{f}}-\dot{C}_{\mathrm{fg}}+\left(1-\chi_{\mathrm{AHS}}\right)\dot{Z}_{\mathrm{TOT}}}{\dot{C}'_{\mathrm{f}}-\dot{C}_{\mathrm{fg}}+\dot{C}_{\mathrm{q,AHS}}+\dot{Z}_{\mathrm{TOT}}}\right].\end{aligned} \tag{9.97}$$

Using Eq. (9.79), the difference between the numerator and denominator of Eq. (9.97) is

$$\Delta = 0.07\left(\dot{C}_{\mathrm{f}} + 1.375 c_{\mathrm{CO}_2}\dot{m}_{\mathrm{f}} - \dot{C}_{\mathrm{fg}}\right) - \left[\left(1.07\chi_{\mathrm{AHS}} - 0.07\right)\dot{Z}_{\mathrm{TOT}} + \dot{C}_{\mathrm{q,AHS}}\right] \tag{9.98}$$

and

$$c_{\mathrm{P,h}} < c_{\mathrm{P,0}}, \text{ if } \Delta > 0 \tag{9.99}$$

$$c_{\mathrm{P,h}} > c_{\mathrm{P,0}}, \text{ if } \Delta < 0 \tag{9.100}$$

According to Eq. (9.99), $c_{\mathrm{P,h}}$, the LEC for the hybrid system tends to become lower than $c_{\mathrm{P,0}}$, that for the reference system, when

1) $\left(\dot{C}_{\mathrm{f}} + 1.375 c_{\mathrm{CO}_2}\dot{m}_{\mathrm{f}} - \dot{C}_{\mathrm{fg}}\right)$ (the fuel price, carbon tax rates and externality cost) increases; and/or

2) χ_{AHS} (the cost rate fraction of the additional heat source) decreases; and/or

3) $\dot{Z}_{\mathrm{TOT}}$. (the total cost rate of the hybrid system) decreases; and/or

4) $\dot{C}_{\mathrm{q,AHS}}$ (the price of the additional heat source device) decreases.

Since $0 < \chi_{\mathrm{AHS}} < 1$,

$$1.07\chi_{\mathrm{AHS}} - 0.07 \approx \chi_{\mathrm{AHS}}. \tag{9.101}$$

Using Eq. (9.95), $c_{\mathrm{p,h}} < c_{\mathrm{p,0}}$, if

$$0.07\left(\dot{C}_{\mathrm{f}} + 1.375 c_{\mathrm{CO_2}} \dot{m}_{\mathrm{f}} - \dot{C}_{\mathrm{fg}}\right) > \dot{Z}_{\mathrm{AHS}} + \dot{C}_{\mathrm{q,AHS}}, \tag{9.102}$$

or written as

$$\dot{C}_{\mathrm{f}} > \frac{1}{0.07}\left(\dot{Z}_{\mathrm{AHS}} + \dot{C}_{\mathrm{q,AHS}}\right) - 1.375 c_{\mathrm{CO_2}} \dot{m}_{\mathrm{f}} + \dot{C}_{\mathrm{fg}}. \tag{9.103}$$

Thus we have found the condition under which the LEC for the hybrid system is lower than that for the reference system. In fact, Eq. (9.103) has a similar form as for SOLRGT.

Using Eqs (9.88), (9.78) and (9.28), Eq. (9.103) can be rewritten as

$$c_{\mathrm{f}} > \frac{\dot{Z}_{\mathrm{AHS}} + c_{\mathrm{q,AHS}} \dot{B}_{\mathrm{AHS}}}{0.07 \dot{m}_{\mathrm{f}} b_{\mathrm{f}}} - 1.375 c_{\mathrm{CO_2}} + \frac{1+\alpha}{\alpha} c_{\mathrm{fg}} b_{\mathrm{fg}} \tag{9.104}$$

It can be seen that Eq. (9.104) and Eq. (9.40) have similar forms as

$$c_{\mathrm{f}} > \frac{\dot{Z}_{\mathrm{AHS}} + c_{\mathrm{q,AHS}} \dot{B}_{\mathrm{AHS}}}{a_1 \dot{m}_{\mathrm{f}} b_{\mathrm{f}}} - a_2 c_{\mathrm{CO_2}} + a_3 c_{\mathrm{fg}} b_{\mathrm{fg}}, \tag{9.105}$$

in which a_i $(i=1,2,3)$ are different for SOLRGT and SOLRMCC and are summarized in Table 9-5.

Table 9-5. Summary table for a_i in comparison between SOLRGT and SOLRMCC

	SOLRGT	SOLRMCC
a_1	$(\alpha_0 - \alpha)$	0.07
a_2	-2.75	-1.375
a_3	1	$\frac{1+\alpha}{\alpha}$

Not all thermochemical hybrid systems are studied here, but it can be reasonably deduced that Eq. (9.105) may apply for most, if not all, of the thermochemical hybrid systems. Since there are too many different current and potential configurations of thermochemical hybrid system it is, however, unlikely that a universal equation for this purpose can be established.

Since Eqs (9.104) and (9.40) have similar forms, the sensitivity analysis of the LEC for SOLRMCC to fuel price, carbon tax and the solar collection equipment price is similar to that from SOLRGT as discussed in Section 9.4. Also, Eqs (9.80) and (9.21) have the same form except that Eq. (9.80) doesn't have the term $\dot{C}_{\mathrm{w}}$ that stands for the cost rate

associated with the water needed in reforming methane in SOLRGT, which is not required in the methanol decomposition process.

Equation (9.105) can be rewritten using the carbon tax rate c_{CO_2} as

$$c_{\mathrm{CO}_2} > \frac{1}{a_2}\left(\frac{\dot{Z}_{\mathrm{AHS}} + c_{\mathrm{q,AHS}}\dot{B}_{\mathrm{AHS}}}{a_1 \dot{m}_{\mathrm{f}} b_{\mathrm{f}}} + a_3 c_{\mathrm{fg}} b_{\mathrm{fg}} - c_{\mathrm{f}} \right), \tag{9.106}$$

indicating that the LEC for the hybrid system is lower than that for the reference when the carbon tax rate c_{CO_2} is higher than a certain value and provides an easy way to determine it.

Equation (9.106) gives guidance for determining the carbon tax rate. It indicates that the LEC for the hybrid system is lower than that for the reference system when the carbon tax rate is higher than a certain value that can be easily calculated. Considering the fact that imposing a carbon tax rate that is too small won't help the thermochemical hybrid system compete with the reference system economically too much and imposing a much larger carbon tax rate may not be needed, Eq. (9.106) provides an easy way in helping determine the appropriate carbon tax value.

The equations derived for the dependence of the thermochemical hybrid systems' electricity costs are functions of the systems' governing parameters and can thus be easily used for price sensitivity analysis. For example, Eqs (9.80) and (9.21) can be differentiated

to determine the sensitivity of the LEC for both hybrid systems, $c_{\mathrm{P,h}}$, to the fuel price, c_{f}, which is functionally expressed by

$$\frac{\partial c_{\mathrm{p,h}}}{\partial c_{\mathrm{f}}} = \frac{1}{\dot{W}_{\mathrm{net}}} \frac{\partial \dot{C}_{\mathrm{f}}}{\partial c_{\mathrm{f}}} = \frac{1}{\dot{W}_{\mathrm{net}}} \dot{m}_{\mathrm{f}} b_{\mathrm{f}}, \tag{9.107}$$

since the other terms in the numerator of Eqs (9.80) and (9.21) don't change with the fuel price.

Similarly, it can be found that

$$\frac{\partial c_{\mathrm{p,h}}}{\partial c_{\mathrm{ct}}} = \frac{1}{\dot{W}_{\mathrm{net}}} \frac{\partial \dot{C}_{\mathrm{ct}}}{\partial c_{\mathrm{ct}}} = \frac{1}{\dot{W}_{\mathrm{net}}} \dot{m}_{\mathrm{CO_2}} \tag{9.108}$$

$$\frac{\partial c_{\mathrm{p,h}}}{\partial \dot{Z}_{\mathrm{AHS}}} = \frac{1}{\dot{W}_{\mathrm{net}}} \tag{9.109}$$

Since c_{f}, c_{ct} and $\dot{Z}_{\mathrm{AHS}}$ have different units and are independent of each other, evaluation of the relative impact of these factors on the LEC for the hybrid system, $c_{\mathrm{P,h}}$, can only be determined by finding and using their values in Eqs (139) and (140). According to Eq. (9.77), $\dot{m}_{\mathrm{f}}$ is proportional to $\dot{m}_{\mathrm{CO_2}}$. Equation (9.107) and (9.108) thus showed that the partial derivative of the fuel price c_{f} and the carbon tax rate c_{ct} both increase with the mass flow rate of the fuel, $\dot{m}_{\mathrm{f}}$. As more AHS is added, less fuel is needed in the power

systems when the total heat input remains the same. This means that the impact of c_f and c_{ct} become smaller as more AHS is added in the hybrid system. The impact of the cost rate of the AHS equipment, $\dot{Z}_{AHS}$, on the $c_{P,h}$ however, doesn't change with $\dot{m}_f$, meaning that more focus should be put on reducing $\dot{Z}_{AHS}$ when the mass flow rate of fuel become smaller.

9.6. Conclusions of the exergo-economic analysis of thermochemical hybrid systems

Exergo-economic analysis is used in this study to derive expressions for calculating the levelized costs of electricity (LEC) from two thermochemical hybrid power generation systems and for comparing them with the corresponding conventional single heat source systems and a reference non-thermochemical hybrid system.

- While it is obvious that when the fuel price and carbon tax is high enough and/or the cost associated with the additional heat source is low enough, the LEC for the hybrid system will be lower than that for the reference system, this study, however, developed the equations that can be used to determine under which conditions the thermochemical hybrid systems becomes economically competitive with the corresponding reference; in the considered specific example based on current prices of fuel, carbon tax and equipment costs, it is found that the LEC for the hybrid system is smaller than the reference one when fuel price is higher than 2.3×10^{-6}

$/kJ, or carbon tax is higher than 0.0113 $/$kg_{CO_2}$, or the cost rate of AHS equipment is less than 0.323$/s.

- A sensitivity analysis of the LEC for the SOLRGT and SOLRMCC to fuel price, carbon tax and the solar collection equipment price, respectively, was performed. The partial derivative of the LEC ($/kWh) from the SOLRGT with respect to the fuel price is 1.73 $/(kJ-exergy) and to the carbon tax rate is 0.093 $/(tonne CO_2). The partial derivative of the LEC ($/kWh) from the SOLRMCC with respect to the fuel price is 1.52 $/(kJ-exergy) and to the carbon tax rate is 0.072 $/(tonne CO_2).

- A summary of the equation numbers derived for determining the conditions under which the LEC for the thermochemical hybrid system will be lower than that for the chosen reference systems along with the results for the sensitivity analysis, are given in Table 9-6.

- It was found that the conditions under which the LEC for the thermochemical hybrid system will be lower than that for the chosen reference systems for both the SOLRGT and SOLRMCC are similar, suggesting that other thermochemical hybrid systems also may lead to similar results.

Table 9-6. Main conclusions of the exergo-economic analysis for SOLRGT and SOLRMCC.

	Condition under which the LEC for the hybrid system is lower than that for the reference system	Partial derivative of LEC for the hybrid system with respect to		
		Fuel price	Carbon tax	Cost of AHS
SOLRGT	Eqs (9.40) and (9.65)	Eq. (9.107)	Eq. (9.108)	Eq. (9.109)
SOLRMCC	Eq. (9.104)			

- A comparison between the energo-economic analysis method and the exergo-economic analysis method was made to show the differences between them, which demonstrated some of the advantages of the latter for comparing the LEC for the thermochemical hybrid system with that for the reference ones (single heat source system or non-thermochemical hybrid system) without thorough knowledge of the cost of each equipment item, but with help of only a few thermodynamic parameters, and the ability to calculate the externalities of power systems.
- The effect of the cost penalty or profit of the flue gas on the economic performance of the power generation systems was included in the analysis.

9.7. Recommendations and future

In addition to the equations developed in this study for facilitating the calculation of the exergo-economic condition that make hybrid power systems competitive with conventional (non-hybrid) ones, the results from this study for the two types of thermochemical hybrid systems show that to make thermochemical hybrid systems economically competitive with the corresponding fuel-only conventional power generation system, the fuel price has to be high enough. Our study showed that the thermochemical hybrid system becomes economically competitive with the assumed fuel-only reference system when the fuel price rises by 17%, which is not hard to achieve.

Considering the fact that the current fuel prices do not in most cases include even a small fraction of the cost of the fuel externalities (such as, but not limited to, carbon tax), inclusion of these would help not only make hybrid systems more economically competitive but also clean the environment. Our study showed that even imposing half of the carbon tax rate of British Columbia [21], the thermochemical hybrid systems will become economically competitive with the fuel-only ones. While fuel price is largely determined by the market and carbon tax by policy, more effort should also be made for decreasing the cost associated with the components that collect and use the additional heat source, such as solar collection equipment when solar heat is used as the additional heat source. For example, the LEC for the hybrid system becomes lower than that for the reference single-heat-source system when the cost rate of the AHS equipment is 26% lower

than its assumed current value shown in Table 9-3. As technology advances, there is still much room to decrease the cost of using the additional heat source (AHS), compared with the fuel-only thermochemical systems, which have been developed for decades and may have less room for reducing theirs.

Predicting rising fuel price in the long term, higher carbon tax, and decreasing cost for implementing additional heat sources, thermochemical hybrid systems using additional heat sources will, therefore, become more economically competitive compared with the conventional systems, especially for the hybrid systems that use AHS, which don't generate CO_2 and other undesirable emissions.

References for Chapter 9

[1] El-Sayed Y.M., The Thermoeconomics of Energy Conversions. Oxford, UK: Elsevier Ltd;2003.

[2] Szargut J., Exergy Method. WIT:2005.

[3] Carbon Tax Center (British Columbia) - Available at:<http://www.carbontax.org/where-carbon-is-taxed/british-columbia/> [accessed 28.2.2016]

[4] U.S. Energy Information Administration 2015 “Natural Gas Weekly Update,” http://www.eia.gov/naturalgas/weekly/ 2015.12.14.

[5] Kliemke H, Johnke T. Gas Turbine Modernization - Fuel Conversion and Special Fuel Applications for the Asian Market POWER-GEN Asia 2012 Bangkok Thailand October 03-05 2012 http://www.energy.siemens.com/us/pool/hq/energy-topics/pdfs/en/techninal%20paper/Siemens-Technical%20Paper-Gas-Turbine-Modernization.pdf

CHAPTER 10

CONCLUSIONS AND RECOMMENDATIONS

Past studies on hybrid power cycles using multiple heat sources of different temperatures focused mainly on case studies and almost no general theory about this type of systems has been developed. This dissertation mainly examined the thermodynamic and economic performance of hybrid power generation systems simultaneously using multiple heat sources of different temperatures. Two types of hybrid systems were examined: thermal hybrid systems that involve chemical reactions only in the fuel combustion process, and thermochemical hybrid systems that involves chemical reactions other than the fuel combustion process.

For the first type of hybrid systems, thermal hybrid power generation systems, the method used in the dissertation is step-wise: to first analyze the major, most commonly used, hybrid power generation systems thermodynamically, without involving specific operation parameter values. In this way, some generalized theory that is at least applicable to *this* type of system can be developed. The second step is to perform such an analysis for all the major types of power generation systems (e.g. Rankine, Brayton, Combined Cycles, and their main variants). The third step is to find commonalities between these theories (if any). The fourth and last step is to develop the sought generalized theory based on these commonalities. As shown in this dissertation, this approach indeed worked and led to the discovery of such a theory.

Based on the major types of power generation methods, the hybrid power generation systems based on Rankine cycles, Brayton cycles and combined cycle were analyzed in sequence.

For the hybrid power generation systems based on the simple Rankine cycle, it was found that for the same enthalpy states in the hybrid and reference systems, the energy efficiency of the hybrid system is higher than that of the reference single heat source system if and only if the energy conversion efficiency (defined in Eq. (4.1)) of the AHS is larger than that of the heat source used in the reference single heat source system, i.e. $\eta_{\mathrm{h}} < \eta_0$ for $\eta_{\mathrm{AHS}} < \eta_{\mathrm{HTHS}}$, $\eta_{\mathrm{h}} = \eta_0$ for $\eta_{\mathrm{AHS}} = \eta_{\mathrm{HTHS}}$ and $\eta_{\mathrm{h}} > \eta_0$ for $\eta_{\mathrm{AHS}} > \eta_{\mathrm{HTHS}}$; and for the same enthalpy states in the hybrid and reference systems, the exergy efficiency of the hybrid system is higher than that of the reference single heat source system if and only if the exergy conversion efficiency (defined in Eqs (4.21) and (4.22)) of the AHS is larger than that of the heat source used in the reference single heat source system, i.e. $\varepsilon_{\mathrm{h}} < \varepsilon_0$ for $\eta'_{\mathrm{AHS}} < \eta'_{\mathrm{HTHS}}$, $\varepsilon_{\mathrm{h}} = \varepsilon_0$ for $\eta'_{\mathrm{AHS}} = \eta'_{\mathrm{HTHS}}$ and $\varepsilon_{\mathrm{h}} > \varepsilon_0$ for $\eta'_{\mathrm{AHS}} > \eta'_{\mathrm{HTHS}}$. The results from the sensitivity analysis (derived from the thermodynamic analysis and confirmed by the simulation results) showed the relations between the temperature, T_{AHS}, and heat addition rate of the AHS, $\dot{Q}_{\mathrm{AHS}}$, and the energy/exergy efficiency of the hybrid system, based on different η_{AHS}. These relations can be used to help design the hybrid systems to achieve higher energy and/or exergy efficiencies before detailed design or simulation or experiment.

The thermodynamic analysis and simulation for the hybrid power generation systems based on the Rankine cycle with reheat showed similar characteristics with the hybrid systems based on the simple Rankine cycle.

The thermodynamic analysis for the hybrid power generation systems based on the Rankine cycle with heat regeneration showed that replacing higher pressure extracted steam will achieve higher system energy efficiency than replacing lower pressure extracted steam, when both extracted steams, if replaced, increase the same amount of net power output. When solar heat is used as the AHS and the temperature of the solar heat is defined as the sun surface, this result also applies to the exergy efficiency of the hybrid system. The results suggested that it is better to replace the higher pressure extracted steams with the AHS than the lower pressure ones in terms of energy efficiency. From the exergy point of view, however, it is not always the case and a simple criterion to decide which extracted steam to replace is Eq. (4.127).

The thermodynamic analysis for the hybrid power generation systems based on the simple Brayton cycle, Brayton cycle with intercooling, Brayton cycle with reheat and Brayton cycle with heat regeneration was done, respectively. The results showed that the energy efficiency of the hybrid system is lower that of the single heat source reference system when $\eta_{\mathrm{AHS}} < \eta_{\mathrm{CC}} - \dfrac{h_4 - h_7}{\mathrm{LHV}}$. Considering that $\eta_{\mathrm{CC}} - \dfrac{h_4 - h_7}{\mathrm{LHV}}$ is close to 1 and $\eta_{\mathrm{AHS}} \le 1$, adding the AHS to the single heat source Brayton cycles will lower the energy efficiency of the reference system as Table 3-2 showed in the background review. The exergy

efficiency, however, is not the case, and $\varepsilon_h > \varepsilon_0$ when $\eta'_{AHS} < \eta'_{CC} - \frac{h_4 - h_7}{b_f}$ or roughly $\eta_{AHS} > 1 - \frac{T_0}{T_{AHS}}$. For example, when $T_{AHS} = 800\ ^\circ\text{C}$ and $T_0 = 15\ ^\circ\text{C}$, $\varepsilon_h > \varepsilon_0$ when $\eta_{AHS} > 0.73$.

Following the validation, a detailed simulation for the hybrid power generation systems based on the Brayton cycle with intercooling, reheat and heat regeneration was done in the dissertation. The results were compared for with and without the consideration of pressure drops in the system and showed that the energy efficiency dropped 3.1% if pressure drops were considered in the system. The results from the exergy analysis for each major component of the single heat source reference system showed that the majority (68.1%) of the exergy destructions happened in the combustors, in which fuel was burned. Considering that, using the AHS to help heat the working fluid may decrease the exergy destruction in the combustors and raise the exergy efficiency of the system. Another simulation was thus done to test the performance of the hybrid system. The results showed that the total exergy destruction of the system decreased by 16% (when the temperature of the solar heat is defined as the sun surface temperature), or 28% (when the temperature the AHS is 10 K higher than the temperature of the working fluid at the outlet of the AHSC). The sensitivity analysis of the energy efficiency of the hybrid system with respect to the AHS input fraction of the total energy input, exergy input rate from the AHS and the dimensionless

parameter $\frac{T_6 - T_5}{T_7}$ in Fig. 5-11, for different energy conversion efficiency of the AHS was also done. The results can be used to help researcher study the performance of the hybrid power generation systems based on the Brayton cycles and suggested that effort should be made in increasing η_{AHS}.

The thermodynamic analysis for the hybrid power generation systems based on the combined cycle suggested that its performance characteristics are similar to the hybrid power generation based on the Brayton cycles, when the AHS is added in the topping cycle (the fuel-saving mode). When the AHS is added in the bottoming cycle (power-boost mode), the results showed that $\eta_{\text{h}} < \eta_0$ and η_{h} increases with η_{AHS} but decreases with the AHS input fraction of total energy input, X_{AHS} (defined in Eq. (2.16)). From the exergy point of view, however, the exergy efficiency of the hybrid system is larger than that of the conventional single heat source system, $\varepsilon_{\text{h}} > \varepsilon_0$, when $T_{\text{AHS}} < \frac{T_0}{1 - \eta_{\text{AHS}} \frac{\psi_{\text{f}} \eta_{\text{bc}}}{\eta_0}}$. This result suggests that the temperature of the AHS, T_{AHS}, should be designed so that it is smaller than $\frac{T_0}{1 - \eta_{\text{AHS}} \frac{\psi_{\text{f}} \eta_{\text{bc}}}{\eta_0}}$, from the perspective of exergy efficiency of the system. This result thus saves lots of work before detail design of the hybrid power generation systems based on the combined cycle when the AHS is added in the bottoming cycle. For

example, when $\eta_{\mathrm{AHS}} = 0.8$, $\psi_{\mathrm{f}} = 1.04$, $\eta_{\mathrm{bc}} = 0.4$, $\eta_0 = 0.55$ and $T_0 = 15$ °C, the maximum AHS temperature is 456 °C for $\varepsilon_{\mathrm{h}} > \varepsilon_0$.

For the second type of hybrid power generation systems using multiple heat sources of different temperatures, the thermochemical hybrid power generation systems, two representative systems were chosen for analysis. One (SOLRGT) using methane as fuel and the other (SOLRMCC) using methanol as fuel, which are the two most widely used types of fuel in thermochemical hybrid power generation systems by researchers. Both of the systems use low temperature solar heat (at ~220 °C) to help reform or decompose the fuel to syngas, which is then used for power generation. The main conclusions were summarized in Section 7.6 and are not repeated here.

Besides thermodynamic analysis of the hybrid power generation systems, the exergo-economic analysis was also done to complement the analysis, since there is usually a tradeoff between the thermodynamic performance and the economic performance of the power generation systems. Using the SPECO method that is widely accepted and used by researchers for exergo-economic analysis, it was found that the difference between the levelized electricity cost (LEC) of the thermal hybrid system and the corresponding single heat source reference system can be grouped into two equations based on whether the AHS is used to save fuel (fuel-saving mode, Eq. (8.194)) or to increase the power output (power-boost mode, Eq. (8.195)). The results also showed the simple criteria to determine whether the LEC of the hybrid system is lower than that of the reference system (Eqs (8.196) and

(9.105)). The exergo-economic analysis method was compared with the conventional energo-economic analysis method. The externalities and carbon tax (or other monetary penalty for CO_2 emissions) were also considered in the exergo-economic analysis. Details are available in Sections 8.6 and 9.6 are not repeated here.

The conclusions summarized here are the main contributions from the author of the dissertation to the state of knowledge. None of this work has been done by others, to the best of the author's knowledge.

The results found in the dissertation give the following recommendations:

1) Effort should be made on increasing the energy conversion efficiency of the AHS, η_{AHS}, since higher η_{AHS} increases the energy efficiencies of the hybrid systems. Using the definition of η_{AHS} (Eq. (4.1)), it means that the heat loss from the AHS to the working fluid of the power cycle should be minimized, which can be done by increasing the AHSC efficiency (such as solar collector efficiency when solar heat is used as the AHS), adding insulation to the pipes, reducing the length of pipes and minimizing the use of heat exchangers that transfer heat from the AHS to the working fluid in the power cycle.
2) Effort should be made on increasing the exergy conversion efficiency of the AHS, η'_{AHS}, since higher η'_{AHS} increases the exergy efficiencies the hybrid systems. Using the definition of η'_{AHS} (defined in Eqs (4.21) and (4.22)), it means that the

energy conversion efficiency η_{AHS} should be maximized, and the exergy factor of fuel, ψ_{f} (defined in Eq. (2.9)), and the temperature of the AHS, T_{AHS}, should be minimized. This suggests that besides the measures mentioned above to increase η_{AHS}, fuels that have lower ψ_{f}, such as biomass, instead of fossil fuel, should be used, and additional effort should be made on reducing T_{AHS}, such as reducing the pinch point temperature in the heat exchanger that transfer heat from the AHS to the working fluid in the power cycle or even heating the working fluid directly without the use of the heat exchangers.

3) When the AHS is used to replace the feedwater heater in the Rankine cycles with heat regeneration, the results suggest that it is better to replace the higher pressure extracted steams with the AHS than the lower pressure ones in terms of energy efficiency. From the exergy point of view, however, it is not always the case and a simple criterion to decide which extracted steam to replace is Eq. (4.127).

4) When adding the AHS to the bottoming cycle (Rankine cycle) of the combined cycle, the temperature of the AHS should be lower than $\dfrac{T_0}{1-\eta_{\text{AHS}}\dfrac{\psi_{\text{f}}\eta_{\text{bc}}}{\eta_0}}$, so that the exergy efficiency of the hybrid system is higher that of the original combined cycle system.

5) It is necessary to distinguish between different solar exergy or solar heat temperature definitions before comparing results from different sources. The results

are different even for the same system with different solar exergy definitions. There is no “solar thermal upgrading” for solar thermochemical hybrid systems if solar exergy is defined using sun surface temperature.

6) Forecasting rising fuel price in the long term, higher taxing of externalities, and decreasing cost for implementing additional heat sources, hybrid systems using multiple heat source of different temperatures will increasingly become more economically competitive when compared with the conventional systems, especially for the hybrid systems that use heat sources that reduce generation of greenhouse gases and other undesirable emissions.

Nomenclature

A	Area, m^2
AHS	Additional heat source
AHSC	Addition heat source collection equipment
AHSP	Addition heat source pump
b	Specific exergy, kJ/kg
b_f	Specific exergy of fuel, kJ/kg
B	Exergy, kJ
$\dot{B}$	Exergy flow rate, kW
c	Specific cost, $/kJ
c'_{ash}	Ratio between cost of ash and fuel price
c'_{ct}	Ratio between cost of carbon tax and fuel price
c'_f	Specific cost associated with fuel, $/kJ (Eq. (8.33))
c'_{fg}	Ratio between cost of flue gas and fuel price
c_p	Specific heat capacity, kJ/kg-K
c_p	Levelized electricity cost (LEC), $/kJ
C_f	Annual fuel cost, $

$\dot{C}_f$ Fuel cost rate, \$/s

C_p Heat capacity, kJ/kg

C_{inv} Total investment cost, \$

$C_{O\&M}$ Annual operation and maintenance (O&M) cost, \$

g Gravitational acceleration, m/s^2

f Fuel-air ratio

h Specific enthalpy, kJ/kg

H Operation time, h; Flow enthalpy, kJ

HHV Higher heating value, kJ/kg

HS Heat source

$HTHS$ Higher temperature heat source

i Interest rate

I_s Energy density of solar radiation, kW/m^2

LHV Fuel Lower heating value, kJ/kg

$\dot{m}$ Mass flow rate, kg/s

n_{HE} Exponent relating the heat transfer rate and the cost of heat exchangers

p Pressure, kPa

Q Heat transfer, kJ

$\dot{Q}$ Heat transfer rate, kW

$\dot{Q}_{\text{ADD}}$ Heat transfer rate to the working fluid from the heat source, kW

r_{cf} Ratio between the assumed fuel price and the current fuel price

R_{sm} Ratio between steam and methane mass flow rates

s specific entropy, kJ/kg-K

S_{f} Fuel savings ratio (Eq. (2.18))

T Temperature, K

T_0 Dead state temperature, K

X Fraction; Height above the lowest level prevailing near the considered device, m

X_{AHS} AHS heat input fraction of total heat input (Eq. (2.16))

X_{sol} Solar share (Eq. (2.17))

X'_{AHS} AHS exergy input fraction of total exergy input (Eq. (6.26))

y Extraction fraction of the extracted steams

$\dot{W}$ Power, kW

Z Cost of component, $

$\dot{Z}$ Cost rate of component, $/s

$\dot{Z}_0$ Change of cost rate of the equipment that both the hybrid and the reference system have, $/s

Greek symbols

η Energy efficiency

ε Exergy efficiency

ψ Exergy factor (Eqs (8.46) and (8.47))

Δ Difference

φ Maintenance factor (Eq. (8.7))

κ Capital recovery factor (Eq. (8.3))

χ_{AHS} Capital cost fraction of the AHS relative to the total capital cost of the system (Eq. (9.95))

Λ Energy level (Eq. (7.7))

Subscripts and superscripts

0 Reference (non-hybrid, single heat source) system

a Air

AHS Additional heat source

AHSC Additional heat source collection equipment

AHSP Additional heat source pump

ash Ash

bc	Bottoming cycle
B	Boiler
BFP	Boiler feedwater pump
CC	Combustor
CEP	Condensate extraction pump
ch	Chemical
COMP	Compressor
COND	Condenser
ct	Carbon tax
cw	Cooling water
d	Destruction
ea	Energy acceptor
ed	Energy donor
eff	Effective
ex	Turbine exhaust gas
E	Economizer
f	Fuel (material)
F	Fuel of a component
FC	Fuel compressor

fg	Flue gas
gen	Generator
GT	Gas turbine
h	Hybrid system; heat
H	Heater
HE	Heat exchanger
HP	High-pressure
HPC	High-pressure compressor
HPF	High-pressure feedwater heater
HR	Heat Recuperator
HRSG	Heat recovery steam generator
HS	Heat source
HT	Higher temperature
HTHS	Higher temperature heat source
IC	Intercooler
i	Inlet
in	input
net	Net
LP	Low-pressure

LPC	Low-pressure compressor
LPF	Low-pressure feedwater heater
LT	Lower temperature
LTHS	Lower temperature heat source
nu	Nuclear
net	Net
o	Outlet
O&M	Operation and Maintenance
P	Pump, Product of a component
R	Reactor; Regenerator
rad	Solar radiation
REC	Recuperator
REF	Reformer
ph	Physical
rad	Solar radiation
s	Steam
sc	Solar collector
se	Solar-to-electricity
sol	Solar

ss	Solar surface
ST	Steam turbine
syn	Syngas
T	Turbine
TI	Turbine inlet
TOT	Total
w	Working fluid, water
'	Non-thermochemical hybrid system